Human Brain Project

EBRAINS

Human Brain Project Summit 2023

Palais du Pharo, Marseille
28-31 March 2023

Book of Abstracts

Presented during Poster Sessions on 29 and 30 March

Co-funded by the European Union

Table of Contents

Please note that abstracts have been added to this document in the format they were submitted, and that there may be differences in layout.

1. openMINDS SANDS - a metadata model for ontology-based brain atlas definitions in graph databases

Lyuba Zehl[1,*], Ulrike Schlegel[2], Tom H. Gillespie[3], Heidi Kleven[2], Oliver Schmid[4], Stefan Köhnen[1], Jan G. Bjaalie[2], Katrin Amunts[1,5], Trygve B. Leergaard[2], Timo Dickscheid[1,6]

Affiliations: [1]Institute of Neuroscience and Medicine (INM-1), Research Centre Jülich, Jülich, Germany [2]Institute of Basic Medical Sciences, University of Oslo, Oslo, Norway [3]Department of Neurosciences, University of California San Diego, San Diego, USA [4]EBRAINS AISBL, Brussels, Belgium [5]C. and O. Vogt Institute for Brain Research, University Hospital Düsseldorf, Heinrich Heine University Düsseldorf, Düsseldorf, Germany [6]Institute of Computer Science, Heinrich Heine University Düsseldorf, Düsseldorf, Germany

*l.zehl@fz-juelich.de

INTRODUCTION/MOTIVATION

openMINDS (open Metadata Initiative for Neuroscience Data Structures) is a community-driven, open-source metadata framework for graph database systems. It is composed of linked metadata models, libraries of serviceable metadata instances, and supportive tooling. Each openMINDS metadata model covers certain aspects of neuroscience data (e.g., generic bibliographic records or modality-specific data provenance) with schemas that foster data findability, accessibility, interoperability and reusability (FAIR) [1]. For selected schemas, the openMINDS libraries offer serviceable metadata instances intended to be commonly used across database systems. Here we will present the metadata model and library for SANDS (Spatial Anchoring of Neuroscience Data Structures). SANDS covers ontology-based in-depth definitions for brain atlases enabling precise references of anatomical annotations, as well as spatial integration of atlas and non-atlas data within any graph database system.

METHODS

The SANDS metadata model closely follows the ontological definitions of the Atlas Ontology Model (AtOM) [2]. AtOM identifies a (brain) atlas as reference data in a common coordinate system presenting a set of anatomical annotations with a given terminology. In fact, any specific combination of these elements constitutes a unique atlas configuration, or version. For SANDS we translated these ontological requirements into a modular set of metadata schemas (Fig.1) that integrate with the other openMINDS metadata models covering all neuroscience data structures. Within the openMINDS framework, all schemas are implemented in a lightweight, JSON-based syntax which is automatically transformed to common schema formats, such as JSON-Schema [3]. As an ongoing effort, we identify metadata of community-wide accepted brain atlases, including common coordinate spaces, and provide a SANDS library of well-defined atlas descriptions as a collection of linked metadata instances (Fig. 2) formatted as JSON-LD files [4]. All openMINDS efforts are open-source, accepting requests and contributions from the whole scientific community.

RESULTS AND DISCUSSION

openMINDS SANDS offers a metadata model to consistently define brain atlases (and their versions) in accordance with AtOM (Fig. 1). SANDS also enables to define semantic and coordinate based relations between atlases and non-atlas, anatomically anchored data. Moreover, it includes a library of linked metadata instances describing an increasing number of community-wide accepted brain atlases (Fig. 2). All integrated openMINDS metadata models and libraries are ready-to-use and freely available on GitHub (https://github.com/HumanBrainProject/openMINDS). While the SANDS metadata model defines brain atlases and their individual components, the SANDS library offers a collection of serviceable atlas elements fostering the FAIRness of brain atlases across database systems and related services (Fig. 1, 2). In 2019, openMINDS (incl. SANDS) was adopted by EBRAINS (https://ebrains.eu/), a European neuroscience research infrastructure. It is currently in the process of being adopted by Brain/MINDS (https://brainminds.jp/en/), a Japanese national brain research project. Within EBRAINS, SANDS facilitates the interoperability between the EBRAINS Knowledge Graph (https://kg.ebrains.eu/) and other data services, in particular the EBRAINS Atlases (https://ebrains.eu/services/atlases/).openMINDS is a mature, open-source metadata framework for graph database systems. openMINDS SANDS, in particular, offers an ontology-based metadata model for defining brain atlases and anatomical locations of non-atlas data. Moreover, the SANDS library offers human and machine- readable atlas descriptions that are referenceable, facilitating integrations of brain atlases across scientific studies and software services. Through SANDS, brain atlases become more FAIR between different brain initiatives worldwide.

Keywords: atlasing, FAIR, graph database, metadata model, ontology

ACKNOWLEDGEMENTS

openMINDS is developed in the Human Brain Project, funded from the European Union's Horizon 2020 Framework Programme for Research and Innovation under Specific Grant Agreements No. 720270, No. 785907, and No. 945539 (Human Brain Project SGA1, SGA2, and SGA3). We also thank the EBRAINS Curation team, the EBRAINS Knowledge Graph team and other regular contributors for their constant support and feedback.

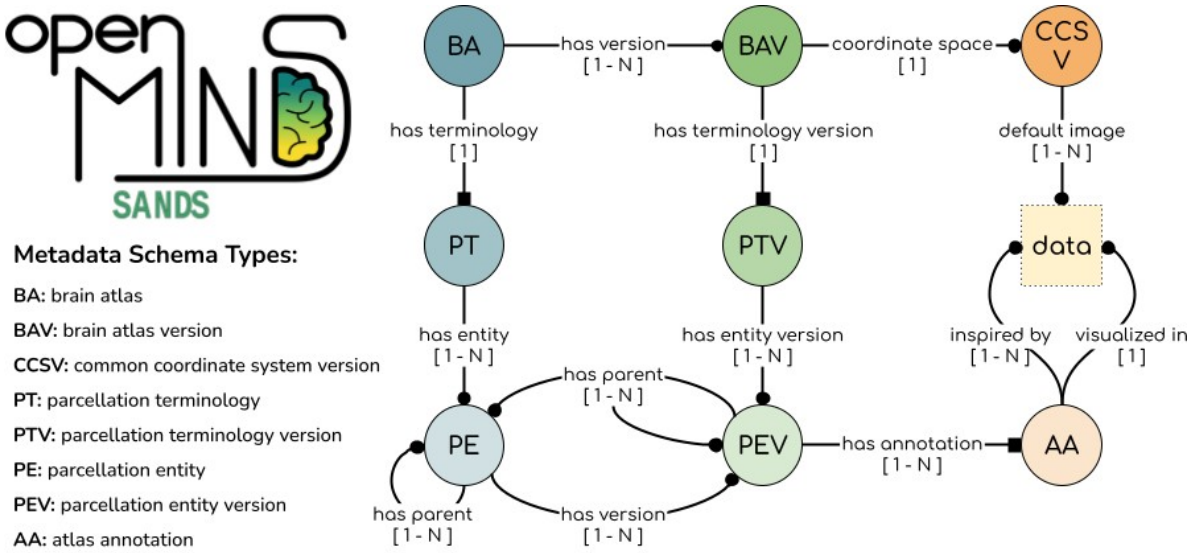

Figure 1: Simplified SANDS metadata model for defining brain atlas components. The figure shows a simplified version of the SANDS metadata model for defining brain atlas components. Metadata schema types are indicated as circles. How schema types are linked within the metadata model is indicated through connectors (square head: embedded schema type; round head: linked schema type; square bracket: possible number of embedded/linked schema types). Note that data are not represented as metadata schema types, because they can be linked in various ways (e.g., via URL).

Brain Atlas	Brain Atlas Version	Common Coordinate System
Julich-Brain Atlas [5]	Julich-Brain Atlas (v3.0, bigbrain)	BigBrain Model (2015) [6]
	Julich-Brain Atlas (v3.0, mni152)	MNI ICBM 152 (2009c Nonlin Asym) [7]
Waxholm Space Rat Brain Atlas [8]	Waxholm Space Rat Brain Atlas (v3)	Waxholm Space Rat Brain (v1.01) [8]
	Waxholm Space Rat Brain Atlas (v4)	
Allen Mouse Brain Atlas [9]	Allen Mouse Brain Atlas (2015)	Allen Mouse Brain CCF (v3) [10]
	Allen Mouse Brain Atlas (2017)	

Figure 2: Extract of the SANDS library for brain atlas components. The figure shows an extract from the SANDS library listing serviceable metadata instances for a selection of community-wide accepted brain atlases and common coordinate spaces. Each item represents a JSON-LD file with metadata stored as key-value pairs according to the respective SANDS schema type.

[5] Amunts, K. et al. (2020); [6] Amunts, K. et al. (2013); [7] Fonov, V.S. et al. (2009); [8] Papp, E. A. et al. (2014); [9] Lein, E.S. et al. (2007); [10] Wang, Q. et al. (2020)

REFERENCES

[1] Wilkinson M et al. (2016) *The FAIR Guiding Principles for scientific data management and stewardship.* Scientific Data, 3(160018), DOI: 10.1038/sdata.2016.18

[2] Kleven H et al. (2023) *AtOM, an ontology model for standardizing use of brain atlases in tools, workflows, and data infrastructures.* bioRxiv 2023.01.22.525049, DOI: 10.1101/2023.01.22.525049

[3] Pezoa F et al. (2016) *Foundations of JSON Schema.* in Proceedings of the 25th International Conference on World Wide Web, IW3C2 (Republic and Canton of Geneva, CHE), pp. 263–273, DOI: 10.1145/2872427.2883029

[4] Lanthaler M and Gütl, C. (2012). *On using JSON-LD to create evolvable RESTful services.* in Proceedings of the Third International Workshop on RESTful Design, ACM (New York, NY, USA), pp. 25–32, DOI: 10.1145/2307819.2307827

[5] Amunts K et al. (2020) *Julich-Brain: A 3D probabilistic atlas of the human brain's cytoarchitecture.* Science, 369(6506): 988-992, DOI: 10.1126/science.abb4588

[6] Amunts K et al. (2013) *BigBrain: An Ultrahigh-Resolution 3D Human Brain Model.* Science, 340 (6139): 1472–1475, DOI: 10.1126/science.1235381

[7] Fonov VS et al. (2009) *Unbiased nonlinear average age-appropriate brain templates from birth to adulthood.* NeuroImage, 47(S1): S39-S41, DOI: 10.1016/S1053-8119(09)70884-5

[8] Papp EA et al. (2014) *Waxholm Space atlas of the Sprague Dawley rat brain.* NeuroImage, 97: 374-386, DOI: 10.1016/j.neuroimage.2014.04.001

[9] Lein ES et al. (2007) *Genome-wide atlas of gene expression in the adult mouse brain.* Nature 445: 168–176 (2007). https://doi.org/10.1038/nature05453

[10] Wang Q et al. (2020) *The Allen Mouse Brain Common Coordinate Framework: A 3D Reference Atlas.* Cell, 181(4): 936-953.e20, DOI: 10.1016/j.cell.2020.04.007

2. TVBase: Utilizing Computational Semantics to Map Biomedical Knowledge onto the Brain

Leon Martin[1,2†], Leon Stefanovski[1,2†], Konstantin Bülau[1,2†], Chloê Langford[1,2], Jessica Palmer[1,2], Roopa Kalsank Pai[1,2,3], Marc Sacks[1,2], Lion Deger[1,2], Marius Pille[1,2], Marc Jacobs[4], Jürgen Klein[4], Alpha Tom Kodamullil[4], Martin Hofmann-Apitius[4,5], Michael Schirner[1,2], Jil Meier[1,2], Petra Ritter [1,2,3*]

[1]Berlin Institute of Health at Charité – Universitätsmedizin Berlin, Berlin, Germany
[2]Department of Neurology with Experimental Neurology, Brain Simulation Section, Charité – Universitätsmedizin Berlin, corporate member of Freie Universität Berlin and Humboldt-Universität zu Berlin, Berlin, Germany
[3]Bernstein Center for Computational Neuroscience Berlin, Berlin, Germany
[4]Department of Bioinformatics, Fraunhofer Institute for Algorithms and Scientific Computing (SCAI), 53757 Sankt Augustin, Germany,
[5]Bonn-Aachen International Center for Information Technology (B-IT), University of Bonn, 53113 Bonn, Germany

[†] LM, LS, and KB contributed equally to this work.

*corresponding author: petra.ritter@bih-charite.de

INTRODUCTION/MOTIVATION

Biomedical knowledge about the brain is increasing daily, alongside a rapidly growing number of scientific publications. While a holistic understanding of this plethora of information by mere reading becomes impossible, recent developments in information science and computational linguistics aim to make this knowledge programmatically accessible by adding a semantic understanding of publications via literature mining and entity recognition algorithms. However, these linguistic methods have not been sufficiently integrated into current brain imaging data standards, hindering researchers from harnessing the full potential of computational semantics in neuroscience.

METHODS

Therefore, we developed the text-mining-based semantic meta-analysis platform The Virtual Brain Adapter of Semantics (TVBase) that projects biomedical knowledge preserved in over 36 million scientific articles onto a 3D standard brain in MNI space. The literature-mining platform SCAIView [1] was used to extract ontologically defined biomedical entities, and their associations with brain anatomy, from abstracts and full texts of the PubMed database. By querying each concept, its association strength with each anatomical term, defined in the Uberon-ontology [2], was calculated using information entropy measures. To project the data onto a standard brain, we created a unique transformation matrix that links over 800 unique anatomical terms to the voxel coordinates of a parcellated brain. Our new methodology creates semantic brain maps that depict which areas of the brain a particular biomedical concept is associated with in the scientific literature and quantifies the relevance of this association by measures of information entropy.

In this study, a first external validation of semantic TVBase maps show their concordance with empirical brain maps derived from the neuromaps database [3]. Maps created from various imaging modalities were investigated, from magnetoencephalography (MEG) data to positron emission tomography imaging of tracers for neurotransmitter receptors. Statistical robustness was quantified using spatially and functionally constrained permutation testing.

RESULTS AND DISCUSSION

Using the proposed methodology, we mapped over 100,000 biomedical concepts unambiguously defined in state-of-the-art ontologies and nomenclatures from the Medical Subject Headings (MeSH) [4], Gene Ontology (GO) [5] and the Hugo Gene Nomenclature (HGNC) [6]. Validation with conceptually equivalent empirical maps shows substantial overlap with semantically extracted brain regions, mainly for MEG power distributions and dopamine, glutamate, and serotonin receptor maps, as well as for maps of cerebral blood flow and glucose metabolism. This unlocks the potential for using TVBase as proxy for empirical data and further for the integration of biological knowledge into brain network models by introducing mechanistically plausible spatial heterogeneity.

In summary, TVBase extracts region-specific information about biomedical concepts from the literature to support translational multi-scale approaches to computational neuroscience. It allows for hypothesis-free neuroimaging pattern interpretation, hypothesis generation, and applications in personalised medicine. TVBase is available as a python package or as an application programming interface (API) connected to a centralized database.

Keywords: Literature research, biomedical knowledge, computational semantics, meta-research, brain mapping, software framework, python, The Virtual Brain

ACKNOWLEDGEMENTS

Computation of underlying data has been performed on the HPC for Research cluster of the Berlin Institute of Health. PR acknowledges support by EU H2020 Virtual Brain Cloud 826421, Human Brain Project SGA2 785907; Human Brain Project SGA3 945539, ERC Consolidator 683049; German Research Foundation SFB 1436 (project ID 425899996); SFB 1315 (project ID 327654276); SFB 936 (project ID 178316478; SFB-TRR 295 (project ID 424778381); SPP Computational Connectomics RI 2073/6-1, RI 2073/10-2, RI 2073/9-1; PHRASE Horizon EIC grant 101058240; Berlin Institute of Health & Foundation Charité, Johanna Quandt Excellence Initiative; ERAPerMed Pattern-Cog.

REFERENCES

[1] Dörpinghaus, J., Klein, J., Darms, J., Madan, S., & Jacobs, M. (2018). SCAIView-A Semantic Search Engine for Biomedical Research Utilizing a Microservice Architecture. Paper presented at the SEMANTICS Posters&Demos.

[2] Mungall, C.J., Torniai, C., Gkoutos, G.V. et al.Uberon, an integrative multi-species anatomy ontology. Genome Biol 13, R5 (2012). https://doi.org/10.1186/gb-2012-13-1-r5

[3] Markello, R.D., Hansen, J.Y., Liu, ZQ. et al. (2022). neuromaps: structural and functional interpretation of brain maps. Nat Methods 19, 1472–1479. https://doi.org/10.1038/s41592-022-01625-w

[4] Rogers, F.B. (1963). Medical subject headings. Bulletin of the Medical Library Association, 51, 114-116.
[5] Gene Ontology Consortium. (2004). The Gene Ontology (GO) database and informatics resource. Nucleic acids research, 32(suppl_1), D258-D261. https://doi.org/10.1093/nar/gkh036
[6] Povey, S., Lovering, R., Bruford, E., Wright, M., Lush, M., & Wain, H. (2001). The HUGO gene nomenclature committee (HGNC). Human genetics, 109, 678-680. https://doi.org/10.1007/s00439-001-0615-0

3. EBRAINS datasets reveal region, sex and age differences in dopamine receptor cell densities in the mouse forebrain

Bjerke IE[1#], Carey H[1], Leergaard TB[1], Bjaalie JG[1], Kim JH[2,3*]

[1] *Neural Systems Laboratory, Institute of Basic Medical Sciences, University of Oslo, Norway*

[2] *The Florey Department of Neuroscience and Mental Health, University of Melbourne, Victoria, Australia*

[3] *IMPACT – the Institute for Mental and Physical Health and Clinical Translation, School of Medicine, Deakin University, Geelong, VIC, Australia*

Presenting author

** Correspondence:* drjeehyunkim@gmail.com

INTRODUCTION / MOTIVATION

The dopaminergic system undergoes major developments during adolescence, a period especially vulnerable to mental disorders. Cells expressing dopamine 1 and 2 receptors (D1R and D2R, respectively), are particularly sensitive to dopaminergic input. These neurons are distributed across the forebrain and contribute to higher cognitive functions such as attention, goal-directed behavior, and motivation. The typical development of the dopaminergic system is poorly understood, with its information sparse and scattered across publications investigating one or at most a few brain regions. This gap in knowledge should be filled to understand the ontogeny of brain function and dysfunction. Here, we perform a comprehensive analysis of D1R and D2R cell densities, using a collection of high-resolution microscopic images available from the EBRAINS Knowledge Graph[1]. We use these data to ask how the density of the dopamine receptor positive cells vary across brain regions, sex, and through development.

METHODS

A comprehensive collection of microscopic images of immunohistochemically stained sections from 152 male and female mice at five stages of development (P17, P25, P35, P49, and adult) was used. These images show D1R and D2R expressing neurons across the forebrain and are shared through the DOPAMAP collection available through the EBRAINS Knowledge Graph[1]. We analyzed all images using the semi-automated QUINT workflow[2], combining atlas defined regions-of-interest and image segmentation to extract and quantify D1R and D2R positive cells across sex and age groups. First, all images were registered to the Allen Mouse brain Common Coordinate Framework (CCF) tools using linear and non-linear registration with the QuickNII (RRID:SCR_016854) and VisuAlign (RRID:SCR_017124) tools[3], respectively, resulting in custom atlas maps corresponding to each image. To account for differences between young and adult brains, images from the P17-P35 age groups were registered to spatially modified atlas delineations matching the morphology of young brains[4]. Secondly, to extract labelled cell bodies, images were segmented using ilastik (RRID:SCR_015246)[5]. Lastly, custom atlas maps

and segmented images were combined using Nutil Quantifier (RRID:SCR_017183)[6], where all extracted cells are quantified per brain region and assigned coordinates in the Allen CCF. Based on these comprehensive data, we explored the regional changes of D1R and D2R cell densities across development and sex. The derived data set will be shared via EBRAINS.

RESULTS AND DISCUSSION

We observed distinct dominance of D1R densities in rostral regions of the forebrain, which switched to D2R dominance in more caudal forebrain regions: D1R cells were most prevalent in isocortical and olfactory areas, while D2R cells were more dominant in hypothalamic and midbrain regions. This pattern was observed at all ages examined. We further observed that D1R cell densities were highest at P17 or P49 in most regions. By contrast, D2R cell densities were typically highest at P17, showing a steady decline to adult levels in most regions. Interestingly, female mice had higher D1R cell densities than males in most regions at P17, while males had higher D2R cell densities than females across development in most regions. Surprisingly, D1R and D2R densities became comparable between the sexes with maturation towards adulthood, suggesting gene-driven sex differences in the dopaminergic system early in life. Our data provide a novel quantitative overview of the regional maturation and spatial distributions of dopaminergic neurons in the mouse forebrain. Our findings show profound sex and age differences in the dopaminergic system, which challenge previous reports on D1R and D2R expression in the forebrain. The high densities of D2R cells at P17 are particularly interesting, and future studies might investigate whether the densities peak around this age or even earlier.

Keywords: dopamine; dopamine 1 receptor; dopamine 2 receptor; mouse; brain development; immunohistochemistry; atlas registration; data sharing; neuroimaging

Acknowledgements: This work was funded from EU Horizon 2020, Specific Grant Agreement No. 945539 (Human Brain Project SGA3) and the HBP voucher program.

References:

1. Bjerke I, Cullity E, Kjelsberg K, Charan K, Leergaard T, Kim J. DOPAMAP, high- resolution images of dopamine 1 and 2 receptor expression in developing and adult mouse brains. *Sci Data*. 2022;9(1):1-11. doi:10.1038/s41597-022-01268-8

2. Yates S, Groeneboom N, Coello C, et al. QUINT: Workflow for Quantification and Spatial Analysis of Features in Histological Images From Rodent Brain. *Front Neuroinform*. 2019;13(75):1-14. doi:10.3389/fninf.2019.00075

3. Puchades M, Csucs G, Ledergerber D, Leergaard T, Bjaalie J. Spatial registration of serial microscopic brain images to three-dimensional reference atlases with the QuickNII tool. *PLoS One*. 2019;14(5). doi:10.1371/journal.pone.0216796

4. Newmaster K, Nolan Z, Chon U, et al. Quantitative cellular-resolution map of the oxytocin receptor in postnatally developing mouse brains. *Nat Commun*. 2020;11(1):1-12. doi:10.1038/s41467-020-15659-1

5. Berg S, Kutra D, Kroeger T, et al. Ilastik: Interactive machine learning for (bio)image analysis. *Nat Methods*. 2019;(16):1226–1232. doi:10.1038/s41592-019-0582-9

6. Groeneboom N, Yates S, Puchades M, Bjaalie J. Nutil: A Pre- and Post-processing

Toolbox for Histological Rodent Brain Section Images. *Front Neuroinform*. 2020;14:37. doi:10.3389/fninf.2020.00037

4. Efferent connections of the orbitofrontal, posterior parietal and insular cortices in the rat

Ingrid Reiten[1], Grethe Olsen[2], Jan G Bjaalie[1], Menno P Witter[2], Trygve B Leergaard[1]

Affiliations:

1. Department of Molecular Medicine, Institute of Basic Medical Sciences, University of Oslo, Norway
2. Kavli Institute for Systems Neuroscience, NTNU Norwegian University of Science and Technology, Trondheim, Norway

Presenting Author: Ingrid Reiten, ingrid.reiten@medisin.uio.no
Corresponding author: Trygve B. Leergaard, t.b.leergaard@medisin.uio.no

Keywords: anterograde labelling, tract tracing, data sharing, biotinylated dextran amine, phaseolus vulgaris leucoagglutinin, orbitofrontal cortex, posterior parietal cortex, insular cortex

Acknowledgements: We thank the EBRAINS data curation team for expert data management, curation and data sharing, Mathias Mathiasen, and Hideki Kondo for carrying out the original experiments, with help from Liliane Hansen, Terri Sakshaug, and Hanne Sømme. We further thank Michele Gianatti, Arthur Laja, and Bruno Monterotti for acquisition of histological section images presented here. This work was supported with funding from the European Union's Horizon 2020 Framework Program for Research and Innovation under the Specific Grant Agreement No. 785907 (Human Brain Project SGA2), Specific Grant Agreement No. 945539 (Human Brain Project SGA3) to JGB and TBL; The Research Council of Norway under Grant Agreement Nos. 223262; 197467, 227769, and the Kavli Foundation to MPW; and Grant Agreement No. 269774 (INCF Norwegian Node) to JGB, MPW, and TBL.

Introduction: In mammalian brains, association areas such as the orbitofrontal (OFC), posterior parietal (PPC), and insular (IC) cortices are sites of higher-order cognitive processing implicated in a wide range of behaviours, including working memory, attention guiding, decision making, and spatial navigation. To better understand how these regions contribute to these functions, it is of interest to map their structural connectivity throughout the brain. Several tract-tracing studies have investigated specific aspects of orbitofrontal, posterior parietal and insular connectivity, but a detailed overview of the totality of the cortical and subcortical projections from these areas is not available. We have therefore accumulated, organised and publicly shared a comprehensive collection of experimental rat brain tract tracing data in which the efferent connections the OFC, PPC, and IC have been anterogradely labelled.

Methods/results: The data collection comprises a selection of brightfield and fluorescence microscopic images of brain sections from 41 adult female Sprague Dawley rats (Charles River, Sulzfeld/Kisslegg, Germany, body weight range 180-390g), in which 49 discrete tracer injections were placed in the OFC (n = 26; 30 injections), IC (n = 8; 8 injections), and PPC (n = 7; 11 injections). The tract tracing experiments were performed at the Kavli Institute for Systems Neuroscience, Centre for Neural Computation, Trondheim, Norway, and results have been partially reported in five previous studies[1-5]. The images were organised (renamed, rotated and flipped to assure correct anteroposterior order and similar positioning for all images) using Nutil[6] software (RRID: SCR_017183), and thereafter

spatially registered to the Waxholm Space Rat brain atlas v4 (RRID: SCR_017124[7-9]) using QuickNII[10] (RRID:SCR_016854) and VisuAlign (RRID:SCR_017978). The data collections (images and atlas registration files) are shared as three datasets on EBRAINS, grouped by the location of the injections in the experiments[11-13]. The EBRAINS Curation services ensures the datasets are discoverable through sufficient and standardised metadata according to openMINDS (https://github.com/HumanBrainProject/openMINDS), a comprehensive metadata model for neuroscience data structures that is linked to taxonomies and ontologies. Figure 1 provides overview of the experimental design, from tract tracing experiments to published datasets on EBRAINS. The atlas-registered images were used to create a semiquantitative overview of the presence of labelling throughout the brain for each experiment. Individual brain regions, defined based on the WHSv4 atlas registration, were graded on a scale from 0-4 based on the density of labelling that was observed. This table is shared on EBRAINS[14], where its relationship to the previously mentioned image collection datasets is outlined.

Discussion: Using EBRAINS as a repository for our data ensures the data are shared according to the FAIR[15] principles and are discoverable in a repository with multi-modal research data through standardised metadata descriptions. The data can be found through customizable filters via a Search UI (https://search.kg.ebrains.eu) or programmatically via an API by searching for their related metadata. The images are easily available for download or for immediate view in an online microscopy viewer. The semiquantitative overview table provides a useful starting point for exploring the image collection based on a region of interest. The image collection, with corresponding reference atlas maps, is suitable as a reference framework for investigating the brain-wide efferent connectivity of these cortical association areas.

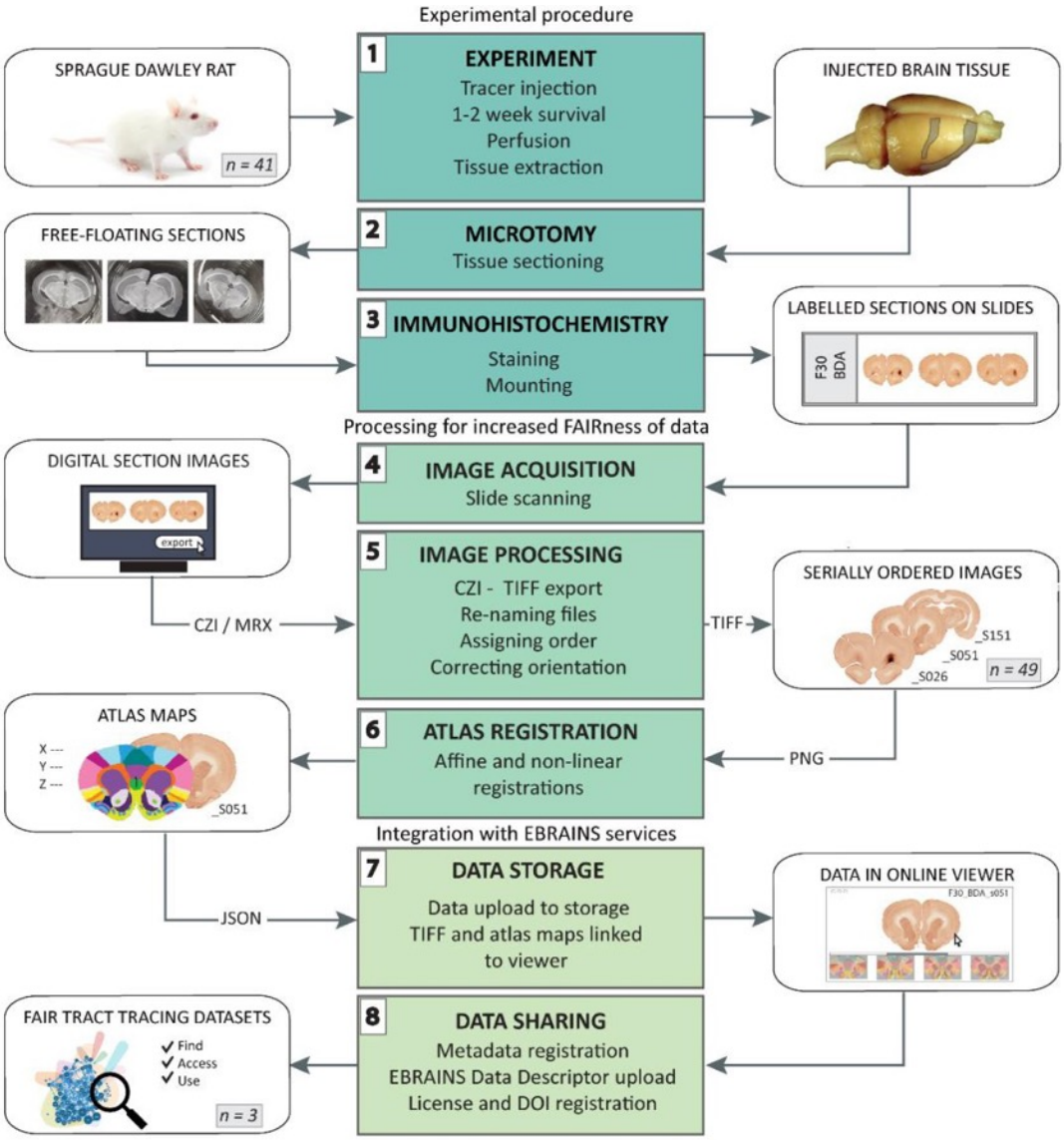

Figure 1. Workflow for tract-tracing experiments, data processing, and integration with EBRAINS services

Diagram showing the process from data generation to digitisation and sharing; starting with the rats used in the tract-tracing experiments to the result consisting of metadata and data shared via the EBRAINS Knowledge Graph. The workflow consists of 8 modules, each containing a set of methodological processes with a set input and output (white boxes). Module 1-3 (teal boxes) represent the experimental procedures (using n=41 subjects), module 4-6 (dark green boxes) represent the steps taken to digitise and process the data for increased level of FAIR[15] (using n=49 series), and module 7-8 represent the sharing and integration of data in EBRAINS (resulting in n=3 datasets). Altogether, the processing and sharing of data lead to 1) collections of organised and digitised photomicrographs, 2) reference atlas maps for each collection, 3) links for all collections pointing to the photomicrographs and atlas maps in the online image viewer, and 4) data and metadata available from ebrains.eu. Image credits: colourbox.com (photograph of rat). (Figure 1 in Reiten et al. 2023 (in review)).

References

1. Olsen, G. *et al.* Organization of Posterior Parietal–Frontal Connections in the Rat. *Front. Syst. Neurosci.* 13, (2019).

2. Kondo, H. & Witter, M. Topographic organization of orbitofrontal projections to the parahippocampal region in rats. *J. Comp. Neurol.* 522, 772–793 (2014).

3. Olsen, G., Ohara, S., Iijima, T. & Witter, M. Parahippocampal and retrosplenial connections of rat posterior parietal cortex. *Hippocampus* 27, 335–358 (2017).

4. Olsen, G. & Witter, M. Posterior parietal cortex of the rat: Architectural delineation and thalamic differentiation. *J. Comp. Neurol.* 524, 3774–3809 (2016).

5. Mathiasen, M., Hansen, L., Witter, M. & Leergaard, T. Insular projections to the parahippocampal region in the rat. *J. Comp. Neurol.* 523, 1379–1398 (2015).

6. Groeneboom, N., Yates, S., Puchades, M. & Bjaalie, J. Nutil: A Pre- and Post-processing Toolbox for Histological Rodent Brain Section Images. *Front. Neuroinform.* 14, 1–9 (2020).

7. Papp, E., Leergaard, T., Calabrese, E., Johnson, G. & Bjaalie, J. Waxholm Space atlas of the Sprague Dawley rat brain. *Neuroimage* **97**, 374–386 (2014).

8. Osen, K., Imad, J., Wennberg, A., Papp, E. & Leergaard, T. Waxholm Space atlas of the rat brain auditory system: Three-dimensional delineations based on structural and diffusion tensor magnetic resonance imaging. *Neuroimage* **199**, 38–56 (2019).

9. Kjonigsen, L., Lillehaug, S., Bjaalie, J., Witter, M. & Leergaard, T. Waxholm Space atlas of the rat brain hippocampal region: Three-dimensional delineations based on magnetic resonance and diffusion tensor imaging. *Neuroimage* **108**, 441–449 (2015).

10. Puchades, M., Csucs, G., Ledergerber, D., Leergaard, T. & Bjaalie, J. Spatial registration of serial microscopic brain images to three-dimensional reference atlases with the QuickNII tool. *PLoS One* 14, 1–14 (2019).

11. Kondo, H. *et al.* Anterogradely labeled axonal projections from the orbitofrontal cortex in rat. (2022) doi:10.25493/2MX9-3XF.

12. Mathiasen, M. *et al.* Anterogradely labeled axonal projections from the insular cortex in rat. (2020) doi:10.25493/WK4W-ZCQ.

13. Olsen, G. *et al.* Anterogradely labeled axonal projections from the posterior parietal cortex in rat. (2020) doi:10.25493/FKM4-ZCC.

14. Reiten, I. & Leergaard, T. Semiquantitative overview of efferent projections from the orbitofrontal, posterior parietal and insular cortices in rat. *EBRAINS* (2022) doi:https://doi.org/10.25493/Q73Z-83J.

15. Wilkinson, M. *et al.* The FAIR Guiding Principles for scientific data management and stewardship. *Sci. Data* **3**, 1–9 (2016).

Reiten, I., Olsen, G., Bjaalie, J., Witter, M. & Leergaard, T. The efferent connections of the orbitofrontal, posterior parietal, and insular cortex of the rat brain. *Sci. Data, in review* (2023).

5. Changes in synaptic dynamics underlies benzodiazepine resistance in paediatric status epilepticus

T. Fedele[1], R.J. Burman[2], A. Steinberg[1], G. Selmin[1], G. Ramantani[1], R. Rosch[3]

[1] - Department of Neuropediatrics, University Children's Hospital Zurich and University of Zurich, Switzerland

[2] - Nuffield Department of Clinical Neurosciences, University of Oxford, Oxford, UK

[3] - Department of Clinical Neurophysiology, King's College Hospital NHS Foundation Trust, London, UK

Abstract

Over a third of children in status epilepticus (SE) do not respond to first-line treatment with benzodiazepines. Experimental data from animal models has suggested that dynamic changes in fast synaptic inhibitory signalling may lead to benzodiazepine resistance. However, it is unknown whether these synaptic mechanisms are indeed relevant in paediatric patients. Here we utilise EEG recordings as a clinically accessible insight into pathological brain dynamics that occur during SE. Through dynamic causal modelling (DCM) we then infer excitatory-inhibitory coupling parameters of cortical microcircuits in different brain states.

We use DCM to test key hypotheses regarding benzodiazepine effects directly on EEG data recorded in patients during SE: (1) that benzodiazepines modulate inhibitory coupling in SE, (2) that there are differences in the balance of excitatory-inhibitory coupling in benzodiazepine responders vs non- responders. We investigated a cohort of 26 paediatric patients (8 benzodiazepine responders) who were managed at the University Children's Hospital Zürich for SE. Using the DCM framework, we fitted hierarchical neural mass models to (1) identify which synaptic parameters best explain the observed EEG changes, and (2) infer group differences in synaptic parameters between responders and non- responders.

The fitted DCMs captured the following changes in EEG broadband spectra associated with benzodiazepine treatment: (1) the observed changes across conditions were best explained through alterations in inhibitory coupling; (2) responders and non-responders differed in the modulation of inhibitory synaptic connections in the neural mass model.

Overall, this study demonstrates that the effect of benzodiazepines on macroscopic brain dynamics in paediatric patients with SE is best explained by dynamic shifts in inhibitory cortical synaptic signalling. The described group differences suggest that there may be baseline differences in cortical synaptic coupling which may be captured by DCM and used to help predict and optimise treatment responses in patients with paediatric SE.

6. Topographic variation in neurotransmitter receptor densities explain differences in intracranial EEG spectra

Ulrich Stoof[1*], Karl Friston[1], Martin Tisdall[2], Gerald Cooray[2], and Richard Rosch[3]

[1] University College London, Wellcome Trust Centre for Human Neuroimaging, London, GB
[2] Great Ormond Street Hospital for Children, NHS Foundation Trust, London, GB
[3] King's College London, MRC Centre for Neurodevelopmental Disorders, London, GB

Corresponding author: Ulrich Stoof, ulrich.stoof.20@ucl.ac.uk

HBP Summit 2023 – Abstract for Poster Session / Presentation

Introduction

The causes of epilepsy and its defining symptom – seizures – lie in cellular and architectural features of brain tissue. Though, for clinical diagnoses, electrophysiological measurements, e.g., intracranial electroencephalography (iEEG), are used to infer causes of seizures. Therefore, understanding how brain tissue generates (pathological) electrophysiological signals is essential. We aim to bridge this explanatory gap using biophysically informed meso-scale neural mass models (NMM) and dynamic causal modelling (DCM).

We developed an approach to integrate electrophysiological data as iEEG recordings, and microscale synaptic data such as neuroreceptor density (RD) maps, to derive a normative map of effective synaptic parameters across the cortical surface.

Methods

We asked how RD from autoradiography studies are related to 'healthy' cortex iEEG activity recorded in individuals with epilepsy remote from the putative epileptogenic zone. We first tested if a canonical microcircuit NMM replicates electrophysiological (iEEG) data using DCM. We then asked if receptor densities can be predicted by iEEG signals, and if regional receptor compositions ('fingerprints') can explain regional variation in iEEG spectra. In addition, to illustrate the wider applicability of our findings, we used mismatch negativity (MMN) as a case study to show improved predictions with our informed connectivity parameter priors.

Results

First, our DCM replicated ongoing awake cross spectral densities of iEEG signals (1770 data series) highly accurately; with 40 exceptions (≅ 2.3% of the total number) DCM was able to explain key components of regional cortical signal variability.

Second, we tested the hypothesis that RD variance across the cortical surface explains regional differences in DCM parameters through a parametric empirical Bayesian hierarchical model. We compared Bayesian model fits of these hierarchical models using different combinations of RD priors – including those driven only be the main excitatory (AMPA, NMDA) and inhibitory (GABA) subclasses. However, the winning model contained the full set of RD values across 15 receptor types.

Third, using principal component analysis (PCA) we captured regional receptor composition variability with a reduced dimensionality, and showed that the principal components of receptor density fingerprints can explain regional variation in the generation of SEEG spectra, i.e., including receptor density fingerprints improves model evidence (free energy ≈ accuracy – complexity).

Fourth, we showed that NMM parameter priors, which include NR information, are informative for modelling the MMN and lead to higher model evidence and fit, and significantly improved parameter posteriors.

Discussion

In summary, we show how tissue characteristics (i.e., receptor density) can be incorporated to improve biophysically grounded models and explain regional variations in electrophysiology. The results will be part of a toolbox (published on GitHub and EBRAINS) that enables integration of normative datasets as prior information to generate patient specific models of (pathophysiological) cortical dynamics, for example in epilepsy.

Subsequent parts for this project will focus on clinical case studies, primarily on iEEG of children with refractory epilepsy, especially focal cortical dysplasia, who undergo pre-surgical evaluation.

Keywords

Epilepsy, FCD, iEEG/SEEG, Neuroreceptors, Biomarkers, Modelling, Translational, Personal Medicine

Figure 1: Illustration: Methodology and Results

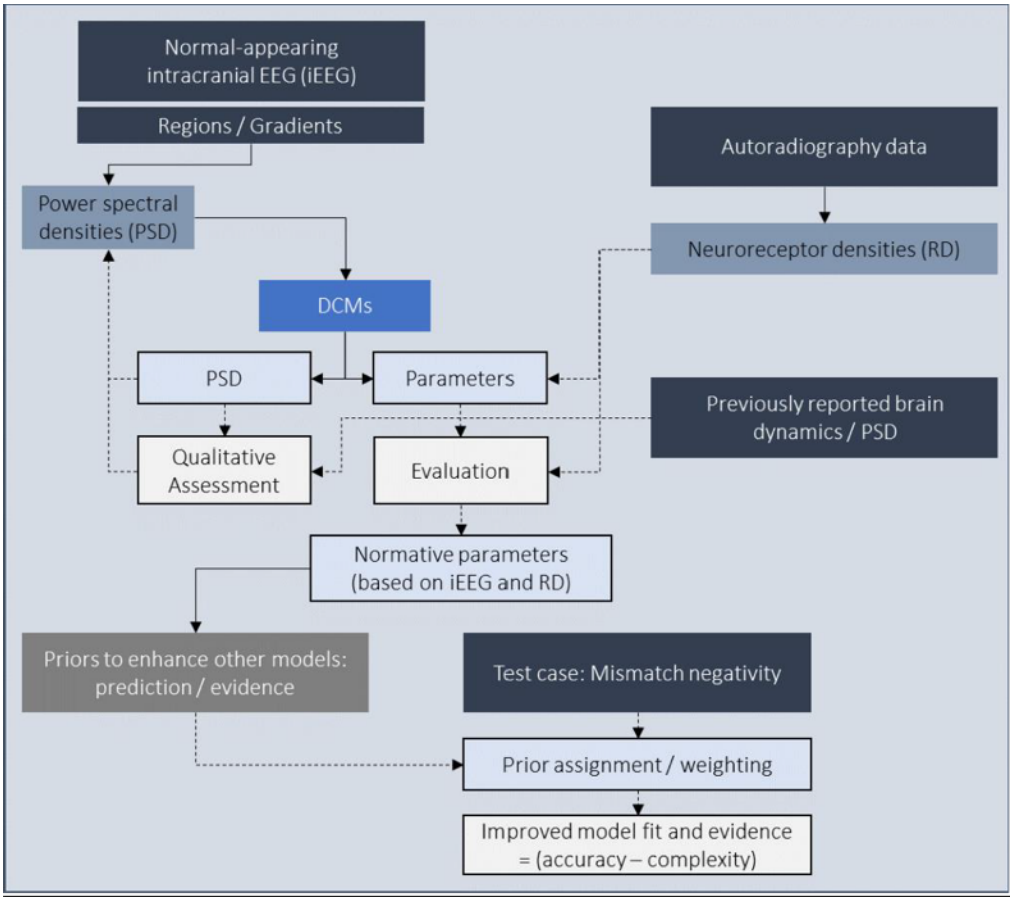

Figure 2: Illustration: Methodology and Results

A) DCM CMC model accuracy (1770 iEEG channels, 38 regions)

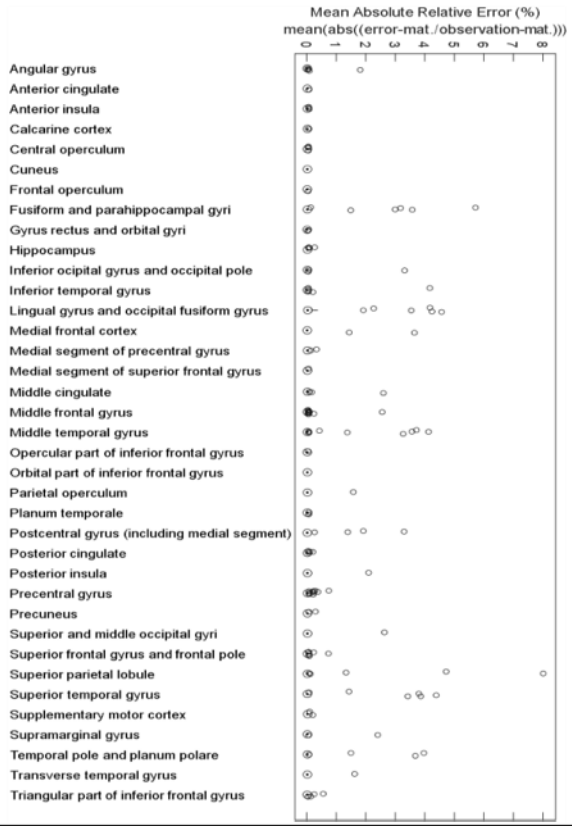

B) Model evidence comparison: 4, 6 receptors, PCs

Rank	Model	Receptors	F	ΔFE
1st		PC1-4	172974	8.2
2nd		PC1-6	172966	2.8
3rd		PC1-2	172963	2.4
4th	59	ANkGaGb	172961	1.4
5th	43	ANkGa	172959	1.6
6th	64	All	172958	6.8
7th	24	ANGa	172951	1.2

C) Mismatch negativity case study: Model evidence comparison

Model	Evidence (F)	Probability (softmax)
CMC PDF (μ=0, σ=1)	176	1
ERP Baseline	-179	0
CMC Hanning	-225	0
CMC Baseline	-436	0

Description: A) DCM CMC showed excellent fit for about 97% of channels; B) Comparison of model evidence (Free Energy) of neuroreceptor density (RD) informed models: log Bayes factor >5 indicates very strong evidence in favour of model with four PCs; C) Mismatch negativity case study: model which used RD priors outperforms baseline models (standard ERP and CMC) as well as CMC with Hanning filter

References

Frauscher B, von Ellenrieder N, Zelmann R, et al. Atlas of the normal intracranial electroencephalogram: neurophysiological awake activity in different cortical areas. Brain. 2018;141(4):1130-1144. doi:10.1093/brain/awy035

Hansen JY, Markello RD, Tuominen L, et al. Correspondence between gene expression and neurotransmitter receptor and transporter density in the human brain. Neuroimage. 2022;264:119671. doi:10.1016/j.neuroimage.2022.119671

Hansen JY, Shafiei G, Markello RD, et al. Mapping neurotransmitter systems to the structural and functional organization of the human neocortex. Nat Neurosci. 2022;25(11):1569-1581. doi:10.1038/s41593-022- 01186-3

Moran RJ, Stephan KE, Seidenbecher T, Pape HC, Dolan RJ, Friston KJ. Dynamic causal models of steady-state responses. Neuroimage. 2009;44(3):796-811. doi:10.1016/j.neuroimage.2008.09.048

Nørgaard M, Beliveau V, Ganz M, et al. A high-resolution in vivo atlas of the human brain's benzodiazepine binding site of GABAA receptors. Neuroimage. 2021;232:117878. doi:10.1016/j.neuroimage.2021.117878

Zilles K, Palomero-Gallagher N. Multiple Transmitter Receptors in Regions and Layers of the Human Cerebral Cortex. Front Neuroanat. 2017;11:78. Published 2017 Sep 20. doi:10.3389/fnana.2017.00078

7. The Brain Scaffold Builder: a component framework for large multiscale brain models and rapid prototyping

Robin Gilbert De Schepper[1]*, Francesco Sheiban[2], Alessio Marta[1], Dimitri Rodarie[1,3], Igor Cantele[1], Claudia Casellato[1], Egidio D'Angelo[1,4]

[1] Department of Brain and Behavioural Sciences, University of Pavia, Italy

[2] Department of Electronics, Information and Bioengineering Politecnico di Milano, Italy

[3] Enrico Fermi Study and Research Center, University of Rome, Italy

[4] Brain Connectivity Center IRCCS Mondino Foundation, Pavia, Italy

*robingilbert.deschepper@unipv.it

INTRODUCTION

The challenges facing modern neuroscientists that wish to model the brain[1] are precluded by a long list of requirements that to a researcher may seem more akin to housekeeping chores than science: writing code to create abstractions for cells, morphologies, biophysical properties, and their connections, validating, organizing, and maintaining code to keep up with modern demands of software quality. Here we present the latest major version of The Brain Scaffold Builder (BSB), starting its public beta release of version 4, with new features that let scientists dive straight into writing the scientific parts of the model, while promoting best software development practices. The BSB is an EBRAINS component[2] and can be conveniently installed on any machine or platform where Python is available.

METHODS

The framework uses a black box component approach, where the invariant part of the modelling task is provided by the framework to the user as a class. The class can be inherited from and the variant model-specific part can be defined in the child class. The framework revolves around the configuration and strategy design patterns: A configuration file in which declarations of components and their respective parameters are explicitly stated, is parsed, and so too are any file, morphology, dataset, code dependencies, or online data sources (e.g., atlas-based volumes and cell densities) of the model. This makes the configuration file a total and sufficient description of the model, to be reified from its portable abstract configuration description to a concrete, possibly very large, simulatable model – anywhere – without additional, unknown, or missing dependencies. Using the strategy pattern, each component declaration can bootstrap itself and is given the already parsed and validated parameters by the framework. When the command is received to reconstruct the model, each component fulfills its interface

with the framework which manages a job pool to run parallel tasks until the reconstruction is complete. The job pool can run in series on a single process or be scaled up to distributed HPC clusters, without any changes to the model description code: write once, run anywhere. User code is by design parallel: placement strategy components are given a placement context, consisting of a description of the cell types to be placed, and the volume in which to place them. The placement strategy is then asked to fill a subset of the volume within certain boundaries. These tasks can be parallelized by tiling a rectangular grid over the total volume and asking each parallel process to fill a tile. Similarly, each connection strategy component is asked to determine the postsynaptic region of interest for each presynaptic tile, and are parallelized as such. The reconstructed cell types and connections can then be simulated on any of the supported simulation backends (NEST, Arbor, and NEURON), by defining a simulator specific representation for each of the following: cell models to represent cell types, synaptic models to represent connection types, and input/output devices to set up experimental protocols such as voltage probes, poisson spike generators, etc (Fig. 1).

RESULTS AND DISCUSSION

As a usecase, the BSB was applied to the mouse cerebellar cortical network[3], which has a geometrically organized architecture that has been suggested to imply its computational properties. Morphology-based reconstruction and simulations as multicompartmental (NEURON) and point-neuron (NEST) networks were carried out. Both cerebellar general-purpose microcircuit and atlas-based specific region models using orientation field were developed. The BSB has been applied also for the reconstruction of thalamic nuclei and hippocampal regions.

Given the "scaffold" design, new neurons and mechanisms can be plugged-in to address ontogenesis, species differences (for example in humans) and pathology.

Figures

Figure 1. Core BSB operations. In the reconstruction phase, the BSB proceeds by sequentially defining the network volume, cell types, cell placement, cell connectivity. Once neurons and fibers are positioned, their geometries/morphologies are imported, and connection rules allow to wire them up and to build the network connectome. In the simulation phase, neuron and synapse models are linked to simulators by a specific adapter and interfaced to a set of devices for stimulation and recording. This workflow is applicable to any kind of brain neuronal network

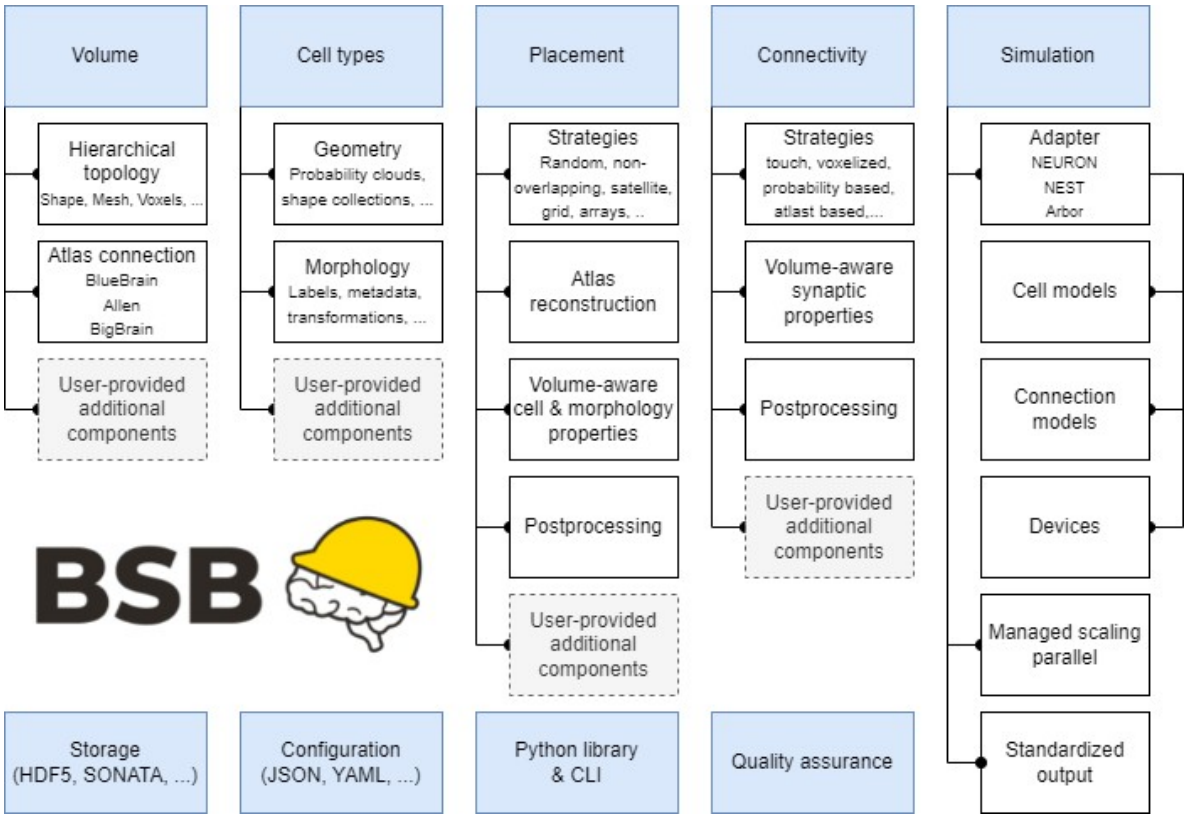

ACKNOWLEDGEMENTS

This research has received funding from: i) European Union's Horizon 2020 Research and Innovation programme under Human Brain Project SGA3 No. 945539, ii) the National Recovery and Resilience Plan (NRRP), Mission 4 Component 2 Investment 1.3 - Call for tender No. 341 of 15/03/2022 of Italian Ministry of University and Research funded by the European Union – NextGenerationEU. Award Number: Project code PE0000006, Concession Decree No. 1553 of 11/10/2022 adopted by the Italian Ministry of University and Research, CUP D93C22000930002, "A multiscale integrated approach to the study of the nervous system in health and disease" (MNESYS).

Special acknowledgement to EBRAINS and FENIX for informatic support and infrastructure.

REFERENCES

1. Egidio D'Angelo, Viktor Jirsa, The quest for multiscale brain modeling, Trends in Neurosciences, Volume 45, Issue 10, 2022, Pages 777-790, ISSN 0166-2236, doi: 10.1016/j.tins.2022.06.007.
2. https://ebrains.eu/service/brain-scaffold-builder/
3. De Schepper R, Geminiani A, Masoli S, Rizza MF, Antonietti A, Casellato C and D'Angelo E. Model simulations unveil the structure-function-dynamics relationship of the cerebellar cortical microcircuit. NAT COMMS BIOL. 2022; doi: 10.1038/s42003-022-04213-y

…

8. Analyzing thalamocortical tract-tracing experiments in a common reference space

Nestor Timonidis[1*], Mario Rubio-Teves[2], Carmen Alonso-Martínez[2], Rembrandt Bakker[1,3], María García-Amado[2], César Porrero[2], Paul Tiesinga[1], Francisco Clascá[2]

[1]Donders Centre for Neuroscience, Radboud University Nijmegen, Nijmegen, The Netherlands.
[2]Department of Anatomy and Neuroscience, School of Medicine, Autónoma de Madrid University, Madrid, Spain.
[3]Inst. of Neuroscience and Medicine (INM-6), Forschungszentrum Jülich, Jülich, Germany.

*nestor.timonidis@donders.ru.nl

INTRODUCTION/MOTIVATION

The thalamus is considered the gate for most sensory information on its way to the cortex. In the case of the somatosensory system, that role is played specifically by the ventral posterior complex (VP) [1]. The axonal projections from the neurons of these nuclei are extremely precise, and they manifest as column- and layer-specific. While tract-tracing experiments are the gold standard for revealing thalamocortical connectivity, only a few such experiments can be performed in the same brain without invalidating their interpretation. Therefore, thalamocortical network analysis would benefit from accurately registering many individual experiments to a common reference space serving as an anatomical template.

The Human Brain Project has developed robust software tools for the registration of mouse brain sections to the Allen Common Coordinate Framework (CCF) [2]. Integrated as the QUINT workflow [3], they allow the registration of brain regions from the CCF to experimental sections to subsequently count labeled somas and neurites in each of these regions. Here we develop an alternative pipeline that inverts the first step of QUINT: it registers connectivity data to the CCF, and then counts labeled neurites. The advantage is that the registered data can now be integrated with other data or used with updated brain parcellations. The pipeline is built as a Jupyter notebook and relies on the same tools as the QUINT workflow.

METHODS

Our use case consists of a series of evenly-spaced histological sections from the mouse brain, in which an anterograde tracer was injected in the somatosensory thalamus. This resulted in the labeling of 10-100 closely located cell bodies and their complete axonal arborizations. For each experiment, we acquired stacks of images covering whole sections at 10x magnification on a brightfield microscope (Neurolucida, MBF Bioscience). Minimum-intensity projection

(MIP) images were produced from the stacks (Fig. 1A). For each MIP image, we used Ilastik's Pixel Classification workflow (Fig. 1E-F)[4] to segment the labeled neurites from the background. In parallel, we performed linear registration of the images to CCF using the DeepSlice deep learning algorithm, which we manually curated via the QuickNii tool [5,6]. We then applied the VisuAlign tool for refined non-linear registration by manually placing histological landmarks over the atlas delineation (Fig. 1B-D). Subsequently, we computed the inverse registration of the segmented images to CCF in order to map the labelled pixels to the 3D brain template. Lastly, we produced 2D cortical and thalamic flatmaps [7] overlaid with anatomical boundaries to visually inspect the topographical organization of the registered populations (Fig. 2).

RESULTS AND DISCUSSION

After the registration, we identified an organization of VPM that mirrors that of the cortex: populations specifically targeting SSp were located rostrally in the nucleus, whereas those targeting SSs were more caudal. Each of these sectors can be further subdivided based on the precise somatotopic organization of its cortical target: from dorsal to ventral, sectors are related to whiskers, nose and mouth, respectively. A third population in ventrolateral VPM projects to both SSp and SSs. In SSp, the axonal layer distribution is markedly different.

Furthermore, registering the dataset allowed us to incorporate it into a virtual atlas that is to be shared, expanded and improved by the neuroscientific community. This can set the basis for multimodal data integration to a whole-brain connectivity matrix that can potentially correlate anatomical and physiological data.

Despite requiring some coding knowledge by the user, our pipeline offers extensive visualization options such as cortical flatmaps, 2D representations of subcortical nuclei and interactions with the Scalable Brain Atlas Composer 3D visualization tool [8]. Lastly, it is fully compatible with the QUINT workflow, allowing further analyses of previously registered datasets.

Keywords: QUINT workflow, Common Coordinate Framework, registration, somatosensory system, thalamus, cortex

ACKNOWLEDGEMENTS

This work was supported by the FLAG-ERA grant NeuronsReunited, by NWO (680-91-318), by Spain's MICINN-AEI (PCI2019-111900-2) and PID2020-115780GB-I00), and by the
European Union's Horizon 2020 Framework Programme for Research and Innovation under Specific Grant Agreement No. 945539 (Human Brain Project SGA3).

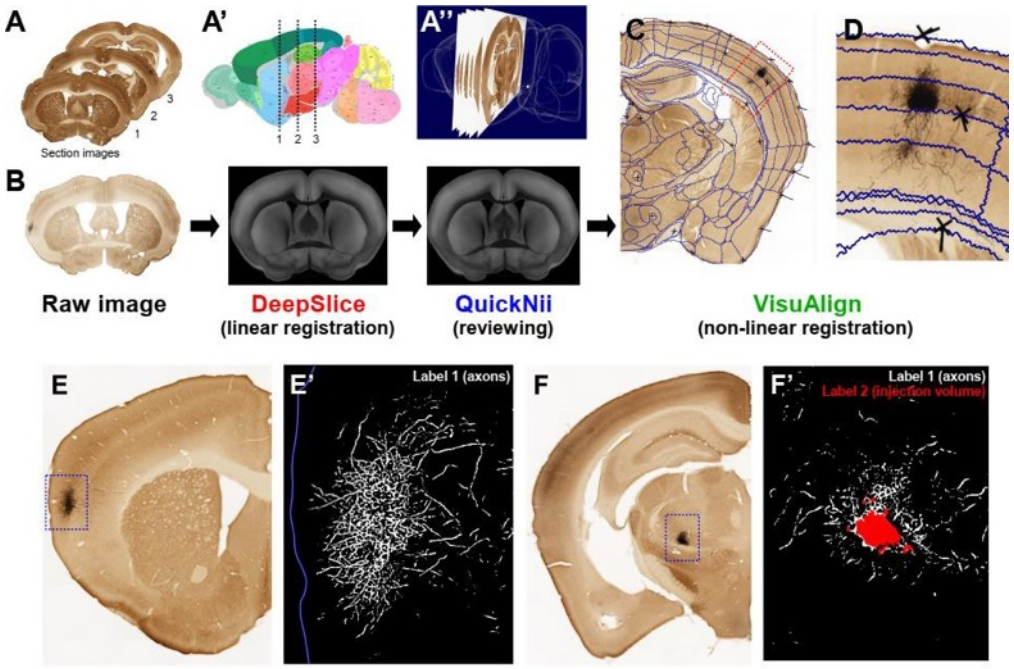

Figure 1: Illustration of the 3D registration pipeline presented in this work. (A-A'') Conceptual illustration of the registration process. (B) Linear registration of a coronal slice to the Allen CCF with DeepSlice and QuickNii. (C, D): Non-linear registration with VisuAlign. (E-E') Segmentation of the axons using the ilastik toolbox. (F-F') Segmentation of the injection volume.

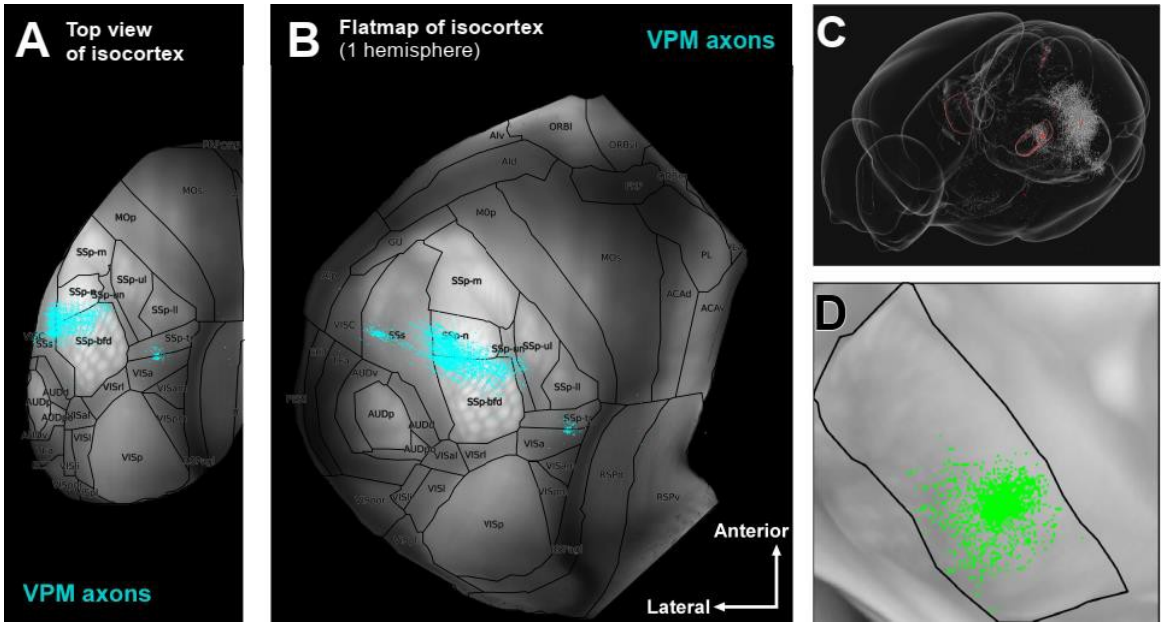

Figure 2. Custom plots for data visualization. (A) Top view of the isocortex showing the distribution of thalamic axons coming from VPM. (B) A dorsal flatmap of one hemisphere of the cortex, illustrating the same projection as in A.(C) Integration with the Scalable Brain Atlas allows for 3D visualization capabilities. (D) Maximum projection plot across the coronal planes defining the anatomical boundaries, the intensity volume and the somatodendritic distribution of the VPM.

REFERENCES

[1] O'Reilly et al., 2021. Rodent somatosensory thalamocortical circuitry: Neurons, synapses, and connectivity. Neuroscience & Biobehavioral Reviews 126 (2021): 213-235.

[2] Wang et al., 2020. The allen mouse brain common coordinate framework: A 3d reference atlas. Cell, 181(4):936 – 953.

[3] Yates et al., 2019. QUINT: Workflow for Quantification and Spatial Analysis of Features in Histological Images From Rodent Brain. Frontiers in Neuroinformatics 13:1662- 5196.

[4] Berg et al., 2019. ilastik: interactive machine learning for (bio)image analysis. *Nat Methods* 16:1226–1232.

[5] Carey et al., 2022. DeepSlice: rapid fully automatic registration of mouse brain imaging to a volumetric atlas. bioRxiv 2022.04.28.489953.

[6] Puchades et al., 2019. Spatial registration of serial microscopic brain images to three- dimensional reference atlases with the QuickNII tool. PLOS ONE 14(5): e0216796.

[7] Knox et al., 2018. High resolution data-driven model of the mouse connectome. Network Neuroscience. 3(1):217–236.

[8] Bakker, R., Tiesinga, P., and Kotter, R., 2015. The scalable brain atlas: Instant web- based access to public brain atlases and related content. Neuroinformatics, 13(3):353:366.

[9]

9. Showcase 1 - the virtual aging brain: structure-function relationship and cognitive decline

Mario Lavanga[†1], Johanna Stumme[†2,3], Jan Fousek[†1], Bahar Hazal Yalcinkaya[1], Christiane Jockwitz[2,3], Hiba Sheheitli[1], Nora Bittner[2,3], Meysam Hashemi[1], Spase Petkoski[1], Svenja Caspers[†2,3], Viktor Jirsa*[†1]

[1]Institut de Neurosciences des Systèmes (INS), Inserm, Aix-Marseille University, Marseille, France

[2]Institute of Neuroscience and Medicine (INM-1), Research Centre Jülich, Jülich, Germany

[3]Institute for Anatomy I, Medical Faculty & University Hospital Düsseldorf, Heinrich-Heine University Düsseldorf, Düsseldorf, Germany

*Corresponding author: VJ (viktor.jirsa@univ-amu.fr)

[†]These authors contributed equally.

INTRODUCTION/MOTIVATION

The human brain changes during healthy aging with large individual variation in the cognitive decline [1]. Sources and mechanisms of this variability are not understood and have been previously linked with whole-brain reorganisation, specifically in terms of the white-matter fibre tracts (structural connectivity, SC), and functional co-activations (functional connectivity, FC) of brain regions [2,3], e.g. hemispheric asymmetry reduction. Here we present a causal framework of virtual twin modelling where the individual SC informs a computational brain network model [4]. Within this framework we can integrate structural and functional cohort-level trends, and also operationalize hypothesised mechanisms of aging individually by modifying specific SC links, and systematically evaluate the impact on the brain dynamics. This Showcase employs whole-brain modelling on structural variability to formulate causal hypotheses about brain mechanisms and to explain functional variability across individuals based on cutting edge datasets. Its implementation is fully embedded in EBRAINS and freely available, providing a reusable template for researchers aiming to use EBRAINS services in their work.

METHODS

We used the SC and regional BOLD signal of older subjects from the 1000BRAINS dataset [5] (n=649, age range [51.1−85.4], $n_{females}$=317). From the BOLD time series we computed data features based on both the static FC, and the time-variant FC dynamics (FCD).

Based on The Virtual Brain, the brain network model [6] was constructed from individual SC with the neural mass model [7] governing the node dynamics enabling simulation of resting-state BOLD data. For each subject we performed a parameter sweep over coupling parameter *G* to identify the optimal working point of the system where FCD fluidity σ^2 is maximised and computed the same functional features as for the empirical data. Next, we have virtually aged the 50

youngest subjects by gradually decreasing the interhemispheric connections and repeating the procedure for each time point. Finally, Simulation Based Inference (SBI) was used to compute the posterior estimate of the global modulation from the empirical data [8] to validate the proposed framework..

The showcase is implemented as a series of jupyter notebooks in the interactive computing environment of the EBRAINS Collaboratory [9]. These integrate a broad spectrum of EBRAINS services including the Knowledge Graph, The Virtual Brain, data analytics, and offloading the computations to the HPC infrastructure.

RESULTS AND DISCUSSION

Across the 1000BRAINS dataset, we identified a strong decline in interhemispheric SC connections over age accompanied with decline both in homotopic FC and FCD fluidity. The trends for both these functional features were recovered in simulated resting state data within the virtual model . The same effect was observed for the virtually aged subjects along the individual trajectories.

The working point value of the connectivity modulation *G* increased over age on the individual level, both in the virtually aged as well as in the empirical setting. The increase of *G* was steeper in the subjects with lower cognitive performance.

Taking advantage of the EBRAINS infrastructure, we demonstrate how brain modeling can benefit from a coordinated effort of data integration and availability within the same framework as the modelling algorithms. Our results indicate that the deterioration of the interhemispheric SC is accompanied by increased modulation of the functional brain dynamics. The SC reorganisation might reflect a potential scaffolding of the brain during the ageing process. This effect is weaker for the cognitively well performing subjects, which suggests a process of brain maintenance. The here established mechanistic framework lays the ground for extending such modelling both towards longitudinal datasets as well as inclusion of other factors beyond 'age', which is currently being pursued.

Keywords: Brain Network Model, Aging, The Virtual Brain, EBRAINS, Showcase

ACKNOWLEDGEMENTS

This project was partially funded by the German National Cohort and the 1000BRAINS-Study of the Institute of Neuroscience and Medicine, Research Centre Jülich, Germany. We thank the Heinz Nixdorf Foundation (Germany) for the generous support of the Heinz Nixdorf Study. We thank the investigative group and the study staff of the Heinz Nixdorf Recall Study and 1000BRAINS. This project/research has received funding from the European Union's Horizon 2020 Framework Programme for Research and Innovation under the Specific Grant Agreement No. 945539 (Human Brain Project SGA3). The authors also wish to acknowledge the financial support of the following agencies: the French National Research Agency (ANR) as part of the second "Investissements d'Avenir" program (ANR-17-RHUS-0004, EPINOV), PHRC-I 2013 EPISODIUM (grant number 2014–27), the Fondation pour la Recherche Medicale (DIC20161236442), Virtual-BrainCloud (grant number 826421), the SATT Sud-Est (827-SA-16- UAM) for providing funding for this research project.

REFERENCES

5[1] Oschwald, J., Guye, S., Liem, F., Rast, P., Willis, S., Röcke, C., Jäncke, L., Martin, M., & Mérillat, S. (2020). Brain structure and cognitive ability in healthy aging: a review on longitudinal correlated change. *Reviews in the Neurosciences*, *31*(1), 1–57. https://doi.org/10.1515/revneuro-2018-0096

[2] Suárez, L. E., Markello, R. D., Betzel, R. F., & Misic, B. (2020). Linking Structure and Function in Macroscale Brain Networks. *Trends in Cognitive Sciences*, *24*(4), 302–315. https://doi.org/10.1016/j.tics.2020.01.008

[3] Cabeza, R. (2002). Hemispheric asymmetry reduction in older adults: The HAROLD model. *Psychology and Aging*, *17*(1), 85–100. https://doi.org/10.1037/0882-7974.17.1.85

[4] Lavanga, M., Stumme, J., Yalcinkaya, B. H., Fousek, J., Jockwitz, C., Sheheitli, H., Bittner, N., Hashemi, M., Petkoski, S., Caspers, S., & Jirsa, V. (2022). The virtual aging brain: a model-driven explanation for cognitive decline in older subjects. In *bioRxiv* (p. 2022.02.17.480902). https://doi.org/10.1101/2022.02.17.480902

[5] Caspers, S., Moebus, S., Lux, S., Pundt, N., Schütz, H., Mühleisen, T. W., Gras, V., Eickhoff, S. B., Romanzetti, S., Stöcker, T., Stirnberg, R., Kirlangic, M. E., Minnerop, M., Pieperhoff, P., Mödder, U., Das, S., Evans, A. C., Jöckel, K.- H., Erbel, R., … Amunts, K. (2014). Studying variability in human brain aging in a population-based German cohort- rationale and design of 1000BRAINS. *Frontiers in Aging Neuroscience*, *6*, 149. https://doi.org/10.3389/fnagi.2014.00149

[6] Schirner, M., Domide, L., Perdikis, D., Triebkorn, P., Stefanovski, L., Pai, R., Prodan, P., Valean, B., Palmer, J., Langford, C., Blickensdörfer, A., van der Vlag, M., Diaz-Pier, S., Peyser, A., Klijn, W., Pleiter, D., Nahm, A., Schmid, O., Woodman, M., … Ritter, P. (2022). Brain simulation as a cloud service: The Virtual Brain on EBRAINS. *NeuroImage*, *251*, 118973. https://doi.org/10.1016/j.neuroimage.2022.118973

[7] Montbrió, E., Pazó, D., & Roxin, A. (2015). Macroscopic Description for Networks of Spiking Neurons. *Physical Review X*, *5*(2), 021028. https://doi.org/10.1103/PhysRevX.5.021028

[8] Gonçalves, P. J., Lueckmann, J.-M., Deistler, M., Nonnenmacher, M., Öcal, K., Bassetto, G., Chintaluri, C., Podlaski, W. F., Haddad, S. A., Vogels, T. P., Greenberg, D. S., & Macke, J. H. (2020). Training deep neural density estimators to identify mechanistic models of neural dynamics. *eLife*, *9*. https://doi.org/10.7554/eLife.56261

[9] SGA3 D1.2 Showcase 1 Collaboratory. https://wiki.ebrains.eu/bin/view/Collabs/sga3-d1-2-showcase-1/

10. Bayesian inference on virtual brain models to reveal the causal mechanisms of disorders

M. Hashemi[1], A. Ziaeemehr, A.N. Vattikonda[1], V. Sip[1], H.E. Wang, S. Petkoski[1],
M.M. Woodman[1], and V. Jirsa[1]

[1] Aix Marseille Univ, INSERM, INS, Inst Neurosci Syst, UMR 1006, Marseille, France

Meysam.hashemi@univ-amu.fr, Vikotr.jirsa@univ-amu.fr

Keywords : Bayesian estimation, likelihood function, virtual brain models, causal inference, brain disorders.

Abstract

Virtual brain modeling is a data-driven approach that combines personalized anatomical information with mathematical models of brain activity to generate spatiotemporal patterns as observed in brain imaging signals. This parametric simulator is equipped with a stochastic generative process, which provides the basis for inference and prediction on the local and global brain dynamics, such as those affected by disorders. Inference algorithms are required to efficiently estimate the unknown parameters (such as regional excitability parameters and global scaling factor), ideally including the uncertainty. In this work, we provide flexible and efficient Bayesian inference on virtual brain models using state-of-the-art algorithms from likelihood-based and likelihood-free approaches. We show the benefits of incorporating prior information and inference diagnostics, using self-tuning Monte Carlo strategies for automatic and principled statistical inference, and deep learning algorithms for fast and efficient model inversion. The performance of these methods is then demonstrated on causal inference and prediction in various brain disorders.

INTRODUCTION/MOTIVATION

In contrast to forward modeling, which is a top-down approach, model inversion is a bottom-up strategy that infers hidden causes from observed effects [1]. We aimed at making flexible, efficient, and accurate inference on the local and global brain dynamics, to reveal the mechanism underlying disorders, such as epilepsy, alcohol use disorders, and Alzheimer's disease. This requires the integration of various sources of information, such as neural

networks, anatomical data, empirical observations, and advanced probabilistic machine learning techniques, in a unified framework called Bayesian inference, as we aim to perform in this work.

METHODS

In practice, to carry out Bayesian model inversion, we can use either Monte Carlo sampling (such as Hamiltonian Mote Carlo, in automatic tools such as Stan) which is asymptotically unbiased, or simulation-based inference (using deep neural networks), which is computationally fast and efficient.

RESULTS AND DISCUSSION

Our results indicate that SBI and HMC can efficiently estimate the full posterior distribution of virtual brain parameters (a local bifurcation parameter at each brain region characterizing the regional epileptogenicity and a global coupling parameter scaling the structural connectivity of patients), from LFP/sEEG/EEG/MEG/fMRI recordings, but each has its own advantages and disadvantages, depending on the type of neuroimaging measurements (Refs 2-6). Also, the calculation of likelihood function —an essential ingredient for both frequentist and Bayesian inference methods—determines to which algorithm is more efficient for a specific neuroimaging data set. The methodology is illustrated for in-silico dataset and then, applied to infer the personalized model parameters based on the empirical stereotactic electroencephalography recordings of retrospective patients. In sum, our Bayesian methodology can deal with non-linear latent dynamics and parameter degeneracy, paving the way for fast and reliable inference on brain disorders from neuroimaging modalities.

ACKNOWLEDGEMENTS

This project was funded by the European Union's Horizon 2020 research and innovation programme under grant agreement No. 785907 (SGA2), and No. 945539 (SGA3) Human Brain Project, and Virtual-BrainCloud (grant number 826421).

Refs:

[1] D'Angelo, Egidio, and Viktor Jirsa. "*The quest for multiscale brain modeling*." Trends in Neurosciences (2022).

[2] M. Hashemi, AN. Vattikonda, V. Sip, M. Guye, F. Bartolomei, M.M. Woodman, and V. Jirsa. "*The Bayesian Virtual Epileptic Patient: A probabilistic framework designed to infer the spatial map of epileptogenicity in a personalized large- scale brain model of epilepsy spread".* NeuroImage. 2020 Aug 15;217:116839. DOI: https://doi.org/10.1016/j.neuroimage.2020.116839

[3] M. Hashemi, AN. Vattikonda, J. Jha, V. Sip, MM. Woodman, F. Bartolomei, V. Jirsa. "*Simulation-Based Inference for Whole-Brain Network Modeling of Epilepsy using Deep Neural Density Estimators*". medRxiv. 2022 Jan 1. DOI: https://doi.org/10.1101/2022.06.02.22275860

[4] M. Hashemi, AN. Vattikonda, V. Sip, M. Guye, F. Bartolomei, MM. Woodman, and V. Jirsa. "*On the influence of prior information evaluated by fully Bayesian criteria in a personalized whole-brain model of epilepsy spread".* PLoS Computational Biology. 2021 Jul 14;17(7):e1009129. DOI: https://doi.org/10.1371/journal.pcbi.1009129

[5] J. Jha, M. Hashemi, AN. Vattikonda, H. Wang, V. Jirsa. "*Fully Bayesian estimation of virtual brain parameters with self-tuning Hamiltonian Monte Carlo".* Machine Learning: Science and Technology. 2022 Sep 26;3(3):035016. DOI: 10.1088/2632-2153/ac9037

[6] N. Baldya, M. Hashemi, N. Simon, V. Jirsa. *"Bayesian Pharmacometrics Analysis of Baclofen for Alcohol Use Disorder".* bioRxiv. 2022 Jan 1. DOI: https://doi.org/10.1101/2022.10.25.513675

BH. Yalcinkaya, A. Ziaeemehr, J. Fousek, M. Hashemi, M. Lavanga, A. Solodkin, AR. McIntosh, V. Jirsa, S. Petkoski. *"Personalized virtual brains of Alzheimer's Disease link dynamical biomarkers of fMRI*

11. Inferring the micro-circuitry of mere presence

Amirhossein Esmaeili[1,2*], Meysam Hashemi[2], Frank Zaal[3], Driss Boussaoud[1], Viktor Jirsa[2]

1. *Aix-Marseille University, Dynamics of Cognitive Processes Group, Institute of Systems Neuroscience, Marseille, France.*
2. *Aix-Marseille University, Theoretical Neuroscience Group, Institute of Systems Neuroscience, Marseille, France.*
3. *University Medical Center Groningen, Faculty of Medical Sciences, Department of Human Movement Sciences, Groningen, Netherlands.*

*Amirhossein.ESMAEILI@univ-amu.fr

Introduction

Isolation wreaks havoc upon the human brain. Keeping in mind our gregarious nature it would stand to reason that social stimuli could significantly modulate our cognition. Mere presence is the most fundamental form of social stimuli and it's been shown to improve behavioral performance depending in simple tasks (social facilitation) [1]. However, the literature surrounding the neurobiological bases of social facilitation is rather sparse, with one of the most promising findings being the discovery of presence/absence sensitive reward-oriented neurons in dorsolateral prefrontal cortex (dlPFC), and anterior cingulate cortex (ACC) of Rhesus monkeys[4]. Based on the same primate dataset, we identified a similar context-dependent trend in the feedback-locked event-related potentials (ERPs), with increased ERP amplitude in the presence condition. We employ the framework of Dynamical Causal Modelling (DCM) in order to infer the parameters of a neural mass [3] (Jansen-Rit) between the two experimental conditions. Our results show that synaptic model parameters are significantly different between the presence and absence conditions. We hypothesize that this difference in the parameter distributions leads to changes in the postsynaptic excitation/inhibition (E/I) balance in the region.

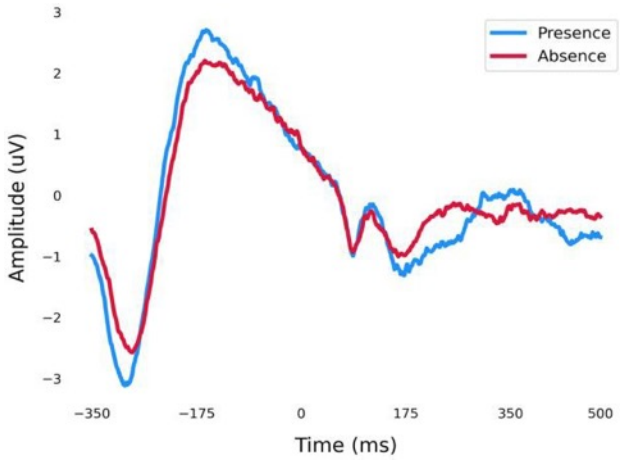

Figure 1 Feedback-locked ERPs obtained from absence & presence condition during successful trials.

Methods

We model the activity of a region via a modification of the Jansen-Rit model, a neural mass model of three subpopulations in a cortical micro-column [3]. The model is capable of producing sustained oscillations, evoked responses, and epileptic-like activity, with the LFP signal assumed to be proportional to the

depolarization of pyramidal cells. Dynamical causal modelling allows us to obtain the parameter distributions which best explain the observed data (ERP time series) via Bayesian inference. More formally, given model parameters θ, and observation data y, we update the uncertainty in parameter estimation by multiplying our domain expertise $p(\theta)$ (or prior) with a data generative process $p(y|\theta)$ (likelihood) in order to calculate the posterior probability distribution $p(\theta|y)$:

$$p(\theta \mid y) \propto p(\theta)p(y \mid \theta)$$

However, this data generative process is usually analytically intractable. Markov chain Monte-Carlo algorithms are therefore utilized to draw random samples from the posterior, bypassing the necessity for knowing the entire distribution. A state-of-the-art variation of this algorithm, -namely Hamiltonian Monte-Carlo (HMC)- alleviates the shortcomings of normal Monte-Carlo algorithms such as random walk, and enables us to acquire the true posterior distribution [2,5,6], which is especially critical for models with high degeneracy such as the Jansen-Rit model.

Results & Discussion

The parameter distributions obtained from HMC show that the majority of between-condition changes to model parameters is stemming from rate constants, maximum postsynaptic potential amplitudes (PSPs), external current, and initial conditions. In the presence condition inhibitory rate constant and excitatory postsynaptic amplitude is increased while the excitatory rate constant is decreased. An opposite trend is seen in the absence condition. Changes to these parameters lead to alterations to the ratio of excitatory and inhibitory postsynaptic potentials with presence exhibiting a lower E/I ratio. In fact, the larger pyramidal activity in the presence condition might be a compensatory response to the increased IPSP.

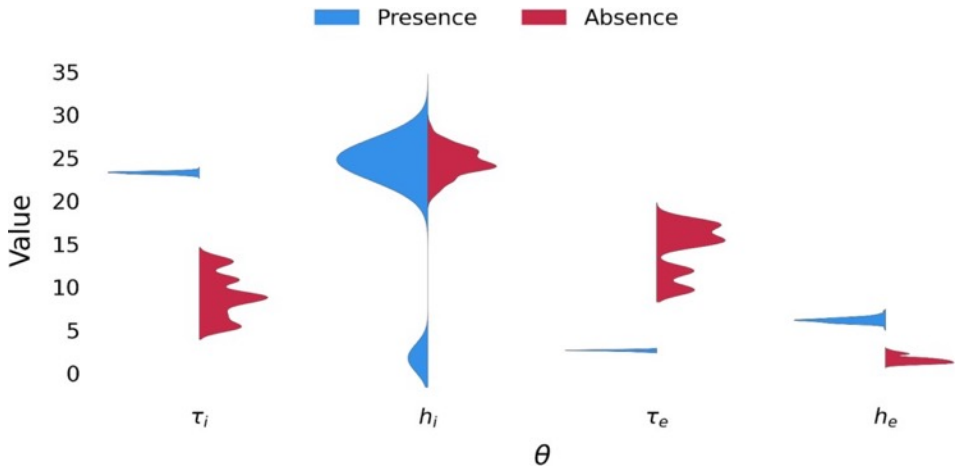

Figure 2 HMC-derived distributions of excitatory (e) & inhibitory (i) synaptic parameters. Here, T represents rate constant and h the maximum amplitude of PSPs.

We suggest a novel analysis pipeline in order to non-invasively investigate how mere presence of conspecifics alters dynamical -synaptic- characteristics of a cortical microcolumn. The caveat to use of the Jansen-Rit model however, is the high correlation between parameters. This signifies that changes to the synaptic conductance should best be evaluated by calculating the *collective* effect of the parameters.

Keywords: Social facilitation, Event-Related Potentials, Dynamical Causal Modelling, Excitation/Inhibition Balance

Bibliography

1. Bond CF Jr, Titus LJ. Social facilitation: a meta-analysis of 241 studies. Psychol Bull. 1983;94(2):265-292.

2. Cranmer K, Brehmer J, Louppe G. The frontier of simulation-based inference. Proceedings of the National Academy of Sciences. 2020;117(48):30055-30062. doi:10.1073/pnas.1912789117

3. David O, Kilner JM, Friston KJ. Mechanisms of evoked and induced responses in MEG/EEG. Neuroimage. 2006;31(4):1580-1591. doi:10.1016/j.neuroimage.2006.02.034

4. Demolliens M, Isbaine F, Takerkart S, Huguet P, Boussaoud D. Social and asocial prefrontal cortex neurons: a new look at social facilitation and the social brain. Soc Cogn Affect Neurosci. 2017;12(8):1241-1248. doi:10.1093/scan/nsx053

5. Neal RM. MCMC using Hamiltonian dynamics. arXiv:12061901 [physics, stat]. Published online May 10, 2011. doi:10.1201/b10905

6. Conference on Neural Information Processing Systems. NIPS'17. Curran Associates Inc.; 2017:2335-2344

7. Bond CF Jr, Titus LJ. Social facilitation: a meta-analysis of 241 studies. Psychol Bull. 1983;94(2):265-292.

8. Cranmer K, Brehmer J, Louppe G. The frontier of simulation-based inference. Proceedings of the National Academy of Sciences. 2020;117(48):30055-30062. doi:10.1073/pnas.1912789117

9. David O, Kilner JM, Friston KJ. Mechanisms of evoked and induced responses in MEG/EEG. Neuroimage. 2006;31(4):1580-1591. doi:10.1016/j.neuroimage.2006.02.034

10. Demolliens M, Isbaine F, Takerkart S, Huguet P, Boussaoud D. Social and asocial prefrontal cortex neurons: a new look at social facilitation and the social brain. Soc Cogn Affect Neurosci. 2017;12(8):1241-1248. doi:10.1093/scan/nsx053

11. Neal RM. MCMC using Hamiltonian dynamics. arXiv:12061901 [physics, stat]. Published online May 10, 2011. doi:10.1201/b10905

12. Conference on Neural Information Processing Systems. NIPS'17. Curran Associates Inc.; 2017:2335-2344

12. Data-driven signaling pathway modelling

Andrei Kramer[1&], Federica Milinanni[2&], Pierre Nyquist[2], Jeanette Hellgren Kotaleski[3], Alexandra Jauhiainen[4#], Olivia Eriksson[3#*]

[1] Science for Life Laboratory, Karolinska Institutet, Solna, Sweden

[2] Department of Mathematics, KTH Royal Institute of Technology, Stockholm, Sweden

[3] Electrical Engineering and Computer Science, KTH Royal Institute of Technology, Stockholm, Sweden

[4] Biometrics, Early Clinical Development, IMED Biotech Unit, AstraZeneca, Gothenburg, Sweden

[&] Have contributed equally to this work as first authors

[#] Have contributed equally to this work as last authors

* e-mail-address of corresponding author: olivia@kth.se

INTRODUCTION/MOTIVATION

Subcellular signaling pathways describe how a series of molecular reactions within the cell regulates some cellular function, like modifying the strength of a synapse. Such pathways are often modeled on a resolution corresponding to concentrations of molecules and the dynamic quantitative data they reproduce can consist of time series experiments e.g., measuring protein activity using FRET technology or similar. It is crucial to understand signaling pathways to understand cellular function and thereby the effects of different drugs or disease mechanisms.

Mathematically, pathway models consist of a set of interacting species, often represented by a graph, together with corresponding dynamical equations describing the rate of change of species concentration or activity. Pathway models thus have the potential to integrate bioinformatics data on e.g., protein interactions and function with dynamical data on protein activity in a data-driven fashion. Data-driven modelling requires efficient and automatic methods for model calibration and validation, as well as a structured way of representing the model, experimental data and calibration process. Within this project we have developed a toolset, UQSA, that can achieve this. UQSA stands for Uncertainty Quantification (UQ) and Sensitivity Analysis (SA). UQ is important to validate a model. Typically, this means that in the parameter estimation process, the estimates are given together with descriptions of their uncertainty (Figure 1). This uncertainty can then next be propagated to the predictions from the model (Figure 1) and allow for well informed comparison with experiments. SA is another tool for model assessment.

METHODS

This toolset includes *methodological developments* concerning efficient and statistically relevant approaches for UQ and SA based on Bayesian methodologies [1]. It also includes *technical developments* mainly concerning the FAIR management [2] of not only experimental data and models, but also the whole workflow (model setup, calibration and model validation) [3, 4].

Concerning methodology, UQSA performs UQ by sampling from a distribution of good parameter values (the posterior

distribution), rather than providing a single optimal point. This sampling is implemented via Markov Chain Monte Carlo (MCMC) methods, using an Approximate Bayesian Computation (ABC) scheme. A so called copula [1] is then fitted to the MCMC samples. This offers the possibility to add datasets sequentially to fit a model, by using the posterior of previous datasets as the prior for UQ with new datasets. The UQ procedure can next be followed by a variance-decomposition based global SA to quantify the uncertainty in the model predictions (Figure 1).

Concerning technical developments, UQSA adopts SBtab [5], an easy-to-use, human and machine readable format to store information about reaction based models and calibration data. A software is also available for transferring the SBtab files to SBML [6] or MOD [7] and thus provides the possibility to run the same model in simulators like e.g. STEPS, COPASI, NEURON or Matlab. SBtab therefore contributes to making the UQSA workflow fulfill the FAIR principles.

The main part of the code is written in R. R, apart from being a user-friendly language, allows the use of sophisticated statistical methods. The core part of the code is, however, in C in order to be computationally efficient.

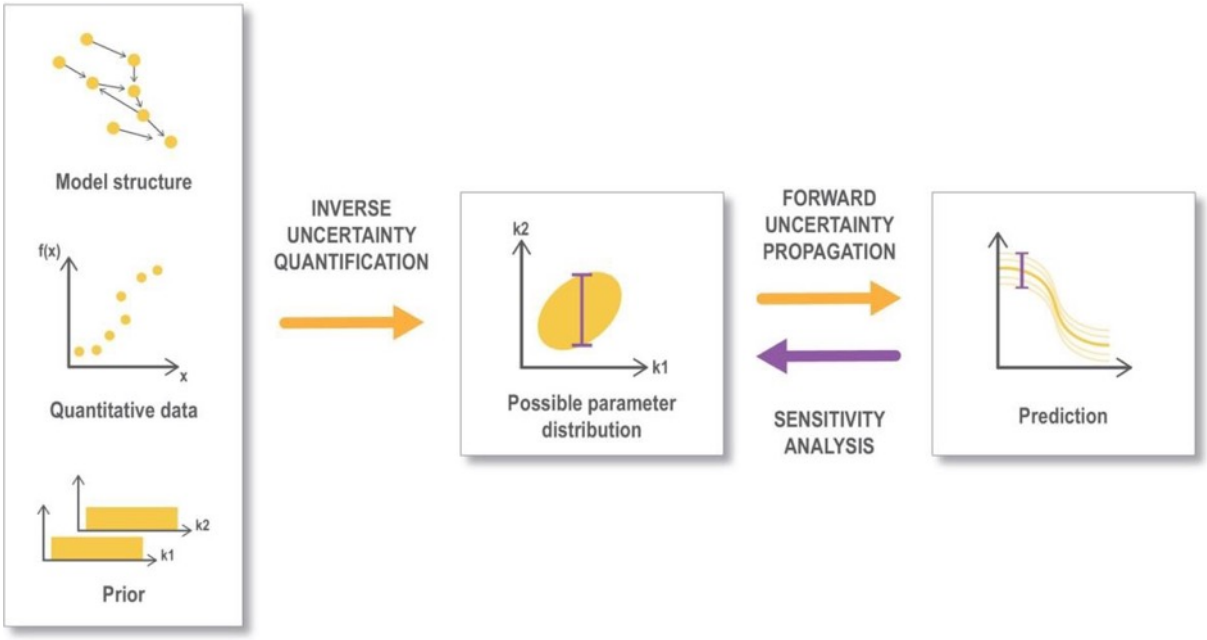

Figure 1 The uncertainty quantification starts from a model structure, quantitative data and prior (starting) assumptions on parameter distributions, then parameter estimation and uncertainty quantification are performed giving rise to a possible parameter distribution (posterior), which is in agreement with the quantitative data. Finally, a sample from the posterior distribution is propagated to the predictions of the model, and thereby describing the uncertainty of the model predictions. A sensitivity analysis can also be performed to e.g. guide further experiments. *The figure is reproduced from [3]*.

RESULTS AND DISCUSSION

We present a toolset for data-driven pathway modelling, that includes Bayesian UQ and global SA. It has been tested on a number of different models and experimental data, including a model for PKA binding to AKAP79 [8], a model on CaMKII dynamics [1], and a model for AKAR4 activation. Source code and more information are available as part of the EBRAINS Subcellular pathway model building and calibration toolset: https://wiki.ebrains.eu/bin/view/Collabs/subcellular-modeling-and-simulation/.

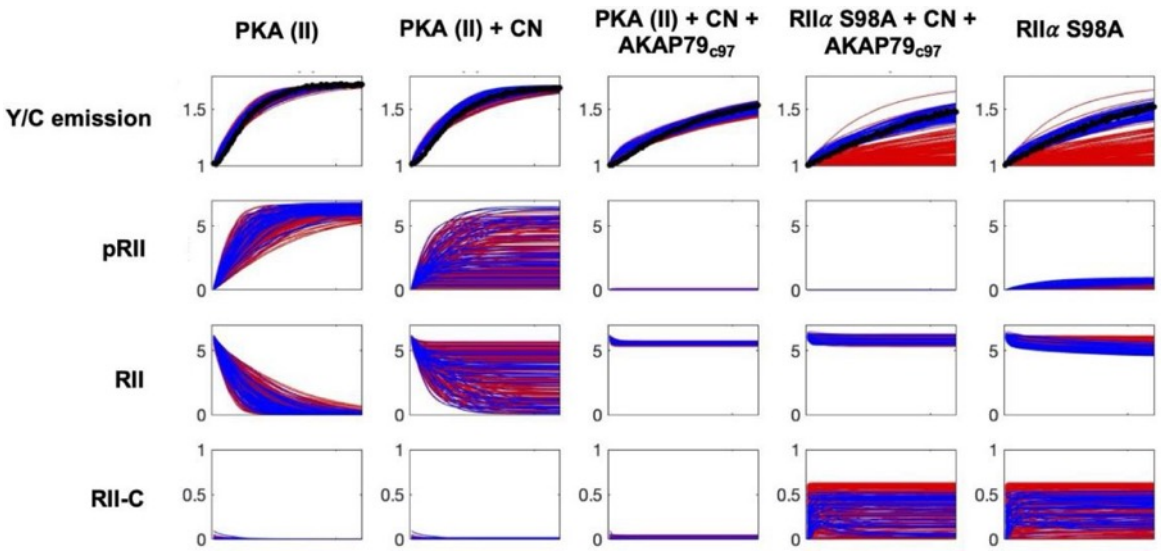

Figure 2 Uncertainty in the predictions from the AKAP79 model [8], corresponding to an ensemble model. The experimental data (black dots, first row, first three columns) have not constrained the model enough to give e precise prediction (first row last two columns). Blue and red correspond to a further classification of "good" and "bad" fits. *Figure is an excerpt from [8]*.

Keywords: Data-driven modelling, Signaling Pathway, Uncertainty Quantification, Global Sensitivity Analyses, FAIR, Workflow, Dynamical modelling

ACKNOWLEDGEMENTS

This work was supported by the European Horizon2020 Framework Programme under grant agreement 945539 (The Human Brain Project, SGA3); the Swedish Research Council; the Swedish e-Science Research Centre (SeRC); AstraZeneca provided support in the form of salary for author AJ. Simulations were performed on resources provided by the Swedish National Infrastructure for Computing (SNIC) at the PDC center for High Performance Computing.

REFERENCES

[1] Eriksson, O., Jauhiainen, A., Maad Sasane, S., Kramer, A., Nair, A. G., Sartorius, C., & Hellgren Kotaleski, J. (2019). Uncertainty quantification, propagation and characterization by Bayesian analysis combined with global sensitivity analysis applied to dynamical intracellular pathway models. *Bioinformatics*, 35(2), 284-292. doi: https://doi.org/10.1093/bioinformatics/bty607

[2] Wilkinson, M. D., Dumontier, M., Aalbersberg, I. J., Appleton, G., Axton, M., Baak, A., ... & Mons, B. (2016). The FAIR Guiding Principles for scientific data management and stewardship. *Scientific data*, 3(1), 1-9. doi: https://doi.org/10.1038/sdata.2016.18

[3] Eriksson, O., Bhalla, U. S., Blackwell, K. T., Crook, S. M., Keller, D., Kramer, A., ... & Hellgren Kotaleski, J. (2022). Combining hypothesis-and data-driven neuroscience modeling in FAIR workflows. *Elife*, 11, e69013. doi: https://doi.org/10.7554/eLife.69013

[4] Santos, J. P., Pajo, K., Trpevski, D., Stepaniuk, A., Eriksson, O., Nair, A. G., ... & Kramer, A. (2022). A Modular Workflow for Model Building, Analysis, and Parameter Estimation in Systems Biology and Neuroscience. *Neuroinformatics*, 20(1), 241-259. doi: https://doi.org/10.1007/s12021-021-09546-3

[5] Lubitz, T., Hahn, J., Bergmann, F. T., Noor, E., Klipp, E., & Liebermeister, W. (2016). SBtab: a flexible table format for data exchange in systems biology. *Bioinformatics*, 32(16), 2559-2561. doi: https://doi.org/10.1093/bioinformatics/btw179

[6] Hucka, M., Finney, A., Sauro, H. M., Bolouri, H., Doyle, J. C., Kitano, H., ... & Wang, J. (2003). The systems biology markup language (SBML): a medium for representation and exchange of biochemical network models. *Bioinformatics*, 19(4), 524-531. doi: https://doi.org/10.1093/bioinformatics/btg015

[7] Hines, M. L., & Carnevale, N. T. (2000). Expanding NEURON's repertoire of mechanisms with NMODL. *Neural computation*, 12(5), 995-1007. doi: https://doi.org/10.1162/089976600300015475

[8] Church, T. W., Tewatia, P., Hannan, S., Antunes, J., Eriksson, O., Smart, T. G., ... & Gold, M. G. (2021). AKAP79 enables calcineurin to directly suppress protein kinase A activity. *Elife*, 10, e68164. doi: https://doi.org/10.7554/eLife.68164

13. Neural correlates of predictions and prediction errors during multisensory object discrimination in the rat somatosensory barrel cortex

Francesco Mannella[1*], Thijs R. Ruikes[2*], Pietro Marchesi[2], Julien Fiorilli[2], Federico Maggiore [1], Cyriel M.A. Pennartz[2], Giovanni Pezzulo[1]

1 Institute of Cognitive Sciences and Technologies, National Research Council, Rome, Italy

2 Swammerdam Institute for Life Sciences, Center for Neuroscience, Faculty of Science, University of Amsterdam, Science Park 904, 1098 XH, Amsterdam, the Netherlands.

Corresponding Authors: francesco.mannella@gmail.com, t.r.ruikes@uva.nl

Keywords: whisking, active inference, prediction error, barrel cortex

INTRODUCTION/MOTIVATION

Rodents actively sense their environment through whisking. During whisking the animals maintain an internal belief about their distance from the objects in their environment. Recently, we proposed a computational model based on the active inference framework, which characterizes rodents anticipatory and error-correction dynamics during whisking [1]. The model explains whisking behaviour and neural activity in terms of prediction error minimization dynamics [2]. During simulations of the model, internal variables are updated based on multisensory input from proprioceptive, tactile and visual modalities. Errors between predicted and sensed observations are used to update probabilistic beliefs about object identity and to adjust whisking amplitude in object-dependent ways. In the current project, we fit the model parameters to empirical data recorded from free behaving rats performing a multisensory object-discrimination task. Rats were tasked with discriminating between two objects using tactile, visual or both modalities [3]. High-speed videography of whisker kinematics and neural recordings from somatosensory cortex were simultaneously recorded. By fitting the animal's whisking kinematics on a trial-by-trial basis, the computational model generates synthetic timeseries (i.e., trial- specific series of predictions and prediction-errors during animal-object interactions) that we aim to compare with neuronal activations in somatosensory barrel cortex.

METHODS

Computational model of prediction and prediction errors in the somatosensory barrel cortex

The computational used for the analysis casts whisking behavior in terms of active inference [1]. Fig. 1 shows the key variables of the active inference agent's generative model (Fig. 1 right) and their putative links with neuroanatomy (Fig. 1, left). The circles shown in the right part of Fig. 2 represent the model variables (which correspond to probabilistic beliefs), whereas the edges correspond to statistical relations between variables. The variables comprise sensory observations (in different modalities, touch, proprioception and vision) and a hierarchy of hidden states and causes at two levels, sensorimotor and decision-level. The left part of Fig. 1 schematically maps some of the key model variables to the neuroanatomy of rats. Colored circles represent the variables of the generative model, whereas the ξ symbols represent prediction errors. Colored edges show the putative (neuronal) message passing between the model variables. The most notable aspect is the presence of reciprocal, top-down and bottom-up messages across hierarchical levels. For example, the red edge originating from the v (causal) variable represents a top-down signal. Blue edges originating from the ξ symbols represent prediction errors that are propagated bottom-up. See [1] for more details about the model.

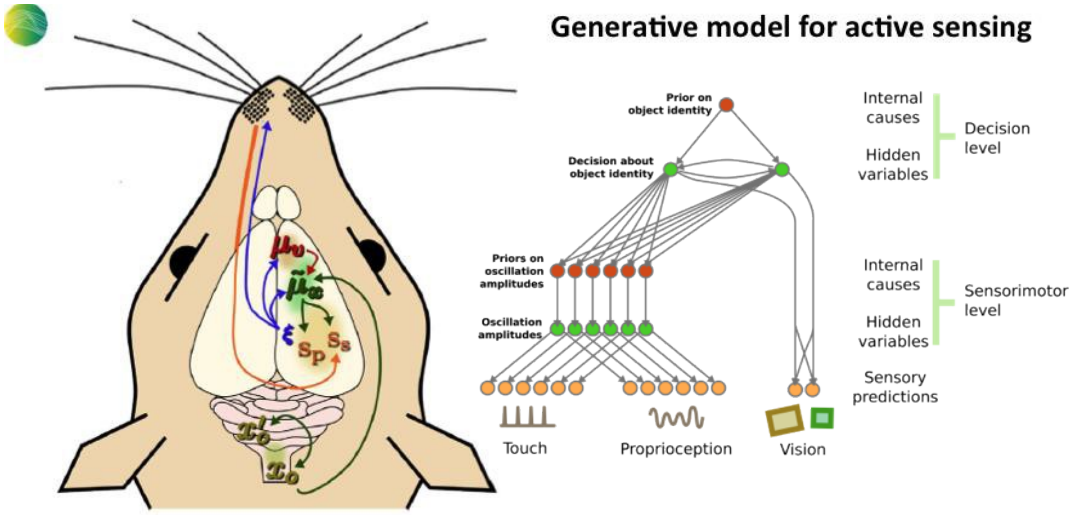

Figure 1. Schematic of the computational model of whisking behavior used for the analysis. Left: schematic overview of the neuroanatomy associated with each model variable. Right: overview of the generative model for active sensing.

Neural recordings from rat somatosensory barrel cortex during object discrimination

Neural activity from somatosensory barrel cortex (S1BF) was recorded from free behaving rats (167 cells), which performed a multimodal object recognition task on an elevated T-maze (Fig. 2). Objects were presented in visual (light on), tactile (object in reaching distance) or visual & tactile (both light on and object in reaching distance) modalities. Upon object presentation, the animal was tasked to navigate to the arm of the maze associated with the presented object. Animal behaviour was tracked using photo-diode sensors and high- speed videography during object detection. The latter allowed us to tracking whisking movements during object detection.

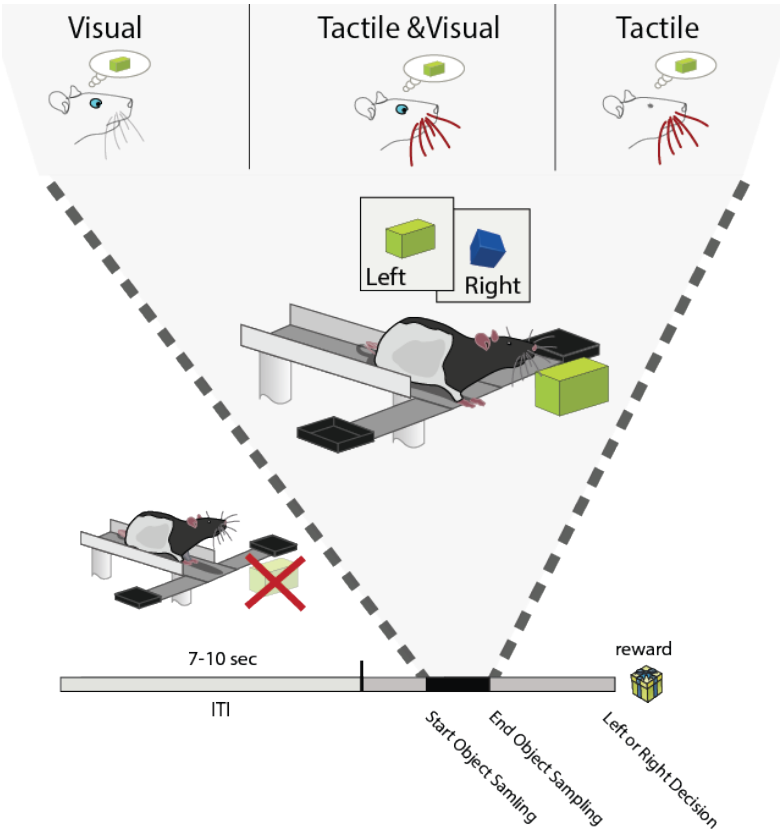

Figure 2; multisensory object detection task. Following a 7-10 second inter trial interval (ITI), to rats could access the object sampling area. Here, an object was presented in Visual, Tactile & Visual or Tactile modality. Following the detection of the object, the animal should report its choice by poke the reward site (black, on either side of the maze) associated with the presented object.

Estimating prediction errors during whisking

The prediction errors during whisking can be estimated based on the animal behaviour. When the animal approaches the object for detection, it will generate a default whisking amplitude and frequency (predictive whisking). Upon touching the object, the whisking motion is interrupted and the animal updates its whisking cycle (reactive whisking). This causes desynchronization of the whiskers due to deceleration. We quantify whether the animal is whisking predictively or reactively by measuring the desynchronization, which can be used to estimated prediction errors inferred by the active inference model.

Results and Discussion

We have completed data acquisition from our experiments and setup our analytical methods to use the model predictions to investigate the neural data. During the poster presentation, we will present the first outcomes of our ongoing research.

REFERENCES

[1] Mannella, F., Maggiore, F., Baltieri, M., & Pezzulo, G. (2021). Active inference through whiskers. Neural Networks, 144, 428–437. https://doi.org/10.1016/j.neunet.2021.08.037

[2] Parr T., Pezzulo G., Friston K. (2022) Active Inference. The Free Energy Principle in Mind, Brain, and Behavior. MIT Press

[3| Fiorilli, J., Ruikes, T., Huis In 'T Veld, Gerjan, & Pennartz, C. M. A. (2022). Sensory, perirhinal and hippocampal tetrode recordings during visual, tactile and visuotactile discrimination task in the freely moving rat (v1) [Data set]. EBRAINS. https://doi.org/10.25493/AM91-2D

14. Decorrelation as a principle for the emerging of Structured Flows on Manifolds

Claudio Runfola[1*], Hiba Sheheitli[1], Viktor Jirsa[1]

[1]Aix-Marseille Université, Institut de Neurosciences des Systèmes (INS), Marseille , France

*e-mail-address of corresponding author: claudio.runfola@univ-amu.fr

INTRODUCTION/MOTIVATION

Structured flows on attractive manifolds prescribe the evolution of low-dimensional dynamic systems, which can be interpreted as internal models in cognitive theories. We identify basic properties of neuronal populations leading to an equivariant matrix in a network, in which complex behaviors can naturally be represented through structured flows on manifolds. We propose a neural mechanism for the generation of structured flows on manifolds from symmetry breaking in the connectivity of brain networks. We show in particular how decorrelation of oscillatory behaviors of the network nodes is essential for the emergence of the manifold and its flows.

METHODS

We elaborate on the analysis of a minimal simple toy model in which a single node dynamics allows for jumpings between an up and a down state (bistable system). We present a numerical exploration of the dynamics, in which we further apply different manifold extracting techniques to extract the resulting low-dimensional topology and the associated flows; first for the case of a two-node system, and then for the more complex case of a high- dimensional network on which the two-nodes dynamics emulate the dynamics of two-modes of behavior that are distributed through an orthogonal projection across a network on a full connectome.

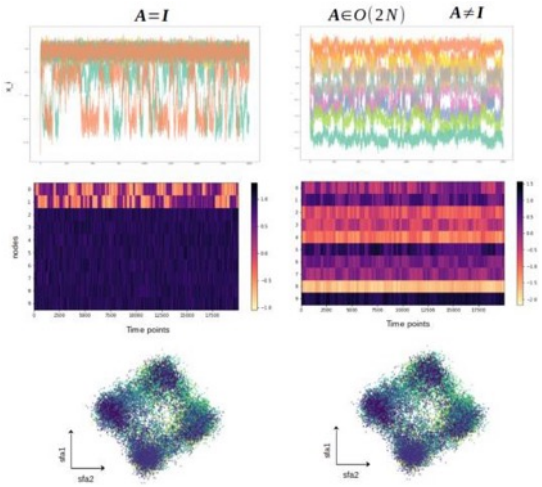

Two coupled nodes are embedded in a larger network through an orthogonal transformation. SFA uncovers the low-dimensional manifold comprised of the 4 original subspaces around the equilibrium points of the embedded two-modes system. Simulated time series are generated tuning the coupling (G=0.07) and the noise (v=0.03) and by using standard parameters of sksfa.SFA function in the sklearn-sfa package.

RESULTS AND DISCUSSION

Narrowed down to the forces present in brain networks, we linked basic properties of neural masses and networks to the emergence of invariant manifolds in state space, which are the carrier of structured flows known from behavioral

neurosciences. The flows on the low-dimensional task-specific manifolds capture, in abstract state space, the mechanistic manifestation of entropy as constructive irreversibility in the brain, and thus, serveas a principal enabling link between neural activity and behavior. In this work, in particulare, we want to serve a proof- of-concept demonstration of the action of decoupling (decorrelation) through frequency separation as a mechanism for the generation of low-dimensional subspaces in high-dimensional systems.

Keywords: symmetry breaking, emergence, structured flows on manifolds, brain networks, oscillations, averaging

15. Generating High Performance Simulations from a Portable Data Format using Arbor

T. Hater[1]*, B. Huisman[1], L. P. L. Landsmeer[1]

[1]JSC Forschungszentrum Jülich Germany

*t.hater@fz-juelich.de

INTRODUCTION/MOTIVATION

Computational neuroscience is experiencing a steady growth in available simulation tools applicable to morphologically detailed cell descriptions [5, 1, 9, 3, 7, 8]. However, the development of portable models lags behind. NeuroML2 (NML) is one of the few comprehensive approaches in this area, but its reference implementation lacks in performance and scalability [2]. Our goal is to enable Arbor, a performance -portable library for simulating morphologically detailed neurons to consume NML models. We present nmlcc, a tool to generate optimised, full scale simulations from a description in NML. It produces bespoke dynamics tailored to the input, resulting in performance metrics comparable to hand-optimised code. Through Arbor, the generated simulation package is able to utilise modern hardware, including large-scale GPU clusters, scaling to millions of cells [7].

METHODS

nmlcc needs to produce inputs tailored to Arbor, that is: cell morphologies, ion channels, cell parameterisations, and network connectivity. As NML can synthesise new ion channels on the fly, nmlcc cannot rely on a static list of channel descriptions. As simulations in an NML description provide a fully integrated picture, nmlcc can exploit this holistic view to optimise input decks beyond what is possible for Arbor out-of-the-box. Ion channels are typically among the most demanding parts of the simulation, thus an emphasis is placed on making them as performant as possible.

RESULTS AND DISCUSSION

As can be seen in Fig. 1 nmlcc can generate an input deck that runs roughly nine times faster on Arbor (arbor+nmlcc) than NEURON using the jnml NML reference implementation (baseline). Part of this is a performance advantage intrinsic to Arbor, which runs about four times faster than the baseline. However, even with the CVODE timestepping available to NEURON, the arbor+nmlcc simulation – using a fixed timestep – is still substantially faster. The advantage of the CVODE scheme will degrade when exposed to high-frequency inputs, which makes it unattractive in network simulation. We have demonstrated a way to convert generic, high-level descriptions into bespoke simulations competitive with hand-optimised code. This is made possible by exploiting the holistic view provided by NML. Further, tailoring generic ion channels to a specific simulation is only feasible via automated translation and optimisation. Overall, nmlcc enables researchers to convert NML models to Arbor using a single command and expect to obtain a high-performance simulation that can trivially be adapted to (GPU-accelerated) HPC systems.

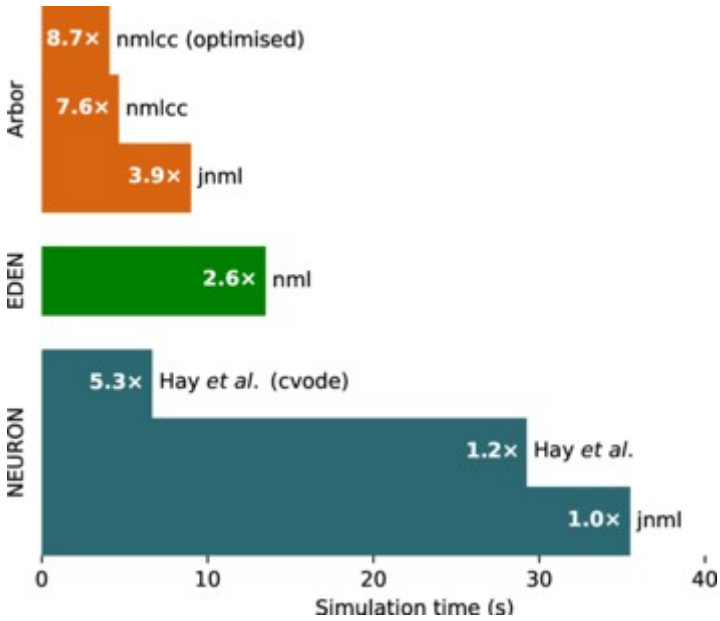

Keywords: HPC, Neural Networks, Simulation, Portable Models

ACKNOWLEDGEMENTS

We are grateful to P. Gleeson for many insightful discussions on the internals of NML2. This research has received funding from the European Union's Horizon 2020 Framework Programme for Research and Innovation under the Specific Grant Agreements No. 720270 (HBP SGA1), No. 785907 (HBP SGA2), and No. 945539 (HBP SGA3).

REFERENCES

[1] Roy Ben-Shalom et al. "NeuroGPU: Accelerating multi-compartment, biophysically detailed neuron simulations on GPUs". In: Journal of Neuroscience Methods, 2022 (10.1016/j.jneumeth.2021.109400)

[2] Robert C Cannon et al. "LEMS: a language for expressing complex biological models in concise and hierarchical form and its use in underpinning NeuroML 2". In: Frontiers in neuroinformatics, 2014 (10.3389/fninf.2014.00079)

[3] Dan FM Goodman and Romain Brette. "The Brian simulator". In: Frontiers in neuroscience, 2009 (10.3389/neuro.01.026.2009)

[4] Etay Hay et al. "Models of neocortical layer 5b pyramidal cells capturing a wide range of dendritic and perisomatic active properties". In: PLoS computational biology 7.7, 2011 (10.1371/journal.pcbi.1002107)

[5] Sotirios Panagiotou et al. "EDEN: A high-performance, general-purpose, NeuroML-based neural simulator". In: Frontiers in Neuroinformatics, 2022 (10.3389/fninf.2022.724336)

[6] url: https://github.com/OpenSourceBrain/L5bPyrCellHayEtAl2011.

[7] N. Abi Akar et al. Arbor — A Morphologically-Detailed Neural Network Simulation Library for Contemporary High-Performance Computing Architectures. IEEE, 2019 (10.1109/EMPDP.2019.8671560).

[8] N. T. Carnevale and M. L. Hines. The NEURON book. Cambridge University Press, 2006. (10.1017/CBO9780511541612)

[9] L. Niedermeier et al. "CARLsim 6: An Open Source Library for Large-Scale, Biologically Detailed Spiking Neural Network Simulation". In: International Joint Conference on Neural Networks, 2022 (10.1109/IJCNN55064.2022.9892644)

16. State-dependent brain responsiveness at the level of local circuits and mesoscale (part A Live Paper T2.5)

Arnau Manasanch[1], Anna L Allegra Mascaro[2], Alessandro Arena[3], Alessandra Camassa[1], Cristiano Capone[4], Leonardo Dalla Porta[1], Olivier David[6], Giulia De Bonis[4], Chiara De Luca[4], Abhilash Dwarakanath[6], Jan Fousek[5], Andrea Galluzzi[7], Jennifer Goldman[8], Espen Hagen[3], Maciej Jedynak[6], Bjorn Erik Juel[3], Ezequiel Mikulan[9], Elena Montagni[2], Antonio Pazienti[7], Spase Petkoski[5], Andrea Pigorini[9], Francesco Resta[2], Axel Roques[8], Johanna Senk[10], Núria Tort-Colet[8], Markuss Diesmann[10], Viktor Jirsa[5], Marcello Massimini[9], Maurizio Mattia[7], Fanis Panagiotaropoulos[6], Pier Stanislao Paolucci[4], Francesco S Pavone[2], Mavi Sánchez-Vives[1], Johann F Storm[3] & Alain Destexhe[8]

[1]IDIBAPS: Systems Neuroscience, Institute of Biomedical Investigations August Pi I Sunyer, Barcelona, Spain [2]LENS: European Laboratory for Non-Linear Spectroscopy, Via Nello Carrara 1, 50019 Sesto Fiorentino, Italy. [3]UIO: Department of Molecular Medicine, University of Oslo, Oslo, Norway

[4]INFN: Istituto Nazionale di Fisica Nucleare (INFN), Sezione di Roma, Rome, Italy

[5]AMU: Institut de Neurosciences des Systèmes, Aix Marseille Université, Marseille, France

[6]CEA: Cognitive Neuroimaging unit, CEA, Universite PAris-Saclay, Neurospin Center, 91191, Gif/Yvette, France

[7]ISS: Center for Radioprotection and Computational Physics, Istituto Superiore di Sanità, Rome, Italy

[8]CNRS: Paris-Saclay Institute of Neuroscience (NeuroPSI), Paris-Saclay University, 91400 Saclay, France;

[9]UMIL: Department of Biomedical and Clinical Sciences "L. Sacco" Universit a degli Studi di Milano, Milan, Italy

[10]FZJ: Institute of Neuroscience and Medicine (INM-6), Institute for Advanced Simulation (IAS-6), JARA-Institute Brain Structure- Function Relationships (INM-10), Jülich Research Centre, Jülich, Germany

INTRODUCTION/MOTIVATION

The brain can be seen as a highly interconnected network, that generates spontaneous activity and expresses its own spatiotemporal dynamics even in the absence of inputs. This network can express different brain states, characterized not only by their different emergent patterns but also by the resulting behavior. The responses to stimulation (endogenous or exogenous) or responsiveness is also highly informative regarding the state of the underlying network, its excitability and encoding capabilities, between others. Therefore, stimulation or perturbation, is an efficient way to probe the functional state of the network, having a diagnostic power in the clinical realm, but also a great value from the experimental and computational perspective.

It is known that the brain's spontaneous activity emerges as the result of the integration of multiple factors, including, among many, the intrinsic electrophysiological properties of single neurons [1] and the synaptic interactions among them [2], which are modulated by neuromodulatory systems [3] and reflected in the behaviour [4]. Here, we aim to investigate the relation between spontaneous activity and brain responsiveness at the micro and mesoscale levels from both experimental and computational perspectives.

METHODS

This study is the first part of a large-scale collaboration across different HBP-member laboratories. Our aim together has been to integrate knowledge, in the form of a Live paper (EBRAINS Live Papers), of the state-dependent brain responsiveness across different scales and species and its dependence on the brain state. "Live" figures will be hosted in EBRAINS accompanied by the data and models allowing to reproduce them. The aim of the Live figures is to create an environment where one will be able to directly interact with the data and models, enabling an online execution of the analysis pipelines and simulations, providing then an avenue for new discoveries.

RESULTS AND DISCUSSION

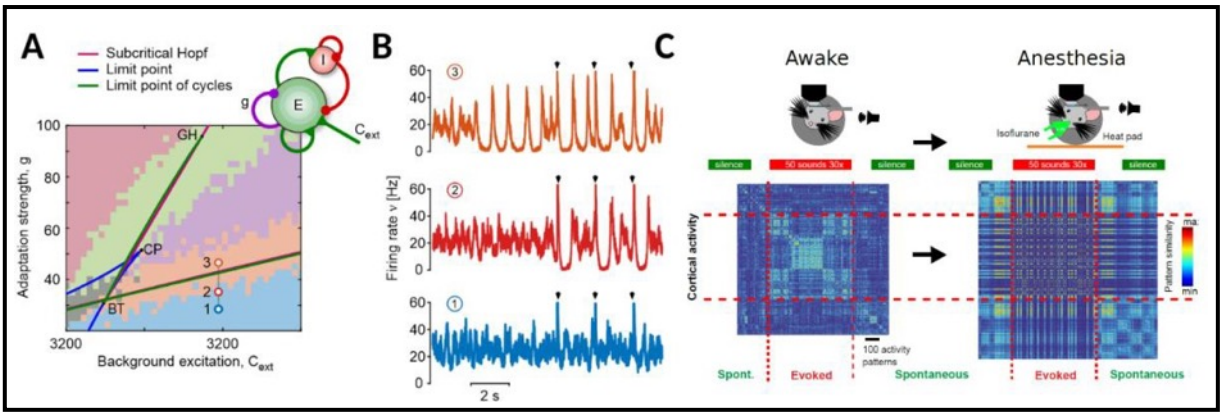

Fig.1 A: Bifurcation diagram with the different dynamical regimes when moving in the excitation or adaptation directions. B: Representative traces of simulated activity from points in panel A. C: Patterns of response to auditory stimulation.

Cortical responsiveness at the level of simulated networks of cortical neurons is first examined. To have a computational approach to the dynamic space ranging from synchronous (e.g., sleep) to asynchronous states (e.g., awake), we first present a dynamic phase diagram, that covers different dynamical regimes observed across brain states can be achieved by modulating two specific features of the microscopic circuit: the strength of the firing-rate adaptation and the excitation level [5]. An excitation-adaptation plane [6] **(Fig.1A)** can be worked out and the network can be trapped in an asynchronous irregular regime or express slow oscillations (SO), for example. By perturbing the network, different state-dependent evoked responses are obtained. When the adaptation is higher, the stimulation elicits synchronized off-periods (or Down states), not visible in the lower adaptation (wake-like) scenario **(Fig. 1B).**

If we investigate sensory stimulation, the patterns of evoked auditory responses vary with the brain state, and this is illustrated when imaging the same population of neurons in the primary auditory cortex of awake and anesthesized mice **(Fig. 1C)**. The correlation between spontaneous and evoked patterns was high in anesthesia and low during awake, suggesting that the fine structure of the evoked responses can reveal if the stimulus has been perceived or not [7] **(Fig.1C)**.

We investigated the visual-evoked responses in the primary visual cortex of awake monkeys, which triggered travelling waves [8], providing mesoscale information about the cortical area. Spontaneous travelling waves had their origin at random sites, while evoked ones were more homogeneously organized **[8] (Fig.2A)**. To explore this phenomenon, a mean field model was employed [9], where simulated travelling waves, evoked by a single input, were compared with more complex patterns of travelling waves evoked by multiple inputs. Finally, another mean-field model, whose connectivity is inferred from experimental data [10], reproduced how the response to focal stimulation is also state- dependent, with no propagation at low excitability, and a global wave pattern when excitability is high **(Fig. 2C).**

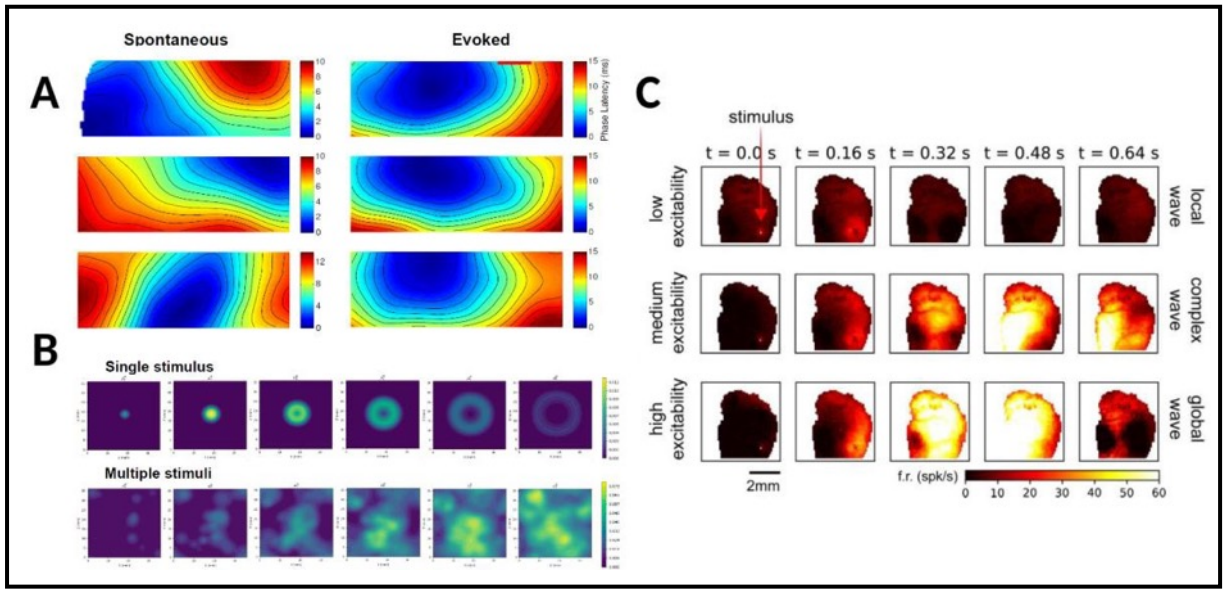

Fig.2 A: Spontaneous versus evoked travelling waves. B: Modelled travelling waves. C: Simulated evoked responses under different levels of excitability.

As mentioned above, the responsiveness of the network depends on different factors, including network excitability, adaptation or spatial functional connectivity. A measure capable of integrating various of these factors and the complexity of evoked responses is the Perturbational Complexity Index (PCI), which has been used in different systems, both experimental and computational. PCI- related data and models at the meso and whole-brain scales will be shown in the accompanying poster (part B).

Keywords: Brain states, responsiveness, circuit, cortical network, model, imaging, awake, anesthesia

Acknowledgements This project/research has received funding from the European Union's Horizon 2020 Framework Programme for Research and Innovation under the Specific Grant Agreement No. 945539 (Human Brain Project SGA3).

REFERENCES

[1] Llinás RR. The intrinsic electrophysiological properties of mammalian neurons: insights into central nervous system function. Science. 1988 Dec 23;242(4886):1654-64. doi: 10.1126/science.3059497. DOI: 10.1126/science.3059497

[2] Steriade M., Corticothalamic resonance, states of vigilance and mentation. Neuroscience2000;101(2):243-76. doi: 10.1016/s0306-4522(00)00353-5. DOI: 10.1016/s0306-4522(00)00353-5

[3] McCormick DA. Neurotransmitter actions in the thalamus and cerebral cortex and their role in neuromodulation of thalamocortical activity. Prog Neurobiol. 1992 Oct;39(4):337-88. doi: 10.1016/0301-0082(92)90012-4.

[4] Stringer C, Pachitariu M, Steinmetz N, Reddy CB, Carandini M, Harris KD. Spontaneous behaviors drive multidimensional, brainwide activity. Science. 2019 Apr 19;364(6437):255. doi: 10.1126/science.aav7893.

[5] Mattia, M., & Sanchez-Vives, M. V. (2012). Exploring the spectrum of dynamical regimes and timescales in spontaneous cortical activity. Cogn Neurodyn, 6(3), 239–250. DOI: 10.1007/s11571-011-9179-4

[6] Cattani, Anna & Galluzzi, Andrea & Fecchio, Matteo & Pigorini, Andrea & Mattia, Maurizio & Massimini, Marcello. (2022). Adaptation shapes local cortical reactivity: from bifurcation diagram and simulations to human physiological and pathological responses. DOI 10.1101/2022.06.11.493219.

[7] Filipchuk, A., Schwenkgrub, J., Destexhe, A. and Bathellier, B. Awake perception is associated with dedicated neuronal assemblies in cerebral cortex. Nature Neuroscience 25, 1327-1338 (2022). DOI: 10.1038/s41593-022-01168-5

[8] Muller, L., Reynaud, A., Chavane, F. *et al.* The stimulus-evoked population response in visual cortex of awake monkey is a propagating wave. *Nat Commun* 5, 3675 (2014). https://doi.org/10.1038/ncomms4675

[9] : Zerlaut Y, Chemla S, Chavane F, Destexhe A. Modeling mesoscopic cortical dynamics using a mean-field model of conductance-based networks of adaptive exponential integrate-and-fire neurons. J Comput Neurosci. 2018 Feb;44(1):45-61. doi: 10.1007/s10827-017-0668-2.

[10] Capone, C. et al. (2021) Simulations Approaching Data: Cortical Slow Waves in Inferred Models of the Whole Hemisphere of Mouse. (accepted in Communications Biology) arXiv, 2104.07445 DOI 10.48550/arXiv.2104.07445

17. State-dependent brain responsiveness: from meso to macroscale level (part B Live Paper T2.5)

Andrea Pigorini, Anna L Allegra Mascaro, Alessandro Arena, Alessandra Camassa, Cristiano Capone, Leonardo Dalla Porta, Olivier David, Giulia De Bonis, Chiara De Luca, Abhilash Dwarakanath, Jan Fousek, Andrea Galluzzi, Jennifer Goldman, Espen Hagen, Maciej Jedynak, Bjorn Erik Juel, Arnau Manasanch, Ezequiel Mikulan, Elena Montagni, Antonio Pazienti, Spase Petkoski, Francesco Resta, Axel Roques, Johanna Senk, Núria Tort-Colet, Markuss Diesmann, Viktor Jirsa, Marcello Massimini, Maurizio Mattia, Fanis Panagiotaropoulos, Pier Stanislao Paolucci, Francesco S Pavone, Mavi Sánchez- Vives, Johann F Storm & Alain Destexhe

[1]IDIBAPS: Systems Neuroscience, Institute of Biomedical Investigations August Pi I Sunyer, Barcelona, Spain LENS:

[2]European Laboratory for Non-Linear Spectroscopy, Via Nello Carrara 1, 50019 Sesto Fiorentino, Italy. UIO: Department of Molecular Medicine, University of Oslo, Oslo, Norway

[3]INFN: Istituto Nazionale di Fisica Nucleare (INFN), Sezione di Roma, Rome, Italy

[4]AMU: Institut de Neurosciences des Systèmes, Aix Marseille Université, Marseille, France

[5]CEA: Cognitive Neuroimaging unit, CEA, Universite PAris-Saclay, Neurospin Center, 91191, Gif/Yvette, France ISS: Center for Radioprotection and Computational Physics, Istituto Superiore di Sanità, Rome, Italy

[6]CNRS: Paris-Saclay Institute of Neuroscience (NeuroPSI), Paris-Saclay University, 91400 Saclay, France

[7]UMIL: Department of Biomedical and Clinical Sciences "L. Sacco" Università degli Studi di Milano, Milan, Italy

[8]FZJ: Institute of Neuroscience and Medicine (INM-6), Institute for Advanced Simulation (IAS-6), JARA-Institute Brain Structure- Function Relationships (INM-10), Jülich Research Centre, Jülich, Germany

INTRODUCTION/MOTIVATION

The brain can be seen as a highly interconnected network, which generates spontaneous activity and expresses its own spatiotemporal dynamics even in the absence of inputs. The brain network can express different brain states, which can be characterized not only by their different emergent patterns but also by the resulting behavior. The responses to stimulation (endogenous or exogenous) or responsiveness is also highly informative regarding the state of the underlying network, its excitability, or encoding capabilities, between others. Therefore, stimulation or perturbation, is an efficient way to probe the functional state of the network, having a diagnostic power in the clinical realm, but also a great value from the experimental and computational perspective. It is known that the brain's spontaneous activity emerges as the result of the integration of multiple factors, including, among many, the intrinsic electrophysiological properties of single neurons [1] and the synaptic interactions among them [2], which are modulated by neuromodulatory systems [3] and reflected in the behaviour [4]. Here, we aim to provide a review on the relation between spontaneous activity, brain responsiveness and complexity at the whole-brain level. Importantly, the first part of this review, regarding the study of responsiveness from micro to meso-scale, is available in the accompanying poster (part A).

METHODS

This study is the second part of a large-scale collaboration across different HBP-member laboratories. Our aim together has been to integrate knowledge, in the form of a Live paper (EBRAINS Live Papers), of the state-dependent brain responsiveness across different scales and species and its dependence on the brain state. "Live" figures will be hosted in EBRAINS accompanied by the data and models allowing to reproduce them, hence the name "Live" figures. The aim of the Live figures is to create an environment where one will be able to directly interact with the data and models, enabling an

online execution of the analysis pipelines and simulations, providing then an avenue for new discoveries.

RESULTS AND DISCUSSION

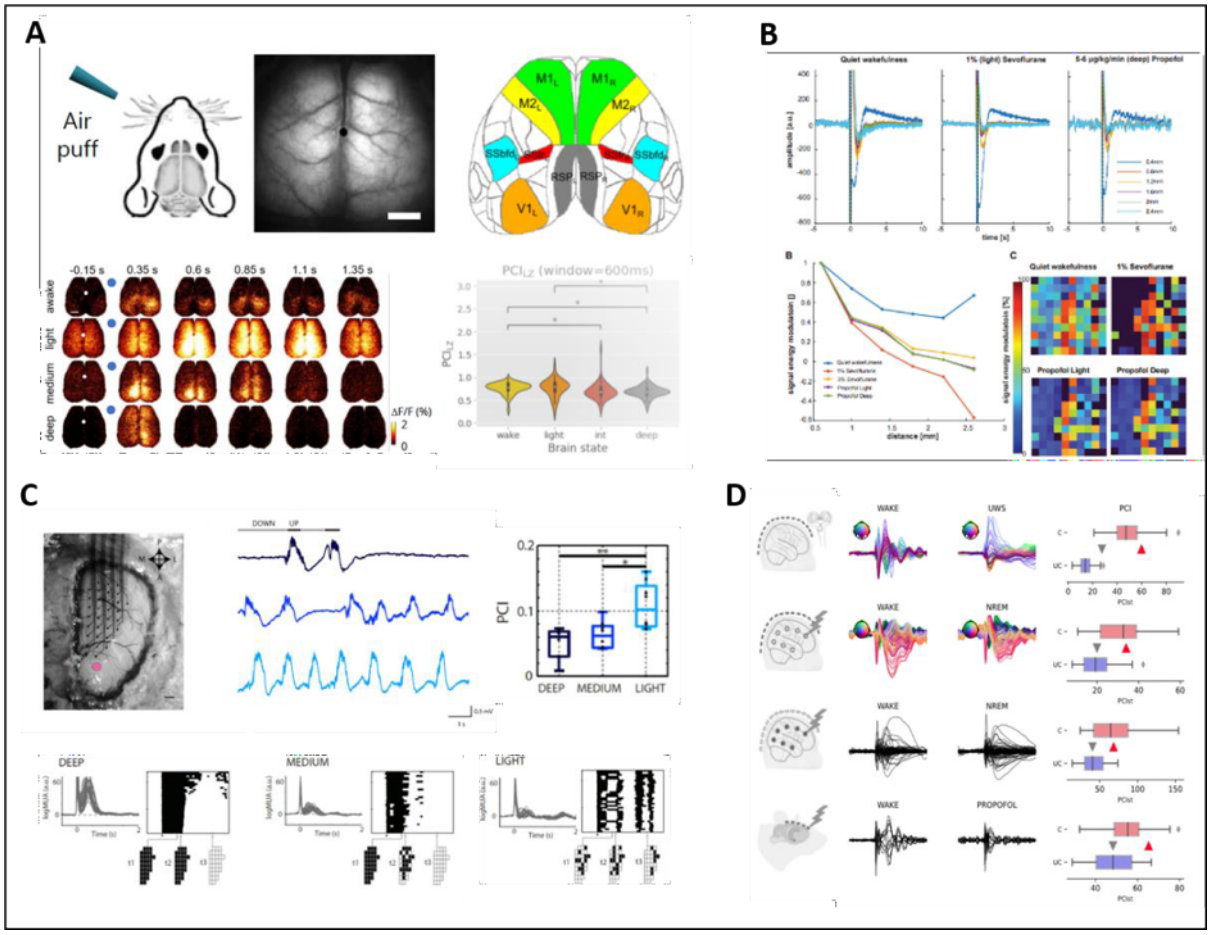

Fig.1. Experimental Data. A: Calcium imaging experimental setup, representative activations across different anesthesia levels and corresponding PCI values. B: Representative traces collected during electrical stimulation from a Utah array implanted in prefrontal cortex of a monkey. C: Electrophysiological stimulation and recordings in rodents: experimental setup, representative activations across different anesthesia levels and corresponding PCI values. D: Electrophysiological recordings in human across scales and stimulation methods (magnetic vs electric), and corresponding PCI values.

In our review we report a set of experiments which studied the brain's responsiveness at the meso and macro scale. Different experimental models such as calcium imaging in rodents **(Fig1A)** and electrophysiological recordings in non-human primates **(Fig1B)**, rodents **(Fig1C**) and humans **(Fig1D)** were used . A variety of techniques were used to stimulate the brain, including both peripheral and direct stimulation as well as invasive (single pulse electrical stimulation) and non-invasive (transcranial magnetic stimulation) stimulation. The complexity of the brain response to stimulation was gauged by means of Perturbational Complexity Index (PCI), a theory-based measure of clinical disorders of consciousness [5]. This set of experiments has provided valuable insights into the complexity of the brain's response to stimulation.

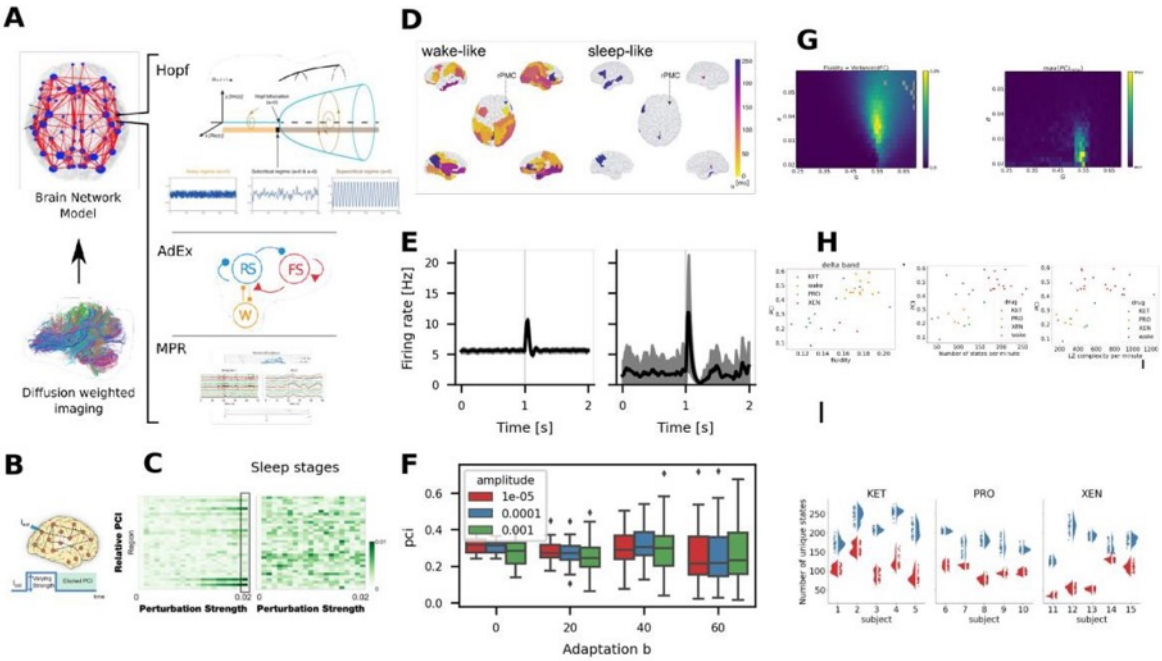

Fig.2 Simulation at the whole-brain level. Brain network model with nodes equipped with three models: Hopf (B,C), MPR (G,H,I), and AdEx (D,E,F) used to ask mechanistic questions. Hopf tuned to sub-/super-critical regimes and perturbed with varying strength; PCI varied in sub-crit. regime, no response in super-crit. (D) Wake-/sleep-like states for spatio-temporal prop. of stimulus. (E) Excitatory firing rate before/after stimulus. (F) Perturbation complexity index in b & strength. (G) MPR measures fluidity & Lempel-Ziv complexity. (H) Three EEG measures track PCI in 18 subjects. (I) Stimulus trials separate from 1-min. segments in # unique states.

Computational models of the brain at the whole-brain level have the capacity to capture various aspects of brain responsiveness. Three models are discussed: the Hopf model [6], the AdEx model [7], and the Montbrio-Pazo-Roxin (MPR [8]) model **(Fig2A)**. The Hopf model has been used to reproduce resting state neuroimaging data **(Fig2B-C)**, while the AdEx model has been used to explore the effect of varying the adaptation and stimulus strength **(Fig2D-F)**. The MPR model has been used to explore the relationship of the complexity of the stimulus-response to complexity-based measures of spontaneous activity **(Fig2G-I)**. Each model has been used to examine the role of structural connectivity, spatial gradients of brain organization, and brain dynamical states in the shaping of the response to stimulus. These and other examples will be shown in the poster along with interactive executions of the live figures.

Keywords: Brain states, responsiveness, complexity, cortical network, model, imaging, awake, sleep

Acknowledgements This project/research has received funding from the European Union's Horizon 2020 Framework Programme for Research and Innovation under the Specific Grant Agreement No. 945539 (Human Brain Project SGA3).

REFERENCES

[1] Llinás RR. The intrinsic electrophysiological properties of mammalian neurons: insights into central nervous system function. Science. 1988 Dec 23;242(4886):1654-64. doi: 10.1126/science.3059497. PMID: 3059497.

[2] Steriade M., Corticothalamic resonance, states of vigilance and mentation. Neuroscience2000;101(2):243-76. doi: 10.1016/s0306-4522(00)00353-5. PMID: 11074149.

[3] McCormick DA. Neurotransmitter actions in the thalamus and cerebral cortex and their role in neuromodulation of thalamocortical activity. Prog Neurobiol. 1992 Oct;39(4):337-88. doi: 10.1016/0301-0082(92)90012-4. PMID: 1354387.

[4] Stringer C, Pachitariu M, Steinmetz N, Reddy CB, Carandini M, Harris KD. Spontaneous behaviors drive multidimensional, brainwide activity. Science. 2019 Apr 19;364(6437):255. doi: 10.1126/science.aav7893. Epub 2019 Apr 18. PMID: 31000656; PMCID: PMC6525101.

[5] Casali AG, Gosseries O, Rosanova M, Boly M, Sarasso S, Casali KR, Casarotto S, Bruno MA, Laureys S, Tononi G, Massimini M. A theoretically based index of consciousness independent of sensory processing and behavior. Sci Transl Med. 2013 Aug 14;5(198):198ra105. doi: 10.1126/scitranslmed.3006294. PMID: 23946194.

[6] Deco G, Kringelbach ML, Jirsa VK, Ritter P. The dynamics of resting fluctuations in the brain: metastability and its dynamical cortical core. Sci Rep. 2017 Jun 8;7(1):3095. doi: 10.1038/s41598-017-03073-5. PMID: 28596608; PMCID: PMC5465179.

[7] Zerlaut Y, Chemla S, Chavane F, Destexhe A. Modeling mesoscopic cortical dynamics using a mean-field model of conductance-based networks of adaptive exponential integrate-and-fire neurons. J Comput Neurosci. 2018 Feb;44(1):45-61. doi: 10.1007/s10827-017-0668-2. Epub 2017 Nov 15. PMID: 29139050.

[8] E. Montbrió, D. Pazó, and A. Roxin, *Macroscopic Description for Networks of Spiking Neurons*, Phys. Rev. 021028 (2015).

18. Multiscale sinusoidal perturbation of slow cortical spontaneous dynamics

Martina Cortada[1*], Joana Covelo[1], Gianni V. Vinci[2], Maurizio Mattia[2], Maria V. Sanchez-Vives[1,3]

[1]Institut d'Investigacions Biomèdiques August Pi i Sunyer (IDIBAPS), Barcelona, Spain, [2] Istituto Superiore di Sanita, Rome, Italy, [3]Institució Catalana de Recerca i Estudis Avançats (ICREA), Barcelona, Spain

*e-mail address of corresponding author(s): martinacortadaperez@gmail.com

INTRODUCTION/MOTIVATION

Stimulation plays a key role in advancing our understanding of cortical dynamics. By perturbing the brain, we are able to obtain an insight into the mechanisms and functions that regulate cortical activity and to detect differences across various brain states [1] or within individual dynamical regimes [2, 3]. Furthermore, we also get valuable information about potential therapeutical tools to modulate brain activity and their precise mechanisms.

Emergent collective behavior in cortical networks can be entrained by sinusoidal electric fields with an intensity similar to its endogenous electric field [4, 5]. As such, transcranial alternate current stimulation (tACS) has the potential to modulate brain oscillations in a frequency-specific manner, offering the possibility to demonstrate a causal nature of oscillation behavior relationships [6]. However, the exact mechanism by which weak electric fields can modulate the dynamics of cortical networks at different scales, including the microscopic, mesoscopic and macroscopic, remains unclear.

Using a perturbative approach (tACS), we examined a particular brain state that arises under unconscious states, such as in slow wave sleep or under anesthesia: the slow oscillation (SO), which is a global and synchronized network phenomenon that engages neurons throughout the cortical system and has been suggested to be the default mode of the cerebral cortex [7].

By means of recording local field potentials in the cerebral cortex *in vitro,* we investigated the emergent collective behavior of cortical networks resulting from the modulation with sinusoidal electric fields. Computational simulations were also performed in order to better understand how neurons are orchestrated to reproduce the experimental observed phenomena.

METHODS

To study the effects of tACS at the population level in the cerebral cortex, we applied a set of amplitudes ranging from ±1 to 5 V/m within a low-frequency range (0.05-1 Hz) of alternating current electric fields to *in vitro* cortical slices exhibiting spontaneous SO.

To obtain a better understanding of the cellular, network, and AC-intrinsic rhythm interaction, we used a model of the cortical network composed of excitatory and inhibitory spiking neurons that can reproduce the spontaneous activity of cortical slices [8]. This model enabled us to explore whether frequency-varying stimulation modulating single-neuron excitability can replicate the collective behavior observed in experiments.

RESULTS AND DISCUSSION

We quantified the amplitude- and frequency-dependent modulation of cortical spatiotemporal patterns. Entrainment with the exogenous sinusoidal current injection occurred in a specific range of frequencies, depending on the electric field strength. For example, a minimum intensity of 2 V/m was required for entrainment to occur at approximately 0.5 Hz. Furthermore, the larger the perturbation amplitude, the broader the range of frequencies in which the system synchronizes with the sinusoidal stimulation.

Additionally, using the model we found that even small changes at the microscopic level in neuronal excitability can be amplified by the nonlinear and collective dynamics of cortical networks, leading to phase locking between sinusoidal field stimulation and spiking activity. This supports the idea of a true multiscale phenomenon.

The results highlight the opportunity for a frequency-specific modulation of the states exhibited by the cortical network at both the micro and mesoscopic levels. The next question to address is: to what extent can we also modulate the macroscopic state and transition to different regimes?

Keywords: tACS, entrainment, electric fields, cortical network, computational model

ACKNOWLEDGEMENTS

This research has received funding from the European Union's Horizon 2020 Framework Programme for Research and Innovation under the Specific Grant Agreement no. 945539 (Human Brain Project SGA3) and from PID2020-112947RB-I00 financed by MCIN/ AEI /10.13039/501100011033.

REFERENCES

[1] Casali, A. G., Gosseries, O., Rosanova, M., Boly, M., Sarasso, S., Casali, K. R., ... & Massimini, M. (2013). A theoretically based index of consciousness independent of sensory processing and behavior. *Science translational medicine*, *5*(198), 198ra105-198ra105. https://doi.org/10.1126/scitranslmed.3006294

[2] D'Andola, M., Rebollo, B., Casali, A. G., Weinert, J. F., Pigorini, A., Villa, R., ... & Sanchez-Vives, M. V. (2018). Bistability, causality, and complexity in cortical networks: an in vitro perturbational study. *Cerebral cortex*, *28*(7), 2233-2242. https://doi.org/10.1093/cercor/bhx122

[3] Barbero-Castillo, A., Mateos-Aparicio, P., Dalla Porta, L., Camassa, A., Perez-Mendez, L., & Sanchez- Vives, M. V. (2021). Impact of GABAA and GABAB inhibition on cortical dynamics and perturbational complexity during synchronous and desynchronized states. *Journal of Neuroscience*, *41*(23), 5029- 5044. https://doi.org/10.1523/JNEUROSCI.1837-20.2021

[4] Fröhlich, F., & McCormick, D. A. (2010). Endogenous electric fields may guide neocortical network activity. *Neuron*, *67*(1), 129-143. https://doi.org/10.1016/j.neuron.2010.06.005

[5] Rebollo, B., Telenczuk, B., Navarro-Guzman, A., Destexhe, A., & Sanchez-Vives, M. V. (2021). Modulation of intercolumnar synchronization by endogenous electric fields in cerebral cortex. Science Advances, 7(10), eabc7772. https://doi.org/10.1126/sciadv.abc7772

[6] Neuling, T., Rach, S., & Herrmann, C. S. (2013). Orchestrating neuronal networks: sustained after- effects of transcranial alternating current stimulation depend upon brain states. *Frontiers in human neuroscience*, *7*, 161. https://doi.org/10.3389/fnhum.2013.00161

[7] Sanchez-Vives, M. V., & Mattia, M. (2014). Slow wave activity as the default mode of the cerebral cortex. *Arch Ital Biol*, *152*(2-3), 147-155. https://doi.org/10.4449/aib.v152i2/3.3677

[8] Mattia, M., and Sanchez-Vives, M. V (2012). Exploring the spectrum of dynamical regimes and timescales in spontaneous cortical activity. Cogn. Neurodyn. 6, 239–250. https://doi.org/10.1007/s11571-011-9179-4

19. Multiscale dynamical characterization of spontaneous cortical brain states: from synchrony to asynchrony

Mavi Sanchez-Vives[1,2] Alessandro Arena[3], Alessandra Camassa[1], Cristiano Capone[4], Leonardo Dalla Porta[1], Giulia De Bonis[4], Chiara De Luca[4], Andrea Galluzzi[5], Jennifer Goldman[6], Bjorn Erik Juel[3], Arnau Manasanch[1], Ezequiel Mikulan[7], Antonio Pazienti[5], Andrea Pigorini[7], Marcello Massimini[7], Maurizio Mattia[5], Pier Stanislao Paolucci[4], Johann F Storm[3], Alain Destexhe[6]

Affiliations:

[1] IDIBAPS: Institut d'Investigacions Biomèdiques August Pi i Sunyer (IDIBAPS), Barcelona, Spain
[2] ICREA: Institució Catalana de Recerca i Estudis Avançats (ICREA), Barcelona, Spain
[3] UIO: Department of Molecular Medicine, University of Oslo, Oslo, Norway
[4] INFN: Istituto Nazionale di Fisica Nucleare (INFN), Sezione di Roma, Rome, Italy
[5] ISS: Center for Radioprotection and Computational Physics, Istituto Superiore di Sanità, Rome, Italy
[6] CNRS: Paris-Saclay Institute of Neuroscience (NeuroPSI), Paris-Saclay University, 91400 Saclay, France
[7] UMIL: Dept of Biomedical and Clinical Sciences "L. Sacco" Universit a degli Studi di Milano, Milan, Italy

*e-mail-address of corresponding author(s): sanchez.vives@gmail.com

INTRODUCTION/MOTIVATION

The brain expresses a variety of states that are associated with different consciousness levels, behavioural states (quiet wakefulness, sleep, attentive...), or cognitive states (such as attention, memory, and decision-making). The cerebral cortex spontaneously elicits different spatiotemporal patterns of activity that changes over time according to the brain state. Brain state transitions from unconscious to conscious states are accompanied by changes in parameters such as cortical complexity, connectivity, synchronization, and by a modulation of the excitatory-inhibitory network balance. In this work we have focused on the multiscale characterization of brain states and their transitions, since it is a fundamental link between experimental, theoretical, and clinical observations, as well as to the development of strategies to restore physiological activity in pathological conditions. The phenomenological correlates of such transitions have been observed in the cerebral cortex at multiple scales, i.e., at microscale in cortical slices in vitro, at mesoscale in cortical areas in vivo and at macroscale at whole brain level.

METHODS

This work comprises experimental, clinical, and computational investigation and modelling for the investigation of different brain states. The different included brain states were physiological (natural sleep stages), drug-induced (e.g., anaesthesia) or clinical cases (e.g., disorders of consciousness). In short, experimental data acquisition included cortical preparations in vitro and in vivo. Recording technologies were electrophysiology (local field potential,

multielectrode arrays, EEG) and calcium imaging. Clinical data acquisition included high density EEG and intracranial EEG. Computational modelling includes spiking models, mean field models and whole brain networks (The Virtual Brain).

RESULTS AND DISCUSSION

We depart this investigation from the most synchronized physiological activity in the cerebral cortex, slow oscillations (SO), the activity that dominates slow wave sleep, deep anaesthesia, and the activity in areas around some brain lesions [1, 2]. Slow oscillations (0.5-4 Hz in humans) are a default activity pattern of the cortical network to which cortical circuits tend to converge when structurally or functionally disconnected [3]. This activity is of cortical origin, and depending on the brain states, the thalamus and other connected nuclei modulate them. SO collectively emerge as traveling waves of activity across the cortex. We describe how the different parameters that characterize wave propagation act as biomarkers of the cortical state [4]. The precise underlying mechanisms were explored in a cortical spiking model, in which changes in the local excitability of cortical assemblies explained most slow wave features, characterizing brain state changes without modifications of the network connectivity [5]. In this work we systematically compared different computational models that have reproduced SO, since these dynamics can be observed consistently in very different systems and simulations. Our own computational models show that the critical mechanisms consist in a combination of recurrent connectivity and adaptation [5, 6]. As the arousing neuromodulatory input from the brainstem and thalamus increases, and modulation from the ascending reticular activation system is altered, cortical circuits and neurons tend to transition out of their default state. This transition is associated with measurable signatures across scales: single cells start firing in an asynchronous manner, slow waves become less frequent, more asynchronous, high frequency, low amplitude activity becomes dominant, and the spectral slope of the EEG flattens. In anesthetized animal models, when the depth of general anesthesia decreased towards wakefulness, the slow oscillations measured with local field potential gradually became faster and the firing rate of underlying multi-unit activity increased, while the silent periods in between Up states gradually decrease in duration [7]. Awakening from NREM sleep or general anesthesia is associated with a transition from EEG activity dominated by slow, high-power oscillations to a sustained, high frequency activity, with reduced low frequency power. This pattern is consistent across species [8]. The synchronous to asynchronous transition can also be seen in whole-brain models, and we have reproduced it for three species. The simulations used the AdEx mean-field model which was implemented in the TVB [9]. In the AdEx mean-field, each node can potentially display asynchronous-irregular activity or slow oscillations with Up and Down states, by adjusting the strength of spike-frequency adaptation, which we illustrate as well in Showcase 3. Finally, we relate all these findings in experimental and computational models to clinical conditions, such as patients that show slow wave activity during wakefulness – i.e., they can open their eyes, wake up and fall asleep at regular intervals, have basic reflexes, but they do not show any signs of awareness; for this reason, they have been named Vegetative State, or Unresponsive Wakefulness Syndrome patients. It has been recently proposed that this disruption of brain function might be due to a massive intrusion of sleep-like dynamics into an awake brain [10].

Keywords: brain states, cortical dynamics, slow oscillations, asynchronous activity, Up states, spontanous actvity, computational models

ACKNOWLEDGEMENTS

Funded by HBP-SGA3 No.945539

REFERENCES

[1] Steriade, M., Nunez, A., & Amzica, F. (1993). A novel slow (< 1 Hz) oscillation of neocortical neurons in vivo: depolarizing and hyperpolarizing components. Journal of neuroscience, 13(8), 3252-3265 https://doi.org/10.1523/JNEUROSCI.13-08-03252.1993

[2] Rosanova, M., & Sarasso, S. (2021). Sleep-like cortical bistability after focal and multifocal brain lesions. Brain Stimulation: Basic, Translational, and Clinical Research in Neuromodulation, 14(6), 1743. https://doi.org/10.1016/j.brs.2021.10.518

[3] Sanchez-Vives, M. V., & Mattia, M. (2014). Slow wave activity as the default mode of the cerebral cortex. Arch Ital Biol, 152(2-3), 147-155.doi 10.12871/000298292014239

[4] Pazienti, A., Galluzzi, A., Dasilva, M., Sanchez-Vives, M. V., & Mattia, M. (2022). Slow waves form expanding, memory-rich mesostates steered by local excitability in fading anesthesia. Iscience, 25(3), 103918. https://doi.org/10.1016/j.isci.2022.103918

[5] Mattia M, Sanchez-Vives MV. Exploring the spectrum of dynamical regimes and timescales in spontaneous cortical activity. Cogn Neurodyn. 2012 Jun;6(3):239-50. doi: 10.1007/s11571-011-9179-4

[6] Capone et al. "Simulations Approaching Data: Cortical Slow Waves in Inferred Models of the Whole Hemisphere of Mouse." arXiv preprint arXiv:2104.07445 (2021) doi 10.48550/arXiv.2104.07445)

[7] Tort-Colet, N., Capone, C., Sanchez-Vives, M. V., & Mattia, M. (2021). Attractor competition enriches cortical dynamics during awakening from anesthesia. Cell Reports, 2021. https://doi.org/10.1016/j.celrep.2021.109270.

[8] Arena, A., Comolatti, R., Thon, S., Casali, A. G., & Storm, J. F. (2021). General anesthesia disrupts complex cortical dynamics in response to intracranial electrical stimulation in rats. eneuro, 8(4). doi: 10.1523/ENEURO.0343-20.2021

[9] Goldman et al. (2021) A comprehensive neural simulation of slow-wave 1 sleep and highly responsive wakefulness dynamics, biorXiv, https://doi.org/10.1101/2021.08.31.458365

[10] Sarasso, S., D'Ambrosio, S., Fecchio, M., Casarotto, S., Viganò, A., Landi, C., & Massimini, M. (2020). Local sleep-like cortical reactivity in the awake brain after focal injury. Brain, 143(12), 3672-3684. doi.org/10.1093/brain/awaa338

20. Showcase #1 – Modelling regional variance

Ignacio Martin[1], Gustavo Patow[1,2], Sandra Diaz-Pérez[3], Timo Dickscheid[4], Michiel van der Vlag[3], Damien Depannemaecker[5], Viktor Jirsa[5], Gustavo Deco[2,6], Gorka Zamora-López[2], Jan Fousek[5]

[1]ViRVIG, Universitat de Girona,Girona, 17003, Spain.
[2]Center for Brain and Cognition, Department of Information and Communication Technologies, Pompeu Fabra University, Barcelona - 08002, Spain.
[3]SimLab Neuroscience, Jülich Supercomputing Centre (JSC), Institute for Advanced Simulation, JARA, Forschungszentrum Jülich GmbH, Jülich, Germany.
[4]Institute of Neuroscience and Medicine (INM-1), Research Centre Jülich, Jülich, Germany. [5]Institut de Neurosciences des Systèmes UMR INSERM 1106, Aix-Marseille Université, Marseille, France.
[6]Institució Catalana de la Recerca i Estudis Avançats (ICREA), Barcelona - 08010, Spain.

Introduction:
The dichotomy of brain structure and function is one of the oldest enigmas in neuroscience. On the one hand, individual brains differ from each other while maintaining full functionality within a range of normal variability. On the other hand, brain regions themselves differ from each other in different aspects, e.g., neuronal densities, cytoarchitecture, or characteristic neuroreceptors [1,2]. State-of-the-art whole-brain network models (as those previously defined during SGA1 and SGA2) assume cortical regions to have identical properties [3]. Showcase 1 addresses this enigma, trying to provide mechanistic explanations through the simulation of anesthetic effects.

Methods:
This part of Showcase 1 deals with the scientific and technical challenges faced in the definition of whole-brain network models that account for the regional heterogeneity of the brain. We do so by developing workflows that integrate several ingredients developed within the HBP: (i) neuroscience data – as organized in the brain reference space – in order to account for the region-wise properties, (ii) extracted via the Siibra interface [4] from the brain atlases in EBRAINS, (iii) regional dynamics are governed by the mean-field AdEx population model, (iv) definition of the whole-brain network model within the TVB, and (v) running computationally demanding parametric fitting in the HPC facilities of EBRAINS via the FENIX infrastructure.

Results and Discussion:
To demonstrate the enhancement of the explanatory power of the models accounting for regional variability we simulate whole-brain resting-state activity in healthy participants in normal awake and during anesthesia (in collaboration with WP2). We show how considering the levels of GABAa and NMDA receptor densities [5] different for each cortical region, the models more accurately reproduce the anesthetic effect of propofol and ketamine.

Keywords: Whole-Brain Modelling, Large-scale Simulations, Brain States – Anaesthesia, Neuroreceptor Maps, EBRAINS, The Virtual Brain, HPC Computing, Human Brain Atlas.

ACKNOWLEDGEMENTS

This project/research has received funding from the European Union's Horizon 2020 Framework Programme for Research and Innovation under the Specific Grant Agreement No. 945539 (Human Brain Project SGA3). This project/research has received a Voucher from the European Union's Horizon 2020 Framework Programme for Research and Innovation under the Specific Grant Agreement No. 945539 (Human Brain Project SGA3).

REFERENCES

[1] S.F. Beul, and C.C. Hilgetag. Systematic modelling of the development of laminar projection origins in the cerebral cortex: Interactions of spatio-temporal patterns of neurogenesis and cellular heterogeneity. *PLoS Comput. Biol*. 2021; 16(10):e1007991. doi: https://doi.org/10.1371/journal.pcbi.1007991.

[2] J.M.Huntenburg, P.L Bazin, and D.S.Margulies. Large-Scale Gradients in Human Cortical Organization. Trends. Cogn. Sci. 2018; 22(1): 21-31. doi: https://doi.org/10.1016/j.tics.2017.11.002.

[3| G. Deco, V.K. Jirsa, and A.R. McIntosh. Resting brains never rest: computational insights into potential cognitive architectures. *Trends. Neurosci*. 36(5): 268-274. doi: http://dx.doi.org/10.1016/j.tins.2013.03.001.

[4] siibra - Software interface for interacting with brain atlases. URL: https://siibra-python.readthedocs.io/en/latest/index.html

[5] D. Zachlod, N. Palomero-Gallagher, T. Dickscheid, and K. Amunts. Mapping cyto-and receptor architectonics to understand brain function and connectivity. Biol. Psychiatry. 2022; 93(5):471-479. doi: https://doi.org/10.1016/j.biopsych.2022.09.014.

21. Exploring the coupling between electrophysiology and hemodynamics during slow wave activity in the neocortex

Alex Suarez-Perez[a*], Diana Casas-Torremocha[a], Sumana Chetia[b], Giulia De Bonis[c], Pier Stanislao Paolucci[c], Turgut Durduran[b,d], Maria V. Sanchez-Vives[a,d]

[a]*Institut d'Investigacions Biomèdiques August Pi i Sunyer (IDIBAPS), Barcelona, Spain*
[b]*ICFO-Insitut de Ciències Fotòniques, The Barcelona Institute of Science and Technology, Barcelona, Spain*
[c]*INFN, 00185 Rome, Italy*
[d]*Institució Catalana de Recerca i Estudis Avançats (ICREA), Barcelona, Spain*
**Corresponding author: suarez@recerca.clinic.cat*

INTRODUCTION/MOTIVATION

The hemodynamical changes (blood flow, blood oxygenation) are an indirect measure of neural activity that is at the basis of the main brain imaging techniques, such as functional magnetic resonance imaging (MRI). Being a noninvasive measure that provides detailed information of function at high spatial resolution (mm), it became a standard method used both in research and in the clinic, despite its limitation in the temporal domain. Instead, electrophysiology provides a temporally precise (ms or even µs) neural activity detail, about neuronal and even ionic channels mechanisms. Still, the exact relation between imaging -or hemodynamics- and electrophysiology is not understood in detail, in part for the difficulties imposed using electric cables and equipment in the MRI magnetic field.

Here, we investigate the precise relationship between the blood flow and the electrophysiology, to quantify how is their temporal and amplitude relationship, and whether we can predict one from the other. We used a prominent brain activity, highly synchronized, that has been proposed to be the "default activity pattern" of the cerebral cortex [1], the slow oscillations (SO) or slow waves. Not only they occur during slow wave sleep and anesthesia, but also in pathological situations associated to stroke, brain lesions or in unresponsive wakefulness syndrome [2], being characterized by a slow oscillation (≤1Hz) that synchronizes large populations of neurons. Not only slow waves are a good model for the investigation of the electrical and hemodynamic coupling, but this understanding is highly relevant for the clinical translation of diagnostic and therapeutic experimental interventions.

Our objective has been to investigate the spatiotemporal relationship between extracellular neuronal activity and hemodynamics during SO. Additionally, we aimed to unveil what features of the hemodynamics can be predicted from the electrophysiology signals. For this, the relative cerebral blood flow (rCBF) and 32-local field potentials (LFPs) were simultaneously monitored during spontaneous SO activity to explore the underlying correspondence between hemodynamics and neural activity.

METHODS

The rCBF and electrophysiology were simultaneously monitored using a synchronized laser speckle flowmetry (LSF) and a 32-channel multielectrode array (MEA) covering the entire exposed area of the cortex (Figure 1A, B). SO activity was recorded in deeply anesthetized *C57BL/6J* mice. All procedures were approved by

the local Ethics Committee.

RESULTS AND DISCUSSION

Slow oscillations consist of periods of activity (Up states) and silent periods (Down states). Up states were observed during spontaneous SO activity as low-pass filtered fluctuations in the rCBF signal (Figure 1B). To analyze the relationship between the LFP and rCBF we computed the power spectral density (PSD) for both the LFP and rCBF signals (Figure 1C). In both cases (rCBF and LFP PSD) we found a peak around 0.25 Hz corresponding to SO frequency. A smaller peak around 1 Hz in both PSDs could be due to the occurrence of doublet Up-states. The peak around 2.3 Hz is attributed to the respiration while the peak around 4.5 Hz correspond to the heartbeat. We block-averaged the rCBF and LFP responses from all the isolated Up-states onset (Figure 1D) and observed that the peak in the rCBF signal was delayed by ~3s on average from the LFP peak.

Figure 1. (A) Experimental setup consisting of the synchronized systems for optical imaging and electrophysiology. (B)

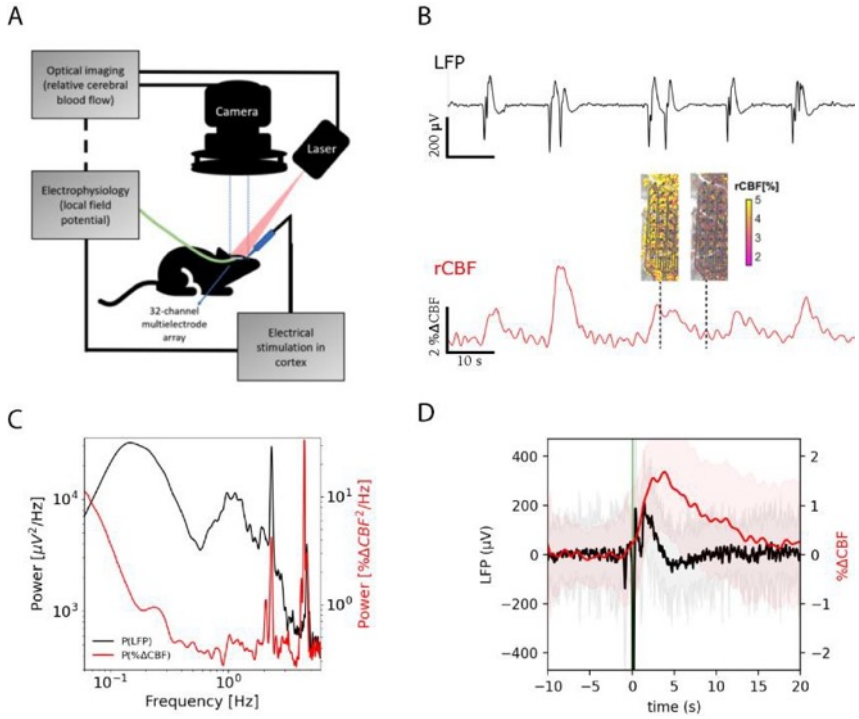

Simultaneous recorded LFP and rCBF signals. Middle panels represent an example of the rCBF imaging in the cortex during and Up-state and a Down-state, respectively. (C) Power spectrum density for the LFP and rCBF. (D) LFP (in black) and rCBF (in red) waveform average around down to up transitions.

Considering that the rCBF represents a convolution of the LFP we developed a kernel estimator to recover the rCBF from the LFP signal. With a simple model based on a first order differential equation with adaptation and using the experimental LFP signal as input, we effectively predicted with high degree of accuracy the dynamics of the measured rCBF (not shown).

Together, our results demonstrate that the hemodynamics generated by each spontaneous slow wave can be detected and measured by means of rCBF. We have also quantified the amplitude, the frequency and the spatiotemporal relationship between the neuronal activity and the hemodynamic activity for spontaneous waves. A simple kernel predicts the hemodynamics from the electrical activity, which can be used in clinical applications. Our

results create bridges between neuronal activity and brain imaging with promising implications for basic and clinical neuroscience.

Keywords: Slow neural oscillations, relative cerebral blood flow, local field potential, cerebral cortex

ACKNOWLEDGEMENTS

Funded by European Union's Horizon 2020 research and innovation programme under Marie Sklodowska-Curie grant agreement No 847517 and Human Brain Project SGA3, no. 945539.

REFERENCES

1. Sanchez-Vives, M. V., Massimini, M., & Mattia, M. (2017). Shaping the default activity pattern of the cortical network. Neuron, 94(5), 993-1001.

2. Sanchez-Vives MV. Origin and dynamics of cortical slow oscillations. *Current Opinion in Physiology*. 2020;15:217-223. doi:10.1016/j.cophys.2020.04.005

3. Dasilva M, Camassa A, Navarro-Guzman A, et al. Modulation of cortical slow oscillations and complexity across anesthesia levels. NeuroImage. 2021;224:117415. doi:10.1016/j.neuroimage.2020.117415

4. Durduran T, Choe R, Baker WB, Yodh AG. Diffuse optics for tissue monitoring and tomography. Reports on Progress in Physics. 2010;73(7):076701. doi:10.1088/0034-4885/73/7/076701

22. AKAP79 enables calcineurin to directly suppress protein kinase A

Timothy W. Church[1], Parul Tewatia[2], Saad Hannan[1], João Antunes[2], Olivia Eriksson[2], Trevor G. Smart[1], Jeanette Hellgren Kotaleski[2], Matthew G. Gold[1]

[1]Department of Neuroscience, Physiology & Pharmacology, University College London, United Kingdom
[2]Science for Life Laboratory, School of Electrical Engineering and Computer Science, KTH Royal Institute of Technology, Sweden; Department of Neuroscience, Karolinska Institute, Sweden

Introduction

Interplay between the second messengers cAMP and Ca^{2+} is a hallmark of dynamic cellular processes. A common motif is the opposition of the Ca^{2+}-sensitive phosphatase calcineurin and the major cAMP receptor, protein kinase A (PKA). Calcineurin dephosphorylates sites primed by PKA to bring about changes including synaptic long-term depression (LTD) [1]. AKAP79 supports signaling of this type by anchoring PKA and calcineurin in tandem [2]. This postsynaptic anchoring protein positions calcineurin [3] and PKA type II regulatory subunits
[4] in close proximity via short linear motifs separated by ~ 50 amino acids. Knockout studies are consistent with the notion that AKAP79 positions calcineurin to dephosphorylate sites primed by protein kinase A to bring about long-term depression [5]. In this study, we investigated the hypothesis that AKAP79 also enables calcineurin to directly inhibit PKA in the induction of LTD.

Methods

We applied a combination of experimental and computational approaches. We measured calcineurin and PKA activities *in vitro* using radiometric assays and FRET-based plate-reader assays respectively. We used lentiviral delivery of shRNA/replacement sequences to mutate PKA type II regulatory (RII) subunits in primary hippocampal neurons, and monitored structural long-term depression in dendritic spines using confocal imaging. We simulated direct suppression of PKA by calcineurin after building a kinetic model. Parameters were estimated using an approximate Bayesian computation (ABC) approach, which included copulas for merging of different experimental data sets, and guided by the results of our experimental values [6, 7]. All model variants were built using the MATLAB Simbiology toolbox (MathWorks).

Results

Recent observations have shown that PKA RII subunits that have been dephosphorylated at the inhibitor site (IS) capture PKA catalytic (C) subunits ~ 50 times faster than phosphorylated pRII subunits [8]. In theory, calcineurin could act on pRII subunits to suppress PKA activity. However, pRII subunits are poor substrates for calcineurin in the absence of additional factors. We reasoned that the anchoring protein AKAP79 might facilitate efficient pRII dephosphorylation by calcineurin by increasing the effective protein concentration of pRII for the phosphatase. We confirmed experimentally that AKAP79 increases the rate of calcineurin dephosphorylation of type II PKA regulatory subunits by an order of magnitude. Fluorescent PKA activity reporter assays, supported by kinetic modelling (summarised in **Figure 1**), show how AKAP79-enhanced calcineurin activity enables suppression of PKA without altering cAMP levels by increasing PKA catalytic subunit capture rate. Experiments with hippocampal neurons indicated that this mechanism contributes toward LTD [9].

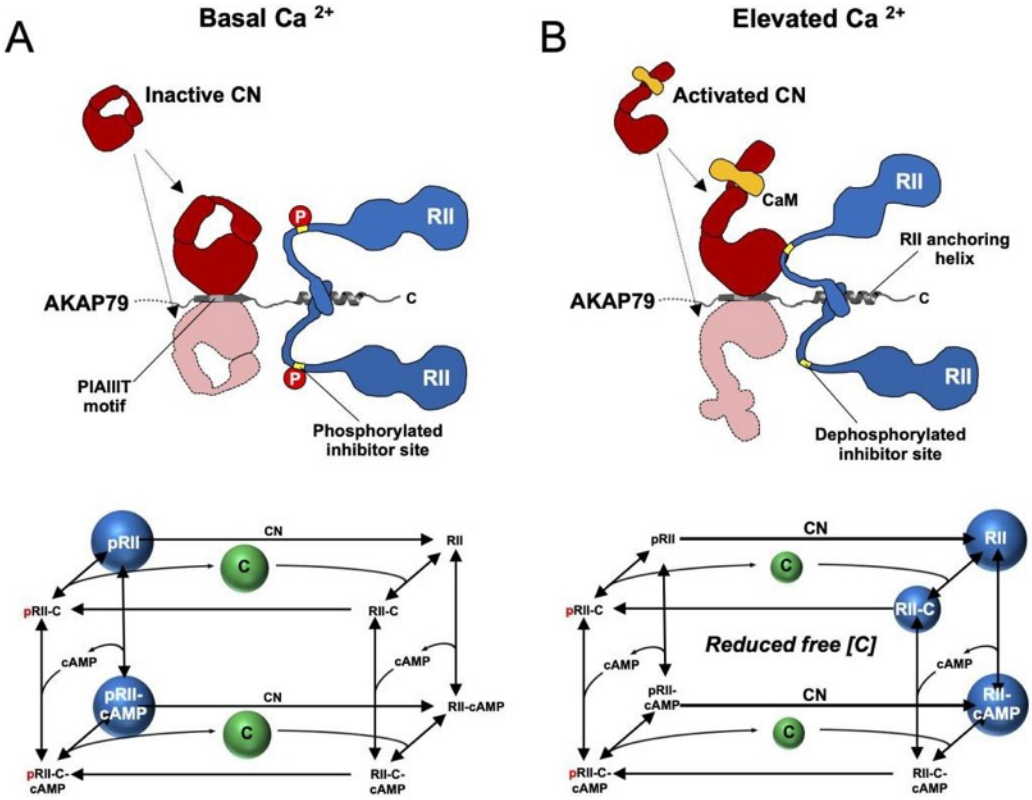

Figure 1. Summary model of PKA suppression by CN within the AKAP79 complex. Structural and kinetic models (upper and lower panels, respectively) of signaling within the AKAP79 complex are shown under conditions of either low (A) or elevated Ca2+ (B). Elevated Ca2+ triggers CN (red) dephosphorylation of pRII (blue) which shifts C subunit capture from the left- hand square of the kinetic scheme to the right-hand square, which features dephosphorylated forms of RII. The overall effect is a reduction in the concentration of free C subunits.

Discussion

The observations in this study support a revised mechanism for long-term depression, a fundamental neuronal process. Furthermore, this non-canonical mode of PKA regulation may underlie many other cellular processes including immune responses and insulin secretion.

References

1. Bear, M.F., *Bidirectional synaptic plasticity: from theory to reality.* Philos Trans R Soc Lond B Biol Sci, 2003. **358**(1432): p. 649-55.
2. Coghlan, V.M., et al., *Association of protein kinase A and protein phosphatase 2B with a common anchoring protein.* Science, 1995. **267**(5194): p. 108-11.
3. Dell'Acqua, M.L., et al., *Mapping the protein phosphatase-2B anchoring site on AKAP79. Binding and inhibition of phosphatase activity are mediated by residues 315-360.* J Biol Chem, 2002. **277**(50): p. 48796-802.
4. Gold, M.G., et al., *Molecular basis of AKAP specificity for PKA regulatory subunits.* Mol Cell, 2006. **24**(3): p. 383-95.
5. Tunquist, B.J., et al., *Loss of AKAP150 perturbs distinct neuronal processes in mice.* Proc Natl Acad Sci U S A, 2008. **105**(34): p. 12557-62.
6. Eriksson, O., et al., *Uncertainty quantification, propagation and characterization by Bayesian analysis combined with global sensitivity analysis applied to dynamical intracellular pathway models.* Bioinformatics, 2019. **35**(2): p. 284-292.
7. Gutierrez-Arenas, O., O. Eriksson, and J.H. Kotaleski, *Segregation and crosstalk of D1 receptor-*

mediated activation of ERK in striatal medium spiny neurons upon acute administration of psychostimulants. PLoS Comput Biol, 2014. **10**(1): p. e1003445.

8. Zhang, P., et al., *Single Turnover Autophosphorylation Cycle of the PKA RIIbeta Holoenzyme.* PLoS Biol, 2015. **13**(7): p. e1002192.
9. Church, T.W., et al., *AKAP79 enables calcineurin to directly suppress protein kinase A activity.* Elife, 2021. **10**.

23. Variability of Reaching Trajectories in Hand Space and Joint Space

Shrabasti Jana[1*], Frederic Barthelemy[1,2], Lucio Condro[1], Alexa Riehle[1,2], Thomas Brochier[1*]

[1]Institut de Neurosciences de la Timone UMR 7289, Aix-Marseille University, Marseille, France
[2]Institute of Neuroscience and Medicine (INM-6), Computational and Systems Neuroscience, Research Center Jülich, Jülich, Germany
* shrabasti.jana@univ-amu.fr, thomas.brochier@univ-amu.fr

INTRODUCTION/MOTIVATION

Comprehension of Movement Variability is essential for exploring motor performance and motor skill learning. Even very trivial movements have considerable variability when repeated across trials (1). Earlier studies, which have explored trajectory planning in humans, have shown that the motor control system optimizes the trajectories (produce straight and less jerky movements) in a specific reference frame (either the joint-space or the hand-space/workspace) (3,4). The current study aims at understanding if the choice of such a reference frame for movement execution could in turn lead to variability across different movement components at the joint and the end-effector levels, using non-human primate model.

METHODS

The kinematic data for this study were recorded from two rhesus macaques during their performance of a visuo-motor (sequential landing) task using an exoskeleton robotic arm (Kinarm, Bkin). In parallel, extracellular multi-electrode recordings were obtained from multiple cortical areas along the visuo-motor pathway (motor areas M1/PMd, parietal areas DP, 7A and visual areas V1, V2).

In order to build a deep understanding of the origin of movement variability, the variability of different kinematic parameters at joint and end-effector levels were investigated. For a set of predefined movements, variability for hand-space/workspace trajectory, joint-trajectory (trajectories formed on a 2D abstract space with elbow and shoulder movements being the 2 axes) and movement energy demands were characterized and compared, over sessions recorded across months.

RESULTS AND DISCUSSION

Our results show that for each individual movement, the spatial variability of the hand space and joint space trajectories have a global covariation across sessions. Yet, this covariation differs between movements (Figure 1). We also observe that the relationship between hand and joint space variability for each movement tend to be similar for the movements in similar direction. The empirical directional tuning of the hand trajectory variability, which we observe exaggerated along the NW-SE axis for our data, validates the above-mentioned directional effect (Figure 2). Further investigation of the potential reasons behind the directional effect on trajectory variability demonstrate a clear correlation between the end-effector variability and rotational kinematic energy, suggesting that energy cost (a measure for biomechanical complexity) plays a major role in defining the patterns of trajectory variability.

These results show that the origin of movement variability has a complex nature and there are different processes spanning through planning, preparation and execution of movements, which contribute to movement variability. Further exploration of the cortical data (recorded simultaneously with the kinematic data) using the cues from the kinematic results, will help us to identify the cortical areas leading to the variability of specific components of movement. The insights from this study can be potentially used to trace the sources and therapeutic solutions to the neuro-degenerative disorders (e.g., Parkinson's disease, Essential Tremors etc) which cause abnormal levels of movement variability.

Keywords: movement variability, trajectory planning, joint-space, hand-space, energy demand, motor control, kinarm

FIGURES

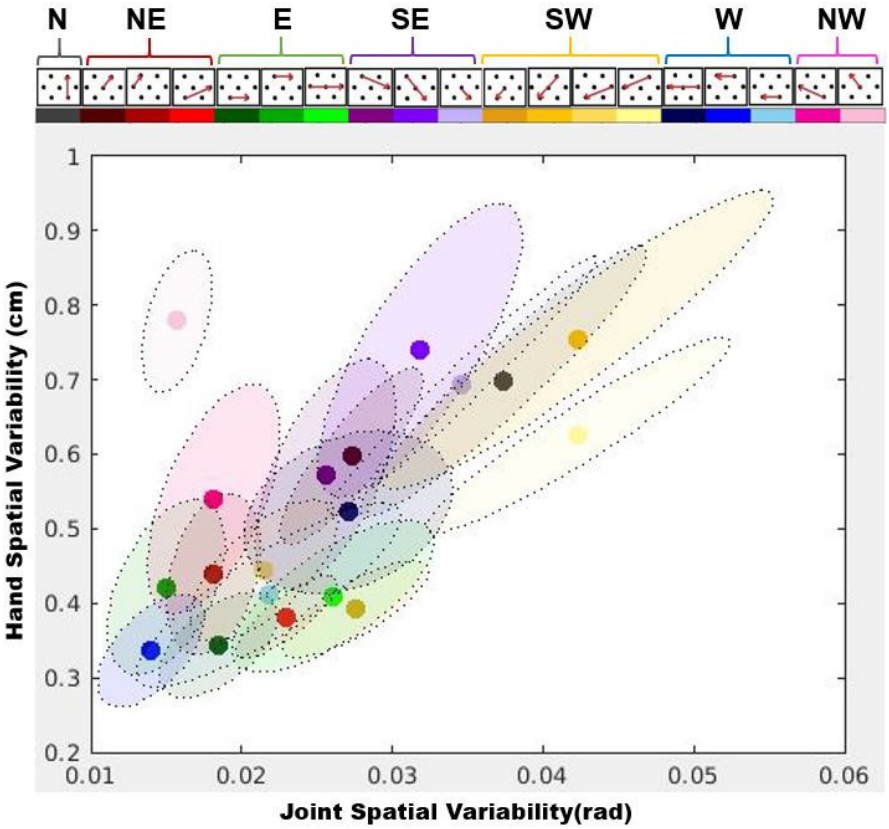

Figure 1- **Hand-space and joint space spatial variability covariation:** The main panel shows the covariation between hand-space and joint-space trajectory variability across session. Each shaded ellipse with a dashed border shows the distribution of the covariation of the hand and joint space variability across sessions for an individual movement, color-coded according to the color palette shown in the top panel. The solid circles represent the average covariation for each movement group.

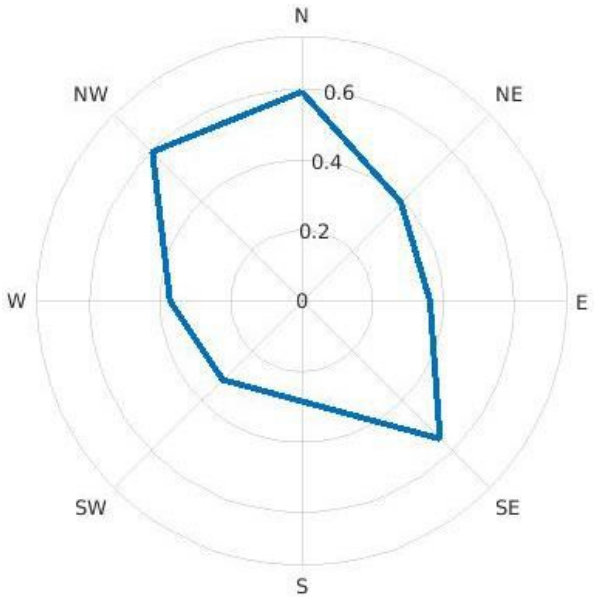

Figure 2- Directional tuning of hand-space trajectory variability: The average hand-space variability (in cm) is shown for each of the seven movement groups oriented along one of the seven directions (N: north, NE: north-east, E: east, SE: south-east, S: south, SW: south-west, W: west, NW: north-west)

ACKNOWLEDGEMENTS

We would like to thank the entire CoMCo team at INT for their rich insights and valuable suggestions, which added richness to this study.
Funding by FLAG-ERA JTC 2019 (supports research projects in synergy with the two FET flagships: Graphene Flagship and the Human Brain Project).

REFERENCES

[1] Haar S, Donchin O, Dinstein I. Individual movement variability magnitudes are explained by cortical neural variability. Journal of Neuroscience. 2017 Sep 13;37(37):9076-85. DOI: https://doi.org/10.1523/JNEUROSCI.1650-17.2017

[2] Orth D, Van der Kamp J, Memmert D, Savelsbergh GJ. Creative motor actions as emerging from movement variability. Frontiers in psychology. 2017 Oct 31;8:1903. DOI: https://doi.org/10.3389/fpsyg.2017.01903

[3] Flash T, Hogan N. The coordination of arm movements: an experimentally confirmed mathematical model. Journal of neuroscience. 1985 Jul 1;5(7):1688-703. DOI: https://doi.org/10.1523/JNEUROSCI.05-07-01688.1985

[4] Uno Y, Kawato M, Suzuki R. Formation and control of optimal trajectory in human multijoint arm movement. Biological cybernetics. 1989 Jun;61(2):89-101. DOI: https://doi.org/10.1007/BF00204593

24. Structuring cortical wave analysis with Cobrawap: a modular and adaptable pipeline for heterogeneous datasets

Robin Gutzen[1,2*], Giulia De Bonis[3], Chiara De Luca[3,4], Cosimo Lupo[3], Irene Bernava[3], Elena Pastorelli[3], Cristiano Capone[3], Anna Letizia Allegra Mascaro[5,6], Francesco Resta[5,7], Arnau Manasanch[8], Francesco Saverio Pavone[5,7,9], Maria V. Sanchez-Vives[8,10], Maurizio Mattia[11], Sonja Grün[1,2], Pier Stanislao Paolucci[3], Michael Denker[1]

[1] Institute of Neuroscience and Medicine (INM-6) and Institute for Advanced Simulation (IAS-6) and JARA-Institute Brain Structure-Function Relationships (INM-10), Jülich Research Centre, Jülich, Germany
[2] Theoretical Systems Neurobiology, RWTH Aachen University, Aachen, Germany
[3] Istituto Nazionale di Fisica Nucleare (INFN), Sezione di Roma, Rome, Italy
[4] Ph.D. Program in Behavioural Neuroscience, "Sapienza" University of Rome, Rome, Italy
[5] European Laboratory for Non-linear Spectroscopy (LENS), University of Florence, Florence, Italy
[6] Neuroscience Institute, National Research Council, Pisa, Italy
[7] Department of Physics and Astronomy, University of Florence, Florence, Italy
[8] Institut d'Investigacions Biomèdiques August Pi i Sunyer (IDIBAPS), Barcelona, Spain
[9] National Institute of Optics, National research Council, Sesto Fiorentino, Italy
[10] Institució Catalana de Recerca i Estudis Avançats (ICREA), Barcelona, Spain
[11] Natl. Center for Radiation Protection and Computational Physics, Istituto Superiore di Sanità (ISS), Rome, Italy

*r.gutzen@fz-juelich.de

INTRODUCTION/MOTIVATION

As neuroscientific research offers a growing wealth of data and methodologies, it becomes increasingly relevant to develop integrative approaches that consolidate evidence from multiple experiments, species, and measurement techniques. A challenge in understanding brain function is quantitatively comparing and combining conclusions from heterogeneous data. Here, we address this challenge in the context of slow wave activity (<1 Hz) [1], which is persistently observed across experimental approaches during sleep or anesthesia and is a dynamic feature expressed in various network models of neuronal activity. With this expression of a single phenomenon across multiple domains, various analytical methods, tools, data formats, metadata, and terminologies have emerged. This heterogeneity

and the intrinsic differences in the recorded data modalities make it difficult to aggregate knowledge across scientific studies quantitatively and form a coherent understanding.

METHODS

This study presents the Collaborative Brain Wave Analysis Pipeline (Cobrawap) [2] as an adaptable and reusable analysis approach. By bringing together existing methods [e.g. 3,4], standards, and tools in a modular fashion, the pipeline is able to serve a wide range of datasets and research questions. In Cobrawap, the heterogeneous input data is aligned to a common representation and description of slow wave activity. This allows generalized methods to extract common characteristic measures (e.g., wave planarity, frequency, velocity, and direction). This approach allows the semiautomatic analysis and characterization of heterogeneous slow wave activity data, providing the basis for rigorous comparisons across datasets due to the consistent reuse of methodology. The pipeline is Python-based and builds on open-source software tools, such as the workflow manager Snakemake [5], EBRAINS tools for handling representation (Neo [6]) and analytics (Elephant [7]) of electrophysiology data, and the EBRAINS Knowledge Graph (https://kg.ebrains.eu) for capturing the pipeline execution. We highlight ongoing efforts towards making Cobrawap available on EBRAINS resources, such as HPC systems using the Unicore engine and the emerging workflow execution engine.

RESULTS AND DISCUSSION

In demonstrating the application of Cobrawap, we pool multiple open-access ECoG and calcium imaging datasets and perform comparisons of slow wave characteristics across the corresponding experimental conditions (Figure 1). In particular, we evaluate the influences of the anesthetic type and dose, replicate previously reported trends [8,9], and examine differences between the measurement techniques due to their different spatial resolution. Furthermore, we exploit the pipeline's modular structure by switching between two alternative methods for up-transition detection to enable a method benchmarking application. Finally, we discuss the reusability of the presented analysis pipeline components for similar analysis applications and model development [10] to promote the collaborative effort of distilling consistent and comparable conclusions from diverse experimental approaches.

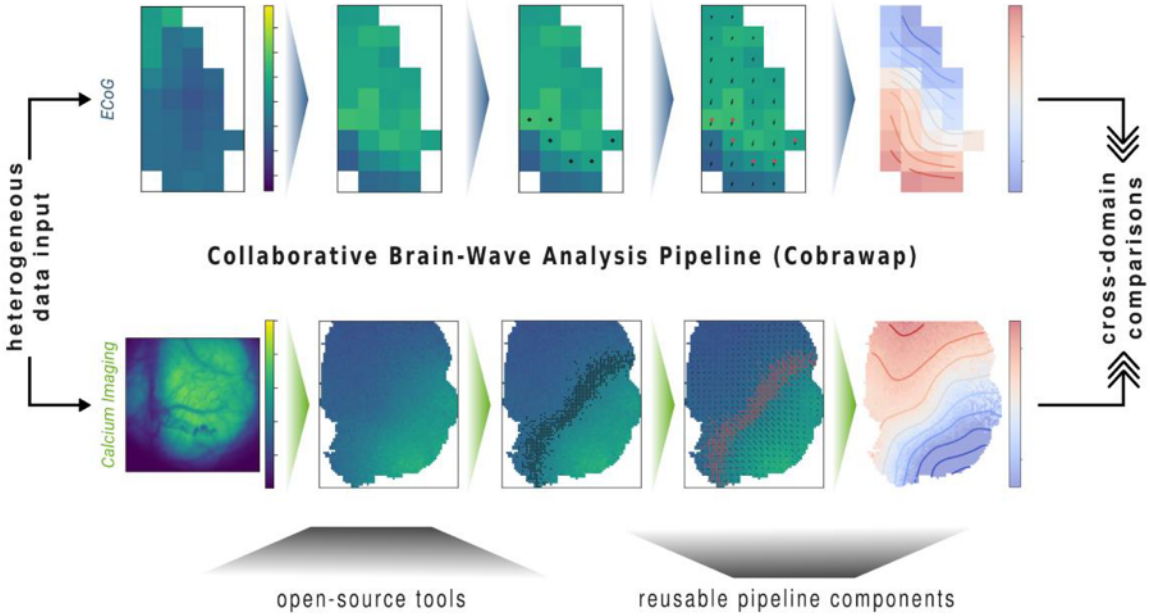

Figure 1: Heterogeneous input data, for example, from ECoG or widefield calcium imaging recordings, are processed and analyzed analogously in Cobrawap to extract quantitative characterizations of slow wave activity as the basis for cross-domain comparisons.

Keywords: cerebral cortex, cortical oscillations, slow wave activity, data analysis, software tools, workflow, reproducibility, validation, wide-field calcium imaging, ECoG

ACKNOWLEDGEMENTS

This research was funded by the European Union's Horizon 2020 Framework Programme for Research and Innovation under Specific Grant Agreements No. 785907 (HBP SGA2) and No. 945539 (HBP SGA3); the Joint Lab "Supercomputing and Modeling for the Human Brain; and the Ministry of Culture and Science of the State of North Rhine-Westphalia, Germany, under NRW-network 'iBehave' grant number NW21-049.

REFERENCES

[1] Steriade, M., Nunez, A., & Amzica, F. (1993). Intracellular analysis of relations between the slow (<1 Hz) neocortical oscillation and other sleep rhythms of the electroencephalogram. *Journal of Neuroscience*, *13*(8), 3266–3283. https://doi.org/10.1523/JNEUROSCI.13-08-03266.1993

[2] Gutzen, R., De Bonis, G., De Luca, C., Pastorelli, E., Capone, C., Allegra Mascaro, A. L., Resta, F., Manasanch, A., Pavone, F. S., Sanchez-Vives, M. V., Mattia, M., Grün, S., Paolucci, P. S., & Denker, M. (2022). *Comparing apples to apples—Using a modular and adaptable analysis pipeline to compare slow cerebral rhythms across heterogeneous datasets* (arXiv:2211.08527). arXiv. https://doi.org/10.48550/arXiv.2211.08527 (RRID:SCR_022966)

[3] Mattia, M., Ferraina, S., & Del Giudice, P. (2010). Dissociated multi-unit activity and local field potentials: A theory inspired analysis of a motor decision task. *NeuroImage*, *52*(3), 812–823. https://doi.org/10.1016/j.neuroimage.2010.01.063

[4] De Bonis, G., Dasilva, M., Pazienti, A., Sanchez-Vives, M. V., Mattia, M., & Paolucci, P. S. (2019). Analysis Pipeline for Extracting Features of Cortical Slow Oscillations. *Frontiers in Systems Neuroscience*, *13*, 70. https://doi.org/10.3389/fnsys.2019.00070

[5] Mölder, F., Jablonski, K. P., Letcher, B., Hall, M. B., Tomkins-Tinch, C. H., Sochat, V., Forster, J., Lee, S., Twardziok, S. O., Kanitz, A., Wilm, A., Holtgrewe, M., Rahmann, S., Nahnsen, S., & Köster, J. (2021). Sustainable data analysis with Snakemake. *F1000Research*, *10*, 33. https://doi.org/10.12688/f1000research.29032.2 (RRID:SCR_003475)

[6] Garcia, S., Guarino, D., Jaillet, F., Jennings, T. R., Pröpper, R., Rautenberg, P. L., Rodgers, C., Sobolev, A., Wachtler, T., Yger, P., & Davison, A. P. (2014). Neo: An object model for handling electrophysiology data in multiple formats. *Frontiers in Neuroinformatics*, *8*(February), 10. https://doi.org/10.3389/fninf.2014.00010 (RRID:SCR_000634)

[7] Denker, M., Yegenoglu, A., & Grün, S. (2018). *Collaborative HPC-enabled workflows on the HBP Collaboratory using the Elephant framework*. Neuroinformatics. https://doi.org/10.12751/incf.ni2018.0019 (RRID:SCR_003833)

[8] Pazienti, A., Galluzzi, A., Dasilva, M., Sanchez-Vives, M. V., & Mattia, M. (2022). Slow waves form expanding, memory-rich mesostates steered by local excitability in fading anesthesia. *IScience*, *25*(3), 103918. https://doi.org/10.1016/j.isci.2022.103918

[9] Dasilva, M., Camassa, A., Navarro-Guzman, A., Pazienti, A., Perez-Mendez, L., Zamora-López, G., Mattia, M., & Sanchez-Vives, M. V. (2021). Modulation of cortical slow oscillations and complexity across anesthesia levels. *NeuroImage*, *224*, 117415. https://doi.org/10.1016/j.neuroimage.2020.117415

[10] Capone, C., De Luca, C., De Bonis, G., Gutzen, R., Bernava, I., Pastorelli, E., Simula, F., Lupo, C., Tonielli, L., Mascaro, A. L. A., Resta, F., Pavone, F., Denker, M., & Paolucci, P. S. (2022). *Simulations Approaching Data: Cortical Slow Waves in Inferred Models of the Whole Hemisphere of Mouse* (arXiv:2104.07445). arXiv. https://doi.org/10.48550/arXiv.2104.07445

25. Tracking the pre-processing and analysis of electrophysiological data with Elephant and Alpaca

Cristiano Köhler[1,2,3,4], Moritz Kern[1,2,3], Julia Sprenger[5], Alexander Kleinjohann[1,2,3,4], Frédéric Barthélemy[1,2,3], Sonja Grün[1,2,3,4], Michael Denker[1,2,3*]

[1] Institute of Neuroscience and Medicine (INM-6), Jülich Research Centre, Jülich, Germany

[2] Institute for Advanced Simulation (IAS-6), Jülich Research Centre, Jülich, Germany

[3] JARA-Institute Brain Structure-Function Relationships (INM-10), Jülich Research Centre, Jülich, Germany

[4] Theoretical Systems Neurobiology, RWTH Aachen University, Aachen, Germany

[5] Institut de Neurosciences de La Timone, CNRS & Aix-Marseille University, Marseille, France

*m.denker@fz-juelich.de

INTRODUCTION/MOTIVATION

Workflows for the processing and analysis of electrophysiology data are often implemented as one or multiple scripts that read input datasets and produce result files [1]. To increase the reuse and rigour of such scripts, the code should rely on software libraries that provide the analysis methods operating on a data model suitable for the representation of neuronal data. Even at such a high level of standardisation, several challenges remain for the analyst. (i) Relevant parameters are often probed interactively, such that subsequent results depend on the details of this interactive process. Keeping track of the parameters used for a specific result becomes difficult. (ii) Results are often used in shared collaborative environments. All collaborators need to have detailed knowledge of the analysis process to understand and interpret the results. (iii) Finding specific results in a large repository of analysis results is difficult, as several parameters may be stored in a custom or non-machine-readable fashion inside the result file. Overall, the exact analysis processes starting from the experimental dataset to the final results may not be clear when looking at a result file alone.

METHODS

Provenance information describes data manipulations and parameters throughout the analysis [2,3]. Comprehensive capture of provenance information during execution of analysis scripts will help to address those challenges. Available workflow management systems can capture high-level parts of the provenance, such as which scripts were executed, the corresponding execution environment, and their dependencies on input files and parameters. However, the details about the analyses carried out inside the executed script are missing and the results can only be understood by source code inspection or documentation. In this work, we aimed to capture such fine-grained provenance within Python scripts. To test our approach, we designed two use case scenarios that implement processing of electrophysiology data. In the first scenario, a multichannel electrophysiological dataset recorded in a behavioural task [4] is analysed by means of a Python script. The use case consists of typical

analysis steps, such as data selection, multi-step processing of the data, aggregation of data across trials, and producing a plot. In the second scenario, we consider modules of a preprocessing pipeline for electrophysiological data based on snakemake [5] that performs specific transformations in the data to generate a final dataset for analysis. The codes of both use cases utilise the Elephant library [6] and the Neo data model [7] as an EBRAINS software basis to standardise data representations and analysis functions.

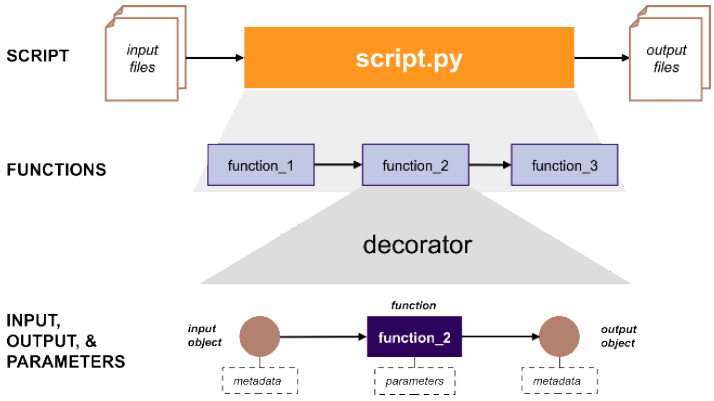

Using decorators, Alpaca captures the provenance of Python scripts including the data flow, used functions, object metadata and function parameters.

RESULTS AND DISCUSSION

We implemented the Alpaca (Automatic Lightweight Provenance Capture) toolbox to capture provenance requiring minimal user intervention when running Python analysis scripts [8]. Alpaca records the inputs, outputs, and parameters of the functions called within a script. We demonstrate how this information is structured according to the W3C PROV standard [9] and serialised as metadata files together with the results. We detail the extent to which Alpaca tracks the data flow during the program execution in the two use case scenarios. Properties and metadata provided by Elephant and Neo are retained in the captured provenance information. Based on these results, we discuss how the provenance information and its graphical representation address the initial challenges for preprocessing and analysis workflows by exposing the details of the result generation. This will help to share results according to the FAIR principles [10], improve research reproducibility and form the basis for intuitive provenance exploration via graphical interfaces.

Keywords: provenance, electrophysiology, workflows, data analysis, preprocessing, metadata, software, visualization, neuroscience, Python, Knowledgegraph

ACKNOWLEDGEMENTS

This work was performed as part of the Helmholtz School for Data Science in Life, Earth and Energy (HDS-LEE) and received funding from the Helmholtz Association of German Research Centres, from the European Union's Horizon 2020 Framework Programme for Research and Innovation under Specific Grant Agreements No. 785907 (Human Brain Project SGA2) and 945539 (Human Brain Project SGA3), by the Helmholtz Association Initiative and Networking Fund under project number ZT-I-0003, and the NRW network iBehave (NW21-049).

REFERENCES

[1] Denker and Grün (2016) Designing Workflows for the Reproducible Analysis of Electrophysiological Data. In Brain-Inspired Computing, Amunts et al., eds. (Cham: Springer International Publishing), 58-72. https://doi.org/10.1007/978-3-319-50862-7_5

[2] Ragan, E.D., Endert, A., Sanyal, J., Chen, J., 2016. Characterizing Provenance in Visualization and Data Analysis: An Organizational Framework of Provenance Types and Purposes. IEEE Transactions on Visualization and Computer Graphics 22, 31–40. https://doi.org/10.1109/TVCG.2015.2467551

[3] Pimentel, J.F., Freire, J., Murta, L., Braganholo, V., 2019. A Survey on Collecting, Managing, and Analyzing Provenance from Scripts. ACM Comput. Surv. 52, 47:1-47:38. https://doi.org/10.1145/3311955

[4] Brochier, T., Zehl, L., Hao, Y., Duret, M., Sprenger, J., Denker, M., Grün, S., Riehle, A., 2018. Massively parallel recordings in macaque motor cortex during an instructed delayed reach-to-grasp task. Scientific Data 5, 180055. https://doi.org/10.1038/sdata.2018.55

[5] Mölder, F., Jablonski, K.P., Letcher, B., Hall, M.B., Tomkins-Tinch, C.H., Sochat, V., Forster, J., Lee, S., Twardziok, S.O., Kanitz, A., Wilm, A., Holtgrewe, M., Rahmann, S., Nahnsen, S., Köster, J., 2021. Sustainable data analysis with Snakemake. https://doi.org/10.12688/f1000research.29032.2

[6] https://python-elephant.org

[7] Garcia, S., Guarino, D., Jaillet, F., Jennings, T., Pröpper, R., Rautenberg, P.L., Rodgers, C.C., Sobolev, A., Wachtler, T., Yger, P., Davison, A.P., 2014. Neo: an object model for handling electrophysiology data in multiple formats. Frontiers in Neuroinformatics 8, 10. https://doi.org/10.3389/fninf.2014.00010

[8] https://alpaca-prov.readthedocs.io

[9] https://www.w3.org/TR/prov-overview

[10] Wilkinson, M.D., Dumontier, M., Aalbersberg, Ij.J., Appleton, G., Axton, M., Baak, A., Blomberg, N. et al., 2016. The FAIR Guiding Principles for scientific data management and stewardship. Scientific Data 3, 160018. https://doi.org/10.1038/sdata.2016.18

26. Pioneering open neuroscience - the role of the curation services

Authors: Sophia Pieschnik[1], Archana Golla[1], Ingrid Reiten[1], Ulrike Schlegel[1], Eivind Hennestad[1], Saira Hussain[1], Stefan Köhnen[2], Camilla H. Blixhavn[1], Heidi Kleven[1], Eszter A. Papp[1], Andrew P. Davison[4], Peyman Najafi[4], Florent Bonnier[4], Oliver Schmid[3], Sara Zafarina[2], Timo Dickscheid[2], Lyuba Zehl[2], Trygve B. Leergaard[1], Jan G. Bjaalie[1*]

Affiliations:
[1]Institute of Basic Medical Sciences, University of Oslo, Norway
[2]Institute for Neuroscience and Medicine (INM-1), Jülich Research Centre, Jülich, Germany
[3]EBRAINS AISBL
[4]Paris-Saclay Institute of Neuroscience, CNRS/Université Paris-Saclay, Saclay, France

*Corresponding author: j.g.bjaalie@medisin.uio.no

Introduction: The transition to open science lays the foundation for exploring the wealth of data produced within neuroscience. Sharing research outputs in a systematic and standardised manner is crucial to repeat, replicate, and reuse scientific outputs. However, the wide variety of data types and formats produced by neuroscience research constitutes a major challenge. The EBRAINS Data and Knowledge Services enable researchers to discover, access, and interpret neuroscience data, computational models, and code, and share their own via the EBRAINS research infrastructure. Here we present the curation service, where data curation scientists of diverse neuroscience backgrounds provide tailored support to researchers sharing their research outputs via EBRAINS. In what follows, we use the word "data" to include data, models, and code. The data curation services ensure that the data is organised in an understandable and consistent manner, that the data are annotated with sufficient metadata, and that the curated data are connected to an ecosystem of tools and services facilitating its reuse and analysis.

Methods/Results: Using the FAIR data guiding principles (Findability, Accessibility, Interoperability, Reusability)[1]as a backbone, the EBRAINS Data & Knowledge Services split into three components: the neuroscience metadata framework, openMINDS (https://github.com/HumanBrainProject/openMINDS, RRID:SCR_023173), the flexible graph database Knowledge Graph, and the curation service. Through established workflows and documentation, the curation service ensures that data is annotated with relevant and sufficient metadata following the openMINDS framework. Curated data is stored as nodes on the Knowledge Graph, making it Findable and Accessible to the broader research community via our search engine (https://search.kg.ebrains.eu) or programmatically via an API. Alongside the annotated data, the Data Descriptor, a document describing data acquisition methods and data organisation, increases the Reusability of the data. Researchers are encouraged to use community standards for data organisation (e.g., BIDS, NWB) to increase the Interoperability of the shared data.

Discussion: Our mission is to ensure viable data sharing and data discovery. We collect, organise and combine multifaceted data to accelerate reproducible research. We aim to unify all neuroscience research by making it as openly available as possible, and by enabling analysis and comparison of brain data across modalities.

Keywords: neuroscience, open science, FAIR data, data sharing, data curation

Acknowledgments: This project received funding from the European Union's Horizon 2020 Framework Program for Research and Innovation under the Specific Grant Agreement No. 720270 (Human Brain Project SGA1), Specific Grant Agreement No. 785907 (Human Brain Project SGA2) and Specific Grant Agreement No. 945539 (Human Brain Project SGA3).

References

1. Wilkinson, M., Dumontier, M., Aalbersberg, I. *et al.* The FAIR Guiding Principles for scientific data management and stewardship. *Sci Data* 3, 160018 (2016). https://doi.org/10.1038/sdata.2016.18

27. Building Responsible Data Governance into EBRAINS

William Knight*[1], Damian Eke[1], Simisola Akintoye[1], Peter Gierow[2]

Affiliations: [1]Centre for Computing and Social Responsibility, De Montfort University, Leicester, United Kingdom.

[2]Department of Medicine and Optometry, Faculty of Life Sciences, Linnaeus University, Sweden.

*William.Knight@dmu.ac.uk

INTRODUCTION/MOTIVATION

As a world-leading research infrastructure facilitating the curation, archiving, and sharing of neuroscience data from all over the globe, EBRAINS processes huge amounts of brain data. Many of these are health data and potentially sensitive or special category data. To be socially acceptable, ethically responsible and legally compliant, this requires appropriate governance mechanisms[1]. EBRAINS is the first infrastructure to develop a responsible, and responsive, model of Data Governance and Ethics Compliance that align with the EU's GDPR. These governance mechanisms are based on a decade of Responsible Research and Innovation research activities by academics and scientists in The Human Brain Project [2]. Our work has garnered a great deal of attention worldwide, and the models, policies and approaches to data governance and ethics compliance we have developed can be replicated in similar international infrastructures.

Meanwhile, researchers still struggle to deal with these complex issues; the question of how data can be ethically collected, stored, and shared is a not a solved one, and so EBRAINS has developed a model which makes the handling of these pivotal concepts simple and straightforward.

This poster will highlight the models for Data Governance and Ethics Compliance which we have developed and will inform researchers on the good practices that those innovative models encourage and support.

METHODS

Current EBRAINS practices, policies and procedures were developed by a multidisciplinary team of ethicists, lawyers, and scientists. They are the result of a great deal of academic inquiry, dialogue, and research in the fields of data ethics, neuroethics, research integrity, law and international policy, to name a few [3].

The content of this poster is derived from a decade of insights and experiences of those professionals over the course of the Human Brain Project.

RESULTS AND DISCUSSION

EBRAINS has developed a data governance framework based upon three core pillars: People, Processes and Technology (PPT). This framework, developed by researchers in WP4, WP9 and the Data Governance Working Group, ensures that data governance issues are addressed at each stage of the data lifecycle[4] .

Within the PPT framework the *People* include all identified stakeholders within all the data processing pipelines in EBRAINS who are responsible for creating, applying, and maintaining data governance procedures. It also includes the identification of data subjects whose rights must always be upheld in a dialogical approach[5]. Most importantly for HBP/EBRAINS, there are established stakeholders, groups or committees to consider the interests of the data subjects. For instance, the Data Governance Working Group: This Includes representatives from all the service categories and Work Packages (WPs). The DGWG works closely with other bodies in the HBP, notably the Science and Infrastructure Board (SIB), the Directorate, the Data Protection Officer (DPO), the Scientific and Technical coordinators and other relevant bodies such as the Compliance, Data Governance, Data Protection and Data Management Task (T4.5), and the independent Ethics Advisory Board (EAB).

There are also *Processes* - referring to the diverse technical, legal, and ethical policies, procedures and practical processes set up to ensure responsible data governance. An example of the processes developed to handle data in EBRAINS is the Ethics Compliance Traffic Lights system developed to assess the compliance requirements for data progressing through the data curation pathway.

Finally, there is also *Technology* which includes all technologies developed and applied in EBRAINS workflows to ensure usability, FAIR and compliance to relevant laws and ethical principles.

This framework, which addresses every stage of the data lifecycle, allows EBRAINS to ensure that ethics and law are embedded in the design process, encompassing a "Responsibility-by- design" approach [6]. Implementation of this framework has highlighted the importance of taking a dialogical approach to the implementation of ethics compliance, data governance and data protection in such a large venture as The Human Brain Project and EBRAINS, where just as important as the application of laws and regulations is the establishment of a network of informed, supported and responsible researchers.

Keywords: Data Governance, Ethics Compliance, Data Protection, Responsibility, Innovation

ACKNOWLEDGEMENTS

This project/research has received funding from the European Union's Horizon 2020 Framework Programme for Research and Innovation under the Grant Agreements No. 720270 (HBP SGA1), 785907 (HBP SGA2), 945539 (HBP SGA3) and the Framework Partnership Agreement No. 650003.

REFERENCES

[1] Fothergill BT, Knight W, Stahl BC and Ulnicane I (2019) Responsible Data Governance of Neuroscience Big Data. Front. Neuroinform. 13:28. doi: 10.3389/fninf.2019.00028

[2] Bernd Carsten Stahl, Simisola Akintoye, Lise Bitsch, Berit Bringedal, Damian Eke, Michele Farisco, Karin Grasenick, Manuel Guerrero, William Knight, Tonii Leach, Sven Nyholm, George Ogoh, Achim Rosemann, Arleen Salles, Julia Trattnig & Inga Ulnicane (2021) From Responsible Research and Innovation to responsibility by design, Journal of Responsible Innovation, 8:2, 175-198, DOI: 10.1080/23299460.2021.1955613

[3| Stahl BC, Akintoye S, Fothergill BT, Guerrero M, Knight W, Ulnicane I. Beyond Research Ethics: Dialogues in Neuro-ICT Research. Front Hum Neurosci. 2019 Mar 29;13:105. doi: 10.3389/fnhum.2019.00105. PMID: 30983981; PMCID: PMC6449836.

[4] Damian O. Eke, Amy Bernard, Jan G. Bjaalie, Ricardo Chavarriaga, Takashi Hanakawa, Anthony J. Hannan, Sean L. Hill, Maryann E. Martone, Agnes McMahon, Oliver Ruebel, Sharon Crook, Edda Thiels, Franco Pestilli (2022) International data governance for neuroscience. Neuron, 110(4), pp. 600–612.

[5] Bernd Carsten Stahl, Stephen Rainey, Emma Harris, B Tyr Fothergill, The role of ethics in data governance of large neuro-ICT projects, Journal of the American Medical Informatics Association, Volume 25, Issue 8, August 2018, Pages 1099–1107, https://doi.org/10.1093/jamia/ocy040

[6] Bernd Carsten Stahl, Simisola Akintoye, Lise Bitsch, Berit Bringedal, Damian Eke, Michele Farisco, Karin Grasenick, Manuel Guerrero, William Knight, Tonii Leach, Sven Nyholm, George Ogoh, Achim Rosemann, Arleen Salles, Julia Trattnig & Inga Ulnicane (2021) From Responsible Research and Innovation to responsibility by design, Journal of Responsible Innovation, 8:2, 175-198, DOI: 10.1080/23299460.2021.1955613

28. Formal and Informal Infrastructures of Collaboration in the Human Brain Project

Christine Aicardi[1], Tara Mahfoud[2*]

Affiliations: [1]Department of Global Health and Social Medicine, King's College London, London, UK

[2]Department of Sociology, University of Essex, Colchester, UK

*tara.mahfoud@essex.ac.uk

INTRODUCTION/MOTIVATION

To stimulate the hoped-for ground-breaking science that will address societal "grand challenges," science policy makers and research funding bodies increasingly stress the need to create wide interdisciplinary networks of researchers and durable research infrastructures. While interdisciplinary collaboration and research infrastructures are well explored topics in the social study of science and technology, we know little about whether and how research infrastructures foster and support interdisciplinary collaboration. The HBP is an unprecedented large-scale project involving more than 500 scientists and engineers in more than 100 institutions across Europe. This presents unique challenges to the management of the collaborations necessary to achieve its scientific goals. As such, it is an experiment in large-scale collaborations and in the development of infrastructure to create, monitor, and measure those very collaborations. Therefore, we use the HBP as a case study to explore the relationships and dynamics between collaboration and infrastructure in large-scale science.

METHODS

Research was conducted continuously between 2014 and 2020 by the Foresight Lab at King's College London as part of its work in the Ethics and Society sub-project of the HBP. More specifically, the research draws on participant observation of meetings between scientists, engineers, and project administrators; a total of eighteen interviews with infrastructure users and developers; and analysis of HBP and EC documents relating to community building, collaboration, and infrastructure development conducted in 2017-2019. We conducted a thematic analysis of our interview data and used inductive coding to identify themes.

RESULTS AND DISCUSSION

The overarching themes we identified in our data were a distinction between formal and informal infrastructure by the research participants, as well as their concerns about the visibility or invisibility of collaborations in the HBP. Our results suggest that the formal infrastructure built to facilitate and structure collaboration within large-scale interdisciplinary research projects can be in tension with the ways researchers collaborate. The interviews we conducted highlighted the coexistence of a formal infrastructure whose design has evolved from being user-led by internal HBP users to being primarily targeted at external users. The formal infrastructure has co-existed with

an informal bricolage infrastructure that researchers and engineers in the HBP are using to collaborate— a parallel, informal, infrastructural patchwork that can go unnoticed by HBP management and EC project officers and reviewers. In some cases, the informal infrastructure is facilitating the development of the official HBP infrastructure and expanding the membership of the project beyond the existing communities that launched it. However, in some cases, the tools that have been put in place to underpin a formal infrastructure are actually perceived by scientists and engineers within and outside of the project as hindering collaboration. We identify a tension between the development of infrastructures of collaboration as a bureaucratic form of accountability and visibility, and the bureaucratic labour involved in enacting this visibility which in itself can fail to see the very collaborations it is meant to monitor and/or enforce. As the HBP formal infrastructure continues to develop and becomes EBRAINS, it will be important to continue to explore the (evolving) relationship between the formal and informal infrastructures of collaboration and what forms of knowledge will be made durable. In the future, it will be important for the EBRAINS research infrastructure to grow its research and innovation communities in a way that respects existing informal collaborations while also ensuring a more inclusive membership and governance.

Keywords: infrastructure, interdisciplinary, collaboration, ethics, society

ACKNOWLEDGEMENTS

This research has received funding from the EU's Horizon 2020 Research and Innovation Programme under Grant Agreements No. 720270 (HBP SGA1) and No.785907 (HBP SGA2).

29. KnowledgeSpace: a global portal for discovering and integrating FAIR data from around the world

Visakh Muraleedharan[1,2], Thomas Gillespie[2,3], Mathew Birdsall Abrams[1,2*]

[1]Department of Neuroscience, Karolinska Institutet, Stockholm, Sweden

[2]International Neuroinformatics Coordinating Facility, Stockholm, Sweden [3]FAIR Data Informatics Lab, University of California, San Diego, USA

*e-mail-address of corresponding author: mathew@incf.org

The FAIR Guiding Principles for scientific data management and stewardship in neuroscience is partnership between researchers, repositories, indexes/aggregators coordinated by community organizations. In this partnership, community organizations are responsible for developing the discipline specific standards and best practices the guide the data management practices of the researchers and serve as the standards for domain- specific data repositories. Indexers/aggregators serve as portals that integrate data and models from different repositories and make them discoverable through a centralized search interface. In an effort to make the research outputs of the global neuroscience community available through the EBRAINS RI, we developed KnowledgeSpace (KS), a global indexing service and encyclopaedia that links neuroscience research concepts to the data, models, and literature from FAIR-compliant data repositories that supports them. As a service, KS ingests metadata from 20 of the world's leading neuroscience repositories to create a catalogue of publicly available datasets and the literature that supports the data. In addition, KS also ingests descriptions of neuroscience terms found in Wikipedia and displays them in the "KS encyclopaedia view" which merges Wikipedia with PubMed and the KS data catalogue. The KS data catalogue can be semantically queried in a multitude of ways: by repository, data type, region of interest, or disease. To our knowledge, KS is the only service that indexes datasets generated by the world's large-scale brain projects (Human Brain Project, BRAIN Initiative, Brain/MINDS, and the Canadian Open Neuroscience Platform). Of special note, KS provides the BRAIN Initiative with a search interface that indexes BRAIN Initiative supported repositories, DANDI Archive and OpenNeuro—a service not provided by the BRAIN Initiative. In addition to indexing publicly available datasets

from the world's leading neuroscience data repositories, KS also indexes abstracts published in PubMed and the educational materials published in the INCF TrainingSpace. In practical terms, this enables a user to query a region of interests and receive results displaying: a. publicly available datasets, b. the literature related to the region of interest in PubMed, c. educational resources related to the region of interest in TrainingSpace, and d. an "encyclopaedia view" of the region of interest which combines Wikipedia, PubMed, and the KS data catalogue. Programmatically, KS APIs that enable 3rd party research infrastructures with the ability to leverage the various components of KS, mappings between data repositories, and all NINDS Common Data Elements. In closing, KS provides the EBRAINS research infrastructure with the 3rd pillar of the FAIR partnership, an indexing- aggregating service, that serves as "proof of the international FAIRness" of the EBRAINS research infrastructure.

Keywords: FAIR data, Data aggregator, Data indexer, Encyclopaedia, Data discovery portal, FAIR models

ACKNOWLEDGEMENTS

This project/research has received funding from the European Union's Horizon 2020 Framework Programme for Research and Innovation under the Specific Grant Agreement No. 945539 (Human Brain Project SGA3).

.

30. Data Movement to Facilitate Scientific Workflows in the Fenix Research Infrastructure

Shiting Long[1*], Martin Lischewski[1]

[1]Forschungszentrum Jülich, Jülich Supercomputing Centre (JSC), Jülich, Germany

*s.long@fz-juelich.de

INTRODUCTION/MOTIVATION

Neuroscience communities in the Human Brain Project (HBP) often rely on e-infrastructure services to access, process and analyse data in a collaborative manner. As a result, a federated research e- infrastructure is proposed, namely Fenix, which is based on a consortium of 6 leading European supercomputing centres integrated into a common AAI [1].

In addition to workflows that utilize high-performance computing resources, there is an increasing number of workflows that extend beyond HPC and involve cloud resources to consume and generate data [2]. Hence, Fenix provides computing and storage services that address not only traditional HPC but also on-demand cloud technologies. This necessitates the use of efficient services to move data across various components. In this abstract, we focus on the Fenix data services, which enable 1) data movement between HPC and cloud environments, and 2) data transfer across different Fenix sites.

METHODS

The Fenix research infrastructure categorises its services into two domains: HPC environment and cloud environment. To address the challenge of providing both high I/O bandwidth access to the data stores in massively parallel HPC systems and federated access to the data stores in the cloud, Fenix introduces two corresponding storage types, namely *Active Data Repository* (ACD) to store short-term data and *Archival Data Repository* (ARD) to store long-term data. To further ease the workflows concerning the two environments, Fenix delivers data services including the *Data Mover* to perform intra-site ACD-to-ARD data movement and the *Data Transfer Service* to perform inter-site ARD-to-ARD data movement.

ACDs describe those POSIX file systems that are close to the compute resources. We consider access to ACDs to be local to a single site. ARDs follow the Openstack Swift object store protocol, which optimises durability, availability and concurrency. Unlike ACDs, we consider access to ARDs to be federated by Fenix AAI, meaning that users can be authenticated by either a Fenix partner site identity provider (IdP) or a community IdP (such as the HBP IdP).

The Data Mover is implemented as a software named Nodeum [3], which is developed by MT-C [4] with the goal of offering programmable, high-speed, scalable and secure data movement between ACDs and ARDs as shown in Figure 1. In addition to Command Line Interface (CLI), the Data Mover allows data movement via the SLURM workload manager. Thus, the service offers 1) automated stage-in of data from ARD to ACD prior to the execution of a batch job, and 2) automated stage-out of data from ACD to ARD following the execution of a batch job.

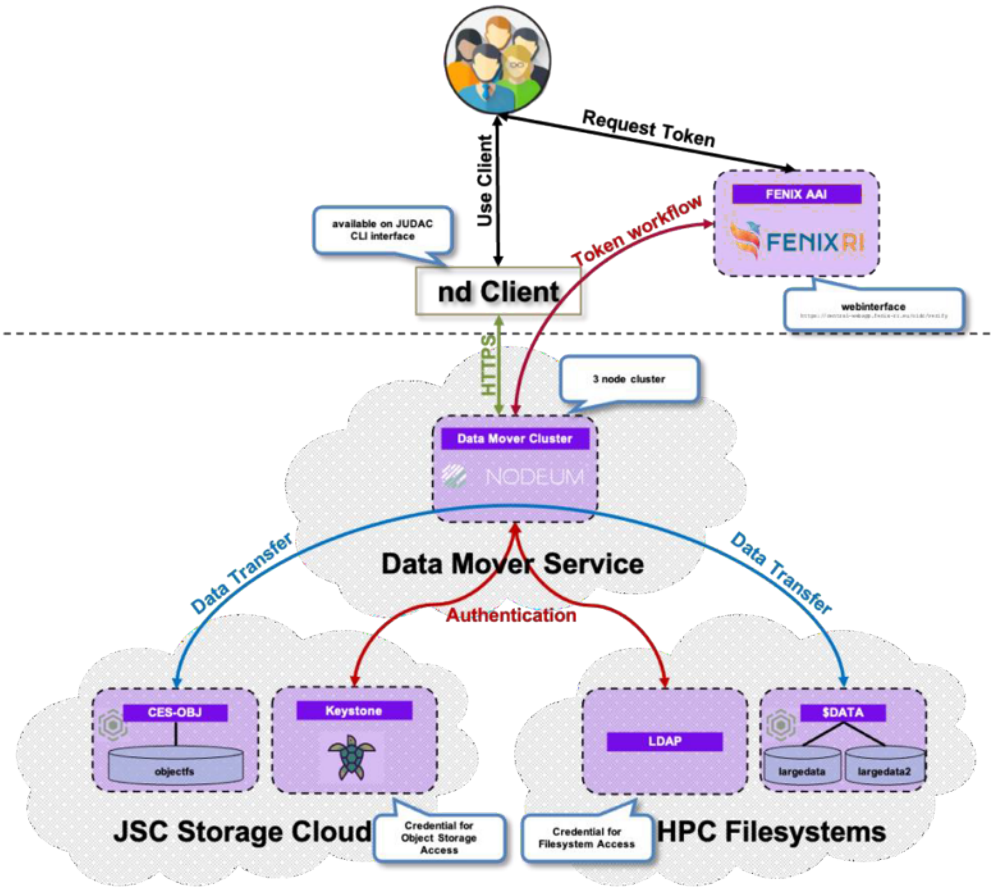

Figure 1. Example Data Mover workflow at JSC.

The Data Transfer Service aims to enable the orchestration of data transfers across ARDs. For this purpose, the File Transfer Service 3 (FTS3) [5] developed by CERN was selected as the service. To realise the Fenix use cases, we added Openstack Swift support to the FTS3 stack so that ARDs can be used as storage endpoints in a data transfer job. Since FTS3 is extended with a web-oriented interface WebFTS, we also added Swift protocol support there so that the service can be easily reached with a browser aside from the CLI.

RESULTS AND DISCUSSION

The Data Mover service is available at JSC on the Jülich Data Access servers (JUDAC). Other sites are currently testing and evaluating the service. There is an FTS3 instance running at Barcelona Supercomputing Center (BSC) that functions as the Data Transfer Service (illustrated in Figure 2). We are also setting up a WebFTS server at BSC to provide an extensive web interface. These data services are undergoing real-world integration and we aim to enhance their capabilities to realise their full potential for the HBP community and beyond.

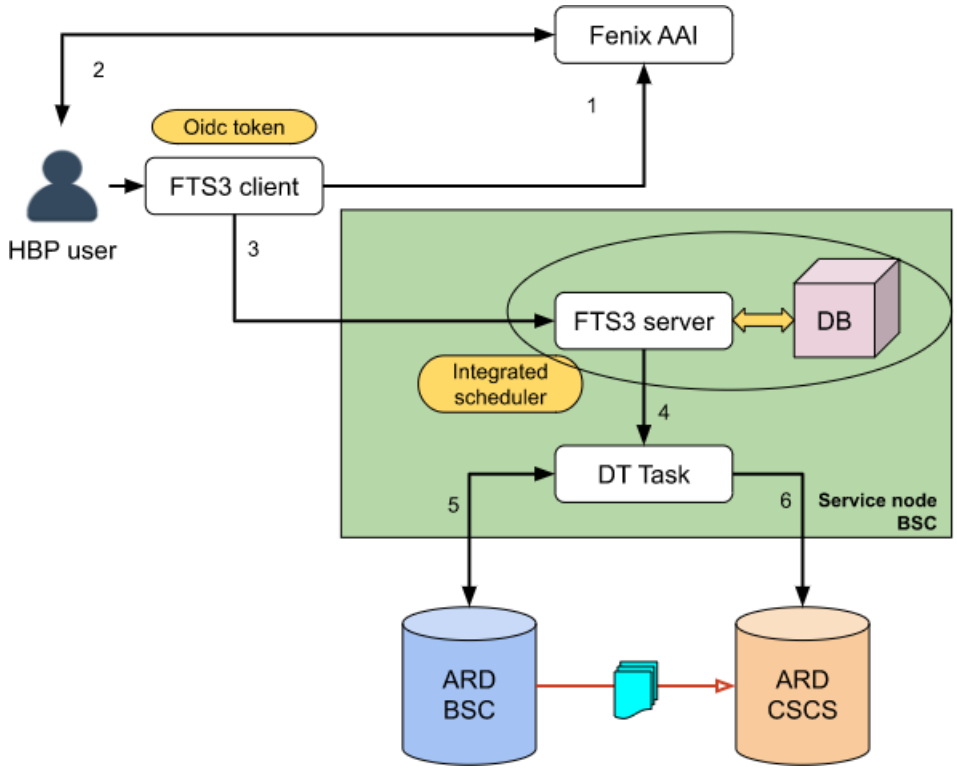

Figure 2. Deployment of the FTS3 service at BSC.

Keywords: HPC, Cloud, e-Infrastructure, Data management, HBP

ACKNOWLEDGEMENTS

Funding for the work is received from the European Commission H2020 program under Specific Grant Agreement No. 800858 (ICEI).

REFERENCES

[1] Alam, Sadaf, et al. "Fenix: distributed e-infrastructure services for ebrains." Brain-Inspired Computing: 4th International Workshop, BrainComp 2019, Cetraro, Italy, July 15–19, 2019, Revised Selected Papers 4. Springer International Publishing, 2021. doi: 10.1007/978-3-030- 82427-3_6

[2] Alam, Sadaf R., et al. "Archival data repository services to enable HPC and cloud workflows in a federated research e-infrastructure." 2020 IEEE/ACM International Workshop on Interoperability of Supercomputing and Cloud Technologies (SuperCompCloud). IEEE, 2020. doi: 10.1109/SuperCompCloud51944.2020.00012.

[3] Nodeum [online] Available: https://www.nodeum.io/.

[4] MT-C [online] Available: https://www.mt-c.com/.

[5] Kiryanov, Andrey, Alejandro Alvarez Ayllon, and Oliver Keeble. "FTS3/WebFTS–a powerful file transfer service for scientific communities." *Procedia Computer Science* 66 (2015): 670-678. doi: 10.1016/j.procs.2015.11.076.

31. Garment EEG: a novel textile system to monitor electroencephalographic activity

Eduardo López-Larraz[1*], Carlos Escolano[1], Almudena Robledo, Leyre Morlas, Alexandra Alda, Javier Minguez

[1]Bitbrain, Zaragoza, Spain

*eduardo.lopez@bitbrain.es

INTRODUCTION/MOTIVATION

Measurement of brain activity with electroencephalography (EEG) can be useful in a broad range of contexts, including research, patient assessment, or brain computer interfaces. Traditionally, this has been done using wet electrodes. These systems are expensive, difficult to place and require a trained specialist to set them up. During the last decades, a lot of effort has been placed on developing mobile dry EEG devices with improved usability and reduced cost, while trying to preserve signal quality [1]. Conductive textiles are a promising alternative for creating garment-like EEG systems that could take on textile qualities such as being breathable and washable. The use of conductive textiles to develop the sensor layer of EEG systems constitutes a relevant step in the field of neurotechnology, that improves the manufacturing process and features like comfort, ergonomics, and cost. [2]. In this work, we present an EEG system whose electrodes (textrodes), transmission and cap support are fully implemented and assembled using elements and materials from textile industry (Garment-EEG). EEG systems encapsulated in garments have the potential to enable a neurotechnology that is naturally accepted by people in their daily lives. The relevance of this research for HBP is that it has the potential to collect massive amounts of EEG data in real-world conditions to expand the contexts of existing EEG databases.

METHODS

We designed an EEG sensor layer that only uses smart textiles to monitor the brain activity from the forehead (see Figure 1A). It includes 4 recording electrodes, plus reference and ground, and a connector at the back part, where the amplifier is attached. The amplifier samples the signals at 256 Hz and uses Bluetooth Low Energy to send the data to a laptop. For comparison, we designed a second headband with the same configuration, but using standard dry Ag/AgCl electrodes (Dry-EEG) and coaxial cables (see Figure 1B). We compared the signals measured with both systems in an experimental study with ten healthy participants. They performed the same tasks using both systems: (1) 3 minutes resting with eyes closed; (2) 3 minutes resting with eyes open; (3) artifact induction, where different movements were executed to contaminate the EEG signals. The obtained signals were compared in terms of power spectral density, and statistical tests were used to compare the power in delta, theta, alpha, beta, and electrical noise (50 Hz) bands for each condition.

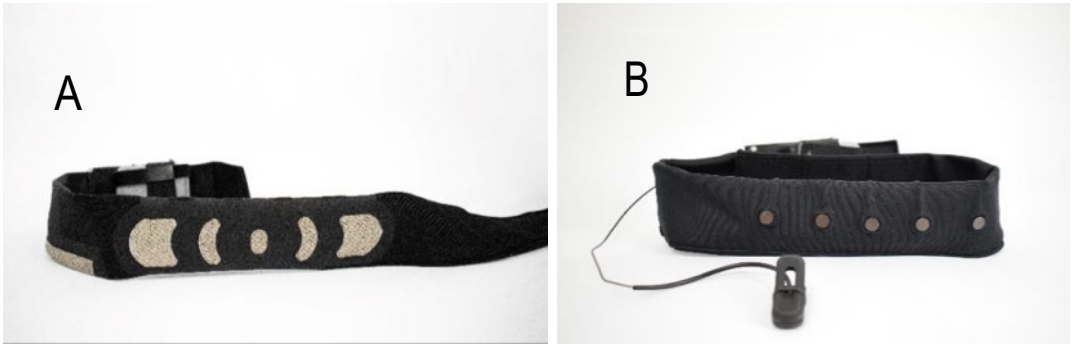

Figure 1. Garment-EEG (A) and Dry-EEG (B) headbands.

RESULTS AND DISCUSSION

Figure 2 shows the spectral analysis of the EEG signals recorded with both headbands during eyes-closed resting state (Figure 2A), eyes-open resting state (Figure 2B), and during the generation of artifacts (Figure 2C). In both resting state measurements, the EEG power in delta, theta, alpha and beta frequencies was not significantly different between the Garment-EEG and the Dry-EEG (Figure 2A-B; $p>0.05$ in all cases). In contrast, the power during the induction of artifacts (Figure 2C), as well as in the electrical-noise band for all conditions, was significantly higher for the Garment-EEG headband than for the Dry-EEG headband.

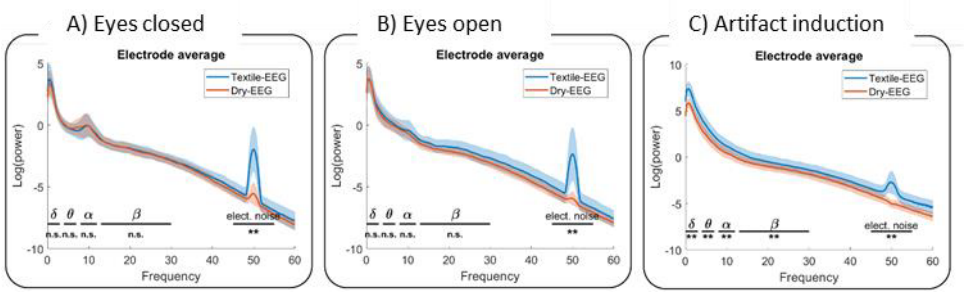

Figure 2. Average power spectral density comparison between the EEG activity measured with the 4 electrodes of the Garment-EEG and Dry-EEG during (A) eyes-closed, (B) eyes-open, and (C) artifact induction. n.s. = non- significant; ** $p<0.01$.

In summary, we have presented the first EEG system conceived as a garment, and compared its signals with respect to a state-of-the-art, metal-based dry EEG system. Our results show that, under a well-controlled scenario (i.e., in resting state), the signals achieved with the Garment-EEG are comparable to those of the Dry-EEG system; however, the textile system is more prone to artifacts in adverse recording conditions due to poorer contact impedances.

Keywords: electroencephalography (EEG), textile EEG, dry EEG, wearable EEG, smart textiles, neurotechnology, brain-computer interface (BCI).

ACKNOWLEDGEMENTS

This study has been funded with grants by the Eureka-Eurostars program (SubliminalHomeRehab: E! 113928; and Hypnos: E! 115062), Penta call 5 – Joint call – Euripides (pAvIs), Programa Misiones de I+D en Inteligencia Artificial (AI4HEALTHYAGING: MIA.2021.M02.0007), EUHubs4Data (EUH4D/OP1/22) and SmartX (824825).

REFERENCES

[1] Casson, A. J. (2019). Wearable EEG and beyond. Biomed. Eng. Lett. 9, 53–71. doi: 10.1007/s13534-018-00093- 6.

[2] Tseghai, G. B., Malengier, B., Fante, K. A., and Van Langenhove, L. (2020). The Status of Textile-Based Dry EEG Electrodes. Autex Res. J. 21, 63–70. doi: 10.2478/aut-2019-0071.

32. Automatic and manual prediction of epileptic seizures based on ECG

Manef BEN MBAREK[1,2], Ines ASSALI[1,2], Salah HAMDI[1], Asma BEN ABDALLAH[1,3], Olivier DAVID[4], Mouna AISSI[5], Marcel CARRERE[4*], Mohamed HEDI BEDOUI[1]

1 Laboratoire de Technologie et Imagerie Médicale, Faculté de Médecine de Monastir, Université de Monastir, 5019, Monastir, Tunisie
2 Faculté des Sciences de Monastir, Université de Monastir, 90 Ave Mohamed V, Monastir 1002, Tunisie
3 Institut supérieur d'informatique et de Mathématiques, Université de Monastir, 5019 Monastir, Tunisie
4 Institut de Neurosciences des Systèmes - Inserm UMR1106 - Aix-Marseille Université - Faculté de Médecine, 27, Boulevard Jean Moulin, 13005, Marseille, France
5 Hôpital Universitaire Fattouma Bourguiba, Monastir, 5019, Tunisie

manef2009@gmail.com, inesassali@gmail.com, salah.hamdi@isffs.u-sousse.tn, assoumaba@yahoo.com, Olivier.David@univ-amu.fr, aissi6mouna@gmail.com, marcel.carrere@univ-amu.fr*, medhedi.bedoui@fmm.rnu.tn

INTRODUCTION/MOTIVATION

Epilepsy is one of the most common neurological disorders. This disorder is mainly characterized by a perdurable predisposition to generate epileptic seizures. In general, doctors use the EEG signal to diagnose patients with epilepsy. Moreover, a lot of work studied the feasibility of predicting seizures based on EEG signals. Indeed, there are some disadvantages that make it hard to use EEG signal for real use such as signal recording, number of electrodes used, finding the appropriate epileptogenic region, etc… In counter, other works showed that epileptic seizures affect not only brain but also anatomic nervous system, in particular heartbeat. In addition, ECG signal is easier to manipulate than the EEG and easier to record with an available sensor and mobile device that can record perfectly the ECG signal at any time. For that reason, this work aimed to study changes in the ECG signal in the pre-ictal period to explore the feasibility of creating an automatic epileptic seizure prediction approach

METHODS

The proposed approach starts with a pre-processing where notch, high pass, and low pass filters were used. The next step consists of detecting the R peaks and then computing the distance between each two consecutive R peaks (RRi). To study the changes on the ECG signal, we studied 1h of ECG signal before the seizures. Moreover, each input signal is divided into sub-segments of 120 seconds with 10 seconds of overlap. For each sub-segment,

two temporal and non-linear features were computed which are the NRRi and the non-linear feature Approximate entropy. Next, from each 5 min of feature vector computed, we compute the standard deviation (STD) with an overlapping of 1 min.

In order to certify a crisis alert, the STD calculation results calculated from these two features were combined. In addition, the threshold algorithm was used on the STD results to ensure crisis prediction for each patient separately. In order to select the threshold value automatically, the following equation is used:

$$Thresh = Mean + \beta \quad (1)$$

- Where $Mean$ presents the mean value of the input data segment.
- β is a value computed from $Mean$ where the value of β will be in the range of values [0 – $Mean$], where the min value of β will equal to 0 and the max will equal to the value of $Mean$
- For selecting the β value, a Grid-search algorithm will be used to test all the possible threshold values.
- Both pre-ictal and inter-ictal period was used to select the best threshold value.
- The β value will be selected for each patient separately.

RESULTS AND DISCUSSION

To measure the performance of the proposed approach, three databases sienna scalp EEG [1], post-ictal [2] and a local database were used. The prediction performance of the proposed approach is listed in the table below.

Table 1. The performance of the automatic threshold approach using the three databases

	Sensitivity	Specificity	Accuracy
The local Database	85%	81%	82%
Siena Scalp EEG Database	75%	85%	82%
Post-ictal Database	90%	83%	85%

The figure bellow presents an example of the automatic thresholding prediction of a patient from the Sienna scalp EEG database

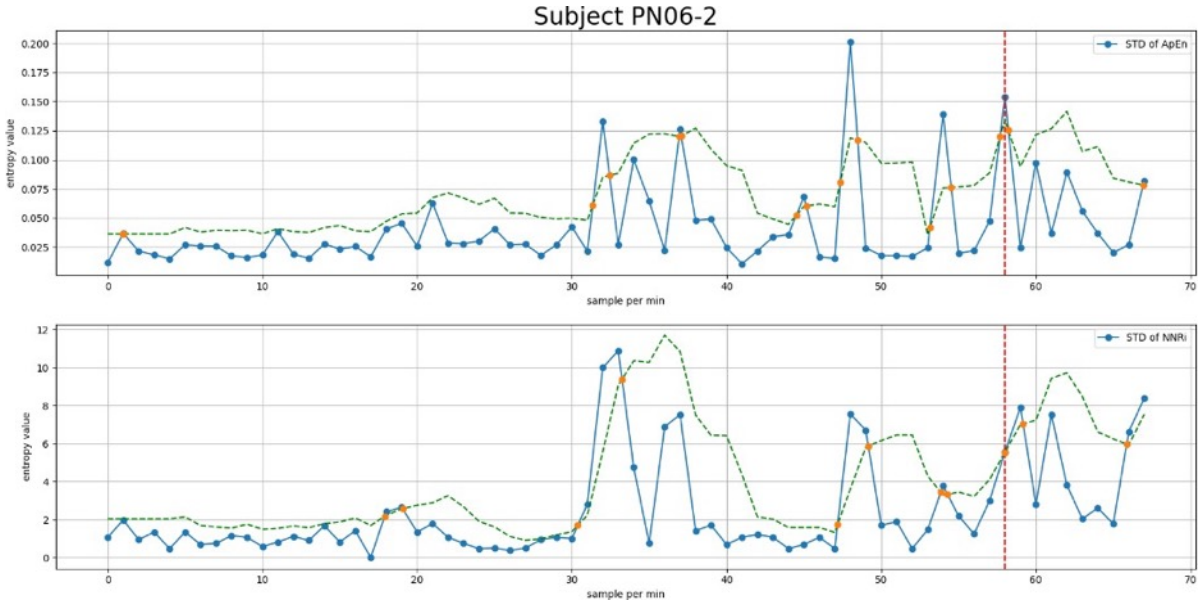

Fig. 1 An example of applying the automatic threshold prediction approach on the acquisition PN06-2

Keywords Electrocardiogram, Epilepsy, Prediction, Epileptic Seizures, threshold, Heart rate variability analysis

ACKNOWLEDGEMENTS REFERENCES

[1] Detti, Paolo, "Siena Scalp EEG Database." PhysioNet. doi: 10.13026/5D4A-J060.

[2] I. C. Al-Aweel *et al.*, "Post-Ictal Heart Rate Oscillations in Partial Epilepsy: Data and Analysis." physionet.org, 1998. doi: 10.13026/C2QC72.

33. Quantitative Susceptibility Mapping and χ-separation method: how MRI can help us understand COVID-19

Elena Grosso[1*], Antonio Ricciardi[2], Fulvia Palesi[1], Claudia AM Gandini Wheeler-Kingshott[2,1,3]

1 Department of Brain and Behavioural Sciences, University of Pavia, Pavia, Italy;
2 NMR Research Unit, Queen Square MS Centre, Department of Neuroinflammation, UCL Institute of Neurology, London, United Kingdom.
3 Brain Connectivity Centre Research Unit, IRCCS Mondino Foundation, Pavia, Italy
* elena.grosso01@universitadipavia.it

INTRODUCTION

After almost three years since the start of the COVID-19 pandemic, people are aware of the possible neurological consequences of the SARS-COV-2 infection[1]. The underlying biological mechanisms of such consequences can be investigated with magnetic resonance imaging (MRI). Quantitative susceptibility mapping (QSM) is an established MRI technique that estimates the distribution of local magnetic susceptibility (χ) of tissue[2], which is directly related to its chemical composition. In the brain, iron and myelin[3] are the two main sources of magnetic susceptibility having opposite characteristics: iron is paramagnetic (positive susceptibility, χ_{pos}) and myelin is diamagnetic (negative susceptibility, χ_{neg}). Both have been suggested as biomarkers for neurological disorders[4,5], however traditional QSM is unable to differentiate between the two. Therefore, new models[6] have been developed to separate the χ_{pos} and χ_{neg} contributions, generating the voxel-wise distributions of the two sources.
Here, one specific model[7] has been used to evaluate local alterations of the total χ as well as of the iron and myelin components in a cohort of subjects previously affected by COVID-19.

METHODS

Subjects & Acquisition

Subjects were divided into four groups: 16 healthy controls (HC; 7 females; 35±12y), 11 subjects recovered from COVID-19 (COVID; 9 females; 28±10y), 8 subjects with persistent anosmia (COVID-P; 7 females; 52±12y), 16 subjects recovered from anosmia (COVID-R; 7 females; 39±8y), 8 young subjects recovered from anosmia (COVID-Y; 4 females; 22±1y). MRI data were acquired with a 3T Philips Ingenia CX scanner with a very rich protocol[8]. The protocol included: 1) multi-echo 3D tilted sagittal spoiled gradient-echo (SPGR) (8 echoes, $TE_1/\Delta TE$=2.3/3.3ms, TR=28.5ms, flip angle=24°, 1x1x1mm^3) for QSM and T^* calculations; 2) 3D sagittal T1-weighted (3DT1) ultrafast gradient echo (TE=3.2ms, TR=6.9ms, flip angle=8°, 1x1x1mm^3) for tissue segmentation.

Preprocessing & Metrics Analysis

For each subject, QSM and local field maps were reconstructed from the complex SPGR data with the Morphology Enabled Dipole Inversion (MEDI) toolbox. T2* was calculated from the magnitude of the SPGR data using the MyRelax toolbox[9]. Brain parcellation was performed on the 3DT1 volume using Geodesic Information Flows (GIF)[10]. Regions of interest (ROIs) of cortical grey matter (CGM), deep grey matter (DGM), white matter (WM) and brain steam (BS) were extracted. QSM maps and ROI masks were registered to SPGR space of each subject using NiftyReg.

The mean values of QSM, χ_{pos}, χ_{neg} and χ_{tot} were calculated for all the ROIs. Linear regression models using one metric at a time as dependent variable, and age and gender as covariates, were performed to assess differences between HC and COVID as a whole, between HC and each COVID subgroup and between COVID-P and recovered anosmia subjects (COVID-R+Y).

RESULTS AND DISCUSSION

All the significative results are reported in Figure2. In particular, they show that mean QSM is greater in COVID-P respect to COVID-R+Y in WM, while it is lower in the DGM and in the CGM. Also, mean QSM is lower in COVID-R respect to HC in WM and it is greater in COVID-Y respect to HC in CGM.

χ_{tot} linear regression analysis gives the same results as the QSM analysis between COVID-P and COVID-R+Y; it additionally showes greater values in COVID-P respect to HC in WM and a lower value in COVID-R respect to HC in the CGM.

χ_{pos} and χ_{neg} analysis give no significant results.

We can conclude that QSM and χ-separation are confident in finding the same differences between groups in the same ROIs of these COVID subgroups. The χ-separation method may require larger sample size groups to capture alterations in the content of iron and myelin in the brain, as these may be subtle. Future work will include investigating other emerging χ -separation models or combining QSM with complementary MRI techniques to obtain more detailed information.

Keywords: MRI, QSM, susceptibility, human brain, iron, myelin. ACKNOWLEDGEMENTS

EG receives funding from TDC Technology Dedicated to Care. FP receive funding from H2020 Research and Innovation Action Grants Human Brain Project (#785907, SGA2 and #945539, SGA3). CGWK receives funding from Horizon2020 (*Human Brain Project SGA3, Specific Grant Agreement No. 945539)*, BRC (#BRC704/CAP/CGW), MRC (#MR/S026088/1), Ataxia UK, MS Society (#77), Wings for Life (#169111). CGWK is a shareholder in Queen Square Analytics Ltd. We thank the MODEL-COV team for support to the study.

REFERENCES (10)

[1] Baig, A.M., 2022. Counting the neurological cost of COVID-19. *Nature Reviews Neurology*, *18*(1), pp.5-6.

[2] Wang Y, Liu T. Quantitative susceptibility mapping (QSM): decoding MRI data for a tissue magnetic biomarker. Magn Reson Med 2015; 73(1):82–101.

[3] Duyn, J.H., Schenck, J., 2017. Contributions to magnetic susceptibility of brain tissue. NMR Biomed. 30, e3546. doi:10.1002/nbm.3546.

[4] Stephenson, E., Nathoo, N., Mahjoub, Y., Dunn, J.F., Yong, V.W., 2014. Iron in multiple sclerosis: roles in neurodegeneration and repair. Nat. Rev. Neurol. 10, 459–468. doi:10.1038/nrneurol.2014.118.

[5] Nave, K.-A., 2010. Myelination and support of axonal integrity by glia. Nature 468, 244–252. doi:10.1038/nature09614.

[6] Schweser, F., Deistung, A., Lehr, B. W., Sommer, K., & Reichenbach, J. R. (2011, May). SEMI-TWInS: simultaneous extraction of myelin and iron using a T2*-weighted imaging

sequence. In Proceedings of the 19th Meeting of the International Society for Magnetic Resonance in Medicine (p. 120).
[7] Shin,H.G, Lee, J. et al., χ-separation: Magnetic susceptibility source separation toward iron and myelin mapping in the brain, NeuroImage, Volume 240, 2021, 118371, ISSN 1053- 8119, https://doi.org/10.1016/j.neuroimage.2021.118371.
[8] Gandini Wheeler-Kingshott, C.A.M, et al., Advanced magnetic resonance imaging to study brain tissue alterations in people infected with SARS-COV-2, ISMRM 2021
[9] Francesco Grussu. (2021). fragrussu/MyRelax: Public API 1.0.0 (1.0.0). Zenodo. https://doi.org/10.5281/zenodo.4561898
[10] Cardoso MJ, Modat M, et al., Geodesic Information Flows: Spatially-Variant Graphs and Their Application to Segmentation and Fusion. IEEE Trans Med Imaging. 2015 Sep;34(9):1976-88. doi: 10.1109/TMI.2015.2418298. Epub 2015 Apr 14. PMID: 25879909.

FIGURES

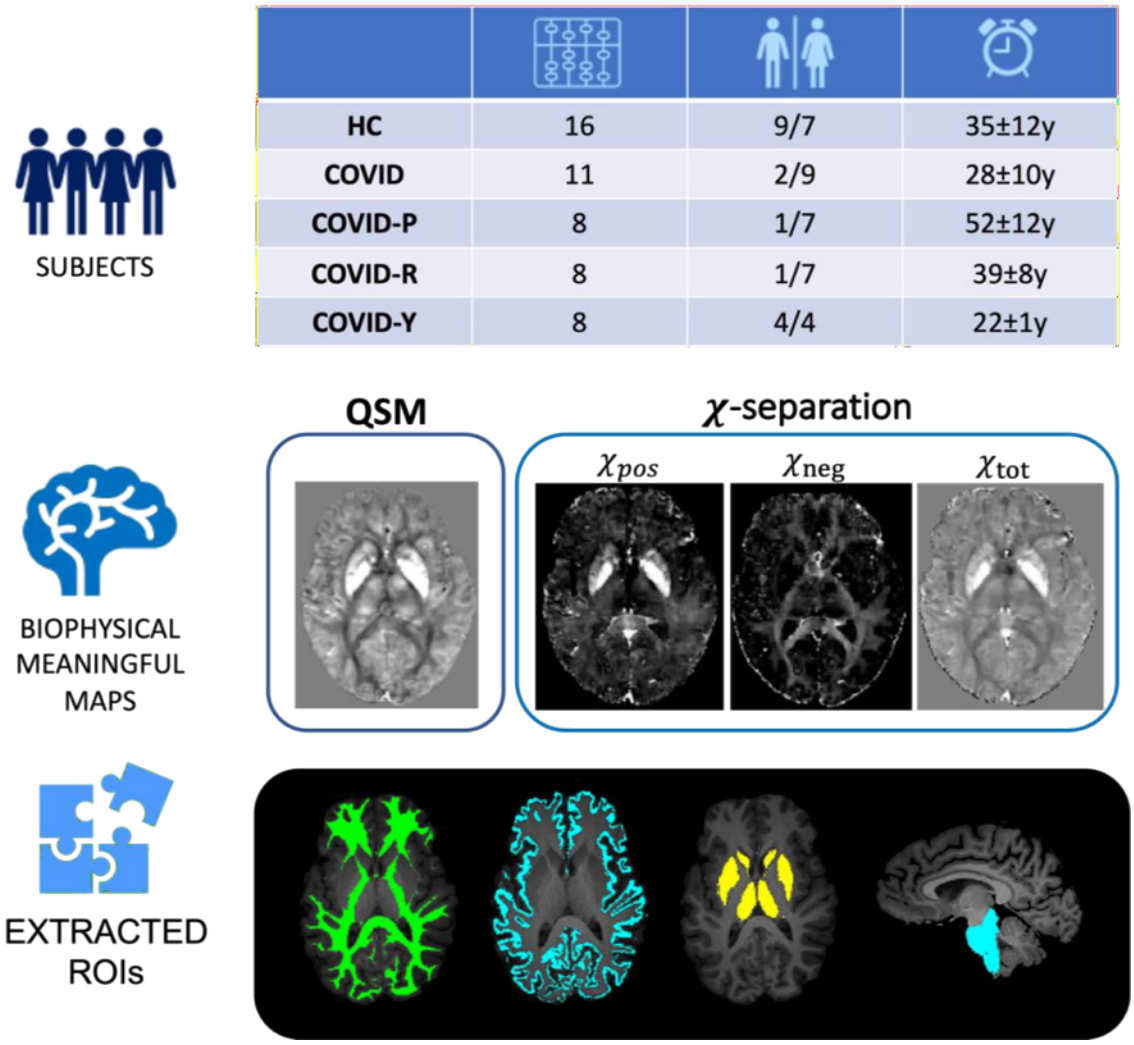

Figure 1| Method pipeline. In the first row it is shown a table of the subjects we recruited for this study (HC = healthy controls, COVID = recovered from COVID-19, COVID-P = persistent anosmia, COVID-R = recovered from anosmia, COVID-Y = young subjects recovered from anosmia). In the second row are reported the biophysical meaningful maps we analysed: quantitative susceptibility mapping (QSM) and χ-positive, χ-negative and χ-total maps (χ_{pos}, χ_{neg}, χ_{tot}) obtained with the χ-separation method. In the last row all the extracted and analyzed regions of interest (ROIs) have been reported.

	χ_{tot}	QSM
HC vs COVID-P	WM ↑	
HC vs COVID-R	CGM ↑	WM ↓
HC vs COVID-Y		CGM ↑
COVID-P vs COVID-R+Y	WM ↓ DGM ↑	WM ↓ DGM ↑ CGM ↑

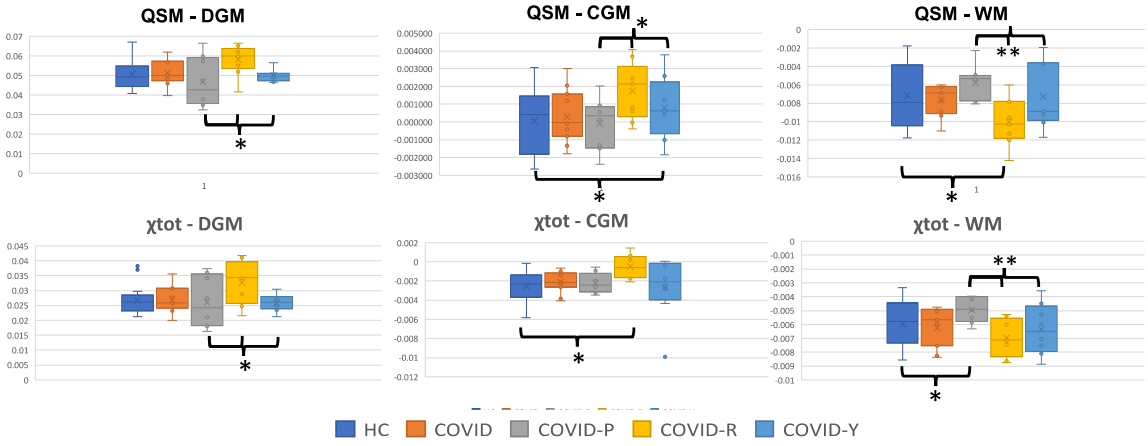

Figure 2| Statistical Results. In the table on the first row are reported all the results of the linear regression betweeen groups. The second row represents boxplots of the analyzed metrics in every region of interest. In every boxplot all the groups are represented (HC = healthy controls, COVID = recovered from COVID-19, COVID-P = persistent anosmia, COVID-R = recovered from anosmia, COVID-Y = young subjects recovered from anosmia). Significant results ($p<0.05$) between groups are marked with an asterisk, results with $p<0.01$ are marked with two asterisks.

34. The Virtual Brain Ontology – Towards a Semantic Web for Brain Simulation

Christoph **Hüttl**[1,2], Leon **Stefanovski**[1,2], Konstantin **Bülau**[1,2], Leon **Martin**[1,2], Rico André **Schmitt**[1,2], Julie **Courtiol** [1,2], Petra **Ritter**[1,2,3*]

[1]Berlin Institute of Health at Charité – Universitätsmedizin Berlin, Berlin, Germany

[2]Department of Neurology with Experimental Neurology, Brain Simulation Section, Charité – Universitätsmedizin Berlin, corporate member of Freie Universität Berlin and Humboldt-Universität zu Berlin, Berlin, Germany

[3]Bernstein Center for Computational Neuroscience Berlin, Berlin, Germany

*Corresponding Author: petra.ritter@bih-charite.de

INTRODUCTION/MOTIVATION

In the field of computational neuroscience, brain simulations with the neuroinformatics platform The Virtual Brain (TVB; www.thevirtualbrain.org) have proven to be a powerful tool both for deepening our understanding of neuronal mechanisms [1], as well as improving our capability to diagnose [2] and treat patients [3]. The employed mathematical models allow for the computation of patient-specific, individualized brain models, aiming for clinical hypothesis testing in silico [4]. The mathematical framework incorporates various local dynamic models of neural behavior, each characterized by numerous parameters governing their dynamics. But while this complexity allows for a wide range of applications, the systematic comparison between results from different models remains challenging. One potential solution is offered by highly structured knowledge representations as available in knowledge bases and ontologies, going back to Tim Berner-Lee's vision of a semantic web [5]. We therefore suggest a novel ontology incorporating both the mathematical and the biological framework of TVB and aiming to serve as a central knowledge hub for brain modelling and simulation with TVB.

METHODS

We have developed The Virtual Brain Ontology (TVB-O): the first knowledge representation that formalizes the mathematical framework at the core of TVB by annotating it in a hierarchically structured manner. Additionally, we have integrated the Gene Ontology (GO, [6]), a biological knowledge graph, into TVB-O. This was achieved using a semi-automatic approach reducing the 1,117,589 biological processes from GO to 215 biochemical pathways and electrophysiological processes that have a potential surrogate in brain modelling. These 215 processes were clustered by their function and linked to the relevant large-scale brain network model (BNM) components of TVB, i.e., model parameters and variables. As an additional function for interoperability, we have implemented full compatibility with the standardized XML-based language Low Entropy Model Specification language (LEMS, [7]) for defining BNMs succinctly.

RESULTS AND DISCUSSION

TVB-O is a central knowledge resource for brain modelling that provides standardization and information for over 370 parameters across 8 biological and 9 phenomenological models. The rich annotation of multimodal information in TVB-O ranges from synonyms, definitions, explanations and further resources over default values to biological surrogates of BNM components. This link between modelling parameters and biological processes is achieved by the annotation of 215 biological processes from GO. The relationship between entities is described by 43 newly defined properties, e.g., "is_coefficient_of".

As an example, we identified the process "positive regulation of neuronal action potential" from GO as electrophysiologically relevant and assigned it to the cluster "Excitation". One of the model parameters annotated to the cluster "Excitation" was the amplitude of the excitatory postsynaptic potential "A_JR" from the Jansen-Rit model [8].

TVB-O is providing its information in a mathematically rigorous machine- and human-readable way. It therefore allows for new inferences of relationships between biological entities and BNM components, based on formal logics and computational semantics. It is also capable of the automated generation of executable code for brain simulations with TVB using LEMS. Furthermore, a key feature of TVB-O is to provide suggestions for candidate mechanisms based on a protein, process or pathology of interest.

TVB-O is providing a novel integrated knowledge resource with a growing number of annotated neural models for the general neuroscientific community, from scientists to clinicians, that paves the way for a better understanding of the neuronal mechanisms involved in specific pathologies and aims to improve standardization and reproducibility in computational neuroscience.

Keywords: brain modelling, biological pathways, ontology, The Virtual Brain, semantic web, knowledge graphs, gene ontology

ACKNOWLEDGEMENTS

Computation of underlying data has been performed on the HPC for Research cluster of the Berlin Institute of Health. PR acknowledges support by EU H2020 Virtual Brain Cloud 826421, Human Brain Project SGA2 785907; Human Brain Project SGA3 945539, ERC Consolidator 683049; German Research Foundation SFB 1436 (project ID 425899996); SFB 1315 (project ID 327654276); SFB 936 (project ID 178316478; SFB-TRR 295 (project ID 424778381); SPP Computational Connectomics RI 2073/6-1, RI 2073/10-2, RI 2073/9-1; PHRASE Horizon EIC grant 101058240; Berlin Institute of Health & Foundation Charité, Johanna Quandt Excellence Initiative; ERAPerMed Pattern-Cog.

REFERENCES

[1] Schirner, M., McIntosh, A. R., Jirsa, V., Deco, G., & Ritter, P. (2018). Inferring multi-scale neural mechanisms with brain network modelling. eLife, 7, e28927. doi:10.7554/eLife.28927

[2] Triebkorn, P., Stefanovski, L., Dhindsa, K., Diaz-Cortes, M. A., Bey, P., Bülau, K., . . . Ritter, P. (2022). Brain simulation augments machine-learning-based classification of dementia. Alzheimers Dement (N Y), 8(1), e12303. doi:10.1002/trc2.12303

[3] Meier, J. M., Perdikis, D., Blickensdörfer, A., Stefanovski, L., Liu, Q., Maith, O., . . . Ritter, P. (2022). Virtual deep brain stimulation: Multiscale co-simulation of a spiking basal ganglia model and a whole-brain mean-field model with The Virtual Brain. Exp Neurol, 354, 114111. doi:10.1016/j.expneurol.2022.114111

[4] Wang, H. E., Woodman, M., Triebkorn, P., Lemarechal, J. D., Jha, J., Dollomaja, B., . . . Jirsa, V. (2023). Delineating epileptogenic networks using brain imaging data and personalized modeling in drug-resistant epilepsy. Sci Transl Med, 15(680), eabp8982. doi:10.1126/scitranslmed.abp8982

[5] Berners-Lee, T. I. M., Hendler, J., & Lassila, O. R. A. (2001). THE SEMANTIC WEB. Scientific American, 284(5), 34-43. Retrieved from www.jstor.org/stable/26059207

[6] Gene Ontology Consortium. (2004). The Gene Ontology (GO) database and informatics resource. Nucleic acids research, 32(suppl_1), D258-D261.

[7] Cannon, R. C., Gleeson, P., Crook, S., Ganapathy, G., Marin, B., Piasini, E., & Silver, R. A. (2014). LEMS: a language for expressing complex biological models in concise and hierarchical form and its use in underpinning NeuroML 2.
Front Neuroinform, 8, 79. doi:10.3389/fninf.2014.00079

[8] Jansen, B. H., & Rit, V. G. (1995). Electroencephalogram and visual evoked potential generation in a mathematical model of coupled cortical columns. Biol Cybern, 73(4), 357-366.

35. Small changes in brain state affect the global cortical functional networks and how sensory inputs are processed

Elena Montagni[1*], Francesco Resta[1], Alessandro Scaglione[2], Giacomo Mazzamuto[2], Núria Tort-Colet[3], Alain Destexhe[3], Francesco Saverio Pavone[1,2,#], Anna Letizia Allegra Mascaro[1,4,#]

[1] European Laboratory for Non-Linear Spectroscopy (LENS), Sesto Fiorentino Italy;

[2] Department of Physics and Astronomy, University of Florence, Sesto Fiorentino Italy;

[3] Paris-Saclay University, CNRS, Institut des Neurosciences (NeuroPSI), Saclay, France;

[4] Neuroscience Institute, National Research Council, Pisa, Italy;[3 #]

Equal contribution

*montagni@lens.unifi.it

INTRODUCTION/MOTIVATION

Functional connectivity (FC) reflects the synchronization of neuronal activity among anatomically separated brain regions. The alteration of spontaneous and perturbed FC has been used to investigate the effects of the brain state on the functional cortical network, demonstrating how sensory responses observed in the neocortex are strongly influenced by changes in brain state[1]. These studies have been generally conducted via functional Magnetic Resonance Imaging (fMRI)[2], which is a measure of blood flow changes rather than neuronal activity, or by comparing awake state with just one anaesthetic condition[3]. Here we described the impact of four distinct brain states, generated with isoflurane anaesthesia, on large-scale spontaneous and perturbed FC in mice expressing fluorescent calcium indicator GCaMP6f in pyramidal neurons.

METHODS

We performed wide-field calcium imaging of the entire dorsal cortex of transgenic mice expressing GCaMP6f in excitatory neurons. Mice were anesthetized with isoflurane (3% for induction, 1–2% for maintenance) and placed in a stereotaxic apparatus (KOPF, model 1900). The skin and the periosteum were cleaned and removed. Bregma was signed with a black fine-tip pen. A custom-made aluminium head-bar placed behind lambda and the exposed skull were sealed using transparent dental cement (Super Bond C&B – Sun Medical). After the post-surgical recovery period (3 days), wide-field imaging was performed through the intact skull using a custom-made microscope.

The awake imaging records consisted by 50-60 minutes of imaging session in which both spontaneous (38 s-long, 5 repetitions) and perturbed activity (24 s-long, 30 repetitions) were recorded. Mice were also anesthetised by isoflurane to investigate three brain states: DEEP (1.71 ± 0.08 %), MEDIUM (1.49 ± 0.06 %) and LIGHT anaesthesia (1.32 ± 0.12 %). Deep and medium anaesthesia were recorded consecutively on the same imaging session per mouse, shifting from the higher isoflurane concentration to the lower. Stimulation was delivered to the left whiskers through a tubing system using an electrically gated pressure injector (Picospritzer III—Science Products). Whiskers were deflected ~1 cm in the rostro-caudal direction. A single stimulation trial consisted of 24 s designed as: 13 s rest, 1 s of stimulation with a blowing time of 60 ms, 10 s rest.

RESULTS AND DISCUSSION

Based on the level of isoflurane concentration, we initially classified four brain sates: (i) wakefulness, (ii) light, (iii) medium and (iv) deep anaesthesia. Then, we characterized and compared the network architecture and properties of both spontaneous and perturbed FC in the four brain states.

Our preliminary results indicate that light anaesthesia caused the most significant changes in spontaneous FC at both the global and the regional level when compared not only to deeper levels of anaesthesia but also to wakefulness. Instead, FC after sensory stimulation exhibited different properties only in awake and light anaesthesia while medium and deep anaesthesia results were comparable. Interestingly, the PCI (Perturbation Complexity Index) analysis of the perturbed activity showed instead a drop of the response complexity for deeper anaesthesia levels. Consequently, we performed a region-specific single-trial peak analysis, which revealed that medium and deep anaesthesia were characterized by a primary stereotyped early response followed by a more time-distributed late response, the probability of which was affected by the brain state. In fact, there were two activation peaks in the single-trial response, and the probability of this secondary response was lower in deep than in medium anaesthesia.

Keywords: wide-field imaging, whisker stimulation, in vivo, isoflurane, anaesthesia, functional connectivity

ACKNOWLEDGEMENTS

This research was supported by the European Union's Horizon 2020 Research and Innovation Framework Program under grant agreements 945539 (HBPSGA3). This research was supported by the EBRAINS research infrastructure, funded from the European Union's Horizon 2020 Framework Programme for Research and Innovation under the Specific Grant Agreement No. 945539 (Human Brain Project SGA3). This research was also supported by the Italian Ministry for Education, University, and Research in the framework of the Advance Lightsheet Microscopy Italian Mode of Euro-bioimaging ERIC.

REFERENCES

[1] Tomokazu Tsurugizawa, Daisuke Yoshimaru. Impact of anesthesia on static and dynamic functional connectivity in mice. NeuroImage 241 (2021) https://doi.org/10.1016/j.neuroimage.2021.118413.

[2] Bukhari, Q., Schroeter, A. & Rudin, M. Increasing isoflurane dose reduces homotopic correlation and functional segregation of brain networks in mice as revealed by resting-state fMRI. Sci Rep 8, 10591 (2018). https://doi.org/10.1038/s41598-018-28766-3.

[3] Jaakko Paasonen, Petteri Stenroos, Raimo A. Salo, Vesa Kiviniemi, Olli Gröhn. Functional connectivity under six anesthesia protocols and the awake condition in rat brain. NeuroImage 172 (2018). https://doi.org/10.1016/j.neuroimage.2018.01.014.

36. Interactively exploring metadata with Beaverdam

Heather More[1,2,3,4,*], Volker Hofmann[4], Stefan Sandfeld[4], Sonja Grün[1,2,3,5], Michael Denker[1,2,3]

[1]Institute of Neuroscience and Medicine (INM-6), Jülich Research Centre, Jülich, Germany
[2]Institute for Advanced Simulation (IAS-6), Jülich Research Centre, Jülich, Germany
[3]JARA-Institute Brain Structure-Function Relationships (INM-10), Jülich Research Centre, Jülich, Germany
[4]Institute for Advanced Simulation (IAS-9), Jülich Research Centre, Jülich, Germany
[5]Theoretical Systems Neurobiology, RWTH Aachen University, Aachen, Germany
* h.more@fz-juelich.de

INTRODUCTION/MOTIVATION

In most scientific disciplines, researchers increasingly rely on data from large numbers of experiments, often containing extensive metadata describing the context of each experiment's individual trials. However, it can be difficult or impossible for a scientist to obtain an overview of these vast quantities of information (e.g. [1]) and to identify sets of experiments based on criteria (e.g. to plan further analyses). Simple user interfaces to inspect metadata can help solve this problem, but scientists don't always have the time or experience to create such software themselves.

Here we present a prototype of our in-development software Beaverdam (Build, Explore, And Visualize ExpeRimental DAtabases of Metadata), which helps researchers interactively explore collections of metadata and summarize subsets of experiments.

METHODS

Beaverdam combines metadata from multiple experiments into a database, then builds an user interface with forms showing options for selection criteria, graphs showing a high-level overview, and a table showing details of each experiment. Users can explore their experiments by interacting with the forms and graphs; visualizations update on the fly as selection criteria change.

We use the programming language Python to develop Beaverdam, and the database system MongoDB for creating and working with unstructured databases. Using unstructured databases enables multiple metadata files to be stored and accessed in a single database even if they don't contain identical fields – this allows metadata from experiments which share a subset of parameters to be compared. Beaverdam currently uses Plotly Dash to build its user interface, which users interact with in a web browser.

Because Beaverdam visualizes results in a web interface, it is suitable for use at multiple scales – individual researchers can build and access a database locally on their laptop, or a research group can maintain a joint database which members access remotely.

RESULTS AND DISCUSSION

While we envision Beaverdam to ultimately be useful for all research disciplines, we are currently testing i t on metadata from multi-electrode recordings from the brains of macaque monkeys performing delayed reaching tasks [2,3]. In this project, each individual recording is accompanied by metadata describing over 1,000 aspects of the experimental setup and procedure. This metadata is stored in odML format [4,5]. Each experiment is rigorously described, but the sheer amount of metadata is too complex to be used as-is. Beaverdam condenses the metadata to show only information chosen by the user.

In future, we plan to integrate support into Beaverdam for additional metadata standards that are commonly used, such as the BIDS metadata structure [6], the openMINDS metadata models [7], and triplestore databases. Not only will this make using Beaverdam easy for researchers using these frameworks for their own metadata, supporting the openMINDS models and additional backends (e.g. triplestores) would give scientists more ways to explore metadata from EBRAINS datasets and knowledge graphs.

By condensing large sets of metadata and making them easy to explore, we envision that Beaverdam will help scientists gain insights into their own work and discover related works of others.

Keywords: database, metadata, software, visualization, neuroscience, Python, MongoDB, EBRAINS, openMINDS, knowledge graph

ACKNOWLEDGEMENTS

This work is supported by the Helmholtz Metadata Collaboration (HMC), EU Grant 945539 (HBP SGA3), and the NRW network iBehave (NW21-049).

REFERENCES

[1] Zehl L, Jaillet F, Stoewer A et al. Handling Metadata in a Neurophysiology Laboratory. *Front. Neuroinf.* 2016;10. doi: 10.3389/fninf.2016.00026

[2] Brochier T, Zehl L, Hao Y et al. Massively parallel recordings in macaque motor cortex during an instructed delayed reach-to-grasp task. *Sci. Data.* 2018;5(1). doi: 10.1038/sdata.2018.55

[3] Dataset available on EBRAINS knowledge graph: https://search.kg.ebrains.eu/instances/b23a87a2-3079- 46ff-9649-d6a521952e4a

[4] Grewe J, Wachtler T, Benda J. A bottom-up approach to data annotation in neurophysiology. *Front. Neuroinf.* 2011;5. doi: 10.3389/fninf.2011.00016

[5] Sprenger J, Zehl L, Pick J et al. odMLtables: A user-friendly approach for managing metadata of neurophysiological experiments. *Front. Neuroinf.* 2019;13. doi: 10.3389/fninf.2019.00062

[6] Gorgolewski KJ, Auer T, Calhoun VD et al. The brain imaging data structure, a format for organizing and describing outputs of neuroimaging experiments. *Sci. Data.* 2016;3(1). doi: 10.1038/sdata.2016.44

[7] openMINDS (RRID:SCR_023173)

37. MATLAB user interface for openMINDS metadata registration

Eivind Hennestad[1*], Lyuba Zehl[2], Jan Bjålie[1]

[1] Department of Molecular Medicine, University of Oslo, Oslo, Norway
[2] Institute of Neuroscience and Medicine (INM-1), Research Centre Jülich, Jülich, Germany

*eivihe@uio.no

INTRODUCTION

The rapid growth in scientific data volume highlights the urgency and importance of data discoverability. To this end, openMINDS delivers a comprehensive metadata framework for neuroscience data which has been successfully implemented on the EBRAINS Knowledge Graph. However, the comprehensive nature of the models, with highly interlinked schemas and different levels of detail, also imply that there is a steep learning curve for anyone who wishes to apply the models to their data.

This project presents a MATLAB toolbox with user-friendly interfaces that facilitates the creation and viewing of openMINDS metadata, enabling researchers who already use MATLAB to integrate the metadata registration into their experimental workflows. By bringing the descriptive nature of openMINDS into the experimental setting, the toolbox can serve as a digital lab book that increase the FAIRness of datasets, and eventually make it easier to share data through services that supports openMINDS.

METHODS

The toolbox is based on the translation of openMINDS schemas into MATLAB class definitions. All the openMINDS schemas are therefore available as classes which the user can use to create metadata instances in the form of objects. The objects can be added to a metadata collection where objects are linked together in a graph structure. The user can create and explore instances directly on the command line or write scripts where instances are created based on experimental parameters.

There is also graphical user interface consisting of a multi-page application where the user can choose to visualize the metadata collection in a tabular- or a graph-based view. Menus provide access to all the openMINDS schemas for easy creation of new instances. If a user chooses to create a new instance of a schema, an input form appears where the user can enter information for all the fields defined by that schema. Instances can later be edited either from the input form, or from the table view.

Lastly the metadata collection can at any point be converted to the JSON-LD format which is the current requirement when sharing metadata in a graph database like the EBRAINS Knowledge Graph.

RESULTS AND DISCUSSION

MATLAB is a programming and computational platform which is widely used by neuroscientists to process and analyze data, and the presented toolbox adds the openMINDS framework into the arsenal of open-source neuroscience toolkits. The object-oriented nature of the toolbox provides advantages such as modular and functional access to all the model schemas, built-in validation, in-place documentation, and ease of maintenance through the ability to regenerate class definitions from openMINDS source code.

The toolbox provides a plug-and-play like entry point to openMINDS metadata, and researchers with no prior knowledge can start using the metadata models without diving into the technical complexities of openMINDS schemas. By letting researchers easily use openMINDS models in their experiments and data workflows, this toolbox may serve as a digital lab book that help researchers better organize their data and metadata and thereby also increase the FAIRness and discoverability of their datasets.

For users that do not have a MATLAB license, the toolbox can be compiled into a standalone executable application (scripting not available) or run through MATLAB Online, a cloud-based computing platform which provides 20 hours of free use per month.

In summary, the openMINDS MATLAB toolbox provides easy access to the full set of openMINDS metadata models, can serve as a digital lab book, provide extra organization and structure to a dataset, and ultimately, facilitate and accelerate the submission process when sharing data to a service which supports openMINDS, like the EBRAINS Knowledge Graph.

ACKNOWLEDGEMENTS

This project has received funding from the European Union's Horizon 2020 Framework Program for Research and Innovation under the Specific Grant Agreement No. 945539 (Human Brain Project SGA3)

38. Hessian-driven spine neck tracing boosts SENPAI segmentation on super-resolution microscopy images

Ester Bruno[1, 2*], Simone Cauzzo[1], Alejandro Luis Callara[1,2], Lydia Danglot[3], Arti Ahluwalia[1,2], Chiara Magliaro[1,2], Nicola Vanello[1,2]

[1]Research Center "E. Piaggio", University of Pisa, Pisa, Italy [2]Dipartimento di Ingegneria dell'Informazione, University of Pisa, Pisa, Italy

[3]Institut de Psychiatrie et Neurosciences de Paris, INSERM 1266, Paris, France

*ester.bruno@phd.unipi.it

INTRODUCTION/MOTIVATION

Dendritic spines are neural protrusions implied in synaptic function [1]-[2], whose morphology and topology result altered in neuropathies such as Alzheimer and autism spectrum [3]-[4]. However, the detection of spine necks, i.e., the thin connections of the head of the spine to the dendrite shaft, is challenged by optical resolution limits [5]. As a result, spines appear disconnected from the dendrite body. In this context, gold-standard manual segmentation is outstandingly time consuming, motivating the need for automatic solutions. Nonetheless, available neck-tracing algorithms either require large databases to train deep neural networks [6] or fail in detecting spine necks using global metrics of image intensity, since spine necks are characterized by lower signal- to-noise ratio [7]. This sensitivity can be attenuated by relying on the eigenvalue analysis of the Hessian matrix, already adopted for detecting tubular structures [8]. In this scenario, we present a new neck tracing method for reconnecting spines with dendrites. We embed it in the SENPAI framework, which employs Hessian topological information, morphological reconstruction and watershed transform to segment and parcellate neuronal trees and spines [9]. Our neck tracing similarly exploits local Hessian eigenvalue analysis to define iterative steps along the trace. The relevance of the trace initialization step is explored, comparing different approaches.

METHODS

A 3D stack of images of murine Purkinje cells acquired using a STED microscope equipped with 93X objective was processed to identify 5 dendritic portions using SENPAI (SENPAI segmentation, SS). The same portions were also segmented manually (MS) using ManSegTool [10]

The neck tracing algorithm works in two phases (Fig. 1):

- The initialization defines the first voxel of the trace among those composing the outer border (OB) of the disconnected spine. We tested 3 criteria: C1) the voxel in OB closest to the dendrite; C2) the maximum intensity voxel within OB; C3) the voxel in OB intersected by the principal axis of the spine, placed on the side of OB closest to the dendrite.

- The path-finding consists of a one-voxel step procedure starting from the voxel v_1 identified in Phase I. Eigenvalues of the Hessian matrix encode the information on second-order intensity variability. Within a tubular structure, the direction parallel to the main axis is associated with the smallest eigenvalue (Fig. 1). Starting from v_1 (green in Fig. 1), voxel v_2 is chosen in its 26-neighborhood as the one being intersected by the eigenvector associated to the smallest eigenvalue (in absolute value; golden arrow in Fig. 1). The procedure is iterated on each v_i, to define v_{i+1}, until the trace meets the dendrite.

A preliminary validation of this approach is performed on spines that appear detached from the dendrite branch after SS. We compare the results achieved with the three initialization strategies defining d_{MS} the average Euclidean distance from the edge of the MS across the voxels of the considered neck.

RESULTS AND DISCUSSION

In fig. 2A 3D reconstructions of 3 dendrite segments along with the spines are shown. SS and MS segmentations are shown in different colors. The majority of the spines were connected with the proper section of the dendrite. Fig. 2B shows the quantitative evaluation for the 3 initialization criteria. Regardless of initialization, our approach averagely reduces by one third the number of spines left disconnected, with approximately all necks showing d_{MS}<3. C2 is the criterion providing the best results, with d_{MS}<3 for the 97% of necks and d_{MS}≤1 for the 41.2% of them. Being embedded in the SENPAI algorithm, the Hessian-based neck tracing enriches an automatic neuron- reconstruction suite that fulfils the need for the characterization of arborization complexity and spine topology and morphology. Future developments should focus on providing a less local definition of maximum intensity.

Keywords: 3D STED, automatic segmentation, dendritic spines, neck tracing.

ACKNOWLEDGEMENTS

This work was supported by the FLAG-ERA JTC 2019 project SENSEI (Partnering Project of the Human Brain Project). This publication was produced with the co-funding European Union - Next Generation EU, in the context of The National Recovery and Resilience Plan, Investment 1.5 Ecosystems of Innovation, Project Tus cany Health Ecosystem (THE), CUP: I53C22000780001.

REFERENCES

[1] Sala C, Segal M (2014): Dendritic Spines: The Locus of Structural and Functional Plasticity. Physiol Rev 94:141–188. doi: 10.1152/physrev.00012.2013

[2] Citri A, Malenka RC (2008): Synaptic Plasticity: Multiple Forms, Functions, and Mechanisms. Neuropsychopharmacology 33:18–41. doi: 10.1038/sj.npp.1301559

[3| Spires TL (2005): Dendritic Spine Abnormalities in Amyloid Precursor Protein Transgenic Mice Demonstrated by Gene Transfer and Intravital Multiphoton Microscopy. J Neurosci 25:7278–7287. doi: 10.1523/JNEUROSCI.1879-05.2005

[4] Serrano-Pozo A, Frosch MP, Masliah E, Hyman BT (2011): Neuropathological Alterations in Alzheimer Disease. Cold Spring Harb Perspect Med 1:a006189–a006189. doi: 10.1101/cshperspect.a006189

[5] J. Son, S. Song, S. Lee, S. Chang, and M. Kim, "Morphological change tracking of dendritic spines based on structural features," *J. Microsc.*, vol. 241, no. 3, pp. 261–272, 2011

[6] I. Vidaurre-Gallart *et al.*, “A Deep Learning-Based Workflow for Dendritic Spine Segmentation,” *Front. Neuroanat.*, vol. 16, 2022. doi: 10.3389/fnana.2022.817903

[7] C. M. Weaver, P. R. Hof, S. L. Wearne, and W. B. Lindquist, “Automated Algorithms for Multiscale Morphometry of Neuronal Dendrites,” *Neural Comput.*, vol. 16, no. 7, pp. 1353–1383, 2004. doi: 10.1162/089976604323057425

[8] A. F. Frangi, W. J. Niessen, K. L. Vincken, and M. A. Viergever, “Multiscale vessel enhancement filtering,” 1998, pp. 130–137.

[9] S. Cauzzo, M. Basile, E. Bruno, A. L. Callara, L. Danglot, A. Ahluwalia, C. Magliaro, N. Vanello, "SENPAI: SEgmentation of Neurons using PArtial derivatives Information," A tool for neuronal segmentation from confocal microscopy using K-means and topological information", abstract and poster for the FENS Annual Forum (Paris, July 2022)

[10] Magliaro C, Callara AL, Vanello N, Ahluwalia A (2017): A Manual Segmentation Tool for Three-Dimensional Neuron Datasets. Front Neuroinform 11. doi: 10.3389/fninf.2017.00036

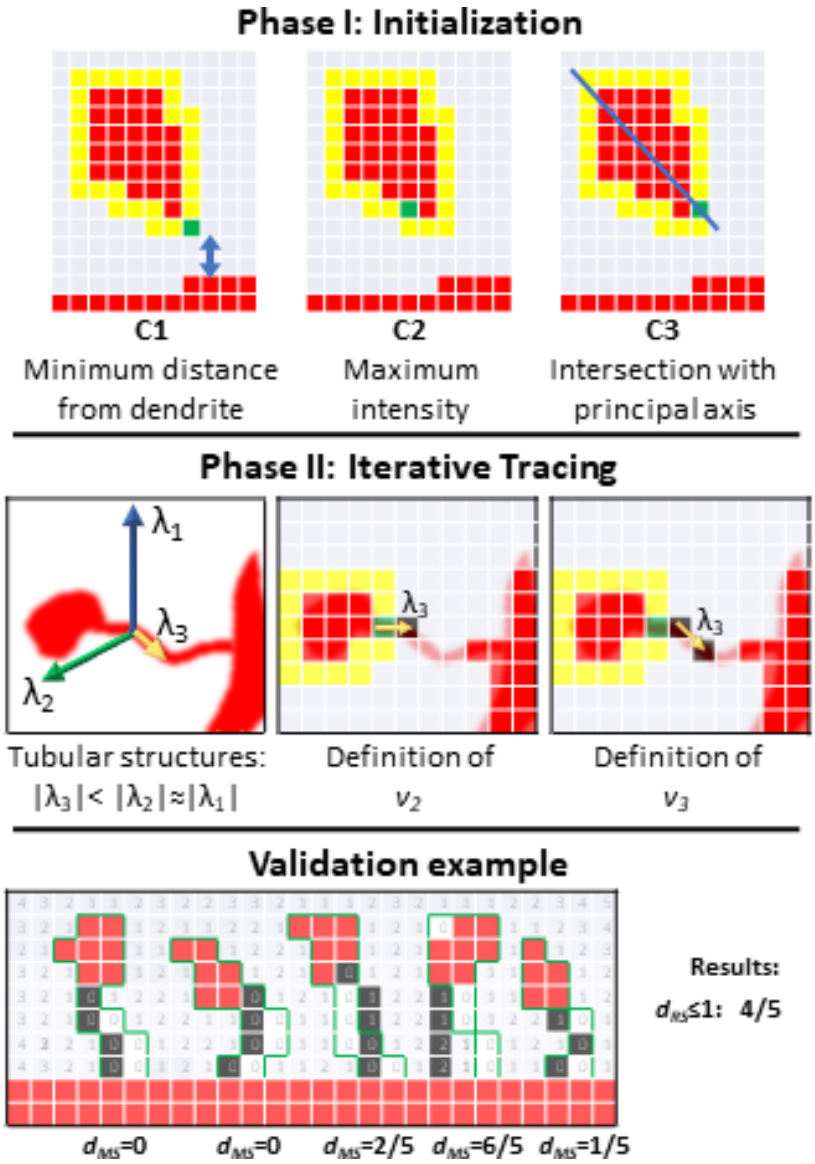

Fig. 1 *Schematization of the neck tracing approach. SS is marked in red, OB in yellow. Phase I) selection of the first voxel v_1 in the trace among those in OB, with the three tested criteria. Phase II) thanks to the properties of the Hessian matrix eigenvalues within tubular structures, the neck can be traced by 1) performing the eigenvalue analysis at voxel v_i; 2) defining v_{i+1} as the neighboring voxel intersected by the smallest eigenvector. Validation example) (simplified in a 2D case): necks (black) connecting disconnected clusters of OS (red) are compared against MS (white with green borders) in terms of average Euclidian distances. Distance values in cells are rounded to the highest integer.*

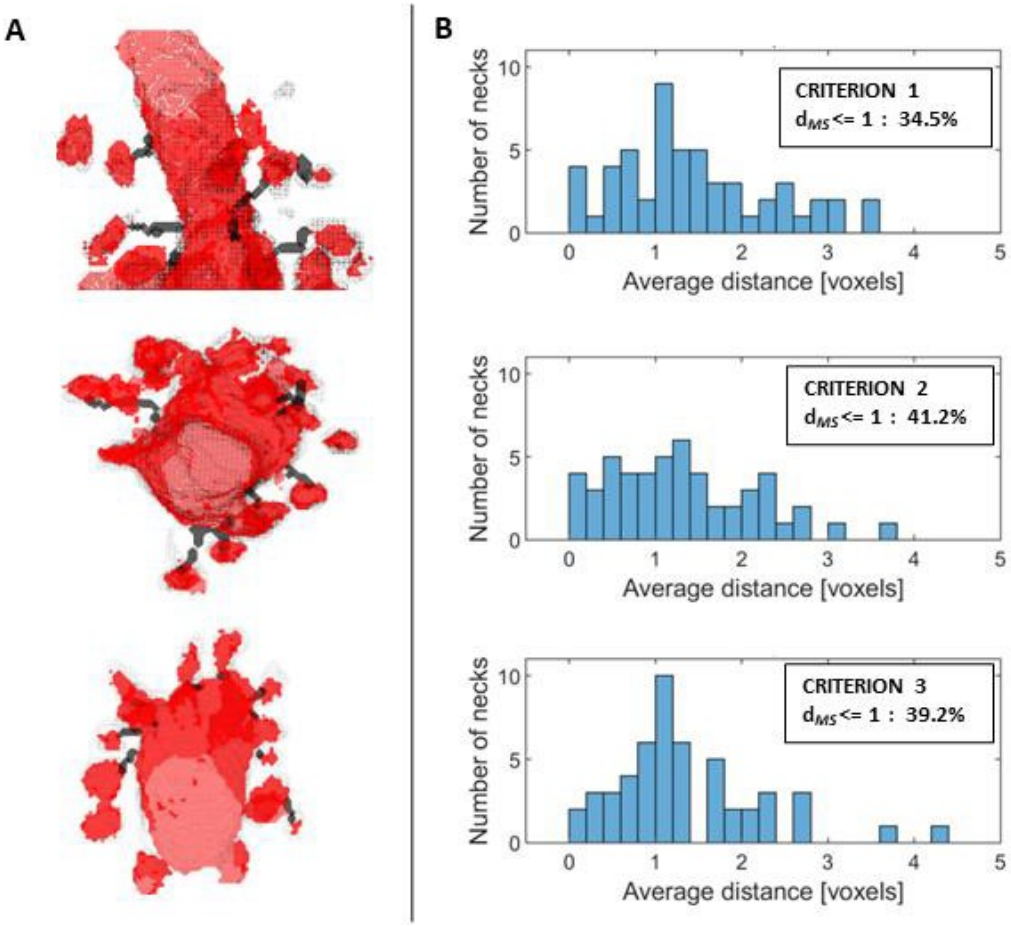

Fig. 2 . **A.** Three examples of necks reconstructed by the algorithm (in black) overlaying SS (red) and MS (gray). **B**. Evaluation of the three initialization approaches of phase I in terms of average distance from MS

39. Advanced magnetic resonance imaging to study brain alterations in people infected with SARS-COV-2

Antonio Ricciardi[1,*], Fulvia Palesi[2,3], Rachel L. Batterham[4,5], Claudia A. M. Gandini Wheeler-Kingshott[1,2,3,6]

1. NMR Research Unit, Queen Square MS Centre, Department of Neuroinflammation, UCL Queen Square Institute of Neurology, Faculty of Brain Sciences, University College London (UCL), London, United Kingdom.
2. Department of Brain & Behavioural Sciences, University of Pavia, Pavia, Italy.
3. Brain Connectivity Center Research Department, IRCCS Mondino Foundation, Pavia, Italy.
4. Centre for Obesity Research, Department of Medicine, University College London, London, United Kingdom.
5. National Institute of Health Research, Biomedical Research Centre at UCLH and UCL, London, United Kingdom.
6. On behalf of the MODEL-COV study team.

*antonio.ricciardi@ucl.ac.uk

INTRODUCTION

SARS-CoV-2 has been associated with neurological diseases, particularly vascular disorders and altered mental status[1,2], and a link between neurological symptoms and the virus induced cytokine storm has been shown[3,4]. People who experienced relatively mild COVID-19 also report persistent symptoms e.g., fatigue, brain fog, anosmia and autonomic dysfunction such as orthostatic hypotension and breathing pattern disorder. These persistent symptoms in otherwise healthy subjects are associated with what has now been defined as “long COVID syndrome”.

The evolving landscape of COVID-19 neurological manifestations requires detailed population-level studies in order to understand the extent of COVID-19 on the brain. Here we report results from a multi-modal quantitative MRI protocol assessing brain alterations in people who have a history of (long) COVID, but were not hospitalised.

METHODS

62 subjects have been recruited between June 2020 and March 2021, of which:

- 18 healthy controls (HC, 9M, 39±11y);
- 8 with persistent anosmia (COVID-P, 1M, 52±12y);
- 20 with recovered anosmia: 10 age-matched with the COVID-PA group (COVID-R, 1M, 51±9y), and 10 younger (yCOVID-R, 4M, 28±2y)
- 16 with no long COVID symptoms (COVID, 3M, 38±9y).

A Philips Ingenia CX 3T was used with a 32-channel head coil. The 1h15" MRI protocol included:

- FLAIR (1×1×1mm^3; TE/TR=266ms/4.8s, TI=1.65s, FA=40°; 3'26") for lesion segmentation/filling[5].
- 3DT1 (1×1×1mm^3; TE/TR=3.1/6.9ms, FA=8°; 1'55") for tissue segmentation[6], producing masks of white matter (WM), cortical/deep grey matter (cGM/dGM) and brain stem (BS).
- fMRI (3×3×3mm^3; TE/TR=25ms/4s, FA=90°, scans=100; 6'47");
- pCASL (3×3×3mm^3; TE/TR=12.1/4266ms, FA=90°, 360 scans; 8') to measure cerebral blood flow (CBF);
- DWI (2×2×2mm^3; TE/TR=96/6287ms, FA=90°, b-values={0, 1000, 2800, 2000}, directions={4, 20, 36, 20}; 9'41"); b0 with inverse phase encoding was also acquired. DTI, DKI and NODDI[7] were performed on the DWI, obtaining maps of mean diffusivity (MD), fractional anisotropy (FA), mean kurtosis (MK), orientation dispersion index (ODI), neurite density index (NDI) and isotropic component volume fraction (Viso).
- IR (2×2×2mm^3; TE/TR=59ms/15s, TI/dTI=[50-1910]/120ms, 12 TIs, FA=90°; 4'28") for T1 mapping[8].
- qMT (2×2×2mm^3; TE/TR=96/6287ms, FA=90°, MT-offset={96(x2), 13.7(x5), 3(x5)}MHz, MT-FAs={100(x2), 890(x5), 593(x5)}°; 4'57") for bound-pool fraction (BPF) and quantitative T2 of the bound component (T2b) mapping[8].
- B1-DAM (2×2×2mm^3; TE/TR=59ms/15s, FA=120/60°; 1') and B1-AFI (4×4×4mm^3; TE=2.2ms, TR=30/180ms, FA=60°; 1'57") for B1 mapping via dual angle method[9] and actual flip angle method[10];
- SPGR-multiTE (1×1×1mm^3; TE/dTE=[2.3-25.4]/3.3ms, 8 TEs, TR=29ms, FA=24°; 4'6") and SPGR (1×1×1mm^3; TE/TR=2.3/29ms, FA=4°; 4'6"), for T2* and macromolecular tissue volume (MTV) mapping[10], and quantitative susceptibility mapping (QSM).
- MRS (20×20×20mm^3; TE/TR=35ms/2s, FA=90°; 4'52") for quantification of metabolite concentration.

DWI, IR, qMT and B1-DAM scans underwent unified pre-processing[10] involving noise, susceptibility distortion, and eddy current correction. B1-DAM and B1-AFI were used for B1 correction on qMT and SPGR, respectively. Approximated T2 maps were calculated from exponential fitting on T2-weighted signal from IR fitting (short TE) and b0 (long TE).

Exploratory statistical assessment of differences between groups was performed via linear regression, uncorrected for multiple comparisons, with age and gender as covariates.

RESULTS AND DISCUSSION

An overview of the extracted maps is shown in Figure 1. Statistically significant differences in regional metrics between groups are reported in Figure 2.

Results indicate the presence of neurological alterations in people previously infected by the SARS-COV-2 virus with respect to HC. These changes were particularly prominent in people with persistent anosmia, including biomarkers of inflammation, iron and myelin alterations.
The possibility of iron overload and demyelination should therefore be further explored. This protocol is now being run as part of the MODEL-COV study on long COVID.

Keywords: COVID-19, anosmia, multimodal, MRI, susceptibility, spectroscopy, functional, diffusion, myelin, iron.

ACKNOWLEDGEMENTS

We thank all the people involved in this study, in alphabetic order:

Daniel C. Alexander, Frederik Barkhof, Marco Battiston, Michael Brightman, Gloria Castellazzi, Olga Ciccarelli, Sara Collorone, Xavier Golay, Louis Grandjean, Francesco Grussu, Yael Hacohen, Baris Kanber, Anita Karsa, Janine Makaronidis, Jim McStravick, James McStravick, Geoff J. M. Parker, Ferran Prados, Rebecca Samson, Madiha Shatila, Karin Shmueli, Bhavana S. Solanky, Jonathan Stutters, Carmen Tur, Jed Wingrove, and Marios C. Yiannakas from UCL; Egidio U. D'Angelo, Elena Grosso, Federico Manai, Anita Monteverdi, and Nicoló Rolandi from University of Pavia.

This study was funded by the H2020 Research and Innovation Action Grants Human Brain Project 945539 (SGA3), WP1 T1.18.

REFERENCES

1. Baig, A.M., 2022. Counting the neurological cost of COVID-19. Nature Reviews Neurology, 18(1), pp.5-6.
2. Ahmed, J.O., Ahmed, S.A., Hassan, M.N., Kakamad, F.H., Salih, R.Q., Abdulla, B.A., Fattah, F.H.R., Mohammed, S.H., Ali, R.K. and Salih, A.M., 2022. Post COVID-19 neurological complications; a meta-analysis. Annals of Medicine and Surgery, p.103440.
3. De Virgiliis, F. and Di Giovanni, S., 2020. Lung innervation in the eye of a cytokine storm: neuroimmune interactions and COVID-19. *Nature Reviews Neurology*, *16*(11), pp.645-652.
4. Espíndola, O.M., Gomes, Y.C., Brandão, C.O., Torres, R.C., Siqueira, M., Soares, C.N., Lima, M.A.S., Leite, A.C.C., Venturotti, C.O., Carvalho, A.J.C. and Torezani, G., 2021. Inflammatory cytokine patterns associated with neurological diseases in coronavirus disease 2019. *Annals of Neurology*, *89*(5), pp.1041-1045.
5. Prados, F., Cardoso, M.J., Kanber, B., Ciccarelli, O., Kapoor, R., Wheeler-Kingshott, C.A.G. and Ourselin, S., 2016. A multi-time-point modality-agnostic patch-based method for lesion filling in multiple sclerosis. *Neuroimage*, *139*, pp.376-384.

6. Cardoso, M.J., Modat, M., Wolz, R., Melbourne, A., Cash, D., Rueckert, D. and Ourselin, S., 2015. Geodesic information flows: spatially-variant graphs and their application to segmentation and fusion. *IEEE transactions on medical imaging*, *34*(9), pp.1976-1988.
7. Zhang, H., Schneider, T., Wheeler-Kingshott, C.A. and Alexander, D.C., 2012. NODDI: practical in vivo neurite orientation dispersion and density imaging of the human brain. *Neuroimage*, *61*(4), pp.1000-1016.
8. Battiston, M., Schneider, T., Grussu, F., Yiannakas, M.C., Prados, F., De Angelis, F., Gandini Wheeler-Kingshott, C.A. and Samson, R.S., 2019. Fast bound pool fraction mapping via steady-state magnetization transfer saturation using single-shot EPI. *Magnetic Resonance in Medicine*, *82*(3), pp.1025-1040.
9. Boudreau, M., Tardif, C.L., Stikov, N., Sled, J.G., Lee, W. and Pike, G.B., 2017. B1 mapping for bias-correction in quantitative T1 imaging of the brain at 3T using standard pulse sequences. *Journal of magnetic resonance imaging*, *46*(6), pp.1673- 1682.
10. Grussu, F., Battiston, M., Veraart, J., Schneider, T., Cohen-Adad, J., Shepherd, T.M., Alexander, D.C., Fieremans, E., Novikov, D.S. and Wheeler-Kingshott, C.A.G., 2020. Multi-parametric quantitative in vivo spinal cord MRI with unified signal readout and image denoising. *Neuroimage*, *217*, p.116884.

Figures

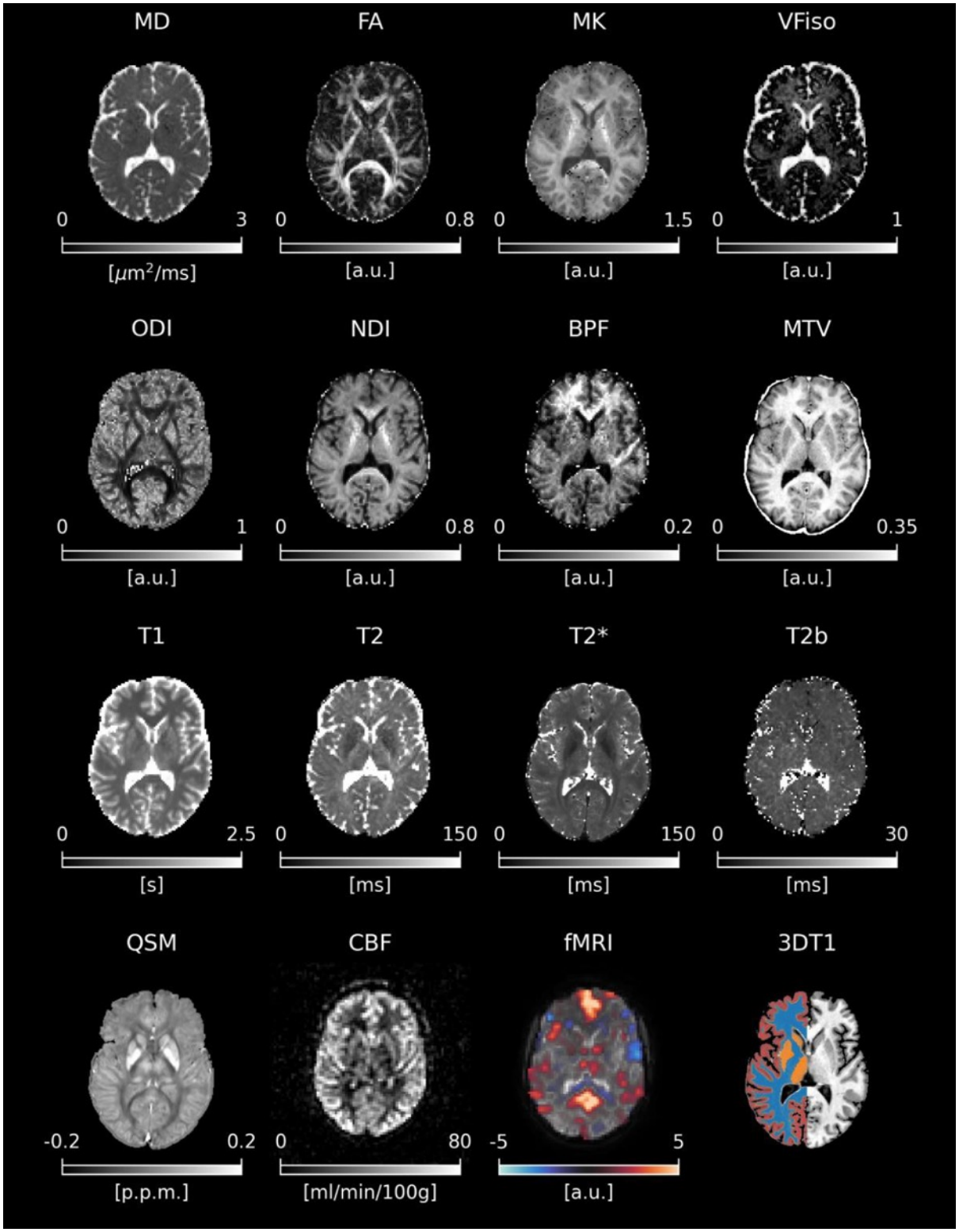

Figure 1. Overview of all the quantitative maps extracted from the multi-modal MRI protocol.

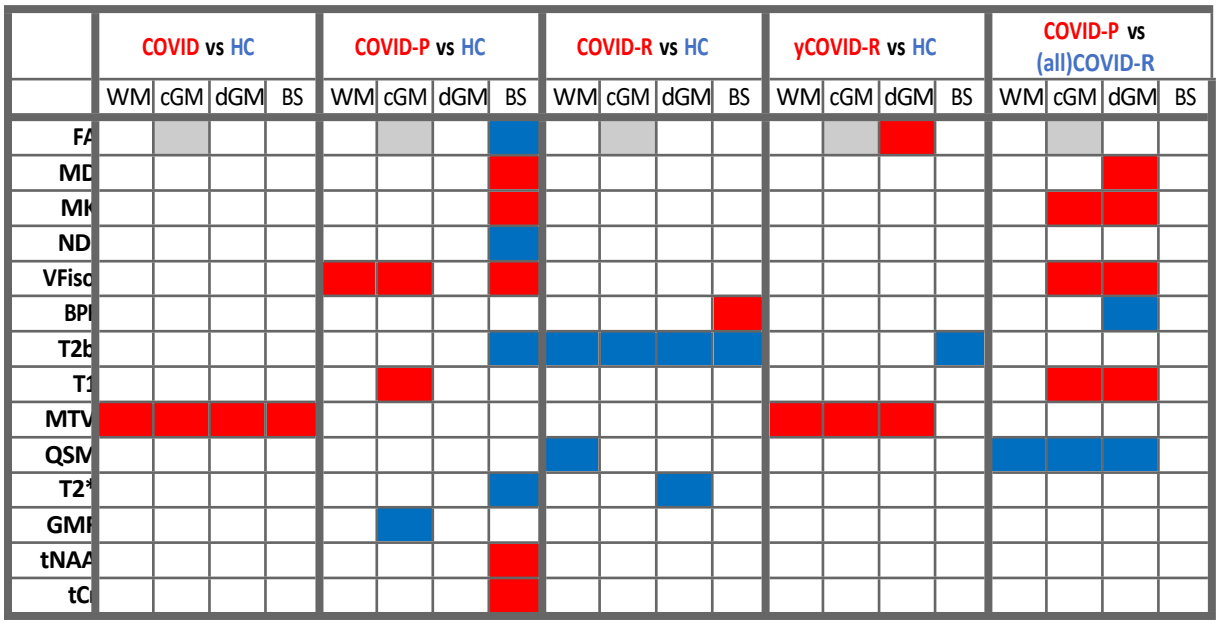

Figure 2. Summary of the significant differences between groups. Red indicates higher scores in the first group, blue indicates higher scores in the second group. FA in the cortex was not considered because not physiologically meaningful. *GMF*: grey matter volume fraction from tissue segmentation; *tNAA* and *tCr*: total N-acetylaspartate and creatine from MRS.

40. Investigating cross-modal contextual effects in human somatosensory cortex with laminar fMRI

Clement Abbatecola[1,2], Lucy S. Petro[1,2], Yulia Lazarova[1,2], A. Tyler Morgan[3], Robert N.S. Sachdev[4], Matthew E. Larkum[4], Lars Muckli[1,2]

[1]Centre for Cognitive Neuroimaging, School of Psychology and Neuroscience, College of Medical, Veterinary and Life Sciences, University of Glasgow, Glasgow, United Kingdom, G12 8QB.
[2]Imaging Centre for Excellence, Queen Elizabeth University Hospital, University of Glasgow, G51 4LB.
[3]Section on Functional Imaging Methods, National Institute of Mental Health, Bethesda, MD 20817, USA.
[4]Neurocure Center for Excellence, Charité Universitätsmedizin Berlin & Humboldt Universität, Berlin, Germany

INTRODUCTION/MOTIVATION

Sensory systems influence one another via cortical feedback and top-down pathways, even at early processing stages. Feedback pathways carry predictions of sensory information based on our internal models learned from prior sensory experiences. Unimodal visual input leads to meaningful sensory representations in the primary somatosensory cortex (S1) in humans (Smith & Goodale, 2013). Predictive processing theories suggest that sensory representations in early sensory cortices following unimodal sensory stimulation are driven by previously formed associative links between the different sensory properties of the stimuli e.g. the visual and haptic experiences associated with a phone. Although the literature indicates the existence of unique visual signatures in S1 due to learned sensory associations (Zhou & Fuster, 2000; Smith & Goodale, 2013), it is unknown if the effects observed in S1 are directly due to prior multi-sensory experience. Here, we investigated how learning through visual- haptic interactions with novel objects influences subsequent neural representations in S1 during unimodal visual stimulation.

METHODS

We divided participants into two groups, either with or without visual-haptic experience. Only the visual-haptic experience group explored two unfamiliar 3D printed objects ("smoothie" and "cubie") visually and haptically, focusing on the object's shape and tactile properties prior to the fMRI experiment. During scanning, images of 4 objects were shown: a hairbrush, mug, "smoothie", "cubie", fig 1). We conducted 3T MRI scanning (N= 10, block-design EPI sequence: 19 slices, TR=1s, TE=20ms, 2x2x2mm) at the CCNi (Glasgow, Siemens Tim Trio), and 7T fMRI scanning at ICE (N = 5, Glasgow, Siemens Magnetom Terra). In 7T MRI, we recorded an anatomical scan (MP2RAGE T1-weighted), a finger tapping localiser scan to identity the cortical representation of each finger in S1 (330 volumes) and 3 functional runs of the main experiment (252 volumes, T2*-weighted gradient echo EPI, with a multiband factor of 2, an echo time (TE) of 26ms, 54 slices with a matrix size of 186 by 186, isotropic resolution 0.8mm, interslice time of 37ms, 2000ms repetition time (TR), and a flip angle of 70 degrees). For functional scans, data were recorded within a slab positioned over the primary and secondary somatosensory cortices, and the motor cortex. During the main functional runs, subjects viewed images of the four objects, presented for 400ms on/off, in a pseudorandom order. Subjects were required to maintain central fixation and passively view the images.

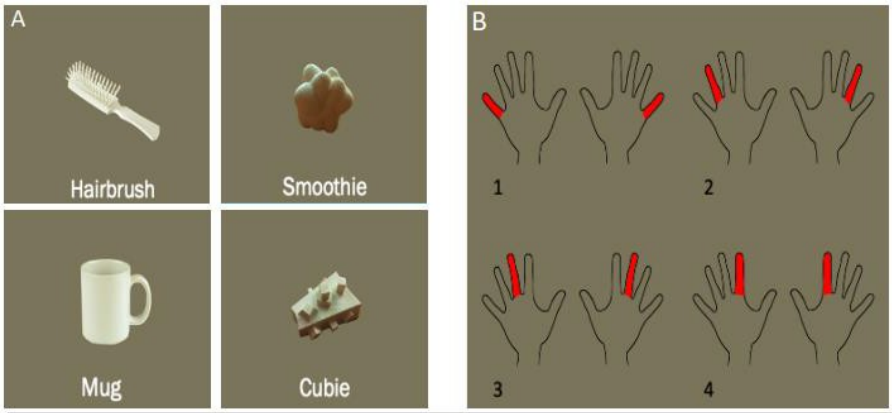

Figure 1: (A) 4 example stimuli presented to participant, 2 familiar ("hairbrush" + "mug"), and 2 abstract unfamiliar objects ("cubie" + "smoothie"). **(B)** Example of stimuli presented for localiser scan, labels 1 – 4 identify "Fingers 1-4" respectively. Each numbered stimulus was presented individually to the participant during the scan.

RESULTS AND DISCUSSION

We investigated whether prior visual-haptic experience with novel objects induced cross-modal contextual effects in S1 even during unimodal visual stimulation. As such, we hypothesised that we would be able to discriminate neuronal representations to unfamiliar objects in response to images of those objects, more so in the participant group with visual-haptic experience. In our 3T data, we used a linear mixed-effects analysis to test the main effects of group type (visual haptic-experience or no visual-haptic experience) and object type (between-category or within-category object comparison). We found preliminary evidence that discriminating between the brain responses was slightly better in the visual-haptic experience group than in the group without visual-haptic experience. Preliminary 7T analysis revealed no content-specific response to visual stimuli in S1 by using a univariate General Linear Model approach, and we are now testing for laminar-specific contextual modulations. We hypothesize that contextual effects might be limited to superficial layers of S1, in line with evidence in mice showing that perirhinal input to layer 1 of S1 modulates learning (Doron et al., 2020).

Keywords: fMRI, cortical layers, somatosensory cortex, cortical feedback processing, internal models, learning

ACKNOWLEDGEMENTS

This project has received funding from the European Union's Horizon 2020 Framework Programme for Research and Innovation under the Specific Grant Agreement No. 720270, 785907 and 945539 (Human Brain Project SGA1, SGA2 and SGA3).

REFERENCES

[1] Zhou, Y. D., & Fuster, J. M. (2000). Visuo-tactile cross-modal associations in cortical somatosensory cells. Proceedings of the National Academy of Sciences, 97(17), 9777-9782.

[2] Smith, F. W., & Goodale, M. A. (2015). Decoding visual object categories in early somatosensory cortex. Cerebral cortex, 25(4), 1020-1031.

[3| Doron, G., Shin, J. N., Takahashi, N., Drüke, M., Bocklisch, C., Skenderi, S., ... & Larkum, M. E. (2020). Perirhinal input to neocortical layer 1 controls learning. Science, 370(6523), eaaz3136.

41. openMINDS extensions for in-depth graph database descriptions of electrophysiology experiments

Peyman Najafi[1]*, Ulrike Schlegel[2], Andrew P. Davison[1], Lyuba Zehl[3]

1 Paris-Saclay Institute of Neuroscience, CNRS/Université Paris-Saclay, Saclay, France

2 Neural Systems Laboratory, Institute for Basic Medical Sciences, University of Oslo, Oslo, Norway

3 Institute for Neuroscience and Medicine (INM-1), Jülich Research Centre, Jülich, Germany

*peyman.najafi@cnrs.fr

INTRODUCTION

openMINDS (open Metadata Initiative for Neuroscience Data Structures) [1] is a metadata framework for graph database systems, composed of linked metadata models, serviceable metadata instances libraries, and supportive tooling. The openMINDS metadata models support a wide range of research products, from experimental/simulated data to computational models and brain atlases, with different levels of granularity (basic, advanced, and in-depth) fostering data findability, accessibility, interoperability and reusability (FAIR) [2]. Here we will focus on electrophysiology data and present the "ephys" metadata model extension, which provides schemas for in-depth descriptions of such data. Additionally, the "specimenPrep", "chemicals", and "stimulation" metadata models are introduced, which are closely linked to the "ephys" extension but provide schemas for in-depth descriptions of techniques used in other research domains.

METHODS

All schemas in the openMINDS framework, including the "ephys", "specimenPrep", "chemicals", and "stimulation" extensions, are implemented in a lightweight, JSON-based syntax which is automatically transformed to common schema formats, such as JSON-Schema [3]. The modular set of metadata schemas of each extension was carefully integrated to fit with the other openMINDS metadata models covering different aspects of neuroscience data structures. As an ongoing effort, we identify electrophysiology relevant terminologies needed by the whole community and provide respective libraries of well-defined terms as a collection of metadata instances formatted as JSON-LD files [4]. If possible, these terms are matched to existing ontological terms of the InterLex project [5].

All openMINDS efforts are open-source, accepting requests and contributions from the whole scientific community [6].

RESULTS AND DISCUSSION

The openMINDS "ephys" extension offers a metadata model to organize and capture information about electrophysiology experiments. The experiments may include patch clamp, intracellular, and extracellular recordings.

The openMINDS "specimenPrep" extension offers a metadata model to organize and capture information about specimen preparations. It is capable of capturing information about all three study design modalities: in vivo, ex vivo, and in vitro. It is interlinked with the openMINDS "ephys" extension to capture metadata information about the preparation of the specimens for electrophysiology experiments, including information about the method of preparation and the conditions under which the preparation took place.

The openMINDS "chemicals" extension offers a metadata model to organise and capture information about chemical compounds and mixtures. It is interlinked with the openMINDS "ephys" extension to define and describe the use of chemical compounds and mixtures in electrophysiology experiments.

The openMINDS "stimulation" extension offers a metadata model to organize and capture information about any stimulation procedure and used stimuli. It covers electrical stimulations as well as sensory and photon stimulations. It is interlinked with the openMINDS "ephys" extension to provide information about the stimulation used during the electrophysiology experiments and how it affects the recorded data. In 2019, openMINDS was adopted by EBRAINS [7], a European neuroscience research infrastructure. It is currently in the process of being adopted by Brain/MINDS [8], a Japanese national brain research project. Within EBRAINS, the integration of the new extensions now facilitates the interoperability between the EBRAINS Knowledge Graph [9] and other services. openMINDS is a mature, open-source metadata framework for graph database systems. In conjunction, the new openMINDS extensions "ephys", "specimenPrep", "chemicals" and "stimulation" offer a comprehensive metadata model for organizing and capturing information about electrophysiology experiments, specimen preparations, chemical compounds and mixtures, and stimulation procedures and stimuli used.

Keywords: **electrophysiology, FAIR, graph database, metadata model, ontology**

ACKNOWLEDGEMENTS

openMINDS is developed in the Human Brain Project, funded from the European Union's Horizon 2020 Framework Programme for Research and Innovation under Specific Grant Agreements No. 720270, No. 785907, and No. 945539 (Human Brain Project SGA1, SGA2, and SGA3).

We would like to thank Oliver Schmid, whose insights were instrumental in the development of openMINDS. We would also like to thank the EBRAINS curation team for their support.

REFERENCES

[1] openMINDS (2023, Feb 01) GitHub. https://github.com/HumanBrainProject/openMINDS

[2] Wilkinson, M. et al. (2016) The FAIR Guiding Principles for scientific data management and stewardship. Scientific Data, 3(160018), DOI: 10.1038/sdata.2016.18

[3] Pezoa, F. et al. (2016) Foundations of JSON Schema. in Proceedings of the 25th International Conference on World Wide Web, IW3C2 (Republic and Canton of Geneva, CHE), pp. 263–273, DOI: 10.1145/2872427.2883029

[4] Lanthaler, M. and Gütl, C. (2012). On using JSON-LD to create evolvable RESTful services. in Proceedings of the Third International Workshop on RESTful Design, ACM (New York, NY, USA), pp. 25–32, DOI: 10.1145/2307819.2307827

[5] InterLex project (2023, Feb 01) SciCrunch. https://scicrunch.org/scicrunch/interlex/dashboard

[6] openMINDS CONTRIBUTING.md (2023, Feb 01) GitHub. https://github.com/HumanBrainProject/openMINDS/blob/main/CONTRIBUTING.md

[7] EBRAINS research infrastructure (2023, Feb 01) EBRAINS. https://ebrains.eu/

[8] Brain Mapping by Integrated Neurotechnologies for Disease Studies (2023, Jan 11) Brain/MINDS. https://brainminds.jp/en/

[9] EBRAINS Knowledge Graph (2023, Feb 01) EBRAINS. https://kg.ebrains.eu/

42. Enhanced simulations of whole-brain dynamics using hybrid resting-state structural connectomes

Thanos Manos[1*], Sandra Diaz-Pier[2], Igor Fortel[3], Ira Driscoll[4], Liang Zhan[5], Alex Leow[3,6]

[1]ETIS Laboratory, CY Cergy-Paris University, ENSEA, CNRS, UMR8051, Cergy, France

[2]Simulation & Data Lab Neuroscience, Institute for Advanced Simulation, Jülich Supercomputing Centre (JSC), Forschungszentrum Jülich GmbH, JARA, Jülich, Germany

[3]Department of Biomedical Engineering, University of Illinois at Chicago, Chicago, IL, USA

[4]Department of Psychology, University of Wisconsin-Milwaukee, Milwaukee, WI, USA [5]Department of Electrical and Computer Engineering, University of Pittsburgh, Pittsburgh, PA, USA [6]Department of Psychiatry, University of Illinois at Chicago, Chicago, IL, USA

*thanos.manos@cyu.fr

INTRODUCTION/MOTIVATION

The human brain is an intricate network coordinating a sophisticated balance of excitatory & inhibitory activity between brain regions. The dynamical balance between excitation and inhibition is vital for adjusting neural input/output relationships in cortical networks and regulating the dynamic range of their responses to stimuli. To infer this balance using connectomics, a computational framework was recently introduced [1] and proposed a novel hybrid resting-state structural connectome (rsSC). One can replicate the time evolution of recordings from brain activity by employing mathematical models [2]. By choosing adequate model parameters, it is feasible to build customised virtual brain activity for individual subjects [3]. A major limitation when using traditional structural connectomes (SCs) to inform the connectivity properties in models, such as the Kuramoto model [4], is that the resulting simulated signals do not produce negative correlations similar to the empirical ones [5]. However, this is not the case in time series obtained by empirical neuroimaging data where both positive and negative correlations coexist. We here show [6] that by using rsSC such dynamical systems are able to produce simulated signals with both positive and negative correlations following the trends of the empirical ones.

METHODS

Structural and functional connectivity for 38 cognitively normal APOE ε4 allele carriers aged 40–60 are compared with 38 age and sex-matched (16 male/22 female) non-carriers (control/non-carriers). Imaging included T1- weighted MRI, resting state fMRI and diffusion weighted MRI (more details in [7]). Freesurfer cortical parcellation and sub-cortical segmentation was performed to derive 80 ROIs registered on the Desikan atlas [8]. We use a

novel approach introduced in [1] to produce rsSC connectomes which has already been used in several studies [9] which considers both structural connectivity and functional time series to form a signed coupling interaction network or signed rsSC to describe neural excitation and inhibition. Fig 1 shows a sample of the empirical SC and

rsSC. We employ the Kuramoto model [4,5] and The Virtual Brain [10] to simulate the network's dynamics and produce simulated BOLD time series. Two cases of connectivity matrices were compared: (i) in the first one the c_{ij} values are defined by simply counting the number of streamlines connecting 2 regions; and (ii) in the second one the c_{ij} values are assigned by the corresponding entries of the hybrid rsSC connectomes.

RESULTS AND DISCUSSION

Fig. 2 shows the superiority of hybrid rsSC over standard SC matrices in generating simulated BOLD time series with the Kuramoto model which better approximate the empirical ones. The upper row refers to simulations performed using the respective subject's standard SC matrix to define the coupling weights. Fig. 2A shows the parameter sweep exploration for the global coupling strength and delay parameters (K, τ) when measuring for correlation coefficient between eFC and sFC (CC_{FC} = corr(sFC, eFC). The 5 white circles on the red regions indicate the highest correlations found. Fig. 2B depicts the eFC calculated from the empirical BOLD signal while Fig. 2C the sFC matrix with the larger CC_{FC}. We can observe that sFC did not capture adequately the negative correlations. In Figs. 2D, we use the respective subject's hybrid rsSC matrix. Note the significant improvement in the maximum value of the $CC_{FC} \approx 0.86$ compared to the one found when using the standard SC matrix ($CC_{FC} \approx 0.33$). Also note the better agreement between the two FC matrices (empirical (D) and simulated (E)) and how better the sFC captures both positive and negative correlations. This novel brain connectome rsSC combines characteristics of both structural and functional information and allowed us to optimize model parameters and tune our model to produce simulated functional connectivity (FC) most similar to actual observed FC [6].

Keywords: Whole brain dynamics, Resting-state brain dynamics, neuroimaging data, functional connectivity, resting-state informed structural connectome, Alzheimer's disease

ACKNOWLEDGEMENTS

We acknowledge the use of Fenix Infrastructure resources, which are partially funded from the European Union's Horizon 2020 research and innovation programme through the ICEI project under the grant agreement No. 800858. In particular, we acknowledge the access to the JUSUF supercomputer at the Jülich Supercomputer Centre. This research was partially funded by the Helmholtz Association through the Helmholtz Portfolio Theme "Supercomputing and Modeling for the Human Brain". This project was also received funding from the European Union's Horizon 2020 Research and Innovation Program under grant agreement no. 945539 (Human Brain Project SGA3). TM and AL were also supported by the Labex MME DII (ANR-11-LBX-0023-01) French national funding program. Additionally, LZ and AL were partially supported by NIH RF1MH125928 and R01AG071243. Moreover, LZ was also partially supported by NSF IIS 2045848.

REFERENCES

[1] Ajilore O, Zhan L, GadElkarim J, et al. Constructing the resting state structural connectome. *Frontiers in Neuroinformatics* 2013; 7. doi:10.3389/fninf.2013.00030.

[2] Jirsa V, Proix T, Perdikis D, et al. The virtual epileptic patient: Individualized whole-brain models of epilepsy spread. *NeuroImage* 2017; 145:377-388. doi:https://doi.org/10.1016/j.neuroimage.2016.04.049.

[3 | Deco G, Jirsa V, Robinson P, et al. The dynamic brain: From spiking neurons to neural masses and cortical fields. *PLOS Computational Biology* 2008; 4:1-35. doi:10.1371/journal.pcbi.1000092.
[4 | Kuramoto Y, Chemical Oscillations, Waves, and Turbulence, Dover Books on Chemistry Series, Dover Publications; 2003.
[5 | Popovych O, Jung K, Manos T, et al. Inter-subject and inter-parcellation variability of resting-state whole-brain dynamical modelling. *NeuroImage* 2021; 236:118201. doi:https://doi.org/10.1016/j.neuroimage.2021.118201.
[6 | Manos T, Diaz-Pier S, Fortel I, et al. Enhanced simulations of whole-brain dynamics using hybrid resting-state structural connectomes. (Submitted - under review) 2023.
[7] Korthauer L, Zhan L, Ajilore O, et all. Disrupted topology of the resting state structural connectome in middle- aged apoe ε4 carriers, *NeuroImage* 2018; 178:295-305. doi:https://doi.org/10.1016/j.neuroimage.2018.05.052.
[8] Desikan RS, Ségonne F, Fischl B, et al. An automated labeling system for subdividing the human cerebral cortex on mri scans into gyral based regions of interest, *NeuroImage* 2006; 31:968-980. doi:https://doi.org/10.1016/j.neuroimage.2006.01.021.
[9] Fortel I, Korthauer LE, Morrissey Z, et al. Connectome Signatures of Hyperexcitation in Cognitively Intact Middle-Aged Female APOE-ε4 Carriers. *Cerebral Cortex*. 2020; 30:6350-6362. doi:10.1093/cercor/bhaa190. [10 | Sanz-Leon P, Knock SA, Spiegler A, et al. Mathematical framework for large-scale brain network modeling in the virtual brain. *NeuroImage* 2015; 111:385-430. doi:10.1016/j.neuroimage.2015.01.002.

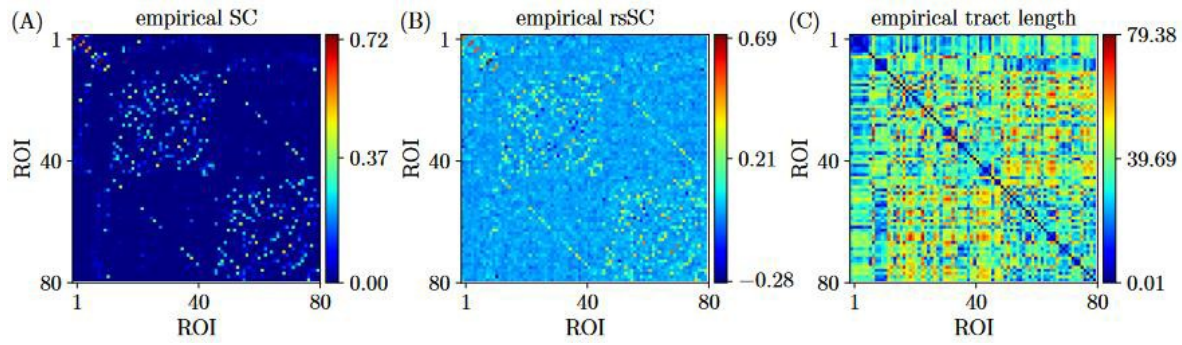

Figure 1. Empirical connectivity matrices example (non-carrier subject). (A) Weights of SC matrix. (B) Hybrid rsSC matrix. (C) Tract length (mm) matrix L based on the euclidean distance of the nodes on the Desikan atlas (same for all simulations and subjects).

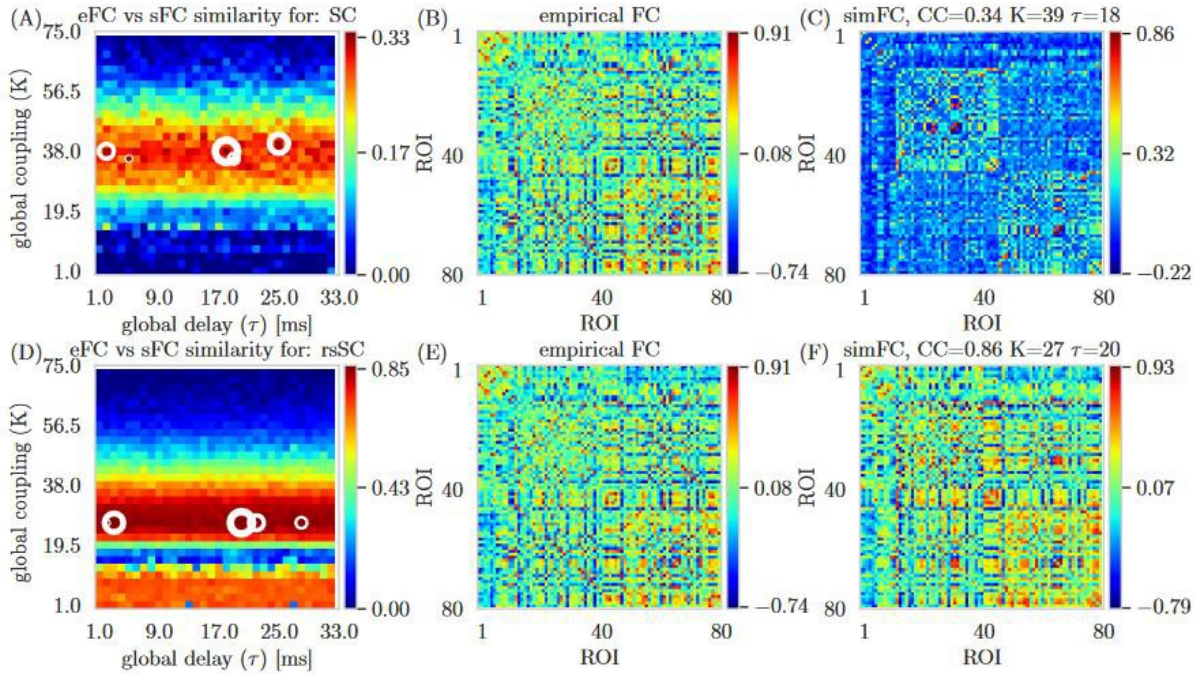

Figure 2. Parameter Sweep Exploration for eFC vs. sFC example. Upper row (using the respective subject's standard SC matrix to define the weights). Lower row (using the respective subject's hybrid rsSC matrix to define the weights).

43. Multiscale Modelling of the Cerebellum: structure-dynamics-function

Claudia Casellato[1], Alessio Marta[1], Robin De Schepper[1], Dimitri Rodarie[1,2], Dianela Osorio[1], Marialaura De Grazia[1], Alice Geminiani[1], Stefano Masoli[1], Egidio D'Angelo[1,3]

[1] Department of Brain and Behavioural Sciences, University of Pavia, Pavia, Italy
[2] Enrico Fermi Study and Research Center, University of Rome, Italy
[3] Brain Connectivity Center IRCCS Mondino Foundation, Pavia, Italy

Keywords: multiscale brain modelling, cerebellum, mouse, human, atlas-based mapping, pathological alterations, signal propagation, sensorimotor tasks, whole-brain integration

Introduction

The cerebellar network is renowned for its regular architecture that has inspired foundational computational theories. However, the relationship between circuit structure, function and dynamics remains elusive[1]. To tackle the issue, we developed an articulate pipeline: i) reconstruct and simulate the mouse cerebellar cortex, using morphologically realistic multi-compartmental neuron models[2],
ii) introduce pathology-specific neural dysfunctions and predict the propagation of these alterations, ii) build an equivalent spiking network with point-neurons and, after introducing plasticity rules, simulate it in long-lasting learning sensorimotor tasks[3], iv) embed the cerebellar circuit in The Virtual Brain (TVB) and predict its impact on whole-brain dynamics. The same pipeline is applied for the human cerebellum.

Methods

The computational framework is the Brain Scaffold Builder[4], flexibly designed to be applied for different species (e.g., rodent, human) and pathological states. The interfaces with several simulators (NEURON, NEST, Arbor) allow investigation of the same brain region at different resolutions. The direct interface with atlases allows to reconstruct full-scale cerebellar lobules with region-specificities (e.g., voxel-based density and cell composition data).

Some brain disorders are under investigations, e.g., autism, where an hyperexcitability of the cerebellar granule cells disrupts signal transfer in mice; the granule cell model was manipulated (ionic and synaptic properties) to reproduce such electrophysiological patterns, and then tested in the cerebellar microcircuit.

Furthermore, the cerebellar microcircuit in spiking version was connected with deep cerebellar nuclei and inferior olive, at a mesoscale level (microcomplex). Long-term plasticity rules were embedded at multiple connection sites. Eye-blink classical conditioning (EBCC) was simulated, in order to match behavioral recordings in mice, also bearing synapse-specific alterations.

Finally, the spiking cerebellar microcomplex model was connected in a mouse TVB framework, simulating a free whisking task. The model parameters and the spike-analog interfaces were tuned

on experimental datasets (resting-state fMRI, baseline discharges…).

Results and discussion

From the mouse cerebellar cortex simulations, the emerging spatio-temporal dynamics provided functional model validation against recordings in vivo, beyond constructive validity based on internal connectivity and single neuron responses (Fig 1A). Neural correlates of behavior were explored by tuning the synapse strengths (Fig. 1B). The "pathological" simulations allowed to predict the impact of detailed lesions at network level.

The EBCC simulations predicted the interplay of different forms of plasticity in the cerebellar cortex, shedding light on the neural activities underlying learning in healthy and knock-out behaving mice (Fig. 1C).

The co-simulations in the TVB highlighted the cerebellar role as a key integrator between primary motor (M1) and sensory (S1) cortices during sensorimotor integration tasks: the M1-S1 spectral coherence showed an increase in gamma-band driven by the cerebellar activity (Fig. 1D).

Starting from the mouse cerebellar cortex reconstruction, the human network parameters were tailored on the available information, e.g., volume and layer thickness, cell morphologies (experimental images or geometrical shapes of the dendritic tree and axonal span), cell and synapse densities. Therefore, the generated connectome unifies a collection of scattered experimental data into a coherent construct and provides a new model-based ground-truth about human cerebellar organization (Fig. 2).

This pipeline connects multiscale elements, from intracellular mechanisms to behavior generation, considering the cerebellar detailed local connectome and the extracerebellar one. It is a powerful workflow to explore and predict mechanisms of pathologies and of possible treatments such as neuromodulation.

Acknowledgment

This research has received funding from: i) European Union's Horizon 2020 Research and Innovation programme under **Human Brain Project** SGA3 No. 945539, ii) **Centro Fermi project** "Alterations in autistic spectrum disorders- multiscale modelling of microcircuit", iii) European Union's Horizon 2020 research and innovation programme under the Marie Skłodowska-Curie (**CEN** No 956414), iv) the National Recovery and Resilience Plan (NRRP), Mission 4 Component 2 Investment 1.3 - Call for tender No. 341 of 15/03/2022 of Italian Ministry of University and Research funded by the European Union – NextGenerationEU. Award Number: Project code PE0000006, Concession Decree No. 1553 of 11/10/2022 adopted by the Italian Ministry of University and Research, CUP D93C22000930002, "A multiscale integrated approach to the study of the nervous system in health and disease" (**MNESYS**).
Special acknowledgement to **EBRAINS and FENIX** for informatic support and infrastructure.

References

1. Egidio D'Angelo, Viktor Jirsa, The quest for multiscale brain modeling, Trends in Neurosciences, Volume 45, Issue 10, 2022, Pages 777-790, ISSN 0166-2236, doi: 10.1016/j.tins.2022.06.007.
2. De Schepper R, Geminiani A, Masoli S, Rizza MF, Antonietti A, Casellato C and D'Angelo E. Model simulations unveil the structure-function-dynamics relationship of the cerebellar cortical microcircuit. NAT COMMS BIOL. 2022; doi: 10.1038/s42003-022-04213-y

3. Geminiani A, Pedrocchi A, D'Angelo E, Casellato C. Response Dynamics in an Olivocerebellar Spiking Neural Network With Non-linear Neuron Properties. FRONT. COMPUT. NEUROSCI. 2019; 13:68; doi: 10.3389/fncom.2019.00068
4. https://ebrains.eu/service/brain-scaffold-builder/

Figures

Figure 1) A) Reconstruction and simulation of a mouse cerebellar cortex volume. Multicompartment morphology-based neuron models are embedded. The Brain Scaffold Builder (BSB) is used, interfacing it with NEURON simulator. A whisker air-puff stimulus (a burst) is delivered to 4 adjacent mossy fibers. Propagation goes along a vertical neuronal column (granule cells – red; Golgi cell – blue; Purkinje cell – green; stellate cell- yellow; basket cell – orange). **B)** The microcircuit model emulates an EBCC paradigm, in which a conditioned stimulus (tone) is delivered to the mossy fibers. The simulations reproduce the final state ("post-learning") by exploring multiple levels of parallel fibers – Purkinje cells (pf-PC) long-term depression (LTD). **C)** Microcomplex model in EBCC trials. The synaptic connections undergoing long-term plasticity are as dashed arrows. CS = conditioned stimulus, US = unconditioned stimulus; CR = conditioned response (eyeblink anticipating the US onset). **D)** Co-simulations with the spiking cerebellar network (in NEST simulator) in the TVB, focusing on the sensorimotor integration.

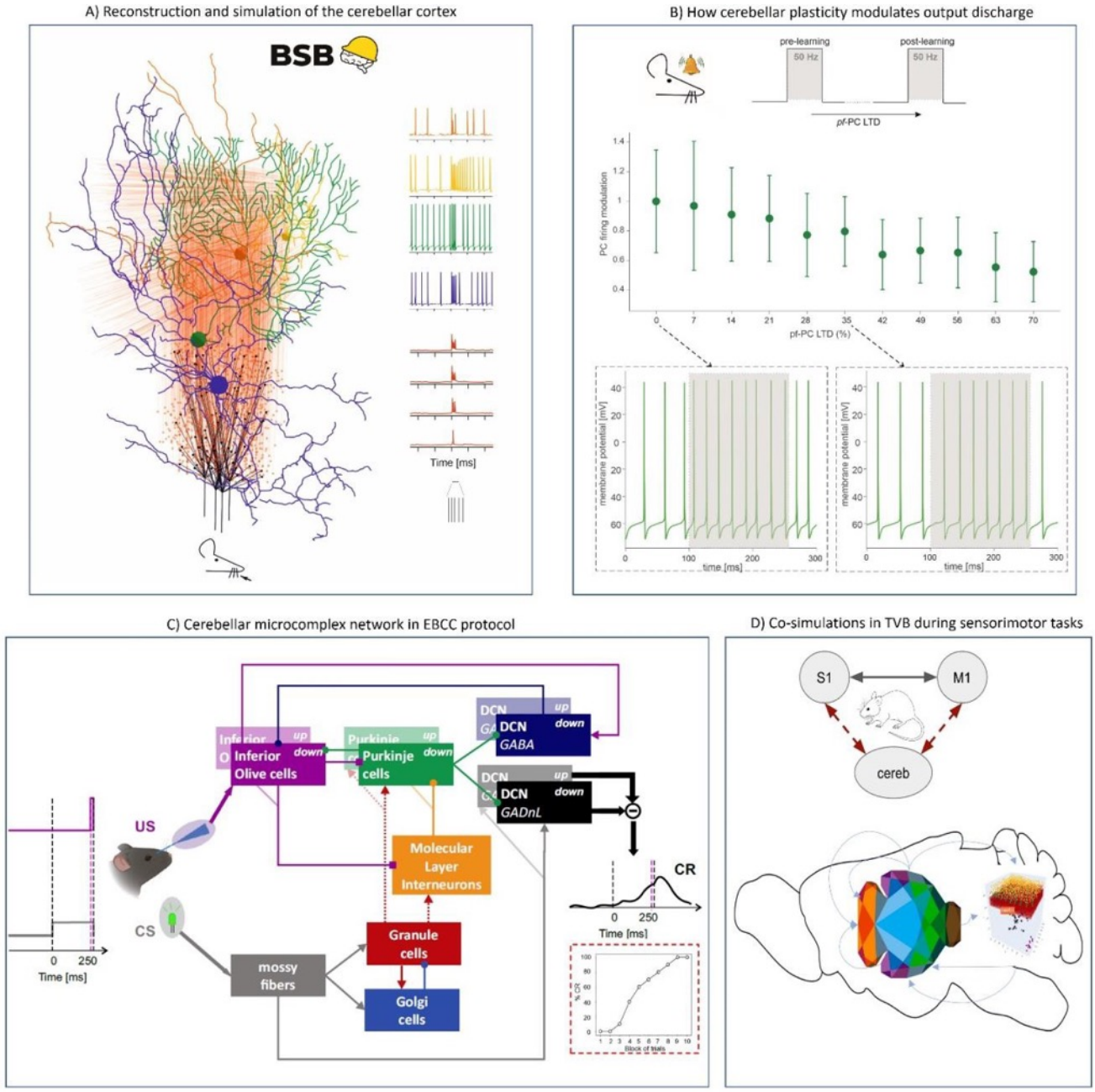

Figure 2) Reconstruction of the human cerebellar microcircuit. **A)** morphologies when available, and point clouds for stellate and basket cells, **B)** excitatory synapses (yellow dots) from parallel fibers on apical dendrites of a Golgi cell (voxel intersection strategy between 2 morphologies), **C)** inhibitory synapses (yellow dots) from stellate cells on a Purkinje cell (intersection strategy from a point cloud to a morphology)

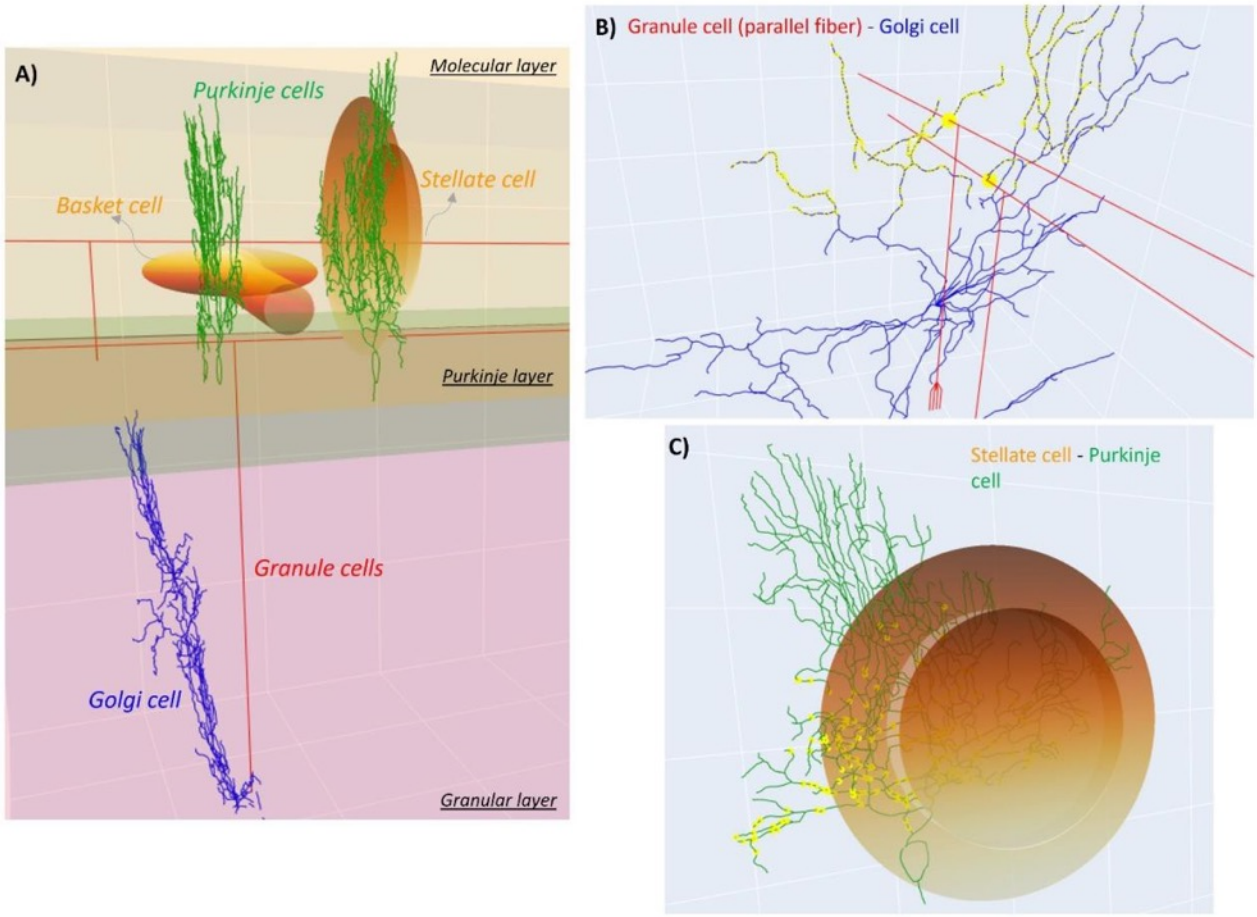

44. Mouse cerebellum reconstruction: declive model with structural and functional regional specificity

Dimitri Rodarie[1,2*], Dianela Osorio[1], Claudia Casellato[1], Egidio D'Angelo[1,3]

1 Department of Brain and Behavioral Sciences, University of Pavia, Pavia, Italy

2 Enrico Fermi Study and Research Center, University of Rome, Italy

3 Brain Connectivity Center IRCCS Mondino Foundation, Pavia, Italy

* dimitri.rodarie@cref.it

Keywords: multiscale brain modelling, cerebellum, mouse, human, atlas-based mapping, pathological alterations, signal propagation, sensorimotor tasks, whole-brain integration

Introduction

We aim to reconstruct and simulate atlas-mapped cerebellar regions of the mouse, capturing the relationship between structure, dynamics, and function. Numerous experimental and clinical evidence in both humans and rodents show that lobule VI plays a relevant role in many functions including motor, cognitive, emotional, and social tasks[1–3]. Lobule VI is made up of a vermis part (declive) and a hemispheric part (simple lobule). We present here a pipeline to reconstruct the declive of the mouse, based on the Blue Brain Cell Atlas model[4] and the Brain Scaffold Builder (BSB) tool[5]. With this pipeline, we were able to estimate for the first time the specific densities of each cell type, including granule, golgi, unipolar brush, lugaro, globular, Purkinje, candelabrum, basket, and stellate cells. In the BSB we placed, oriented, and connected the neurons. The output of this pipeline is a circuit that can be simulated and validated against functional experimental findings.

Methods

We build here a 3D representation of the mouse declive region, embedded into an anatomically realistic whole mouse brain structure (Figure 1). We based our model on the Blue Brain Cell Atlas pipeline[4], which we extended with the Purkinje layer at the boundary between granular and molecular layers. We also added Unipolar brush cells and lugaro cells based on regional densities from Sekerková et al.[6] and Dieudonné and Dumoulin[7], respectively. Moreover, we proposed a new strategy to place Purkinje, candelabrum and globular cells based on linear density from Osorno et al.[8] (Figure 1A). The remaining cell types and their numbers were estimated using regional distributions from the Blue Brain Cell Atlas.

To reconstruct local connectivity, we computed the orientations of each morphology (Figure 1BC) using Rodarie et al.'s method[4]. We leveraged this information to orient neurons including granule cells and their ascending axons. Additionally, it will be used to bend the parallel fibers of our model following the external surface of the region. We applied voxel intersection and point clouds connection strategies and synaptic in- and out-degree ratios reported in De Schepper et al.[5].

We assigned point-neuron electrical parameters to each cell type, and synaptic parameters to each connection type, according to Geminiani et al.[9]. The resulting scaffold model has been simulated using the

BSB interfacing with the NEST simulator[5]. The model will be structurally and functionally refined as more data become available.

Results and Discussion

The final scaffold model has 3,113,153 neurons, with 2,877,812 Granule cells, 45257 Golgi cells, 10956 Unipolar brush cells, 234 Lugaro cells, 3240 Globular cells, 3512 Purkinje cells, 3875 Candelabrum cells, 80952 Basket cells and 87314 Stellate cells (see Figure 1D).

The connectome defines a precise picture of the local connectivity.

Preliminary simulations are ongoing, to validate the dynamics of the declive region in resting-state and under proper stimulations. Our goal is to leverage this circuit to study fear conditioning and emotions responsible circuits in cerebellum. Moreover, our strategy can be extended to reconstruct other cerebellar regions. A full-scale cerebellum network will allow us to analyze subregions specificities and their interactions. Finally, we will investigate mechanisms to simulate pathological states such as autism[10].

Acknowledgements

This research has received funding from: i) European Union's Horizon 2020 Research and Innovation program under **Human Brain Project** SGA3 No. 945539, ii) **Centro Fermi project** "Alterations in autistic spectrum disorders-multiscale modelling of microcircuit", iii) European Union's Horizon 2020 research and innovation program under the Marie Skłodowska-Curie (**CEN** No 956414)

Figures

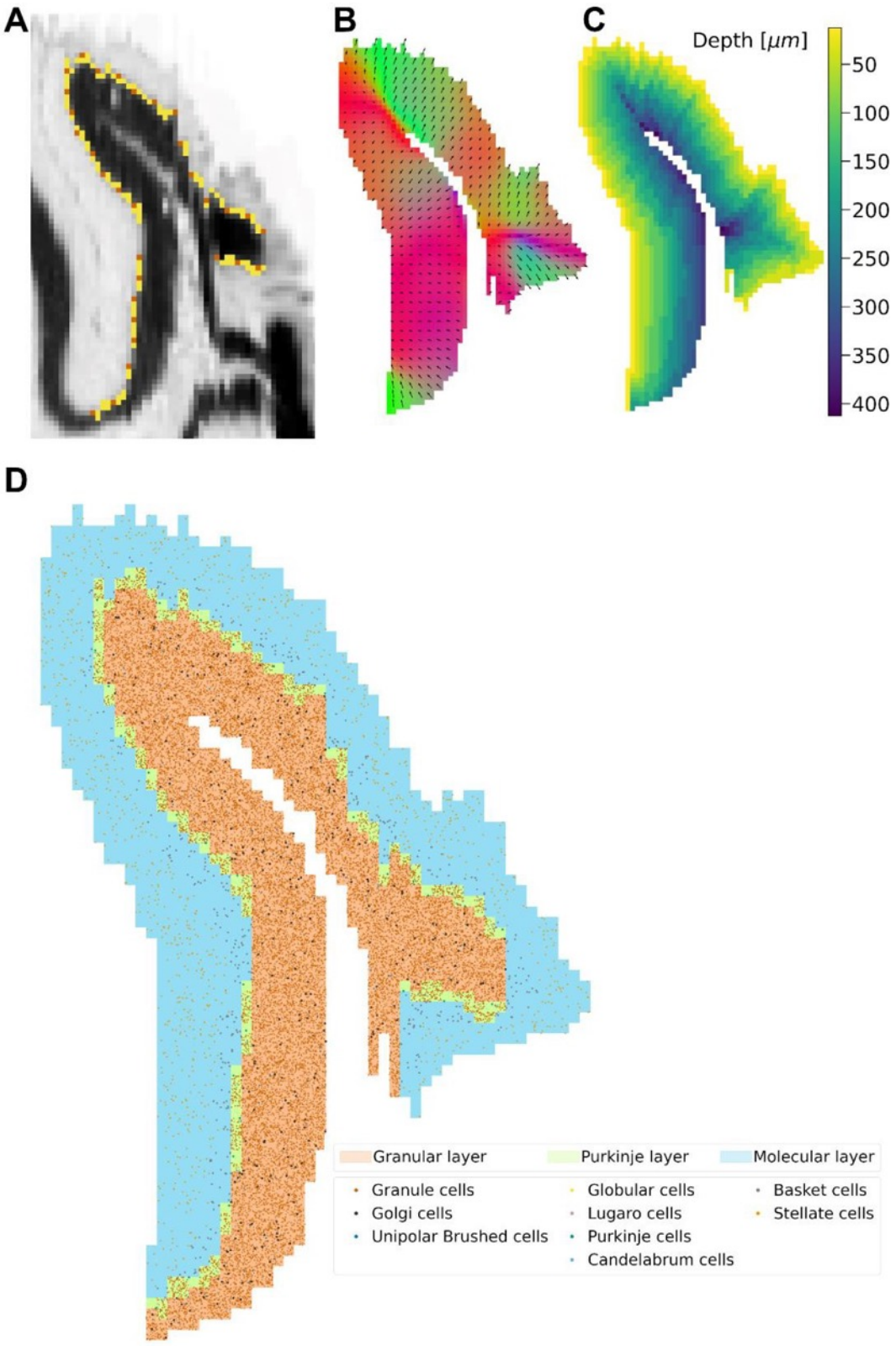
A
B
C
Depth [μm]
50
100
150
200
250
300
350
400
D
Granular layer
Purkinje layer
Molecular layer
Granule cells
Golgi cells
Unipolar Brushed cells
Globular cells
Lugaro cells
Purkinje cells
Candelabrum cells
Basket cells
Stellate cells

Figure 1: Sagittal views of the declive model.

A - Placement of the Purkinje Cells in the newly created Purkinje Layer based on linear density. A sagittal slice of the Nissl volume from the Allen institute is displayed in levels of grey with the overlaid annotated Purkinje layer in yellow. The granular layer is clearly visible as a darker band due to its high cell density. Placed Purkinje cells are displayed in orange.

B - Orientation field defined by one vector for each voxel of the volume. Orientations of the ascending axons were calculated following a gradient from the arbor vitae fibers towards the molecular layer.

C - Depth for each voxel of the volume. This corresponds to the distance between each voxel and the outer border of the molecular layer following the orientation field. The depth of each voxel in the molecular layer is used determine whether the neurons in it are stellate or basket cells.

D - Cell positions. Placement of the different cell types of the declive.

References

1. Hwang KD, Kim SJ, Lee YS. Cerebellar Circuits for Classical Fear Conditioning. *Front Cell Neurosci*. 2022;16. Accessed February 7, 2023. https://www.frontiersin.org/articles/10.3389/fncel.2022.836948

2. Manto M, Gruol D, Schmahmann J, Koibuchi N, Sillitoe R, eds. *Handbook of the Cerebellum and Cerebellar Disorders*. Springer International Publishing; 2020. doi:10.1007/978-3-319-97911-3

3. Adamaszek M, Manto M, Schutter DJLG, eds. *The Emotional Cerebellum*. Vol 1378. Springer International Publishing; 2022. doi:10.1007/978-3-030-99550-8

4. Rodarie D, Verasztó C, Roussel Y, et al. A method to estimate the cellular composition of the mouse brain from heterogeneous datasets. Marinazzo D, ed. *PLOS Comput Biol*. 2022;18(12):e1010739. doi:10.1371/journal.pcbi.1010739

5. De Schepper R, Geminiani A, Masoli S, et al. Model simulations unveil the structure-function-dynamics relationship of the cerebellar cortical microcircuit. *Commun Biol*. 2022;5(1):1-19. doi:10.1038/s42003-022-04213-y

6. Sekerková G, Watanabe M, Martina M, Mugnaini E. Differential distribution of phospholipase C beta isoforms and diaglycerol kinase-beta in rodents cerebella corroborates the division of unipolar brush cells into two major subtypes. *Brain Struct Funct*. 2014;219(2):719-749. doi:10.1007/s00429-013- 0531-9

7. Dieudonné S, Dumoulin A. Serotonin-Driven Long-Range Inhibitory Connections in the Cerebellar Cortex. *J Neurosci*. 2000;20(5):1837-1848. doi:10.1523/JNEUROSCI.20-05-01837.2000

8. Osorno T, Rudolph S, Nguyen T, et al. Candelabrum cells are ubiquitous cerebellar cortex interneurons with specialized circuit properties. *Nat Neurosci*. 2022;25(6):702-713. doi:10.1038/s41593-022-01057-x

9. Geminiani A, Pedrocchi A, D'Angelo E, Casellato C. Response Dynamics in an Olivocerebellar Spiking Neural Network With Non-linear Neuron Properties. *Front Comput Neurosci*. 2019;13. doi:10.3389/fncom.2019.00068

10. Fatemi SH, Aldinger KA, Ashwood P, et al. Consensus Paper: Pathological Role of the Cerebellum in Autism. *The Cerebellum*. 2012;11(3):777-807. doi:10.1007/s12311-012-0355-9

45. A semi-automated pipeline for cell detection and white matter segmentation in the macaque brain

Nathan Vinçon[1*], Yujie Hou[1], Pierre Misery[1], Camille Lamy[1], Kenneth Knoblauch[1], Julien Vezoli[1], Henry Kennedy[1]

[1]Stem-cell and Brain Research Institute, University of Claude Bernard Lyon 1, Lyon, France
*nathan.vincon@inserm.fr

INTRODUCTION/MOTIVATION

Cell detection and white matter segmentation are crucial steps for the creation of precise connectivity datasets in the macaque brain. However, they are time-consuming procedures and constitue a bottleneck to the creation of large size connectivity datasets. The open source histology viewer QuPath along with deep learning methods enable automated and semi-automated processing of histological slides, opening the way to high throughput imaging in histology. Many segmentation approaches have been developed for human and mouse MRI images[1,2], but few are available for macaque MRI[3]. Additionally, such processing pipelines are not available for macaque histology. Here, we developed a semi-automated pipeline for cell detection and white matter segmentation in the macaque brain that reduces the processing time and improves the reliability of parcel annotation.

METHODS

Histological sections were obtained from macaque brains following injection of fluorescent retrograde tracers in target areas[4], and mounted on individual slides and cover slipped for scanning. Fluorescence images were first obtained with a x20 objective using a high-throughput slide-scanner[5]. Histological sections were stained with Nissl in order to be rescanned with a bright field (x5 objective), for delimiting the white-matter/gray-matter boundary.

Fluorescence images

For the tissue segmentation, we created annotations inside and outside the tissue (N = 1 slides) to train a pixel classifier using QuPath with a multi-layer perceptron classifier. For labelled cell detection, we created a permissive cell detector for each channel and refined the detection with a random-tree classifier. Each object classifier was trained on 200 objects classified as “cell” or “artefact” (N = 3 entire sections) under the supervision of human experts for validation.

Nissl images

We manually annotated the regions corresponding to white-matter, tissue and background (as three binary masks) for 79 slides and divided them into 14191 tiles to train a multiresolution (x5, x1.25, x0.3125) convolutional neural network. Binary masks were then converted to polygons using the pypotrace library[6]. Polygons from the fluorescent image and the Nissl image were merged using linear registration[7] on the rasterized tissue polygon.

We used QuPath version 0.4.1, Python 3.9, keras 2.3.0, SimpleElastix 2.0.0 and pypotrace 0.2.

RESULTS AND DISCUSSION

We evaluated the efficiency of the pipeline for (i) time saved on manual annotations and (ii) precision of the fluorescence to Nissl registration and merger. In the first configuration (fully manual), the operator draws the white matter contour without any automated approximation. In the second configuration (semi-automated), the operator starts from the automatically generated contour and refines it. Using 3 slides, the second configuration reduced the time needed per slide by 3.6-fold. We also evaluated the precision of the automated merging of fluorescence-related annotations and Nissl-related annotations and showed that the deviation in white-matter boundary is minimal when comparing the two procedures (21.8 ± 14.35 µm). The automated segmentation will be improved iteratively through a human feedback loop. We will extend the training to the claustrum region[8] where there are numerous white matter neurons, which makes segmentation very challenging. Further validations of the accuracy and precision of the semi-automated white matter segmentation and the cell detection methods will be done by comparing the variability between fully manual and semi-automated processing. This pipeline will strongly accelerate and facilitate the processing of retrograde labelling enabling the host team to: (i) construct a large connectivity dataset; (ii) develop a multimodal atlas of the macaque brain; (iii) complete a study on claustrum cortical neurons and adjacent white matter cortical projecting neurons in a study looking at claustrum hub functions in the cortex.

Keywords: pipeline, cell detection, brain segmentation, macaque

ACKNOWLEDGEMENTS

LABEX CORTEX (ANR-11-LABX-0042 to H.K.), Claustrum_Hub (ANR-22-CE92-0010-01 to H.K.), National Institute of Health (NIH award UM1MH130981, subaward 2022-0618 to H.K.), DUAL_STREAMS (ANR-19-CE37-0000 to K.K.).

REFERENCES

1. Yamanakkanavar N, Choi JY, Lee B. MRI Segmentation and Classification of Human Brain Using Deep Learning for Diagnosis of Alzheimer's Disease: A Survey. *Sensors*. 2020;20(11):3243. doi:10.3390/s20113243
2. Feo R, Giove F. Towards an efficient segmentation of small rodents brain: A short critical review. *J Neurosci Methods*. 2019;323:82-89. doi:10.1016/j.jneumeth.2019.05.003
3. Geffroy D, Rivière D, Denghien I, Souedet N, Laguitton S, Cointepas Y. BrainVISA: a complete software platform for neuroimaging.
4. Wang M, Hou Y, Magrou L, et al. *Retinotopic Organization of Feedback Projections in Primate Early Visual Cortex: Implications for Active Vision*. Neuroscience; 2022. doi:10.1101/2022.04.27.489651
5. Zeiss. *Microsc Today*. 2016;24(S1):8-9. doi:10.1017/S155192951600002X
6. Rouch L. potrace Python bindings. Published online January 22, 2023. Accessed January 26, 2023. https://github.com/flupke/pypotrace
7. What is SimpleElastix? Published online January 26, 2023. Accessed January 27, 2023. https://github.com/SuperElastix/SimpleElastix
8. Jackson J, Smith JB, Lee AK. The Anatomy and Physiology of Claustrum-Cortex Interactions. *Annu Rev Neurosci*. 2020;43:231-247. doi:10.1146/annurev-neuro-092519-101637

46. Online workflows for analysing murine brain images

Maja A. Puchades*, Sharon C Yates, Nicolaas Groeneboom, Gergely Csucs, Dmitri Darine, Harry Carey, Trygve B. Leergaard & Jan G. Bjaalie

Institute of Basic Medical Sciences, University of Oslo, Norway

*Presenting author: majap@uio.no

Keywords: Brain, volumetric atlas, image registration, machine learning, quantification, cell count, analysis, coordinates.

Introduction: Research in small animals often depends on comparisons of cellular and molecular features in animal cohorts, requiring precise localizations of the observed differences. While numerous methodologies are available to enumerate labelled features visualized in microscopic images, it remains difficult to combine them into coherent and reproducible workflows. The EBRAINS research infrastructure now offers a robust, open and low-threshold analytic environment tailored for analysis of experimental mouse and rat brain image data in atlas context.

Methods: The EBRAINS atlas services (https://ebrains.eu/services/atlases) offer several workflows for organizing, analyzing and sharing brain research data. Users can create their own workspace and combine methods for 1) interactive inspection of high-resolution images;
2) automatic[1] and user-guided spatial registration[3,4] of brain section images to a volumetric reference atlas; 3) annotation of atlas-aligned image series[5]; 4) extraction[5] of spatial coordinates for features of interest; 5) whole brain labelled object distribution analysis[7], with metadata management according to the FAIR principles.

Results: We present examples of typical analytic workflows[2], illustrating how the available suite of tools were combined and which results were obtained. One example workflow is to apply atlas overlays to histological images using WebAlign[3] and WebWarp[4], to inspect and map tract-tracing connections in the images using the LocaliZoom[5] annotation tool, and to visualise resulting point clouds in the Meshview[6] 3D viewer. Comparison and contrast of point clouds obtained by this or other methods with MeshView is yet another possible approach. Users may also count cells and examine distributions across brain regions by combining the registration tools with the Nutilweb[7] tool that supports quantification. All the tools have user-friendly web interfaces, with extensive online user manuals and user support.

Discussion: The online tools and workflows presented are based on standalone software versions[8,9,10] already available on EBRAINS, with the addition of new features such as online annotations and extraction of feature coordinates. To our knowledge, these tools represent

the first fully open access online service for neuroscientists, developed in close interaction with users in the neuroscience community.

Acknowledgements: Funded from EU Horizon 2020, Specific Grant Agreement No. 945539 (Human Brain Project SGA3)

References:

1. Carey H, et al. 2022. DeepSlice: rapid fully automatic registration of mouse brain imaging to a volumetric atlas. BioRxiv preprint version posted April 30, 2022.;https://doi.org/10.1101/2022.04.28.489953

2. Puchades et al. 2023. EBRAINS tools for rodent image data atlasing and analyses, in preparation

3. https://webalign.readthedocs.io/en/latest/

4. https://webwarp.readthedocs.io

5. https://localizoom.readthedocs.io/en/latest/

6. https://meshview-for-brain-atlases.readthedocs.io/en/latest/

7. https://quint-webtools.readthedocs.io/en/latest/NutilWeb.html

8. Puchades MA, et al 2019. Spatial registration of serial microscopic brain images to three-dimensional reference atlases with the QuickNII tool. PLosONE, 14(5): e0216796. https://doi.org/10.1371/journal.pone.0216796

9. Yates SC, et al. 2019. QUINT: Workflow for quantification and spatial analysis of features in histological images from rodent brain. Front Neuroinform. 2019 Dec 3;13:75. doi: 10.3389/fninf.2019.00075

10. Groeneboom NE, et al. 2020. Nutil: A Pre- and Post-processing Toolbox for Histological Rodent Brain Section Images. Front. Neuroinform. 14:37. doi: 10.3389/fninf.2020.00037

47. DeepSlice: Atlas registration of mouse and rat brain sections with deep learning

Harry Carey*[1], Gergely Csucs[1], Simon McMullan[2], Maja Puchades[1] and Jan Bjaalie[1]

[1] Institute of Basic Medical Sciences, University of Oslo, Norway
[2] Macquarie Medical School, Faculty of Medicine, Health & Human Sciences, Macquarie University,

Marsfield, NSW 2109, Australia

Keywords:

Neural network models; Machine learning; registration, brain atlases, Murine

Introduction:

The increase in both rat and mouse brain datasets has made it crucial to integrate and analyze the data within a common spatial reference frame. However, the current process of registering histological brain section images to volumetric brain atlases is time-consuming and requires anatomical expertise. To address this challenge, we have trained a deep neural network, DeepSlice[1], to automatically recognize the atlas position of coronally cut histological sections from both rat and mouse brains.

Methods

The DeepSlice toolbox was created to anchor mouse and rat brain histology to the Waxholm Space atlas of the rat brain and Allen Mouse Brain Common Coordinate Framework. The accuracy of the algorithm was compared to human anatomists for mice. DeepSlice is based on the Xception neural network architecture[2] and trained on data from the Allen Institute for the mouse and data from Ebrains for the rat.

Results and Discussion:

DeepSlice achieved accurate anchoring of rat brain histology in seconds, while a human anatomist would take hours to perform the same task. The output of DeepSlice is compatible with the QUINT

workflow[3], including QuickNII[4] (RRID: SCR_016854), allowing predictions to be modified by users, and VisuAlign (RRID: SCR_017978) enabling further user defined non-linear deformations. DeepSlice is freely available as both a Python package and web application.

We are yet to quantify performance of the rat but the mouse performs comparably to human neuroanatomists.

Keywords: DeepSlice, rat brain histology, Waxholm Space atlas, deep learning, reference space

Acknowledgements:

This project has received funding from the European Union's Horizon 2020 Framework Program for Research and Innovation under the Specific Grant Agreement No. 945539 (Human Brain Project SGA3).

References:

1. Carey et al. "DeepSlice: rapid fully automatic registration of mouse brain imaging to a volumetric atlas." bioRxiv preprint version posted April 30, 2022. https://doi.org/10.1101/2022.04.28.489953.
2. Chollet, François. "Xception: Deep learning with depthwise separable convolutions." *Proceedings of the IEEE conference on computer vision and pattern recognition*. 2017.
3. Yates, Sharon C., et al. "QUINT: workflow for quantification and spatial analysis of features in histological images from rodent brain." *Frontiers in Neuroinformatics* 13 (2019): 75.
4. Puchades, Maja A., et al. "Spatial registration of serial microscopic brain images to three-dimensional reference atlases with the QuickNII tool." *PloS one* 14.5 (2019): e0216796.

48. Reconstructing axonal arborizations from sectioned mouse brains through alignment and stitching

Rembrandt Bakker[1,2*], Mario Rubio-Teves[3], Nestor Timonidis[1], María García-Amado[3], Francisco Clascá[3], Paul Tiesinga[1]

[1]Donders Centre for Neuroscience, Radboud University Nijmegen, Nijmegen, The Netherlands. [2]Inst. of Neuroscience and Medicine (INM-6), Forschungszentrum Jülich, Jülich, Germany. [3]Department of Anatomy and Neuroscience, School of Medicine, Autónoma de Madrid University, Madrid, Spain.

*rembrandt.bakker@donders.ru.nl

INTRODUCTION/MOTIVATION

Since the turn of this century, new and powerful cell labeling techniques have allowed the consistent and complete labeling of axonal arborizations of individual long range projection neurons (LRPNs) in mouse [1]. The prospect of creating a connectome at the cellular level, together with new developments in the automated scanning of whole (rodent) brain volumes, has resulted in a the release of thousands of fully reconstructed LRPNs [2,3,4]. In parallel with this number-driven 'industrial' approach, there are smaller scale, hypothesis-driven projects that focus on particular populations of neurons, perform targeted single-cell labeling experiments and explore the resulting data to the maximum possible extent. In this setting, axons are traced from a stack of brain slices, stained to highlight particular features and mounted on a glass slide. Tracing axons from this data is a two step process:

1. Find all pieces of axon in each individual section.
2. Connect pieces of axon across adjacent sections to create a full axonal reconstruction, a process that we refer to as *alignment and stitching*.

The first step is a manual procedure that can be carried out in commercially available microscope-attached software such as Neurolucida [MBF Bioscience]. In this work we present a workflow to automate the second step which, when performed manually, is the most tedious part of the process.

METHODS

Our alignment and stitching approach consists of:

1. **Preparation** of a structured dataset that contains for each section all pieces of axon and a section image in a shared coordinate system. Implemented in Python.
2. **Alignment** of sections using two complementary methods:

   a. For sections that contain only a few pieces of axon: use a tissue-based alignment tool that presents the user with the overlay of (a) a tissue section, (b) the contours of the adjacent section, and (c) all pieces of axon that are traced in the two sections. The user manually rotates and shifts the overlay to obtain the best possible match. Implemented as a web-based tool.
   b. For sections with many pieces of axon: align sections to create a maximum number of matching pieces, using a modified version of the Dercksen [5] algorithm. Implemented in Python.
3. **Stitching** pieces of neuron using a greedy approach that starts with an initial segment (the soma), and at each iteration connects a piece from the set of unconnected pieces to one of the endings of the growing neuron, in such a way that the added axonal length is minimal, and permitting only stitches between adjacent sections. Implemented in Python.
4. **Validation**: visualize the applied stitches in step 3 as arrows, and allow the user to mark incorrect stitches, before re-running step 3. This makes use of the HBP Morphology Viewer [6].

RESULTS AND DISCUSSION

The use-case that we present here concerns a thalamocortical neuron that is present in 14 coronal sections of 50 micron thickness. In 10 sections, the number of axon pieces is sufficient for piece-matching alignment (step 2a, Fig 1a), while in the remaining sections we rely on tissue-based alignment (step 2b, Fig. 1b). In the validation, a few stitches are to be discarded (Fig. 2). In the end result we apply nearly 500 stitches with an average length of 12 microns, which sums up to 18% of the neuron's total axonal length.

Applying the pipeline not only saves days of work, it is also reproducible in that it keeps track of where stitches have been made, and it results in a known correspondence between axon segments and tissue sections. The pipeline is currently extended for the use case where multiple neurons are present in the stack, and integrated with a pipeline to register the neuron to a common reference space [7].

Keywords: Long range projection neuron, axonal reconstruction, neuronal morphology, stitching, thalamus, cortex

ACKNOWLEDGEMENTS

This work was supported by the FLAG-ERA grant NeuronsReunited, by NWO (680-91-318), by Spain's MICINN-AEI (PCI2019-111900-2), and by the European Union's Horizon 2020 Framework Programme for Research and Innovation under Specific Grant Agreement No. 945539 (Human Brain Project SGA3).

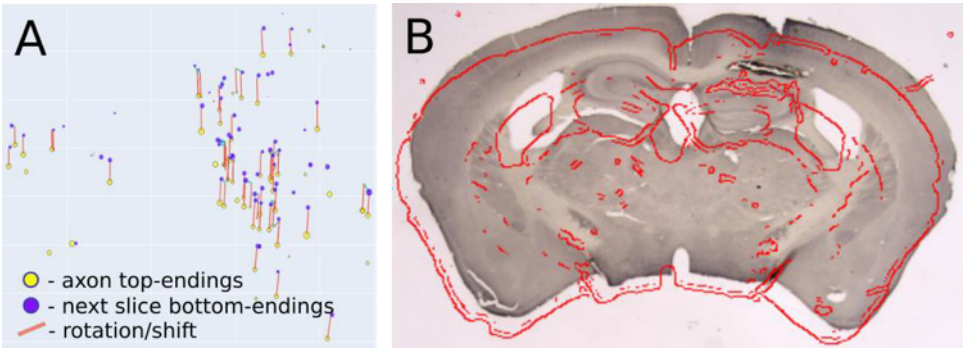

Figure 1: Alignment of the neuron. (A) Automatically position adjacent slices to maximize the number of matching pieces of axon. Red lines indicate the optimal rotation/shift to be applied. (B) In case of too few pieces of axon, manually align tissue sections using a web-based tool. Shown is a tissue section with the next (to be aligned) section in the form of an edge-detected contour on top of it.

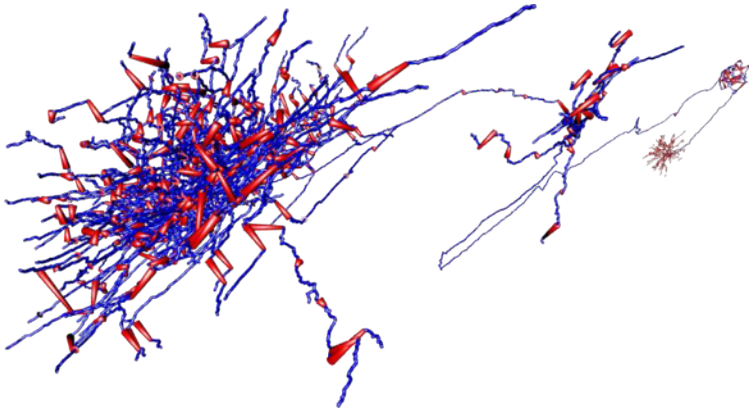

Figure 2: Stitching validation. 3D render of a stitched thalamocortical neuron using the HBP Morphology Viewer [6]. Stitches (red cones) are enlarged so they can be marked as 'not allowed' for a re-run of the optimization process.

REFERENCES

[1] Furuta et al, 2001. In vivo transduction of central neurons using recombinant Sindbis virus: Golgi-like labeling of dendrites and axons with membrane-targeted fluorescent proteins. J Histochem Cytochem 49(12):1497-508. doi: 10.1177/002215540104901203.

[2] Peng et al. 2021. Morphological diversity of single neurons in molecularly defined cell types. Nature. 598(7879):174-181. doi: 10.1038/s41586-021-03941-1.

[3] Winnubst et al. 2019. Reconstruction of 1,000 Projection Neurons Reveals New Cell Types and Organization of Long-Range Connectivity in the Mouse Brain. Cell. 179(1):268-281. doi: 10.1016/j.cell.2019.07.042.

[4] Neuronsreunited neuron database viewer web site. https://neuroinformatics.nl/HBP/neuronsreunited-viewer/.

[5] Dercksen et al. 2009. Automatic alignment of stacks of filament data, 2009 IEEE International Symposium on Biomedical Imaging, 971-974. doi: 10.1109/ISBI.2009.5193216.

[6] HBP Morphology Viewer web site. https://neuroinformatics.nl/HBP/morphology-viewer/.

[7] Piastra et al. 2021. INCF Neuroinformatics Assembly, Poster 91, https://neuroinformatics.incf.org/node/259.

49. Where structure meets function: human brain connectivity from dMRI and intracerebral electrical stimulation

Maciej Jedynak[a,b], Anthony Boyer[a,b] , Lena Trebaul[b], Jean-Didier Lemarechal[a,b], Nicole Labra[c], Manik Bhattacharjee[a,b], François Tadel[b,d], Blandine Chanteloup-Forêt[b], Cyril Poupon[c], Jean-François Mangin[c], Olivier David[a,b,*] F-TRACT Consortium

a) Aix Marseille Université, Inserm, INS, Institut de Neurosciences des Systèmes, Marseille, France
b) Grenoble Institut Neurosciences, Université Grenoble Alpes, Inserm, U1216, 38000, Grenoble, France
c) Université Paris-Saclay, CEA, CNRS, Neurospin, UMR9027 Baobab, Gif-sur-Yvette, France
d) Signal and Image Processing Institute, University of Southern California, Los Angeles, USA

Introduction

Connectivity of the human brain can be studied by a number of techniques in different modalities. In particular, diffusion MRI allows to map structure of white matter fascicles connecting gray matter areas. At the same time, anatomo-functional connectivity can be estimated by means of functional tractography of intracerebral electrical stimulation. Here, we present integration and cross validation of connectivity maps provided by those two modalities. Moreover, we leverage their complementarity, i.e. we combine the geometry of connectivity pathways obtained from diffusion-MRI with signal propagation time obtained from electrical stimulation. As the result we obtain speeds of signal propagation in white matter and timescales of local processing in gray matter. These results are differentiated with respect to specific brain areas and connections.

Methods

Our study is based on multi-subject analysis engaging two disjunctive cohorts of humans. The first cohort, CONNECT/Archi dataset [1], provides diffusion MRI HARDI data of 77 healthy subjects. These data have been clustered in order to obtain white matter pathways repetitive between the subjects [2, 3] what allowed us to use them in the context of the second cohort: brought together by the F-TRACT project (http://f-tract.eu) [4, 5] over one thousand pharmaco-resistant epileptic patients who, in the course of preparation to a brain resection surgery, underwent intracerebral implantation with stereoencephalographic EEG (SEEG) electrodes.

In order to increase spatial resolution, we divided white matter pathways according to their ending gray matter parcels as defined by the AAL parcellation [6]. We obtained 322 white matter bundles. For each bundle we identified nearby SEEG electrodes and considered stimulations performed at the end of the bundle – in gray matter - and recorded anywhere near the bundle. We computed spatially dependent distribution of probability of registering a significantly strong response to stimulation. Stimulations in each direction were considered independently, resulting in two distributions per bundle. We introduced normalization methods based either on an inter-bundle comparison or on a null distribution. Finally, following the assumption that signal propagation speed is constant along a bundle, we performed linear regression and obtained speed per white matter bundle (in each direction) and time constants of local processing in gray matter per AAL parcel.

Results

We found that the probability of observing a significant response to SEEG stimulation is greater when the stimulating and recording intracerebral electrodes are likely to be connected by a white matter pathway. This result holds regardless of distance between the stimulation and recording sites, although probability strongly decays with this distance.

Projection of the probability onto individual bundles yields 644 distributions. Here, as an example, we present results obtained from stimulation performed to the left middle temporal pole. The bundles mediating direct propagation of the signal resulting from such stimulation are presented in Figure 1. Color coded is probability of observing a significant response to stimulation and maroon codes for no data. Speed of signal propagation from this site to e.g. occipital inferior left parcel was found to be 13 m/s +/- 3 m/s. Finally, in accordance with earlier studies [5], the map of local processing time constants suggests that primary brain areas respond faster than higher brain areas.

Conclusions

We integrated structural and functional connectivity data obtained from two different modalities – diffusion MRI and SEEG-based connectivity mapping – and two disjunctive large cohorts of humans. We found concordance between the modalities and we computed quantities not accessible from each modality alone, namely speed of signal propagation in the white matter and timescale of processing in the gray matter. The brain atlas with our results will be shared online.

Acknowledgements

The research leading to these results has received funding from the European Research Council under the European Union's Seventh Framework Programme (FP/2007–2013)/ERC Grant Agreement no. 616268 F-TRACT, the European Union's Horizon 2020 Framework Programme for Research and Innovation under Specific Grant Agreement No. 785907 and 945539 (Human Brain Project SGA2 and SGA3), and from the Agence Nationale de la Recherche grant number ANR-21-NEUC-0005-01.

Figures

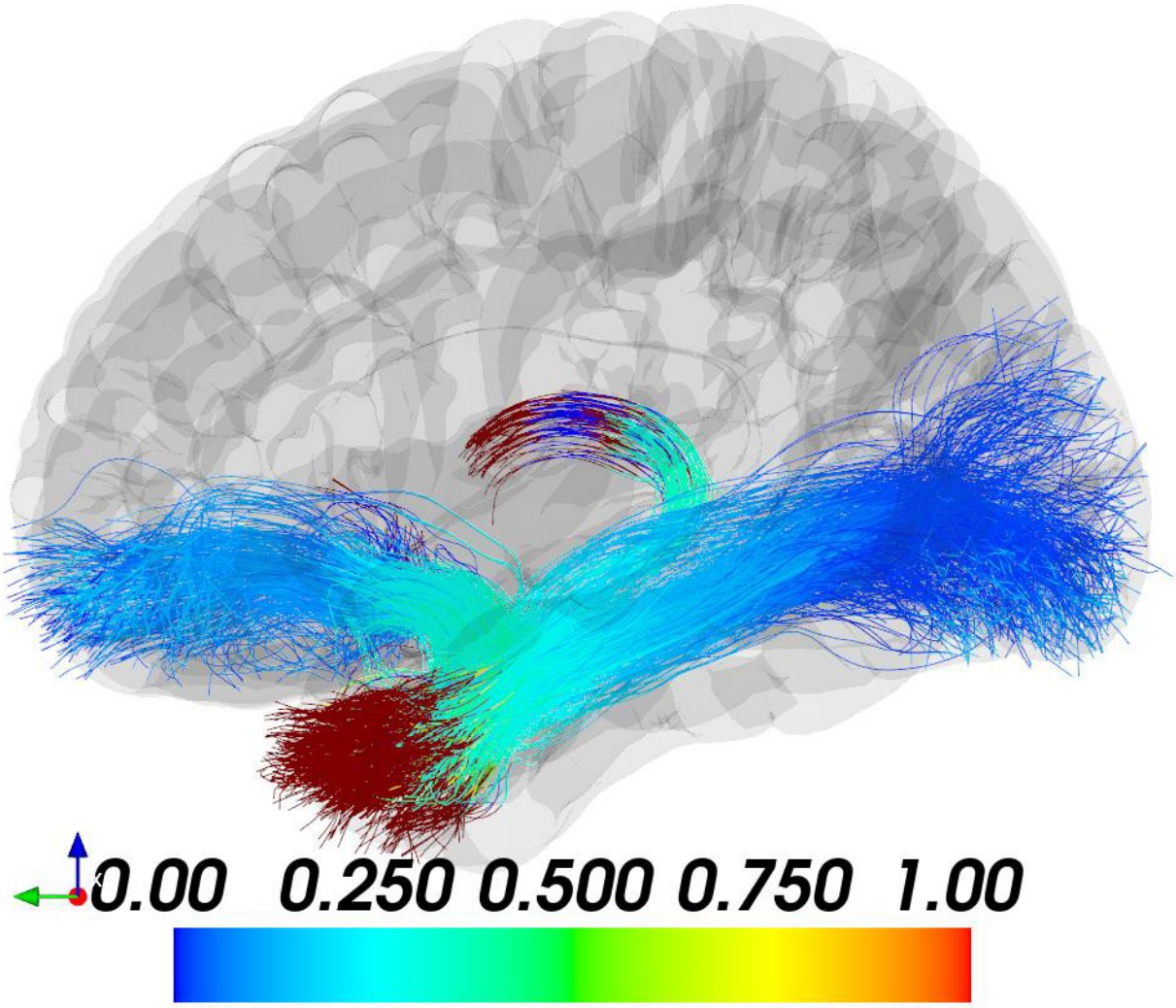

Figure 1. Projection onto white matter bundles of the probability of observing a significant response to SEEG stimulation in the left middle temporal pole. Maroon codes missing data

References

[1] Schmitt B et al. (2012), “CONNECT/ARCHI: an open database to infer atlases of the human brain connectivity”, ESMRMB.

[2] Guevara P et al. (2011) “Robust clustering of massive tractography datasets” Neuroimage vol. 54, pages 1975-1993.

[3] Guevara P et al. (2012), “Automatic fiber bundle segmentation in massive tractography datasets using a multi-subject bundle atlas”, NeuroImage vol. 61, pages 1083-1099

[4] Trebaul L et al. (2018) “Probabilistic functional tractography of the human cortex revisited”, NeuroImage vol. 181, pages 414-429.

[5] Lemaréchal J-D et al. (2022) A brain atlas of axonal and synaptic delays based on modelling of cortico-cortical evoked potentials. Brain 145(5):1653–1667.

[6] Tzourio-Mazoyer N et al. Automated Anatomical Labeling of Activations in SPM Using a Macroscopic Anatomical Parcellation of the MNI MRI Single-Subject Brain. *NeuroImage* 2002, 15 :273-289

50. Nested parcellations connectome delivered for one large dataset using Constellation algorithm

C. Langlet[1*], D. Rivière[1], A. Grigis[1], V. Frouin[1], S. Bludau[2], T. Dickscheid[2], K. Amunts[2,3] and J.-F. Mangin[1]

1: Université Paris-Saclay, CEA, CNRS, Neurospin, Saclay, France

2: Institute of Neuroscience and Medicine (INM-1), Research Centre Jülich, 52425 Jülich, Germany 3:

Cecile und Oskar Vogt Institut für Hirnforschung, Heinrich-Heine Universität Düsseldorf, Germany

*clement.langlet@cea.fr

INTRODUCTION/MOTIVATION

The Human Brain Project aims to decrease the gap between microscopic and macroscopic features of the brain, by defining the structure of a multiscale connectome and its inherent variability between individuals. One of the components of this target connectome is the structural connectivity induced by millions of white-matter fibers linking regions across the brain, that diffusion MRI can highlight. With the potential of the large Human Connectome Project[1] dataset and the innovative algorithm Constellation[2], we first constructed an adequate structural connectome atlas and then obtained individual parcellations and connectomes for each individual of the dataset by applying a projection method.

METHODS

Preprocessing steps consisted in generating the tractographies from the outstanding diffusion MRI data of 1004 subjects of the S1200 HCP release using FSL probtrackx2[3] mode and resampling the Freesurfer[4] meshes, extracted from the 3T-MRI images, of these subjects to the fs_LR 32K referential, according to HCP guidelines.

Using a group of 200 of these subjects, we used Constellation software to subdivide both the Desikan-Killiany atlas[5] and the GapMaps of the Julich-Brain[6] atlas (v2.9[7]) projected onto the surface[8]. For each region of interest, by applying a machine learning-based approach on the connectivity fingerprints of the subjects of the group, various numbers of subregions were considered. The selection of the most adequate number of such regions yielded an optimal parcellation, in the sense that each parcel corresponds to a region whose connectivity to the rest of the brain is stable throughout the population.

For each atlas, the optimal parcellation was then projected onto individual subjects of the database by determining the most probable label of each vertex. Therefore, by taking into account the fibers organization of each subject, we obtained 1004 fine-tuned individual parcellations that were used to compute macroscopic structural connectomes stable across the population. These individual parcellations were also coupled with resting-state functional MRI images to compute functional connectomes that describe probable communications between the corresponding parcels.

Additionally, as part of the Brainvisa suite[8], Constellation was adapted to CEA's supercomputing center, one of the flagships of Fenix Infrastructure.

RESULTS AND DISCUSSION

Hence, we obtained two atlases (*Figure 1*): Constellation, a whole-brain structural-based connectivity atlas, and a Constellation-augmented Julich-Brain atlas by integrating the parcellated GapMaps to the original atlas. For each of these atlases, we provide to the modeling community[9] the 1004 individual parcellations conjointly with their corresponding structural and functional connectomes[10] (*Figure 2*).

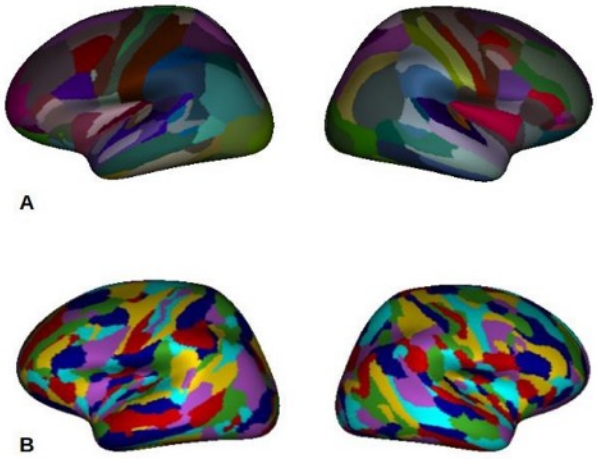

Figure 1 : Constellation atlas (A). Constellation-augmented Julich-Brain (B)

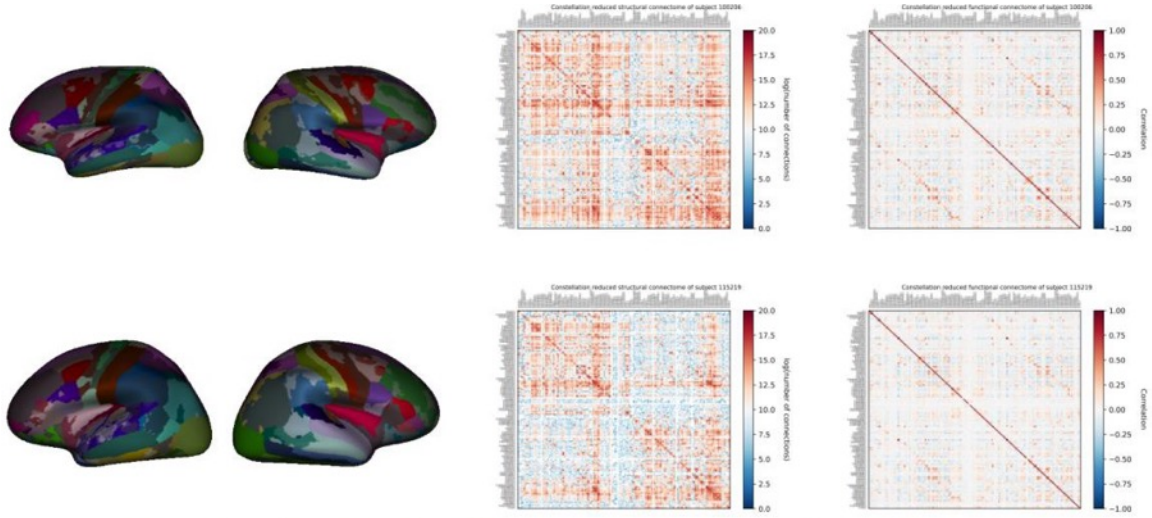

Figure 2 : Fine-tuning of a parcellation to individuals to achieve stable structural and functional connectomes

This work provides solid foundations for the study of the human connectome and opens new perspectives for the understanding of the brain's intrinsic variability both in terms of parcellations and connectomes. The choice of the optimal parcellation as base for the projection process can still be refined, especially in conjunction with current cytoarchitectonics mapping. Finally, in the short term, these connectivity-consistent parcellations will give rise to heritability studies as a validation entrypoint for larger surface region-based genetic studies.

Keywords: **brain mapping, parcellations, Constellation, Julich-Brain, Desikan, diffusion MRI, structural connectome, functional connectome, Human Connectome Project, Fenix Infrastructure**

ACKNOWLEDGEMENTS

This research received funding from the European Union's Horizon 2020 Research and Innovation Programme under Grant Agreement No. 945539 (HBP SGA3).

Data were provided in part by the Human Connectome Project, WU-Minn Consortium (Principal Investigators: David Van Essen and Kamil Ugurbil; 1U54MH091657) funded by the 16 NIH Institutes and Centers that support the NIH Blueprint for Neuroscience Research; and by the McDonnell Center for Systems Neuroscience at Washington University.

REFERENCES

[1] David C. Van Essen, Stephen M. Smith, Deanna M. Barch, Timothy E.J. Behrens, Essa Yacoub, Kamil Ugurbil, for the WU-Minn HCP Consortium. (2013). The WU-Minn Human Connectome Project: An overview. NeuroImage 80(2013):62-79. DOI: 10.1016/j.neuroimage.2013.05.041
[2] S. Lefranc, P. Roca, M. Perrot, C. Poupon, D. L. Bihan, J.-F. Mangin, and D. Rivière. Groupwise connectivity-based parcellation of the whole human cortical surface. Medical Image Analysis, 30:11– 29, 2016. DOI: 10.1016/j.media.2016.01.003
[3] Dale AM, Fischl B, Sereno MI. Cortical Surface-Based Analysis: I. Segmentation and Surface Reconstruction. NeuroImage. 1999;9(2):179-194. DOI: 10.1006/nimg.1998.0395
[4] Behrens TEJ, Berg HJ, Jbabdi S, Rushworth MFS, Woolrich MW. Probabilistic diffusion tractography with multiple fibre orientations: What can we gain? NeuroImage. 2007;34(1):144-155. DOI: 10.1016/j.neuroimage.2006.09.018
[5] Desikan RS, Ségonne F, Fischl B, et al. An automated labeling system for subdividing the human cerebral cortex on MRI scans into gyral based regions of interest. NeuroImage. 2006;31(3):968-980. DOI: 10.1016/j.neuroimage.2006.01.021
[6] Amunts, K., Mohlberg, H., Bludau, S., & Zilles, K. (2020). Julich-Brain: A 3D probabilistic atlas of the human brain's cytoarchitecture. Science, 369(6506), 988–992. DOI: 10.1126/science.abb4588
[7] Amunts, K., Mohlberg, H., Bludau, S., Caspers, S., Eickhoff, S. B., & Pieperhoff, P. (2021). Whole- brain parcellation of the Julich-Brain Cytoarchitectonic Atlas (v2.9) [Data set]. EBRAINS. DOI: 10.25493/VSMK-H94
[8] Mangin, J. F., Rivière, D., & Amunts, K. (2021). Surface projections of Julich-Brain cytoarchitectonic maps (v2.9) [Data set]. EBRAINS. DOI: 10.25493/2FNZGY-6AS
[9] Sanz Leon P, Knock S, Woodman M, et al. The Virtual Brain: a simulator of primate brain network dynamics. Frontiers in Neuroinformatics. 2013;7. Accessed February 2, 2023. DOI: 10.3389/fninf.2013.00010
[10] Langlet, C., Rivière, D., & Mangin, J.-F. (2022). Nested parcellations connectome delivered for one large dataset using Constellation algorithm (v1.1) [Data set]. EBRAINS. DOI: 10.25493/5RCR-GS

51. Multi-scale multi-modal connectomic and cytoarchitectonic mapping in the same human brain section

Roxana N. Kooijmans[1,2*], Irene Costantini[3,4,5], Markus Axer[2,6]

[1]Vision and Cognition, Netherlands Institute for Neuroscience, The Dutch Academy for Arts and Science, Amsterdam, The Netherlands

[2]Institute of Neuroscience and Medicine-1 (INM-1), Forschungszentrum Jülich, Jülich, Germany

[3]European Laboratory for Non-Linear Spectroscopy, University of Florence, Florence, Italy

[4]Department of Biology, University of Florence, Florence, Italy

[5]National Institute of Optics, National Research Council, Sesto Fiorentino, Italy

[6]Department of Physics, School of Mathematics and Natural Sciences, Bergische Universität Wuppertal, Wuppertal, Germany

*r.kooijmans@nin.knaw.nl

INTRODUCTION/MOTIVATION

We need new labelling and imaging protocols to be able to extend detailed human brain mapping (Amunts et al., 2020) and atlasing (https://ebrains.eu/service/human-brain-atlas) with high-resolution fibre (Axer & Amunts, 2022), and molecular information originating in animal research. Such developments would facilitate better understanding of the interplay between cell diversity and connectivity, and how it gives rise to the described functional specificity of cytoarchitectonically defined brain areas.

We combine multiple independent optical imaging techniques to acquire high-resolution data of different scales (micron and sub-micron) as well as different modalities (fibre and cell type) of the same human brain section to address their relationship.

METHODS

We used 3 different methods to generate independent information channels mapping fibre-, as well as cell-architecture in the same human brain section. We acquired 3D-PLI (3D Polarised Light Imaging, Axer et al., 2011) data for micron, and TPFM (two photon fluorescence microscopy, Costantini et al., 2021) for sub-micron fibre resolution, followed by bright field light microscopy of molecularly identified cell types, sequentially, at precisely the same location.

RESULTS AND DISCUSSION

We show that it is feasible to image both fibres (at multiple scales), as well as molecularly identified cell types, in the same human brain section. This will enable us to further explore their contribution to the differences between cytoarchitectonic areas, and mapped borders.

Keywords: 3D-Polarized Light Imaging, Immunohistochemistry, Two-Photon-Fluorescence Microscopy, Multimodality, connectome, cytoarchitecture

ACKNOWLEDGEMENTS

This work was supported by the European Union's Horizon 2020 Framework Programme for Research and Innovation (grant no. 945539: "Human Brain Project" SGA3) in the context of WP1(Tasks 1.1 & 1.3).

REFERENCES

[1] Amunts, K., Mohlberg, H., Bludau, S., Zilles, K., 2020. Julich-Brain: A 3D probabilistic atlas of the human brain's cytoarchitecture. Science 369, 988-992.

[2] Axer, M., Amunts, K., 2022. Scale matters: The nested human connectome. Science 378, 500-504.

[3| Axer, M., Amunts, K., Grassel, D., Palm, C., Dammers, J., Axer, H., Pietrzyk, U., Zilles, K., 2011. A novel approach to the human connectome: ultra-high resolution mapping of fiber tracts in the brain. NeuroImage 54, 1091-1101. [4| Costantini, I., Baria, E., Sorelli, M., Matuschke, F., Giardini, F., Menzel, M., Mazzamuto, G., Silvestri, L., Cicchi, R., Amunts, K., Axer, M., Pavone, F.S., 2021. Autofluorescence enhancement for label-free imaging of myelinated fibers in mammalian brains. Sci Rep 11, 8038.

52. VoluBA: Interactive registration of high-resolution volumes to 3D reference atlases

Timo Dickscheid[1, 2 *], Julia Thönnißen[1], Xiao Gui[1], Yann Leprince[3], Pavel Chervakov[1], Daviti Gogshelidze[1], Katrin Amunts[1, 4]

[1] Institute of Neuroscience and Medicine (INM-1), Forschungszentrum Jülich, Germany

[2] Institute of Computer Science, Heinrich-Heine-University Düsseldorf, Germany

[3] Neurospin, CEA, Gif-sur-Yvette, France

[4] C. & O. Vogt Institute for Brain Research, University Hospital Düsseldorf, Heinrich-Heine-University Düsseldorf, Germany

* t.dickscheid@fz-juelich.de

INTRODUCTION/MOTIVATION

Spatial anchoring of high-resolution volumes of interest (VOIs) from different imaging experiments into the detailed anatomical context of a high-resolution reference model such as the BigBrain[1] became an important practical problem with increasingly available datasets during recent years. Typical examples include the integration of high-resolution MRI, 3D Polarized Light Imaging, or X-ray computed tomography measurements of brain tissues, which would be appropriately organised in the detailed anatomical context of the BigBrain model. However, working on a proper anchoring of such imaging data to the full-resolution reference template is out of reach for many neuroscientists due to the sheer size of the datasets, the lack of available tools, but also the problem to identify correspondences between the datasets in a reliable and reproducible way. Here we present a new release of the interactive volumetric alignment tool VoluBA, which allows anchoring of volumetric image data to reference volumes at microscopical spatial resolutions. VoluBA is implemented as an online web service and enables interactive manipulation of image position, scale, and orientation, flipping of coordinate axes, and entering of anatomical point landmarks in 3D. The resulting transformation parameters can be downloaded in JSON format or used to view the anchored image volume in the interactive atlas viewer siibra-explorer.

METHODS

VoluBA offers a highly interactive workflow. Users can log in with their ORCID or EBRAINS account to upload a dataset into a private working space to perform the anchoring process. The BigBrain model serves as the default reference volume. The input volume is presented as a graphical overlay in a 3D view with orthogonal cross sections, which utilizes Google's neuroglancer engine[2] (Fig. 1). The latest VoluBA release provides options to finetune the overlay by customizing contrast, brightness, colormaps, and intensity thresholds. The 3D view can be used to directly manipulate the relative position and orientation of the input volume. A dialogue window further enables adjustment of its voxel scaling and axis orientations. These settings determine a rigid transformation between the two volumes, which is modelled as a 3D affine matrix. A 3D landmark editor can then refine the

transformation by specifying pairs of corresponding points between the volumes. This is further facilitated by an optional side-by-side navigation mode, where the incoming and reference volume are shown in two separate views. From a set of landmarks, the affine transformation matrix can be recalculated with additional degrees of freedom, including shearing. Alignment actions can be performed and repeated in arbitrary order, supported through a history browser which allows to undo individual anchoring steps.

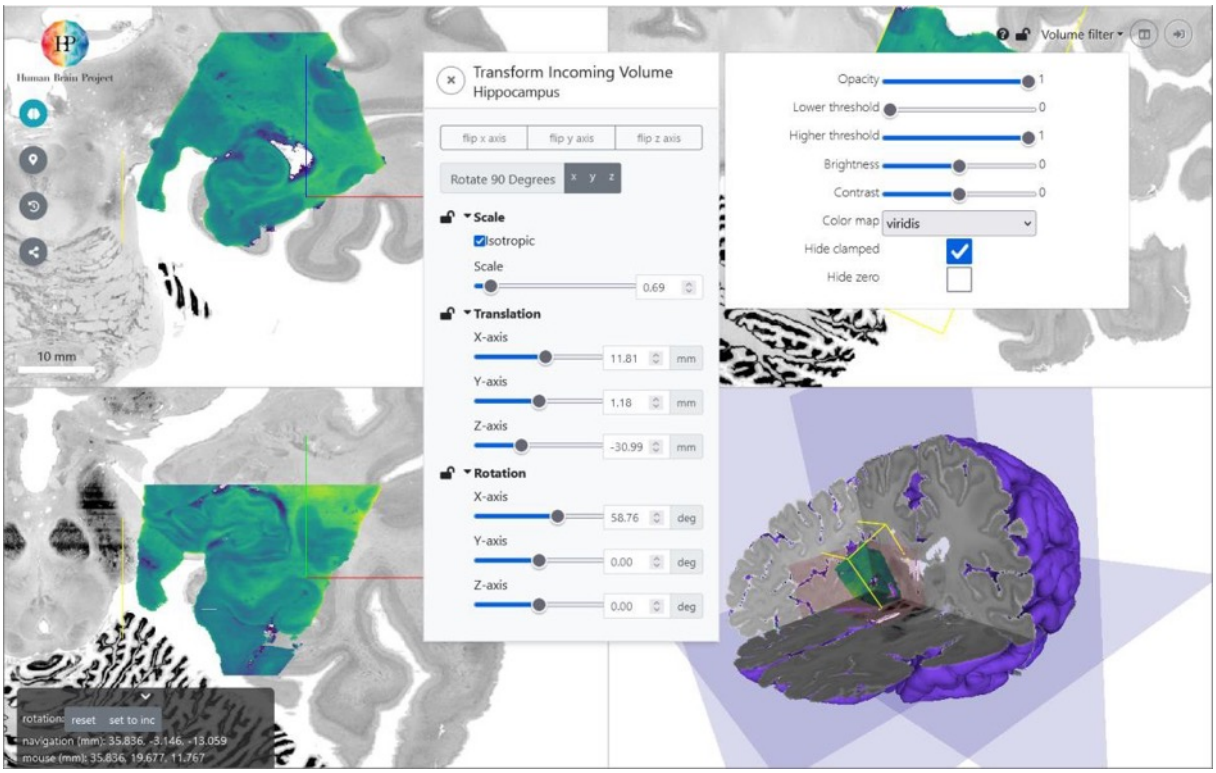

Fig. 1: After uploading a volumetric dataset, various filters like contrast or colour maps allow to configure the presentation of the data. The user can position the volume on top of a reference brain (here: the BigBrain model) by shifting and rotating the input in any of the 3 planar views. Further linear geometric alignments can be adjusted in a parameter window. For more detailed affine adjustment, corresponding point landmarks can be entered.

RESULTS AND DISCUSSION

Anchoring results from VoluBA can be used in several ways. First, users can download the parameters of the affine transformation matrix as a JSON file for reference. The stored transformation file can be re-imported in VoluBA, and due to its simple structure be utilized in other tools and workflows. Furthermore, VoluBA can generate a private URL to view and share the anchored volume as a remote dataset in neuroglancer-based image viewers. Most importantly, VoluBA offers a direct link to open the anchored volume as a semi-transparent layer in the interactive atlas viewer siibra-explorer (Fig. 2). VoluBA has been used successfully by EBRAINS curation teams and different research labs to anchor volumes of interest to BigBrain reference space. Examples include a hippocampus sample imaged with MRI and 3D Polarized Light Imaging[3], a hippocampus sample imaged with phase-contrast computed tomography[4], and a 3D model of the human brain stem[5]. VoluBA is openly accessible in its most recent version at http://voluba.apps.hbp.eu. Detailed documentation is available at https://voluba.readthedocs.io/en/latest/.

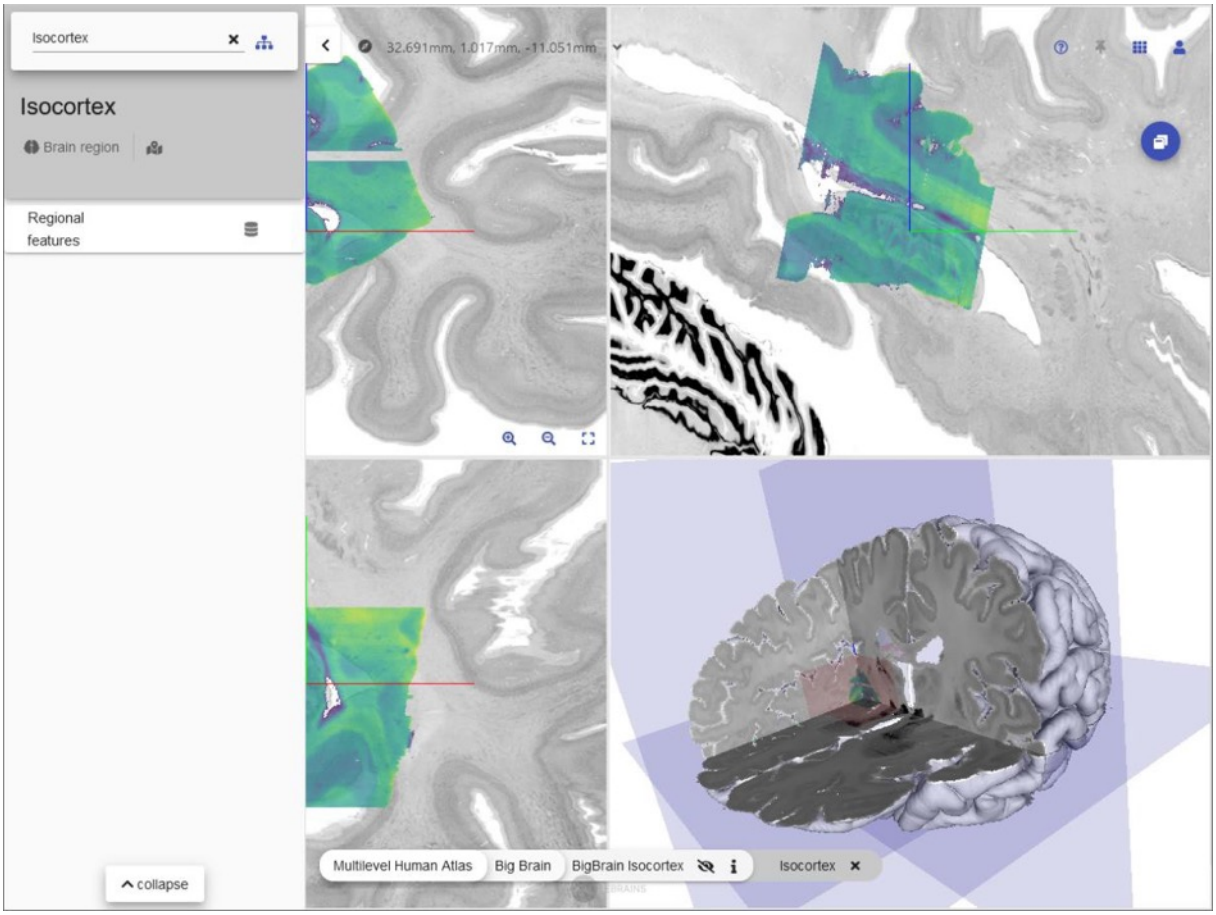

Fig. 2: Users can view the anchoring result as an overlay in the interactive atlas viewer siibra-explorer. Thus, the user can directly inspect the aligned data superimposed with the full atlas context and compare it to atlas regions as well as other data linked to the same reference space.

Keywords: brain atlasing, spatial anchoring, image registration

ACKNOWLEDGEMENTS

This project received funding from the European Union's Horizon 2020 Research and Innovation Programme, grant agreement 945539 (HBP SGA3), and Priority Program 2041 (SPP 2041) "Computational Connectomics" of the German Research Foundation (DFG), as well as the Helmholtz Association's Initiative and Networking Fund through the Helmholtz International BigBrain Analytics and Learning Laboratory (HIBALL) under the Helmholtz International Lab grant agreement InterLabs-0015.

REFERENCES

[1] Amunts K, Lepage C, Borgeat L, Mohlberg H, Dickscheid T, Rousseau MÉ, Bludau S, Bazin PL, Lewis LB, Oros-Peusquens AM, Shah NJ, Lippert T, Zilles K, Evans AC. BigBrain: An Ultrahigh-Resolution 3D Human Brain Model. Science. 2013;340(6139):1472-1475. doi:10.1126/science.1235381

[2] Maitin-Shepard J, Baden A, Silversmith W, Perlman E, Collman F, Blakely T, Funke J, Jordan C, Falk B, Kemnitz N, tingzhao, Roat C, Castro M, Jagannathan S, moenigin, Clements J, Hoag A, Katz B, Parsons D,

Wu J, Kamentsky L, Chervakov P, Hubbard P, Berg S, Hoffer J, Halageri A, Machacek C, Mader K, Roeder L, Li PH. google/neuroglancer: Published online October 16, 2021. doi:10.5281/zenodo.5573294

[3] Axer M, Poupon C, Costantini I. Fiber structures of a human hippocampus based on joint DMRI, 3D-PLI, and TPFM acquisitions. Published online January 29, 2020. doi:10.25493/JQ30-E08

[4] Eckermann M, Schmitzer B, van der Meer F, Franz J, Hansen O, Stadelmann C, Salditt T. Three-dimensional virtual histology of the human hippocampus based on phase-contrast computed tomography. Proc Natl Acad Sci. 2021;118(48):e2113835118. doi:10.1073/pnas.2113835118

[5] Lechanoine F, Jacquesson T, Beaujoin J, Serres B, Mohammadi M, Planty-Bonjour A, Andersson F, Poupon F, Poupon C, Destrieux C. WIKIBrainStem: An online atlas to manually segment the human brainstem at the mesoscopic scale from ultrahigh field MRI. NeuroImage. 2021;236:118080. doi:10.1016/j.neuroimage.2021.118080

53. Linking the multilevel human brain atlas to neuroscience workflows with siibra

Timo Dickscheid[1, 2 *], Sebastian Bludau[1], Xiao Gui[1], Katrin Amunts[1, 3]

1 Institute of Neuroscience and Medicine (INM-1), Forschungszentrum Jülich, Germany

2 Institute of Computer Science, Heinrich-Heine-University Düsseldorf, Germany

3 C. & O. Vogt Institute for Brain Research, University Hospital Düsseldorf, Heinrich-Heine-University Düsseldorf, Germany

* t.dickscheid@fz-juelich.de

INTRODUCTION/MOTIVATION

Studying the human brain requires to capture its structural and functional organization in a common spatial framework. Despite progress in imaging and mapping however, access to information of different scales and modalities for applications ranging from visual exploration to computational workflows remains a challenge. We present siibra, a tool suite that implements a multilevel atlas of the human brain by providing streamlined access to reference templates at different spatial scales, complementary parcellation maps, and multimodal data features. The tool suite includes a web-based 3D viewer and a Python library to support a broad range of use cases. It utilizes EBRAINS as a hosting platform and implements interfaces to established neuroscience resources. Tools and contents are freely available.

METHODS

siibra-explorer is the interactive 3D atlas viewer in EBRAINS hosted at https://atlases.ebrains.eu/viewer. It integrates neuroglancer [10] and a custom surface view to navigate brain templates and parcellation maps at multiple resolutions. siibra-python (https://siibra-python.readthedocs.io) is a software library for using the atlas framework in computational workflows, well compatible with established tools such as nibabel and pandas. It exposes the core functionality to siibra-explorer through a REST API. Motivated by community ideas [3], siibra implements semantic concepts for parcellations and reference spaces, and separates them from their spatial representations in image and surface form. It builds on Julich-Brain cytoarchitectonic maps [4], complements them with functional modules [5] and fiber structures [8], and integrates the microscopic BigBrain model [2] with the MNI152, Colin27 [7] and fsaverage [6] spaces. Regions and locations are linked with data of molecular, cellular, and functional architecture, connectivity and population variance (Fig. 1). A unified interface provides straightforward access to 3D volumes in different forms, including NIfTI images, various meshes, and Terabyte- sized multiresolution data. Content is stored as public datasets on FENIX (https://fenix-ri.eu) with metadata curated in the EBRAINS knowledge graph (https://kg.ebrains.eu) according to FAIR principles. This is complemented by interfaces to additional resources such as the Allen brain atlas [1].

RESULTS AND DISCUSSION

siibra supports a range of neuroscientific use cases. Workflows often start with specifying locations in the brain, e.g by interactive navigation in the 3D viewer, providing 3D coordinates, or loading a NIfTI file (Fig. 1A). Siibra then assigns regions from different parcellations to coordinates, peaks or 3D structures (Fig. 1B). Assignment utilizes probabilistic maps (e.g. functional, cyto- or fiber architectonic maps), and distinguishes between incidence,

correlation and overlap of structures. To evaluate structures defined in different spaces, siibra automatically warps locations between reference templates using precomputed diffeomorphic transformations [9]. Resulting matched brain regions and coordinates can then be used to query features that capture various regional aspects of brain organization (Fig. 1C), so far covering cellular (cell densities; staining profiles) and molecular architecture (receptor densities; gene expressions), structural and functional connectivity from different cohorts, and dynamic access to a growing set of histological data. Data structures are tagged with comprehensive metadata and use established standards for tabular and image data. In summary, siibra facilitates multimodal neuroscience analyses by offering streamlined access to a multilevel human brain atlas framework that covers different resolutions and complementary aspects of brain organization. With an interactive web interface and Python client, it supports a broad range of workflows from neuroimaging, AI, and computational neuroscience. siibra is unique in linking brain features from molecular to microanatomical level into a common atlas framework, and designed to be extended with new datasets, maps, and routines.

[1] Allen Institute for Brain Science, Allen Brain Atlas API, © 2015 Allen Institute for Brain Science. Available from: brain-map.org/api/index.html

[2] Amunts, K. et al. (2013), 'BigBrain: An Ultrahigh-Resolution 3D Human Brain Model', Science 340, 1472– 1475

[3] Amunts, K. et al. (2014), 'Interoperable atlases of the human brain', NeuroImage 99, 525–532

[4] Amunts, K. et al. (2020), 'Julich-Brain: A 3D probabilistic atlas of the human brain's cytoarchitecture', Science 369, 988–992

[5] Dadi, K. et al. (2020), 'Fine-grain atlases of functional modes for fMRI analysis', NeuroImage 221, 117126

[6] Fischl, B. et al. (1999), 'High-resolution intersubject averaging and a coordinate system for the cortical surface', Human Brain Mapping 8, 272-284

[7] Fonov, V. et al. (2011), 'Unbiased average age-appropriate atlases for pediatric studies', Neuroimage 54, 313–327

[8] Guevara, M. et al. (2016), 'Reproducibility of superficial white matter tracts using diffusion-weighted imaging tractography', NeuroImage 147, 703–725

[9] Lebenberg, J. et al. (2018), 'A framework based on sulcal constraints to align preterm, infant and adult human brain images acquired in vivo and post mortem', Brain Structure and Function, 223, 4153–4168

[10] Maitin-Shepard, J. et al. (2021), google/neuroglancer: Published online October 16, doi:10.5281/zenodo.55732949. Maitin-Shepard, J. et al. (2021), google/neuroglancer: Published online October 16, doi:10.5281/zenodo.5573294

A | **Input: Brain locations** in **MNI,** BigBrain or freesurfer space

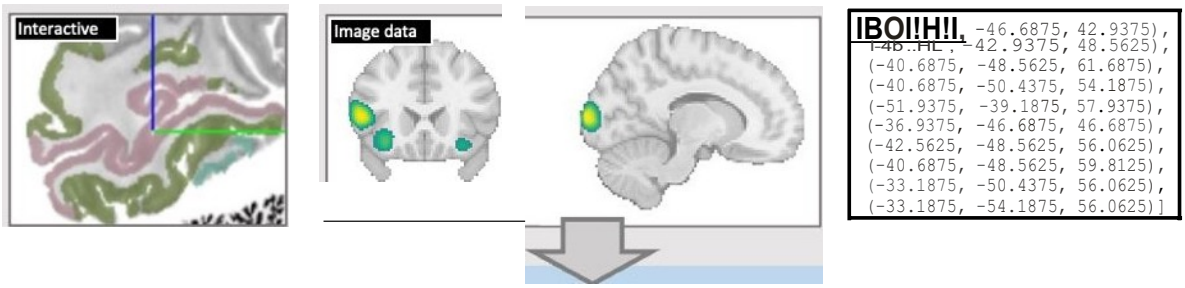

B | **Assign locations to brain regions** using probabilistic maps

Structure	Region	Correlation
	Area Id1o (Insula) len	0.64
5	Area ICl10 {Insuta) rtght	0.55
	Area44 (IFG) left	0.38
3	Area hOC1 I\11, 17, GalCS) left	0.3
3	AreahOC2 Nf2, 18) len	0.3
	AreaOp9 (Frontal Operculum) left	0.26
	Area opa (Frontal Operculum) len	0.25

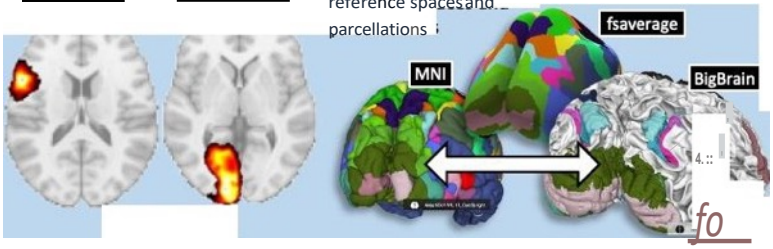

C | **Collect multimodal regional** features capturing regional and population variance

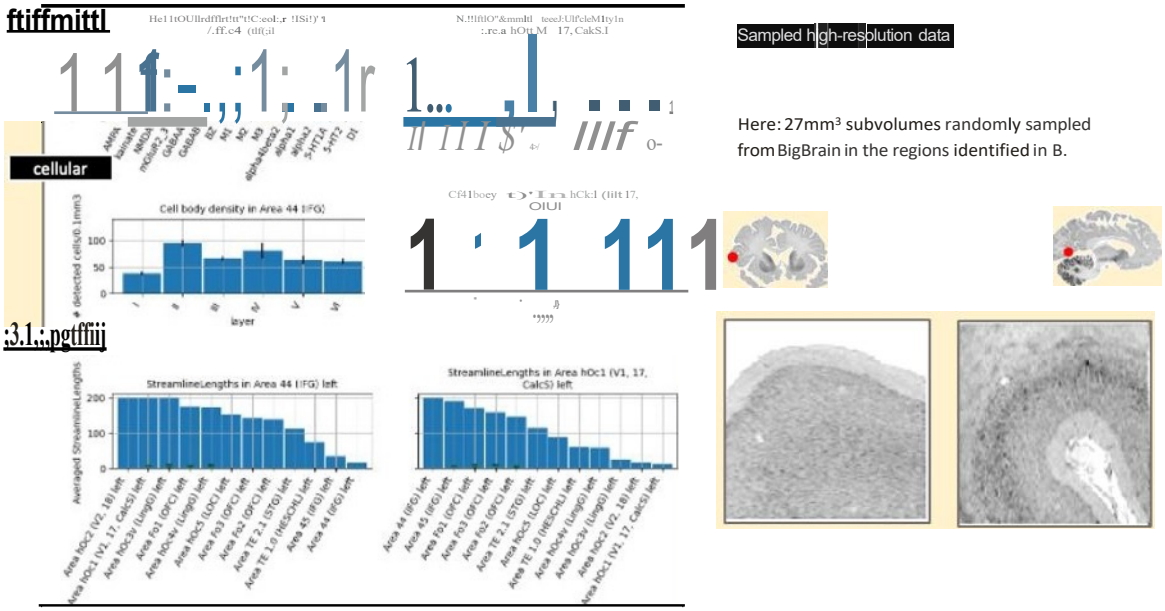

A notebook reproducing the main parts of this figure is available at https://github.com/FZJ-INM1-BDA/siibra-tutorials.

54. A conceptual framework for integrating and positioning brain data in murine 3D brain atlases

Camilla H. Blixhavn, Ingvild E. Bjerke, Ingrid Reiten, Heidi Kleven, Ulrike Schlegel, Maja A. Puchades, Jan G. Bjaalie, Trygve B. Leergaard*

Affiliation: Neural Systems Laboratory, Institute of Basic Medical Sciences, Department of Molecular Medicine, University of Oslo, Oslo, Norway
Corresponding author: Trygve B. Leergaard, t.b.leergaard@medisin.uio.no

INTRODUCTION: Neuroscientists use a range of experimental methods generating increasing amounts of data describing the brain. The multimodality and abundance of brain data pose a challenge for efforts to organize, query, analyze and integrate data in a meaningful way. To achieve this, it is necessary to represent different types of data in a standardized way to allow comparison of anatomical locations and to ultimately ensure data findability and reusability[1]. The EBRAINS research infrastructure employs three-dimensional (3D) brain atlases to organize, combine, and compare multimodal and multilevel neuroscience data. For the atlases to support data integration, spatial queries and co-visualization, we propose using positions defined in a 3D brain atlas as common denominators for representing different types of data as geometric objects in 3D atlases. We here present a conceptual framework, *Locāre* (latin: to place), for positioning and integrating brain data within atlas coordinate systems[2] for the mouse and rat brain (Fig. 1).

METHODS AND RESULTS: Assessing a range of openly available murine neuroscience datasets, we find that information describing data positions in the brain can be sorted into three categories: images, spatial coordinates, and/or semantic descriptions (Fig. 1, step 1). For each of the three information categories, we have specified a process for defining positions in atlases, using image registration software, extracting spatial coordinates, and deduction of positions from atlas terms or semantic descriptions (Fig. 1, step 2). Following these processes, it is possible to derive combinations of atlas coordinates specifying data locations as points, segments, polygons, or polyhedrons, within a 3D brain atlas (Figure 1, step 3). We exemplify how multimodal and multilevel datasets can be combined and co-visualized in the Waxholm Space rat brain atlas (v4, RRID: SCR_017124[3,4,5,6]; Fig. 2).

DISCUSSION: This conceptual framework allows inherently disparate data to be spatially integrated, as the process relies on information *documenting* data locations (images, spatial coordinates, and semantic information), which is independent of the type and format of the data. We discuss the use of community standards (openMINDS: open Metadata Initiative for Neuroscience Data Structures, https://github.com/HumanBrainProject/openMINDS/; SANDS: Spatial Anchoring of Neuroscience Data Structures, https://github.com/HumanBrainProject/openMINDS_SANDS/) to format the output from the integration process, and how the standardized output may be used to increase findability and reusability of open data in the EBRAINS Knowledge Graph (https://search.kg.ebrains.eu/) and the Siibra Explorer (https://atlases.ebrains.eu/viewer/) by enabling data visualization and spatial queries. The *Locāre* framework thus streamlines the process of integrating experimental brain data into atlases, facilitating reusability and findability of open data.

Keywords: brain atlas, FAIR data, data integration, open data, rat brain, mouse brain

Acknowledgements: This work was funded from EU Horizon 2020, Specific Grant Agreement No. 945539 (Human Brain Project SGA3).

References:

1. Wilkinson, M., Dumontier, M., Aalbersberg, I. et al. The FAIR Guiding Principles for scientific data management and stewardship. Sci Data 3, 160018 (2016). https://doi.org/10.1038/sdata.2016.18
2. Kleven, H., Gillespie, T. H., Zehl, L., Dickscheid, T., and Bjaalie, J. G. (2023). AtOM , an ontology model for standardizing use of brain atlases in tools , workflows , and data infrastructures. bioRxiv, 1–24. doi: 10.1101/2023.01.22.525049.
3. Papp, E., Leergaard, T., Calabrese, E., Johnson, G., and Bjaalie, J. (2014). Waxholm Space atlas of the Sprague Dawley rat brain. Neuroimage 97, 374–386. doi: 10.1016/j.neuroimage.2014.04.001.
4. Kjonigsen, L., Lillehaug, S., Bjaalie, J., Witter, M., and Leergaard, T. (2015). Waxholm Space atlas of the rat brain hippocampal region: Three-dimensional delineations based on magnetic resonance and diffusion tensor imaging. Neuroimage 108, 441–449. doi: 10.1016/j.neuroimage.2014.12.080.
5. Osen, K., Imad, J., Wennberg, A., Papp, E., and Leergaard, T. (2019). Waxholm Space atlas of the rat brain auditory system: Three-dimensional delineations based on structural and diffusion tensor magnetic resonance imaging. Neuroimage 199, 38–56. doi: 10.1016/j.neuroimage.2019.05.016.
6. Kleven, H., Bjerke I.E., Clascá, F., Groenewegen, H.J., Bjaalie, J.G., Leergaard, T.B. (2023) Waxholm Space atlas of the rat brain: A 3D atlas supporting data analysis and integration. Research Square (preprint). https://doi.org/10.21203/rs.3.rs-2466303/v1.

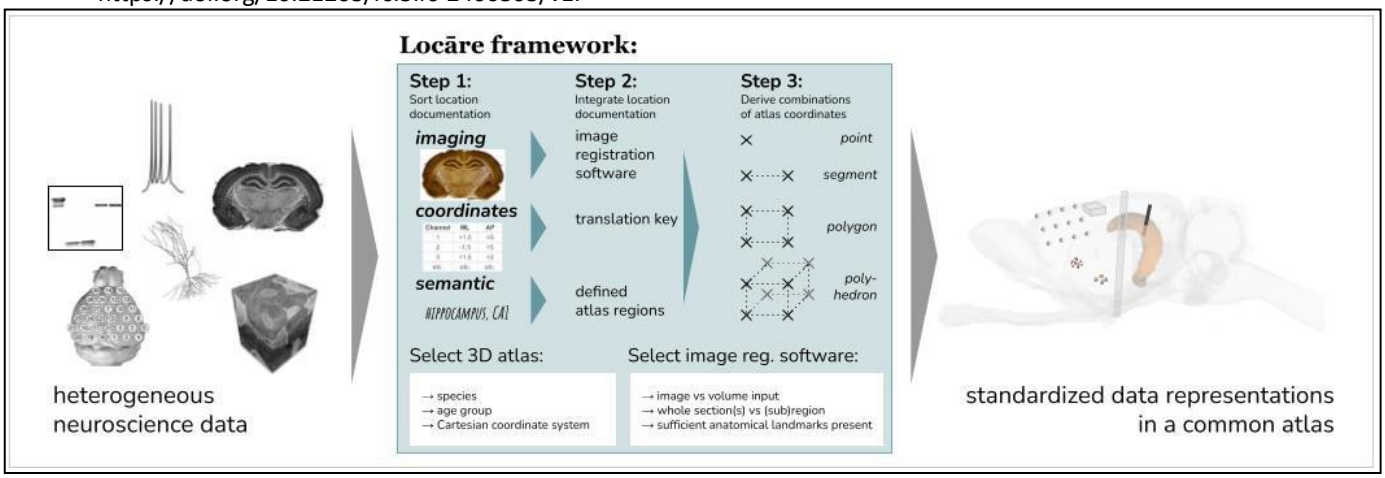

Figure 1. Framework overview. Multimodal and multilevel neuroscience data are subjected to the *Locāre* framework to

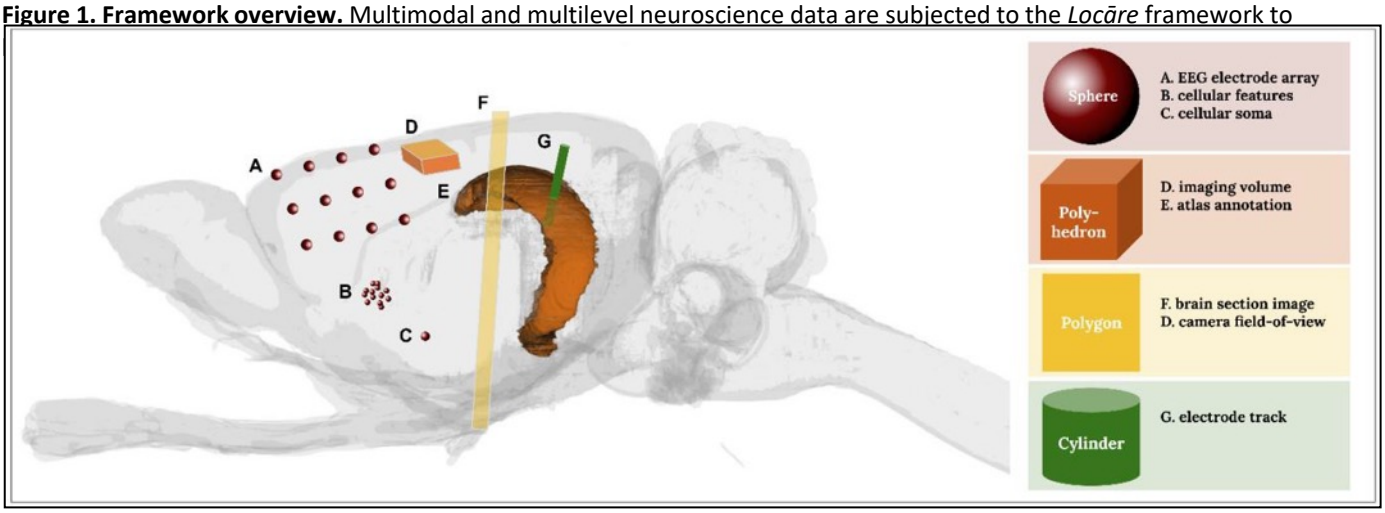

Figure 2. Spatial representations of data within the Waxholm Space rat brain atlas v4. Examples of data represented by a sphere, a polyhedron, a polygon or a cylinder: A) EEG electrode array. B) Cellular features. C) Cellular soma. D) Imaging volume (orange box); camera field-of-view (yellow top layer). E) Atlas annotation (*cornu Ammonis* 1, CA1). F) Brain section image (coronal orientation). G) Electrode track.

55. Interactive brain image segmentation with webilastik

Tomaz Vieira[1], Emil Melnikov[1], Dominik Kutra[1], Anna Kreshuk[1*]

Cell Biology and Biophysics Unit, European Molecular Biology Laboratory, Heidelberg, Germany

*anna.kreshuk@embl.de

INTRODUCTION/MOTIVATION

Image segmentation is a common task in biomedical image analysis. In neuroscience, it is frequently used to find features in brain images acquired at mesoscopic, microscopic or nanoscopic resolution. The goal of our contribution is to automate this task with machine learning, while allowing users retain control over the algorithm performance through interactive training on their own data. Our software ilastik [1] has already been successfully used as a standalone tool for segmentation in a wide variety of biological domains, ranging from cryogenic electron tomography to regular camera images. Here, we present the integration of ilastik with the EBRAINS platform, allowing users to leverage the computational resources provided through EBRAINS HPC centres directly from their browser. Furthermore, webilastik is integrated with other brain atlas analysis tools in the EBRAINS ecosystem.

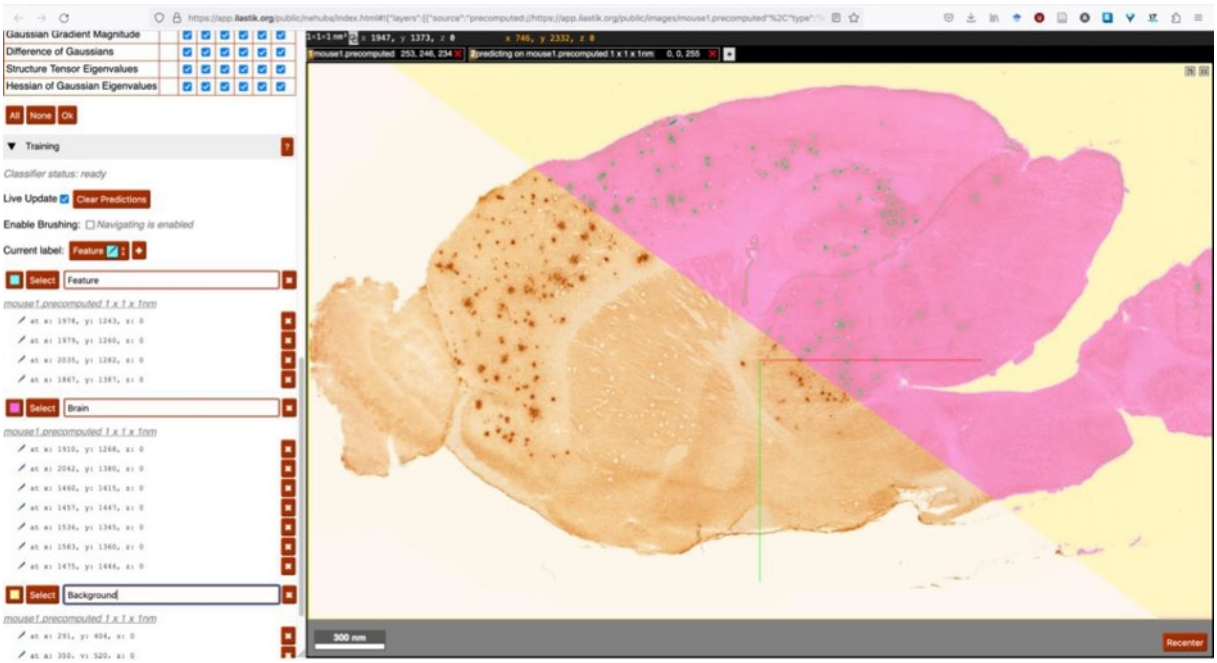

Figure 1 ilastik uses machine learning to automatically segment brain images, interactively guided by user brushstrokes

METHODS

Webilastik is implemented on the basis of the Neuroglancer viewer[2] which is also used in the EBRAINS siibra explorer[3]. The web-based viewer has been extended by interactive segmentation capabilities of ilastik, allowing users to process 2D or

3D data available through EBRAINS, including private data uploaded to Collab Buckets. While the computations are executed on the HPC resources, a simple EBRAINS account is sufficient to launch a webilastik session, interactively train a classifier on a representative sub-volume of the data and submit a larger dataset for offline processing. The bespoke webilastik backend automatically distributes the computations over dynamically allocated HPC resources, maintaining the interactive user feedback loop even for very large brain images. The results can be downloaded from the Collab Bucket or used as input for other EBRAINS analysis tools such as nutilweb.

RESULTS AND DISCUSSION

Webilastik is freely available to EBRAINS users at https://app.ilastik.org or as part of the QUINT workflow Collab (https://wiki.ebrains.eu/bin/view/Collabs/quint-demo). Users can upload their own data or use one of the curated EBRAINS datasets. The computations are performed remotely on the HPC centers compute resources, allowing user annotation and training sessions to persist when the user is offline. This development constitutes a major advance over the monolith ilastik application as described in [1] which is limited to interactive sessions on a single machine. Ilastik documentation is available at https://www.ilastik.org/documentation/index.html. Its use as part of the QUINT workflow (Quantification and Spatial Analysis of Features in Histological Images From Rodent Brain) is described in [3].

Keywords: image analysis, software, EBRAINS

ACKNOWLEDGEMENTS

We gratefully acknowledge financial support by H2020 Research and Innovation Action grants Human Brain Project SGA2 785907, SGA3 945539. We thank the QUINT team for our fruitful collaboration, the EBRAINS infrastructure team for continuous support and all ilastik users for encouraging us to keep developing this software.

REFERENCES

[1] Berg, S., Kutra, D., Kroeger, T., Straehle, C. N., Kausler, B. X., Haubold, C., ... & Kreshuk, A. (2019). Ilastik: interactive machine learning for (bio) image analysis. Nature methods, 16(12), 1226-1232.

[2] https://github.com/google/neuroglancer

[3| Yates, S. C., Groeneboom, N. E., Coello, C., Lichtenthaler, S. F., Kuhn, P. H., Demuth, H. U., ... & Bjaalie, J. G. (2019). QUINT: workflow for quantification and spatial analysis of features in histological images from rodent brain. Frontiers in Neuroinformatics, 13, 75.

56. High-throughput method for brain-wide characterisation of genetically diverse AD mice

Sharon C Yates[1]*, Brianna Gurdon[2,3], Gergely Csucs[1], Nicolaas E Groeneboom[1], Maja A Puchades[1], Catherine Kaczorowski1[2,3,4], Jan G Bjaalie[1].

[1]Neural Systems Laboratory, Institute of Basic Medical Sciences, University of Oslo, Oslo, Norway

[2]The Jackson Laboratory, Bar Harbor, ME, US

[3]The University of Maine Graduate School of Biomedical Sciences and Engineering, Orono, ME

[4]Tufts University Graduate School of Biomedical Sciences, Medford, MA

*s.c.yates@medisin.uio.no

INTRODUCTION/MOTIVATION

The observed variation in the age at onset, severity of pathology and rate of cognitive decline in Alzheimer's disease (AD) patients, despite presence of risk mutations, suggest that background genetic variability may confer protection in some individuals. The AD-BXD mouse population[1] that incorporates 5 familial AD mutations (5XFAD) with genetic diversity reflects this variation in symptom; and provides a unique platform for exploring genotype-phenotype interactions, with potential for revealing resilience genes and pathways[2]. While immunohistochemistry (IHC) is the gold standard for revealing pathological features, new methods are needed to support brain-wide characterization in high-throughput studies. In the BRAINSPACE project, we aimed to develop such new methodologies and have applied them to a subset of AD-BXD mice.

METHODS

Here, we utilize a new atlas-based method (the QUINT workflow)[3] to establish brain-wide alterations in neurons, microglia, reactive astrocytes and beta-amyloid across 40 mice of multiple AD-BXD strains at two ages (6 and 14 months). The method uses the Allen Mouse Brain Common Coordinate Framework version 3 (CCFv3)[4] to define customized regions for the quantification. To meet the needs of the present high-throughput study, new functionality for quality control is added to the workflow to 1. Screen section images to test their suitability for QUINT analysis, and to 2. Assess the quality of the atlas-registration to each region as performed in the workflow (QCAlign software, RRID: SCR_023088). The second assessment is performed at a customized level of the atlas- hierarchy that supports verification based on the manual assessment of overlap between delineations supplied by the atlas and the boundaries revealed by labelling. The tools in the QUINT workflow are shared through the EBRAINS platform (ebrains.eu/service/quint), and are developed to support open and FAIR science[5].

RESULTS AND DISCUSSION

Here, we demonstrate near-global increases in microglia, reactive astrocytes and beta-amyloid across the brains with

increasing age, with little effect on neuronal loads. Despite small sample size, there were also suggestions of individual differences in NeuN loads amongst strains. With the addition of the new QCAlign tool, we were able to remove damaged sections from the analysis according to strict criteria, and to document high-quality registration across the customized regions that were used for the quantification. In a future study, the results will be used together with behavioural and transcriptomic data to stratify AD-BXD strains as resilient or vulnerable, and to reveal gene expression differences across resilient and vulnerable strains that may represent novel targets for therapeutic intervention. In conclusion, we demonstrate that the QUINT workflow is a highly effective method for registering and quantifying pathological changes in genetically diverse rodent models.

ACKNOWLEDGEMENTS

This project has received funding from the European Union's Horizon 2020 Framework Programme for Research and Innovation under the Specific Grant Agreement No. 945539 (Human Brain Project SGA3).

REFERENCES

1. Neuner SM, Heuer SE, Huentelman MJ, O'Connell KMS, Kaczorowski CC. Harnessing Genetic Complexity to Enhance Translatability of Alzheimer's Disease Mouse Models: A Path toward Precision Medicine. *Neuron*. 2019;101(3):399-411.e5. doi:10.1016/j.neuron.2018.11.040
2. Neuner SM, Telpoukhovskaia M, Menon V, O'Connell KMS, Hohman TJ, Kaczorowski CC. Translational approaches to understanding resilience to Alzheimer's disease. *Trends Neurosci*. 2022;45(5). doi:10.1016/j.tins.2022.02.005
3. Yates SC, Groeneboom NE, Coello C, et al. QUINT: Workflow for Quantification and Spatial Analysis of Features in Histological Images From Rodent Brain. *Front Neuroinform*. 2019;13(December):1-14. doi:10.3389/fninf.2019.00075
4. Wang Q, Ding SL, Li Y, et al. The Allen Mouse Brain Common Coordinate Framework: A 3D Reference Atlas. *Cell*. 2020;181(4):936-953.e20. doi:10.1016/j.cell.2020.04.007
5. Chue Hong NP, Katz DS, Barker M, et al. FAIR principles for research software (FAIR4RS principles). *Research Data Alliance*. 2022;(2022):1-32. doi:10.15497/RDA00068

57. Cytoarchitectonic Maps of Five New Areas in the Human Dorsolateral Prefrontal Cortex

K. Lothmann*[1,2], A. Bruno*[1,2], S. Bludau[1], H. Mohlberg[1], K. Amunts[1,2]

1 Institute of Neuroscience and Medicine (INM-1), Research Centre Jülich, Jülich, Germany

2 C. & O. Vogt Institute for Brain Research, University Hospital Düsseldorf, Heinrich-Heine-University Düsseldorf, Düsseldorf, Germany

*K. Lothmann: ki.lothmann@fz-juelich.de

*A. Bruno: a.bruno@fz-juelich.de

INTRODUCTION/MOTIVATION

The dorsolateral prefrontal cortex (DLPFC) is involved in executive functions, including working memory, value encoding, attention, and decision-making[1]. Recent studies supported the notion that the DLPFC is not a single unit but consists of an anterior-posterior and dorsal- ventral axis including small functionally differentiated regions[2,3]. This functional heterogeneity does not correspond to existing parcellation schemes, varying additionally among each other, e.g., regarding their number of areas. Cytoarchitectonic mapping studies showed a subdivision of the DLPFC, for example, into two (area 9 and 46[4]), three (area 9, 9-46, and 46[5]), or four (area 9, 46, 9/46d, and 9/46v[6]). Macroanatomical parcellations are based only on gyri and sulci[7,8], that hardly reflect the underlying microstructural organization. Therefore, there is a need for a detailed cytoarchitectonic parcellation in 3D, that integrates variations in brain structure.

METHODS

For cytoarchitectonic analyses, serial cell body-stained sections of ten human post-mortem brains (five male, five female; age range from 30 to 86 years) from the Body Donor Program of the Department of Anatomy of the University of Düsseldorf were analyzed. Methods described in detail in[9]. Borders between areas were identified by image analysis and a multivariate, statistically reliable mapping approach based on grey-level index (GLI-) profiles that reflect the cytoarchitecture. Area volumes were calculated and compared for putative interhemispheric and sex differences. Considering interindividual variability, probability maps were created for each area in stereotaxic space, assessing the variance between the individual brains.

RESULTS AND DISCUSSION

Five new cytoarchitectonic areas, SFG2, SFG3, SFG4, MFG4, and MFG5, were mapped in serial sections over their full extent in both hemispheres of the sample. The areas were located mainly on the superior and middle frontal gyrus but also reached the neighboring inferior and superior frontal sulci. A hierarchical cluster analysis based on GLI profiles revealed cytoarchitectonic similarities and dissimilarities within this group of areas and with respect to neighboring ones. Neighboring frontal pole areas Fp1 and Fp2, more posterior areas 8d1, 8d2, 8v1, and 8v2 and areas 44 and 45 (Broca-region) were clearly separable[10]. Similarities to previously identified frontal areas[10] were observed: Area SFG3 and area MFG5, mainly situated within the inferior frontal sulcus, clustered with area SFS2 because of different thickness in layer II and IV. Area SFG4 formed a cluster with area MFG4. Both areas had characteristics of BA9 and BA46. This could be interpreted as the previously outlined transition area[5], which could now be subdivided into two parts: area SFG4 with loosely packed cells and sharp borders and area MFG4 with densely packed cells and a rather diffuse layering.

The analysis of volumes revealed neither statistically significant gender nor interhemispheric differences.

All five areas were superimposed in stereotaxic reference spaces (MNI Colin27 and ICBM152casym), and probability maps were created as a microstructural reference for the brain function. According to the assumption of a functional subdivision into anterior and posterior subregions[2,3], SFG2 and SFG3 could be assigned to anterior DLPFC areas, whereas SFG4, MFG4, and MFG5 correspond to posterior areas. While anterior DLPFC areas are attributed to episodic control for action selection based on ongoing context in relation to more complex cognitive thinking, posterior parts correspond to action selection based on sensory input[2,3]. Activation patterns of the posterior subregion have been related to the execution of movement as well as working memory processes[2], which correlate with the position of areas SFG4 and MFG4. What the internal differences of the areas in the anterior and posterior subregions means in terms of function remains a project of future research.

REFERENCES

1. Friedman NP, Robbins TW. The role of prefrontal cortex in cognitive control and executive function. *Neuropsychopharmacology.* 2022;47(1):72-89. doi:10.1038/s41386-021-01132-0.
2. Cieslik EC, Zilles K, Caspers S, et al. Is there "one" DLPFC in cognitive action control? Evidence for heterogeneity from co-activation-based parcellation. *Cereb Cortex.* 2013;23(11):2677- 2689. doi:10.1093/cercor/bhs256.
3. Jung J, Lambon Ralph MA, Jackson RL. Subregions of DLPFC Display Graded yet Distinct Structural and Functional Connectivity. *J Neurosci.* 2022;42(15):3241-3252. doi:10.1523/jneurosci.1216-21.2022.
4. Brodmann K. Vergleichende Lokalisationslehre der Großhirnrinde in ihren Prinzipien dargestellt auf Grund des Zellenbaues. *Leipzig (DE): Johann Ambrosius Barth.* 1909.
5. Rajkowska G, Goldman-Rakic PS. Cytoarchitectonic definition of prefrontal areas in the normal human cortex: I. Remapping of areas 9 and 46 using quantitative criteria. *Cereb Cortex.* 1995;5(4):307-322. doi:10.1093/cercor/5.4.307.
6. Petrides M. Lateral prefrontal cortex: architectonic and functional organization. *Philos Trans R Soc Lond B Biol Sci.* 2005;360(1456):781-795. doi:10.1098/rstb.2005.1631.
7. Desikan RS, Ségonne F, Fischl B, et al. An automated labeling system for subdividing the human cerebral cortex on MRI scans into gyral based regions of interest. *Neuroimage.* 2006;31(3):968-980. doi:10.1016/j.neuroimage.2006.01.021.
8. Destrieux C, Fischl B, Dale A, Halgren E. Automatic parcellation of human cortical gyri and sulci using standard anatomical nomenclature. *Neuroimage.* 2010;53(1):1-15. doi:10.1016/j.neuroimage.2010.06.010.
9. Amunts K, Mohlberg H, Bludau S, Zilles K. Julich-Brain: A 3D probabilistic atlas of the human brain's cytoarchitecture. *Science.* 2020;369(6506):988-992. doi:10.1126/science.abb4588.
10. Amunts K, Mohlberg H, Bludau S, et al. Julich-Brain Atlas, cytoarchitectonic maps (v3.0) [Data set]. *EBRAINS.* 2022. doi:10.25493/MGKP-Z5T.

58. The Waxholm Space rat brain atlas v4 - a 3D atlas for efficient analysis and transparent reporting

Heidi Kleven[1#], Ingvild E. Bjerke[1], Francisco Clascá[2], Henk J. Groenewegen[3], Jan G. Bjaalie[1], Trygve B. Leergaard[1*]

1. Department of Molecular Medicine, Institute of Basic Medical Sciences, University of Oslo, Norway
2. Department of Histology and Neuroscience, Autonomous University of Madrid, Spain
3. Department of Anatomy and Neuroscience, Amsterdam University Medical Center, The Netherlands

[#]Presenting author
*Corresponding author: t.b.leergaard@medisin.uio.no

INTRODUCTION/MOTIVATION

Three-dimensional (3D) brain atlases provide spatial reference for experimental neuroscience data shared via the EBRAINS research infrastructure. Atlases are used to assign anatomical location to data, enabling researchers to interpret, integrate, and compare observations and measurements collected from different brains. The Waxholm Space (WHS) rat brain atlas (RRID: SCR_017124) is an open source 3D atlas based on a high-resolution magnetic resonance imaging (MRI) and diffusion tensor imaging (DTI) dataset acquired ex-vivo from an adult male Sprague Dawley rat brain[1,2,3]. An important limitation for this atlas has been lack of detailed subdivisions of several major brain regions, such as the thalamus, basal ganglia and cerebral cortex. We have revised and expanded the atlas with more than 100 detailed subdivisions, and here present the first version the WHS rat brain atlas with brain-wide coverage. This atlas is a comprehensive open-access resource incorporated in the EBRAINS atlas services, and several analytic tools.

METHODS

Brain region delineations were manually defined using the ITK-SNAP software[4] (version 3.8.0, http://www.itksnap.org/). The criteria for defining and delineating a brain structure were based on interpretation of the atlas MRI/DTI data set combined with spatially registered cyto-, chemo-, and myeloarchitecture data, other reference atlases, and literature.

RESULTS AND DISCUSSION

The Waxholm Space rat brain atlas v4 comprises an atlas reference MRI/DTI data set in which the Waxholm Space coordinate system is applied, and a whole-brain annotation set which is named and organized by a hierarchical terminology (Fig.1). The atlas contains 222 brain structure delineations, including detailed and revised subdivisions of the cerebral cortex, striatopallidal region, midbrain dopaminergic system, and thalamus[5]. The atlas has been incorporated in tools for registration of images to atlases, planning spatial position of recording electrodes or viral expression, brain-wide analysis, search for data associated with specific brain regions, and visualization of brain atlases, regions and data points. The atlas provides a spatial framework for integration of the multifaceted neuroscience data shared via the EBRAINS platform (http://ebrains.eu) developed by the EU Human Brain Project. It is shared under a CC-BY-SA license via EBRAINS and the Neuroimaging Informatics Tools and Resources Clearinghouse (www.nitrc.org), and has been downloaded >11.000 times since its release on October 1, 2021. In summary, the Waxholm Space rat brain atlas is openly available, contains detailed brain structure delineations and has been incorporated in several tools. We therefore believe that the updated fourth version of the atlas is an important resource for efficient analysis and transparent reporting.

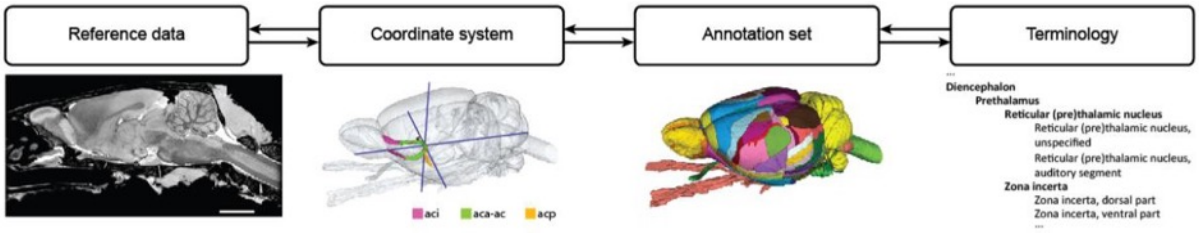

Figure 1: The Waxholm Space atlas of the Sprague Dawley rat brain v4, presented according to the atlas ontology model (AtOM)[6].

Keywords: brain atlases, rat, neuroanatomy, neuroinformatics, spatial registration,

ACKNOWLEDGEMENTS
Funded from the European Union's Horizon 2020 Framework Program for Research and Innovation under the Specific Grant Agreement No. 785907 (Human Brain Project SGA2), Specific Grant Agreement No. 945539 (Human Brain Project SGA3

REFERENCES

1. Papp, E., Leergaard, T., Calabrese, E., Johnson, G., and Bjaalie, J. (2014). Waxholm Space atlas of the Sprague Dawley rat brain. Neuroimage 97, 374–386. doi: 10.1016/j.neuroimage.2014.04.001.
2. Kjonigsen, L., Lillehaug, S., Bjaalie, J., Witter, M., and Leergaard, T. (2015). Waxholm Space atlas of the rat brain hippocampal region: Three-dimensional delineations based on magnetic resonance and diffusion tensor imaging. Neuroimage 108, 441–449. doi: 10.1016/j.neuroimage.2014.12.080.
3. Osen, K., Imad, J., Wennberg, A., Papp, E., and Leergaard, T. (2019). Waxholm Space atlas of the rat brain auditory system: Three-dimensional delineations based on structural and diffusion tensor magnetic resonance imaging. Neuroimage 199, 38–56. doi: 10.1016/j.neuroimage.2019.05.016.
4. Yushkevich, P.A., Piven, J., Hazlett, H.C., Smith, R.G., Ho, S., Gee, J.C., Gerig, G. (2006). User- guided 3D active contour segmentation of an atomical structures: significantly improved efficiency and reliability. Neuroimage 31, 1116–1128. doi: 10.1016/j.neuroimage.2006.01.015.
5. Kleven, H., Bjerke, I., Clascá, F., Groenewegen, H., Bjaalie, J., and Leergaard, T. (2023). Waxholm Space atlas of the rat brain: A 3D atlas supporting data analysis and integration. 07 February 2023, PREPRINT (Version 1) available at Research Square. doi: 10.21203/rs.3.rs-2466303/v1.
6. Kleven, H., Gillespie, T. H., Zehl, L., Dickscheid, T., and Bjaalie, J. G. (2023). AtOM, an ontology model for standardizing use of brain atlases in tools, workflows, and data infrastructures. bioRxiv, 1–
   24. doi: 10.1101/2023.01.22.525049.

59. Accelerated inference on fields: virtual brains in JAX

Marmaduke Woodman[1*], Meysam Hashemi[1], Abolfazl Ziaamehr[1], Anirudh Vattikonda[1], Jan Fousek[1], Viktor Jirsa[1]

[1]Aix Marseille Univ, INSERM, INS, Inst Neurosci Syst, Marseille, France

*e-mail-address of corresponding author(s) marmaduke.woodman@univ-amu.fr

INTRODUCTION/MOTIVATION

Statistical inference for whole brain modelling is a recent breakthrough enabling personalized models for varied applications. The tractability of model inference has been limited so far by the computational scalability of the models for both forward computation but also backwards passes for gradient computation, required for variational and full Markov Chain Monte Carlo (MCMC) algorithms [1,2], while the need to increase spatial and temporal resolution has stretched available resources. In parallel, the deep learning community has built significant computational infrastructure for complex models, which can be repurposed for (a) the needs of personalized whole brain network modelling at high spatial and temporal resolutions [3] and (b) developing and deploying new inference techniques for wider EBRAINS community use.

METHODS

In this work we present an implementation of virtual brain modelling with significant feature parity with the widely used The Virtual Brain (TVB) simulator but builds on the JAX library for NumPy-style tensor computations [4] on both CPU and accelerators such as GPU and TPU; JAX transparently provides efficient autodifferentiation and just- in-time compiling, which enables use of flexible inference schemes. Extended with scalable, GPU friendly inference in mind, the new implementation adds techniques for high spatial and temporal resolution models. A TVB plugin allows users to reuse existing TVB models while smooths the transition to statistical modelling. The resulting library significantly simplifies use cases for HBP and EBRAINS users. The implementation is developed in the open (github.com/ins-amu/vbjax), easily installable, with an open-source yet business-friendly license.

RESULTS AND DISCUSSION

Several use cases from TVB and HBP are presented ranging from rest state aging to virtual epilepsy patient use cases, and the resulting library is shown to support all use cases with similar or better performance. We additionally present for the first time full MCMC inference for a realistic neural field model applied to clinical epilepsy patient data. While the current aim of the library to cover existing use cases, we wish to use it as a test bed for developing further theory innovation on the structure of brain dynamics, as well as integrate with deep learning innovations in flexible parameterizations and approximations, allowing for significant acceleration of model inference.

Keywords: computational neuroscience, machine learning, artificial intelligence

ACKNOWLEDGEMENTS

This research has received funding from the European Union's Horizon 2020 Framework Programme for Research and Innovation under the Specific Grant Agreement No. 945539 (Human Brain Project SGA3).

REFERENCES

[1] Stan Development Team. 2023. Stan Modeling Language Users Guide and Reference Manual, 2.31. https://mc- stan.org

[2] Phan, Du, Neeraj Pradhan, and Martin Jankowiak. "Composable effects for flexible and accelerated probabilistic programming in NumPyro." *arXiv preprint arXiv:1912.11554* (2019).

[3] Wang, Huifang E., et al. "Virtual Epileptic Patient (VEP): Data-driven probabilistic personalized brain modeling in drug-resistant epilepsy." *medRxiv* (2022): 2022-01.

[4] Bradbury et al 2018. "JAX: composable transformations of Python+NumPy programs". http://github.com/google/jax.

...

60. Model driven data analysis on the Human Intracereberal Platform: a Virtual Brain app

Marmaduke Woodman[1*], Jan Fousek[1], Viktor Jirsa[1]

[1]Aix Marseille Univ, INSERM, INS, Inst Neurosci Syst, Marseille, France

*e-mail-address of corresponding author(s) marmaduke.woodman@univ-amu.fr

INTRODUCTION/MOTIVATION

Data recorded from intracereberal electroencephalography (iEEG) has been in use for several decades in the context of clinical epilepsy to assess in detail the origin of a patient's seizures. Despite the high interest of the data for fundamental neuroscience research, the modality has never been employed at large scale in systematic ways. The new Human Intracerebral Platform resolves several technological issues in one platform, enabling participating clinics to work with their data without needed to manage installation of many cutting edge softwares. The majority of the softwares available enable important analyses of patient data, however none of them bring computational modelling techniques to the platform. The Virtual Brain is a software for efficient whole brain modelling, including network-mediated seizure propagation as frequently seen in clinical epilepsy [2]. We present an application, the HIP TVB app in short, to enable interested HIP users to discover their data through the lens of a computational model.

METHODS

The Virtual Brain is a software for whole brain network modelling which simulates realistic neuroimaging data using a patient specific connectome and cortical geometry, which are derived from a patient's MRI scans. The HIP expects apps packaged as container images to be run securely on a HIP deployment. Our app packages TVB along with preprocessing tools like FreeSurfer, FSL & MRtrix3 into a single convenient container image including the JupyterLab Desktop GUI to enable full model-driven workflows for simulation and inference [1] on iEEG data.

RESULTS AND DISCUSSION

We use the HIP TVB app to preprocess and simulate seizures for the HIP demo datasets. The app along with this tutorial are available on the production HIP instance. While the current set of workflows is restricted, it will be extended in the future towards virtual resection and high resolution modelling workflows.

Keywords: intracereberal data, computational neuroscience, machine learning

ACKNOWLEDGEMENTS

This research has received funding from the European Union's Horizon 2020 Framework Programme for Research and Innovation under the Specific Grant Agreement No. 945539 (Human Brain Project SGA3).

REFERENCES

[1]Stan Development Team. 2023. Stan Modeling Language Users Guide and Reference Manual, 2.31. https://mc- stan.org
[2|Wang, Huifang E., et al. "Virtual Epileptic Patient (VEP): Data-driven probabilistic personalized brain modeling in drug-resistant epilepsy." medRxiv (2022): 2022-01.

…

61. Co-simulation workflow for brain simulations: a multi-scale mouse brain model with TVB and NEST

Kusch lionel[1] , Diaz Sandra[2,3] , Klijn Wouter[2,3] , Sontheimer Kim[2,3] , Christophe Bernard[1] , Abigail Morrison[2,3] & Jirsa Viktor[1]

[1] Inst. de Neurosciences des Systèmes, Aix-Marseille Univ., Marseilles, France;
[2] Software Engineering, Department of Computer Science 3, RWTH Aachen University, Ahornstraße 55, 52074 Aachen, Germany
[3]Forschungszentrum Jülich GmbH, Institute for Advanced Simulation, Jülich Supercomputing Centre (JSC), SimLab Neuroscience, JARA, 52425 Jülich, Germany

Keywords: co-simulation, multi-scale, brain network model, spiking neural network, mouse brain

The brain is a very complex, adaptive and multi-scale system. To better understanding is (dys)function, it required multiscale data acquisition which is possible nowadays with some technology like Opto-E-Dura[5]. The understanding of this new data require multiscale simulators. Previous brain knowledge and models at different scales can be used to understand this new data, but they need to be linked across scales, and the co-simulation is an option.
We present a framework of co-simulation that is applied to the study of brain dynamics for different dynamics of the CA1 in mouse brain. The neural circuit of the CA1 is modelled by a spiking neural network, implemented by Nest[2] which is one of the most efficient simulators for point neuron model. The macro-scopic model of the mouse brain is a network of neural masses connected through the connectome, which is derived using data from Allen Brain Institute[4]. The simulation here is performed using The Virtual Brain [6](TVB) which is one of the most efficient simulators at this level and it has already been used to model the macroscopic dynamics of the mouse brain[3].
The Nest-TVB co-simulation thus allows simulating the whole mouse brain with very detailed CA1. In addition, the co-simulation used sensors model to simulate a recording signal at each scale (Local Field Potential using HybridLFPy[1] at the level of neurons, and ElectroCOrticoGraphy by a forward solution at the level brain regions). Unlike the recordings of state variables whihc have no meaning for the experimental neuroscientists, the simulated recordings can be directly compared with recording from real experiments allows validation of multiscale model.
The co-simulation framework is composed at least 2 simulators (Nest and TVB) which communicate with MPI and translation modules that translate the data from one scale to another as shown by the figure . These modules are composed of an interface for each simulator and a translation component in the middle. To estimate the additional time required by co-simulation and it's limitations, the performance of the actual implementation of the framework was evaluated
on one computer and on a supercomputer.
This new framework is a new tool for research which works on the integration of data and models across scale.

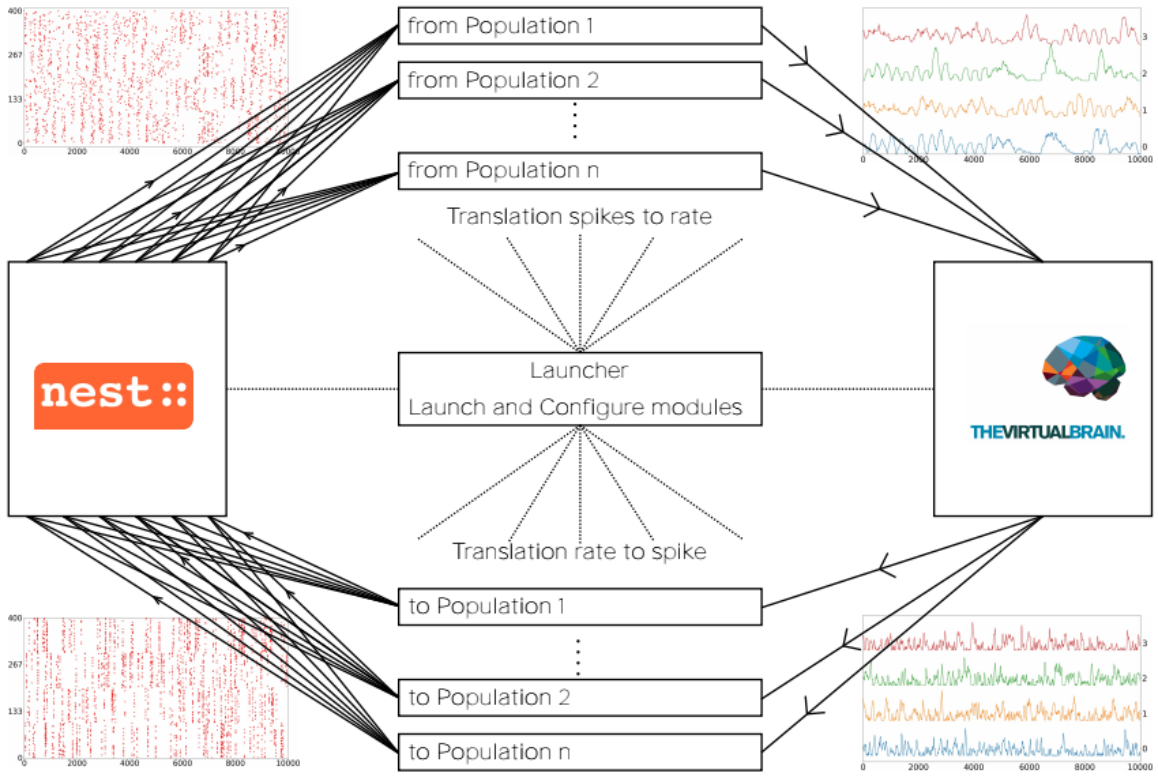

Figure 1: **High-level design of the co-simulation of TVB and Nest showing some of the important functional modules.**

The plots in the four corners illustrate the type of information exchanged in respective information channels. The launcher in the middle starts and handles coordination of simulation parameters. Middle top and bottom of panel B show the translators. These modules translate the mean firing rate information from TVB (module on the right) and spike times from Nest (module on the left). Each population has a specific translator enabling transfer of information from the neurons in the brain regions and vice versa.

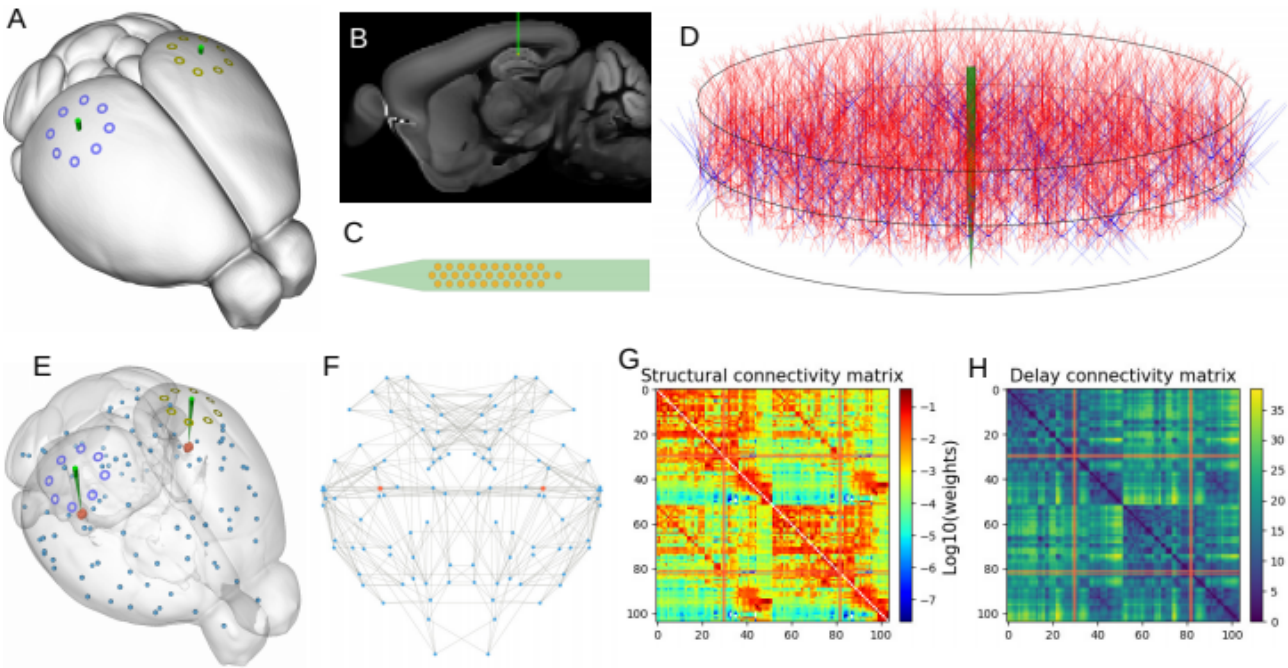

Figure 2: **The virtual mouse brain experience**

A Mouse brain of Allen Institute with the position of the 2 polytrode electrodes and 16 ECOG electrodes. The ECOG electrodes measure the neural field from the surface of the electrode in blue for left hemisphere and yellow for the right hemisphere. B Cross section of the mouse brain with the position of the left implemented electrode. C Position of the site layout of the polytrode (Neuronexus 32 models from MEAutility library). D The position of the probe inside the neural network. The red neurons are pyramidal neurons and the blue neurons are basket cells. E Similar figure than A but with transparent mesh. Blue spheres mark the centres of mouse brain regions and the red spheres a subset of neurons of the CA1. F Spatial representation of the connectome of the mouse brain. The blue dots are brain regions and the red ones are CA1 regions, whose neurons are simulated with NEST. The strongest anatomical connections are highlighted by the grey links. G The weights of the anatomical links in F are shown as an adjacency matrix. H The connection delays associated with F are shown as an adjacency matrix. The anatomical connections are extracted from tracer data of the Allen Institute.

References

[1] Espen Hagen et al. “Hybrid Scheme for Modeling Local Field Potentials from Point-Neuron Networks”. In: Cerebral Cortex 26.12 (Dec. 1, 2016), pp. 4461–4496. issn: 1047-3211. doi: 10 . 1093 / cercor / bhw237. Url: https://academic.oup.com/cercor/article/26/12/4461/2333943.

[2] Jan Hahne et al. NEST 3.0. June 10, 2021. doi: 10.5281/zenodo.4739103. url: https://zenodo.org/record/4739103.

[3] Francesca Melozzi et al. “The Virtual Mouse Brain: A Computational Neuroinformatics Platform to Study Whole Mouse Brain Dynamics”. In: eNeuro 4.3 (May 1, 2017), ENEURO.0111–17.2017. issn: 2373-2822. doi: 10.1523/ENEURO.0111- 17.2017. url: http://www.eneuro.org/content/4/3/ENEURO.0111-17.2017.

[4] Seung Wook Oh et al. “A mesoscale connectome of the mouse brain”. In: Nature 508.7495 (Apr. 2014), pp. 207–214. issn: 1476-4687. doi: 10.1038/nature13186. url: https://www.nature.com/articles/nature13186.

[5] Aline F. Renz et al. “Opto-E-Dura: A Soft, Stretchable ECoG Array for Multimodal, Multiscale Neuroscience”. In: Advanced Healthcare Materials 9.17 (2020). _eprint: https://onlinelibrary.wiley.com/doi/pdf/10.1002/adhm.202000814, p. 2000814. issn: 2192-2659. doi: https : / / doi . org / 10 . 1002 / adhm . 202000814. url: http://onlinelibrary.wiley.com/doi/abs/10.1002/adhm.202000814.

[6] Paula Sanz Leon et al. “The Virtual Brain: a simulator of primate brain network dynamics”. In: Frontiers in Neuroinformatics 7 (2013). issn: 1662-5196. doi: 10.3389/fninf.2013.00010. url: https://www.frontiersin.org/articles/10.3389/fninf.2013.00010/full.

62. A Computational Approach To Investigate Parkinson's Disease Bradykinesia in Reaching Movements

Alessio Fasano[1,2,*], Lorenzo Fruzzetti[1,2], Egidio Falotico[1,2]

[1]The BioRobotics Insitute, Scuola Superiore Sant'Anna, Pisa, Italy,

[2]Department of Excellence in Robotics and AI, Scuola Superiore Sant'Anna, Pisa, Italy

*Corresponding author: alessio.fasano@santannapisa.it

INTRODUCTION/MOTIVATION

Mazzoni et al. [1] have shown that patients with Parkinson's disease (PD) can reach a predefined target with their upper limb as accurately as control subjects, but on average they select speeds that are lower than control ones, because of a greater sensitivity to the movement effort. Their results were in line with the theory of optimal control [2] which postulates that the brain generates trajectories by minimizing a behavioral cost function.

The objective of this work was to build a mechanistic computational model of the neural control exerted by the motor cortex (MC) and the basal ganglia (BG) for goal-directed movements of the upper limb, which may constitute an *in silico* framework to investigate the physiological and pathological reaching movement control. Leveraging the knowledge acquired with literature review [3], a "disease" version of the model was built to simulate the bradykinetic (i.e., abnormally slow) movements of PD patients.

METHODS

The motor controller was simulated as a fully-connected, continuous-time recurrent neural network of leaky integrator neurons, trained to send motor commands to a biomechanical model of the human upper limb [4] for reaching circular targets on a bidimensional workspace. The task was to reach the target as accurately and fast as possible and then hold

the final posture until a predefined time limit (T_{lim}).

We developed two instances of the model. In a first implementation, the control policy generated by the motor cortex (MC) was updated via optimization of an objective function *l* of the network parameters which is thought to be computed by the BG:

$$l = \frac{1}{T_{lim}} \sum_{t=0}^{T_{lim}} \beta \left[1 - \exp\left(-r \frac{\| y^* - y \|^2}{2(W_i^2)}\right)\right] + \alpha_1 \| u \|^2 + \alpha_2 \| z \|^2$$

Where *i* is the current movement trial, y_t the hand position at time *t* and y_i^* the target center, W_i its width, *r* a constant. The exponential term presents a saturation at 1, as a motivational drive that is maintained during the movement until the vicinity of the target [5]. The second term is a neuromuscular cost, penalizing high neural z and muscular activity u. α and β are hyper-parameters which regulate the relative importance given by the subject to accuracy and effort. We

modelled the PD condition as an imbalance between these hyper-parameters.

In the second implementation, we have incorporated a second network in loop with the cortical one, simulating the BG modulation of MC activity. At cortico-striatal synapses we introduced a multiplicative gain, which value was proportional directly to fixed dopamine level, and inversely to the index of difficulty of the task [6]. The PD condition was mimicked directly as decreased dopamine level.

RESULTS AND DISCUSSION

In the first implementation, we obtained straight reaching trajectories and bell-shaped velocity profiles, as experimentally observed [1] (fig. 1). We also obtained realistic multiphasic muscular activities, revealing synergies between shoulder and biarticular extensors in the acceleration phase, and shoulder and biarticular flexors in the deceleration phase. The shift in the hyper-parameters led to similar trajectories, but lower peak velocities and longer movement durations, mimicking PD bradykinesia [1]. In muscular activity, the first agonist burst was reduced, and a bigger level of coactivation was present in the deceleration phase, as experimentally observed [7]. Simulation results on the second model instance showed realistic velocity profiles and a reduced vigor of movement when the dopamine level was decreased, simulating the PD condition (fig.2).

With respect to previous studies [8], we conceived ours as a mechanistic model of reaching control in an infinite-horizon framework to predict the movement duration as an emergent feature of the optimization, given that the literature of interest concerned the distorted modulation of this variable in PD. Our model was able to handle scenarios of speed-accuracy tradeoffs, with a task-related modulation of the effort and accuracy, reproducing recent experimental results on PD bradykinesia.

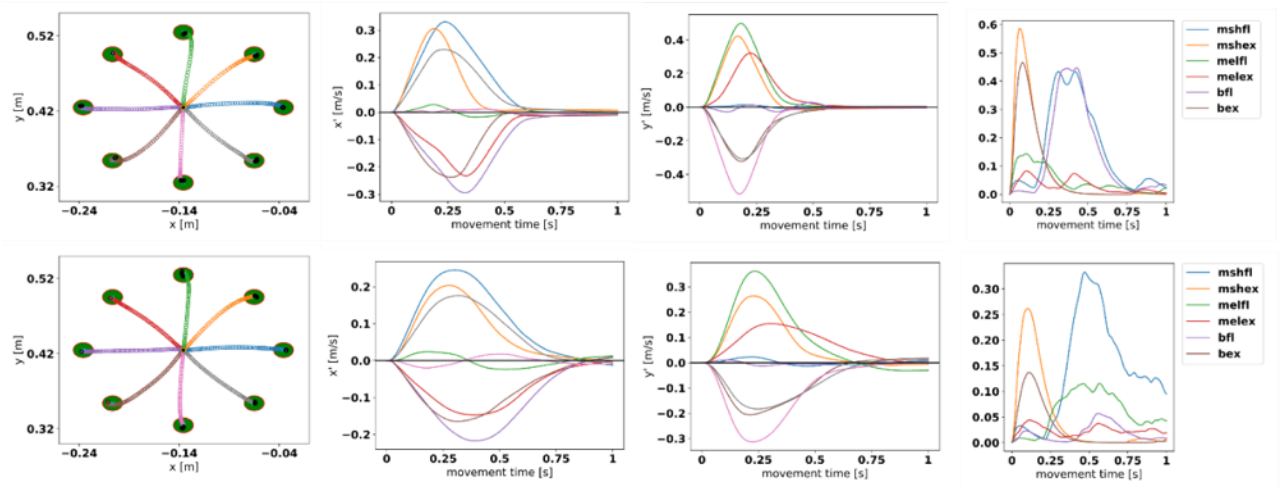

FIGURE 1 – Hand reaching trajectories (first column), hand velocity profiles (second and third columns), and muscular activations (last column), for a simulated "healthy" subject (first row) and for a simulated "PD" patient (second row), obtained with the first implementation. mshfl = monoarticular shoulder flexors; mshex = monoartic. shoulder extensors; melfl = monoartic. elbow flexors; melex = monoartic. elbow extensors; bfl = biarticular flexors; bex = biarticular extensors.

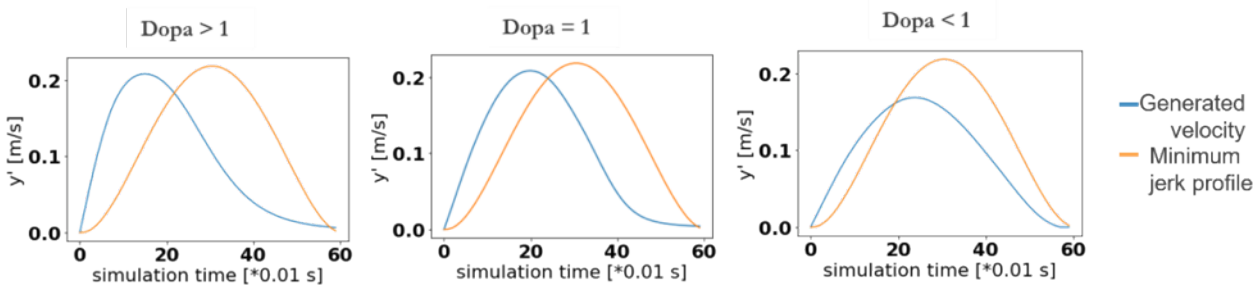

FIGURE 2 – Hand velocity profiles generated by the second implementation, for decreasing level of dopamine (Dopa). The neural model generates more realistic velocity profiles compared to a minimum jerk model. PD is simulated in the third column.

Keywords: Parkinson's disease, Reaching movement, Artificial Neural Network, computational modelling, basal ganglia

ACKNOWLEDGEMENTS

This work has received funding from the European Union's Horizon 2020 Framework Programme for Research and Innovation under the Specific Grant Agreements No. 785907 (Human Brain Project SGA2) and No. 945539 (Human Brain Project SGA3).

REFERENCES

[1] Mazzoni, P., Hristova, A., & Krakauer, J. W. (2007). Why don't we move faster? Parkinson's disease, movement vigor, and implicit motivation. *Journal of neuroscience*, *27*(27), 7105-7116. https://doi.org/10.1523/JNEUROSCI.0264-07.2007

[2] Todorov, E., & Jordan, M. I. (2002). Optimal feedback control as a theory of motor coordination. *Nature neuroscience*, *5*(11), 1226-1235. https://doi.org/10.1038/nn963

[3] Fasano, A., Mazzoni, A., & Falotico, E. (2022). Reaching and Grasping Movements in Parkinson's Disease: A Review. *Journal of Parkinson's Disease*, (Preprint), 1-31. https://doi.org/10.3233%2FJPD-213082

[4] Brown, I. E., Cheng, E. J., & Loeb, G. E. (1999). Measured and modeled properties of mammalian skeletal muscle. II. The effects of stimulus frequency on force-length and force-velocity relationships. *Journal of Muscle Research & Cell Motility*, *20*, 627-643. https://doi.org/10.1023/A:1005585030764

[5] Huh, D., & Todorov, E. (2009, March). Real-time motor control using recurrent neural networks. In *2009 IEEE Symposium on Adaptive Dynamic Programming and Reinforcement Learning* (pp. 42-49). IEEE. https://doi.org/10.1109/ADPRL.2009.4927524

[6] Fitts, P. M., & Peterson, J. R. (1964). Information capacity of discrete motor responses. *Journal of experimental psychology*, *67*(2), 103. https://psycnet.apa.org/doi/10.1037/h0045689

[7] Hallett, M., & Khoshbin, S. (1980). A physiological mechanism of bradykinesia. *Brain*, *103*(2), 301-314. https://doi.org/10.1093/brain/103.2.301

[8] Kalidindi, H. T., Cross, K. P., Lillicrap, T. P., Omrani, M., Falotico, E., Sabes, P. N., & Scott, S. H. (2021). Rotational dynamics in motor cortex are consistent with a feedback controller. Elife, 10, e67256. https://doi.org/10.7554/eLife.67256

63. Learning Sensorimotor-Predictions through Mismatch-Based Hebbian Plasticity

Matthias Brucklacher[1*], Giovanni Pezzulo[2], Francesco Mannella[2], Cyriel M.A. Pennartz[1]

[1]Cognitive and Systems Neuroscience Group, University of Amsterdam, Amsterdam, Netherlands

[2]CONAN LAB, ISTC-CNR, Rome, Italy

*e-mail-address of corresponding author: m.m.brucklacher@uva.nl

INTRODUCTION/MOTIVATION

A key problem any sufficiently complex animal needs to solve when constructing a representation of the external world is to distinguish between self- and externally generated sensory signals. More precisely, the question is how the neural networks of sensory processing can learn to suppress irrelevant predictable outcomes such as the sound of one's footsteps during walking, and when to process them such as when preparing to jump over a known gap occluded by a bush. Here, neuroscientific observations are informative, that extend the traditional understanding of primary visual cortex (V1) as a representational canvas of the world and provide experimental evidence showing a strong influence of motor-related signals on neurons in this area[1–3]. Indeed, some of these observed motor-correlates appear to be predictions about sensory outcomes resulting from egomotion[1,2] and can be used to suppress irrelevant information for more efficient sensory processing[4]. Addressing the vague understanding of the underlying learning rules and neural circuits, we show that neuronal activity patterns suggestive of such predictive mechanism are readily explained by a Hebbian covariance learning rule between neurons in motor areas and mismatch neurons in V1. Out model thus provides a mechanism to address the computational challenge of identifying non-self-generated components in the visual input stream.

METHODS

A minimal circuit of mismatch computation. Based on the observations of [2], a minimal model of mismatch computation between visual input and predictions from motoric areas was constructed. As shown in Figure 1a,

the model circuit consists of three populations of neurons. The motor units shown in red control the speed of movement, linearly encoding it as a scalar value $y_m \in [0,1]$. Direction-selective neurons shown in blue are sensitive to caudally moving patterns, and linearly reflect the speed of pattern motion. Thus their activity is given

as $y_v \in [0,1]$, with higher values corresponding to faster pattern motion. Mismatch neurons depicted as a square in Figure 1 compute the difference between motor prediction and sensory input, the latter is scaled by a synaptic weight w. The firing rate e of mismatch neurons is thus defined as

$$e(y_m, y_v) = \phi(y_m - w \cdot y_v)$$

with a rectified sigmoid as saturating activation function:

$$\phi(x) = \max\left(0, \frac{1}{1 + e^{-x}}\right)$$

Lastly, the learning rule adapting the synaptic weight is applied at every based on the covariance rule of [5] and given by:

$$\Delta w = \alpha \cdot (e - \bar{e}) \cdot y_v$$

with learning rate α and temporally averaged mismatch signal $\bar{e}$. The learning rule is applied at every simulation timestep.

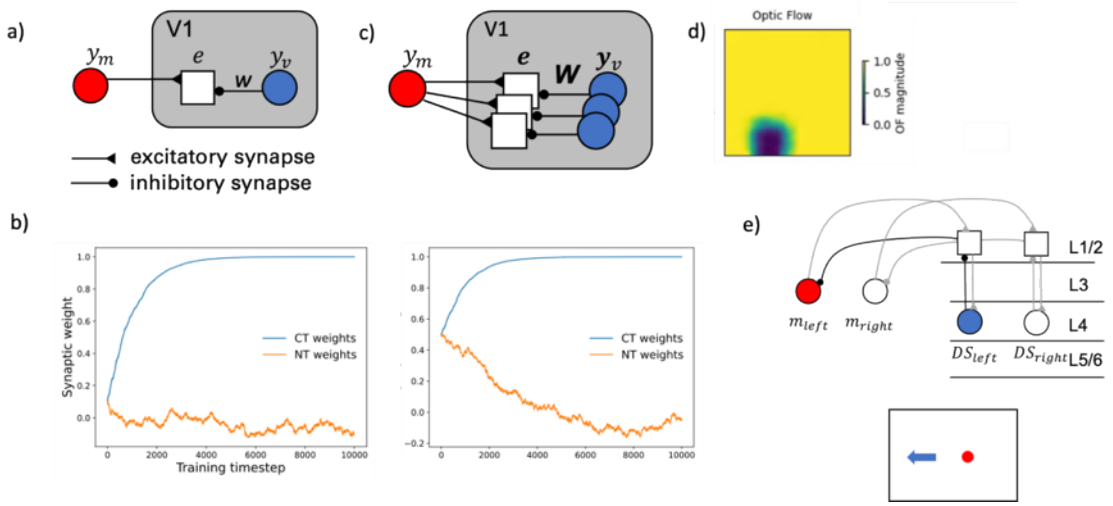

Figure 1. The model is progressively extended from a minimal circuit of sensorimotor mismatch computation to retinotopic mismatch computation and mismatch-based action control. a) In primary visual cortex (V1), mismatch neurons compute the difference e between the corollary discharge from motor neurons y_m and activity of direction selective neuron y_v. The latter is scaled by the synaptic weight w, that is trained in two conditions described in the main text and shown in b) for two different initialization values (left plot: 0.01, right plot: 0.5). c) Extension of the model to retinotopic space through spatial arrangement of mismatch- and direction selective neurons. d) Retinotopic testing paradigm with local halt of optic flow (in the white square). e) Connecting the mismatch neurons back to the respective motor units allows control of simple sensory-guided behavior. Here, two motor units control a shift of gaze direction to the left or right.

Coupled and non-coupled network training. We trained two identically initialized networks as shown in Figure 1a in different environments. For both, motor commands y_v were randomly sampled from $U(0,1)$ at each timestep. Network 1 received visual inputs contingent with this movement, i.e. backward-moving patterns when moving forward and no input to motion selective visual neurons when standing still. In line with [2], we termed this condition in which $y_v = y_m$ *CT* (coupled training). The second network received non-contingent visual input (thus labelled *NT*), with both y_v and y_m sampled independently from $U(0,1)$. Figure 1b shows the evolution of weights for both CT (blue) and NT networks (orange) across training time for two weight initialization values. The learning rule drove

the weight close to the correlation value of the centered visual and motor neuron responses, yielding low values close to zero in the uncorrelated NT condition and high values close to one in the CT condition.

Extension to retinotopic space. According to the measurements of [1], mismatch responses in mouse V1 are retinotopically organized, allowing the animal to precisely locate, and thus react to, the position of non-self-generated motion. The model from Figure 1a is thus extended by multiplying visually tuned neurons and distributing them across retinotopic space, along with the one-to-one connected mismatch neuron (Figure 1c) and trained weights of the CT network. Note that the (global) movement state remains one-dimensionally encoded.

RESULTS AND DISCUSSION

Experience-dependent mismatch responses. Attinger et al. [2] were able to elucidate mismatch in mouse V1 responses during the recording phase by artificially halting optic flow in the VR setup shown in Figure 2a while the mouse was running. In Figure 2, this is termed the mismatch condition. In the playback halt co ndition, the still standing mouse observed a moving visual input that then suddenly stopped. We tested both the CT and NT model (non-retinotopic) described above in the same conditions (Figure 2b) and found a good match to the Ca^{2+} responses from [2] that are shown in Figure 2c. Specifically, the strong response to the mismatch condition also only in the CT-trained model, just as experiments found it to be present only in CT-trained mice. Lastly, after being exposed to the CT training paradigm for another 2000 timesteps, the NT model was tested again and now showed an increase in mismatch neuron activity in the mismatch paradigm (Figure 2d). This, too, is in good agreement with the study of Attinger et al., who found the same recovery pattern in mice, leaving our model as a viable candidate for the underlying learning mechanism.

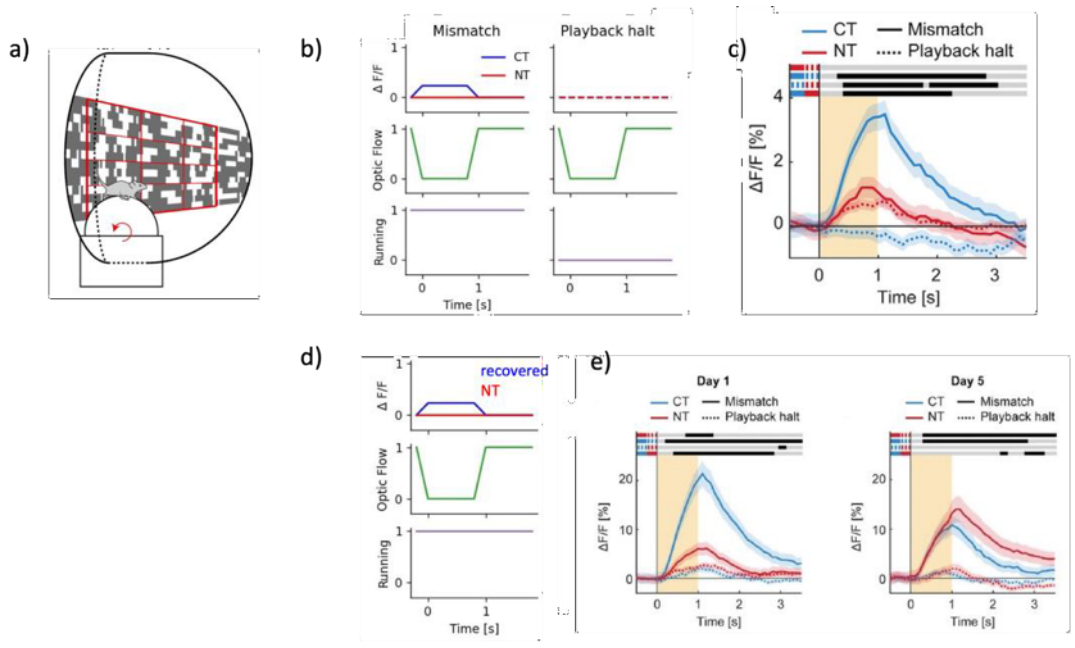

Figure 2. The model reproduces various patterns of experimentally observed mismatch selectivity in mouse V1. a) The experimental VR setup of Attinger et al. [2] allows to raise mice with different types of visual experience. In the CT condition, visual feedback follows running speed on the treadmill. In the NT condition, visual feedback is uncorrelated. b) Response of mismatch

neurons in the trained models from Figure 1b to the mismatch and playback halt conditions described in the main text. c) Neural responses measured by Attinger et al. [2]. d-e) Exposure to the CT paradigm restores mismatch responses in model (d) and mouse (e). Panels a, c and e are reproduced from Attinger, Wang and Keller (2017), Cell, Cell Press.

Spatially tuned mismatch computation. As the nature of motor-correlated feedback to visual areas is a topic of intense discussion, a key factor is the dimensionality of the signals. Zmarz and Keller [1] showed that the information about expected visual flow that is passed on to V1 is retinotopically organized and thus may serve to identify the precise position of externally generated stimulus causes, such as an approaching predator. We tested the retinotopic model introduced in Figure 1c in such a predator-spotting setting, in which part of a visual input stream, moving in accordance with motor neuron activity was perturbed by halting it still, simulating independent motion of an external object. This area, marked by a white square on the right of Figure 1c, indeed elucidated a detectable mismatch pattern shown on the right that is readily decodable for downstream areas such as the selection of the appropriate behavioral response. Our model thus provides a simple, but effective neural mechanism in to disentangle self-generated from externally caused changes in visual inputs.

Mismatch-based action control. The connection from motor to sensory areas investigated above does not need to be unidirectional. By using feedback from mismatch neurons to motor neurons, sensory-guided behavior can be elicited from an extended version of our model. This is shown in Figure 1e, where an ant moving to the left is observed. In V1, this elicits activity in direction-selective cells tuned to the respective direction (shown in blue). The consequently activated mismatch neuron (square), putatively situated in supragranular layers, then activates the motor neuron encoding the motor program for shifting the gaze leftwards. As the gaze shift (blue arrow in the lower panel), the perceived optic flow of the moving and it reduced, thus closing the control loop that minimizes the mismatch response. In combination with the putative arrangement of the circuit in the cortical layers as hinted at in Figure 1e, this fits well with experimentally observed tuning of neurons in supragranular layers in mouse V1 that were tuned to the direction of saccadic eye movements, but not to direction of motion of visual signals [6]. To conclude, the experience-dependent comparison of corollary discharge signals from motor areas with responses of visual neurons is a promising candidate for the challenge of identifying non-trivial components in the visual input stream and fits well into larger and more complex circuits for visually guided behavior.

Keywords: predictive processing, self-supervised learning, unsupervised learning, vision, feedback, sensorimotor, motor control, neural networks, computational model

ACKNOWLEDGEMENTS

This project has received funding from the European Union's Horizon 2020 Framework Programme for Research and Innovation under the Specific Grant Agreement No. 945539 (Human Brain Project SGA3; to C.P. and G.P.).

A research stay in Rome connected to this project was funded for M.B. through the NENS Exchange Grant program of the Federation of European Neuroscience Societies (FENS).

REFERENCES

1. Zmarz P, Keller GB. Mismatch receptive fields in mouse visual cortex. *Neuron*. 2016;92(4):766-772.

2. Attinger A, Wang B, Keller GB. Visuomotor Coupling Shapes the Functional Development of Mouse Visual Cortex. *Cell*. 2017;169(7):1291-1302.e14. doi:10.1016/j.cell.2017.05.023

3. Saleem AB, Ayaz A, Jeffery KJ, Harris KD, Carandini M. Integration of visual motion and locomotion in mouse visual cortex. *Nat Neurosci*. 2013;16(12):1864-1869. doi:10.1038/nn.3567

4. Crapse TB, Sommer MA. Corollary discharge across the animal kingdom. *Nat Rev Neurosci*. 2008;9(8):587-600. doi:10.1038/nrn2457

5. Sejnowski TJ. Storing covariance with nonlinearly interacting neurons. *J Math Biol*. 1977;4(4):303-321. doi:10.1007/BF00275079

6. Miura SK, Scanziani M. Distinguishing externally from saccade-induced motion in visual cortex. *Nature*. 2022;610(7930):135-142. doi:10.1038/s41586-022-05196-w

64. Emergence of oscillations in a biologically realistic model of a V1 cortical column

Giulia Moreni[1*], Cyriel M.A. Pennartz[1], Jorge F. Mejias[1]

[1]Cognitive and Systems Neuroscience Group, University of Amsterdam, Amsterdam, Netherlands
*e-mail-address of corresponding author: g.moreni@uva.nl

INTRODUCTION/MOTIVATION

The local cortical network plays a crucial role in brain function. The relationship between its structure and activity is not yet fully understood, but large scale spiking columnar models can help reveal the correlation between the network's cell-specific structure and neuronal activity. Using existing experimental data, we built a spiking network model of the cortical column microcircuit including biological realistic details such as cell-type specific densities and the presence of AMPA, GABA and NMDA receptors. The model was composed of multiple layers in which different type of neurons are included: in each layer 3 inhibitory neurons populations (PV, SST, and VIP) and one excitatory populations are present.

The models of the cortical column proposed so far in literature (for example [1]) have taken into account only static weights between neurons. However, we know that plasticity is an ongoing process in the brain. For this reason, in the second part of our study we introduced plastic weights using the STDP rule to uncover the effects of stimulus-driven plasticity in the complex spatio-temporal patterns of neuronal activity within the column.

METHODS

All neurons in the model are described by leaky integrate-and-fire neurons.

Each neurons includes dynamics of different postsynaptic receptors (AMPA, GABA, NMDA) with exact equations. The network model is composed by 4 cortical layers each containing pyramidal neurons, PV, SST and VIP cells (layer 2/3, 4, 5, 6). The model has biological realistic constrains: the percentages of neurons in each group and the structural parameters of our multi-laminar column, that is, the connectivity strength and probability of connections between populations are derived from experimental data [2]. This modeling approach minimize the arbitrary choice of parameters and avoids any fitting or tuning of the activity of neurons. The parameters for each neuron type (refractory period, membrane resting potential, membrane threshold, capacitance of the membrane) are also constrained using experimental data.

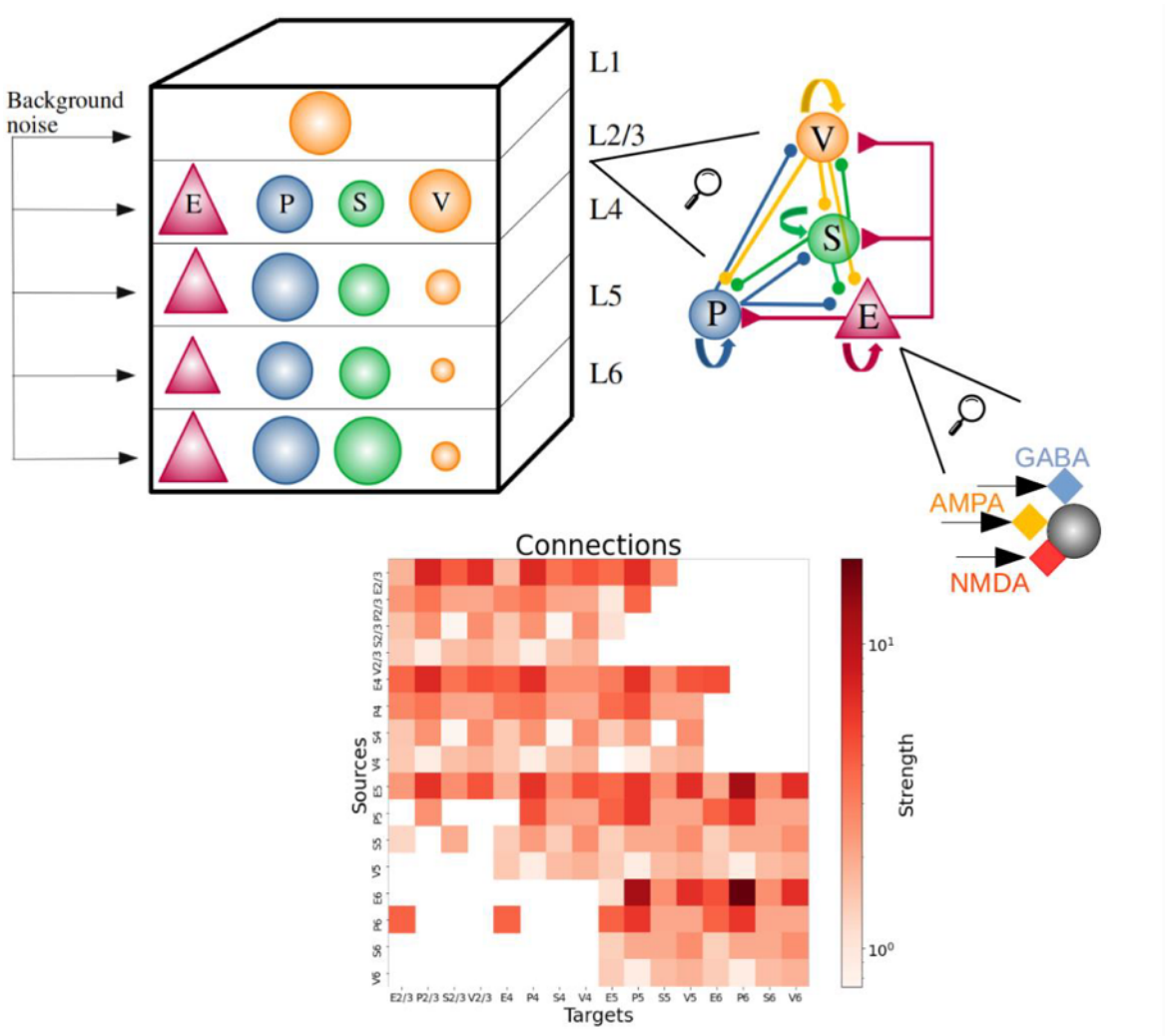

Figure 1. *Model definition. In layers 2/3, 4, 5, and 6 excitatory population (red triangles) and 3 types of inhibitory populations (PV, SST, VIP as blue, green, orange circles respectively) of model neurons are present. In layer 1 only VIP cells are present. The percentage of neurons in each population is reported in Table 1, the size of the circles in the figure represents the relative size of the inhibitory populations. Input to the populations is represented by external background noise to all populations. Connections between groups are not explicitly shown in the cortical column figure, populations are all to all connected according to the probability matrix P. On the right the connection diagram for one layer is shown. Each neuron has 3 types of receptors, AMPA and NMDA for excitatory inputs and GABA for inhibitory inputs. The connection matrix shown is computed as the number of connections between two populations times the strength of each connections.*

RESULTS AND DISCUSSION

Our study is divided in two parts and is structured as follows.

In the first part, we built the cortical column model with static weights derived from experimental data [2], and we analyze the spontaneous activity, the stimulus evoked response patterns. We were able to match the simulations with experimental recordings both in spontaneous and in evoked case (Fig. 3).

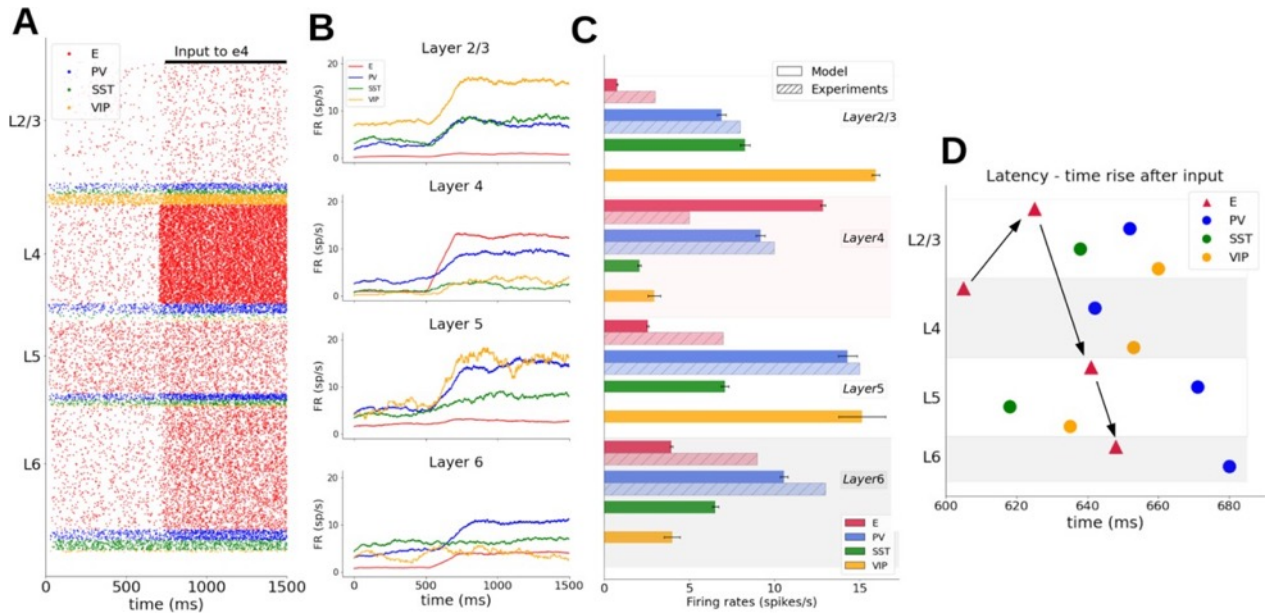

Figure 3: *Simulated evoked cell-type specific activity. (A) Raster plot of spiking activity recorded for 1500 ms of biological time showing the response of neurons after an input current (30pA) is given to E4 at 700 ms. There is a propagation of activity through all the column, all the groups have an increase in their number of spikes. Layers 2/3, 4, 5, and 6 are shown (from top to bottom; red: excitatory, blue: PV, green: SST, yellow: VIP). Number of displayed spike trains corresponds to the number of neurons in the network (total of 5000 shown). (B) Firing rates traces showing the increase of the overall activity when the input current is injected in E4. Computed with a sliding window of 200ms and a time step of 1ms. (C) Mean firing rates for each population in comparison with experimental mean firing rates (dashed bars). Error bars for experimental data are not depicted and are available in Figure 3 of [2]. (D) Propagation order of the input in the column. From layer 4 the input goes to E2/3 then E5 and finally to E6.*

We then studied the response of all the neurons groups in relation to a external stimulation of one target group. We looked at their response both in the spontaneous case (only background noise present) and in the evoked case (background noise + input to layer 4). Depending on the state of the network (spontaneous or evoked) the response of the neurons caused by the same external stimulation can differ. Lastly, we studied the effect of Feed forward (FF) input, i.e. input to layer 4, combined with a Feedback (FB) input, i.e. input targeting layer 5, and we shown they have opposite effects.

In the second part we introduce plasticity to the model, the weights are no longer fixed but are allowed to change according to STDP rule.
In the presence of a constant input to layer 4 plasticity give rise to oscillations in the low gamma range (22 Hz).

Once the model is "trained", i.e. after a phase in which the weights were allowed to change, we fixed the weights again and we studied the behavior of neurons in the model. We show for instance that a stronger input to layer 4 leads to the rise of faster oscillations whereas removing completely the input causes the oscillations to disappear and the neurons to fire again at their basal firing rates.

In the presence of constant Feed forward (FF) input, where the network shows a presence of oscillations, we studied the effect of varying Feedback (FB) input. FB is able to modulate the frequency of the oscillations: a strong FB input drastically reduce the presence of oscillations.

We then studied the origin of the oscillations and which layers are required to have plastic weights to allow the oscillations to appear. Layer 4 is found to be the candidate: plasticity in L4 is crucial for oscillations whereas in the other layers the plasticity can be turned off without major effects on oscillations.
In the last part we studied the role of the different interneurons on oscillations and identify the most relevant ones. Oscillations is found to be a collective property, all interneurons contribute to it. However, according to our model PV seems to be the most important interneuron type involved in oscillations.

In conclusion, the role of FB and FF input, the study of oscillations in the model and the role of the different interneurons gives us insight on the dynamical properties of the cortical micro-circuitry.

Keywords: cortical microcircuit, layered network, specificity of connections, interneurons, Feedback & Feed forward input, plasticity, STDP, oscillations, interneurons's role in oscillations.

ACKNOWLEDGEMENTS

This project has received funding from the European Union's Horizon 2020 Framework Programme for Research and Innovation under the Specific Grant Agreement No. 945539 (Human Brain Project SGA3; to C.P. and G.P.).

REFERENCES

[1] Tobias C. Potjans and Markus Diesmann. The Cell-Type Specific Cortical Microcircuit: Relating Structure and Activity in a Full-Scale Spiking Network Model. March 2014. Cerebral Cortex;24:785–806 doi:10.1093/cercor/bhs358

[2] Yazan N. Billeh et al. Systematic Integration of Structural and Functional Data into Multi-scale Models of Mouse Primary. May 2020. Neuron 106, 388–403 https://doi.org/10.1016/j.neuron.2020.01.040

65. Computational modelling of the pathway between dopamine receptors and Ca2+ channels in layer II stellate cells

Chitaranjan Mahapatra[1]*, Andrew P. Davison[1]

[1]Integrative & Computational Neuroscience, Paris-Saclay Institute of Neuroscience (NeuroPSI), CNRS/Université Paris-Saclay, Saclay, France

*chitaranjan.mahapatra@cnrs.fr

INTRODUCTION/MOTIVATION

Dopamine plays an important role in mediating spatial learning and memory. The firing patterns of stellate cells in layer II of medial entorhinal cortex are also involved in memory, cognition, and perception [1]. These patterns are largely modulated by the underlying subcellular calcium dynamics within the axon initial segment (AIS) [2]. Recent experimental data have suggested a putative coupling between dopamine D2 receptors (D2R) and T-type Ca^{2+} channels as another biophysical explanation for the firing pattern modulation [3]. This computational study aims to enhance our understanding of the subcellular membrane mechanisms within AIS of the layer II stellate cells and their modulating effects on resting membrane potential (RMP) and action potential (AP) plasticity in pathological conditions.

METHODS

The schematic Figure 1 illustrates the G protein coupled receptor (GPCR) pathway between the D2R and T-type Ca^{2+} channel. The computational model is established in three folds. First, the biophysical parameters for various ion channels in the AIS region of layer II stellate cells were combined and adapted from previous models and experimental studies. Second, we developed equations for the GPCR pathway to alter the cAMP concentration, which was merged with the maximum conductance of T type Ca^{2+} channels in a modified Boltzmann equation. Third, various pharmacological agents are simulated to explore new biological insights from our model. Using the NEURON software platform in a single compartmental isolated cell, the RMP, APs and T-type Ca^{2+} channel currents were simulated by utilizing both current clamp (current ramp and current step) and voltage clamp protocols.

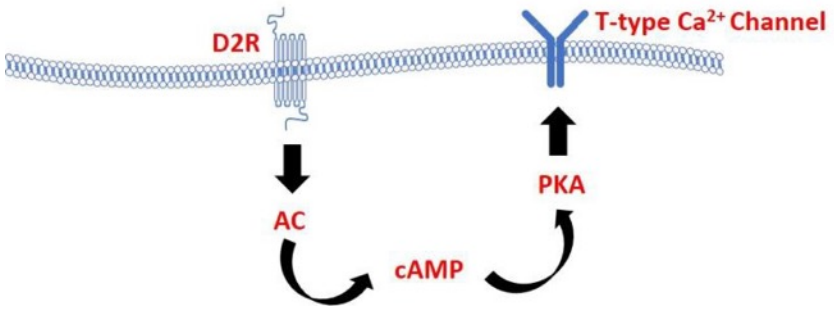

Figure 1: The GPCR pathway between D2R and T-type Ca^{2+} channel

RESULTS AND DISCUSSION

The dopamine agonist bromocriptine (bromo) of 10 µM is mimicked to investigate the altered internal kinetics of the T- type Ca^{2+} channel. Then the APs are evoked from the whole cell model. Figure 2 (a) illustrates the modulating effects of bromo on the steady- state activation and inactivation curves of the T-type Ca^{2+} channel. It shows approximately zero effects on the steady- state inactivation curve, but a positive shift on the steady- state activation curve (black solid line). As a result, the half activation potential of the T-type Ca^{2+} channel is shifted from –36 mV to –32 mV. Figure 2 (B) demonstrates the effects of dopamine agonist on the simulated AP generation with a current injection of 400 pA for a duration of 1 s. It clearly indicates the reduced AP frequency (black solid line) under the effects of dopamine agonist. The window current to maintain the RMP was reduced due to activation of D2R receptors and it was counter balanced by decreasing the A-type K^+ channel conductance. This in silico study suggests that the application of cAMP antagonists and K^+ channel agonists could be used to replace dopamine in certain pathological conditions and in studies of spatial memory performance.

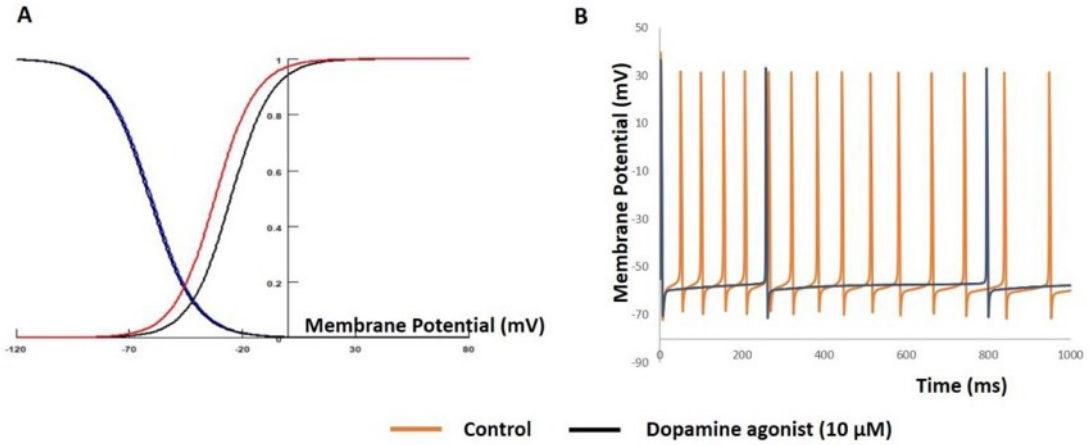

Figure 2: Modulating effects of dopamine agonist bromocriptine on the kinetics of T- type Ca^{2+} channel (A) and action potential generation (B)

Keywords: Layer II Stellate cells, Dopamine receptor, T-type Ca^{2+} channel, Computational model, Action Potential

REFERENCES

[1] Rowland, D. C., Obenhaus, H. A., Skytoen, E. R., Zhang, Q., Kentros, C. G., Moser, E. I., & Moser, M. B. (2018). Functional properties of stellate cells in medial entorhinal cortex layer II. eLife 7.

[2] Lipkin, A. M., Cunniff, M. M., Spratt, P. W., Lemke, S. M., & Bender, K. J. (2021). Functional microstructure of CaV-mediated calcium signaling in the axon initial segment. *Journal of Neuroscience*, *41*(17), 3764- 3776.

[3] Jin, X., Chen, Q., Song, Y., Zheng, J., Xiao, K., Shao, S., ... & Huang, Z. (2019). Dopamine D2 receptors regulate the action potential threshold by modulating T-type calcium channels in stellate cells of the medial entorhinal cortex. *The Journal of Physiology*, *597*(13), 3363-3387.

ACKNOWLEDGEMENTS

This project was developed in part or in whole in the Human Brain Project, funded from the European Union's Horizon 2020 Framework Programme for Research and Innovation under Specific Grant Agreements No. 945539 (Human Brain Project SGA3).

66. Bio-Inspired Backpropagation in Spiking Neural Networks

Fabian Schubert [1*], Thomas Nowotny [1]

[1]School of Engineering and Informatics, University of Sussex, Brighton, UK

*f.schubert@sussex.ac.uk

INTRODUCTION/MOTIVATION

Backpropagation as a method for training artificial neural networks has a long history of successful applications [1, 2]. Due to its biological implausibility, various learning rules and network architectures were suggested that approximate backpropagation while adhering to biological principles.

Sacramento et al. showed that an approximation to backpropagation can be achieved using a simplified multi-compartment model of cortical pyramidal neurons in combination with a local inhibitory circuit [3]. A rate-based network was able to learn a variety of supervised learning tasks by encoding feedback errors in the apical pyramidal compartment.

In our work, we apply this approach to a network of deterministic spiking neurons with threshold dynamics. While it was previously shown that networks of rate neurons or rate-based Poisson spiking neurons can approximate backpropagation [4, 5, 3], our model is, to our knowledge, the first bio-inspired backpropagation model using deterministic threshold-based spiking neurons without separate learning phases.

METHODS

In Fig. 1a, the architecture of each layer in the network is shown, consisting of a pyramidal population (P) and an interneuron population (I), which are recurrently connected. The voltages in the populations of the k-th layer are represented as vectors $\boldsymbol{u}_k^{\mathrm{P}}$ and $\boldsymbol{u}_k^{\mathrm{I}}$ with dynamics given by

$$\begin{aligned}
\dot{\boldsymbol{u}}_k^{\mathrm{P}} &= g_{\mathrm{B}}\boldsymbol{v}_k^{\mathrm{B}} + g_{\mathrm{A}}\boldsymbol{v}_k^{\mathrm{A}} & \qquad \dot{\boldsymbol{u}}_k^{\mathrm{I}} &= g_{\mathrm{D}}\boldsymbol{v}_k + g_{\mathrm{S}}\check{\boldsymbol{v}}_k \\
\dot{\boldsymbol{v}}_k^{\mathrm{B}} &= \left(W_k^{\mathrm{PP}}\boldsymbol{s}_{k-1}^{\mathrm{P}}(t) - \boldsymbol{v}_k^{\mathrm{B}}\right)/\tau_{\mathrm{s}} & \qquad \dot{\boldsymbol{v}}_k &= \left(W_k^{\mathrm{IP}}\boldsymbol{s}_k^{\mathrm{P}} - \boldsymbol{v}_k\right)/\tau_{\mathrm{s}} \\
\dot{\boldsymbol{v}}_k^{\mathrm{A}} &= \left(W_k^{\mathrm{PI}}\boldsymbol{s}_k^{\mathrm{I}}(t) + \widetilde{W}_k^{\mathrm{PP}}\boldsymbol{s}_{k+1}^{\mathrm{P}}(t) - \boldsymbol{v}_k^{\mathrm{A}}\right)/\tau_{\mathrm{s}} & \qquad \dot{\check{\boldsymbol{v}}}_k &= \left(\widetilde{W}_k^{\mathrm{PP}}\boldsymbol{s}_{k+1}^{\mathrm{P}} - \check{\boldsymbol{v}}_k\right)/\tau_{\mathrm{s}}
\end{aligned}$$

A voltage reset $\boldsymbol{u}^{\mathrm{P/I}} \rightarrow 0$ is triggered if $\boldsymbol{u}^{\mathrm{P/I}} \geq u^{\theta}$. The spike population vectors $\boldsymbol{s}$ contain the corresponding spike events as delta pulses given by $s_i(t) = \sum_i \delta(t - t_i^{\mathrm{spk}})$. Note that the feedback matrix $\widetilde{W}_k^{\mathrm{PP}}$ was always set to a one-to-one connection matrix.

Plasticity in this setup was present in all except matrices except for $\widetilde{W}^{\mathrm{IP}}$ and $\widetilde{W}^{\mathrm{PP}}$, with the latter group being randomly initialised. The plasticity rules were given by

$$\dot{W}_k^{\mathrm{PP}} = \mu_{\mathrm{PP}} \left(\boldsymbol{r}_k^{\mathrm{P}} - \boldsymbol{v}_k^{\mathrm{B}} g_{\mathrm{B}} / u^{\theta} \right) \otimes \boldsymbol{s}_{k-1}^{\mathrm{P}} \qquad \dot{W}_k^{\mathrm{IP}} = \mu_{\mathrm{IP}} \left(\boldsymbol{r}_k^{\mathrm{I}} - \boldsymbol{v}_k g_{\mathrm{D}} / \left(u^{\theta} - g_{\mathrm{S}} \right) \right) \otimes \boldsymbol{s}_k^{\mathrm{P}}$$
$$\dot{W}_k^{PI} = -\mu_{\mathrm{PI}} \boldsymbol{v}_k^{\mathrm{A}} \otimes \boldsymbol{s}_k^{\mathrm{I}} \qquad \dot{\boldsymbol{r}}_k^{\mathrm{P/I}} = \left(\boldsymbol{s}_k^{\mathrm{P/I}} - \boldsymbol{r}_k^{\mathrm{P/I}} \right) / \tau_{\mathrm{r}} \quad ,$$

where $\otimes$ denotes the outer product. The $\boldsymbol{r}$ variables are exponentially filtered version of the spike trains. Crucially, the presented learning rules are computationally efficient as updates on individual weights only need to be invoked if a presynaptic spike event occurs.

RESULTS

The network was implemented using the GeNN simulator [6], allowing us to efficiently run the full network on a GPU. We trained a three-layer network with layer dimensions 30-50-10, see Fig. 1b, on a supervised learning task where pairs of inputs and target output samples were randomly generated using an additional three-layer teacher network of the same size. The output targets induced a current in the apical voltage of the output layer given by $\boldsymbol{r}_{\mathrm{target}} - \boldsymbol{r}^{\mathrm{P}}$. Only the hidden layer contained an inhibitory population.

Fig. 1c and 1d show the resulting mean square loss in the output layer during training and the resulting output prediction of the network. Since estimating the rate required low pass filtering the output spike trains, a certain delay can be observed between the target rates and the resulting output. Therefore, the loss for a given sample was determined as the square error of the rate estimate and the target after the network and the firing rate estimate had reached a stationary state. The network successfully learned to reproduce the desired output rates. To demonstrate that changes in the weights to the hidden units indeed contribute to reducing the error, we also trained the network with plasticity only being active at the readout weights, which led to an increased loss as shown in Fig. 1c.

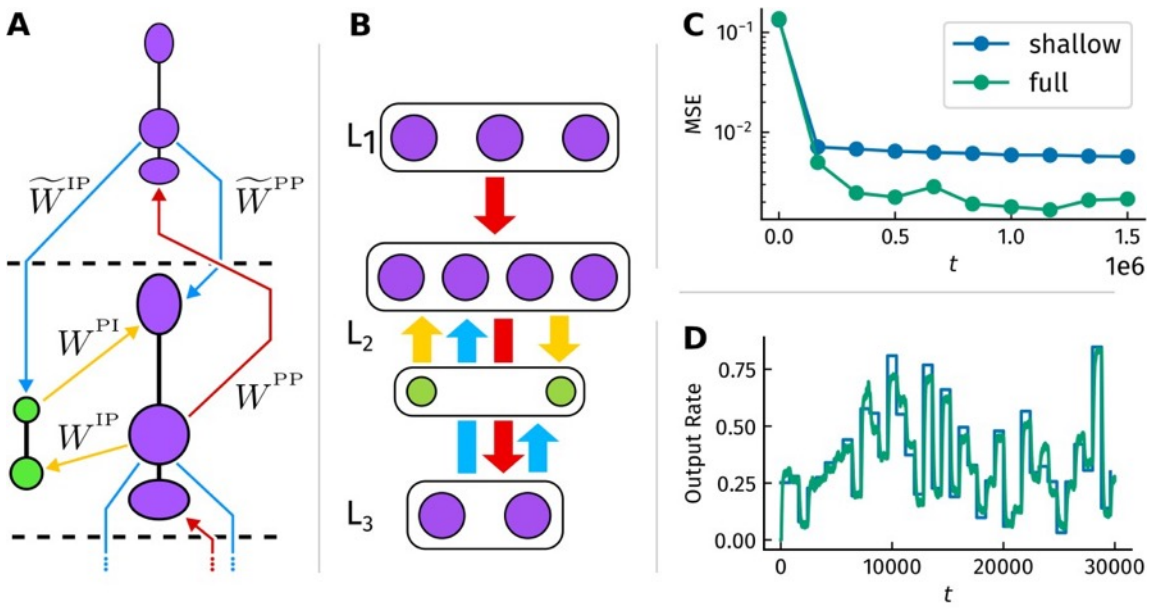

Figure 1: A) Network architecture of a single layer. B) Schematic of the three-layer network architecture used in the training task. C) Mean square error training loss, full plasticity and shallow learning, i.e. training only the output weights. D) Output prediction (green) and target output (blue) for the fully trained network.

DISCUSSION

On a computational level, spiking neural networks can be considered a double-edged sword: Increased efficiency in running SNNs on dedicated neuromorphic hardware goes along with less efficient training methods. A common method for training SNNs that encode information via spike rates is to train a conventional artificial neural network on the same task and transfer the resulting weights onto the spiking system [7]. The presented model is a step towards bridging the gap between learning methods and inference in spiking networks. Therefore, potential use cases could include spiking networks that continuously learn while processing sensory information. To that end, future research should also investigate the capabilities of the proposed model in unsupervised setups, where no additional training input is presented to the output layer.

Keywords: Spiking Neural Networks, Backpropagation, Pyramidal Neurons, Dendritic Compartments, GeNN

ACKNOWLEDGEMENTS

This work was funded by the EU, under Grant Agreement 945539 (HBP SGA3).

REFERENCES

[1] Rumelhart DE, Hinton GE, Williams RJ. *Learning internal representations by error propagation.* MIT Press; 1986: 318-362.

[2] Krizhevsky A, Sutskever I, Hinton GE. *ImageNet Classification with Deep Convolutional Neural Networks.* Curran Associates, Inc.; 2012.

[3] Sacramento J, Costa RP, Bengio Y, Senn W. *Dendritic cortical microcircuits approximate the backpropagation algorithm.* Curran Associates, Inc.; 2018.

[4] Guerguiev J, Lillicrap TP, Richards BA. *Towards deep learning with segregated dendrites.* ELife 2017; *doi: 10.7554/eLife.22901.*

[5] Whittington JCR, Bogacz R. *An Approximation of the Error Backpropagation Algorithm in a Predictive Coding Network with Local Hebbian Synaptic Plasticity.* Neural Computation 2017; 29: 1229-1262. doi: 10.1162/NECO a 00949

[6] Knight JC, Komissarov A, Nowotny T. *PyGeNN: A Python Library for GPU-Enhanced Neural Networks.* Frontiers in Neuroinformatics 2021; 15. doi: 10.3389/fninf.2021.659005.

[7] Xu Q, Peng J, Shen J, Tang H, Pan G. Deep CovDenseSNN: *A hierarchical event-driven dynamic framework with spiking neurons in noisy environment.* Neural Networks 2020; 121: 512-519. doi: 10.1016/j.neunet.2019.08.034

67. Gradient free optimization of neuroscience models at different scales with L2L

Alper Yeğenoğlu[1,3,*], Cristian Jimenez Romero[1], Aarón Pérez Martín[1], Michiel van der Vlag[1], Wouter Klijn[1], Thorsten Hater[1], Abigail Morrison[1,2,4], Sandra Diaz-Pier[1]

1. SDL Neuroscience, Institute for Advanced Simulation, Jülich Supercomputing Centre (JSC),
2. Institute of Neuroscience and Medicine (INM-6), Institute for Advanced Simulation (IAS-6), Theoretical Neuroscience, Computational and Systems Neuroscience, Forschungszentrum Jülich and JARA, Jülich, Germany;
3. Institute of Geometry and Applied Mathematics, Department of Mathematics, RWTH Aachen, Aachen, Germany
4. Department of Computer Science 3, Faculty 1, RWTH Aachen, Aachen, Germany

*a.yegenoglu@fz-juelich.de

INTRODUCTION/MOTIVATION

Models in neuroscience have a high number of degrees of freedom. Often only specific parameter regions are of interest, which emphasizes the need of developing tools to efficiently find these regions and advance brain research. In computational neuroscience techniques to explore high dimensional spaces have been used more frequently. In addition, high performance computing (HPC) can provide an infrastructure to efficiently run these computational heavy exploration methods to increase our general understand of the model behavior within reasonable times. In this work we present the parameter optimization of different neuroscientific models at different scales with the framework L2L.

METHODS

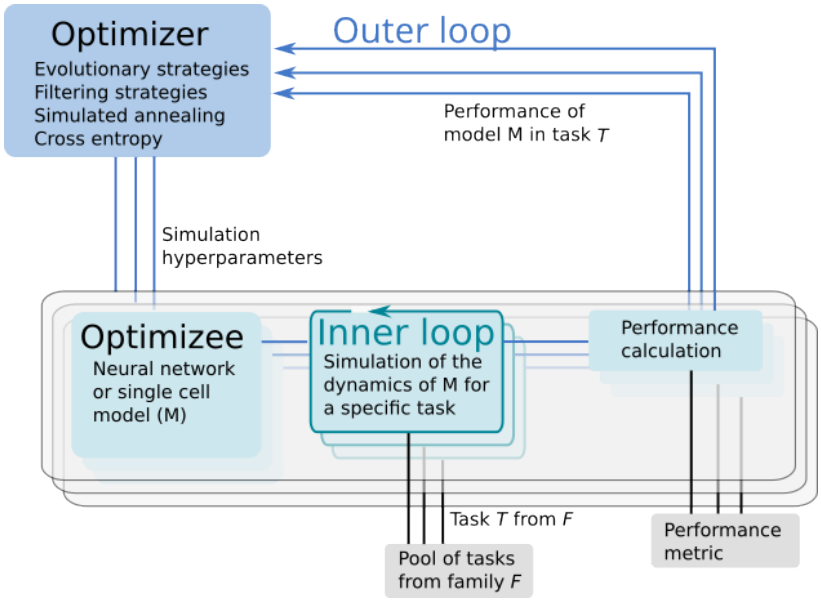

Figure 1: The two loop structure of learning to learn. In the inner loop a model can be trained or simulated on a task from a family of tasks. A task specific fitness function evaluates the performance. The outer loop optimizes the parameters of the inner loop model.

Learning to learn or meta-learning is a well-known concept in machine learning (ML) [1]. It is a specific method to improve learning performance by optimizing hyper-parameter and parameters of the model. The concept is divided into a two loop optimization process as depicted in Figure 1. The optimizee, i.e. the optimization target, in the inner loop can consist of any program such as an artificial neural network, a spiking network, a single cell model, or a whole brain simulation. This program is trained or just simulated on a task from a family of tasks. A fitness function, designed specifically for the task, assesses the performance. The (hyper-)parameters of the model and the fitness value are sent to the outer loop optimizer, which adapts the parameters using population based decision algorithms such as evolutionary algorithms or filtering techniques.

Here we present L2L [2] as an easy to use framework to perform parameter and hyper- parameter explorations of different neuroscience models utilizing HPC systems. L2L implements the learning to learn concept as an open source framework written in Python. The flexibility of the framework allows to deploy multiple simulations or model instances in a parallel fashion on HPCs.

RESULTS AND DISCUSSION

We highlight a variety of neuroscience models being optimized within the L2L framework. The different types of tasks shown in this work, illustrate the concept of reproducing empirical data or the learning process to solve a complex problem in dynamic environments. Our simulations range from single cell to the whole brain and use a variety of simulation engines such as NEST [3], Arbor [4], TVB [5], and NetLogo [6].

Keywords: simulation, meta learning, hyper-parameter optimization, high performance computing, connectivity generation, parameter exploration

ACKNOWLEDGEMENTS

The research leading to these results has received funding from the European Union's Horizon 2020 Framework Programme for Research and Innovation under the Specific Grant Agreement

No. 945539 (Human Brain Project SGA3). This research has also been partially funded by the Helmholtz Association through the Helmholtz Portfolio Theme "Supercomputing and Modeling for the Human Brain". Open Access publication funded by the Deutsche Forschungsgemeinschaft (DFG, German Research Foundation) - 491111487.

REFERENCES

[1LIST] Sebastian Thrun and Lorien Pratt. Learning to learn. Springer Science & Business Media, 2012.

[2] Alper Yegenoglu et al. “Exploring Parameter and Hyper-Parameter Spaces of Neuroscience Models on High Performance Computers With Learning to Learn”. In: Frontiers in Computational Neuroscience 16 (2022)

[3] Jan Hahne et al. NEST 3.0. Version 3.0. June 2021. doi: 10.5281/zenodo.4739103. url: https://doi.org/10.5281/zenodo.4739103.

[4] N. Abi Akar et al. “Arbor — A Morphologically-Detailed Neural Network Simulation Library for Contemporary High-Performance Computing Architectures”. In: 2019 27th Euromicro International Conference on Parallel, Distributed and Network-Based Processing (PDP). Feb. 2019, pp. 274–282. doi: 10.1109/EMPDP.2019.8671560.

[5] Paula Sanzleon et al. “The virtual brain: A simulator of primate brain network dynamics”. In: Frontiers in Neuroinformatics 7.MAY (2013). issn: 16625196. doi: 10.3389/fninf.2013.00010.

[6] Seth Tisue and Uri Wilensky. “Netlogo: A simple environment for modeling complexity”. In: International conference on complex systems. Vol. 21. Boston, MA. 2004, pp. 16–21.

68. A layered cognitive architecture for motivational control in a navigation task

Alejandro Jimenez Rodriguez[1*], Tony Prescott[2]

[1]Department of Computer Science, University of Sheffield, UK

*a.jimenez-rodriguez@sheffield.ac.uk

INTRODUCTION/MOTIVATION

Recent developments in the neuroscience of motivation have identified the main neural circuits at the interface between physiological needs and behavioural decision making [1]. On the one hand, different hypothalamic circuits interface with the internal millieu in order to encode physiological signals in the activity of neurons. On the other hand, the output of such circuits use neuromodulators like dopamie to influence action selection in downstream areas like the striatum. Among the involved regions, the Lateral Hypothalamus (LH) stands out as a hub that combine signals from all over the mammalian brain along the physiological state to drive the dopaminergic neurons in the Ventral Tegmental Area (VTA) and basal ganglia [2, 5].

In this work we propose a layered cognitive architecture that leverages such circuits to drive exploration and exploitation in a robotic model of hippocampal replay[3]. In previous work we have already showed that such an architecture possess dynamical properties that allow for behavioural switching that satisfies competing needs. This work shows how the brain implements these ideas following the layered architecture paradigm [4] to drive navigation and learning.

METHODS

The hypothalamic circuit is implemented with rate neurons in three different layers. The ventricular layer is composed of independent homeostatic circuits that drive independent signals towards variable set points. The intermediate layer is composed of an I-E balanced network that performs the behavioural switching at the LH level and the exploration-exploitation switch at the level of the Nucleus accumbens. Finally, the monoaminergic layer performs the dopaminergic modulation.

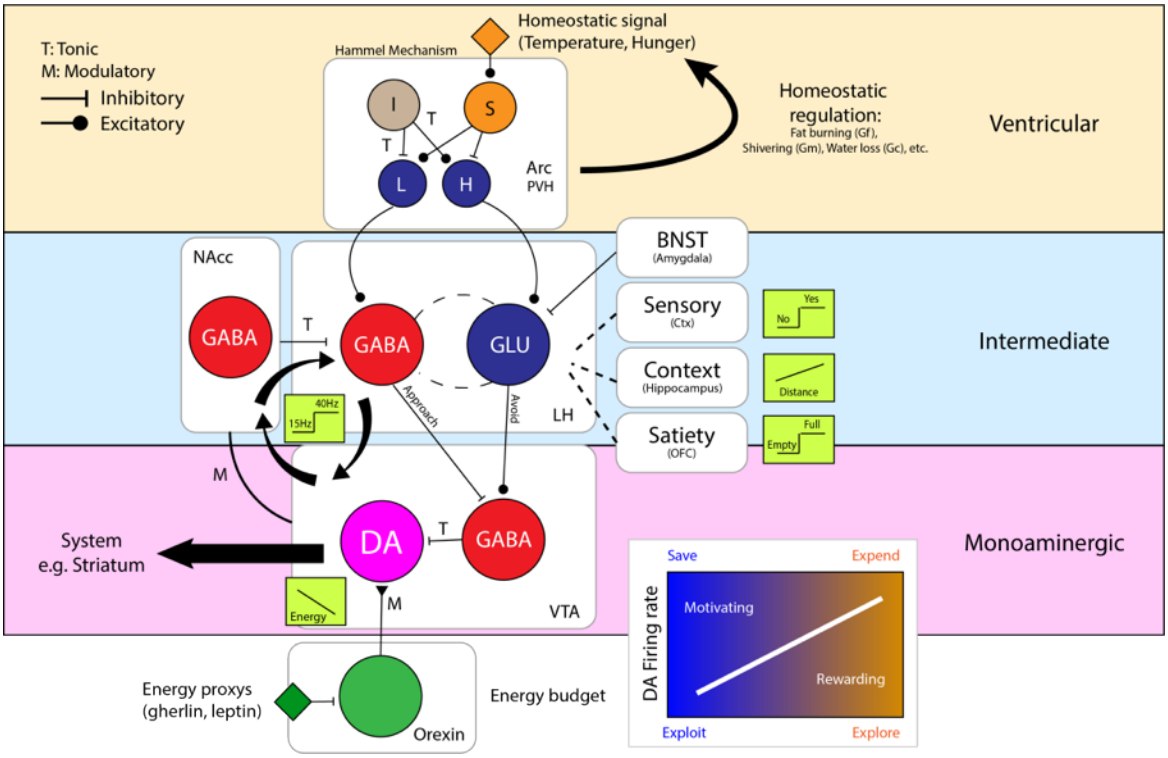

Figure 1: Hypothalamic layered architecture for motivational control

RESULTS AND DISCUSSION

We test our model in a previously published robotic implementation of the Morris Water maze [3]. In such a model, we augment a policy gradient rule with the motivational neuromodulation to satisfy different needs (Figure 2). We show that the motivational state of the agent successfully drive learning and exploration under different conditions. Additionally, we illustrate how the properties of the balanced network of the LH reproduce different aspects of the dopamine signal.

This work is an important step forward in integrating motivational dynamics into functional architectures in robots. Additionally, it provides computational testable hypothesis about the grounding of value and reward in reinforcement learning tasks using principles of homeostasis and energy balance.

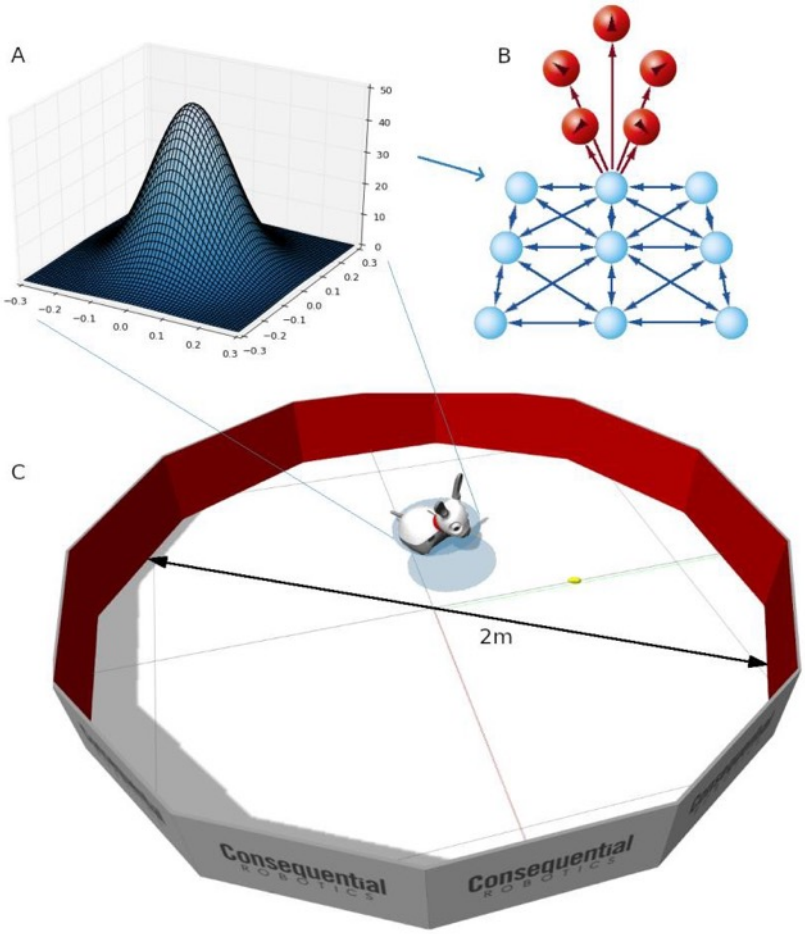

Figure 2: Hippocampal replay implementation with MiRo

Keywords: Dopamine, Hypothalamus, Motivation, Self-regulation, Navigation

REFERENCES

[1] Yapici, N., Zimmer, M., & Domingos, A. I. (2014). Cellular and molecular basis of decision-making. *EMBO reports*, *15*(10), 1023-1035.

[2| Stuber, G. D., & Wise, R. A. (2016). Lateral hypothalamic circuits for feeding and reward. *Nature neuroscience*, *19*(2), 198- 205.

[3] Whelan, M. T., Jimenez-Rodriguez, A., Prescott, T. J., & Vasilaki, E. (2022). A robotic model of hippocampal reverse replay for reinforcement learning. Bioinspiration & Biomimetics, 18(1), 015007.

[4] Jimenez-Rodriguez, A., Prescott, T. J., Schmidt, R., & Wilson, S. (2020). A framework for resolving motivational conflict via attractor dynamics. In *Biomimetic and Biohybrid Systems: 9th International Conference, Living Machines 2020, Freiburg, Germany, July 28–30, 2020, Proceedings 9* (pp. 192-203). Springer International Publishing.

[4] Prescott, T. J., Redgrave, P., & Gurney, K. (1999). Layered control architectures in robots and vertebrates. *Adaptive Behavior*, *7*(1), 99-127.
[5] Swanson, L. W. (2000). Cerebral hemisphere regulation of motivated behavior. Brain research, 886(1-2), 113-164.

69. The virtual multiple sclerosis patient: on the clinical- radiological paradox

Pierpaolo Sorrentino *[1,2], Anagh Pathak[3], Abolfazl Ziaeemehr [1], emahnuel Troisi Lopez [4,5], Lorenzo Cipriano [4,5], Antonella Romano [4,5], Simona Bonavita [6], Mario Quarantelli [7], Arpan Banerjee [3], Giuseppe Sorrentino[4,5] , Meysam Hashemi[1], Viktor Jirsa[1]

1. Institut de Neurosciences des Systèmes, Aix-Marseille Université, Marseille, France
2. Institute of Applied Sciences and Intelligent Systems, National Research Council, Pozzuoli, Italy
3. National Brain Research Centre, Manesar, Gurgaon, Haryana, India
4. Department of Motor Sciences and Wellness, Parthenope University of Naples, Naples, Italy
5. Institute for Diagnosis and Cure Hermitage Capodimonte, Naples, Italy
6. Department of Advanced Medical and Surgical Sciences, University of Campania Luigi Vanvitelli. Caserta, Italy
7. Biostructure and Bioimaging Institute, National Research Council, Naples, Italy

* pierpaolo.SORRENTINO@univ-amu.fr.

INTRODUCTION/MOTIVATION

The structural lesions, typical of Multiple Sclerosis, are a consequence of the damage of the myelin sheath in the central nervous system. However, the lesion load is only a poor predictor of clinical disability [1]. In this paper, we hypothesize that the overall slowing of conduction velocities (i.e., across all brain tracts) is a better predictor of clinical disability as compared to structural damage. However, conduction velocities are typically measured on selected white-matter tracts (e.g., visual evoked potentials), which do not directly relate to clinical impairment. In fact, estimating conduction velocities across the whole brain has not been possible so far.

METHODS

To overcome this obstacle, we estimated patient-specific conduction velocities in MS patients by merging multimodal data (i.e., DTI and source-reconstructed magnetoencephalography) to inform large-scale brain models [2,3], fitted on each individual patient. We started from the known reduction of the power of the alpha frequency band, as well as the shift in its peak, observed in MS patients. We then reproduced these individual spectral features in silico using large-scale models based on the individual connectomes. We then used state-of-the-art deep neural networks for Bayesian model inversion to estimate the most likely average conduction velocity in each patient, given the observed spectral features (and the connectomes). To this end, we used Bayesian inference for model inversion, which is a principled method for updating beliefs with the information provided by the observed data (new evidence) to quantify uncertainty over hidden variables [4,5]. See Fig. 1 for an overview. For the present manuscript a key goal would be to infer patient specific average conduction velocities as the parameter that modulates power spectra in the alpha frequency band. To this end, we used simulation-based- inference (SBI) to estimate the conduction velocities (and a scaling parameter) over the patient's structural information, with the aid of only forward simulations. Finally, we used the inferred conduction velocities to predict the individual clinical disability.>

RESULTS AND DISCUSSION

MS patients displayed significantly attenuated peak alpha amplitudes as compared to controls ($p < 0.01$). Furthermore, the total power in the alpha band, measured as the area under the PSD curve between 8-13 Hz, was significantly lower in MS patients ($p = 0.02$). With respect to the parameter inference, we estimated the posterior distributions over the whole-brain model parameters (the global coupling strength G, and the velocity V), by using SBI against the empirical PSD, pooled over the control and the patient groups. The posterior distribution of parameter G, which scales the structural connectivity of subjects, demonstrated non-significant changes (p-value
= 0.87), whereas the posterior distribution of averaged velocities V significantly decreased (p-value <0.01) in MS patients as compared to the control group (see Fig. 2). Finally, we built a multilinear model to predict clinical disability as measured by the EDSS scale. Gender, age, education level, disease duration and lesion load (i.e., the total volume of lesions), and the inferred conduction velocities were considered as predictors. We found that the model performs well at predicting individual disability ($R2 = 0.595$, Adjusted $R2 = 0.41$). Adding the inferred velocities to the model significantly improves the predictive power over the EDSS ($p=0.028$). To test for the generalizability of our model, we used a leave-one-out cross validation (LOOCV) scheme. Again, adding the estimated speed to the model significantly improved the predictive power ($p=0.0417$). Our results suggest a biologically and physically plausible solution to the "clinico-radiological" paradox, where the inferred, individual changes in conduction velocities across the whole networks are proposed as causative to the clinical disability in multiple sclerosis patients. Furthermore, this new pipeline merges multimodal imaging, large-scale brain models and machine learning in a Neurologically-coherent fashion, providing a new way to investigate large-scale communication of the brain mechanistically.

Keywords: <Multiple sclerosis>, <brain networks>, <conduction delays>, <tractography>, <brain networks>, <brain modelling>, <Bayesian inference>, <virtual patient>.

ACKNOWLEDGEMENTS

This research has received funding from the European Union's Horizon 2020 Framework Programme for Research and Innovation under the Specific Grant Agreement No. 945539 (Human Brain Project SGA3).

REFERENCES

[1] Barkhof, F. (2002). The clinico-radiological paradox in multiple sclerosis revisited. *Current opinion in neurology*, *15*(3), 239-245.

[2] Sorrentino, P., Petkoski, S., Sparaco, M., Troisi Lopez, E., Rucco, R., Signoriello, E., ... & Jirsa, V. (2021). On the topochronic map of the human brain dynamics. *bioRxiv*, 2021-07.

[3| Pierpaolo, S., Caio, S., Rosaria, R., Marianna, L., Emahnuel, T. L., Simona, B., ... & Zalesky, A. (2021). The structural connectome constrains fast brain dynamics. *eLife*, *10*.

[4] Gonçalves, P. J., Lueckmann, J. M., Deistler, M., Nonnenmacher, M., Öcal, K., Bassetto, G., ... & Macke, J. H. (2020). Training deep neural density estimators to identify mechanistic models of neural dynamics. *Elife*, *9*, e56261.

[5] Hashemi, M., Vattikonda, A. N., Sip, V., Guye, M., Bartolomei, F., Woodman, M. M., & Jirsa, V. K. (2020). The Bayesian Virtual Epileptic Patient: A probabilistic framework designed to infer the spatial map of epileptogenicity in a personalized large-scale brain model of epilepsy spread. *NeuroImage*, *217*, 116839.

Fig.1: overview of the pipeline.

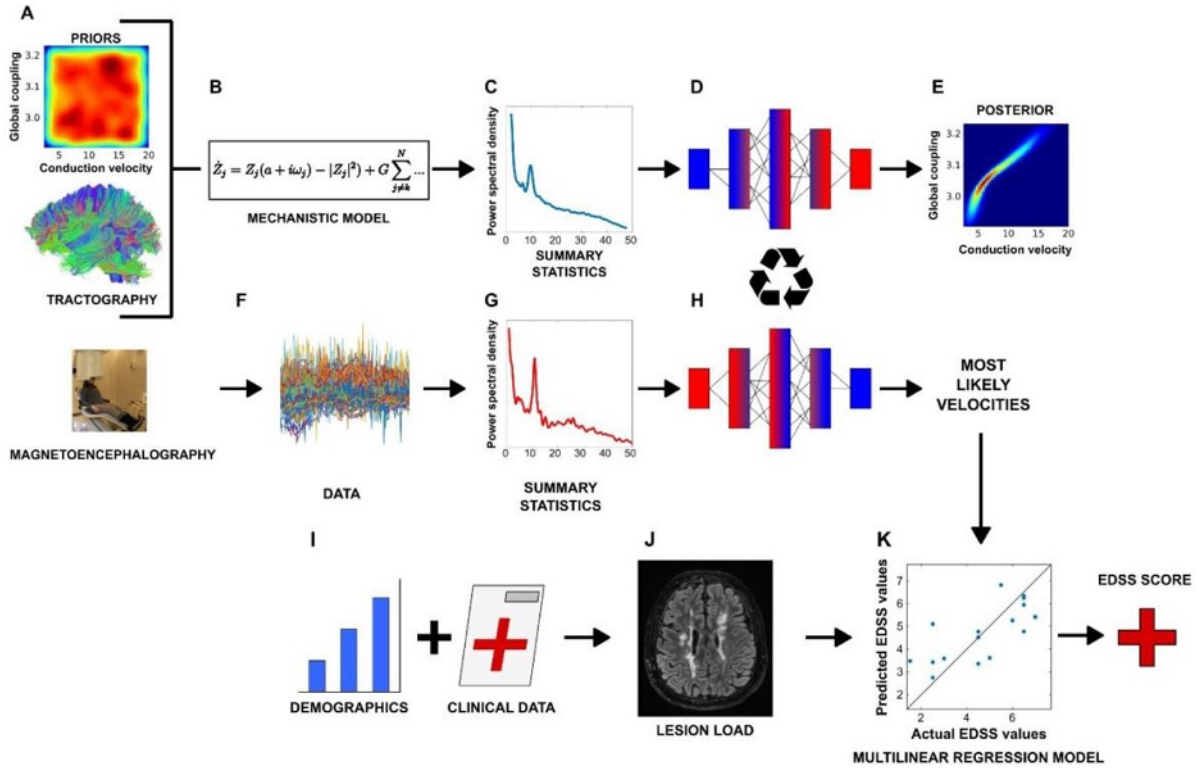

Fig. 2. Main results.

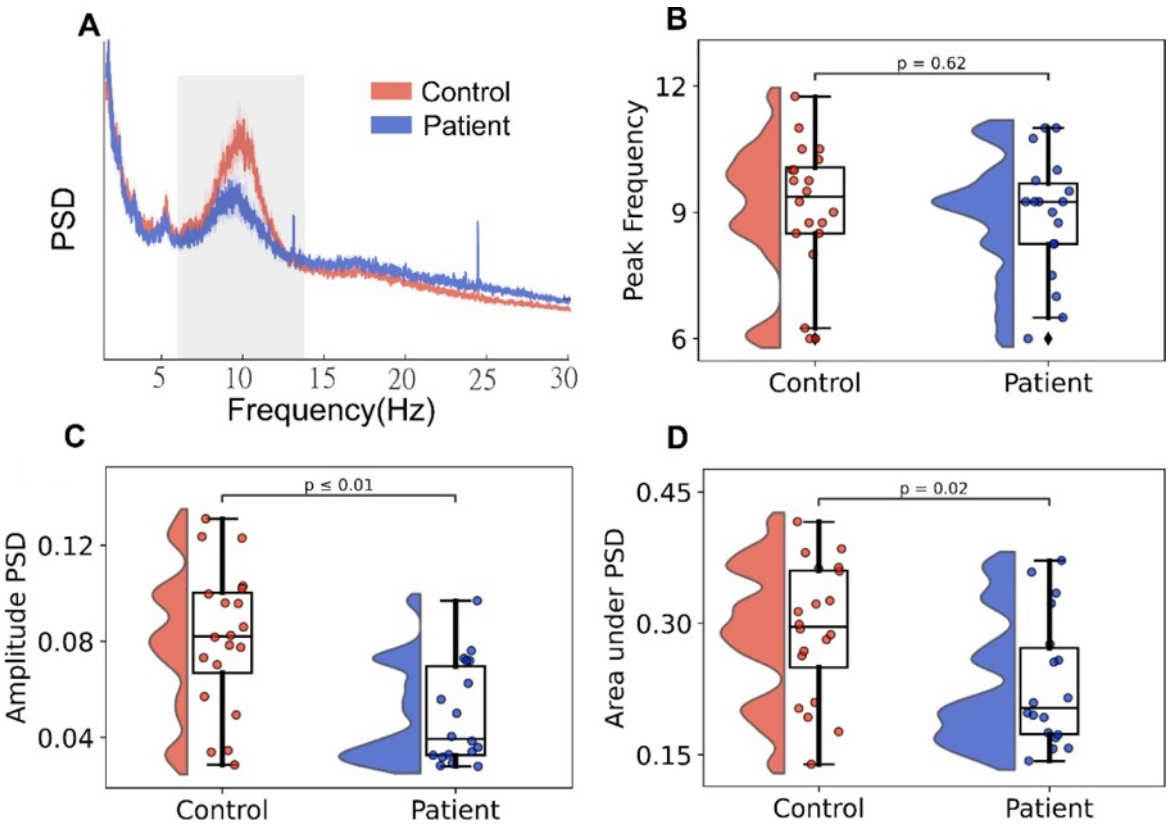

70. Modelling spatio-temporal dynamics of interictal spikes

Jean-Didier Lemaréchal[1*], Paul Triebkorn[1], Gian-Marco Duma[1], Borana Dollomaja[1], Jean-Michel Badier[1], Christian-George Bénar[1], Fabrice Bartolomei[1,2], Huifang Wang[1], Viktor Jirsa[1]

[1.] Institut de Neurosciences des Systèmes, Aix-Marseille Université, Marseille, France.
[2.] Assistance Publique - Hôpitaux de Marseille, Hôpital de la Timone, Service de Neurophysiologie Clinique, CHU, Marseille, France.

* jean-didier.lemarechal@univ-amu.fr

INTRODUCTION

The localization of the epileptogenic network from the analysis of interictal activity is still an open issue for patients with pharmacoresistant epilepsy. Compared with seizure events, interictal activity is also observable with both invasive (stereoelectroencephalography, SEEG) and non-invasive (magnetoencephalography, MEG) techniques, but is usually much easier to record. In this study, we build a whole brain network model personalized with patient specific data to predict spatio-temporal dynamics of interictal spikes.

METHODS

First, we simulated interictal spikes for a single node of the network with Epileptor, a phenomenological neuronal model of epileptic activity (Jirsa et al., 2014). For a single Epileptor model, the generation of spikes depends on the level of noise of the stochastic integrator used to compute the dynamics of the model. Then, we built and simulated a high spatial resolution neural field model composed of 20484 cortical (and 18 subcortical) nodes (Proix et al., 2018). This model embeds long-range and short-range structural connectivity, and accounts for complex spatio-temporal dynamics observed in epilepsy. Finally, we mapped the simulated brain activity to both SEEG and MEG measurements.

RESULTS

For whole brain network modelling, short-range coupling is essential to recruit a sufficient number of nodes and to trigger the emergence of a significant interictal activity which then propagates through the network. Importantly, this activity is also observable in simultaneous SEEG and MEG synthetic data, with specific spatio-temporal patterns. We built personalized whole brain network for 10 patients and showed that the simulated SEEG and MEG signals had similar spatio-temporal patterns as empirical SEEG and MEG observations.

DISCUSSION

This work demonstrates the modelling of spatio-temporal dynamics of interictal spikes for individualized patients. It brings opportunities to better understand the relationships between interictal and ictal discharges using invasive but also non-invasive measurements. Finally, the multimodal dataset of this study is made available to the community.

Keywords : Epileptogenic network, interictal spikes, stereoelectroencephalography, magnetoencephalography, Virtual Epileptic Patient

ACKNOWLEDGEMENTS

This work is partially funded through the European Union's Horizon 2020 Framework Programme for Research and Innovation under the Specific Grant Agreement No. 945539 (Human Brain Project SGA3) and through the French National Research Agency (ANR) as part of the second "Investissements d'Avenir" program (ANR-17-RHUS-0004, EPINOV).

REFERENCES

Jirsa, V.K., Stacey, W.C., Quilichini, P.P., Ivanov, A.I., Bernard, C., 2014. On the nature of seizure dynamics. Brain 137, 2210–2230. https://doi.org/10.1093/brain/awu133

Proix, T., Jirsa, V.K., Bartolomei, F., Guye, M., Truccolo, W., 2018. Predicting the spatiotemporal diversity of seizure propagation and termination in human focal epilepsy. Nat. Commun. 9, 1088. https://doi.org/10.1038/s41467-018-02973-y

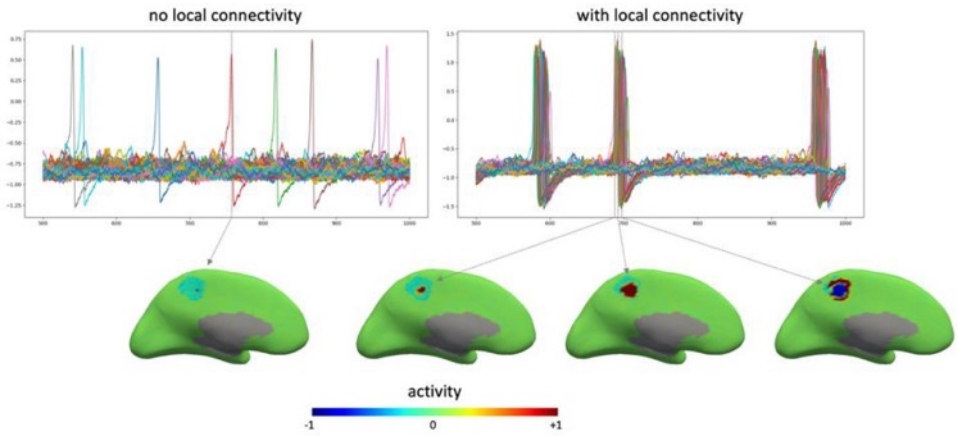

Figure 1 : Without local connectivity, spikes are generated randomly. Adding local connectivity induces a spatio-temporal synchronization of local dynamics and results in the
emergence of a significant spiking activity.

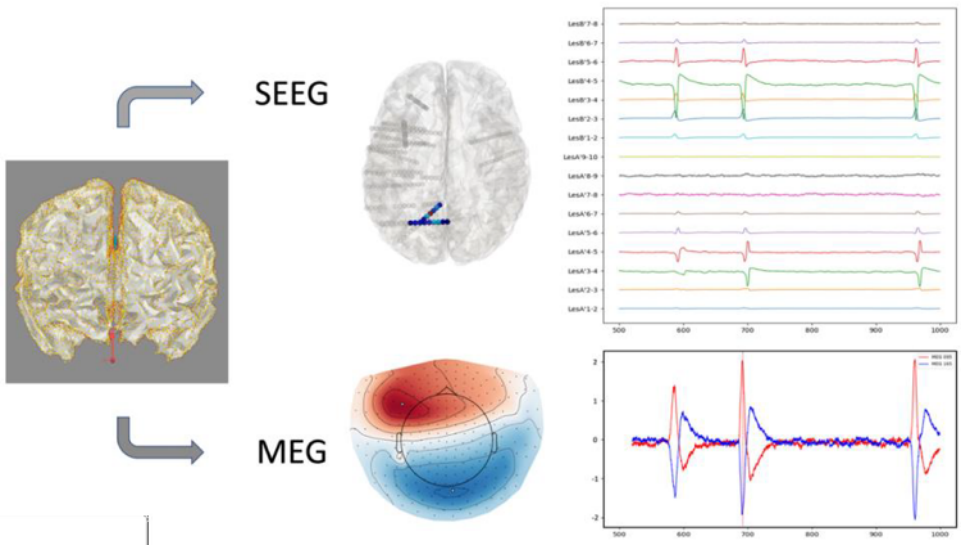

Figure 2 : Simulated brain activity is projected to SEEG and MEG modalities with respect to the specific forward solution and spiking activity is observable in both invasive SEEG and non-invasive MEG measurements.

71. The structured flow on the brain's resting state manifold

Jan Fousek[1], Giovanni Rabuffo[1], Kashyap Gudibanda[1], Hiba Sheheitli[1], Spase Petkoski[1], Viktor Jirsa[1*]

[1]INSERM UMR 1106 Institut de Neurosciences des Systèmes - Aix-Marseille Université, Marseille, France
*viktor.jirsa@univ-amu.fr

INTRODUCTION/MOTIVATION

Fluctuations of brain activity at rest display correlations between areas involved in task conditions, and their temporal variability possesses functional significance. However, our understanding of the mechanisms underlying these spatio-temporal patterns is still incomplete. Here we address the main empirical signatures of brain resting state data: bistability of single region activation, low-dimensionality of the global system dynamics, multistability of recurrent coactivation patterns,and their non-trivial temporal dynamics. These constitute the key features of what we describe as structured flows on manifolds (SFMs) [1,2].

METHODS

We construct a whole brain network model [3] using 2D neural mass model [4] driven by noise to govern the regional dynamics coupled with a DTI-derived connectome from the Human Connectome Project in the Desikan- Killiany parcellation, and equip it with BOLD observer model [5]. From the simulated 10 minutes of noise-driven spontaneous activity we extract time-averaged time series of the state variables of the model (1kHz sampling rate), and the BOLD signal (~0.5 Hz).

First we employ systematic parameter exploration for global coupling scaling factor G and the noise variance σ. For each combination of the two parameters we evaluate the dynamical functional connectivity of the BOLD signal (dFC, correlation between windowed) in terms of its fluidity (variance of the upper triangle), and the dimensionality of the dynamics of the model by computing the variance accounted for (VAF) of the PCA applied to the time series of the state variables of the model. Result of this step provides a working point where the dFC is similar to the empirical data [6].

Additionally, having access to the generating model, we analyse in detail the fixed point skeleton of the networked model and show how the low dimensional manifold and the associated structured flow using linear stability analysis.

Second, we strive to map the attractive manifold of the spontaneous dynamics in the space of the state variables of the system in this working point of the fluid dFC. For this we first compute the edge time-series (dot-product of the z-scored BOLD [7]), apply k-means clustering to separate similar co-activations, and then locate the corresponding time points on the low-dimensional embedding (PCA) of the state variable time-series.

RESULTS AND DISCUSSION

We have observed that the dimensionality of the system state space dynamics reduces for the same intermediate values of G where the main dynamical signatures of the resting state are captured, whereas the decoupled or over-connected system lacks the recurrence in time and exhibits high-dimensional dynamics.

In the working point, we then link the low-dimensional manifold subspaces with the clusters of the dynamic functional connectivity. We find that the structured flow is composed of fluctuation of the system on a slow time- scale between global states of high- and low-activity, and in the subspace of high activity undergoes the high- amplitude co-fluctuations [7]. In addition, applying a convolution kernel similar to the BOLD observer model (in the time width) to the state variables in the low-dimensional projection results to clearer separation of the occupied subspaces, which is consistent with the expected loss of information due to relative slowness of the BOLD compared to the neuronal activity.

These results underscore the central role that the structural connectome plays in the symmetry breaking that shapes the manifold and the resulting structured flow which describes the resting state brain dynamics. All in all, we show in-silico the potential of SFMs formalism as a prime candidate to make current semi-formal descriptions using a variety of mathematical concepts such as attractor landscapes [8] explicit.

Keywords: Resting State, fMRI, Brain Network Model, Structured Flows on Manifolds

ACKNOWLEDGEMENTS

This research has received funding from the European Union's Horizon 2020 Framework Programme for Research and Innovation under the Specific Grant Agreement No. 945539 (Human Brain Project SGA3), and under grant agreement No 826421 (TVB-Cloud).

REFERENCES

[1] Pillai, A. S., & Jirsa, V. K. (2017). Symmetry Breaking in Space-Time Hierarchies Shapes Brain Dynamics and Behavior. *Neuron*, *94*(5), 1010–1026. https://doi.org/10.1016/j.neuron.2017.05.013

[2] Fousek, J., Rabuffo, G., Gudibanda, K., Sheheitli, H., Jirsa, V., & Petkoski, S. (2022). The structured flow on the brain's resting state manifold. In *bioRxiv* (p. 2022.01.03.474841). https://doi.org/10.1101/2022.01.03.474841

[3] Sanz Leon, P., Knock, S. A., Woodman, M. M., Domide, L., Mersmann, J., McIntosh, A. R., & Jirsa, V. (2013). The Virtual Brain: a simulator of primate brain network dynamics. *Frontiers in Neuroinformatics*, *7*, 10. https://doi.org/10.3389/fninf.2013.00010

[4| Montbrió, E., Pazó, D., & Roxin, A. (2015). Macroscopic Description for Networks of Spiking Neurons. *Physical Review X*, *5*(2), 021028. https://doi.org/10.1103/PhysRevX.5.021028

[5] Stephan, K. E., Weiskopf, N., Drysdale, P. M., Robinson, P. A., & Friston, K. J. (2007). Comparing hemodynamic models with DCM. *NeuroImage*, *38*(3), 387–401. https://doi.org/10.1016/j.neuroimage.2007.07.040
[6] Rabuffo, G., Fousek, J., Bernard, C., & Jirsa, V. (2021). Neuronal Cascades Shape Whole-Brain Functional Dynamics at Rest. eNeuro, 8(5), 2020.12.25.424385. https://doi.org/10.1523/ENEURO.0283-21.2021
[7] Zamani Esfahlani, F., Jo, Y., Faskowitz, J., Byrge, L., Kennedy, D. P., Sporns, O., & Betzel, R. F. (2020). High- amplitude cofluctuations in cortical activity drive functional connectivity. *Proceedings of the National Academy of Sciences of the United States of America*, *117*(45), 28393–28401. https://doi.org/10.1073/pnas.2005531117
[8] Shine, J. M. (2021). The thalamus integrates the macrosystems of the brain to facilitate complex, adaptive brain network dynamics. *Progress in Neurobiology*, *199*, 101951. https://doi.org/10.1016/j.pneurobio.2020.101951

72. A multi-layer mean-field model of the cerebellar cortex can faithfully account circuit microscopic properties

Roberta M. Lorenzi[1*], Alice Geminiani[1], Yann Zerlaut[2], Alain Destexhe[3], Claudia A.M. Gandini Wheeler-Kingshott[1,4,5], Fulvia Palesi[1], Claudia Casellato[1], and Egidio D'Angelo[1,5]

[1]Department of Brain and Behavioural Sciences, University of Pavia, Pavia, Italy

[2]Institut du Cerveau - Paris Brain Institute - ICM, Inserm, CNRS, APHP, Hôpital de la Pitié Salpêtrière, Paris, France

[3]Paris-Saclay University, CNRS, Saclay, France

[4]NMR Research Unit, Queen Square Multiple Sclerosis Centre, Department of Neuroinflammation, UCL Queen Square Institute of Neurology, UCL, London, UK

[5]Brain Connectivity Center IRCCS Mondino Foundation, Pavia, Italy

*e-mail-address of corresponding author: robertamaria.lorenzi01@universitadipavia.it

INTRODUCTION

Brain modeling is opening new frontiers for clinical applications and requires specific multiscale strategies. Mean- field (MF) models are a mesoscale formalisms summarizing the interaction of a neuronal population with the mean-field generated by the others[1], providing a statistical approximation that bridges the gap between the underlying microscale effects and macroscale recordings[2]. Isocortical MFs have been integrated in simulators such as The Virtual Brain (TVB)[3]. An effective MF model is now much needed for the cerebellum , given its specific structure that can hardly be accounted for by ordinary neural masses and MFs elaborated for the isocortex [4]. We present here the first model of the cerebellum, based on its realistic multi-layer structure including Granule Cells (GrC), Golgi Cells (GoC), Molecular Layer Interneurons (MLI), and Purkinje Cells (PC). The cerebellar MF was optimized using parameters taken from experimental recordings and was validated against a realistic spiking neural network(SNN) of the cerebellum. The integration of this MF into TVB and its connection with cortical MFs would contribute to the development of advanced brain digital twins toward personalized medicine.

METHODS

The pipeline for implementing a multi-layer MF model is presented (Fig1A) for the specific case of the cerebellum, considering its multi-layer microcircuitry already implemented in a cerebellar SNN (Fig1B)[5]. A Transfer Function (F) formalism transferred neuronal biophysical properties into MF equations[6]. For each neuronal population, an analytical F (F_{PC},F_{MLI},F_{GrC},F_{GoC}) was fitted to the SNN output including connection probabilities, synaptic decay times

and quantal conductances (K,τ,Q)(Fig1C)[7]. The MF time constant (T) that regulates system global dynamics was optimized on Local Field Potentials (LFP) recorded from the granular layer (GrC and GoC) of mice cerebellar slices. The MF was validated against the SNN simulating the responses to composite inputs from intra-cerebral and sensory systems[8]. To investigate the MF predictive capability, inhibition control and PC learning were explored by tuning F_{PC} inputs (MLI-PC and GrC-PC, respectively)[9]. This allowed us to monitoring PC modulation of specific patterns like burst-and-pause and the impact of different levels of Long-Term Depression/Potentiation at the synapses between GrCs and PCs. Area Under Curve (AUC) and peak were reported. PC pause depth was computed for MLI-PC case.

RESULTS AND DISCUSSION

MF activities with an optimal T=3.5ms (MF-LFP Mean Absolute Error=3%) resulted comparable with SNN simulation (Fig2A). Simulations exploring GrC-PC plasticity revealed an AUC linear trend and a peak sigmoidal trend with increasing synaptic strength (Fig2B1). The inhibition control on PC resulted in AUC and peak exponential decay with increasing MLI-PC synaptic strength and a pause depth sigmoidal trend (Fig2B2).

The first complete cerebellar MF was developed with high fidelity to approximate the real biological multi-layer network, with optimal T reflecting the speed of cerebellar dynamics (these are faster compared to the isocortical activity). MF equations reproduced cerebellar oscillations and signal propagation matching the SNN activity in response to cortical input patterns and predicted the modulation of PCs firing depending on cortical plasticity, which drives learning in associative tasks, and feedforward inhibition level. F_{PC} tuning predicted how cerebellar complex synaptic mechanisms impact on the activity underlying motor control and learning. Parameters tuning might pave the way for further manipulation to remap physiological and/or pathological features onto the MF. Once integrated into TVB, the connection of the cerebellar MF with MFs specific for basal-ganglia-thalamocortical loop would remarkably improve the brain dynamics simulation[10], allowing to compare dysfunctional oscillations with physiological activity anticipating the clinical impact of brain digital twin.

Keywords: mean-field; transfer function; brain modelling; multiscale modelling; cerebellum; digital twin

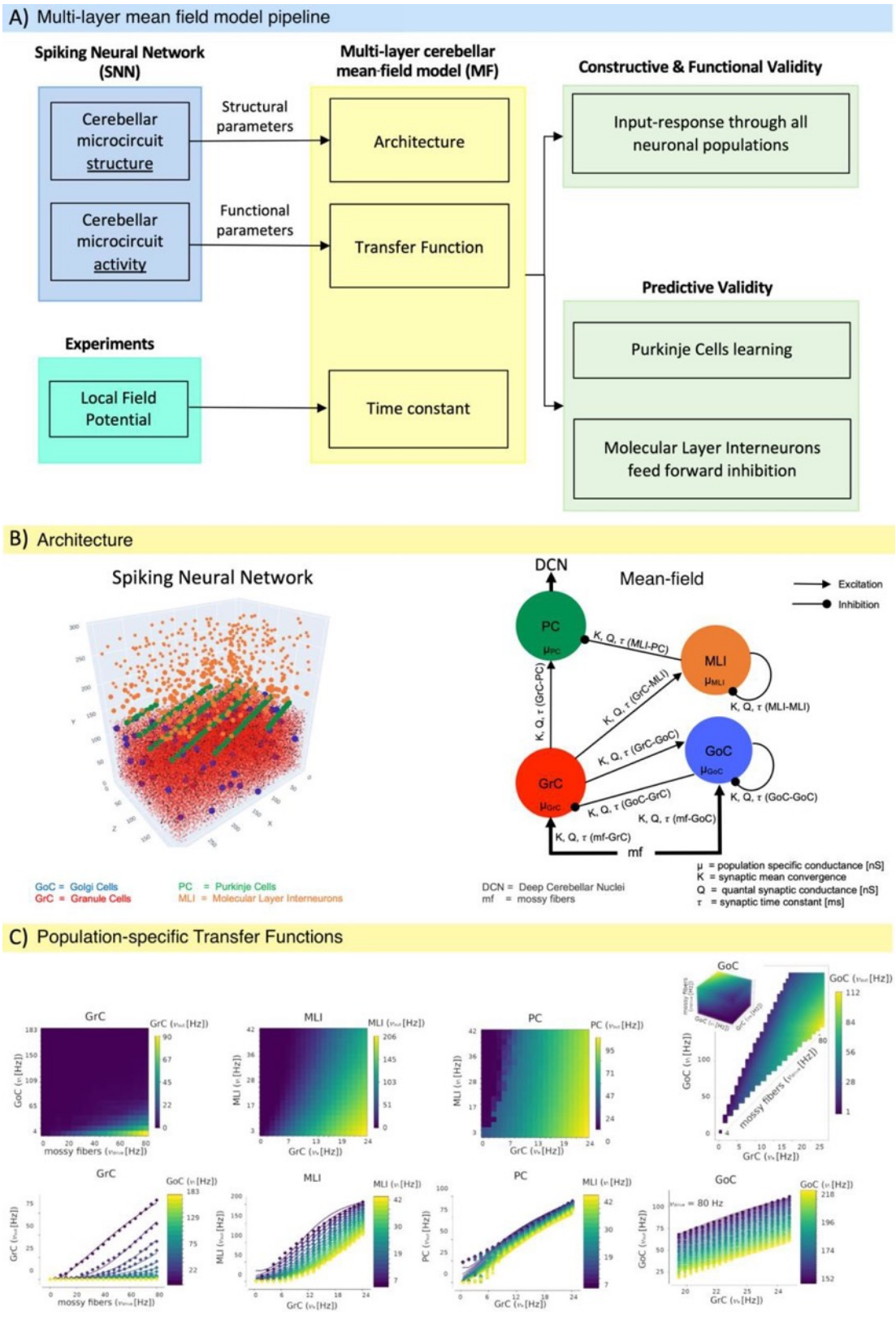

Figure 1) A) Pipeline to develop and optimize a multi-layer mean-field (MF). B) Spiking Neural Network (SNN) was used as a structural and functional template to build up the architecture of the multi-layer interwire cerebellar MF network. For each pre-synaptic connection, presynaptic parameters (connection probability K, synaptic conductance Q and time constant τ) were extracted based on SNN. C) Population-specific TFs are fitted on the numerical template computed with SNN using physiological working frequencies of each presynaptic connection. Semi-analytical TFs captures the differences in input/output relation determined by the population- specific biophysical features. (e.g, sigmoidal for molecular layer interneuron and almost linear for PC)

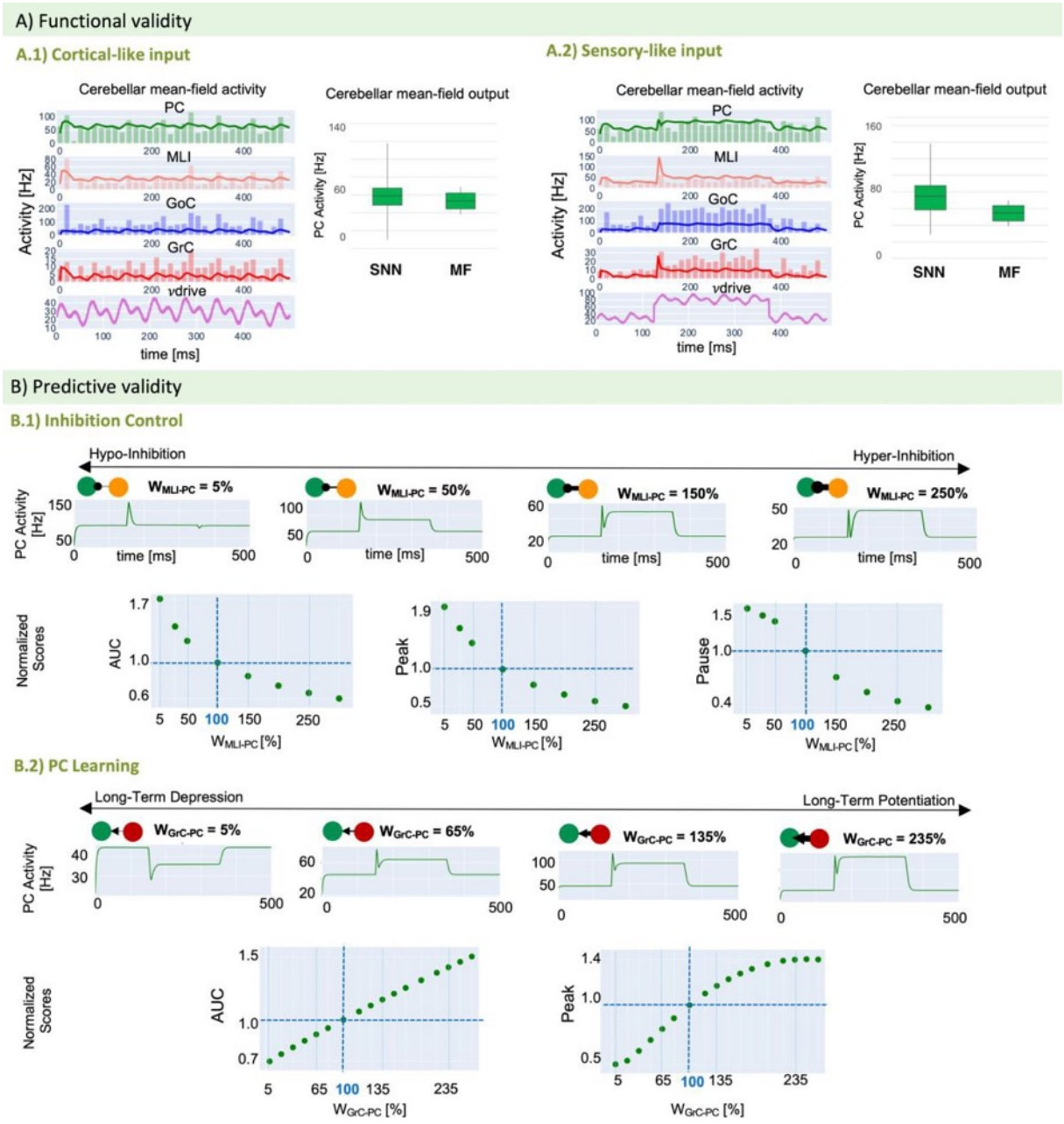

Figure 2) Validation. A1 & A2) Mean-field (MF) predictions (lines) for cortical-like input overlap the validated Spiking Neural Network (SNN - histogram). MF output (PC activity) is within SNN output (boxplots). B1) Inhibition control (wMLI-PC tuning, hypo to hyper inhibition) leads to nonlinear changes in PC activity quantified as Area Under Curve (AUC) and burst-pause dynamics (peak-pause). B2) PC learning (wGrC-PC tuning, Long-Term depression to potentiation) shows AUC linear increase and peak sigmoidal trend.

ACKNOWLEDGEMENTS

This research has received funding from the European Union's Horizon 2020 Framework Program for Research and Innovation under the Specific Grant Agreement No. 945539 (Human Brain Project SGA3) to ED, CGWK, FP and AD, and under the Marie Sklodowska-Curie grant agreement No. 892175 to YZ. CGWK received funding from BRC (#BRC704/CAP/CGW), MRC (#MR/S026088/1), Ataxia UK, MS Society (#77), Wings for Life (#169111). CGWK is a shareholder in Queen Square Analytics Ltd. This research has also received funding from Centro Fermi project "Local Neuronal Microcircuits" to ED. Special acknowledgement to EBRAINS and FENIX for informatic support and infrastructure.

REFERENCES

1. El Boustani S, Destexhe A. A master equation formalism for macroscopic modeling of asynchronous irregular activity states. *Neural Comput*. 2009;21(1):46-100. doi:10.1162/neco.2009.02-08-710
2. D'Angelo E, Jirsa V. Neurosciences The quest for multiscale brain modeling. *Trends Neurosci*. 2022;xx(xx):1-14. doi:10.1016/j.tins.2022.06.007
3. Sanz Leon P, Knock SA, Woodman MM, et al. The virtual brain: A simulator of primate brain network dynamics. *Front Neuroinform*. 2013;7(MAY). doi:10.3389/fninf.2013.00010
4. D'Angelo E. *Physiology of the Cerebellum*. Vol 154. 1st ed. Elsevier B.V.; 2018. doi:10.1016/B978-0-444- 63956-1.00006-0
5. Geminiani A, Pedrocchi A, D'Angelo E, Casellato C. Response Dynamics in an Olivocerebellar Spiking Neural Network With Non-linear Neuron Properties. *Front Comput Neurosci*. 2019;13(October):1-15. doi:10.3389/fncom.2019.00068
6. Zerlaut Y, Chemla S, Chavane F, Destexhe A. Modeling mesoscopic cortical dynamics using a mean-field model of conductance-based networks of adaptive exponential integrate-and-fire neurons. *J Comput Neurosci*. 2018;44(1):45-61. doi:10.1007/s10827-017-0668-2
7. De Schepper R, Geminiani A, Masoli S, et al. Model simulations unveil the structure-function-dynamics relationship of the cerebellar cortical microcircuit. *Commun Biol*. 2022. doi:https://doi.org/10.1038/s42003-022-04213-y
8. Del Percio C, Drinkenburg W, Lopez S, et al. On-going electroencephalographic rhythms related to cortical arousal in wild-type mice: the effect of aging. *Neurobiol Aging*. 2017;49:20-30. doi:https://doi.org/10.1016/j.neurobiolaging.2016.09.004
9. ten Brinke MM, Boele HJ, Spanke JK, et al. Evolving Models of Pavlovian Conditioning: Cerebellar Cortical Dynamics in Awake Behaving Mice. *Cell Rep*. 2015;13(9):1977-1988. doi:10.1016/j.celrep.2015.10.057
10. van Albada SJ, Robinson PA. Mean-field modeling of the basal ganglia-thalamocortical system. I. Firing rates in healthy and parkinsonian states. *J Theor Biol*. 2009;257(4):642-663. doi:10.1016/j.jtbi.2008.12.018

73. Efficient Bayesian Inference for Virtual Brain Modeling: Incorporating Prior Information and automatic Algorithms for Disorder Prediction

A. Ziaeemehr[1] , M. Hashemi[1],, A.N. Vattikonda[1], V. Sip[1], H.E. Wang, S. Petkoski[1], M.M. Woodman[1], and V. Jirsa[1]

[1] Aix Marseille Univ, INSERM, INS, Inst Neurosci Syst, UMR 1006, Marseille, France

Abolfazl.ziaee-mehr@univ-amu.fr, Vikotr.jirsa@univ-amu.fr

Keywords: Simulation based inference, Bayesian estimation, likelihood function, virtual brain models, brain disorders.

Abstract

Whole-brain network modeling combines personalized anatomical information with dynamical models of brain activity to generate spatio-temporal patterns as observed in brain imaging signals. This approach allows for the inference and prediction of local and global brain dynamics in both healthy states and disorders such as Alzheimer's disease, multiple sclerosis and epilepsy. However, the calculation of likelihood function at whole-brain scale is often intractable. Thus, likelihood-free inference algorithms are required to efficiently estimate the parameters pertaining to hypothetical areas in the brain, ideally including the uncertainty. We present the simulation-based inference method for the whole-brain models, which only requires forward simulations, enabling us to amortize posterior inference on parameters from low-dimensional data features representing whole-brain patterns in various brain disorders. We use state-of-the-art deep learning algorithms for conditional density estimation to retrieve the statistical relationships between parameters and observations through a sequence of invertible transformations. This approach enables us to for example predict excitability of lesioned area from new input data. The presented Bayesian methodology can deal with non-linear latent dynamics and parameter degeneracy, paving the way for reliable prediction of neurological disorders from neuroimaging modalities, which can be crucial for planning intervention strategies.

INTRODUCTION/MOTIVATION

The main purpose of this research is to provide a flexible, efficient, accurate and user friendly framework using deep neural network for inferenc of local and global brain dynamics to reveal the mechanism underlying disorder

such as Alzheimer's disease, multiple sclerosis, and epilepsy.

METHODS

In practice, we use simulation-based inference, and low-dimensional data features from hundreds of thousands of simulations and train the deep neural network to produce the posterior distribution of required parameters to fit the mathematical models to local and global brain activity patterns.

RESULTS AND DISCUSSION

Our results indicate that SBI can efficiently estimate the full posterior distribution of virtual brain parameters (Excitability and global coupling in Alzheimer's Disease), from fMRI recordings(Refs 1-4). In sum, our Bayesian methodology can deal with non-linear latent dynamics and parameter degeneracy, paving the way for fast and reliable inference on brain disorders from neuroimaging modalities. We also provide an open-source Python package in Ebrain platform for neuroscience community usage.

ACKNOWLEDGEMENTS

This project was funded by the European Union's Horizon 2020 research and innovation programme under grant agreement No. 785907 (SGA2), and No. 945539 (SGA3) Human Brain Project, and Virtual-BrainCloud (grant number 826421).

Refs:

[1] D'Angelo, Egidio, and Viktor Jirsa. "*The quest for multiscale brain modeling*." Trends in Neurosciences (2022).
[2] M. Hashemi, AN. Vattikonda, J. Jha, V. Sip, MM. Woodman, F. Bartolomei, V. Jirsa. "*Simulation-Based Inference for Whole-Brain Network Modeling of Epilepsy using Deep Neural Density Estimators*". medRxiv. 2022 Jan 1. DOI: https://doi.org/10.1101/2022.06.02.22275860
[3] BH. Yalcinkaya, A. Ziaeemehr, J. Fousek, M. Hashemi, M. Lavanga, A. Solodkin, AR. McIntosh, V. Jirsa, S. Petkoski. *"Personalized virtual brains of Alzheimer's Disease link dynamical biomarkers of fMRI with increased local excitability*". bioRxiv. 2022 Jan 1. DOI: https://doi.org/10.1101/2023.01.11.23284438
[4] A. Ziaeemehr, M Hashemi, M. Woodman, V. Jirsa *"Simulation-Based Inference for Whole-Brain Dynamics: Developing a Python Package for Reliable Prediction of Neurological Disorders".* In preperation.

74. Characterization of regional differences in resting- state fMRI with a network model of brain dynamics

Viktor Sip[1*], Meysam Hashemi[1], Timo Dickscheid[2], Katrin Amunts[2], Spase Petkoski[1], Viktor Jirsa[1]

[1]Aix Marseille Univ, INSERM, INS, Inst Neurosci Syst, Marseille, France

[2]Institute of Neuroscience and Medicine (INM-1), Research Centre Jülich, Jülich, Germany

*viktor.sip@univ-amu.fr

INTRODUCTION/MOTIVATION

One avenue for analysis of resting-state functional magnetic resonance imaging (fMRI) is the use of network models of large-scale brain network dynamics[1]. These models can be constrained by individual brain imaging data; typically, the diffusion-weighted imaging data are used to estimate the edge weights. The local dynamics of brain regions is represented by the so-called neural mass models – low-dimensional models of neuronal population activity. Neural mass models employed in these studies are usually derived through a series of major simplifications in order to arrive to simple, low-dimensional models of neural dynamics. Here we examine whether such neural mass models can be obtained in a data-driven fashion using modern methods of dynamical system identification from resting-state fMRI. We develop a suitable method and use it to characterize the regional differences underlying the large-scale brain dynamics[2].

METHODS

We follow the general framework of large-scale brain network modeling, and we assume that for a specific subject the observations $y_j(t)$ of a brain region j are generated by a dynamical system

$$\dot{\boldsymbol{x}}_j(t) = f\left(\boldsymbol{x}_j(t), \boldsymbol{\theta}_j^r, \boldsymbol{\theta}^s, u_{ext}(t), u_j(t)\right) + \boldsymbol{\eta}_j(t)$$

$$y_j(t) = g\left(\boldsymbol{x}_j(t)\right) + \nu_j(t)$$

where $\boldsymbol{x}_j(t) \in \mathbb{R}^{n_s}$ is the state at time t, $\boldsymbol{\theta}_j^r \in \mathbb{R}^{m_r}$ and $\boldsymbol{\theta}^s \in \mathbb{R}^{m_s}$ are the region-specific and subject-specific parameters. The term $u_{ext}(t)$ is the external input, shared by all regions of a single subject, and

$$u_j(t) = \sum_{i=1}^{n} w_{ji} g_c\left(\boldsymbol{x}_j(t)\right)$$

is the network input to region j with $\{w_{ji}\}_{i,j=1}^{n}$ being the structural connectome matrix of the network with n nodes. The functions f, g, and g_c are initially unknown, and $\boldsymbol{\eta}_j(t)$ and $\nu_j(t)$ is the system and observation noise, respectively. From the observed time series of multiple subjects we wish to infer both the evolution function f and observation function g, which are the same for all subjects, as well as region- and subject-specific parameters $\boldsymbol{\theta}^r$ and $\boldsymbol{\theta}^s$ and the time-dependent external input u_{ext}. To do so, we adopt the general framework of amortized variational inference[3] with hierarchical structure in parameters[4]. We consider the states $\boldsymbol{x}_j$, the

parameters $\boldsymbol{\theta}^{r}{}_{j}$ and $\boldsymbol{\theta}^{s}$, and the external input uext the latent variables, and we seek their approximate posterior distribution represented by multivariate Gaussian distributions. In the spirit of amortized variational inference, we do not optimize their parameters directly, but through encoder functions which transform the data to the latent variables (system states, regional and subject parameters, and external input, respectively).

RESULTS AND DISCUSSION

We applied the developed method to human resting-state fMRI data obtained from 100 subjects from Human Connectome Project[5] (HCP), processed with HCP pipeline and further denoised by DiCER method[6], parcellated into 68 cortical regions of Desikan-Killiany parcellation. The analysis using the developed method indicates that three regional parameters can be robustly identified from the resting-state fMRI data, all with distinct and specific roles in the dynamical model. The first parameter influences the presence of low-frequency oscillations. The second parameter modulates the response to the external input: the simulated time series change from being anti-correlated with the external input for negative values to correlated for positive values. Finally, the third parameter changes the response to the input from the rest of the network, from non-correlated for negative values to correlated for positive values. Furthermore, the first of our inferred parameters is strongly linked to the first component of gene expression spatial map. These results show that the present approach opens a novel way to the analysis of resting-state fMRI with possible applications for understanding the brain dynamics during aging or neurodegeneration.

Keywords: large-scale brain network modeling, model discovery, parameter inference, resting-state fMRI

ACKNOWLEDGEMENTS

This work was supported by a public grant overseen by the French National Research Agency (ANR) as part of the second "Investissements d'Avenir" program (reference: ANR-17-RHUS-0004), by the European Union's Horizon 2020 research and innovation programme under grant agreement No. 945539 (SGA3) Human Brain Project, and by the Fenix infrastructure, funded under the EC's H2020 R&I programme through the ICEI project under the grant agreement No. 800858. Data were provided by the Human Connectome Project, WU-Minn Consortium (Principal Investigators: David Van Essen and Kamil Ugurbil; 1U54MH091657) funded by the 16 NIH Institutes and Centers that support the NIH Blueprint for Neuroscience Research; and by the McDonnell Center for Systems Neuroscience at Washington University.

REFERENCES

1. Breakspear M. Dynamic models of large-scale brain activity. *Nat Neurosci*. 2017;20(3):340-352. doi:10.1038/nn.4497

2. Sip V, Petkoski S, Hashemi M, Dickscheid T, Amunts K, Jirsa V. *Parameter Inference on Brain Network Models with Unknown Node Dynamics and Spatial Heterogeneity*.; 2021. doi:10.1101/2021.09.01.458521

3. Kingma DP, Welling M. An Introduction to Variational Autoencoders. *Found Trends® Mach Learn*. 2019;12(4):307-392. doi:10.1561/2200000056

4. Roeder G, Grant PK, Phillips A, Dalchau N, Meeds E. Efficient Amortised Bayesian Inference for Hierarchical and Nonlinear Dynamical Systems. In: *Proceedings of the 36th International Conference on Machine Learning*. Vol 97. PMLR; 2019:4445-4455. Accessed January 8, 2021. http://arxiv.org/abs/1905.12090

5. Van Essen DC, Ugurbil K, Auerbach E, et al. The Human Connectome Project: A data acquisition perspective. *NeuroImage*. 2012;62(4):2222-2231. doi:10.1016/j.neuroimage.2012.02.018

6. Aquino KM, Fulcher BD, Parkes L, Sabaroedin K, Fornito A. Identifying and removing widespread signal deflections from fMRI data: Rethinking the global signal regression problem. *NeuroImage*. 2020;212:116614. doi:10.1016/j.neuroimage.2020.116614

75. Tuning to resonances: Homeostatic plasticity in the Olivocerebellar system

Elias M. Fernandez Santoro[1*], Aleksandra Badura[1], Mario Negrello[1], Chris I. De Zeeuw[12]

[1]Department of Neuroscience, Erasmus MC, Rotterdam, The Netherlands

[2]Netherlands Institute for Neuroscience, Royal Academy of Arts and Sciences, Amsterdam, The Netherlands

*e.fernandezsantoro@erasmusmc.nl

INTRODUCTION/MOTIVATION

The olivocerebellar system plays a central role in motor learning, crucially contributing to the coordination, precision and accurate timing of movements. Despite early conceptions of the system as strictly feed-forward, the olivocerebellar system is composed of multiple feedforward and feedback loops. The main loop consists of two inhibitory projections from Purkinje cells (PCs) to deep cerebellar nuclei (DCN) to Inferior olive (IO) and a powerful excitatory feedback connection, via climbing fibres. We study the dynamics of plasticity of this closed loop when Purkinje cells are subjected to stochastic input with hidden signals.

METHODS

IO cells in our model are biophysically plausible, with both resonant and oscillatory dynamics[1]. Our modelling experiments inquire on the role of induced IO reverberations and electrotonic coupling on Purkinje cell homeostatic synaptic plasticity, which is incorporated through Bienenstock-Cooper-Munro (BCM) type plasticity with both a homeostatic and LTD/LTP component. We further expand by looking at different PCs from different microzones of the Cerebellum (Zebrin +/- zones)[2].

RESULTS AND DISCUSSION

We uncover that specific resonant frequencies from the olivary nucleus become encoded in the Purkinje cell weights, rendering the system able to promote inputs with specific frequency components. We investigate whether the selectivity for particular frequency components is at the control of resonance and IO synchronicity. Against intuition, we observe that in the presence of strong coupling and synchrony firing patterns of IO cells Purkinje cells effectively decorrelate. This indicates that in the presence of strong coupling PCs are separating temporal patterns. We expand on these results by a parameter space analysis and show the relationship between the selected patterns and IO cell oscillatory and coupling characteristics. In line with experimental results, we find

that during BCM induction, Zebrin - PCs have higher propensity of LTD, while positive zone PCs tend to potentiate. This indicates that various types of signals will be encoded differently in the microzones.

Keywords: Olivocerebellum, Homeostatic plasticity, Microzones

REFERENCES

[1] Jornt R De Gruijl, Paolo Bazzigaluppi, Marcel TG de Jeu, and Chris I De Zeeuw. Climbing fiber burst size and olivary sub-threshold oscillations in a network setting. PLoS computational biology, 8 (12):e1002814, 2012.

[2] De Zeeuw CI. Bidirectional learning in upbound and downbound microzones of the cerebellum. Nat Rev Neurosci. 2021 Feb;22(2):92-110. doi: 10.1038/s41583-020-00392-x. Epub 2020 Nov 17. PMID: 33203932.

76. A generative model for continual learning based on self-organizing maps

Lorenzo Fruzzetti[1,2*], Francesco Iori[1,2], Alessio Fasano[1,2], Egidio Falotico[1,2]

[1]The BioRobotics Insitute, Scuola Superiore Sant'Anna, Pisa, Italy,

[2]Department of Excellence in Robotics and AI, Scuola Superiore Sant'Anna, Pisa, Italy

*Lorenzo.fruzzetti@santannapisa.it

INTRODUCTION

Artificial Neural Networks (ANNs) trained with a shifting sample space (presenting some classes early in training and others later) can forget previously learned information (known as catastrophic forgetting), resulting in the loss of the earlier learned classes[1]. To combat this, one solution is to store all training samples and retrain the network on both stored and new samples, but this approach is not efficient due to increasing memory requirements and longer training time with each iteration. A more efficient alternative is to use memory replay algorithms [2], which store some training samples or generate old samples using a generative model[3].

While neural networks are well-suited for generating data[4], generating new training samples from a previous training distribution can be challenging as it requires training a new generative model for each class, which increases both memory and training time. Relying on a single neural network generative model only moves the problem of catastrophic forgetting to the generative model.

Our proposed solution involves storing a representation of data and a method for generating them. Our system, based on self-organizing maps (SOM)[5], has several advantages, including the ability to generate new samples from stored knowledge, a fixed memory requirement, and the prevention of the network from overwriting important previous memories. METHODS

The generative model has two parts: a self-organizing map (SOM) that holds the data representation and an importance map that holds the significance of each unit in the SOM. The SOM is updated after each training cycle and to keep previously important units from being overwritten, the learning rate for each unit in the SOM is proportional to its importance (the more important a unit, the less it will be updated during training).

The SOM update rule is the following:

$$lr_i = e^{\left(-\frac{D_{iQ}}{\alpha^2}\right)} * (1 - lmp_i) \quad (1)$$

The learning rate of each unit in the SOM lr_i is determined by the unit's distance D_{ic} from the closest unit c to the input, and its importance lmp_i.

The importance of each unit in the SOM increases if it is active during a cycle and the importance map is updated between cycles through an importance function. This function determines the most significant units in each cycle and controls their future changes through the following equation.

$$\Delta \mathrm{Imp_i} = \frac{1}{n} \sum_{a=1}^{n} e^{(-D_{ia})} \quad (2)$$

$$lmp_i = lmp_i + \Delta \mathrm{Imp_i} \quad (3)$$

Where $\Delta \mathrm{Imp_i}$ is the amount of update of unit i, $-D_{ia}$ is the Euclidean distance between the unit i and the unit a, which is one of the n-th (in our case n = 3) most active unit in this cycle, the activity of the i unit and unit a. All units with an importance greater than 1 are reduced to an importance of 1.

Generating new samples involves selecting units from the SOM, where the likelihood of choosing a specific unit is proportional to its importance. This allows the network to produce the most significant memories acquired during the entire learning process.

In this project, we trained the SOM on a portion of the MNIST dataset. The training process was divided into two stages. During the first stage, we fed the SOM only the inputs belonging to the classes associated with numbers 0 and 1. In the second stage, we provided the SOM with inputs associated with classes 1 and 2.

RESULTS AND DISCUSSION

In the study, two variations of the SOM were compared. The first SOM was trained using the previously described algorithm while the second SOM did not consider the importance of each unit as the lmp_i term was removed from the equation 1. The training process was done on the MNIST dataset and was divided into two phases. During the first phase, only classes 0 and 1 from the MNIST dataset were used, while in the second phase, only classes 1 and 2 were included.

The results are illustrated in the following figure: Subfigures a and c were trained in the first cycle, while subfigures b and d were trained in the second cycle. Although there was no significant difference between a and c, the samples obtained after the second cycle showed significant differences. The SOM in b lost the memory of class 0, while in d a representation is maintained.

Our results indicate that incorporating an importance map into SOM can help in generating samples from classes that are no longer available and may reduce the impact of catastrophic forgetting using memory replays algorithms without increasing the memory requirement.

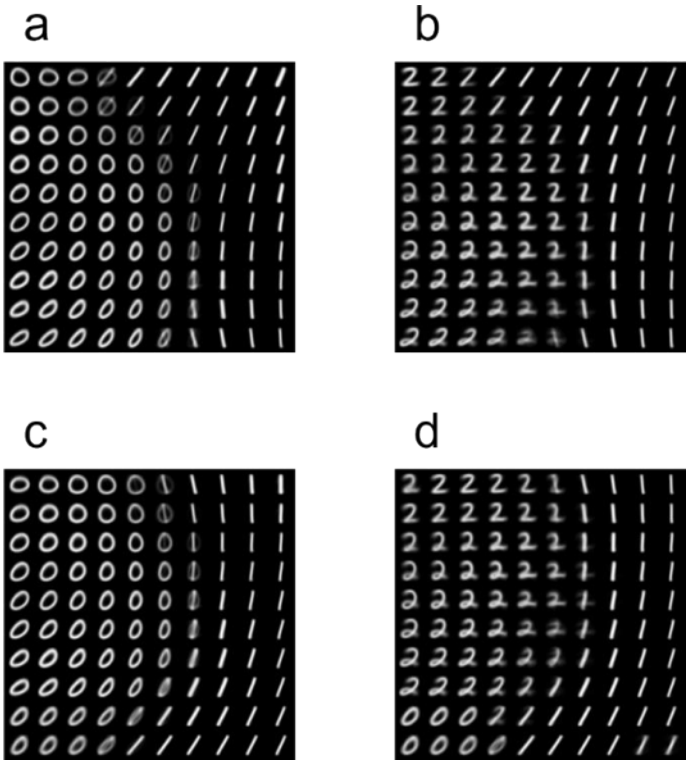

Figure 1: results of training of two SOM. ***a)*** *trained on 0 and 1, no importance map.* ***b)*** *trained on 1 and 2, no importance map.* ***c)*** *trained on 0 and 1, importance map.* ***d)*** *trained on 1 and 2, importance map*

Keywords: Artificial Neural Networks, catastrophic forgetting, memory replay algorithms, self-organizing maps, data representation, data generation

References

1. Parisi GI, Kemker R, Part JL, Kanan C, Wermter S. Continual Lifelong Learning with Neural Networks: A Review. *Neural Netw*. 2019;113:54-71. doi:10.1016/j.neunet.2019.01.012.

2. Wang L, Zhang X, Yang K, et al. Memory Replay with Data Compression for Continual Learning. 2022. Accessed February 9, 2023. https://openreview.net/forum?id=a7H7OucbWaU

3. van de Ven GM, Siegelmann HT, Tolias AS. Brain-inspired replay for continual learning with artificial neural networks. *Nat Commun*. 2020;11(1):4069. doi:10.1038/s41467-020-17866-2

4. Bond-Taylor S, Leach A, Long Y, Willcocks CG. Deep Generative Modelling: A Comparative Review of VAEs, GANs, Normalizing Flows, Energy-Based and Autoregressive Models. *IEEE Trans Pattern Anal Mach Intell*. 2022;44(11):7327- 7347. doi:10.1109/TPAMI.2021.3116668

5. Miljković D. Brief review of self-organizing maps. In: *2017 40th International Convention on Information and Communication Technology, Electronics and Microelectronics (MIPRO)*. ; 2017:1061-1066. doi:10.23919/MIPRO.2017.7973581

77. Fitting finite-size population models to networks of leaky integrate-and-fire neurons with

Jan-Eirik W. Skaar[1]*, Tilo Schwalger[2], Hans E. Plesser[1,3], Gaute T. Einevoll[1,4], Kristin Tøndel[1]

[1] Faculty of Science and Technology, Norwegian University of Life Sciences, Ås, Norway

[2] Technische Universität/Bernstein Zentrum (BCCN) Berlin, Berlin, Germany [3]Institute of Neuroscience and Medicine (INM-6) and Institute for Advanced Simulation (IAS-6) and JARA- Institut Brain Structure-Function

[4] Department of Physics, University of Oslo, Oslo, Norway

*jan-eirik.welle.skaar@nmbu.no

INTRODUCTION/MOTIVATION

Simulating large networks of neurons is computationally demanding. When modelling large networks, one may be mostly interested in one or a specific populations of neurons. Other populations of lesser interest may be modelled at a coarser scale. Signals such as local field potentials (LFPs) can readily be closely approximated by the aggregated activity of populations of neurons without the detailed spiking of individual neurons (Hagen et al. 2022).

Recently developed mesoscopic population models have been shown to accurately be able to capture the population averaged spiking activities of networks of generalized leaky integrate-and-fire (LIF) neurons with escape noise (Schwalger et al. 2017), including fluctuations due to finite-size effects. Yielding an explicit probability distribution over population averaged spiking activity, such mesoscopic models are statistically tractable, and can be used to infer parameter values consistent with observed population spiking activity (René et al. 2020).

In this ongoing work, we develop a mesoscopic population model that can include input noise in the form of a Poisson process, based on previous work by (Chizov & Graham, 2008), as well as taking into account the noise from random connectivity within populations. We aim to implement and systematically compare these low- dimensional population models to their high-dimensional counterparts in larger networks comprising multiple populations.

METHODS

Combining existing work by (Schwalger et al 2017) and (Chizov & Graham, 2008), we formulate a mesoscopic population model based on an underlying LIF neuron model with exponentially correlated synaspses. An escape rate is used such that the spiking statistics matches those from populations receiving random Poisson input. An additional noise term, based on the connection statistics, is introduced to account for the noise resulting from the random network connectivity, The population model is then compared to full simulations of networks of LIF neurons using the NEST simulator (Spreizer et al. 2022). The population model can itself be integrated into the

NEST simulator using NESTML (Linssen et al. 2022). Since the escape rate yields an explicit probability distribution over the population activities, the gradient of the log likelihood of an observed time series of population activities can be found using automatic differentiation libraries such as JAX (Bradbury et al. 2018), and can be used to optimize model parameters.

RESULTS AND DISCUSSION

Our preliminary results are promising, showing that the theoretical approximations can accurately capture the noise present in the networks of LIF neurons.

Keywords: computational neuroscience, population model, inference

ACKNOWLEDGEMENTS

This work has received funding from the European Union's Horizon 2020 Framework Programme for Research and Innovation under Specific Grant Agreement 945539 HBP SGA3 (HEP, GTE).

REFERENCES

René et al. Neural Comput 2020; 32 (8): 1448–1498. https://doi.org/10.1162/neco_a_01292
Schwalger et al. PLoS Comput Biol 2017; 13(4): e1005507.https://doi.org/10.1371/journal.pcbi.1005507 Hagen et al. PLoS Comput Biol 2022; 18(8): e1010353. https://doi.org/10.1371/journal.pcbi.1010353 Chizhov & Graham Phys Rev E Stat Nonlin Soft Matter Phys. 2008 Jan;77(1 Pt 1):011910. doi: 10.1103/PhysRevE.77.011910.
Spreizer et al. (2022). NEST 3.3 (3.3). Zenodo. https://doi.org/10.5281/zenodo.6368024 Linssen et al. (2022). NESTML 5.1.0. Zenodo. doi:10.5281/zenodo.7071624.
Bradbury et al. (2018). http://github.com/google/jax

78. Decreased brain responsiveness to multimodal sensory stimulations during absence seizures in awake rats

Federico TESLER[1], Petteri STENROOS[2,5], Isabelle GUILLEMAIN[2], Olivier MONTIGON[2,3], Nora COLLOMB[3], Vasile STUPAR[2,3], Véronique COIZET[2], Olivier DAVID[2,4], Emmanuel L. BARBIER[2,3], Alain DESTEXHE[1]

[1]- Paris-Saclay University, CNRS, Paris-Saclay Institute of Neuroscience (NeuroPSI), 91400 Saclay, France
[2]- Univ. Grenoble Alpes, Inserm, U1216, Grenoble Institut Neurosciences, Grenoble, France
[3]- Univ. Grenoble Alpes, Inserm, US17, CNRS, UAR 3552, CHU Grenoble Alpes, IRMaGe, Grenoble, France
[4]- Univ. Aix Marseille, Inserm, INS, Institut de Neurosciences des Systèmes, 13000 Marseille, France
[5]- A.I.Virtanen Institute for Molecular Sciences, University of Eastern Finland, P.O. Box 1627, FI,-70211 Kuopio, Finland

INTRODUCTION/MOTIVATION

Absence seizures are a type of generalized epileptic seizures, characterized by a brief loss of consciousness that can last from a few seconds up to tens of seconds. Electrophysiological measurements during ictal periods exhibit a characteristic rhythmic oscillation known as spike-and-wave discharges (SWD), which occur at a frequency of around 3Hz in humans [1]. A recognized animal model for this type of epilepsy is the GAERS rat, which exhibits absence seizures with SWD patterns in a frequency between 5 to 10 Hz and which shows an equivalent response to pharmacological treatments used in humans [2]. The mechanisms behind this type of epilepsy are still under discussion, and in particular the lack of response to external stimulation is still not well understood. One possibility is that the lack of response occurs due to a restricted propagation of information in early stages of the sensory pathways, while another possibility is that the lack of response occurs due to alterations at later stages of motor control and decision making areas [3]. In this work, we evaluate the stimulus response during absence epilepsy via experiments and simulations

METHODS

For simulations we used a whole-brain model built in the EBRAINS platform. The model was built via the use of mean-field models of Adaptive-Exponential LIF (AdEx) neurons in the TVB platform [4, 5], where each node (area/compartment) in a brain connectome is represented by a single mean-field. Each node represents a population of 10000 neurons connected over a random directed network where the probability of connection between two neurons is p = 5%. We considered excitatory and inhibitory neurons, with 20% inhibitory neurons and 80% excitatory (Figure 2.A). To perform the whole brain simulations we made use of the BAMS rat connectome [6], a project of aggregated connectome data which currently contains over 50000 connectivity reports from the rat brain. Experiments were performed in GAERS rats, with simultaneous EEG and functional magnetic resonance imaging (fMRI) measurements at 9.4T. EEG signals were used to identify ictal and inter-ictal periods (Figure 1.A), while fMRI was used to map neuronal derived hemodynamic activity during visual and whisker stimulation performed in ictal and in inter-ictal states.

RESULTS AND DISCUSSION

Statistical activation maps were created from fMRI measurements in response to stimulus during ictal and inter-ictal periods and compared between the two states (Figure 1.B). A general reduced hemodynamic response and limited propagation of activity was observed during ictal periods for both type of stimulation. For visual stimulation, activation changes were seen in the visual, somatosensory, and frontal cortices. For whisker stimulation, activation changes were seen in the somatosensory, auditory and frontal cortices. The number of activated voxels due to stimulation was also substantially lower during ictal periods (136% and 179% more during inter-ictal period for visual and whisker stimulation respectively).

With the use of simulations we showed first that within this whole-brain model normal and ictal neuronal states can be reproduced, exhibiting asynchronous irregular activity (AI) and SWD-like dynamics respectively (Figure 2.B). Then we simulated the effect of an external stimulus during each neuronal state and we observed a restricted propagation of the stimulus during the ictal state in comparison with the AI state, in agreement with experiments. This is explained due to the dominance of the seizure dynamics during ictal periods even under stimulation, added to the periods of low excitability exhibited during the 'wave' phase of the oscillatory dynamics that reduce the responsiveness of the system.

The results obtained in this study suggest that the lack of response may be in part originated due to a limited propagation of information during seizures starting at early stages of the sensory pathways. A better understanding of the stimulus response during ictal states may help to disentangle the processing of information during seizures, which can be of relevance for medical treatments of epilepsy such as a deep brain stimulation.

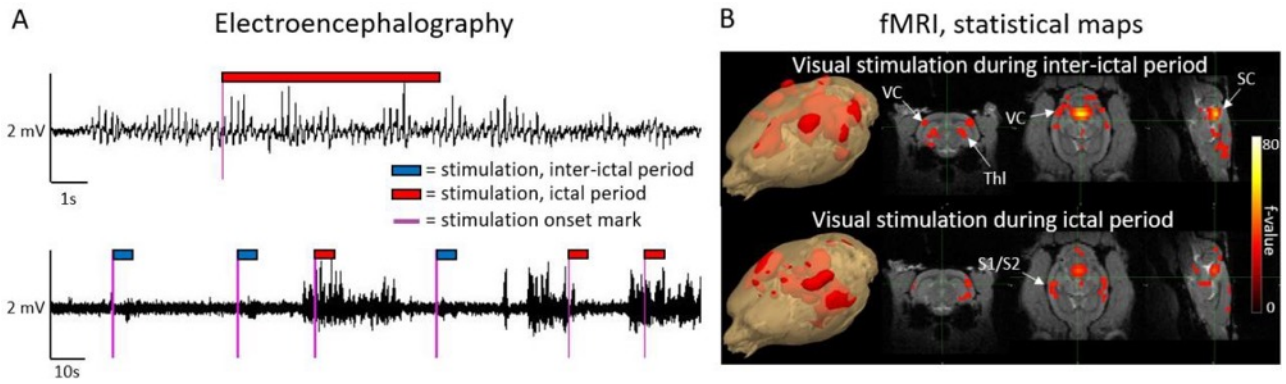

Figure 1: A) EEG recording trace at 2 different temporal scales during ictal and interictal states and with stimulation onset marks B) fMRI statistical F-maps of stimulation during interictal and ictal states. S1/S2 = primary and secondary somatosensory cortex, SC = superior colliculus, Thl = thalamus, VC = visual cortex.

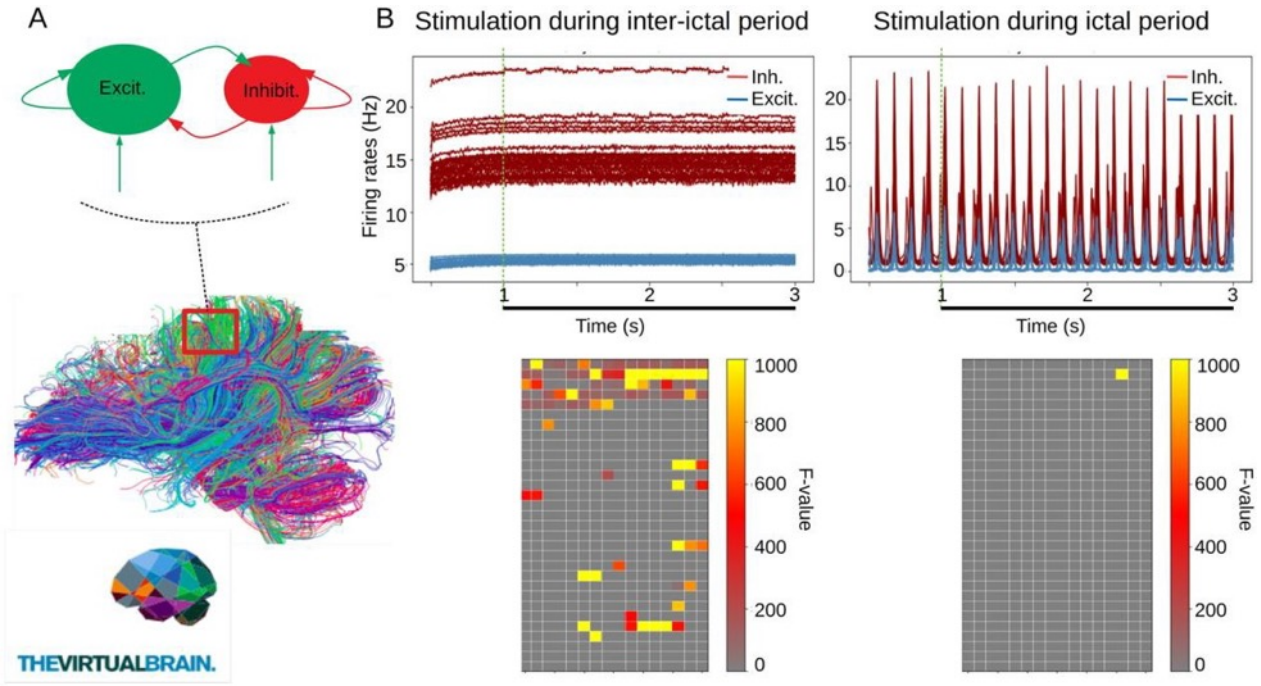

Figure 2: A) Diagram of the model. Mean-field models simulations where performed using the TVB platform in EBRAINS (diagram adapted from Ref.[5]). B) Top: Time-series of neuronal activity under stimulation during inter-ictal (asynchronous irregular) and ictal (spike-and-wave) periods. The vertical dashed line and horizontal black line indicate the beginning and duration of the stimulation. Bottom: statistical maps of neuronal activity during stimulation for each state.

Keywords: functional magnetic resonance imaging, GAERS, absence seizure, brain responsiveness, awake rat, whole-brain simulations, mean-field models

ACKNOWLEDGEMENTS

Research supported by the CNRS and the European Union (Human Brain Project H2020-785907, H2020-945539).

REFERENCES

1 - Loiseau, P., Duché, B., and Pédespan, J. -M. (1995). “Absence Epilepsies”, Epilepsia, 36(12). 1182–1186. https://doi.org/10.1111/j.1528-1157.1995.tb01060.x

2 - Depaulis, A., David, O., and Charpier, S. (2016). “The genetic absence epilepsy rat from Strasbourg as a model to decipher the neuronal and network mechanisms of generalized idiopathic epilepsies”, Journal of Neuroscience Methods, 260, 159–174. https://doi.org/10.1016/J.JNEUMETH.2015.05.022

3 - Blumenfeld, Hal. (2012). “Impaired Consciousness in Epilepsy”, The Lancet Neurology 11(9): 814–26.

4 - M. Di Volo, A. Romagnoni, C. Capone and A. Destexhe (2019), “Biologically realistic mean-field models of conductance-based networks of spiking neurons with adaptation”, Neural Computation, 31, 653–680.

5 - Goldman JS, Kusch L, Aquilue D, Yalçınkaya BH, Depannemaecker D, Ancourt K, Nghiem T- AE, Jirsa V and Destexhe A (2023) A comprehensive neural simulation of slow-wave sleep and highly responsive wakefulness dynamics. Front. Comput. Neurosci. 16:1058957. doi: 10.3389/fncom.2022.1058957

6 - Bota, M., Dong, H. W., and Swanson, L. W. (2012). Combining collation and annotation efforts toward completion of the rat and mouse connectomes in BAMS. Frontiers in neuroinformatics, 6, 2.

79. A fluid hierarchy in multisensory integration properties of large-scale brain networks

Ronaldo V. Nunes[1,2], Marcelo B. Reyes[1], Raphael Y. De Camargo[1], Jorge F. Mejias[2*]

[1]Cognitive and Systems Neuroscience Group, University of Amsterdam, Amsterdam, the Netherlands
[2]Center for Mathematics, Computing and Cognition, Universidade Federal do ABC, Sao Paulo, Brazil
*j.f.mejias@uva.nl

INTRODUCTION/MOTIVATION

A fundamental ingredient for perception is the integration of information from different sensory modalities, also known as multisensory integration (MSI)[1,2]. It is not clear how different brain areas contribute to this process, as identifying MSI areas remains a challenging task due to experimental limitations. Computational models have traditionally focused only on a few areas due to the lack of reliable connectivity datasets, so the implications of brain-wide communication for MSI are still unknown. We present here a theoretical and computational study of the large-scale mechanisms underlying MSI in the mouse brain, by constraining our model with recently acquired anatomical brain connectivity datasets and analyzing the resulting brain dynamics during simulated multisensory perception tasks.

METHODS

We considered connectivity data from the mouse [3,4](Fig. 1A) to build the large-scale structure of our mouse brain model, and combined it with a firing rate approach for the dynamics of each cortical area. Using the resulting large-scale cortical network (*full model*), we simulated a visuotactile stimulation protocol in which a weak, brief somatosensory input and a stronger and longer visual input were presented to the barrel fields of the primary somatosensory cortex (SSp-bfd) and the primary visual cortex (V1), respectively (Fig. 1B). To better understand the origin of the dynamics of this full model, we also built a *simplified model* constituted by N fully connected nodes, and included heterogeneity in their internal properties (such as their activation thresholds).

RESULTS AND DISCUSSION

When both sensory stimuli coincided in time, the full model showed an enhanced firing rate response. Such enhanced response was markedly strong and nonlinear for specific areas, and allowed us to identify those as candidate MSI areas – for example, secondary visual area RL (Fig. 1B), which plays an important role in visuotactile integration [5]. We subsequently used this strong response to weak multisensory stimulation to characterize the crossmodal response of a given area in the model. By computing this quantity for all areas, our simulations revealed the existence of a hierarchy of crossmodal responses, with areas at the top of the hierarchy being the best multisensory integrators. Unexpectedly, our model predicted that the hierarchical rank of any given area is

highly fluid, and depends on the level of visual input (Fig. 1C). The relevance of any area for MSI therefore depends on input strength –and by extension, on any context-dependent signals able to alter the crossmodal responses.

By simulating the simplified model (Fig. 1D) and developing a mean-field approximation, we found that the structural heterogeneity of the network [4,5] was a plausible origin of the hierarchical dynamics. Node heterogeneity induced 'crossing points' between the activation functions of the different nodes (Fig. 1D), i.e. two nodes can switch places if their activation curves are different. The crossing points were more frequent in the vicinity of the onset of activity (Fig. 1D inset), when nonlinear firing properties are more salient. The results were also replicated in other brain models [7,8,9] and further analyzed using refined time-series analysis [10]. Our work provides a compelling explanation as of why it is not possible to identify a unique MSI area even for a well-defined multisensory task, and suggests that MSI circuits are highly distributed and context-dependent.

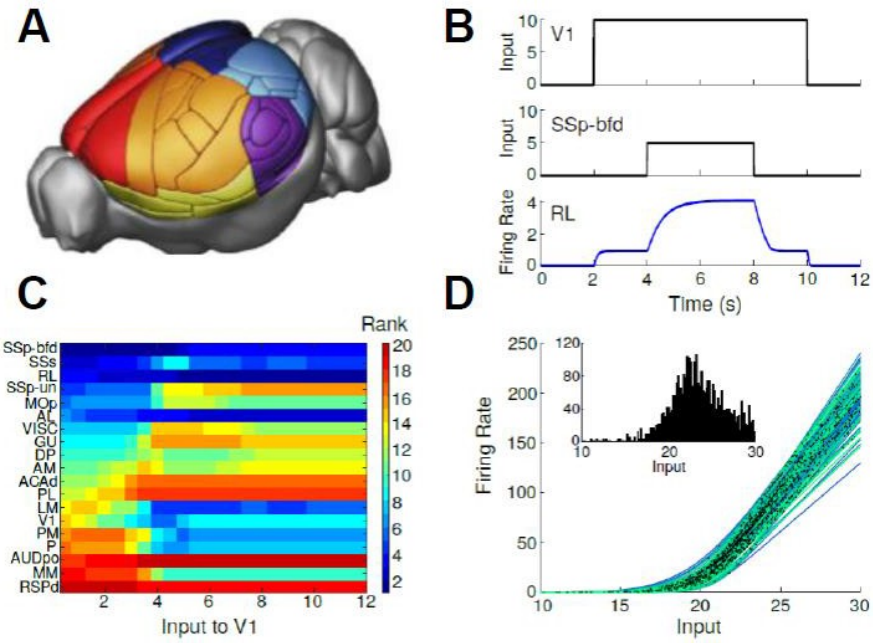

Figure 1: (A) Brain map of the mouse brain used to constrain our large-scale model, from [5]. (B) The network receives baseline visual input, and after a shorter somatosensory input, the response of different areas (here, area RL) is analyzed. (C) Ranks of areas as a function of their crossmodal response, with rank 1 (20) linked to strongest (weakest) response. (D) Input- output functions for the simplified network model reveal that hierarchical switches arise from crossing points (black dots) between curves on the firing onset (inset).

Keywords: computational neuroscience, large-scale brain model, multisensory integration, brain dynamics, mouse, perception, functional hierarchies, mean-field approaches.

ACKNOWLEDGEMENTS

We thank colleagues at the Cognitive and Systems Neuroscience Group for useful discussions.

REFERENCES

[1] Yau JM, DeAngelis GC, Angelaki DE. Dissecting neural circuits for multisensory integration and crossmodal processing. Phil. Trans. Royal Soc. B: Biol. Sci. 370, 20140203, 2015.

[2] Chandrasekaran C. Computational principles and models of multisensory integration. Curr. Op. Neurobiol. 43, 25-34, 2017.

[3] Oh SW et al. A mesoscale connectome of the mouse brain. Nature 508, 207-214, 2014.

[4] Gamanut R et al. The mouse cortical connectome, characterized by an ultra-dense cortical graph, maintains specificity by distinct connectivity profiles. Neuron 97, 698-715, 2018.

[5] Olcese U, Iurilli G, Medini P. Cellular and synaptic architecture of multisensory integration in the mouse neocortex. Neuron 79, 579-593, 2013.

[6] Mejias JF, Longtin A. Differential effects of excitatory and inhibitory heterogeneity on the gain and asynchronous state of sparse cortical networks. Front. Comput. Neurosci. 8, 107, 2014.

[7] Mejias JF, Murray JD, Kennedy H, Wang XJ. Feedforward and feedback frequency-dependent interactions in a large-scale laminar network of the primate cortex. Sci. Adv. 2:e1601335, 2016.

[8] Mejias JF and Wang XJ. Mechanisms of distributed working memory in a large-scale network of macaque neocortex. eLife 11, e72136, 2022.

[9] Feng M, Bandyopadhyay A, Mejias JF. Emergence of distributed working memory in a human brain network model. BioRxiv, 2023.01. 26.525779 .

[10] Nunes RV, Reyes MB, De Camargo RY. Evaluation of connectivity estimates using spiking neuronal network models. Biol. Cybern. 113, 309-320, 2019

80. SpiNNaker 2 Enables Multi-Scale Spiking Neural Network Simulation

Yexin Yan[1*], Bernhard Vogginger[1], Johannes Partzsch[1], Steve Furber[2], Christian Mayr[1]

[1]Chair of Highly Parallel VLSI Systems and Neuro-Microelectronics, TU Dresden, Dresden, Germany

[2]Advanced Processor Technologies Research Group, University of Manchester

*yexin.yan@tu-dresden.de

INTRODUCTION/MOTIVATION

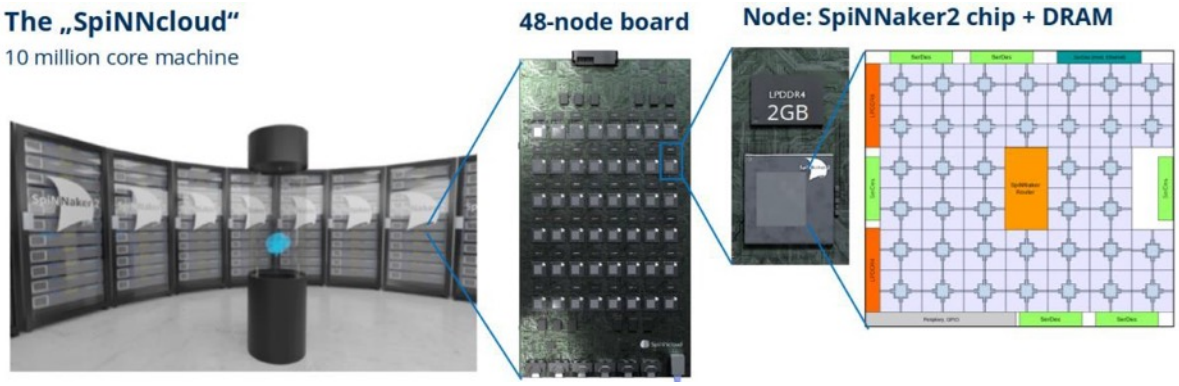

Fig.1 The final SpiNNaker 2 system (SpiNNCloud) is a real-time neuromorphic supercomputer consisting of thousands of SpiNNaker 2 chips.

SpiNNaker 2 [1] is a digital neuromorphic hardware system designed in the Human Brain Project by TU Dresden and the University of Manchester. The final SpiNNaker 2 system contains thousands of interconnected SpiNNaker 2 chips. Each SpiNNaker 2 chip contains 152 Processing Elements (PEs). Each PE contains an ARM core and several hardware accelerators for neural algorithms, including an exponential accelerator, a true random number generator and a MAC array. In addition, each PE can adjust its supply voltage and clock frequency dynamically through Dynamic Voltage and Frequency Scaling (DVFS). These new features enable efficient simulation of spiking neural networks (SNNs) on different abstraction levels, including synaptic dynamics and neural networks consisting of point neurons. Since the simulation runs on the ARM core, SpiNNaker 2 could also be used for the simulation of mean field approximations of neuron populations. In this poster we present efficient simulation of synaptic dynamics and spiking neural networks.

METHODS

Reward-based synaptic sampling [2] is a structural plasticity model which describes the stochastic rewiring of synapses as a random walk guided by reward signals. Computationally, the synaptic weight w_i depends exponentially on the synaptic parameter θ_i, and θ_0 is an offset constant:

$$w_i = \exp(\theta_i - \theta_0)$$

The change of the synaptic parameter is composed of the effects of the prior distribution, the gradient of the value function and the random walk:

$$d\theta_i(t) = \beta \left(\frac{1}{\sigma^2} (\mu - \theta_i(t)) + g_i(t) \right) dt + \sqrt{2\beta T}\, d\mathcal{W}_i(t)$$

where β is a scaling factor, σ and μ are the standard deviation and mean of the prior distribution, g_i is the gradient of the value function, T is the temperature and $d\mathcal{W}_i$ is a random number.

For a conventional CPU without accelerators, the computation of the exponential function and the random number generation dominates the computation time of this synapse model. But with the exponential accelerator and the random number generator in SpiNNaker 2, the computation time and energy consumption can be drastically reduced [3].

In addition to efficient simulation of synaptic plasticity models, with DVFS, SNNs consisting of point neurons can also be efficiently simulated. During an SNN simulation, the number of spikes generated by the network fluctuates over time, which leads to fluctuations of compute workload for the hardware. With DVFS, each PE can dynamically adjust its supply voltage and clock frequency, so that higher power consumption only occurs when there is a higher workload. This is illustrated in a synfire chain simulation with 4 PEs below [4].

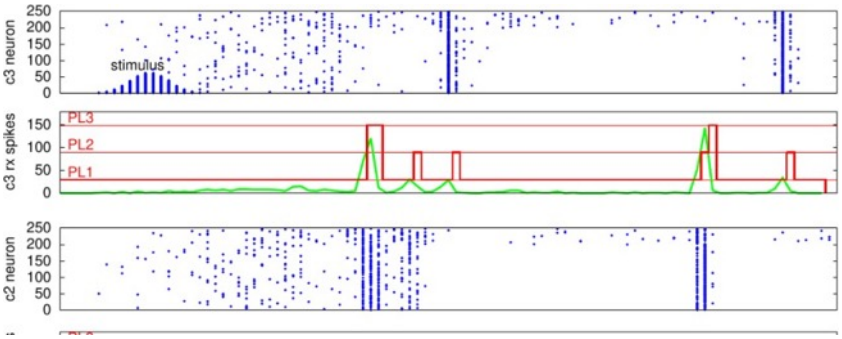

Fig. 2 A synfire chain network is simulated with 4 PEs on a SpiNNaker 2 chip. The blue dots are the spikes, the red lines indicate the Performance Level (PL) of a PE, i.e. the voltage and frequency configuration, and the green lines indicate the number of spikes received by a PE, i.e. the workload. The PL is only increased when more spikes are received, thus consuming more power only when it's necessary.

RESULTS AND DISCUSSION

For the simulation of synaptic sampling, with a conventional CPU, where the exponential function and random number generation are done only with software, one plasticity update takes 236 clock cycles, whereas with the exponential accelerator and random number generator, the simulation with SpiNNaker 2 takes only 110 clock cycles, achieving a 2X speedup [3].

For the simulation of synfire chain, where the spike activities fluctuate over time, if no DVFS is available, the PE has to always run with the highest clock frequency and supply voltage. But with DVFS, 60.4% power reduction is achieved compared to without DVFS [4].

In addition, since the simulation in SpiNNaker 2 is done with software running on the ARM core, mean field simulation is also possible, and simulation of different levels can be combined in the same simulation, enabling multi-scale simulation of SNNs.

Keywords: SpiNNaker 2, Neuromorphic Computing, Multi-Scale Neural Network Simulation, Synaptic Plasticity, Spiking Neural Network, Hardware Accelerator, True Random Number Generator, Exponential Function Accelerator, Dynamic Voltage and Frequency Scaling

REFERENCES

[1] Christian Mayr, Sebastian Hoeppner, and Steve Furber. SpiNNaker 2: A 10 Million Core Processor System for Brain Simulation and Machine Learning. *arXiv e-prints*, arXiv:1911.02385, November 2019.

[2] David Kappel, Robert Legenstein, Stefan Habenschuss, Michael Hsieh, and Wolfgang Maass. A Dynamic Connectome Supports the Emergence of Stable Computational Function of Neural Circuits through Reward-Based Learning. e*Neuro*, 5(2), 2018.

[3] Yexin Yan, David Kappel, Felix Neumärker, Johannes Partzsch, Bernhard Vogginger, Sebastian Höppner, Steve Furber, Wolfgang Maass, Robert Legenstein, and Christian Mayr. Efficient Reward-Based Structural Plasticity on a SpiNNaker 2 Prototype. *IEEE Transactions on Biomedical Circuits and Systems*, 13(3):579–591, 2019.

[4] S. Höppner, B. Vogginger, Y. Yan, A. Dixius, S. Scholze, J. Partzsch, F. Neumärker, S. Hartmann, S. Schiefer, G. Ellguth, L. Cederstroem, L. A. Plana, J. Garside, S. Furber, and C. Mayr. Dynamic Power Management for Neuromorphic Many-Core Systems. *IEEE Transactions on Circuits and Systems I: Regular Papers*, 66(8):2973–2986, 2019.

81. The human multiscale brain connectome

Viktor Jirsa[*1], Alain Destexhe[2], Egidio D'Angelo[3], Svenja Caspers[4], Spase Petkoski[1], and all members of WP1 in HBP-SGA3

[1]Aix Marseille Univ, INSERM, INS, Inst Neurosci Syst, UMR 1006, Marseille, France

[2] CNRS: Paris-Saclay Institute of Neuroscience (NeuroPSI), Paris-Saclay University, 91400 Saclay, France

[3] University of Pavia, Italy

[4] Universitätsklinikum Düsseldorf, Heinrich-Heine-Universität Düsseldorf, Forschungszentrum Jülich, Germany

*e-mail-address of corresponding author(s) viktor.jirsa@univ-amu.fr

INTRODUCTION/MOTIVATION

Linking neuroscience data with brain models has reached a level of sophistication, which is too complex to handle for individual laboratories in an era of big data, high performance computation and interdisciplinary research [1]. Advances in structural and functional imaging provide huge amounts of data and allow investigating networks of unprecedented degrees of detail and complexity. Large amounts of data alone, even if well analysed, do not necessarily advance our understanding of how the brain works. Adding more data or more modalities of the same event will not alleviate this concern. Virtually indistinguishable network activity can arise from various biophysical mechanisms and genetically identical organisms can show consistently different neuronal activity associated with the same behaviour [2]. Such one-to-many and many-to-one property is well known in complex systems and is the cause of intra- and inter-subject variability, posing challenges for mechanistic identifiability. Causal inference integrating data, models and methods proposes a solution to this basic obstacle to progress in neuroscience.

METHODS

To ensure interoperability of heterogeneous multiscale data, models, and analysis workflows, we have established a brain reference framework organizing data and computational models in the same informatics environment with standardised spatial referencing and verified links between data and model parameters, validated against empirical brain imaging data. We organised, mapped, co-registered structural (molecular, cellular, synaptic and connectome data) and functional brain data (Cortico-Cortical Evoked Potentials, fMRI, simultaneous fMRI/EEG, intracranial and simultaneous scalp-EEG). We mapped regional data features upon detailed mathematical models across scales (cellular to full brain). Missing data and mappings were addressed by gap maps, interpolations, and ML techniques. We integrated multiscale data-driven network models (microcircuit models for cortex, cerebellum, hippocampus, basal ganglia), linking between scales using various simulation engines (Neuron, Arbor, NEST, TVB), and developed specific component workflows for microcircuit reconstruction (BSB, Snudda) [3], strategies to generate mesoscale mean-field models of brain circuits [4] and co-simulation technologies for simultaneous operation on mixed scales [5]. Validation workflows using various types of Bayesian inferences (MCMC, HMC, DCM, SBI) have been developed and integrated in EBRAINS [6, 7]. Figure 1 illustrates the workflows integrated in EBRAINS and showcases in cohort studies of aging populations [8] and epilepsy demonstrate their use.

RESULTS AND DISCUSSION

The systematic integration of multiscale heterogeneous data [9] and models into a common spatial and technological reference framework in EBRAINS enables causal reasoning, promotes the use of digital twin technology and supports end-to-end modelling of the human brain with a promise for pharmacological, clinical and technological translation (e.g. early detection of trajectories of brain disease manifesting at different levels of brain organisation, personalised tracking of brain health, better stratification of patients). Through EBRAINS, the brain reference framework and its validated human brain models will be distributed for immediate usage in everyday basic research and clinical application.

Keywords: multiscale data, brain reference system, brain network model, digital twin, model Inversion.

ACKNOWLEDGEMENTS

This research was supported by the European Union's Horizon 2020 research and innovation program under grant agreement No. 945539 (SGA3) Human Brain Project.

REFERENCES

[1] Amunts, K., Rowald, A., Petkoski, S., Sanchez-Vives, M. V., Axer, M., De Bonis, G., ... & Salles, A. (2022). *The coming decade of digital brain research-A vision for neuroscience at the intersection of technology and computing* (No. FZJ-2022-01628). Computational and Systems Neuroscience

[2] D'Angelo, E., & Jirsa, V. (2022). The quest for multiscale brain modeling. *Trends in Neurosciences*.

[3] De Schepper, R., Geminiani, A., Masoli, S. *et al.* Model simulations unveil the structure-function-dynamics relationship of the cerebellar cortical microcircuit. *Commun Biol* 5, 1240 (2022).

[4] Tesler, F., Tort-Colet, N., Depannemaecker, D., Carlu, M., & Destexhe, A. (2022). Mean-field based framework for forward modeling of LFP and MEG signals. *Frontiers in Computational Neuroscience*

[5] Kusch, L., Diaz, S., Klijn, W., Sontheimer, K., Bernard, C., Morrison, A., & Jirsa, V. (2022). Multiscale cosimulation design template for neuroscience applications. *bioRxiv*, 2022-07

[6] Hashemi, M., Vattikonda, A. N., Sip, V., Guye, M., Bartolomei, F., Woodman, M. M., & Jirsa, V. K. (2020). The Bayesian Virtual Epileptic Patient: A probabilistic framework designed to infer the spatial map of epileptogenicity in a personalized large-scale brain model of epilepsy spread. *NeuroImage*, *217*, 116839

[7] Lavanga, M., Stumme, J., Yalcinkaya, B. H., Fousek, J., Jockwitz, C., Sheheitli, H., ... & Jirsa, V. (2022). The virtual aging brain: a model-driven explanation for cognitive decline in older subjects. *bioRxiv*, 2022-02

[8] Caspers, S., & Schreiber, J. (2020). 1000BRAINS study, connectivity data [Data set]. EBRAINS. DOI: 10.25493/61QA-KP8

[9] Axer, M., & Amunts, K. (2022). Scale matters: The nested human connectome. *Science*, *378*(6619), 500-504

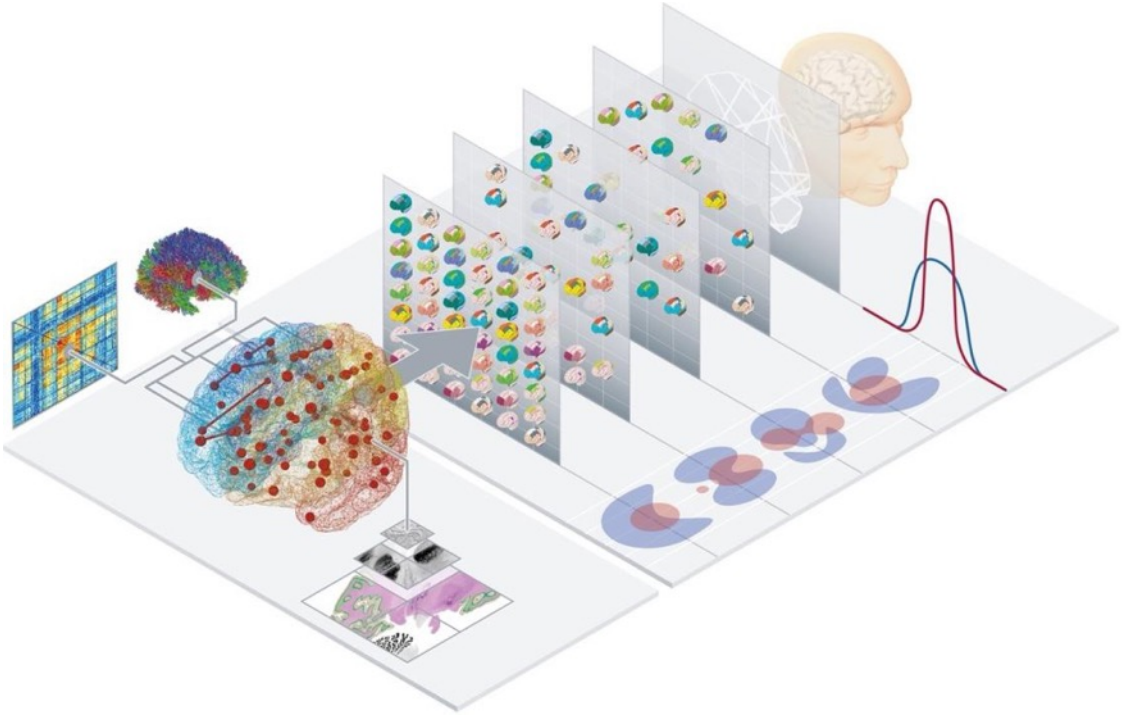

Figure 1. Workflows in WP1. Multiscale data of heterogeneous origin and different scales (molecular, cellular, synaptic and connectome data) are integrated in the same brain reference system (left). Brain models are represented in the same space and brain data are mapped upon the corresponding model parameters. Causal inference techniques are applied to empirical and simulated functional brain data and estimate posterior probability distributions of mechanistic representations of possible causes. This process advances our knowledge from initial premises and empirical observations to logical conclusions by quantifying the uncertainty in a model and data.

82. A computational model of Alzheimer reproduces features of disease severity in EEG recordings

Lorenzo Gaetano Amato[1,2*], Alberto Arturo Vergani[1,2], Michael Lassi[1,2], Riccardo Mannella[3], Valentina Bessi[4], Antonello Grippo[5], Alberto Mazzoni[1,2]

[1]The BioRobotics Institute, Scuola Superiore Sant'Anna, Pisa, Italy

[2]Dept. Of excellence in Robotics and AI, Scuola Superiore Sant'Anna, Pisa, Italy

[3]Dipartimento di Fisica, Università di Pisa, Pisa, Italy

[4]Dept. Of Neuroscience, Psychology, Drug research and child health, Careggi University Hospital, Firenze, Italy

[5]IRCCS Fondazione Don Carlo Gnocchi, Firenze, Italy

*LorenzoGaetano.Amato@santannapisa.it

INTRODUCTION/MOTIVATION

Alzheimer's disease (AD) is the predominant form of dementia, with more that 4 milions new cases each year worldwide. Even though several studies during the past decades focused on the structural alterations induced by the disease, currently, a reliable diagnosis of the disease is still far from being achieved [1]. Additionally, the relationship between structural changes and electrophysiological abnormalities commonly seen in Alzheimer's and pre-Alzheimer's patients remains unclear [2]. Gaining insights into the underlying connections between these anomalies and their causal changes would greatly enhance the diagnostic accuracy using non-invasive, commonly available scans like EEG. Here, we discuss a analysis pipeline in which the degree of structural alterations in pre-AD subjects has been determined by combining experimental EEG recordings with computational modelling of cortical activity, implemented with the EBRAINS The Virtual Brain open-source platform [3].

METHODS

We performed resting-state EEG recordings on 9 individuals with subjective cognitive decline (SCD) [4], 12 with mild cognitive impairment (MCI) [5], and 9 age-matched healthy controls (HC). We computed for each subjects the power spectral density (PSD) and the functional connectivity between EEG electrodes (FC) studying the statistical differences across the three groups with a one-way ANOVA f-test. We then developed a TVB-based multiscale model of the human cortex, altering the parameters to capture the evolution of the disease, modelling both synaptic alterations and connectome degeneration [1]. The first was condensed in a local parameter of degeneration (lp) and the latter in a connectivity parameter of degeneration (cp), both comprised between 0 and 1. With this model, we reproduced for each group the mean values of both FC and PSD by fitting the model parameters to the experimental EEG recordings, thus determining for each group the mean degree of structural alterations.

RESULTS AND DISCUSSION

The PSDs of the three groups were significantly different in the alpha [8-12 Hz] ($f = 6.87$, $p = 0.011$) and theta [4-8 Hz] ($p = 4.88$, $p = 0.37$) bands. In delta [0-4 Hz] and theta bands, average PSD was higher for MCI subjects than for SCD, and for SCD than HC. The inverse ordering is instead present in the alpha band, Figure 1a.

Interestingly, a non-linear evolution of significant functional connections emerged from FC analysis (Figure 1b-c): the HC group had an average of 26.4% significant connections, compared to 28.3% for the SCD group and 23.5% for the MCI group.

Overall, these results are consistent with the literature on evolution of EEG biomarkers in AD [2].

From these EEG features we fitted the model parameters to estimate the values of synaptic and connectome degeneration from the EEG recordings. The results of the fitting procedure are three parameter combinations, one per group, whose ordering is coherent with the severity of the clinical diagnosis. In particular, we found, for HC: lp = 0.52, cp = 0.24; for SCD: lp = 0.64, cp = 0.46; for MCI: lp = 0.74, cp = 0.90.
The model implemented with these parameter values was able to reproduce the experimentally observed PSD ordering in delta, theta and alpha bands, ($f = 3.82$, $p = 0.04$ in the theta band, $f = 3.38$, $p = 0.063$ in delta and $f = 1.69$, $p = 0.22$ in alpha, see Figure 2a). We captured also the non-linearity of FC values (24.0 % relevant functional connections in the modeled HC network, 24.8 % in the SCD, and 19.1 % in the MCI one, Figure 2b-c).

These findings show that computational models can accurately reproduce experimental EEG recordings in AD evolution. Moreover they can shed light on the underlying mechanisms of anomalies.

Keywords: The Virtual Brain, Alzheimer, EEG, Computational model

ACKNOWLEDGEMENTS

This project is funded by Tuscany Region - PRedicting the EVolution of SubjectIvE Cognitive Decline to Alzheimer's Disease With machine learning - PREVIEW - CUP. D18D20001300002.

THE ("Tuscany Health Ecosystem") Project funded by the Italian Ministry of University and Research – PNRR – Next Generation EU Projects.

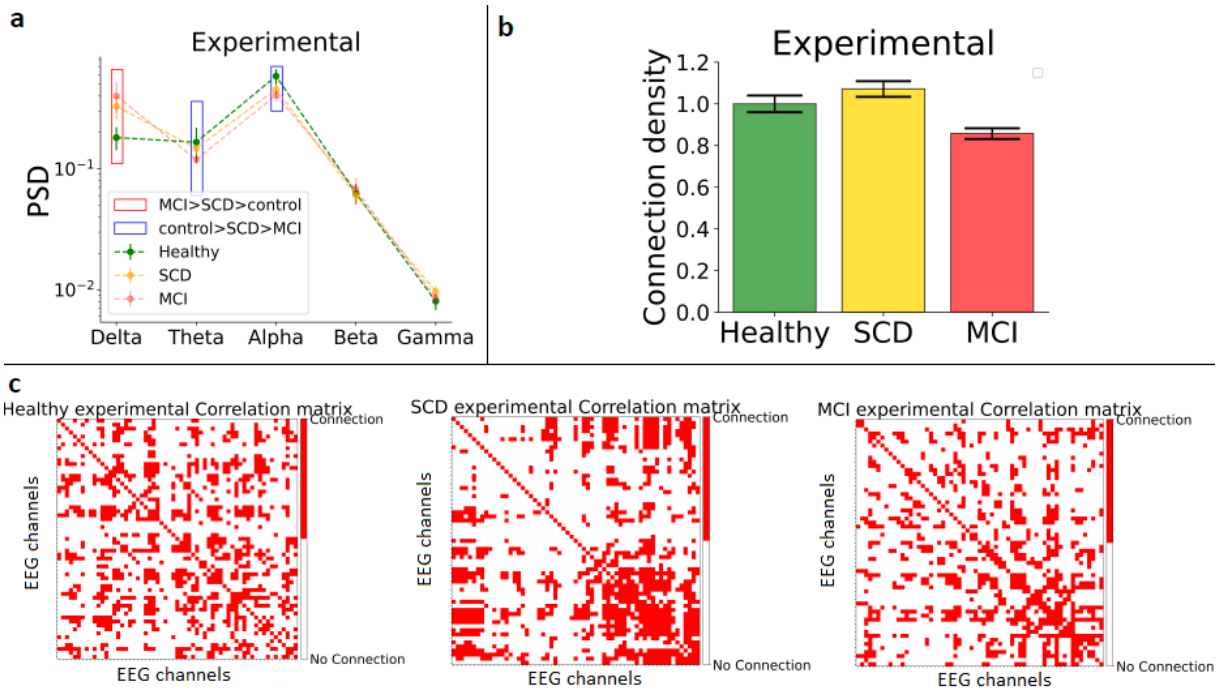

Figure 1: FC and PSD features computed from experimental recordings: a: Band-wise PSD for each group. (= p < 0.05) b: Barplot of the average FC density for each group c: Average thresholded FC matrix for each group*

REFERENCES

[1] Stefanovski, Leon, et al. "Bridging scales in alzheimer's disease: Biological framework for brain simulation with the virtual brain." *Frontiers in Neuroinformatics* 15 (2021): 630172. https://doi.org/10.3389/fninf.2021.630172

[2] Horvath, Andras, et al. "EEG and ERP biomarkers of Alzheimer's disease: a critical review." *Frontiers in bioscience (Landmark edition)* 23 (2018): 183-220. https://doi.org/10.5167/uzh-151582

[3] Sanz Leon, Paula, et al. "The Virtual Brain: a simulator of primate brain network dynamics." *Frontiers in neuroinformatics* 7 (2013): 10. https://doi.org/10.1089/cpb.2005.8.241

[4] Slot, Rosalinde ER, et al. "Subjective cognitive decline and rates of incident Alzheimer's disease and non–Alzheimer's disease dementia." *Alzheimer's & Dementia* 15.3 (2019): 465-476. https://doi.org/10.1016/j.jalz.2018.10.003

[5] Albert, Marilyn S., et al. "The diagnosis of mild cognitive impairment due to Alzheimer's disease: recommendations from the National Institute on Aging-Alzheimer's Association workgroups on diagnostic guidelines for Alzheimer's disease." *Alzheimer's & dementia* 7.3 (2011): 270-279. https://doi.org/10.1016/j.jalz.2011.03.008

83. Simulating ^{18}FDG-PET based on a neurogliovascular ATP model in The Virtual Brain

Halgurd Taher[1,2†], Leon Stefanovski[1,2†], Leon Martin[1,2], Malin Müting[1,2], Michael Schirner[1,2], Sharna Jamadar[3], Gary Egan[3], Petra Ritter[1,2,4*]

[1]Berlin Institute of Health at Charité – Universitätsmedizin Berlin, Berlin, Germany

[2]Department of Neurology with Experimental Neurology, Brain Simulation Section, Charité – Universitätsmedizin Berlin, corporate member of Freie Universität Berlin and Humboldt-Universität zu Berlin, Berlin, Germany

[3]Monash Biomedical Imaging & School of Psychological Sciences, Monash University, Melbourne 3800, VIC, Australia

[4]Bernstein Center for Computational Neuroscience Berlin, Berlin, Germany

[†] The co-first authors HT and LS contributed equally to this work.

*corresponding author: petra.ritter@charite.de

INTRODUCTION/MOTIVATION

While positron emission tomography with [^{18}F]fluorodeoxyglucose (FDG-PET) is an established imaging technique in clinical oncology, it is of emerging relevance in neurology in the field of neurodegenerative diseases. Recent approaches aim to use it as a functional measure of brain activity and connectivity , analogous to electroencephalography (EEG) or functional magnetic resonance imaging (fMRI). From a computational viewpoint, large-scale brain simulation with The Virtual Brain (TVB, www.thevirtualbrain.org) can reproduce such measures through biophysically grounded forward models, linking neuronal activity to EEG and fMRI signals. However, this link is not yet fully understood for FDG-PET. Besides the neuronal energy consumption, it further involves vascular and glial mechanisms. In this work, we propose a mechanistic forward model relating glucose metabolism and hence FDG-PET signals to the underlying electrophysiological activity in a large-scale brain simulation.

METHODS

We employ a bottom-up approach, encompassing the impact of neuronal firing on adenosine triphosphate (ATP) levels and energy metabolism. Therefore, we make use of an existing neurogliovascular model of ATP metabolism [1]. Derived from this, we propose a forward model that takes the simulated raw neuronal activity as an input and outputs a virtual FDG-PET signal, allowing for the calculation of a virtual static PET image and virtual PET-derived functional connectivity (FC). Model optimization and validation are performed based on a data set of simultaneous resting state fMRI and functional FDG-PET [2].

RESULTS AND DISCUSSION

Our model predicts the empirical PET data to a large extent while outperforming an existing forward model that is in use for fMRI. We observe high correlations between simulated and empirical static PET, for which the model was optimized based

on a subset of 3 subjects. Further, the same model reproduces the FDG-PET derived FC, for which the model has not been optimized. We show *in silico* fundamental differences between FDG-PET signal outputs and fMRI, including dependence on amplitude and frequency of the underlying neuronal activity for FDG- PET. Overall, our results suggest that the neurogliovascular ATP model may provide additional insights into brain function compared to other imaging modalities that do not take into account energy metabolism.

The model extends the fields covered with TVB to a larger variety of clinical applications, as PET is more frequently available than fMRI in clinical routine – for example, in the diagnostic workup of neurodegenerative diseases. Moreover, FDG-PET-derived FC promises to complement restrictions that are immanent to fMRI-based approaches, as it inherits a different degree of noise and differs in the resolution of time and space. Ultimately, the presented model is a step towards a better understanding of cerebral glucose metabolism and its relationship to brain activity.

Keywords: FDG, PET, brain simulation, glucose metabolism, The Virtual Brain

FIGURES

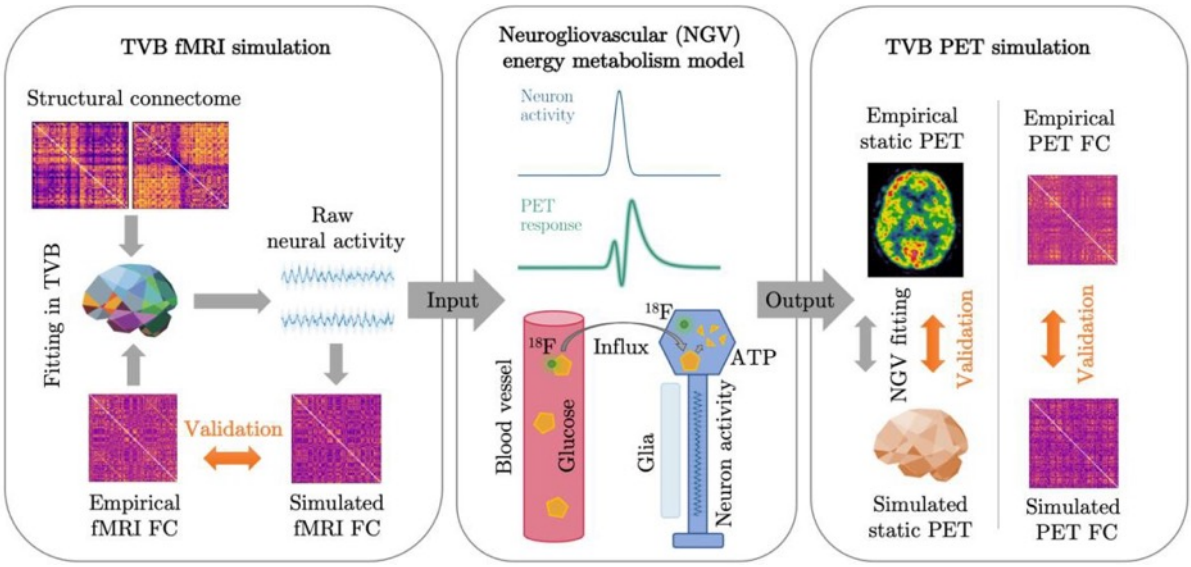

Figure 1: Simulating [^{18}F]fluorodeoxyglucose positron emission tomography (FDG-PET) in The Virtual Brain (TVB). Left: Structural connectomes (SC) are used as an input to TVB, in order to produce raw neural activity. By optimizing model parameters to reproduce functional connectivity (FC) derived from functional magnetic resonance imaging (fMRI), we obtain physiologically plausible raw activity. Center: The simulated neural activity acts as an input to a biophysical forward model of the neurogliovascular (NGV) energy metabolism. Spiking activity is ensued by the consumption of adenosine triphosphate (ATP) and triggers a "hunger" signal. Therefore, glucose and FDG molecules are released from blood vessels into the neuron to compensate for the consumed ATP. The FDG is trapped in the cell and gives a contribution to the FDG-PET signal. Right: This virtual FDG-PET signal is optimized to reproduce empirical static PET data of a subset of subjects. The remaining subjects are used for data validation, taking also into account FDG-PET-derived FC.

ACKNOWLEDGEMENTS

Computation of underlying data has been performed on the HPC for Research cluster of the Berlin Institute of Health. GE & SJ acknowledges support from the Australian Research Council Linkage Grant LP170100494. SJ

acknowledges support from the National Health and Medical Research Council of Australia Fellowship APP1174164. PR acknowledges support by EU H2020 Virtual Brain Cloud 826421, Human Brain Project SGA2 785907; Human Brain Project SGA3 945539, ERC Consolidator 683049; German Research Foundation SFB 1436 (project ID 425899996); SFB 1315 (project ID 327654276); SFB 936 (project ID 178316478; SFB-TRR 295 (project ID 424778381); SPP Computational Connectomics RI 2073/6-1, RI 2073/10-2, RI 2073/9-1; PHRASE Horizon EIC grant 101058240; Berlin Institute of Health & Foundation Charité, Johanna Quandt Excellence Initiative; ERAPerMed Pattern-Cog.

REFERENCES

[1] Chhabria, K., & Chakravarthy, V. S. (2016). Low-Dimensional Models of "Neuro-Glio-Vascular Unit" for Describing Neural Dynamics under Normal and Energy-Starved Conditions. Frontiers in Neurology, 7. doi:10.3389/fneur.2016.00024

[2] Jamadar, S. D., Ward, P. G. D., Close, T. G., Fornito, A., Premaratne, M., O'Brien, K., . . . Egan, G. F. (2020). Simultaneous BOLD-fMRI and constant infusion FDG-PET data of the resting human brain. Scientific Data, 7(1), 363. doi:10.1038/s41597-020-00699-5

84. Concepts for reproducible network connectivity

Johanna Senk[1*], Birgit Kriener[2], Mikael Djurfeldt[3], Nicole Voges[4], Han-Jia Jiang[1,5], Lisa Schüttler[6], Gabriele Gramelsberger[2], Markus Diesmann[1,7,8], Hans E. Plesser[1,9], Sacha J. van Albada[1,5]

[1]Institute of Neuroscience and Medicine (INM-6) and Institute for Advanced Simulation (IAS-6) and JARA-Institute Brain Structure-Function Relationships (INM-10), Jülich Research Centre, Jülich, Germany [2]Institute of Basic Medical Sciences, University of Oslo, Oslo, Norway
[3]PDC Center for High-Performance Computing, KTH Royal Institute of Technology, Stockholm, Sweden
[4]INT UMR 7289, Aix-Marseille University, Marseille, France
[5]Institute of Zoology, University of Cologne, Cologne, Germany
[6]Chair of Theory of Science and Technology, Human Technology Center, RWTH Aachen University, Aachen, Germany
[7]Department of Psychiatry, Psychotherapy and Psychosomatics, School of Medicine, RWTH Aachen University, Aachen, Germany
[8]Department of Physics, Faculty 1, RWTH Aachen University, Aachen, Germany
[9]Faculty of Science and Technology, Norwegian University of Life Sciences, Ås, Norway
*j.senk@fz-juelich.de

INTRODUCTION/MOTIVATION

Constructing a computational model of a neuronal network requires determining which neurons are connected to each other. Connectivity rules either specify explicit pairs of source and target neurons or make statistical assumptions on the connectivity between source and target neuron populations by abstracting from neuroanatomical data. Small differences between such rules may lead to network instances with statistically different dynamics. As the mathematical definition of connectivity forms the basis for algorithmic implementations, sustainable research demands this description to be complete and understandable.

Ambiguities and missing details are unfortunately frequent and hinder the reproducibility and extensibility of models and simulation studies. One possible reason for this observation is that the field of computational neuroscience still lacks standardized means for the description of network models [1].

METHODS

To find out which connectivity structures computational neuroscientists use and how they are described, we first review network models available in the repositories ModelDB [2] and Open Source Brain [3]. Analyzing both manuscript and code, we characterize all selected models according to "Metadata" (When, where, and by whom were article and code published?), "Description" (How does the article describe the connectivity and is the description complete?), "Implementation" (How is the connectivity technically implemented?), "Network" (How are network nodes and edges characterized?), and "Concepts" (Which connectivity concepts are realized?).

Next, we review how connectivity is abstracted in description languages and simulation interfaces: We distinguish between procedural, declarative population-level, and algebraic descriptions and list population-level connection rules of

languages and simulators, e.g., CSA [4] and NEST [5]. Based on this dual review, we derive a set of connectivity concepts together with a graphical notation for the unambiguous description of network models.

RESULTS AND DISCUSSION

Our main result is a proposal for a standardized nomenclature for connectivity concepts and a graphical notation for network diagrams, which we derive by analyzing, unifying, and formalizing approaches in use in the computational neuroscience community [6]. Reviewing a representative number of published network models reveals that the descriptions of connectivity in scientific publications are often insufficient to reproduce the connectivity actually created by accompanying source code. High-level connectivity concepts, defining the connectivity between neuron populations, may serve as concise and informative network specification not only for the textual and mathematical description but also for the implementation of connectivity if an agreement on the precise terminology is achieved. Our proposed guidelines aim to provide a reference for future descriptions of deterministically and probabilistically connected networks, including networks embedded in metric space. We demonstrate and discuss the practical use of the ideas in three examples covering complementary network models. We focus on expressing these networks using our graphical and symbolic notation to facilitate an intuitive understanding of network properties. This notation is already adopted by the graphical user interface NEST Desktop [7]. We hope that the proposed standardizations will advance complete and concise descriptions of network connectivity and also guide the implementation of connection routines in simulation software and neuromorphic hardware systems. Most neuronal network models developed until now have limited complexity, but newly developed research infrastructure such as EBRAINS and more experimental data becoming available will lead to increasingly complex models that need to remain manageable by individual scientists. By promoting consistency, we hope our work provides a contribution toward overcoming the complexity barrier in computational neuroscience.

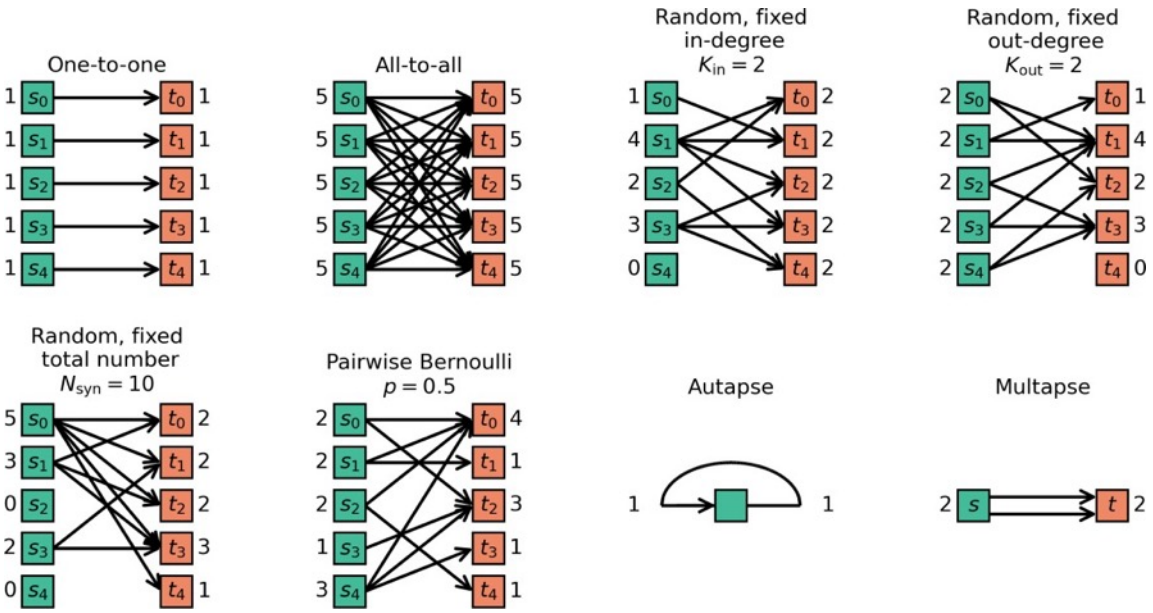

Figure 1: Connectivity patterns reflecting the most common rules.

Keywords: neuronal network connectivity, reproducibility, model description

ACKNOWLEDGEMENTS

This project has received funding from the European Union's Horizon 2020 Framework Programme for Research and Innovation under Specific Grant Agreement 720270 (HBP SGA1), 785907 (HBP SGA2), 945539 (HBP SGA3), and 754304 (DEEP-EST); the Deutsche Forschungsgemeinschaft (DFG, German Research Foundation) - 368482240/ GRK2416: ''RTG 2416 Multi-senses Multi-scales"; the Priority Program (SPP 2041 ''Computational Connectomics") of the Deutsche Forschungsgemeinschaft; the Helmholtz Association Initiative and Networking Fund under project number SO-092 (Advanced Computing Architectures, ACA); the Excellence Initiative of the German federal and state governments (neuroIC001): ''ERS: disziplinärer Paketantrag NeuroIC: NeuroModelingTalk (NMT) Approaching the complexity barrier in neuroscientific modeling"; the Helmholtz Metadata Collaboration (HMC), an incubator platform of the Helmholtz Association within the framework of the Information and Data Science strategic initiative, under the funding ZT-I-PF-3-026; and HiRSE_PS, the Helmholtz Platform for Research Software Engineering - Preparatory Study, an innovation pool project of the Helmholtz Association.

REFERENCES

[1] Nordlie E, Gewaltig MO, Plesser HE. Towards Reproducible Descriptions of Neuronal Network Models. *PLoS Comput. Biol.* 2009;5(8):e1000456. DOI:10.1371/journal.pcbi.1000456

[2] McDougal RA, Morse TM, Carnevale T, Marenco L, Wang R, Migliore M, et al. Twenty years of ModelDB and beyond: building essential modeling tools for the future of neuroscience. *J. Comput. Neurosci.* 2017;42(1):1–10. DOI:10.1007/s10827-016-0623-7

[3] Gleeson P, Cantarelli M, Marin B, Quintana A, Earnshaw M, Sadeh S, et al. Open Source Brain: A Collaborative Resource for Visualizing, Analyzing, Simulating, and Developing Standardized Models of Neurons and Circuits. *Neuron*. 2019;103(3):395–411.e5. DOI:10.1016/j.neuron.2019.05.019

[4] Djurfeldt M. The Connection-set Algebra—A Novel Formalism for the Representation of Connectivity Structure in Neuronal Network Models. *Neuroinformatics.* 2012;10:287–304. DOI:10.1007/s12021-012-9146-1

[5] Gewaltig MO, Diesmann M. NEST (NEural Simulation Tool). *Scholarpedia*. 2007;2(4):1430. DOI:10.4249/scholarpedia.1430

[6] Senk J, Kriener J, Djurfeldt M, et al. Connectivity concepts in neuronal network modeling. *PLoS Comput Biol.* 2022;18(9):e1010086. DOI:10.1371/journal.pcbi.1010086

[7] Spreizer S, Senk J, Rotter S, Diesmann M, Weyers B. NEST Desktop, an Educational Application for Neuroscience. *eNeuro*. 2021;8(6):ENEURO.0274-21.2021. DOI:10.1523/ENEURO.0274-21.2021

85. Inferring the mechanisms of resting-state network reconfiguration upon focal region silencing

Giovanni Rabuffo[1*], Houefa-Armelle Lokossou[2], Zengmin Li[3], Abolfazl Ziaee-Mehr[1], Meysam Hashemi[1], Pierpaolo Sorrentino[1], Antoine Ghestem[1], Pascale Quilichini[1], Kai-Hsiang Chuang[3], Teodora-Adriana Perles-Barbacaru[2], Angele Viola[2], Viktor Jirsa[1], Christophe Bernard[1]

[1]Institute de Neuroscience des Systems, UMR 1106, INSERM, Aix Marseille University, Marseille, France

[2]Center for Magnetic Resonance in Biology and Medicine, CNRS, Aix-Marseille University, Marseille, France

[3]Queensland Brain Institute, The University of Queensland, Brisbane, Australia

*giovanni.rabuffo@univ-amu.fr

INTRODUCTION/MOTIVATION

Silencing specific regions of the brain has become a popular approach for studying brain function and its underlying mechanisms [1], yet its effect on the whole-brain activity remains largely unknown. This study aims to shed light on the mechanistic relationship between focal brain region silencing and whole-brain activity, providing a deeper understanding of the effects of local modulation on brain function.

We investigate two mouse fMRI datasets upon focal silencing of brain sites, obtained by either lesioning thalamic nuclei or by chemogenetic shutdown of cortical hubs (Fig.1,a).

We report a structured and widespread reconfiguration of functional connectivity in all experiments, showing that decreased correlations occur along specific networks, and are paralleled by increased correlations in other channels (Fig.1,b-c).

A robust mechanistic interpretation of the processes underlying this structured re-organization is achieved via a simulation-based inference (SBI) approach [2,3], where brain activity is simulated in-silico and model parameters are inferred to best match the observed data (Fig.2,a). The model predicts increased neuronal excitability in the silenced region, paralleled by increased segregation of brain regions (Fig.2,b).

Our results provide a solid mathematical grounding to recent evidence on the effects of neuronal silencing [4] and pave the way to developing personalized predictions of local modulation effects over large-scale brain organization.

METHODS

In two independent experiments, we performed mouse brain imaging 10min before and 10min after region silencing (Fig.1,a). The 1st dataset was obtained by DREADDs inhibition of the retrosplenial cortex (RSC; 14 mice) or anterior cingulate area (ACA; 7 mice), which are generally considered functional hubs in the mouse brain. The data was acquired using a multiband EPI (TR=0.3s) [5]. The 2nd dataset was obtained from 6 C57Bl/6J mice with irreversible lesions in thalamic nuclei (Th) induced by i.c. injections of NMDA under ketamine + xylazine or isoflurane, and BOLD rs-fMRI acquisitions (TR=2s) were performed before and 6 wk after surgery under light anesthesia.

Both datasets were registered onto a parcellation of the Allen Mouse brain consisting of 148 regions of interest (ROIs). Tracer structural connectivity was imported from the Allen Institute [6].

In whole-brain simulations, the activity of each ROI is described by suitable dynamical equations [7]. The brain regions are connected through the Allen mouse connectome, resulting in a system of coupled equations. Simulated activity is obtained by numerical integration in The Virtual Mouse Brain (TVMB) [8] and depends on the choice of local and global parameters (Fig.2,a). The parameter η measures the neuronal excitability within the lesioned region. The coupling G measures the impact of structure over the local dynamics, with low- and high-G values indicating network segregation and integration, respectively.

In this work we exploited a simulation-based inference (SBI) approach [2,3], using deep artificial neural networks (ANNs) to infer the best parameter configuration that explains the observations (Fig.2,a).

RESULTS AND DISCUSSION

Analyzing empiric datasets we show that focal region silencing results in significant network-wide reconfiguration (Fig.1,b). While local silencing induces loss of functional connectivity on average, we show that decreased correlations along specific networks are paralleled by increased correlations in other channels (Fig.1,c).

We simulated brain activity in TVB and explored the parameter space by varying global and local model parameters. For each mouse, we used SBI to spot the parameter configuration producing the best fitting of simulations to observations for pre- and post-silencing recordings. We show that the silencing of a brain region results in a paradoxical increase of neuronal excitability (higher η parameter), and increased network segregation (lower G parameter) (Fig.2,b).

Our results ascribe the complex reconfiguration of large-scale networks to the adaptation of both local and global mechanistic factors, which emphasize the necessity of concurrent multilevel investigation of brain modulation, for both research and clinical assessments.

Keywords: Mouse fMRI, Resting-state, Thalamic lesion, chemogenetic shutdown, Brain simulations, Inference

ACKNOWLEDGEMENTS

This research has received funding from the European Union's Horizon 2020 Framework Programme for Research and Innovation under the Specific Grant Agreement No. 945539 (Human Brain Project SGA3) and 826421 Agence Nationale de la Recherche (ANR) Grants ANR-17-CE37-0001-CONNECTOME and ANR-20-NEUC-0005-01- Brainstim. ANR (grant ANR-17-CE37-0001-03), France Life Imaging (grant ANR-11-INBS-0006)

REFERENCES

[1] Rocchi F, Canella C, Noei S, et al. Increased fmri connectivity upon chemogenetic inhibition of the mouse prefrontal cortex. *Nature Communications*. 2022;13(1). doi:10.1038/s41467-022-28591-3

[2] Cranmer K, Brehmer J, Louppe G. The frontier of simulation-based inference. *Proceedings of the National Academy of Sciences*. 2020;117(48):30055-30062. doi:10.1073/pnas.1912789117

[3| Hashemi M, Vattikonda AN, Jha J, et al. Simulation-based inference for whole-brain network modeling of epilepsy using deep neural density estimators. 2022. doi:10.1101/2022.06.02.22275860

[4] Thiebaut de Schotten M, Foulon C, Nachev P. Brain disconnections link structural connectivity with function and behaviour. *Nature Communications*. 2020;11(1). doi:10.1038/s41467-020-18920-9

[5] Lee H-L, Li Z, Coulson EJ, Chuang K-H. Ultrafast fmri of the rodent brain using simultaneous multi-slice epi. *NeuroImage*. 2019;195:48-58. doi:10.1016/j.neuroimage.2019.03.045

[6] Oh SW, Harris JA, Ng L, et al. A mesoscale connectome of the Mouse Brain. *Nature*. 2014; 508(7495): 207-214. doi:10.1038/nature13186

[7] Montbrió, E., Pazó, D. and Roxin, A. (2015) "Macroscopic description for networks of spiking neurons," *Physical Review X*, 5(2). Available at: https://doi.org/10.1103/physrevx.5.021028.

[8] Melozzi F, Woodman MM, Jirsa VK, Bernard C. The virtual mouse brain: A computational neuroinformatics platform to study whole Mouse Brain Dynamics. *eneuro*. 2017;4(3). doi:10.1523/eneuro.0111-17.2017

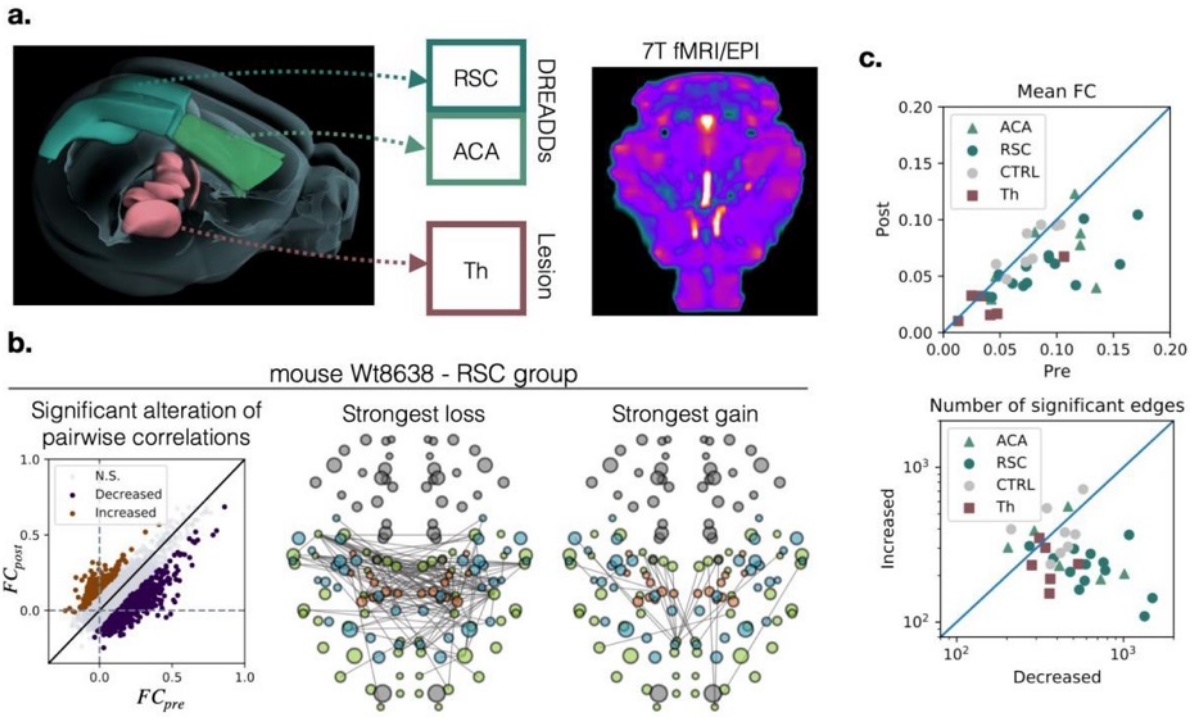

Figure 1: Widespread network effects of focal region silencing. **(a)** We recorded whole-brain activity before and after silencing of brain sites. In a first dataset, either the retrosplenial cortex (RSC) or the anterior cingulate area (ACA) were chemogenetically shutdown and the data was recorded using ultrafast fMRI (EPI). In a second dataset, thalamic nuclei (Th) of the mouse were lesioned and data was recorded using 7T fMRI. **(b)** Network reconfiguration after focal silencing is widespread as observed by the increase and decrease of pairwise correlations. **(c)** In most subjects average Functional Connectivity (FC) decreases in post-lesion recordings, consistent with the higher number of decreasing pairwise correlations versus increasing ones. These effects are not consistently observed in a control group (CTRL).

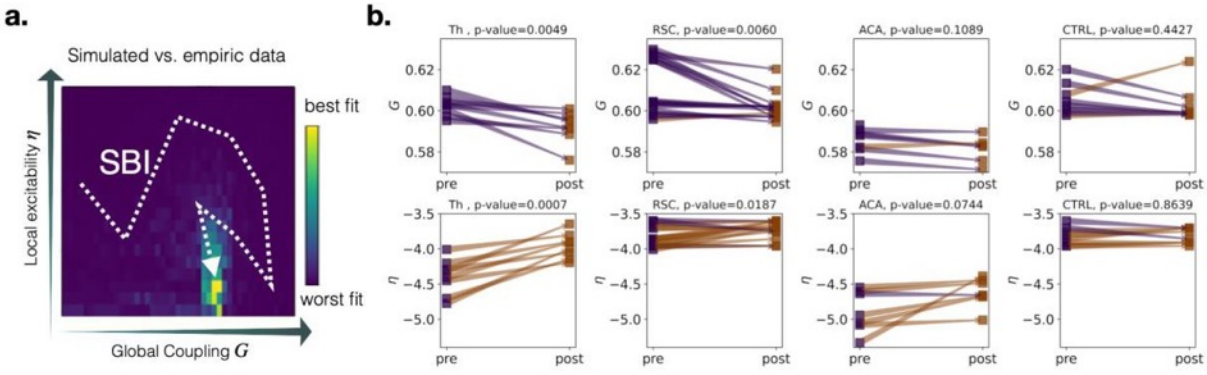

Figure 2: Mechanistic analysis of brain networks reconfiguration after focal silencing. **(a)** For each recording, simulation-based inference (SBI) was used to search for the (G, η) parameters configuration producing simulations that best match the empiric data features. **(b)** The estimation of parameters shows that pre- and post- lesion regimes change in a consistent way across subjects and datasets. Namely, the global coupling G decreases and the local excitability η of the silenced region increases, consistently across subjects and silencing modalities.

86. Simulating deep brain stimulation using a multiscale model in The Virtual Brain

Jil Meier[1,2,*], Jan Stasinski[1,2], Marius Pille[1,2], Timo Hofsähs[1,2], Anaïs Halimi[1,2], André Blickensdörfer[1,2], Lion Deger[1,2], Leon Martin[1,2], Dionysios Perdikis[1,2], Johannes Busch[3], Johannes Achtzehn[3], Lucia Feldmann[3], Roxanne Lofredi[3], Patricia Krause[3], Nanditha Rajamani[3], Bassam Al-Fatly[3], Christopher Güttler[3], Andrea Kühn[3], Petra Ritter[1,2,*]

[1] Berlin Institute of Health at Charité – Universitätsmedizin Berlin, Berlin, Germany

[2] Charité – Universitätsmedizin Berlin, corporate member of Freie Universität Berlin and Humboldt-Universität zu Berlin, Department of Neurology with Experimental Neurology, Brain Simulation Section, Berlin, Germany [3] Charité – Universitätsmedizin Berlin, Department of Neurology, Movement Disorders and Neuromodulation Unit, Berlin, Germany

*e-mail-addresses of corresponding authors: jil-mona.meier@bih-charite.de and petra.ritter@bih-charite.de

INTRODUCTION

Deep brain stimulation (DBS) is a successful symptom-relieving neuromodulation technique established for many different neurodegenerative diseases. However, the effects of DBS on the local scale around the electrode and on the global scale of macroscopic brain regions are still insufficiently understood. Recently, we established a multiscale model for DBS that combines fine-grained spiking modeling for the surrounding areas of the electrode and coarse-grained mean-field modeling to offer a whole-brain perspective on the effects of DBS [1]. The code of this model and the data used in this previous study are publicly available on EBRAINS. We provided proof of concept for virtual DBS in a co-simulation multiscale environment with The Virtual Brain (TVB). However, bringing such a virtual DBS model to the clinic for improving and accelerating DBS programming for the individual Parkinson's disease patient warrants extensive validation. Furthermore, our previous model was not sensitive to the exact 3D location of the electrode, which is a crucial factor for the successfulness of DBS.

METHODS

In this study, we compared our multiscale DBS model with empirical DBS ON and OFF resting-state fMRI BOLD data (N=2, biphasic stimulation). We also extended our previous multiscale model to allow for a high-resolution modeling around the DBS electrode by interfacing TVB with electrical field (E-field) modeling, which includes the electromagnetic properties of the surrounding tissue of the electrode and estimates the electrical field changes due to the DBS pulses. To this end, we adapted the surface-based modeling approach of An et al. [2] to include high-resolution modeling around the DBS electrode and traced the activations of the fibers towards cortical

regions. Inputting the localizations of Sensight directional DBS leads (N=9, Medtronic Percept), we simulated local field potentials and BOLD data.

RESULTS AND DISCUSSION

Virtual DBS showed increases as well as decreases in BOLD activity and correlations among sensorimotor and basal ganglia (BG) regions (Fig. 1ACD). For some single regional and selective pairwise correlations, those stimulation effects seem to be congruent with decreases or increases in empirical data (Fig. 1ACD). Further, we established a first link between the individual simulated dynamics (local field potentials based on the individual localizations of the Sensight DBS lead, N=9) and the clinical improvements of patients after DBS using principal component analysis (PCA) (Fig. 1B). Our results are still preliminary and warrant further testing and validation on larger sample sizes. With the virtual DBS model, we can observe the local and global dynamics simultaneously (Fig. 1C-E) which has the potential to identify DBS network effects and generate new hypotheses for the mechanisms of DBS. Our extended multiscale model is sensitive to different parameters of the E-field (amplitude/frequency of the stimulus, precise location) and can be used in the future to test different DBS programming and/or surgical targeting which may determine optimal clinical outcome tailored to individual symptomatic profiles.

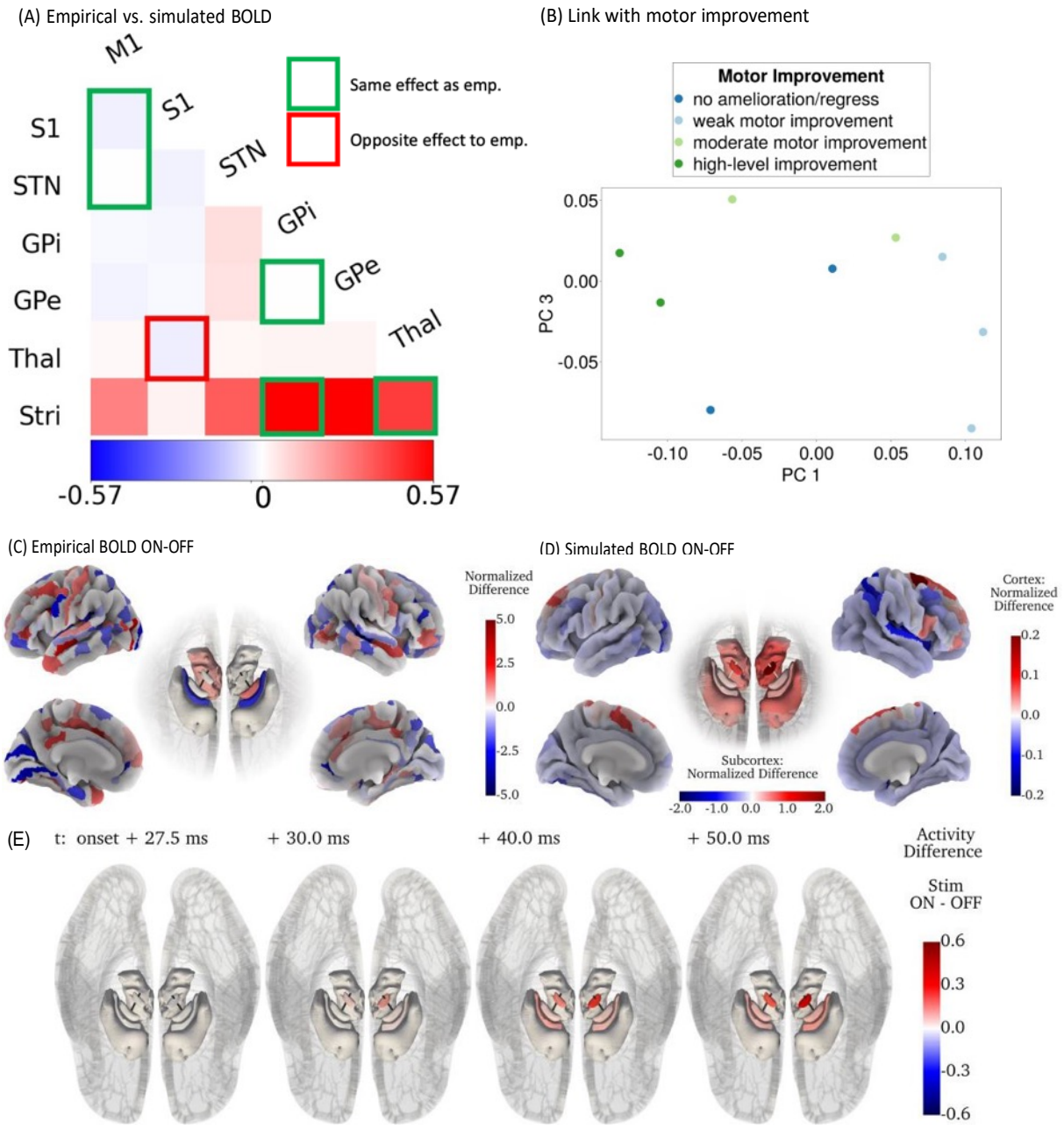

Figure 1: Comparison of simulated DBS effects with empirical BOLD data and first link of simulated dynamics with clinical symptoms. (A) Simulated data was able to capture 5 out of 6 increases/decreases of BOLD correlations under DBS ON (in the left hemisphere). (B) PCA on the simulated dynamics shows a reasonable classification of patients based on their motor improvement under DBS ON. (C) Empirical and (D) simulated BOLD activity fluctuations due to DBS. (E) Snapshots of the simulated LFP signal in the BG regions after stimulus onset.

Keywords: The Virtual Brain, multiscale modelling, electric-field modelling, deep brain stimulation

ACKNOWLEDGEMENTS

Computation of underlying data has been performed on the HPC for Research cluster of the Berlin Institute of Health. PR acknowledges support by Digital Europe TEF-Health 101100700, EU H2020 Virtual Brain Cloud 826421, Human Brain Project SGA2 785907; Human Brain Project SGA3 945539, ERC Consolidator 683049; German

Research Foundation SFB 1436 (project ID 425899996); SFB 1315 (project ID 327654276); SFB 936 (project ID 178316478; SFB-TRR 295 (project ID 424778381); SPP Computational Connectomics RI 2073/6-1, RI 2073/10-2, RI 2073/9-1; PHRASE Horizon EIC grant 101058240; Berlin Institute of Health & Foundation Charité, Johanna Quandt Excellence Initiative; ERAPerMed Pattern-Cog.

REFERENCES

[1] Meier, J.M., Perdikis, D., Blickensdörfer, A., Stefanovski, L., Liu, Q., Maith, O., Dinkelbach, H.Ü., Baladron, J., Hamker, F.H. and Ritter, P., 2022. Virtual deep brain stimulation: Multiscale co-simulation of a spiking basal ganglia model and a whole-brain mean-field model with the virtual brain. *Experimental Neurology*, p.114111. https://doi.org/10.1016/j.expneurol.2022.114111

[2] An, S., Fousek, J., Kiss, Z.H., Cortese, F., van Der Wijk, G., McAusland, L.B., Ramasubbu, R., Jirsa, V.K. and Protzner, A.B., 2022. High-resolution virtual brain modeling personalizes deep brain stimulation for treatment-resistant depression: Spatiotemporal response characteristics following stimulation of neural fiber pathways. *NeuroImage*, *249*, p.118848. https://doi.org/10.1016/j.neuroimage.2021.118848

87. The Arbor Simulator: growing a sustainable, portable, and performant ecosystem

B. Cumming[1], F. Bösch[1], S. Frasch[1], L. Drescher[1], A. Küsters[2], T. Hater[2], B. F. B. Huisman[2*], L. P. L. Landsmeer[2]

[1]CSCS - Swiss National Supercomputing Centre and ETHZ - Eidgenössische Technische Hochschule Zürich, Switzerland

[2]JSC - Jülich Supercomputing Centre, Forschungszentrum Jülich, Germany

*b.huisman@fz-juelich.de

INTRODUCTION/MOTIVATION

Computational neuroscience is experiencing a steady growth in available simulation tools applicable to morphologically detailed cell descriptions [1, 2, 3, 4, 5, 6]. Arbor is a relatively recent entry [7] in the competition and is designed to elevate computational neuroscience to the scales of simulation of the human brain. It does so by enabling HPC simulation with the same ease as local simulation. Recent developments include inclusion as backend in BluePyOpt, a parameter optimization library; publication of the Arbor GUI, a graphical front-end to Arbor; nmlcc, a tool to generate optimised simulations from a description in NeuroML; and preliminary results from the BrainScaffoldBuilder, which benchmarks Arbor favorably to competing simulators.

METHODS

1. Packaging and testing

Ensuring reproducible results is aided by using tools and practices common in the development of professional software. Arbor's source code is publicly available and uses the commonly employed CMake build system. Unit tests covering Arbor's functionality are executed upon every code addition to prevent bugs and regressions. Arbor is available as a Python and Spack package. The Spack package is part of the Ebrains Lab. The Arbor GUI has automated builds for MacOS and Linux. We publish an integrated validation and benchmarking framework, called NSUITE, in lockstep with the Arbor library and is used to spot performance regressions and investigate scaling behavior.

2. Accessibility

The Arbor GUI lets the user interactively design a detailed cell. Morphologies can be loaded from a variety of formats, and helps the user visualize regions and location sets where e.g. ion dynamics are painted or bio-physical properties set, and helps with placement of e.g. probes. The result can be exported in Arbor's internal format for simulation elsewhere, such as HPC. The Arbor Playground Arbor compiled to the web, making Arbor accessible to anyone with a web browser, and comes preloaded with select published models.

3. Ecosystem integration

To make more models available to scientists, we designed nmlcc, a translator from NeuroML2 to Arbor's native format(s). It leverages the full-simulation description of NML2 to provide optimised outputs, resulting in significant performance improvements. Arbor is an officially supported backend for BluePyOpt [8], a commonly used package for parameter

optimization.

4. Features

Some recently added features include support for inhomogeneous parameters: selected parameters can be scaled by a function evaluated along a cell. Stochastic differential equations (SDEs) lets users introduce sources of white noise. Plasticity modelling is improved by providing resumable simulations, connection table modifications, and an efficient implementation for dendritic diffusion of ions, which play a role in synapse plasticity.

RESULTS AND DISCUSSION

A published study used the L2L framework to conduct a parameter optimisation study using Arbor [9]. Arbor also became a supported back end in the Brain Scaffold Builder, enabling the simulation of a series of published models [10]. In 2022 a user group around plasticity was kicked off, which will steer Arbor development to support planned original research in the near future. One planned study will investigate structural plasticity: how do spines grow and decay, and in turn modulate the strength of a synapse, as function of ion concentration and endpoints distance? Another planned study has as goal to reproduce evoked EEG responses over the primary somatosensory cortex, measured for known vibratory stimuli in clinical studies.

The Arbor source code now counts contributions from 30 persons, about half of which are people from outside the development team. The Python package is downloaded ~300 times per month and the Arbor community space sees daily discussions, pointing to increased use and a community forming with plans to scale their ambitions and simulations out.

Acknowledgements

This research has received funding from the European Unions Horizon 2020 Framework Programme for Research and Innovation under the Specific Grant Agreement No. 720270 (Human Brain Project SGA1), Specific Grant Agreement No. 785907 (Human Brain Project SGA2), and Specific Grant Agreement No. 945539 (Human Brain Project SGA3).

Keywords: HPC, Neural Networks, Simulation, Portable Models

REFERENCES

[1] Roy Ben-Shalom et al. "NeuroGPU: Accelerating multi-compartment, biophysically detailed neuron simulations on GPUs". In: Journal of Neuroscience Methods, 2022 (10.1016/j.jneumeth.2021.109400)

[2] Dan FM Goodman and Romain Brette. "The Brian simulator". In: Frontiers in neuroscience, 2009 (10.3389/neuro.01.026.2009)

[3] Sotirios Panagiotou et al. "EDEN: A high-performance, general-purpose, NeuroML-based neural simulator". In: Frontiers in Neuroinformatics, 2022 (10.3389/fninf.2022.724336)

[4] N. T. Carnevale and M. L. Hines. The NEURON book. Cambridge University Press, 2006. (10.1017/CBO9780511541612)

[5] L. Niedermeier et al. "CARLsim 6: An Open Source Library for Large-Scale, Biologically Detailed Spiking Neural Network Simulation". In: International Joint Conference on Neural Networks, 2022 (10.1109/IJCNN55064.2022.9892644)

[6] Omar Awile et al. "Modernizing the NEURON Simulator for Sustainability, Portability, and Performance". In: Frontiers in Neuroinformatics, 2022 (10.3389/fninf.2022.884046)

[7] N. Abi Akar et al. Arbor — A Morphologically-Detailed Neural Network Simulation Library for Contemporary High-Performance Computing Architectures. IEEE, 2019 (10.1109/EMPDP.2019.8671560).

[8] Werner Van Geit et al. "BluePyOpt: Leveraging open source software and cloud infrastructure to optimise model parameters in neuroscience."In: Front. Neuroinform., 2016 (doi: 10.3389/fninf.2016.00017)

[9] Alper Yegenoglu et al. “Exploring Parameter and Hyper-Parameter Spaces of Neuroscience Models on High Performance Computers With Learning to Learn”. In Frontiers in computational neuroscience, 2022 (10.3389/fncom.2022.885207)
[10] Robin De Schepper et al. “Cross-comparison of state of the art neuromorphological simulators on modern CPUs and GPUs using the Brain Scaffold Builder”. In: Bioaxiv preprint, 2022 (10.1101/2022.03.02.482285)

88. A biologically plausible decision-making model of interacting cortical columns

Emre Baspinar[1*], Gloria Cecchini[2], Michael DePass[2], Marta Andujar[3], Ignasi Cos[2], Ruben Moreno-Bote[4], Stefano Ferraina[3], Alain Destexhe[1]

[1]NeuroPSI, CNRS, Saclay, France

[2]Dep. of Mathematics and Computer Science, University of Barcelona, Barcelona, Spain

[4]Dep. of Physiology and Pharmacology, University of Rome, Rome, Italy [4]Dep. of Information and Communications Technologies, Pompeu Fabra University, Barcelona, Spain

*Corresponding author, emre.baspinar@cnrs.fr

INTRODUCTION/MOTIVATION

Decision-making refers to making a perceptual or motor choice between alternatives. It requires anticipating consequences of each choice. Previous studies on decision-making focused mostly on paradigms with immediate consequences. However, in many cases, decision-making with consideration of long-term benefits is important for survival of species. This requires control over future planning to identify optimal decision-making strategy. To study behavioural background of such mechanisms, we applied a visual discrimination experiment on human (20 years old female) and monkey (16 years old male). Challenge is to model induced dynamics at behavioural level.

METHODS

The Adaptive Exponential (AdEx) mean-field framework[1] describes the averaged neuronal population behaviour modelled by AdEx network. In the case of cerebral cortex, AdEx networks are used to model two cell types: Regular Spiking (RS) neurons, displaying spike-frequency adaptation as observed in excitatory pyramidal neurons, and Fast Spiking (FS) neurons, with no adaptation, as observed in inhibitory interneurons. AdEx networks are high dimensional, complex and difficult to analyse. AdEx mean-field models are low dimensional, simpler and easier to analyse compared to networks, yet they approximate closely the network dynamics, motivating our choice of model.

We extend the AdEx mean-field framework to model two networks of excitatory-inhibitory neurons, representing two cortical columns, and interconnected with excitatory connections contacting both RS and FS cells (Figure 1). Intercolumnar excitation introduces bi-columnar competition in which winning column makes the decision. This excitation is balanced by intracolumnar inhibition. This is different from previous models[2, 3], which postulate intercolumnar inhibition.

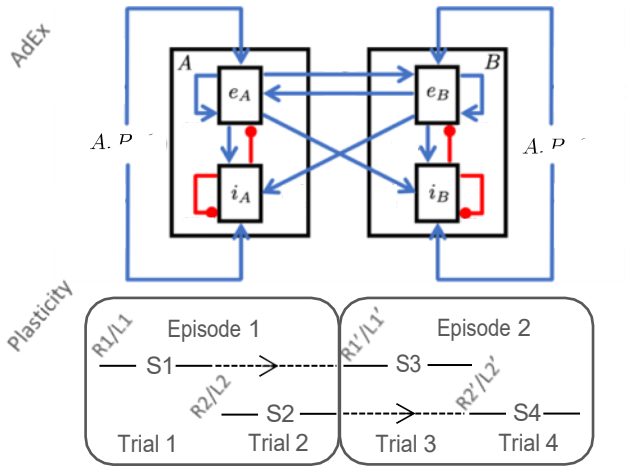

Figure 1: AdEx mean-field double-column model with plasticity. Columns vote for stimuli A or B. They are composed of excitatory (e) and inhibitory (i) populations. Arrow and dot ended lines denote excitatory and inhibitory connections, respectively. Plasticity introduces bias S initialized by reward R or loss L at the beginning of each trial. The columns receive stimuli A and B biased by S.

Experiment task is based on maximizing total reward provided at the end of each episode consisting of two trials. The choices are two different icons. They are randomly generated for each trial and projected on computer screen. The reward at the end of the episode depends on the coherency between choices of the subject and pre-set strategy. A reward-driven plasticity allows the model to learn the implemented strategy, as well as subject exploratory behaviour.

RESULTS AND DISCUSSION

We compare simulations to human and macaque data in terms of performance and reaction times. Quantification of simulation and experiment data is done based on statistical measures of performance and reaction times.

Novelties are several. Firstly, it provides biophysical ground for simpler phenomenological models proposed for similar decision-making tasks. It is directly linked to biological machinery observed in RS and FS cell populations. Secondly, it is based on biologically plausible intercolumnar connectivity. Finally, it is the first time that AdEx mean-field framework is applied to a cognitive task.

This model can produce neurophysiological dynamics of decision-making, proposing two future perspectives. The first is to apply it to multiarray recordings of decision-making macaque brain. The second is to extend it to multiple cortical columns, enabling implementation to whole-brain simulator *The Virtual Brain*.

Keywords: Computational neuroscience, decision-making, cortical column, mean-field, plasticity, AdEx

ACKNOWLEDGEMENTS

This research is supported by Human Brain Project (European Union grant H2020-945539).

REFERENCES

[1] di Volo M, Romagnoni A, Capone C, Destexhe A. Biologically realistic mean-field models of conductance-based networks of spiking neurons with adaptation. *Neural Computation.* 2019;31(4):653-680. doi: 10.1162/neco_a_01173.

[2] Wang XJ. Probabilistic decision making by slow reverberation in cortical circuits. *Neuron*. 2002;36(5):955-68. doi: 10.1016/s0896-6273(02)01092-9.

[3] Marcos E, Pani P, Brunamonti E, Deco G, Ferraina S, Verschure P. Neural variability in premotor cortex is modulated by trial history and predicts behavioral performance. *Neuron.* 2013;78(2):249-255. doi: 10.1016/j.neuron.2013.02.006.

89. Cholinergic neuromodulation of cortical brain states: an experimental and computational study of cellular and network mechanisms

Leonardo Dalla Porta[1], Almudena Barbero-Castillo[2], Jose M. Sanchez-Sanchez[2], Maria V. Sanchez-Vives[1]

[1]IDIBAPS, Spain
[2]Institute of Biomedical Research August Pi i Sunyer, Spain

Introduction

During slow wave sleep (SWS) we are unconscious and disconnected from the outside world, while when we wake up, we are conscious of ourselves and the world around us. Notwithstanding, from a network dynamics perspective, these states are rather different: while SWS is a highly synchronous activity, the awake state is characterized by desynchronized dynamics [1]. However, what are the mechanisms driving the transition between these rather different functional brain states? In the current study we investigated one mechanism that is critical for the sleep to wake transition to occur in the cerebral cortex network: the blockade of muscarinic-sensitive K^+ current (M-current) by cholinergic action. We sought to determine the impact of M-current on cortical dynamics during spontaneous slow oscillations (SO), as well as its interaction with network excitability. We carried out this investigation both in experiments, using visual cortical slices, and in a biophysical detailed recurrent neuronal network. Together, our results indicate that M-current is highly implicated in the maintenance of the slow cortical dynamics, and its blockage results in a progressive elongation of the periods of persistent activity that dominates over the regular presence of silent periods, resembling the transition to wake brain states. Overall, our work bridges one ionic channel with network modulation, providing a mechanistic insight into the network dynamics of awakening and opening the door to link microscopic to whole brain dynamics.

Methods

Local field potentials (LFP) were recorded using a 16-channel flexible microarray from visual cortex slices. Slices were placed in an interface-style recording chamber and superfused with an equal mixture of sucrose solution and artificial cerebrospinal fluid as in [2]. XE991 was used as a specific M-current blocker. For the analysis of spontaneous activity, the MUA signal was used (LFP filtered between 0.2-1.5kHz), once it is a reliable estimation of the population firing rate [3]. For the recurrent network model, we reproduced a model of slow oscillations proposed in [4]. In it, the M-current was newly integrated in the excitatory neurons. To simulate the M-current blockage (increment) in the model we parametrically reduced (increased) its maximal conductance. We also regulated network excitability by controlling the leak currents conductance.

Results and Discussion

In this study we found that M-current has an important role in the mechanisms controlling the Up states, specifically modulating its persistence and termination. Blocking the M-current resulted in a prominent elongation (ca. four times) of the Up states, while the Down states hardly varied in duration (Fig. 1, top). The population firing rate was also increased during both Up and Down states, reflecting the increased excitability of the network. The cortical activity under the M-current blockage was like the so-called microarousals that occur as a result of activation of the arousal systems in the sleep-wake transition [5]. In our computational model we replicated the experimental results (Fig. 1, bottom) and showed that there is a linear relation between the firing rate and up state duration. Furthermore, we showed that for an increment in the M-current higher than 20%, the network was unable to show spontaneous activity. Looking at the individual neuronal level, we observed that just the reduction of this current induced a radical change in network dynamics, going from regular and synchronous SO to more prolonged and desynchronized firing periods, and effect that was more striking for states with higher network excitability. In conclusion, since cholinergic action in the cerebral cortex is critical to induce the transition from sleep to awake, our results suggest a relevant role for M- current blockage by muscarinic action into this transition. On the contrary, the physiological activation of the M-current plays an important role in maintaining a hyperpolarized neuronal membrane potential and facilitating, in the absence of cholinergic inputs, the expression of slow waves in the cortical network.

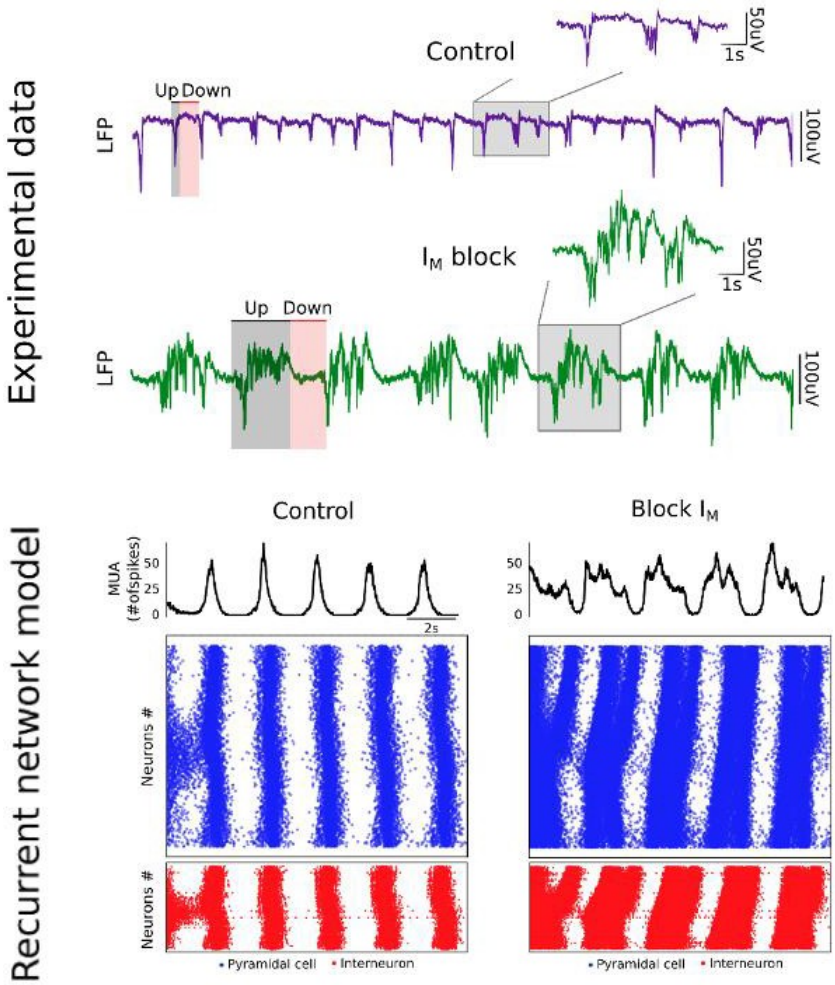

Figure 1 Effect of M-current blockage on spontaneous slow oscillations in cortical slices (LFP, top) and in a recurrent network model (bottom). Notice the prominent elongation of periods of activation (Up states) in both experimental and simulated data.

Keywords: Neuromodulation, cortical networks, slow oscillations, brain states, synchronization, Up states.

Acknowledgements

This research has received funding from the European Union's Horizon 2020 Framework Programme for Research and Innovation under the Specific Grant Agreement no. 945539 (Human Brain Project SGA3) and from PID2020-112947RB-I00 financed by MCIN/ AEI /10.13039/501100011033.

[1] Harris, K.D. and Thiele, A. (2011) "Cortical state and attention," Nature Reviews Neuroscience, 12(9), pp. 509–523. https://doi.org/10.1038/nrn3084.

[2] Sanchez-Vives, M.V. and McCormick, D.A. (2000) "Cellular and network mechanisms of rhythmic recurrent activity in neocortex," Nature Neuroscience, 3(10), pp. 1027–1034. https://doi.org/10.1038/79848.

[3] Mattia, M. and Del Giudice, P. (2002) "Population dynamics of interacting spiking neurons," Physical Review E, 66(5). https://doi.org/10.1103/physreve.66.051917.

[4] Compte, A. et al. (2003) "Cellular and network mechanisms of slow oscillatory activity (<1 Hz) and wave propagations in a cortical network model," Journal of Neurophysiology, 89(5), pp. 2707–2725. https://doi.org/10.1152/jn.00845.2002.

[5] Tort-Colet, N. et al. (2021) "Attractor competition enriches cortical dynamics during awakening from anesthesia," Cell Reports, 35(12), p. 109270. https://doi.org/10.1016/j.celrep.2021.109270.

90. TheVirtualBrain in the Neurorobotics Platform: Haken-Kelso-Bunz bimanual coordination

Dionysios Perdikis[1,2*], Krzysztof Lebioda[3], Erdi Sayar[3], Michael Schirner[1,2], Fabrice O. Morin[3], Petra Ritter[1,2]

[1] Berlin Institute of Health at Charité – Universitätsmedizin Berlin, Berlin, Germany

[2] Brain Simulation Section, Department of Neurology with Experimental Neurology, Charité – Universitätsmedizin Berlin, Berlin, Germany

[3]Chair of Robotics, Artificial Intelligence and Real-Time Systems, Technical University of Munich, Germany

*dionysios.perdikis@bih-charite.de

INTRODUCTION

TheVirtualBrain (TVB) [1] is a computational framework for modelling and simulating whole brain dynamics at the level of large-scale networks, which allows for the integration of structural and functional neuroimaging data [2]. The Neurorobotics Platform (NRP) [3] is a set of software tools to prepare, execute and monitor simulations of virtual agents interacting in a closed loop with their environment. The latter can be implemented in game engines, such as Unity, or in simulation environments such as MuJoCo or Gazebo [4]. We present a first demonstration of an embodied virtual brain simulation that exhibits a phase transition in bimanual sensorimotor coordination following the classical Haken-Kelso-Bunz (HKB) model [5], via closed-loop co-simulation of TVB and Gazebo in the NRP.

METHODS

We embedded the bimanual coordination task dynamics into a TVB network model by (a) augmenting the network with two nodes representing the Gazebo fingers, (b) selecting a HKB like oscillatory model [6] for the dynamics of each network node and their mutual coupling, (c) setting directed connections implementing the loop Left Motor Cortex (LMC) -> Right Finger (RF) -> Left Sensory Cortex (LSC) -> Right Motor Cortex (RMC) -> Left Finger (LF) -> Right Sensory Cortex (RSC) -> LMC (Figure 1), and (d) reducing the weights of all other brain connections and removing all time delays to the TVB time step of integration (0.1 ms). At every time step of simulation, the activity of the motor cortices determines the position and velocity of the Gazebo fingers, acting as motor commands, whereas the actual position and velocity of those fingers update the state of the respective TVB RF and LF nodes (by overwriting it), which then couple to the sensory cortices, acting as proprioception, eventually directed to the motor cortices. The oscillations go through three successively increased frequency plateaus (by modifying accordingly a frequency parameter), the middle of which corresponds to the critical frequency that destabilizes the antiphase mode of coordination.

The NRP platform implements a hub-and-spokes architecture with NRP Core as the hub and distributed "engines" for constituent simulators, employing a client-server paradigm for communications. The NRP core (a) orchestrates the co-simulation of the TVB and Gazebo engines, and (b) carries out the data exchange, as well as mathematical transformations of the data via transceiver functions (in Python).

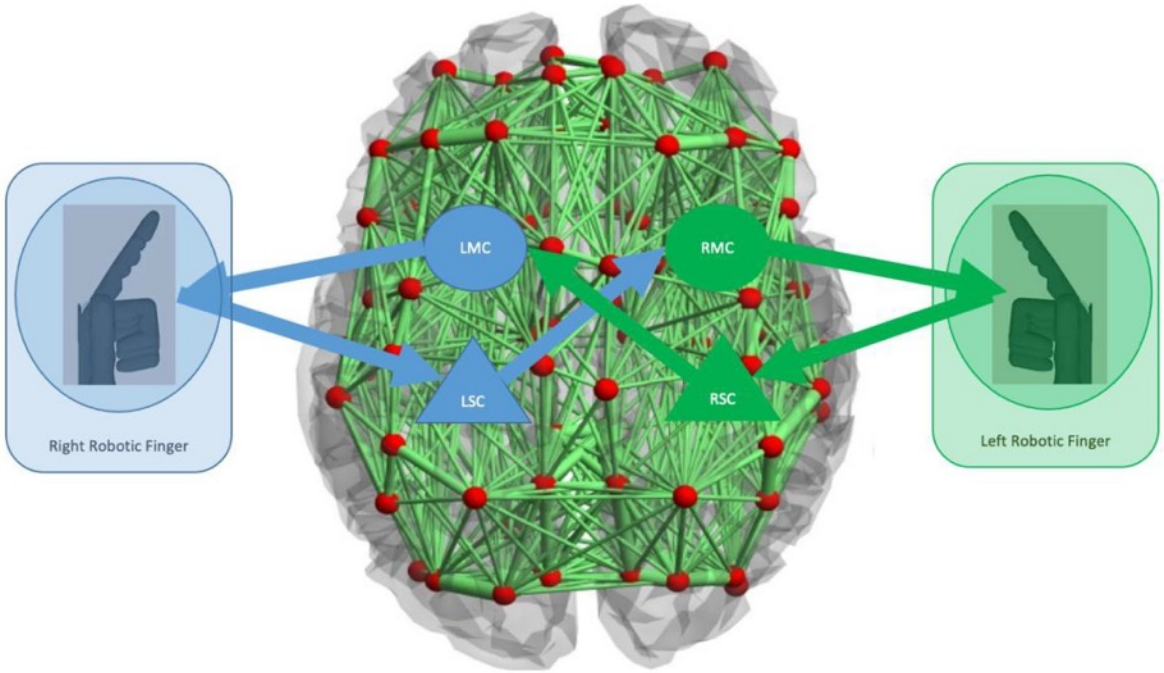

Figure 1: Model architecture. TVB network augmented with two Gazebo fingers. Task related directed connections shown as thick arrows in blue (green) for right the (left) finger.

RESULTS AND DISCUSSION

The co-simulation starts with initial conditions chosen to result to an antiphase mode of bimanual coordination. During the middle (critical) frequency plateau a phase transition takes place to the inphase coordination mode spontaneously, with the assistance of noise (Figure 2; see also [7] for an animation).

Future work can increase the biological realism of both the brain dynamics (e.g., inducing the phase transition due to interhemispheric crosstalk and respective time delays [8]), and on the side of the robotic fingers' biomechanics. Such a co-simulation framework allows researchers to perform in-silico experiments of brain and behaviour interactions for testing hypotheses or making predictions e.g., for lesions or perturbations, while integrating neuroimaging, neuromuscular and behavioural data.

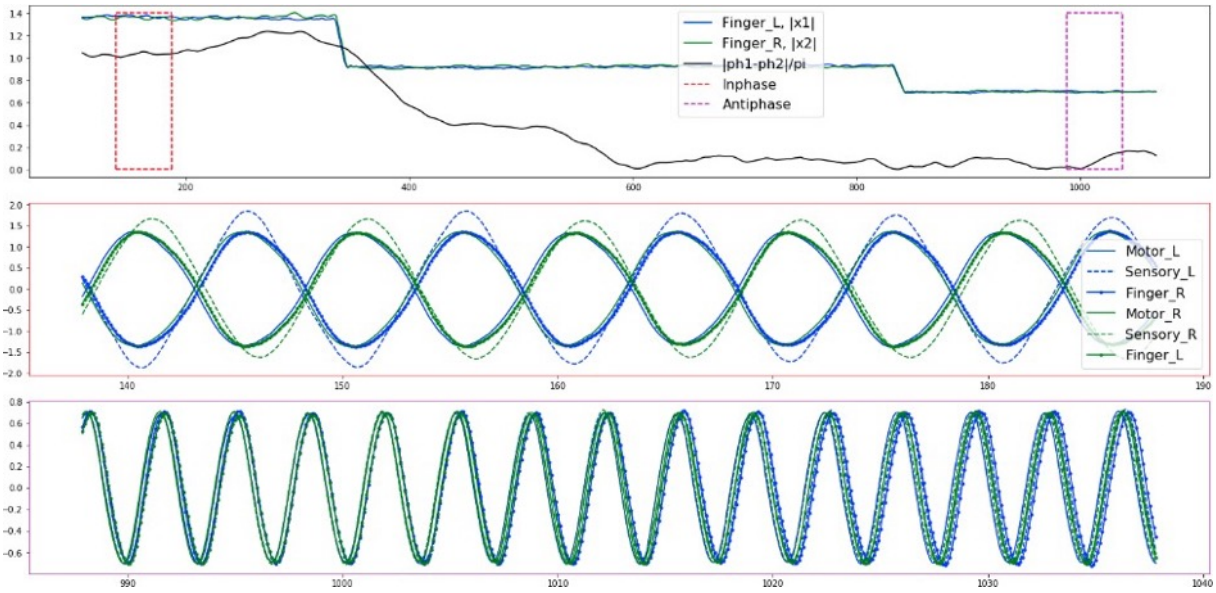

Figure 2: Model simulation. Co-simulation time series exhibiting a phase transition from an antiphase to an inphase mode. Top: Finger position amplitudes and normalized phase difference (black) for three frequency plateaus Middle (bottom): Motor and sensory cortices' activities, and finger positions (see legend for line styles) corresponding to the red (magenta) inserts of the top panel, exhibiting antiphase (inphase) synchronization, respectively. Right (left) finger circuit showed in (blue) green.

Keywords: TheVirtualBrain, Neurorobotics Platform, Gazebo, Haken-Kelso-Bunz model, bimanual coordination, phase transition, Co-Simulation, embodied brain

ACKNOWLEDGEMENTS

H2020 Research and Innovation Action Grant Human Brain Project SGA2 785907 (PR) H2020 Research and Innovation Action Grant Human Brain Project SGA3 945539 (PR)

H2020 Research and Innovation Action Grant Interactive Computing E-Infrastructure for the Human Brain Project ICEI 800858 (PR)

H2020 Research and Innovation Action Grant EOSC VirtualBrainCloud 826421 (PR) H2020 Research and Innovation Action Grant AISN 101057655 (PR)

H2020 Research Infrastructures Grant EBRAINS-PREP 101079717 (PR) H2020 European Innovation Council PHRASE 101058240 (PR)

H2020 Research Infrastructures Grant EBRAIN-Health 101058516 (PR) H2020 European Research Council Grant ERC BrainModes 683049 (PR) JPND ERA PerMed PatternCog 2522FSB904 (PR)

Berlin Institute of Health & Foundation Charité (PR) Johanna Quandt Excellence Initiative (PR)

German Research Foundation SFB 1436 (project ID 425899996) (PR)

German Research Foundation SFB 1315 (project ID 327654276) (PR) German

Research Foundation SFB 936 (project ID 178316478) (PR) German Research

Foundation SFB-TRR 295 (project ID 424778381) (PR)

German Research Foundation SPP Computational Connectomics RI 2073/6-1, RI 2073/10-2, RI 2073/9-1 (PR) Digital Europe

TEF-Health # 101100700

REFERENCES

[1] Sanz-Leon P, Knock SA, Spiegler A, Jirsa VK. Mathematical framework for large-scale brain network modeling in The Virtual Brain. *Neuroimage*. 2015;111:385-430. doi:10.1016/j.neuroimage.2015.01.002.

[2] Ritter P, Schirner M, McIntosh AR, Jirsa VK. The virtual brain integrates computational modeling and multimodal neuroimaging. *Brain connectivity*. 2013;1;3(2):121-45. doi:10.1016/j.neuroimage.2015.01.002.

[3] Falotico E, Vannucci L, Ambrosano A, Albanese U, Ulbrich S, Vasquez Tieck JC, Hinkel G et al. Connecting artificial brains to robots in a comprehensive simulation framework: the neurorobotics platform. *Frontiers in Neurorobotics. 2017*;11:2. doi: 10.3389/fnbot.2017.00002

[4| Koenig N, Howard A. Design and use paradigms for gazebo, an open-source multi-robot simulator. In *2004 IEEE/RSJ International Conference on Intelligent Robots and Systems (IROS) (IEEE Cat. No. 04CH37566)*. 2004 Sep 28 (Vol. 3, pp. 2149-2154). IEEE. doi: 10.1109/IROS.2004.1389727.

[5| Haken H, Kelso JS, Bunz H. A theoretical model of phase transitions in human hand movements. Biological cybernetics. 1985;51(5):347-56. doi: 10.1007/BF00336922.

[6| Jirsa VK, Fuchs A, Kelso JA. Connecting cortical and behavioral dynamics: bimanual coordination. *Neural Computation*. 1998;10(8):2019-45. doi: 10.1162/089976698300016954.

[7| The Virtual Brain - Neurorobotics Platform: Haken-Kelso-Bunz phase transition. Brain Modes YouTube channel. https://www.youtube.com/watch?v=9mSi1OQGj-E&ab_channel=BrainModes. Published 2023. Accessed February 7th, 2023.

[8| Banerjee A, Jirsa VK. How do neural connectivity and time delays influence bimanual coordination?. *Biological cybernetics*. 2007;96(2):265-78. doi: 10.1007/s00422-006-0114-4.

91. The Modular Science Framework: Deployment, Orchestration and Monitoring of Coupled Brain Simulations

Kim Sontheimer*[1], Muhammad Fahad[1], Rolando Inglés Chávez[1], Cristian Jiménez- Romero[1], Wouter Klijn[1], Sandra Díaz[1], Lena Oden[1,4], Abigail Morrison[1,2,3]

1 Forschungszentrum Jülich GmbH, Institute for Advanced Simulation, Jülich Supercomputing Centre (JSC), 52425 Jülich | Germany

2 Forschungszentrum Jülich, GmbH, Institute of Neuroscience and Medicine (INM-6) and Institute for Advanced Simulation (IAS-6), 52425 Jülich | Germany

3 Software Engineering, Department of Computer Science 3, RWTH Aachen University, Ahornstraße 55, 52074 Aachen | Germany

4 Fakultat fur Mathematik und Informatik, Hagen, Germany

*k.sontheimer@fz-juelich.de

INTRODUCTION/MOTIVATION

The brain is an inherently multi-scale and highly complex system. The work in the Human Brain Project (HBP) has resulted in a set of simulation engines which cover a broad spectrum of levels of description ranging from morphologically detailed to the whole brain level. While the efficient simulation at each scale is vitally important, it is not sufficient to address the rather complex research questions such as how to study the global brain behavior while depending on the local morphological details. Such research questions can be feasibly addressed by connecting the multiple simulations of different spatial and temporal scales. However, this results in complex workflows with multiple components to be executed in parallel. These workflows introduce different challenges such as deployment and resource management on HPC systems.

Here, we introduce the Modular Science (MSC) framework which addresses these challenges with a set of microservices. To execute the complex multi-scale co-simulation workflows on HPC systems, the MSC framework deploys different simulators operating across different brain scales, together with visualization, data transport and analysis tools. It provides a handle on the steering, management of the workflow execution, the overall system health and the individual application status during runtime for provenance and failure tracking. Another salient feature of the framework is its capability of monitoring the computational resource usage by individual applications in a non-invasive way and with

negligible overheads on their performance. A set of common APIs and standards are defined in order to ensure the interoperability, reusability and to smoothly integrate the MSC framework with different EBRAINS tools [3]. For example, the monitoring service can be used with any EBRAINS tool using a coupling interface complying with the API of the service.

The framework currently supports the specific examples of implementations including the two-way co-simulation workflow of The Virtual Brain (TVB) [1] and NEST [2] simulators using ELEPHANT library [4] for in transit data analysis. The following use-cases are identified as the target workflows for the Modular Science framework:

1. **Two-way coupling of NEST & TVB**: Parallel simulations of whole-brain behavior in TVB constrained by detailed local behavior in NEST of selected brain regions.
2. **NEST-Arbor co-simulation**: Enabling the description of higher-level network architecture in NEST and local behavior of selected regions in Arbor[3].
3. **In-situ infrastructure**: In-situ data analysis and visualization and common coupling infrastructure.
4. **LFPy [7] as a one-way co-simulation**: Feeding NEST spiking results into a simplified Arbor simulation producing current dipoles fed into an analysis framework to compute EEG & LFP predictions, and extension with TVB coupling.

METHODS

Architecture: Modular structure, micro-services like set of independent applications **Technology stack:** Python, Bash, XML, JSON, ZeroMQ, MPI, UNIX, PSOIX APIs **Platforms:** multi-core CPUs, HPC cluster

RESULTS AND DISCUSSION

Currently, the framework supports the deployment and the execution of use-case-1 (Two way coupling of TVB-NEST) on local systems such as laptops and the JUSUF/JUWELS supercomputers [5]. In this use- case, the Brunel-Alpha balanced network [6] is run as co-simulation with NEST and TVB, both with and without monitoring of resource usage to test the efficacy of the framework and the impact of monitoring on performance. We found that monitoring of the resources usage has no impact on the performance of the simulators. The other use-cases are currently being codeveloped and integrated in MSC. We are also aiming to run the high scaling co-simulations for different brain models available in the simulators.

Keywords: neuroscience, brain simulation, spiking neural network, coupled simulation, multi-scale, high- performance computing

ACKNOWLEDGEMENTS

This project has received funding from the European Union's Horizon 2020 research and innovation programme under grant agreement No 785907 (HBP SGA2).

This project/research has received funding from the European Union's Horizon 2020 Framework Programme for Research and Innovation under the Specific Grant Agreement No. 945539 (HBP SGA3).

This research was supported by the EBRAINS research infrastructure, funded from the European Union's Horizon 2020 Framework Programme for Research and Innovation under the Specific Grant Agreement No. 945539 (Human Brain Project SGA3).

REFERENCES

1. Sanz Leon P, Knock SA, Woodman MM, Domide L, Mersmann J, McIntosh AR and Jirsa V (2013) The Virtual Brain: a simulator of primate brain network dynamics. Front. Neuroinform. 7:10. doi: 10.3389/fninf.2013.00010
2. de Schepper, Robin, Eppler, Jochen Martin, Kurth, Anno, et al. NEST 3.2. Published online January 21, 2022. doi:10.5281/zenodo.588689
3. Ebrains (2023) Simulation, EBRAINS. Available at: https://ebrains.eu/services/simulation/#services (Accessed: February 1, 2023).
4. Denker M, Yegenoglu A, Grün S (2018) Collaborative HPC-enabled workflows on the HBP Collaboratory using the Elephant framework. Neuroinformatics 2018, P19. doi:10.12751/incf.ni2018.0019
5. Jülich Supercomputing Centre (JSC). Supercomputers. https://www.fz-juelich.de/en/ias/jsc/systems/supercomputers. Accessed February 1, 2023.
6. Brunel N, Dynamics of Sparsely Connected Networks of Excitatory and Inhibitory Spiking Neurons, Journal of Computational Neuroscience 8, 183-208 (2000)
7. Hagen E, Næss S, Ness TV and Einevoll GT (2018) Multimodal Modeling of Neural Network Activity: Computing LFP, ECoG, EEG, and MEG Signals With LFPy 2.0. Front. Neuroinform. 12:92. doi: 10.3389/fninf.2018.00092. https://dx.doi.org/10.3389/fninf.2018.00092
8. Nora Abi Akar, John Biddiscombe, Benjamin Cumming, Marko Kabic, Vasileios Karakasis, Wouter Klijn, Anne Küsters, Alexander Peyser, Stuart Yates, Thorsten Hater, Brent Huisman, Espen Hagen, Robin De Schepper, Charl Linssen, Harmen Stoppels, Sebastian Schmitt, Felix Huber, Max Engelen, Fabian Bösch, … Lennart Landsmeer. (2022). Arbor Library v0.8.1 (v0.8.1). Zenodo. https://doi.org/10.5281/zenodo.7473671

92. Cross-comparison of morphologically detailed simulators on modern CPUs and GPUs using the Brain Scaffold Builder

R. De Schepper [1] , N. Abi Akar [2] , T. Hater [3], B. F. B. Huisman [3,*] , E. D'Angelo [1,4], A. Morrison [3,5,6] , C. Casellato [1]

[1] Neurocomputational Unit, Department of Brain and Behavioral Sciences, University of Pavia, Pavia, Italy

[2] Scientific Software & Libraries, Swiss National Supercomputing Centre (CSCS), Zürich, Switzerland

[3] Simulation and Data Lab Neuroscience, Jülich Supercomputing Centre (JSC), Institute for Advanced Simulation, JARA, Forschungszentrum Jülich GmbH, Jülich, Germany

[4] IRCCS Mondino Foundation, Brain Connectivity Center, Pavia, Italy

[5] Institute of Neuroscience and Medicine (INM-6), Institute for Advanced Simulation (IAS-6), Research Centre Jülich, Jülich, Germany

[6] Department of Computer Science 3 - Software Engineering, RWTH Aachen University, Aachen, Germany

*b.huisman@fz-juelich.de

INTRODUCTION/MOTIVATION

A variety of software simulators exist for neuronal networks, and a subset of these tools allow the scientist to model neurons in high morphological detail. The scalability of such simulation tools over a wide range in neuronal networks sizes and cell complexities is predominantly limited by effective allocation of components of such simulations over computational nodes, and the overhead in communication between them. In order to have more scalable simulation software, it is important to develop a robust benchmarking strategy that allows insight into specific computational bottlenecks for models of realistic size and complexity.

METHODS

In this study, we demonstrate the use of the Brain Scaffold Builder [1] as a framework for performing such benchmarks. We perform a comparison between the well-known morphologically detailed simulator NEURON [2], and Arbor [3], a new simulation library developed within the framework of the Human Brain Project. The BSB can construct identical neuromorphological and network setups of highly spatially and biophysically detailed networks for each simulator. This ensures good coverage of feature support in each simulator, and realistic workloads. After validating the outputs of the BSB generated models, we execute the simulations on a variety of hardware configurations consisting of two types of nodes (GPU and CPU). We investigate performance of two different network models, one suited for a single machine, and one for distributed simulation. We investigate performance across different mechanisms, mechanism classes, mechanism combinations, and cell types. **RESULTS AND DISCUSSION**

Our benchmarks show that, depending on the distribution scheme deployed by Arbor, a speed-up with respect to NEURON of between 60 and 400 can be achieved. Additionally, Arbor can be up to two orders of magnitude more energy efficient.

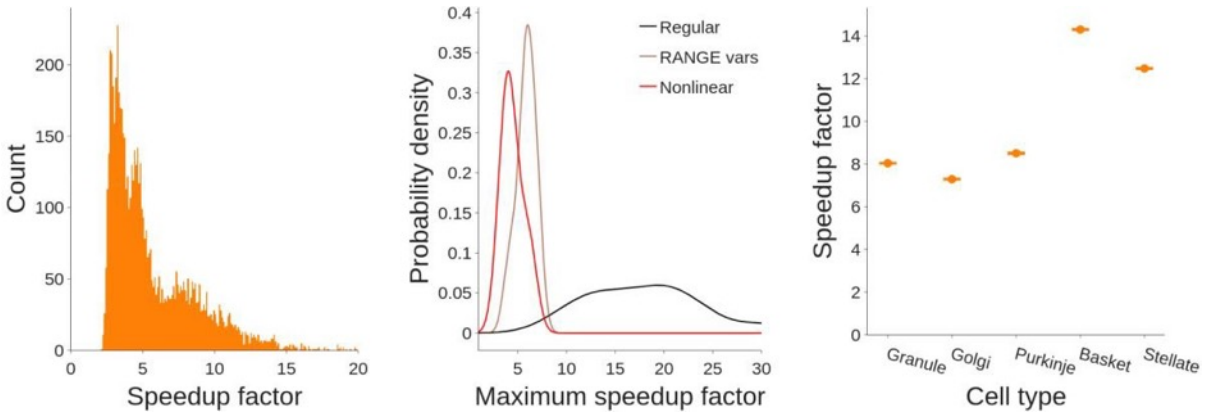

Figure 1 - Left: Histogram of the speed-up factors for Arbor with respect to NEURON of 46,939 mechanism combinations inserted in a single compartment. Each combination was repeated 10 times. The mean is used. Center: Kernel density estimates of the maximum speedup of 3 groups of mechanisms: mechanisms with nonlinear dynamics (labelled *Nonlinear*), such as cdp5, mechanisms with high amounts of RANGE variables (*RANGE vars*), and all other mechanisms lacking extraordinary NMODL features (*Regular*). Right: Comparison of the timestep duration for NEURON and Arbor to solve biological timesteps of the cerebellar single cell models.

During analysis of the mechanism benchmarks several separate distributions were observed in a multimodal distribution. Taken apart they reveal that Arbor speeds up simulation of most mechanisms between 10 to 25 times, while more specific cases with aberrant properties such as high amounts of RANGE variable declarations, or complex nonlinear dynamics, could only be sped up 5 times (Fig 1).

Simulator	Nodes	Tasks /Node	Threads /Task	GPU /Node	Time-to-solution (s)	Timestep dur. ($s_{\text{wall}}/\text{ms}_{\text{bio}}$)	Energy (kJ)
NEURON	20	36	1		17400 ± 300	16.7 ± 0.2	93000 ± 2000
Arbor	20	36	1		3600 ± 600	2.68 ± 0.05	18000 ± 1000
	20	2	18		2270 ± 20	1.99 ± 0.02	6500 ± 100
	20	2	36		2700 ± 200	2.16 ± 0.03	7500 ± 400
Arbor GPU	1	1	12	1	3560 ± 10	3.07 ± 0.01	517 ± 9
	2	1	12	1	1899 ± 6	1.53 ± 0.01	515 ± 4
	4	1	12	1	1110 ± 40	0.77	560 ± 10
	8	1	12	1	760 ± 20	0.39	680 ± 10
	12	1	12	1	590 ± 20	0.28	790 ± 20
	16	1	12	1	650 ± 50	0.28	1090 ± 50
	20	1	12	1	720 ± 80	0.28	1420 ± 110

Table 2 - Benchmark results for the large network of 30,000 cells running on multiple nodes. † corresponds to the configurations optimized for and allocated to a single socket. If no error is given, it was below the measurement threshold. Highlighting indicates the best performance in each section.

Under these realistic large-scale conditions, utilizing the full spectrum of strenuous features available in each simulator, Arbor reached speedups of x10 on CPU and x30 on GPU. This speedup is comparable to the speedup of NEURON versus CoreNEURON under similar conditions [4], and is a good, yet indirect, indication that the simulators are on par in terms of performance (Fig 2).

Acknowledgements

This research has received funding from the European Unions Horizon 2020 Framework Programme for Research and Innovation under the Specific Grant Agreement No. 720270 (Human Brain Project SGA1), Specific Grant Agreement No. 785907 (Human Brain Project SGA2), and Specific Grant Agreement No. 945539 (Human Brain Project SGA3).

Keywords: HPC, Neural Networks, Simulation, Portable Models

REFERENCES

[1] De Schepper, R., Geminiani, A., Masoli, S., Rizza, M. F., Antonietti, A., Casellato, C., et al. (2021). Scaffold modelling captures the structure-function-dynamics relationship in brain microcircuits. bioRxiv doi:10.1101/2021.07.30.454314

[2] Carnevale, N. T. and Hines, M. L. (2006). The NEURON book (Cambridge University Press)

[3] Abi Akar, N., Cumming, B., Karakasis, V., Küsters, A., Klijn, W., Peyser, A., et al. (2019). Arbor — A Morphologically-Detailed Neural Network Simulation Library for Contemporary High-Performance Computing Architectures. In 2019 27th Euromicro International Conference on Parallel, Distributed and Network-Based Processing (PDP). 274–282. doi:10.1109/EMPDP.2019.8671560

[4] Awile, O., Kumbhar, P., Cornu, N., Dura-Bernal, S., King, J. G., Lupton, O., … Schürmann, F. (2022). Modernizing the NEURON Simulator for Sustainability, Portability, and Performance. Frontiers in Neuroinformatics, 16, section 3.3.1-3.3.3 . doi:10.3389/fninf.2022.884046

93. Bridging high-level neural modelling languages and accelerated neural simulation engines

Sotirios Panagiotou*, Rene Miedema, Mario Negrello, Christos Strydis

Department of Neuroscience, Erasmus MC, Rotterdam, The Netherlands

*Correspondence: s.panagiotou@erasmusmc.nl

MOTIVATION

In the recent decades, an increasingly popular approach for the problems of neuroscience is the in-silico method [1]. This method allows exploring the behaviour of neural structures in ways that are not practical or even feasible to do experimentally.

In-silico neuroscience relies on high-performance computing to take on increasingly complex neural models, and unlock insights into the subtle behaviours that they exhibit.

Presently, computational tools for in-silico neuroscience come in two types: general-purpose neuro-simulators and model class-specific ones.

General-purpose simulators can run a rich variety of neuron models, but computational performance is limited by their generality [2].

On the other hand, specialised simulators make extreme speeds and scales of simulation possible, but they work on a specific class of neural models each [3] and their custom and highly optimised internal data formats make it difficult for end-users to customise the parameters for each run.

METHODS

We propose a methodology for making specialised simulators accessible by neuro-modellers, through the use of open data formats and some simple guidelines on how to make the simulators detect compatibility with, and run, neural models in these formats.

RESULTS AND DISCUSSION

We demonstrate our work through an adapter from the NeuroML modelling language to a high-performance reconfigurable hardware engine [4] previously developed in our lab. Performance is identical to when programming the simulator's native data format, but the engine can now readily run all NeuroML models that it can support, thanks to the adapter.

Keywords: high performance computing, simulation, in silico experiment, spiking neural networks, reconfigurable computing, accelerated computing, software, tooling, NeuroML

REFERENCES

1. Markram H, Meier K, Lippert T, et al. Introducing the Human Brain Project. Procedia Computer Science. 2011;7:39-42. doi:https://doi.org/10.1016/j.procs.2011.12.015

2. Wang RM, Thakur CS, van Schaik A. An FPGA-Based Massively Parallel Neuromorphic Cortex Simulator. Frontiers in Neuroscience. 2018;12. doi:https://doi.org/10.3389/fnins.2018.00213

3. A. Pastur-Romay L, B. Porto-Pazos A, Cedron F, Pazos A. Parallel Computing for Brain Simulation. Current Topics in Medicinal Chemistry. 2017;17(14):1646-1668. doi: https://doi.org/10.2174/1568026617666161104105725

4. Miedema R, Smaragdos G, Negrello M, Al-Ars Z, Möller M, Strydis C. flexHH: A Flexible Hardware Library for Hodgkin-Huxley-Based Neural Simulations. IEEE Access. 2020;8:121905-121919. doi:https://doi.org/10.1109/ACCESS.2020.3007019

94. Modernisation of NEURON Simulator toolchain and Deployment on EBRAINS Platforms

Ioannis Magkanaris[1*], Jorge Blanco Alonso[1*], Alexandru Săvulescu[1], Olli Lupton[1], Nicolas Cornu[1], Omar Awile[1], Christos Kotsalos[1], Matthias Wolf[1], Michael L. Hines[2], Pramod Kumbhar[1], James Gonzalo King[1]

[1] Blue Brain Project, École Polytechnique Fédérale de Lausanne (EPFL), Geneva, Switzerland
[2] Department of Neuroscience, Yale University, New Haven, CT, United States

[*]e-mail-address of corresponding authors: ioannis.magkanaris@epfl.ch, jorge.blancoalonso@epfl.ch

INTRODUCTION/MOTIVATION

NEURON is a widely-used simulation environment for computational neuroscience research. In the pursuit of simulating substantially larger and morphologically detailed neuronal circuits built within HBP, the Blue Brain Project (BBP) has been collaborating with Yale University to transform the NEURON simulator into a modern, efficient, scalable and easy-to-use framework.

METHODS

During the past 2 years, the NEURON developer community has undertaken various initiatives to future- proof the simulator. We have significantly improved NEURON's overall code organisation, testing, documentation and build system to increase the code's software sustainability. Also, we have fully integrated the CoreNEURON simulation engine within NEURON source code. Additionally, a modern source-to-source compiler (NMODL) capable of targeting both CPUs and GPUs is now available. We have introduced Python wheels for the NEURON package, easing the installation of the toolchain in various computing platforms. Finally, we have broadened the support of CoreNEURON, enabling the GPU execution of multiple publicly available NEURON models [1,2] and improved the performance of the CPU and GPU execution using the NMODL translation framework [3]. While developing all of the above we have revised the contribution practices with extensive CIs and enhanced the user and developer documentation. All these new features and improvements are made available on multiple EBRAINS platforms [4] via a Spack package manager-based [5] software deployment workflow.

RESULTS AND DISCUSSION

As part of this work, we present the performance of two large-scale models developed within HBP using different multi-CPU and multi-GPU configurations. We showcase our Spack-based deployment workflow on various HBP platforms including Piz-Daint, JUSUF and Marconi100. We also show how NEURON can be easily used on private cloud infrastructure as well as EBRAIN's collaboratory. Moving forward, we will discuss how the core data structures of NEURON are being updated with a tighter and seamless integration of CoreNEURON.

This transformation and advancement of NEURON was achieved through the joint efforts and collaboration of members of the NEURON developers group and users [6]. Since 2020, these members organise monthly meetings to discuss topics for the improvement of NEURON and better enable researchers to further their goals. We encourage others to attend to present their ideas and help drive the roadmap for future features and capabilities.

Keywords: NEURON, CoreNEURON, HBP, EBRAINS, HPC, Simulation

ACKNOWLEDGEMENTS

Research reported here was supported by the National Institute for Neurological Disorders and Stroke, the National Institute for Mental Health, and the National Institute of Biomedical Imaging and Bioengineering of the National Institutes of Health under award numbers R01NS011613, R01MH086638, and U24EB028998, National Science Foundation 1904444-1042C, New York State Spinal Cord Injury Research Board (SCIRB) DOH01-C32250GG-3450000, funding to the Blue Brain Project, a research center of the École Polytechnique Fédérale de Lausanne (EPFL), from the Swiss government's ETH Board of the Swiss Federal Institutes of Technology, the European Union's Horizon 2020 Framework Programme for Research and Innovation under the Specific Grant Agreement Nos. 785907 and 945539 (Human Brain Project SGA2 and SGA3).

REFERENCES

[1] Migliore M, Cavarretta F, Hines ML, Shepherd GM. Distributed organization of a brain microcircuit analyzed by three-dimensional modeling: The olfactory bulb. Frontiers in Computational Neuroscience. 2014;8. doi:10.3389/fncom.2014.00050

[2] Romani A, Ramaswamy S, Kàli S, et al. Simulating a hippocampus microcircuit. edX. https://www.edx.org/course/simulating-a-hippocampus-microcircuit. Updated February 1, 2023. Accessed February 1, 2023.

[3] Awile O, Kumbhar P, Cornu N, et al. Modernizing the neuron simulator for sustainability, portability, and performance. 2022. doi:10.1101/2022.03.03.482816

[4] Ebrains. A key enabler to advance brain science. EBRAINS. https://ebrains.eu/. Published January 29, 2023. Accessed February 1, 2023.

[5] BlueBrain. BlueBrain/Spack: A flexible package manager that supports multiple versions, configurations, platforms, and compilers. GitHub. https://github.com/BlueBrain/spack. Updated February 1, 2023. Accessed February 1, 2023.

[6] Neuronsimulator. Neuronsimulator/NRN: Neuron simulator. GitHub. https://github.com/neuronsimulator/nrn. Updated February 1, 2023. Accessed February 1, 2023.

95. NEST-SONATA: Fast parallel instantiation of explicitly specified large-scale neuronal network models

Nicolai Haug[1], Håkon Bakke Mørk[1], Stine Brekke Vennemo[1], Susanne Kunkel[1,2], Kael Dai[3], Anton Arkhipov[3], Hans Ekkehard Plesser[1,4*]

[1]Faculty of Science and Technology, Norwegian University of Life Sciences, Ås, Norway

[2]Neuromorphic Software Ecosystems (PGI-15), Jülich Research Centre, Jülich, Germany

[3]Allen Institute for Brain Science, Seattle, WA, USA

[4]Institute of Neuroscience and Medicine (INM-6) and Institute for Advanced Simulation (IAS-6) and JARA Institute Brain Structure-Function Relationships (INM-10), Jülich Research Centre, Jülich, Germany

* hans.ekkehard.plesser@nmbu.no

INTRODUCTION

Simulating brain-scale models requires parallel computers to provide enough memory to represent network connectivity and efficient instantiation of complex network connectivity on massively parallel computers. While scalable data structures and algorithms for storing and accessing connections in parallel are available [1 -3], efficient parallel instantiation of such networks has received less attention. Network connectivity can be defined either rule-based [4] or through explicit tabulation of connections, e.g., using the SONATA format [5]. Even for models of limited size and complexity, such as a model of the mouse cortex with more than 9 million point neurons connected by 25 billion synapses, SONATA specification files comprise nearly 500 GB of data in mostly binary format (HDF5). We present here an implementation of direct support for efficient instantiation of networks from SONATA specifications in the NEST simulator [6] as a result of the HBP NEST-SONATA infrastructure voucher.

METHODS

NEST uses a hybrid parallelization strategy combining MPI processes and OpenMP threads, representing connectivity primarily on the thread updating a connection target. Files representing large-scale networks need to be read in chunks due to memory constraints; we implement this using HDF5 hyperslabs of configurable size. Since HDF5 does not provide support for thread-parallel reading, only one thread per MPI process reads connectivity data, before all threads create connection in parallel. We explored two reading schemes:

i. Read datasets sequentially as blocks of contiguous hyperslabs. All MPI ranks thus read all connection data, even though only $1/M^{th}$ of all connections will be stored on any one of M MPI processes.

ii. Using SONATA files with connections sorted by targets and additional index tables, read on each MPI rank only hyperslabs containing data relevant for that rank. In this case, hyperslabs are not contiguous and are read in an irregular pattern.

We tested and benchmarked NEST-SONATA on three network models provided by the Allen Institute: a toy model with 300 point neurons, a mouse V1 model [7] and a yet unpublished mouse cortex model based on the Allen Mouse Brain Connectivity Atlas [8] and the Blue Brain Project's instantiation of cortical connections [9].

RESULTS AND DISCUSSION

Our implementation of SONATA support for NEST is currently under public review[1]. The implementation has been verified against BMTK [10] with the 300 point neuron and V1 models. NEST-SONATA instantiates the V1 model in about 20 seconds compared to BMTK's 80 seconds in simulations with 8 OpenMP threads on a laptop.

On an HPC system with 32 compute nodes (MPI ranks) each providing 128 CPU cores (threads; AMD EPYC Rome; JUSUF, Jülich Supercomputing Centre), using the sequential reading scheme, the mouse cortex model was instantiated in approximately 20 minutes. Performance appears to be constrained by data transfer from the supercomputer's file system. The rank-specific reading scheme performed so much worse that we could not complete any benchmarks with an acceptable use of compute time and energy. This applied for reading one hyperslab at a time as well as reading unions of hyperslabs. This result is surprising, since the rank-specific scheme should on each MPI rank read only 1/32 of the data volume read by the sequential scheme. We suspect that out-of-order reading from hyperslabs encounters performance problems in the HDF5 library.

Further acceleration of network instantiation from explicitly tabulated connections may require replacing HDF5 with data formats more suitable for efficient MPI- and thread parallel reading, e.g., based on SIONlib[2], which is already used by NEST's highly efficient parallel spike recording backend.

Keywords: Simulation, Modeling, Large-scale networks, High-performance computing, Connectome

ACKNOWLEDGEMENTS

This work has received funding from the European Union's Horizon 2020 Framework Programme for Research and Innovation under Specific Grant Agreement 945539 (HBP SGA3; HEP, NH, HBM, SBV, SK) and was supported by the Allen Institute, by the National Institute Of Biomedical Imaging And Bioengineering of the National Institutes of Health under Award Number R01EB029813, and the National Institute Of Neurological Disorders And Stroke of the National Institutes of Health under Award Numbers R01NS122742 and U24NS124001 (KD, AA). The content is solely the responsibility of the authors and does not necessarily represent the official views of the National Institutes of Health. We acknowledge the use of Fenix Infrastructure resources, which are partially funded from the European Union's Horizon 2020 research and innovation programme through the ICEI project under the grant agreement No. 800858.

REFERENCES

[1] Kunkel et al. (2014). Spiking network simulation code for petascale computers. Front. Neuroinform. 8:78. doi: 10.3389/fninf.2014.00078

[2] Ippen et al. (2017). Constructing Neuronal Network Models in Massively Parallel Environments. Front. Neuroinform. 11:30. doi: 10.3389/fninf.2017.00030

[3] Jordan et al. (2018). Extremely Scalable Spiking Neuronal Network Simulation Code: From Laptops to Exascale Computers. Front. Neuroinform. 12:2. doi: 10.3389/fninf.2018.00002

[4] Senk et al. (2022). Connectivity concepts in neuronal network modeling. PLoS Comput Biol 18(9): e1010086 doi: 10.1371/journal.pcbi.1010086

[5] Dai et al. (2020). The SONATA data format for efficient description of large-scale network models. PLoS Comput Biol 16(2): e1007696 doi: 10.1371/journal. pcbi.1007696

[6] Gewaltig & Diesmann (2007). NEST (Neural Simulation Tool) Scholarpedia 2(4):1430 doi: 10.4249/scholarpedia.1430

[1] https://github.com/nest/nest-simulator/pull/2595

[2] https://apps.fz-juelich.de/jsc/sionlib/docu

[7] Billeh et al. (2020). Systematic Integration of Structural and Functional Data into Multi-scale Models of Mouse Primary Visual Cortex. Neuron 106(3), 388–403.e18. doi: 10.1016/j.neuron.2020.01.040

[8] Oh et al. (2014). A mesoscale connectome of the mouse brain. Nature 508, 207–214. doi: 10.1038/nature13186

[9] Reimann et al. (2019). A null model of the mouse whole-neocortex micro-connectome. Nat Commun 10, 3903. doi: 10.1038/s41467-019-11630-x

[10] Dai et al. (2020) Brain Modeling ToolKit: An open source software suite for multiscale modeling of brain circuits. PLoS Comput Biol 16(11): e1008386. doi: 10.1371/journal.pcbi.1008386

96. Enabling Multiscale In-Transit Processing Through Insite Pipeline

Marcel Krüger[1*], Torsten W. Kuhlen[1], Tim Gerrits[1], Benjamin Weyers[2]

[1]Visual Computing Institute, RWTH Aachen University, Aachen, Germany

[2]Human-Computer Interaction, University of Trier, Trier, Germany

*krueger@vis.rwth-aachen.de

INTRODUCTION/MOTIVATION

Simulation of neuronal networks has steadily advanced and now allows for larger and more complex models. However, scaling simulations to such sizes comes with issues and challenges.

Especially the amount of data produced, as well as the runtime of the simulation can be demanding.

Often, it is not even possible to store all data on disk, and users might have to wait for a long time until they can process the data.

A standard solution in simulation science is to use in-transit approaches [8].

In-transit implementations allow users to access data while the simulation is still running and do processing in parallel outside of the simulation.

This allows for early insights into the results, early stopping of simulations that are not promising, or even steering of the simulations.

Existing in-transit solutions, however, are often complex to integrate into the workflow as they rely on integration into simulators and often use data formats that are complex to handle.

This is constraining in the context of multi-disciplinary research conducted in the HBP as such an important feature should be accessible to all users.

Especially domain scientists from neuroscience and visualization providers should be able to leverage in-transit processing.

To remedy this, we developed Insite [1,2], a pipeline that allows easy in-transit access to simulation data of multiscale simulations conducted with TVB [6], NEST [4], and Arbor[5].

METHODS

Insite is designed around providing users with an interface that is easy to integrate into existing workflows and tools.

Two achieve this, Insite uses a modular and tiered architecture consisting of simulator modules and a central access node.

The simulator modules are provided for TVB, NEST, and Arbor and are responsible for collecting the raw data from the simulation and providing them to the access node.
Simulator modules are designed to be as unintrusive as possible and easy for all users to integrate into existing simulation scripts.

The access node acts as a single point of contact for users and provides the data of all simulators and simulator instances from a single source.
Insite allows access to the data via two paradigms.
A push-oriented paradigm via WebSockets where the user gets new data pushed into their application whenever new data is available.
Secondly, users can use a pull-based approach based on an HTTP REST API to query data on demand.

The data returned in both cases can either be encoded as JSON or flatbuffers. JSON
offers a human-readable representation with broad support.
Flatbuffer's binary encoding provides a more performant alternative to JSON.
By offering these standard protocols and data formats, users can easily use the Insite Pipeline in various programming languages and technologies, as plenty of libraries for this are available.

The API provides a variety of parameters that can be used to filter the data making accessing of the data as easy as possible.

Thus, making it easy for users to access the data for further processing like analysis or visualization. RESULTS AND DISCUSSION
With a focus on ease-of-integration and ease-of-use, Insite is accessible to many developers and users.
The Pipeline was successfully integrated into the ViSimpl Visualization Tool [3] and NEST Desktop[7] to add in- transit capabilities, allowing users to get early feedback on their simulations.
Due to the design of Insite, both tools could integrate it into their desktop- and web applications.
Especially considering the emerging eco-system of web-based solutions in the context of EBRAINS, Insite provides a big advantage over classical in-situ/in-transit approaches.
The modular architecture additionally allows extending the access node to provide more data, e.g., metrics or pre- processed data from other sources.
Thus, Insite enriches the capabilities of the computational neuroscience community.

Keywords: in-transit, in-situ, simulation, visualization, computational science, multiscale simulation

ACKNOWLEDGEMENTS
We would like to thank Simon Oehrl, Jan Müller and Ali C. Demiralp for his contribution to the design and implementation of Insite.

This project/research has received funding from the European Union's Horizon 2020 Framework Programme for Research and Innovation under the Specific Grant Agreement No. 945539 (Human Brain Project SGA3) and Specific Grant Agreement No. 785907 (Human Brain Project SGA2).

REFERENCES

[1] Krüger, M. et al. (2022). Insite: A Pipeline Enabling In-Transit Visualization and Analysis for Neuronal Network Simulations. In: Anzt, H., Bienz, A., Luszczek, P., Baboulin, M. (eds) High Performance Computing. ISC High Performance 2022 International Workshops. ISC High Performance 2022. Lecture Notes in Computer Science, vol 13387. Springer, Cham. https://doi.org/10.1007/978-3-031-23220-6_20

[2] Oehrl, S. et al. (2018). Streaming Live Neuronal Simulation Data into Visualization and Analysis. In: Yokota, R., Weiland, M., Shalf, J., Alam, S. (eds) High Performance Computing. ISC High Performance 2018. Lecture Notes in Computer Science(), vol 11203. Springer, Cham. https://doi.org/10.1007/978-3-030-02465-9_18

[3] Galindo, S. E., Toharia, P., Robles, O. D., & Pastor, L. (2016). ViSimpl: multi-view visual analysis of brain simulation data. Frontiers in Neuroinformatics, 10, 44.

[4] Marc-Oliver Gewaltig, & Markus Diesmann (2007). NEST (NEural Simulation Tool). Scholarpedia, 2(4), 1430.

[5] Nora Abi Akar, John Biddiscombe, Benjamin Cumming, Marko Kabic, Vasileios Karakasis, Wouter Klijn, Anne Küsters, Alexander Peyser, Stuart Yates, Thorsten Hater, Brent Huisman, Espen Hagen, Robin De Schepper, Charl Linssen, Harmen Stoppels, Sebastian Schmitt, Felix Huber, Max Engelen, Fabian Bösch, … Lennart Landsmeer. (2022). Arbor Library v0.8.1 (v0.8.1). Zenodo. https://doi.org/10.5281/zenodo.7473671

[6] P. Sanz Leon, S. A. Knock, M. Woodman, L. Domide, J. Mersmann, A. R. McIntosh, V. Jirsa The Virtual Brain: a simulator of primate brain network dynamics
Frontiers in Neuroinformatics 7:10. doi: 10.3389/fninf.2013.00010

[7] Jens Buchertseifer, Sebastian Spreizer, & Benjamin Weyers. (2022). NEST Desktop (v3.1.1). Zenodo. https://doi.org/10.5281/zenodo.6320318

[8] Bennett, J. C., Abbasi, H., Bremer, P. T., Grout, R., Gyulassy, A., Jin, T., … & Chen, J. (2012, November). Combining in-situ and in-transit processing to enable extreme-scale scientific analysis. In SC'12: Proceedings of the International Conference on High Performance Computing, Networking, Storage and Analysis (pp. 1-9). IEEE. DOI: 10.1109/SC.2012.31

97. Brain stimulation effects on seizure dynamics through whole brain modeling for drug-resistant epilepsy

Borana Dollomaja[a], Flavius Bratu[b], Julia Makhalova[a,b], Fabrice Bartolomei[a,b], Huifang Wang[a], Viktor Jirsa[a]*

[a] Aix-Marseille Université, Inserm, INS UMR_1106, Marseille, France
[b] APHM, Timone Hospital, Epileptology and Cerebral Rhythmology, Marseille, France
** borana.dollomaja@univ-amu.fr*

INTRODUCTION/MOTIVATION

The main treatment option for drug-resistant epilepsy patients is resective surgery, with a failure rate of about 50%. Prior to surgery, brain stimulation is applied through invasive-EEG electrodes for functionality mapping of candidate regions. It is also used to delineate the epileptogenic zone by inducing seizures. Clinicians stimulate using an empirical approach which costs an amount of time with patients' additional suffering. Most stimulation parameters do not induce seizures or generate functional effects. We aim to find optimal stimulation parameters that induce seizures through a personalized modeling approach.

METHODS

We virtualized 5 drug-resistant epilepsy patients which have undergone surgery (3 male, 2 female, age 33±14, Engel class I/II). These patients had spontaneous seizures, stimulated seizures and interictal recordings. We build personalized whole-brain models based on patient- specific MRI, diffusive-MRI and CT-scan[1]. To simulate brain activity, we use the Epileptor[2] model which captures seizure dynamics. We extended this model for brain stimulation effects on seizure onset.

Based on theories of reduced resilience of the epileptogenic zone [3,4] and studies which relate the increase in spike frequency and oscillations when an external perturbation is applied to heightened excitability [5,6], we studied parameters in the Epileptor which influence the dynamics of the seizure-like state, in particular, the parameter *m* [7]. We hypothesized that, for stimulation induced seizure, a build-up of ion imbalances reaches a seizure threshold followed by an epileptic seizure. This has also been shown experimentally [8,9,10], however there is no consensus on the precise biophysical mechanism of ion exchanges that lead to seizure onset. We modified the equations by converting the phenomenological parameter *m* to a variable, which accumulates the ionic imbalance effects from the external stimulus. This accumulation when reaching a defined seizure threshold, destabilizes the system by pushing it into a seizure-like state. By modeling the effects of stimulation parameters applied clinically, we study its effects on network dynamics.

RESULTS AND DISCUSSION

We validated our model against empirical recordings where brain stimulation was applied. For personalized whole-brain network models, we generate different seizure dynamics by changing only stimulation parameters. We compared the spatio-temporal patterns of simulated-SEEG

signals against empirical data. After validating the personalized whole-brain models, we designed the optimized stimulation parameters. These parameters include: stimulation site, stimulation amplitude, brain connectivity, brain state.

The personalized whole-brain network models can simulate brain stimulation and help better understand the effects of brain stimulation for epilepsy diagnosis. In addition, we introduced the optimization methods for stimulation parameters.

REFERENCES

1. Wang, H. E. *et al.* Delineating epileptogenic networks using brain imaging data and personalized modeling in drug-resistant epilepsy. *Sci. Transl. Med.* **15**, eabp8982 (2023).
2. Jirsa, V. K., Stacey, W. C., Quilichini, P. P., Ivanov, A. I. & Bernard, C. On the nature of seizure dynamics. *Brain* **137**, 2210–2230 (2014).
3. Chang, W.-C. *et al.* Loss of neuronal network resilience precedes seizures and determines the ictogenic nature of interictal synaptic perturbations. *Nat. Neurosci.* **21**, 1742– 1752 (2018), https://doi.org/10.1038/s41593-018-0278-y.
4. Rich, S., Moradi Chameh, H., Lefebvre, J. & Valiante, T. A. Loss of neuronal heterogeneity in epileptogenic human tissue impairs network resilience to sudden changes in synchrony. *Cell Rep.* **39**, 110863 (2022), https://doi.org/10.1016/j.celrep.2022.110863.
5. Valentin, A. Responses to single pulse electrical stimulation identify epileptogenesis in the human brain in vivo. *Brain* **125**, 1709–1718 (2002), https://doi.org/10.1093/brain/awf187.
6. Valentín, A. *et al.* Single pulse electrical stimulation for identification of structural abnormalities and prediction of seizure outcome after epilepsy surgery: a prospective study. *Lancet Neurol.* **4**, 718–726 (2005), https://doi.org/10.1016/S1474-4422(05)70200-3.
7. Houssaini, K. E., Bernard, C. & Jirsa, V. K. The Epileptor model: a systematic mathematical analysis linked to the dynamics of seizures, refractory status epilepticus and depolarization block. *eNeuro* (2020) doi:10.1523/ENEURO.0485-18.2019.
8. FRÖHLICH, F., BAZHENOV, M., IRAGUI-MADOZ, V. & SEJNOWSKI, T. J. Potassium Dynamics in the Epileptic Cortex: New Insights on an Old Topic. *Neurosci. Rev. J. Bringing Neurobiol. Neurol. Psychiatry* **14**, 422–433 (2008), DOI: 10.1177/1073858408317955.
9. Lillis, K. P., Kramer, M. A., Mertz, J., Staley, K. J. & White, J. A. Pyramidal cells accumulate chloride at seizure onset. *Neurobiol. Dis.* **47**, 358–366 (2012), https://doi.org/10.1016/j.nbd.2012.05.016.
10. Graham, R. T. *et al.* Synergistic positive feedback underlying seizure initiation. 2021.02.28.433224 Preprint at https://doi.org/10.1101/2021.02.28.433224 (2021), https://doi.org/10.1177/15357597221127163.

98. Personalized whole brain network modelling on virtual epilepsy surgery

Huifang E Wang[1]*, Julia Makhalova[2,3,4] , Paul Triebkorn[1], Fabrice Bartolomei[1,2], Viktor Jirsa[1]*

[1]Aix Marseille Université, Institut National de la Santé et de la Recherche Médicale, Institut de Neurosciences des Systèmes (INS) UMR1106; Marseille 13005, France
[2]APHM, Epileptology and Clinical Neurophysiology Department, Timone Hospital; Marseille, 13005, France
[3]Aix Marseille Univ, CNRS, CRMBM ; Marseille, 13005, France
[4] APHM, Timone University Hospital, CEMEREM ; Marseille, 13005, France

*e-mail-address of corresponding author(s):

*Huifang E Wang: huyfang.wang@univ-amu.fr
Viktor Jirsa: viktor.jirsa@univ-amu.fr

INTRODUCTION/MOTIVATION

We aim to use a personalized whole brain network modelling method to aid clinicians in planning surgical interventions for patients with drug-resistant focal epilepsy.

METHODS

For each epilepsy patient, we built a patient's specific whole brain network model. The structural scaffold of the patient-specific whole-brain network model is constructed from anatomical T1 and diffusion-weighted magnetic resonance imaging. Bayesian inference methods sample and optimize key parameters of the personalized model using functional stereoelectroencephalography recordings of patients' seizures. These key parameters determine a given patient's personalized model [1]. We performed virtual resection on this patient's personalized models based on the sampling results of Bayesian inference. We compared the results of virtual resection surgery with the outcome of the real surgery. We also introduced an optimization method for surgical strategies.

RESULTS AND DISCUSSION

We gave three patients examples of performing virtual surgery using different clinical hypotheses and real surgery as well. Then we used optimization methods for the surgical strategies. We performed the virtual surgery workflow retrospectively using 40 patients with drug-resistant focal epilepsy. These 40 patients had epilepsy surgery with at least one-year follow-up outcome. We performed the virtual surgery and compared it with the real surgery, which was consistent with the outcome prediction. Based on the personalized whole brain network modelling, we optimized the best surgery strategy. For each patient, we rank the different surgical strategies by the statistical metrics.

Personalized whole brain network modelling can make a prediction on the outcome of surgery and is able to suggest the surgical strategies by ranking the statistical metrics.

Keywords:

Network modelling, Personalised whole brain network modelling, Virtual surgery, Epilepsy

ACKNOWLEDGEMENTS

This work is partially funded through the European Union's Horizon 2020 Framework Programme for Research and Innovation under the Specific Grant Agreement No. 945539 (Human Brain Project SGA3); This work is partially funded through the French National Research Agency (ANR) as part of the second "Investissements d'Avenir" program (ANR-17-RHUS-0004, EPINOV).

REFERENCES

[1] Wang, H. E., Woodman, M., Triebkorn, P., Lemarechal, J.-D., Jha, J., Dollomaja, B., Vattikonda, A. N., Sip, V., Medina Villalon, S., Hashemi, M., Guye, M., Makhalova, J., Bartolomei, F., & Jirsa, V. (2023). Delineating epileptogenic networks using brain imaging data and personalized modeling in drug-resistant epilepsy. Science Translational Medicine, 15(680). https://doi.org/10.1126/scitranslmed.abp8982

99. A Simulation Based Fractal Feature Paradigm for capturing evolution of Interictal activities

Swati BANERJEE[1,2*], Viktor JIRSA[2]

[1]Laboratoire des Interfaces Sensorielles et Ambiantes, Institut LIST, Commissariat à l'énergie atomique et aux énergies alternatives (CEA), Gif-sur-Yvette Cedex, France.
Theoretical Neuroscience Group, Institut De Neurosciences Des Systémes, Faculté de Medécine, Aix-Marseille Université

*swatibanerjee@cea.fr

INTRODUCTION/MOTIVATION:

Epilepsy is one of the most common severe neurological dis- order characterized by likelihood for the brain to enter seizure states [1]. Prompt and efficient treatment often requires a prior knowledge or predictability, when and where seizures are likely to occur. Developing prediction strategies is extremely challenging due to the patient-specific causes of seizures, and the difficulty in obtaining data from longitudinal study. Interictal spikes(IS) are observed in 1% of non-epileptic population and around 70 to 90 % of epileptic subjects before and after seizure. The interictal discharges are often observed transient changes translating as spikes captured through the sEEG implants before the onset of seizure. The spikes are usually distinguishable as prominent sharp amplitude feature occuring for a short duration of time.

METHOD:

The cause of source level activation pattern and the associated physiological changes is often not known. In this work we attempt to understand the underlying physiological phenomenon using the epileptor model [2, 3]. An extension of this model to connect the epileptic state with the resting state is developed in [4]. The aim is to capture the bursting phenomenon at the source level through the model and translating up to the sensor level i.e at the sEEG level. A relative comparison gives an insight and understanding of the co-activation pattern of the brain regions recruited during an occurrence of seizure in an epileptic brain. To do so it becomes essential to learn more about the evolution and transition of the system from interictal or spiking state to a fully evolved seizure or epileptic state. In this work we tried to quantify the phenomenon using a fractal feature over the LFP network. The simulations were done using the neuro informatic platform The virtual brain (http://www.thevirtualbrain.org). Anatomical MRI data preprocessing and structural reconstruction was performed us- ing an in house pipeline for automatic processing of multimodal neuroimaging data based on publicly available neuro-imaging tools being customized for TVB (https://github.com/the-virtual-brain/tvb-recon) [5]. The connectome

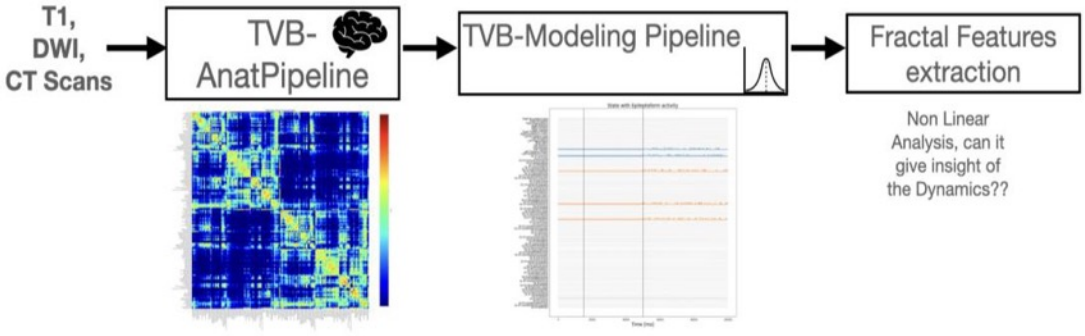

Fig 1: TVB based processing and analysis pipeline.

was obtained using the Virtual Epileptic Patient (VEP) parcellation scheme. Once the connectome is obtained the spiking phenomenon at the source level is being simulated using the model described in [4]. This is followed by estimation of a fractal features namely Higguchi Fractal Dimension (HFD). The complete pipeline as shown in Fig 1 summarizes the schema of current work.

RESULTS AND DISCUSSION:

Fractals dimensions of Dynamical Systems:

Fractals are sets that exhibit self similarity in all levels of magnification and they have noninteger dimension that is typical of strange attractors. Roughly speaking, self similarity means that a set remains qualitatively similar in its spatial characteristics under contraction or magnification. The simplest (first order) geometric property of a fractal is usually measured by its fractal dimen- sion, also called the capacity dimension. Thus fractal based analysis can give us more insight about a systems transition from one state to another. In our case which is the switch from Interictal state identified by Interictal Discharges to Epileptic seizure state. Here we have shown in Fig 2, the evolution of the features using Higuchi Fractal Dimension(HFD), which in turn gives us a predictability of the hidden repertoire in the system.

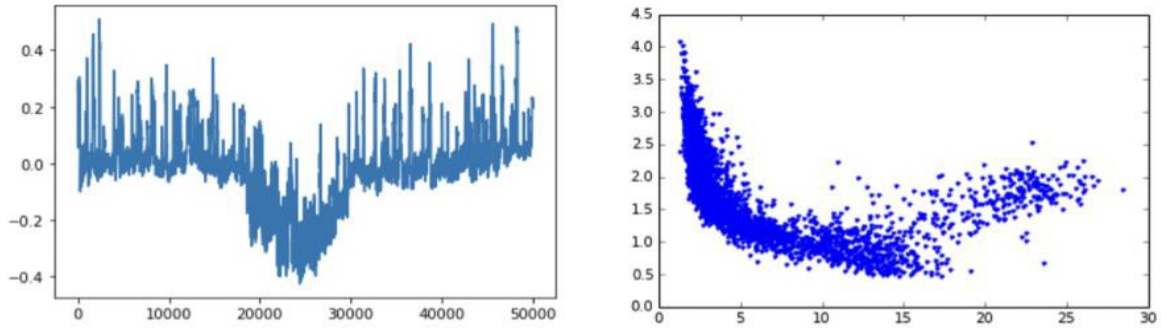

Figure 2: The Left figure shows: A simulated Interictal Discharge in the Interic- tal Zone followed by an Epileptic Seizure. The right figure shows the evolution of the HDF parameter when measured over a 50 sec simulation with a 50 msec epoch.

Keywords: Epilepsy, Whole brain network simulation, Fractals, Clinical features.

ACKNOWLEDGEMENTS: Funding received from HBP and INSERM are thankfully acknowledged.

REFERENCES

[1] Duncan JS, Sander JW, Sisodiya SM, Walker MC., “Adult epilepsy. Lancet. 2006 Apr 1;367(9516):1087-1100. doi: 10.1016/S0140- 6736(06)68477-8. PMID: 16581409.

[2] Jirsa VK, Stacey WC, Quilichini PP, Ivanov AI, Bernard C, “On the nature of seizure dynamics.," Brain 137:2210–2230, 2014.

[3] El Houssaini K, Bernard C, Jirsa VK. The Epileptor Model: A Systematic Mathematical Analysis Linked to the Dynamics of Seizures, Refractory Status Epilepticus, and Depolarization Block. eNeuro. 2020;7(2):ENEURO.0485-18.2019. Published 2020 Mar 24. doi:10.1523/ENEURO.0485-18.2019.

[4] Courtiol Julie, Guye Maxime, Bartolomei Fabrice, Petkoski Spase and Jirsa VK, “Dynamical Mechanisms of Interictal Resting-State Func- tional Connectivity in Epilepsy,", Journal of Neuroscience, 40 (29) 5572- 5588, 15 July 2020.

[5] Proix T, Spiegler A, Schirner M, Rothmeier S, Ritter P, Jirsa VK (2016), “How do parcellation size and short-range connectivity affect dynamics in large-scale brain network models?”, Neuroimage 142:135–149.

100. Multiscale Co-Simulation of TheVirtualBrain with NEST, ANNachy and NetPyNE (NEURON) spiking networks

Dionysios Perdikis[1*], Valeriy Bragin[1,2], André Blickensdörfer[1], Lia Domide[3], Michael Schirner[1], Salvador Dura-Bernal[2], Petra Ritter[1]

[1]Brain Simulation Section, Berlin Institute of Health & Department of Neurology with Experimental Neurology at Charité—Universitätsmedizin, Berlin, Germany

[2] Physiology and Pharmacology Department, State University of New York (SUNY) Downstate Health Sciences University, New York, USA

[3]Codemart, Cluj-Napoca, Romania

*dionysios.perdikis@bih-charite.de

INTRODUCTION

TheVirtualBrain (TVB) [1] is a state-of-the art computational framework for modelling and simulating whole brain dynamics at the coarse level of large-scale networks, which allows for the integration of structural (structural and diffusion MRI) and functional (BOLD/fMRI/PET, EEG/MEG/SEEG/iEEG) neuroimaging data [2]. TVB dynamics results from interactions among network nodes, either whole brain regions or local patches of neural tissue on the surface of brain's grey matter, which are modelled by neural mass population models. Spiking neural network simulators aim at modelling and simulating specific systems or circuits of the brain at a much finer scale, using neuronal models, either point (as for NEST [3] and ANNarchy [4] simulators), or multicompartmental (as for NEURON [5] and its network-building python interface, NetPyNE [6]) as their elementary modelling and computational units, generating spiking dynamics. We introduce TVB-multiscale [7], a new Python toolbox for Co-Simulation of TVB with all three of the above spiking simulators, which facilitates the implementation in a unified and user-friendly manner of so-called interfaces, i.e., data transformations and exchanges between the large-scale activity of the whole brain, as modelled in TVB, and neuronal networks extending on several brain regions.

METHODS

TVB and spiking network models are interfaced at the mesoscale of neuronal population dynamics, as the state variables of the TVB neural mass models capture the average dynamics of neuronal population activity, and statistical averages of the same activity are computed from spiking neural networks. A mapping is formed between TVB state variables and populations modelled as spiking networks, to which a label of the brain region of the TVB network, where they reside, is assigned. Interfaces are implemented in a modular architecture consisting of (a) "transformer" classes for converting average population activity (usually spiking firing rate, as well as current or voltage), to total individual neuronal activity (e.g., spike trains) and vice-versa, employing the software Elephant

[8], (b) “communicator” classes for exchanging data between simulators and transformers, and (c) “TVB proxy” nodes that represent TVB brain regions withing the spiking network. “TVB proxies” act either as stimulating devices, which mimic the transformed dynamical activity of TVB model state variables and couple to target neuronal populations (Figure 1), or as devices, which record the activity of spiking neuronal populations to update

- by overwriting - the respective TVB state variables of the brain region where they reside (Figure 2).

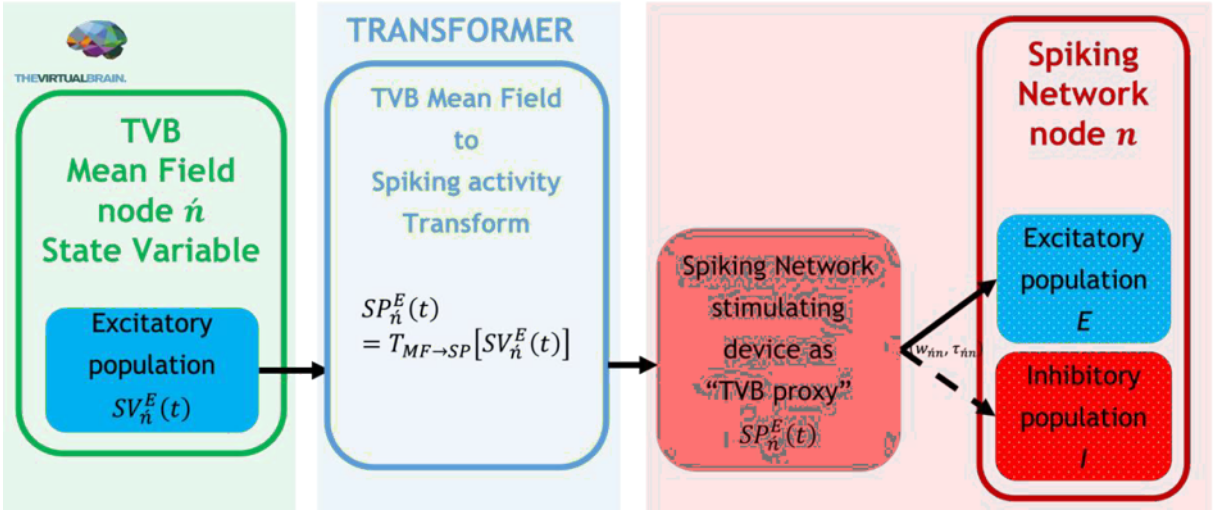

Figure 1. TVB to spiking network coupling.

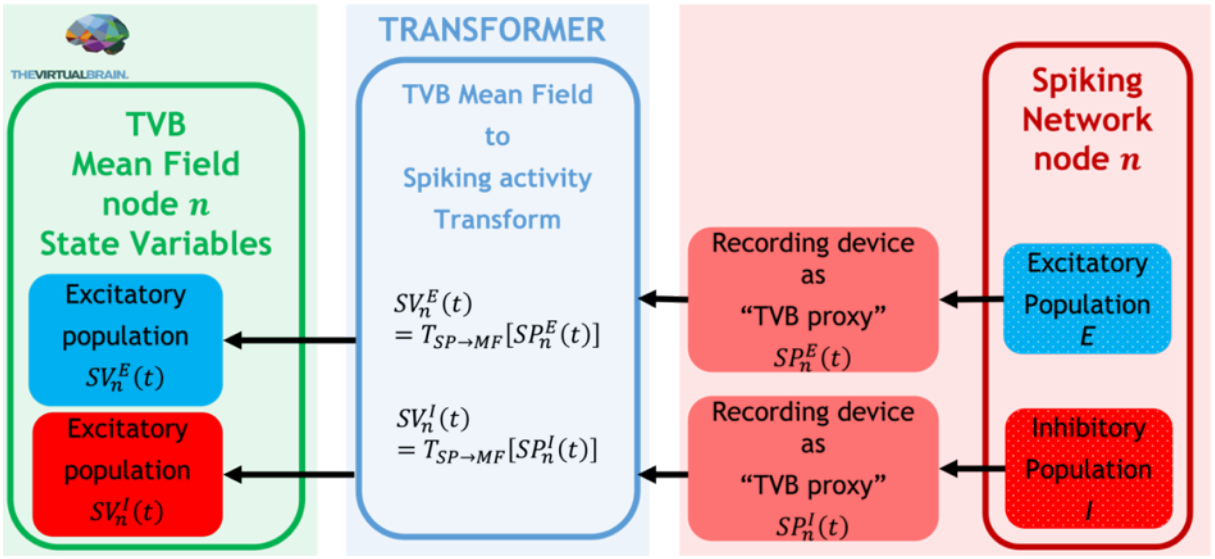

Figure 2. Spiking network to TVB update.

RESULTS AND DISCUSSION

TVB-multiscale opens the possibility for computational studies, in which a specific neural system that is the focus of the scientific inquiry is embedded into a biologically realistic spatio-temporal whole brain context and interacts

with it. TVB provides input to the spiking network differentiated in terms of dynamics (e.g., frequency content) and/or the source brain region, this input is processed by the spiking network implementing functions beyond the complexity and specificity of the TVB neural mass models, and then the output of the spiking network feeds back to the rest of TVB affecting the global brain dynamics. It has already been used to integrate TVB e.g., with an ANNarchy spiking model of basal ganglia for virtual Deep Brain Simulation modelling [9], or with a NEST spiking network model of the cerebellum in a study of sensorimotor integration of freely whisking mice [10]. Ongoing studies model thalamocortical networks using TVB with NetPyNE Co-Simulation. Such use cases further validate the implemented interfaces with neuroimaging and spiking data. Future software development will improve the computational efficiency of Co-Simulation, test (unit and integration) coverage, and documentation.

Keywords: TheVirtualBrain, NEST, ANNarchy, NetPyNE, NEURON, Co-Simulation, brain network models, spiking neural networks, Python, scientific software

ACKNOWLEDGEMENTS

H2020 Research and Innovation Action Grant Human Brain Project SGA2 785907 (PR) H2020 Research and Innovation Action Grant Human Brain Project SGA3 945539 (PR)
H2020 Research and Innovation Action Grant Interactive Computing E-Infrastructure for the Human Brain Project ICEI 800858 (PR)
H2020 Research and Innovation Action Grant EOSC VirtualBrainCloud 826421 (PR) H2020 Research and Innovation Action Grant AISN 101057655 (PR)
H2020 Research Infrastructures Grant EBRAINS-PREP 101079717 (PR) H2020 European Innovation Council PHRASE 101058240 (PR)
H2020 Research Infrastructures Grant EBRAIN-Health 101058516 (PR) H2020 European Research Council Grant ERC BrainModes 683049 (PR) JPND ERA PerMed PatternCog 2522FSB904 (PR)
Berlin Institute of Health & Foundation Charité (PR) Johanna Quandt Excellence Initiative (PR)
German Research Foundation SFB 1436 (project ID 425899996) (PR) German Research Foundation SFB 1315 (project ID 327654276) (PR) German Research Foundation SFB 936 (project ID 178316478) (PR) German Research Foundation SFB-TRR 295 (project ID 424778381) (PR)
German Research Foundation SPP Computational Connectomics RI 2073/6-1, RI 2073/10-2, RI 2073/9-1 (PR) Digital Europe TEF-Health # 101100700
National Institutes of Health (NIH) NIBIB Grant # U24EB028998

REFERENCES

[1] Sanz-Leon P, Knock SA, Spiegler A, Jirsa VK. Mathematical framework for large-scale brain network modeling in The Virtual Brain. *Neuroimage*. 2015;111:385-430. doi:10.1016/j.neuroimage.2015.01.002.

[2] Ritter P, Schirner M, McIntosh AR, Jirsa VK. The virtual brain integrates computational modeling and multimodal neuroimaging. *Brain connectivity*. 2013;1;3(2):121-45. doi:10.1016/j.neuroimage.2015.01.002.

[3] Spreizer S, Mitchell J, Jordan J, Wybo W, Kurth A, Vennemo SB, Pronold J, Trensch G, Benelhedi MA, Terhorst D, Eppler JM, Mørk H, Linssen C, Senk J, Lober M, Morrison A, Graber S, Kunkel S, Gutzen R, Plesser HE. NEST 3.3 (3.3). Zenodo. 2022. doi:10.5281/zenodo.6368024.

[4| Vitay J, Dinkelbach HÜ, Hamker FH. ANNarchy: a code generation approach to neural simulations on parallel hardware. *Frontiers in Neuroinformatics*. 2015; 9:19. DOI:10.3389/fninf.2015.00019.

[5| Carnevale, NT, Hines, ML. *The NEURON Book*. Cambridge, UK: Cambridge University Press; 2006. doi:10.1017/CBO9780511541612.

[6| Dura-Bernal S, Suter BA, Gleeson P, Cantarelli M, Quintana A, Rodriguez F, Kedziora DJ, Chadderdon GL, Kerr CC, Neymotin SA, McDougal RA. NetPyNE, a tool for data-driven multiscale modeling of brain circuits. *Elife*. 2019;e44494. doi: 10.7554/eLife.44494.002.

[7| Co-Simulation The Virtual Brain Multiscale. Dedicated EBRAINS Collaboratory page with many relavant resources (GIthub, Dockerhub, EBRAINS app). wiki.ebrains.eu/bin/view/Collabs/the-virtual-brain- multiscale.

[8| Denker M, Yegenoglu A, Grün S. Collaborative HPC-enabled workflows on the HBP Collaboratory using the Elephant framework. *Neuroinformatics*. 2018;P19. doi:10.12751/incf.ni2018.0019.

[9| Meier JM, Perdikis D, Blickensdörfer A, Stefanovski L, Liu Q, Maith O, Dinkelbach HÜ, Baladron J, Hamker FH, Ritter P. Virtual deep brain stimulation: Multiscale co-simulation of a spiking basal ganglia model and a whole-brain mean-field model with the virtual brain. *Experimental Neurology*. 2022;13:114111. doi: 10.1016/j.expneurol.2022.114111.

[10| Meier JM, Geminiani A, Perdikis D, Ouertani S, Cassellato C, Ritter P, D'Angelo E. Detailed cerebellar models in whole-brain multiscale cosimulations offer perspective on sensori-motor integration. Bernstein Conference 2022; doi: 10.12751/nncn.bc2022.073.

101. Latest developments in the electrical model building toolset

Aurélien Jaquier[1*], Tanguy Damart[1], Lukas Drescher[2], Thorsten Hater[3], Brent Huisman[3], Anil Tuncel[1], Henry Markram[1], and Werner Van Geit[1]

[1] Blue Brain Project, École polytechnique fédérale de Lausanne (EPFL), Campus Biotech, 1202 Geneva, Switzerland

[2] CSCS - Swiss National Supercomputing Centre and ETHZ - Eidgenössische Technische Hochschule Zürich, Switzerland

[3] JSC - Jülich Supercomputing Centre, Forschungszentrum Jülich, Germany

* aurelien.jaquier@epfl.ch

INTRODUCTION

Computational electrical models of biologically detailed cells are valuable to understand the underlying electrophysiological dynamics of the neurons. They can be used in circuit models or for *in silico* experimentation in ways that are today impossible with an *in vitro* cell, and thus expand our understanding of the internal dynamics of neurons.

To build an electrophysiological model using the toolset described here, first electrical features are extracted from experimental traces of the required cell type. Then an evolutionary algorithm is used to adjust the ion channel parameters to fit the *in silico* features to the features extracted from the experimental traces.

A challenge that the computational neuroscientist faces is the sharing of models with other neuroscientists. Multiple tools, formats and standards are used in the field, and using a model from a team that does not use the same standard can be a time-consuming hurdle.

METHODS

The electrical model building toolset consists of 4 software packages designed for electrical model building: eFel, BluePyEfe[1], BluePyOpt[2] and BluePyMM.

eFel is a tool to compute features from electrophysiological trace data.

BluePyEfe is a tool to extract mean and standard deviations values for features from experimental voltage traces. Its latest features include: more robustness to noisy data, allowing it to skip feature values that could not be extracted from the trace, the ability to automatically detect the begin and end time of step stimuli from experimental trace data when they are not provided, and the ability to use current injection stimuli other than step stimuli.

BluePyOpt is a tool to optimize the electrophysiological parameters of a cell using an evolutionary algorithm, aiming to reproduce the experimental features extracted by BluePyEfe.
Developing e-models can take a lot of time and computing resources. Therefore, these models are not reoptimized for every morphology in the circuit model. Instead, we test if an existing e-model matches that particular morphology 'well enough' using the BluePyMM software.

RESULTS

To make electrical models easier to use by the community, BluePyOpt can now export optimized cells using the NeuroML2 format [3], and those cells were able to produce traces similar to the ones produced using BluePyOpt.

The traditional optimization method used in the BluePyOpt package is the Indicator Based Evolutionary Algorithm (IBEA). We have recently added an alternative method, Covariance Matrix Adaptation (CMA). Both a single- and multi-objective version of this algorithm is available. Depending on the use case CMA can generate solutions more efficiently than the original IBEA algorithm.

A new version 2.0 of the BluePyEfe has recently been released. It shows more robustness from noisy experimental data and is less prone to returning corrupted feature extraction. It can also successfully detect the begin and end time of a step stimulus used during the experiment. Finally, the features extracted using non-step stimuli have been successfully used to validate optimised electrophysiological parameters.

Originally the BluePyOpt software only supported detailed neuron models that were implemented in the Neuron simulator. Recently an integration with Arbor[4] was added to the code, allowing users to choose between simulators.

DISCUSSION

This electrical model building toolset already has been used in many publication [5,6]. By providing regular updates we try to improve the usability of the software for a wide area of use cases.

Keywords: model building, software, optimisation, single neuron, NeuroML, Arbor, BluePyOpt, BluePyEfe, eFEL, BluePyMM

ACKNOWLEDGEMENTS

This work has been partially funded by the European Union Seventh Framework Program (FP7/20072013) under grant agreement no. 604102 (HBP), the European Union's Horizon 2020 Framework Programme for Research and Innovation under the Specific Grant Agreement No. 720270, 785907 (Human Brain Project SGA1/SGA2) and by the EBRAINS research infrastructure, funded from the European Union's Horizon 2020 Framework Programme for Research and Innovation under the Specific Grant Agreement No. 945539 (Human Brain Project SGA3). This project/research was supported by funding to the Blue Brain Project, a research center of the École polytechnique fédérale de Lausanne (EPFL), from the Swiss government's ETH Board of the Swiss Federal Institutes of Technology.

REFERENCES

[1] Roessert C, Damart T, Van Geit W. BluePyEfe 0.3.90. Published online February 2022. doi:10.5281/zenodo.6006925.

[2] Van Geit W, Gevaert M, Chindemi G, Rössert C, Courcol J-D, Muller EB, Schürmann F, Segev I and Markram H (2016) BluePyOpt: Leveraging Open Source Software and Cloud Infrastructure to Optimise Model Parameters in Neuroscience. *Front. Neuroinform*. 10:17. doi: 10.3389/fninf.2016.00017.

[3] Gleeson P, Crook S, Cannon RC, et al. NeuroML: a language for describing data driven models of neurons and networks with a high degree of biological detail. *PLoS computational biology*. 2010;6(6):e1000815. doi: 10.1371/journal.pcbi.1000815

[4] Akar NA, Biddiscombe J, Cumming B, et al. Arbor Library v0.8.1. Published online December 2022. doi:10.5281/zenodo.7473671

[5] Blue Brain. Publications that use or mention BluePyOpt. *GitHub*. https://github.com/BlueBrain/BluePyOpt/wiki/Publications-that-use-or-mention-BluePyOpt

[6] Reva M, Rössert C, Arnaudon A, et al. A universal workflow for creation, validation and generalization of detailed neuronal models. *bioRxiv*. Published online 2022:2022-2012. doi: https://doi.org/10.1101/2022.12.13.520234

102. Interplay between synaptic scaling and structural plasticity maintains the robust firing rate homeostasis

Han Lu[1,2,*], Sandra Diaz-Pier[3], Maximilian Lenz[1], Andreas Vlachos[1,2,4,5,*]

[1]Department of Neuroanatomy, Institute of Anatomy and Cell Biology, Faculty of Medicine, University of Freiburg, Freiburg, Germany; [2]Center BrainLinks-BrainTools, University of Freiburg, Freiburg, Germany; [3]Forschungszentrum Jülich, Simulation Lab Neuroscience, Jülich Supercomputing Centre, Institute for Advanced Simulation, Jülich Aachen Research Alliance, Jülich, Germany; [4]Center for Basics in Neuromodulation (NeuroModulBasics), Faculty of Medicine, University of Freiburg, Freiburg, Germany; [5]Bernstein Center Freiburg, University of Freiburg, Freiburg, Germany

[*]han.lu@brainlinks-braintools.uni-freiburg.de

[*]andreas.vlachos@anat.uni-freiburg.de

INTRODUCTION/MOTIVATION Critical network states and neural plasticity are essential for learning and flexible behaviour in changing environments [1,2]. However, associative learning perturbs network dynamics via positive feedback. Adjusting synaptic weights or synapse/spine numbers in a homeostatic manner, i.e., based on negative feedback mechanisms, help restore network stability. Experiments have inconsistent results on the homeostatic nature of spine-number-based structural plasticity [3], unlike homeostatic synaptic scaling. Instead, spine loss, formation, or no changes were reported under different deprivation protocols, making it challenging to understand the function of structural plasticity.

METHODS We combined *in vitro* experiments and point neuronal network modelling to assess the interplay of synaptic scaling and structural plasticity. Time-lapse imaging of eGPF-expressing CA1 pyramidal neurons was conducted in organotypic tissue cultures to track changes in dendritic spine numbers before and after inhibition of AMPA receptors with 200 nM and 50 µM NBQX for three-days. Co-simulation of calcium-based structural plasticity and synaptic scaling models in a spiking neural network was conducted to study their interrelationship under various activity perturbation. Simulations were carried out using NEST [4], part of the EBRAINS infrastructure, and executed on the JUSUF supercomputer at the Jülich Supercomputing Centre under a FENIX/ICEI computing time project.

RESULTS AND DISCUSSION By tracking individual dendritic segments, we showed that dendritic spine density is not linearly regulated after inhibition of excitatory neurotransmission: partial inhibition of AMPA receptors with 200 nM NBQX significantly increased while complete blockade with 50 µM NBQX reduced spine density. Based on these experimental results, we established a bi-phasic structural plasticity rule in a spiking neural network. Our computer simulations showed that this rule maintains homeostatic properties upon stimulation and permits both spine formation and spine loss depending on the degree of deprivation. When silencing-induced spine loss occurs, the product of external stimulation and recurrent connectivity jointly determines the network activity and leads

to further degeneration or regeneration. Homeostatic synaptic scaling, which instantly modulates the recurrent connectivity, accordingly shapes the response of structural plasticity. In summary (Figure 1), we showed that the bi-phasic structural plasticity rule is competitive, redundant, and compensatory to the synaptic-weight-based homeostatic synaptic scaling rule. We conclude that the robust adaptation of network activity is enabled by calcium concentration-based integral feedback control, in the forms of structural plasticity and synaptic scaling.

Keywords: homeostatic structural plasticity, synaptic scaling, firing rate homeostasis, organotypic tissue cultures, CA1 pyramidal neurons, NBQX, spine density, NEST, spiking neural network

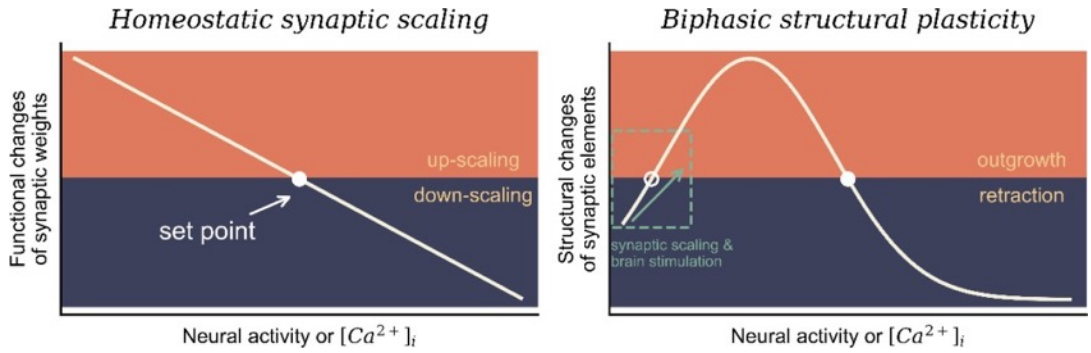

Figure 1: Comparison of the homeostatic synaptic scaling rule and biphasic structural plasticity rule. For the synaptic scaling rule, up-scaling and down-scaling of input synaptic weights are monotonically regulated by neural activity (i.e., intracellular calcium concentration) via a negative feedback control. Therefore, neurons could maintain their activity level around a set point value (solid white circle). For the biphasic structural plasticity model, the outgrowth and retraction of synaptic elements (axonal boutons and dendritic spines) are also regulated by the difference between their activity level and the set point value, but in a more complex manner. Particularly, it displays homeostatic properties when neural activity is above the unstable set point (empty white circle) but when the neural activity drops below that value, degeneration begins. Therefore, neurons may present homeostatic outgrowth or retraction of synapses and silencing-induced degeneration. We showed with computer simulations that synaptic scaling and brain stimulation could shape network connectivity by modulating neural activity via recurrent inputs or external inputs.

ACKNOWLEDGEMENTS

The work was supported by Deutsche Forschungsgemeinschaft (DFG; Project-ID 259373024 B14–CRC/TRR 167 to AV). The research leading to these results has received funding from the European Union's Horizon 2020 Framework Programme for Research and Innovation under the Specific Grant Agreement No. 945539 (Human Brain Project SGA3). This research has also been partially funded by the Helmholtz Association through the Helmholtz Portfolio Theme Supercomputing and Modeling for the Human Brain. We acknowledge the use of Fenix Infrastructure resources, which are partially funded from the European Union's Horizon 2020 research and innovation programme through the ICEI project under the grant agreement No. 800858.

REFERENCES

[1] Shew WL, Yang H, Petermann T, Roy R, Plenz D. Neuronal avalanches imply maximum dynamic range in cortical networks at criticality. *J Neurosci*. 2009;29(49):15595-600.

[2] Shew WL, Plenz D. The functional benefits of criticality in the cortex. *Neuroscientist*. 2013;19(1):88-100.

[3] Moulin TC, Rayêe D, Schiöth HB. Dendritic spine density changes and homeostatic synaptic scaling: a meta-analysis of animal studies. *Neural Regen Res*. 2022;17(1):20.

[4] Fardet T, Vennemo SB, Mitchell J, Mørk H, Graber S, Hahne J, et al. NEST 2.20.2. *Zenodo*. 2021 Aug. Available from: https://doi.org/10.5281/zenodo.5242954.36.

103. Virtual brain simulations reveal subject-specific excitatory/inhibitory profiles of dementia patients

Anita Monteverdi[1*], Fulvia Palesi[2] Michael Schirner[3], Francesca Argentino[2], Mariateresa Merante[2], Alberto Redolfi[4], Francesca Conca[5], Laura Mazzocchi[6], Matteo Cotta Ramusino[2,7], Alfredo Costa[2,7], Anna Pichiecchio[2,6], Lisa Maria Farina[5], Stefano Cappa[5,8], Viktor Jirsa[9], Petra Ritter[3], Claudia A.M. Gandini Wheeler-Kingshott[1,2,10] and Egidio D'Angelo[1,2]

*Corresponding to: anita.monteverdi01@universitadipavia.it

[1] *Brain Connectivity Center, IRCCS Mondino Foundation, Research Department, 27100 Pavia, Italy*

[2] *Dept of Brain and Behavioral Sciences, University of Pavia, 27100 Pavia, Italy*

[3] *Berlin Institute of Health at Charité, Universitätsmedizin Berlin, Charitéplatz 1, Berlin 10117, Germany; Department of Neurology with Experimental Neurology, Charité, Universitätsmedizin Berlin, Corporate member of Freie Universität Berlin and Humboldt Universität zu Berlin, Charitéplatz 1, Berlin 10117, Germany; Bernstein Focus State Dependencies of Learning and Bernstein Center for Computational Neuroscience, Berlin, Germany; Einstein Center for Neuroscience Berlin, Charitéplatz 1, Berlin 10117, Germany; Einstein Center Digital Future, Wilhelmstraße 67, Berlin 10117, Germany*

[4] *Laboratory of Neuroinformatics, IRCCS Istituto Centro San Giovanni di Dio Fatebenefratelli, 25125 Brescia, Italy,*

[5] *IRCCS Mondino Foundation, 27100 Pavia, Italy.*

[6] *Advanced Imaging and Radiomics Center, IRCCS Mondino Foundation, 27100 Pavia, Italy*

[7] *Unit of Behavioral Neurology, IRCCS Mondino Foundation, 27100 Pavia, Italy*

[8] *University Institute of Advanced Studies (IUSS), 27100 Pavia, Italy*

[9] *Institut de Neurosciences des Systèmes, INSERM, INS, Aix Marseille University, 13005 Marseille, France*

[10] *NMR Research Unit, Queen Square MS Centre, UCL Queen Square Institute of Neurology, Department of Neuroinflammation, Russell Square House, Russell Square, WC1B 5EH, London, UK*

Keywords: <Virtual brain modelling> <Brain dynamics> <Excitatory/Inhibitory balance> <Alzheimer's Disease> <Frontotemporal Dementia> <Resting-state networks> <Digital Twins> INTRODUCTION

A disrupted balance between neuronal excitation and inhibition (E/I) lays at the core of neurodegenerative physiopathology[1], but E/I alterations at whole-brain and functional networks levels are hard to unveil in living subjects. Virtual brain modelling[2] is now providing a new tool to non-invasively explore intrinsic subject-specific brain features, such as the E/I balance[3,4]. Our work exploits The Virtual Brain (TVB) capabilities to characterize neurodegenerative pathologies in terms of subject-specific E/I profile, both at whole-brain level and in multiple functional networks. Our results lay the groundwork for customized biomarkers research and define new trajectories for the design of tailored interventional workflows.

METHODS

Two cohorts of healthy controls (HC) and dementia patients (Alzheimer's disease (AD), Frontotemporal Dementia (FTD)) were enrolled: 1) 15 HC (8f, 64±11y), 15 AD (6f, 70±7y), 15 FTD (4f, 69±7y); 2) 10 HC (6f, 67±3y), 16 AD (13f, 70±8y) and 7 FTD (1f, 69±5y) classified into several phenotypes. Subjects underwent neuropsychological examination and MRI data were used to characterize structural and functional connectivity. Brain dynamics were simulated using TVB with the Wong-Wang model[5] both at whole-brain level (first cohort) and in multiple functional networks (second cohort). An iterative optimization[6] of TVB parameters was performed to gain a description of global coupling (G), excitatory (JNMDA) and inhibitory (Ji) synaptic strength, and recurrent excitation (w+).

TVB parameters were compared between groups using non-parametric tests and between networks with general linear model, while the relationship with neuropsychological scores was assessed through multiple regressions. K- mean clustering reconstructed subjects-specific E/I profile.

RESULTS

At whole-brain level, TVB parameters were different between groups, and AD patients showed the highest global coupling and inhibition (Fig1A). Global coupling, excitation and inhibition strength significantly contributed to explain the variation of neuropsychological scores (Fig1B), while clustering analysis revealed the heterogeneity of E/I balance across subjects and groups (Fig1C).

In multiple functional networks, TVB parameters revealed network-dependent E/I and connectivity patterns showing a different impact of neurodegeneration in AD and FTD (Fig2A). Networks-specific excitation, inhibition and global coupling explained neuropsychological performance in the cognitive domains in which the network is involved (Fig2B). Clustering analysis identified TVB parameters of cognitive networks as the most informative features allowing to isolate personalized fingerprints (Fig2C) and reveal the correspondence between cognitive networks properties and clinical severity.

DISCUSSION

Through virtual brain models, we provide a first description of E/I balance in dementia both at whole-brain and functional networks level.

At whole-brain level, the high global coupling characterizing AD underlies the hypersynchrony of disrupted networks, while high inhibition strength supports GABAergic dysfunction in AD pathogenesis. At networks level, TVB parameters capture differential aspects of the two disease conditions, depicting the Default Mode and the Frontoparietal networks as crucial to distinguish dementia patients.

Beside a novel analysis of pathological differences between neurodegenerative diseases, TVB parameters were associated with subjects' neuropsychological performance and underline the link between neurophysiology and cognition.

Therefore, TVB parameters can provide a unique subject-specific description of E/I balance at whole-brain level and unveil E/I patterns in functional networks, proving sensitive to clinical severity in multiple phenotypes.

In conclusion, TVB simulations can reveal subject-specific profiles of dementia patients, opening new perspectives for understanding disease pathophysiology and for designing personalized therapeutic approaches.

FIGURES LEGENDS

Fig.1 | A) Boxplots of optimal TVB parameters (G=global coupling, J_NMDA=excitation, w+=recurrent excitation, Ji=inhibition) across groups (healthy=HC Alzheimer's disease=AD Frontotemporal Dementia=FTD). Asterisks represent significant differences ($p<0.05$). B) In backward regressions a different combination of features including TVB parameters significantly ($p<0.05$) explain the variation (R^2 index) of each neuropsychological domain. C) Top: clusters identified with k-means analysis (left: colour coded) are characterized by a combination of low and high TVB parameters (right: Ji, J_NMDA and w+ on the axis, G values colour coded). Bottom: Visual representation of cluster distributions across groups. Each dot represents a single subject, providing a subject-specific description of the excitatory/inhibitory balance.

Fig.2 | A) Network (DMN=default mode, FPN=frontoparietal, LN=limbic, AN=attention, VN=visual, SMN=somatomotor) specific changes related to neurodegeneration are summarized in the tables. The increase or decrease of TVB parameters (G=global coupling, J_NMDA=excitation, w+=recurrent excitation, Ji=inhibition) in a network with respect to the others is indicated with colored arrows in the pathological groups (AD, FTD). B) In backward regressions networks specific TVB parameters contribute to significantly ($p<0.05$) explain neuropsychological scores variance (R^2 index) in the cognitive domains in which the network is involved. C) Top: Cognitive network properties (Ji in AN, G in LN, G in DMN) are the most informative features to perform patient's labelling and each of the identified clusters is characterized by a combination of low and high TVB parameters. Bottom: The distribution of subjects into the clusters outlines personalized fingerprints based on cognitive networks properties. Each dot represents a subject and dots dimension corresponds to the cognitive status (assessed with MMSE), revealing the correspondence between cognitive networks properties and clinical severity.

Whole-brain

A

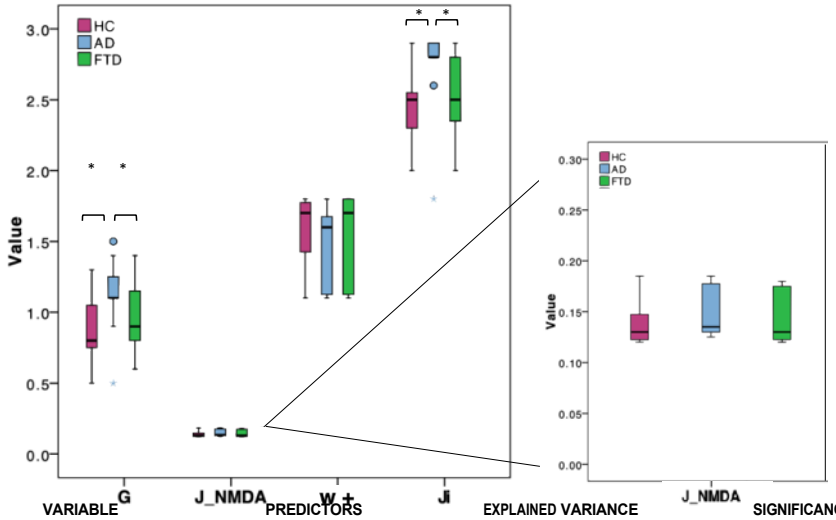

B

VARIABLE	PREDICTORS	EXPLAINED VARIANCE	SIGNIFICANCE
MEMORY	Ji	8.4%	0.028
EXECUTIVE FUNCTION	group, gender, age, w+, G	19.9%	0.037
	group, gender, age, G	19.8%	0.018
	group, age, G	19.5%	0.008
	group, age	18.5%	0.004
ATTENTION	group, Ji, gender, age	16.9%	0.040
	group, Ji, age	16.7%	0.019
	group, Ji	15%	0.011
	group	12%	0.008
LANGUAGE	group, G	10.8%	0.044
	G	8.7%	0.025
VISUO-SPATIAL SKILLS	group, Ji	10.7%	0.045

C

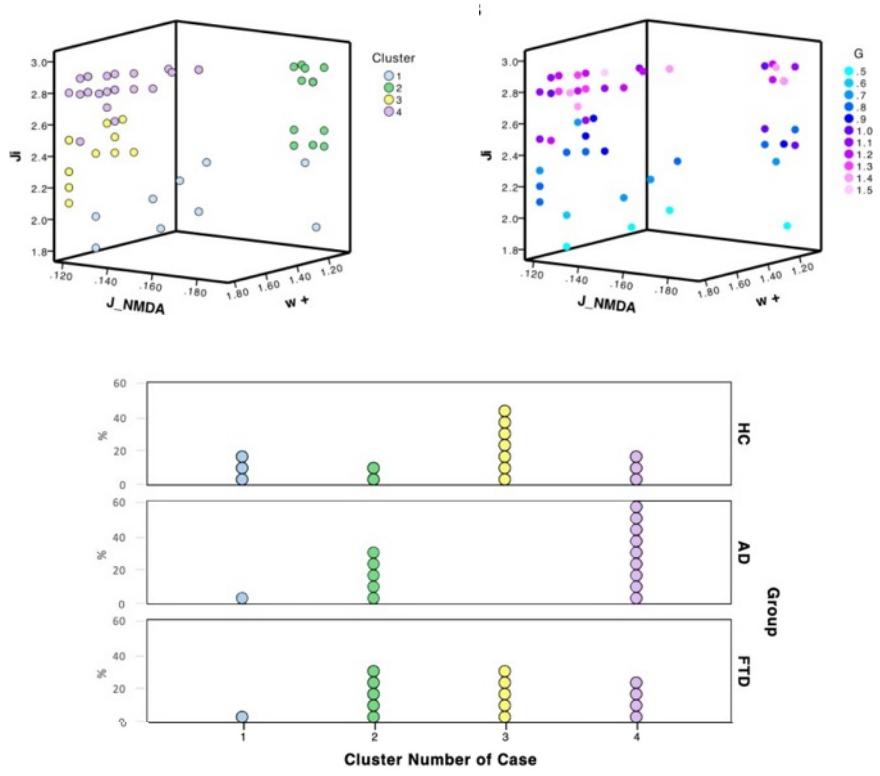

A

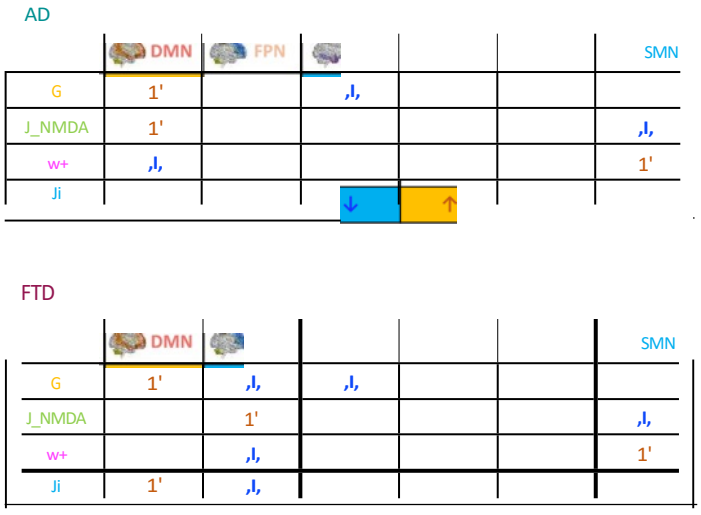

B

NETWORKS	VARIABLE (Neuropsychology)	PREDICTORS (TVS-parameters)	EXPLAINED VARIANCE	SIGNIFICANCE
VISUAL	MEMORY	NMDA	21.3%	0.027
	LANGUAGE-FLUENCY	w+,Ji	30.1%	0.028
SOMATOMOTOR	VISUO-CONSTRUCTIONAL	Ji	21.3%	0.030
ATTENTION	MEMORY	w+, J_NMDA, Ji	33.4%	0.047
LIMBIC	MEMORY	Ji	21.5%	0.026
	ATTENTION	w+,G,J NMDA	42.0%	0.030
	VISUO-CONSTRUCTIONAL	w+, G, J_NMDA,Ji	45.7%	0.027
FRONTOPARIETAL	EXECUTIVE FUNCTION	J NMDA	21.3%	0.027
DMN	LANGUAGE-FLUENCY	G, J_NMDA, Ji	39.1%	0.022

C

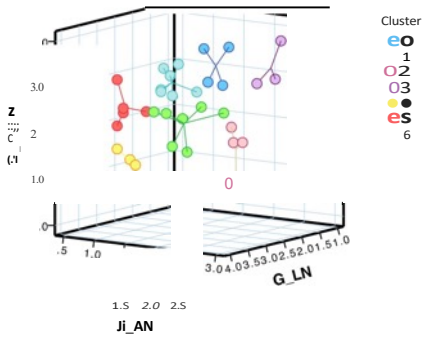

/Div

1st componenl

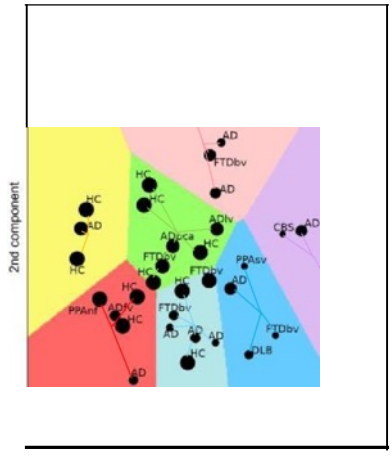
2nd component
AD
FTDbv
HC
HC
AD
HC
AD
ADlv
ADpca
HC
CBS
AD
FTDbv
PPAsv
HC
HC
FTDbv
AD
HC
HC
PPAnf
ADlv
HC
FTDbv
AD
AD
AD
FTDbv
HC
DLB
AD

ACKNOWLEDGEMENTS

This work was performed at the IRCCS Mondino Foundation and was supported by the Italian Ministry of Health (RC2022-2024). ED'A and FP received funding by the H2020 Research and Innovation Action Grants Human Brain Project 785907 and 945539 (SGA2 and SGA3), and ED'A received funding by the MNL Project "Local Neuronal Microcircuits" of the Centro Fermi (Rome, Italy). CG received funding Horizon2020 (Human Brain Project SGA3, Specific Grant Agreement No. 945539), BRC (#BRC704/CAP/CGW), MRC (#MR/S026088/1), Ataxia UK, MS Society (#77), Wings for Life (#169111) and is a shareholder in Queen Square Analytics Ltd.

REFERENCES

1. Maestú F, de Haan W, Busche MA, DeFelipe J. Neuronal excitation/inhibition imbalance: core element of a translational perspective on Alzheimer pathophysiology. *Ageing Res Rev*. 2021;69:101372. doi:10.1016/j.arr.2021.101372
2. Sanz-Leon P, Knock SA, Spiegler A, Jirsa VK. Mathematical framework for large-scale brain network modeling in The Virtual Brain. *Neuroimage*. 2015;111:385-430. doi:10.1016/j.neuroimage.2015.01.002
3. Zimmermann J, Perry A, Breakspear M, et al. Differentiation of Alzheimer's disease based on local and global parameters in personalized Virtual Brain models. *NeuroImage Clin*. 2018;19(April):240-251. doi:10.1016/j.nicl.2018.04.017
4. Monteverdi A, Palesi F, Costa A, et al. Subject-specific features of excitation / inhibition profiles in neurodegenerative diseases. *Front Aging Neurosci 14868342*. 2022;(August). doi:10.3389/fnagi.2022.868342
5. Deco G, Ponce-Alvarez A, Hagmann P, Romani GL, Mantini D, Corbetta M. How local excitation-inhibition ratio impacts the whole brain dynamics. *J Neurosci*. 2014;34(23):7886-7898. doi:10.1523/JNEUROSCI.5068-13.2014
6. Kong X, Kong R, Orban C, et al. Sensory-motor cortices shape functional connectivity dynamics in the human brain. *Nat Commun*. 2021;12(1). doi:10.1038/s41467-021-26704-y

104. Large-scale brain signatures of fluid dynamics and responsiveness linked to consciousness

Martin Breyton[1,2*], Jan Fousek[1], Pierpaolo Sorrentino[1], Giovanni Rabuffo[1], Lionel Kusch[1], Spase Petkoski[1], Viktor Jirsa[1]

[1]INSERM, Institut de Neurosciences des Systèmes, UMR 1106, Aix-Marseille Université, Marseille, France
[2]Service de pharmacologie clinique, AP-HM, Marseille, France
*martin.breyton@univ-amu.fr

INTRODUCTION/MOTIVATION

Neural bases of consciousness have been explored through many different paradigms and the notion of complexity emerged as a unifying framework to characterize conscious experience. To date, the perturbational complexity index (PCI), rooted on information theory, performs best to assess consciousness through brain stimulation. However, the mechanisms underpinning this complexity remain unclear and reliable metrics on spontaneous activity are still missing. In the present study, we explore brain responsiveness and resting-state activity through large-scale brain modelling and prove that complexity and consciousness are directly associated with a fluid dynamical regime (Fig 1). This fluidity is reflected in the dynamic functional connectivity, and other metrics drawn from the theory of dynamical systems and manifolds can capture dynamics in synthetic data. We then validate our findings on a cohort of 15 subjects under anesthesia and wakefulness and show that measures of fluidity on spontaneous activity can distinguish consciousness as good as perturbational complexity.

METHODS

We built a large-scale brain network model with The Virtual Brain (TVB [1]) consisting of 84 cortical and subcortical regions using a connectome from the Human Connectome Project (HCP [2]) and a mean field model [3]. Spontaneous EEG data and maximum PCI values of 15 healthy subjects under anesthesia (Xenon N=5, Propofol N=5 or Ketamine N=5) and wakefulness were provided by [4,5]. In synthetic data, perturbational complexity was assessed by a modified version of PCI [6], coined *simulation PCI* (sPCI). The *fluidity* of spontaneous data is defined by the variance of the upper triangular part of the dynamic functional connectivity (dFC). After binarization, complexity was calculated by Lempel-Ziv (LZ) complexity and the size of the functional repertoire (SFR) was defined by the count of unique avalanche configurations during a recording [7]. The bursting potential (BP) is based on the organization of neuronal activations in short-lived bursts and corresponds to the maximum variation of the bursting profile. Classification accuracy of the resting state metrics was tested using a Support Vector Machine algorithm with a linear kernel. First, grouping all participants in the *wakefulness* condition (N=15) against *anesthesia* (N=15); and second, grouping participants in *conscious report* (N=20) against *no report* (N=10).

RESULTS AND DISCUSSION

Spontaneous activity of the network can show a variety of dynamics depending on two global parameters: the global coupling *G* and noise. Non-trivial behaviour is found around a *working point* where cascades of coactivations of different sizes and durations occur in a complex fashion. *Fluidity* based on dFC is found to be maximal around this *working point,* and so is sPCI when the system is perturbed. LZ complexity, the SFR and BP are found to increase abruptly as global coupling crosses the working point. This suggests that the same dynamical regime might underpin both the highest brain responsiveness and the most fluid spontaneous activity. In empirical data, PCI is systematically higher during wakefulness than under anesthesia for Xenon and Propofol drugs, except for Ketamine. Metrics on spontaneous activity revealed that *fluidity* is also systematically higher during wakefulness than anesthesia (except for Ketamine) with a classification accuracy of 100%. Results for LZ complexity, the SFR and BP were similar (Fig 2). Here, we demonstrated that the symmetry breaking caused by the connectome is

sufficient for setting the global working point of the brain, allowing the generation of complex behavior in different paradigms: rest and stimulation.

In the future, the imperfect separation of groups for some of the metrics could be improved by personalized brain modelling and including more realistic parameters in the models such as neuromodulatory pathways to improve explanatory power.

Keywords: consciousness, dynamics, responsiveness, manifold, functional connectivity ACKNOWLEDGEMENTS
<optional. your text here>

REFERENCES

[1] Sanz Leon P, Knock S, Woodman M, Domide L, Mersmann J, McIntosh A, et al. The Virtual Brain: a simulator of primate brain network dynamics. Front Neuroinformatics 2013;7.

[2] Van Essen DC, Smith SM, Barch DM, Behrens TEJ, Yacoub E, Ugurbil K. The WU-Minn Human Connectome Project: An Overview. NeuroImage 2013;80:62–79. https://doi.org/10.1016/j.neuroimage.2013.05.041.

[3] Montbrió E, Pazó D, Roxin A. Macroscopic Description for Networks of Spiking Neurons. Phys Rev X 2015;5:021028. https://doi.org/10.1103/PhysRevX.5.021028.

[4] Sarasso S, Boly M, Napolitani M, Gosseries O, Charland-Verville V, Casarotto S, et al. Consciousness and Complexity during Unresponsiveness Induced by Propofol, Xenon, and Ketamine. Curr Biol 2015;25:3099–105. https://doi.org/10.1016/j.cub.2015.10.014.

[5] Colombo MA, Napolitani M, Boly M, Gosseries O, Casarotto S, Rosanova M, et al. The spectral exponent of the resting EEG indexes the presence of consciousness during unresponsiveness induced by propofol, xenon, and ketamine. NeuroImage 2019;189:631–44. https://doi.org/10.1016/j.neuroimage.2019.01.024.

[6] Casali AG, Gosseries O, Rosanova M, Boly M, Sarasso S, Casali KR, et al. A Theoretically Based Index of Consciousness Independent of Sensory Processing and Behavior. Sci Transl Med 2013;5:198ra105- 198ra105. https://doi.org/10.1126/scitranslmed.3006294.

[7] Sorrentino P, Rucco R, Baselice F, De Micco R, Tessitore A, Hillebrand A, et al. Flexible brain dynamics underpins complex behaviours as observed in Parkinson's disease. Sci Rep 2021;11:4051. https://doi.org/10.1038/s41598-021-83425-4.

FIGURES

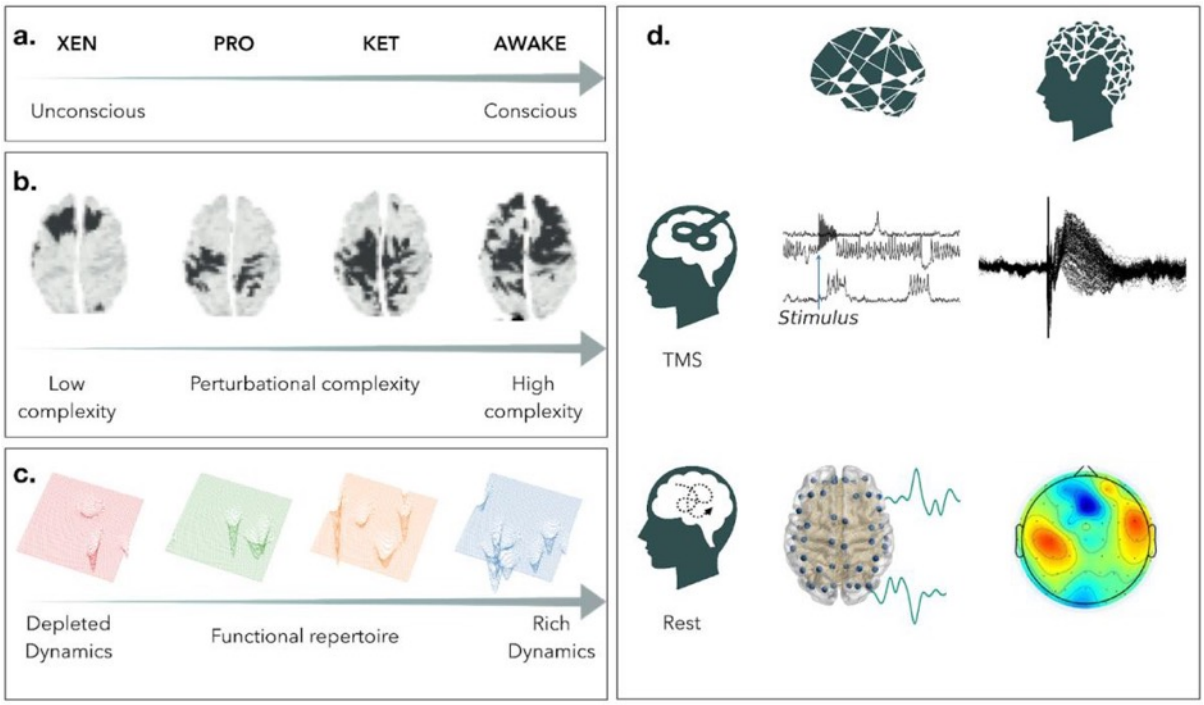

Fig 1: Conceptual framework of the study

(a) Consciousness is a continuum and can be explored with drug-induced coma of various depths (Xenon, Propofol > Ketamine > Wakefulness). We hypothesized a correspondence between the variations in complexity found with PCI and the dynamics of spontaneous activity across the spectrum of consciousness. (b) We sketched various patterns of spatio-temporal activity reflecting changes in perturbational complexity from left to right. In (c) we showed the conceptual shapes of corresponding manifolds of brain activity responsible for different sizes of the functional repertoire (number of wells) and associated with consciousness. (d) The brain is modeled as a network of neural masses coupled by an empirical connectome. This whole-brain model serves as a platform to simulate resting state activity (bottom left) and cortical stimulation (top left, example of firing rate time series with applied stimulus). Dynamical properties of the simulations are studied and compared with data features of human empirical recordings of spontaneous activity (bottom right, EEG during wakefulness and under three anesthetics) and stimulation (top right, TMS-EEG protocol performed in the same conditions).

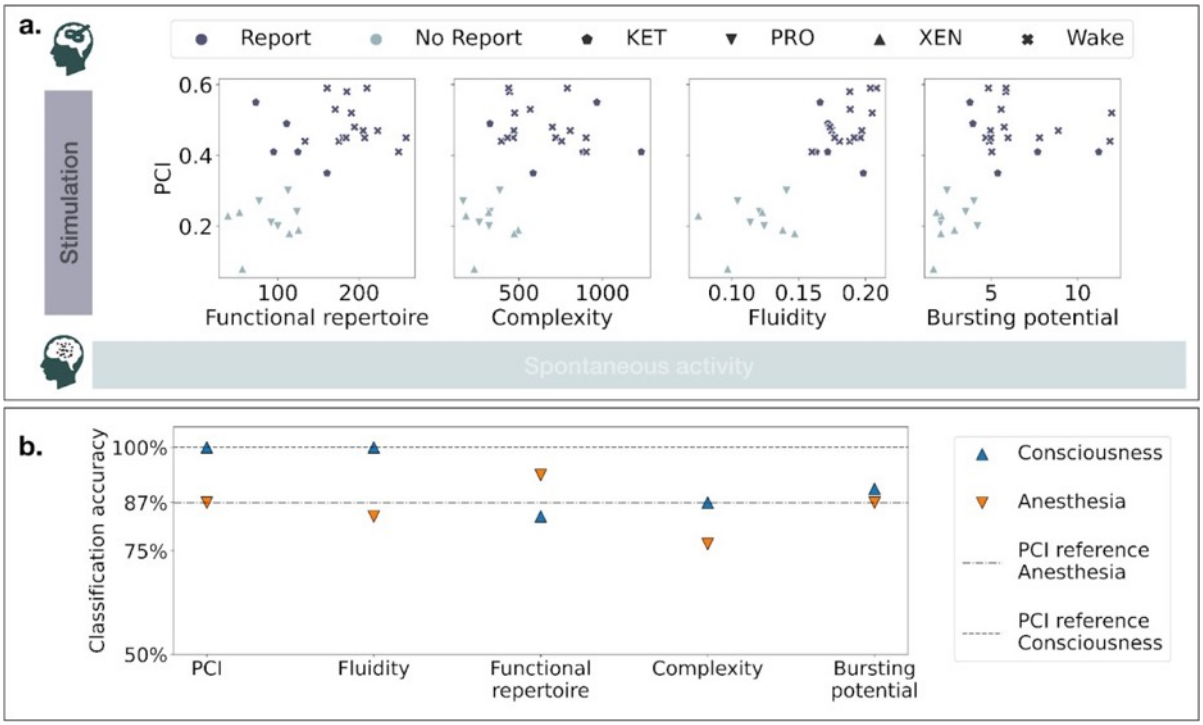

Fig 2: Predictive power of resting-state metrics and PCI

(a) Crossplots between the PCI obtained experimentally during a TMS-EEG protocole and each metric on spontaneous recordings (functional repertoire, complexity, fluidity and bursting potential). Complexity and the size of the functional repertoire were normalized by the length of the recording in minutes. (b) Classification accuracy of a Support Vector Machine classifier with a linear kernel to distinguish either between anesthesia and wakefulness (downward orange triangles) or between conscious report and no report (upward blue triangles). Dashed lines represent the benchmark performances achieved by PCI classification (100% for consciousness and 87% for anesthesia).

105. Now you see it more – Multiscale visualization on EBRAINS

Oscar D. Robles*[1,3], Susana Mata[1,3], Pablo Toharia[2,3], Luis Pastor[1,3], Wouter Klijn[4], Sandra Diaz-Pier[4]

1. Department of Computer Science and Computer Architecture, Rey Juan Carlos University, Madrid, Spain
2. DATSI, ETSIINF, Universidad Politécnica de Madrid, Madrid, Spain
3. Center for Computational Simulation, Universidad Politécnica de Madrid, Madrid, Spain
4. Simulation and Data Lab Neuroscience, Jülich Supercomputing Centre, Institute for Advanced Simulation, JARA, Forschungszentrum Jülich GmbH, Jülich, Germany

* oscardavid.robles@urjc.es

INTRODUCTION/MOTIVATION

The Human Brain Project has the objective of creating a comprehensive digital infrastructure for brain research. This infrastructure is meant to consider the complexity and multi-scale nature of the brain during the co-design of software and hardware tools. Multi-scale modelling and (co-)simulation using the EBRAINS infrastructure is now possible and opens a new avenue to address questions linking relevant features of brain structure and function from the molecular level all the way to whole brain dynamics. Besides simulation, analysis and visualization tools have also been developed to aid the exploration and understanding of the information produced during the scientific workflows. In particular, visualization tools allow end users to explore and explain relevant data features which would otherwise be impossible to see. Understanding the complex structural and functional connections in the brain as well as their changes through time is essential to advance brain research ([1,2,3]). In this work we present an overview of a set of visualization tools which address the challenge of understanding the multiscale brain.

METHODS

We have developed a comprehensive set of visualization tools to provide end users with different perspectives on data produced at different scales of brain simulation and enable multiscale modeling.

First, we present ConGen [4], a framework that facilitates the generation of multiscale connectivity in large neural networks using a symbolic visual language capable of representing the model at different structural levels. At the other end of the in-silico experimentation workflows, we present the ViSimpl [7,8] and NeuroTessMesh [6], a set of tools which allow the visualization using coordinated views on different perspectives on anatomical and neural dynamics data.

The visual front-end of ConGen (Fig. 1) enables the creation of a hierarchy of super-populations and populations and the specification of their connections by establishing the necessary connectivity parameters. This multiscale approach makes it possible to generate large scale scenarios capturing global behavior and local details at the

same time. Its symbolic language allows researchers to create and visually analyze the generated networks independently of the simulator to be used, since the visual model is translated into a simulator-independent language.

ViSimpl (Fig. 1) provides 3D particle-based rendering that allows visualizing simulation data with their associated spatial and temporal information, enhancing the knowledge extraction process. It also provides abstract representations of the time-varying magnitudes supporting different data aggregation and disaggregation operations and giving also focus and context clues.

Finally, NeuroTessMesh (Fig. 1) provides a visual environment for the generation of 3D polygonal meshes that approximate the membrane of neuronal cells. The 3D models can be tessellated at different levels of detail, providing either homogeneous or adaptive resolution along the model at an affordable computational cost, both in terms of memory and rendering time.

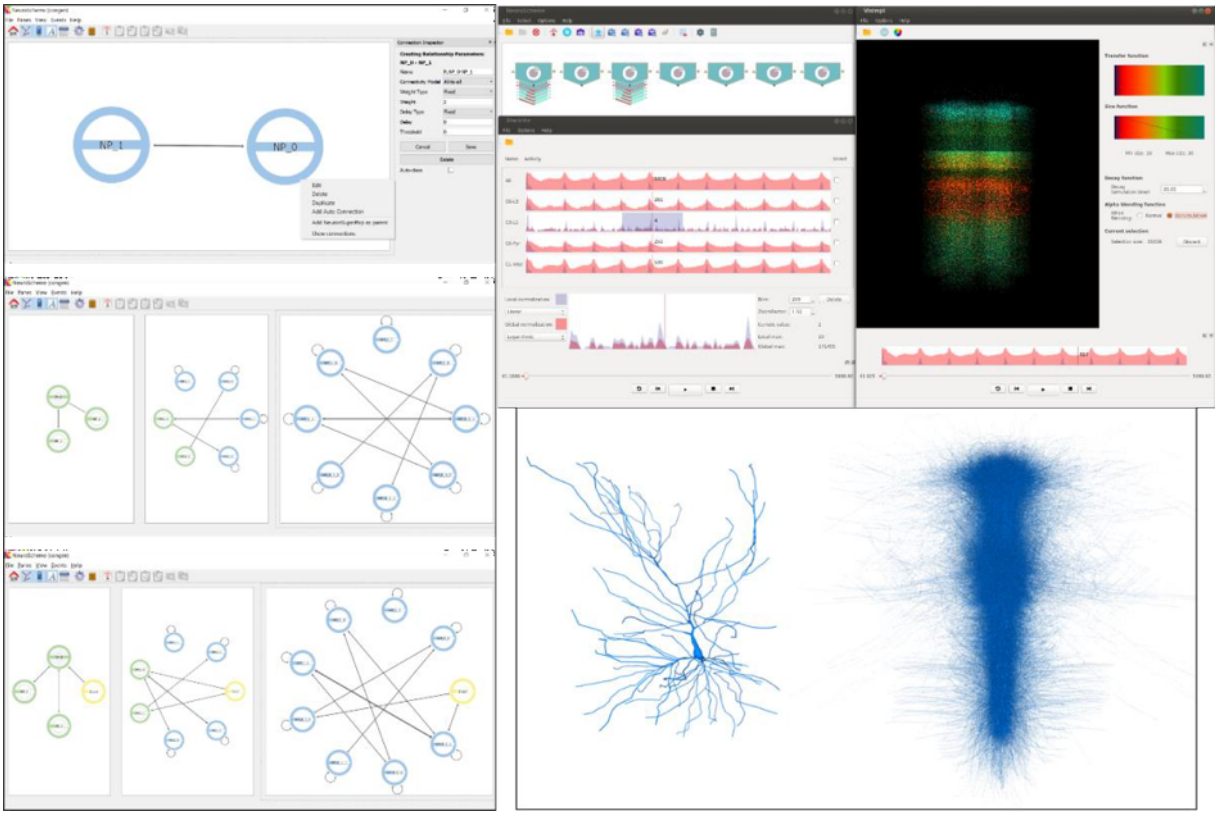

Fig. 1.- Left: Different views of ConGen. Top right: ViSimpl. Bottom right: NeuroTessMesh, showing a single neuron (left) and a cortical column (right).

RESULTS AND DISCUSSION

We have developed the aforementioned tools and deployed them on FENIX, offering them as part of the EBRAINS infrastructure. We have tested these tools using data produced from different work packages within the Human Brain Project, and used them to support scientific use cases as well as training, workshops and dissemination.

These tools have been designed to reduce the complexity of working with large amounts of data and help the users extract meaningful information from it. These tools particularly support the modeling and simulation of the multiscale brain, which requires a combination of hierarchical grouping and visual abstractions in order to convey relevant information.

Keywords: Visualization, Multiscale, Large scale models, Co-simulation, Analysis

ACKNOWLEDGEMENTS

We would like to kindly acknowledge the support and discussions with Viktor Jirsa and Lionel Kusch about the generation of co-simulation scripts with TVB and NEST. The research leading to these results has received funding from the Spanish Ministry of Economy and Competitiveness under grants C080020-09 (Cajal Blue Brain Project, Spanish partner of the Blue Brain Project initiative from EPFL), TIN2017-83132, PID2020-113013RB-C21, and PID2020-113013RB-C22, as well as from the European Union's Horizon 2020 Framework Programme for Research and Innovation under the Specific Grant Agreements No. 785907 (Human Brain Project SGA2) and 945539 (Human Brain Project SGA3). This research has also been partially funded by the Helmholtz Association through the Helmholtz Portfolio Theme Supercomputing and Modeling for the Human Brain.

REFERENCES

[1] Evanko, D., and Pastrana, E. (2013). Why mapping the brain matters. Nat. Methods 10:447. doi: 10.1038/nmeth.2513

[2] D'Angelo, Egidio, and Viktor Jirsa. "The quest for multiscale brain modeling." Trends in Neurosciences (2022). [3| Peyser, A., Diaz Pier, S., Klijn, W., Morrison, A., and Triesch, J. (2019). Linking experimental and computational connectomics. Netw. Neurosci. 3, 902–904. doi: 10.1162/netn_e_00108

[4] Herbers, Patrick, et al. "ConGen—A Simulator-Agnostic Visual Language for Definition and Generation of Connectivity in Large and Multiscale Neural Networks." Frontiers in neuroinformatics 15 (2022): 72.

[5] Pastor, L., Mata, S., Toharia, P., Beriso, S. B., Brito, J. P., and Garcia-Cantero, J. J. (2015). "NeuroScheme: efficient multiscale representations for the visual exploration of morphological data in the human brain neocortex," in XXV Spanish Computer Graphics Conference, CEIG 2015, eds M. Sbert and J. Lopez-Moreno (Benicássim), 117–125.

[6] Garcia-Cantero, J., Brito, J., Mata, S., Bayona, S. and Pastor, L. "NeuroTessMesh: A Tool for the Generation and Visualization of Neuron Meshes and Adaptive On-the-Fly Refinement" in Frontiers in Neuroinformatics 11 (2017). doi: 10.3389/fninf.2017.00038

[7] Galindo Sergio E., Toharia Pablo, Robles Oscar D., Pastor Luis. "ViSimpl: Multi-View Visual Analysis of Brain Simulation Data". Frontiers in Neuroinformatics, 10 (2016). doi: 10.3389/fninf.2016.00044

[8] Galindo Sergio E., Toharia Pablo, Robles Óscar D., Ros Eduardo, Pastor Luis, Garrido, Jesús A. "Simulation, visualization and analysis tools for pattern recognition assessment with spiking neuronal networks". Neurocomputing, 400 (2020), 309-321. doi: https://doi.org/10.1016/j.neucom.2020.02.114.

106. Building detailed neuron models from patch-clamp and MEA data using the BluePyOpt and LFPy libraries

Alessio Paolo Buccino[1], Tanguy Damart*[2], Julian Bartram[1], Darshan Mandge[2], Xiaohan Xue[1], Mickael Zbili[2], Tobias Gänswein[1], Aurélien Jaquier[2], Vishalini Emmenegger[1], Henry Markram[2], Andreas Hierlemann[1], and Werner Van Geit[2]

[1]Bio Engineering Laboratory, Department of Biosystems Science and Engineering, ETH Zurich, Basel, Switzerland

[2]Blue Brain Project, École polytechnique fédérale de Lausanne (EPFL), Campus Biotech, 1202 Geneva, Switzerland

*tanguy.damart@epfl.ch

INTRODUCTION/MOTIVATION

In computational neuroscience, multicompartment models provide arguably one of the most biophysically detailed representations of single neurons. They are built by combining a morphological reconstruction of neurons, obtained through imaging techniques, with electrophysiological characteristics of ion-channel dynamics and their distribution over the neuron morphology. These models have enabled researchers to explore several characteristics of neuronal dynamics, including dendritic and axonal properties. In recent years, computer-based optimization has enabled computational neuroscientists to explore the large parameter space of these models more thoroughly and faster, for example using evolutionary strategies and specialized software such as BluePyOpt.

Still, for the vast majority of models, experimental features used to fit the model are extracted solely from somatic patch-clamp recordings. While the soma clearly is a very important "compartment'', neurons are much more than just their somata. However, quantitative data about of the dynamics taking place in the axonal and dendritic arbors is sparse mainly because performing simultaneous patch-clamp recordings of multiple compartments of the same cell is extremely challenging.
One strategy to capture dynamics over a larger spatial range could be to use extracellular signals, which are generated by transmembrane currents of all neuronal compartments and provide an indirect readout of the intracellular activity. This could be made possible with the advent of high-density micro-electrode arrays (HD- MEAs), which enable the recording of signal of individual neurons at sub-cellular resolution. This richness of information could allow the parameterizing of neuronal compartments which cannot be simultaneously and directly probed by patch-clamp experiments.

In this study, we investigated the potential of extracellular recordings as a data source for multicompartment models building and we extended the software BluePyOpt to allow such simulations to happen.

METHODS

Two cultured cortical neurons were exposed to a set of current stimuli and a simultaneous acquisition of their intracellular and extracellular voltage activity using somatic patch clamp recordings and a HD-MEA were performed. After the electrophysiology data acquisition, the target neurons were imaged to reconstruct their 3D morphology. During this step, the position of the cells relative to the MEAs were also recorded.

In a second step, we implemented the LFPy library as a backend simulator to the BluePyOpt optimization library. In this simulator, we instantiated a replica of each of the morphology reconstructions to which were added a set of mechanisms describing the ionic and calcium dynamics taking place in the cell. In parallel, we designed and extracted meaningful electrical features from both the intra and extracellular recordings. These electrical features were then used as targets during an optimization procedure aiming at finding the optimal parameters for the models for them to reproduce the features observed experimentally when exposed to the same stimuli.

RESULTS AND DISCUSSION

In two cell models, the use of patch-clamp data alone yielded better intracellular features, while the use of MEA data resulted in better extracellular features. In this latter case, the shape characteristics of the extracellular waveforms appear to be reproduced by the optimized cell models, but mismatches are still apparent.

Our study highlights key difficulties associated to the use of MEA both during the data acquisition and simulation steps. Adding extracellular measurements to a patch-clamp experiment adds constraints on the experimental setup and requires a quasi two-dimensional sample. On the simulation side, it implies making approximations about the medium surrounding the cells and requires a significant amount of compute power as the local field potential needs to be computed at each timestep of the simulation.

Keywords: high-density micro-electrode array, single neuron, neuron model building, LFP, LFPy, BluePyOpt

ACKNOWLEDGEMENTS

This study was supported by the ETH Zurich Postdoctoral Fellowship 19-2 FEL-17 (APB), the ERC Advanced Grant 694829 "neuroXscales" (JB, XX, TG, VE, AH), the China Scholarship Council (XX), by funding to the Blue Brain Project, a research center of the École polytechnique fédérale de Lausanne (EPFL), from the Swiss government's ETH Board of the Swiss Federal Institutes of Technology (TD, DM, MZ, AJ, HM, WVG), and by the European Union's

Horizon 2020 Framework Programme for Research and Innovation under the Specific Grant Agreement No. 945539 (Human Brain Project SGA3) (TD, AJ).

107. BRAVE: protecting the brain from COVID-19 mediated neurodegeneration through inflammasome inhibition

Eleonora Gianquinto[1], Emanuele Casali[2], Simone Gastaldi,[1] Giulia Rossetti[3], Paolo Carloni[3], Rebecca Wade[4], Giorgio Colombo[2], Massimo Bertinaria[1], Francesca Spyrakis[1*]

[1]Department of Drug Science and Technology, University of Turin, Turin, Italy.

[2]Department of Chemistry, University of Pavia, Pavia, Italy.

[3]Institute for Neuroscience and Medicine (INM-9), Forschungszentrum Jülich, Jülich, Germany.

[4]Molecular and Cellular Modeling Group, Heidelberg Institute for Theoretical Studies (HITS), Heidelberg, Germany.

*francesca.spyrakis@unito.it

INTRODUCTION/MOTIVATION

BRAVE aims at developing new and safer ligands against neuroinflammation and related diseases, by targeting the NLRP3 inflammasome (Figure 1), whose aberrant activation is strongly associated with neuroinflammation and, therefore, to several neurodegenerative diseases for which effective treatments are still missing. Recently, targeting the NLRP3 inflammasome has also been suggested as a promising and viable strategy to ease acute and long COVID-19 symptoms, again associated to neuroinflammation [1,2].

The NLRP3 inflammasome is formed by the apoptosis-associated speck-like protein containing a caspase-recruiting domain (ASC), procaspase-1, and the NLRP3 protein as the central core. Upon binding of activation signals, NLRP3 protein undergoes a massive conformational change that triggers the production of pro-inflammatory cytokines IL-1β and IL-18, and cell death by pyroptosis. The nucleotide-binding and oligomerization (NACHT) domain binds and hydrolyzes ATP and is primarily responsible for the oligomerization process [3-5]. Inhibition of NLRP3 protein by small molecules binding to an allosteric site in the NACHT domain is a strategy already explored by compounds as MCC950, which, unfortunately, present several toxicity issues [6].

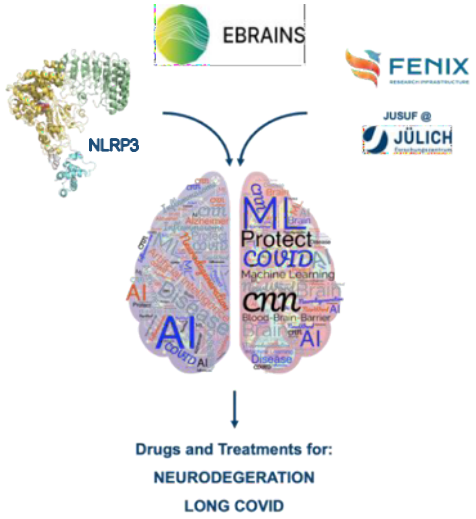

Figure 1. The BRAVE project

METHODS

Building on previous results obtained by our group, we are currently investigating and optimizing a library of in- house synthesized NLRP3 inhibitors by means of *in silico* studies. After a first assessment of the binding pose with docking studies, for the most promising inhibitors molecular dynamics (MD) simulations were set up to evaluate the stability of the ligands and characterizing their interaction in the binding site (Figure 2). As the synthesis of this library of NLRP3 inhibitors and *in vitro* tests are still ongoing, the results of MD simulations are guiding the modulation of scaffolds to maximize their affinity. In parallel, MD simulations of NLRP3 in complex with the known sulfonylurea-based inhibitor MCC950 have been run to clarify, at atomistic details, the allosteric inhibition on the overall architecture of NLRP3, and the interactions established by MCC950 in the NLRP3 binding site.

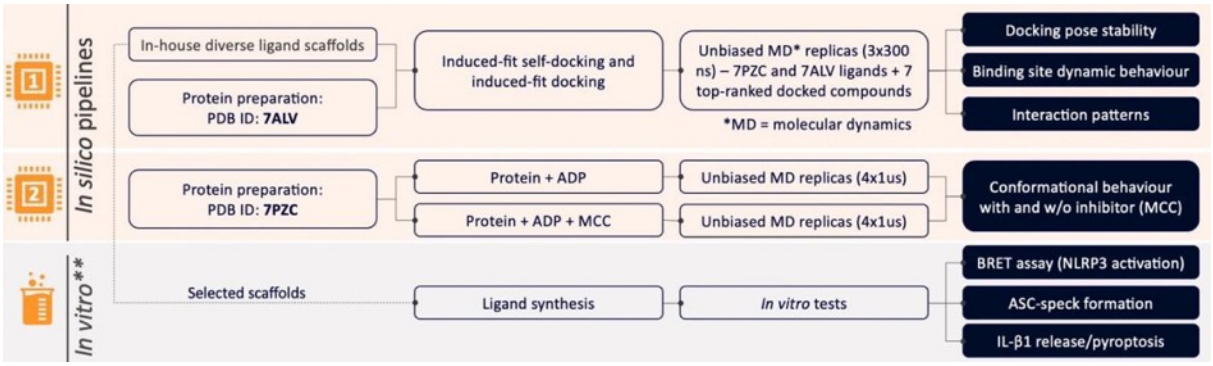

Figure 2. Pipeline for the identification of new NLRP3 allosteric inhibitors.

RESULTS AND DISCUSSION

MD simulations led to the selection and design of different series of ligands characterized by the presence of a polar moiety pointing towards the exterior part of the binding site, a hydrophobic region deeply inserted in the binding pocket and a linker joining the two. In particular, three different linkers have been recognized as more promising when the compounds have been tested in J774A.1 cells, for their capability of reducing the production of interleukin-1β, upon LPS/nigericin stimulation. Indeed, IC_{50} values in the low micromolar range have been determined, identifying these compounds as new promising hits for treating neuroinflammation. A selected number of molecules is currently under hit-to-lead optimization stage and is being tested for basic pharmacokinetic parameters and BBB permeation.

Keywords: Neuroinflammation, neurodegeneration, NLRP3, inflammasome, drug design, molecular dynamics simulations, long COVID

ACKNOWLEDGEMENTS

We kindly acknowledge HBP for supporting the project H2020 BRAVE - Protecting the brain from COVID-19- mediated neurodegeneration through inflammasome inhibition - GA: 945539 -, and EBRAINS for providing the essential calculation recourses at the Fenix research infrastructure, supporting the project number 25681.

REFERENCES.

[1] Freeman TL and Swartz TH. Targeting the NLRP3 inflammasome in severe COVID-19. *Frontiers in Immunology*, 2020, 111:1518; doi: 10.3389/fimmu.2020.01518.

[2] Zeng J et al. Specific inhibition of the NLRP3 inflammasome suppresses immune overactivation and alleviates COVID-19 like pathology in mice. *EBioMedicine*, 2022, 75:103803; doi: 10.1016/j.ebiom.2021.103803.

[3] He Y, Hara H, Nuñez G. Mechanism and regulation of NLRP3 inflammasome activation. *Trends in biochemical sciences*, 2016, 41: 1012-1021; doi: 10.1016/j.tibs.2016.09.002.

[4] Sharif H et al. Structural mechanism for NEK7-licensed activation of NLRP3 inflammasome. *Nature*, 2019, 570: 338-343; doi: 10.1038/s41586-019-1295-z.

[5] Sharma M, De Alba E. Structure, activation and regulation of NLRP3 and AIM2 inflammasomes. *International Journal of Molecular Sciences*, 2021, 22: 872; doi: 10.3390/ijms22020872.

[6] Wu D et al. Target of MCC950 in inhibition of NLRP3 inflammasome activation: a literature review. *Inflammation*, 2020, 43: 17-23; doi: 10.1007/s10753-019-01098-8.

108. Modelling reentry excitation and interventions in a personalized cortical model of epilepsy

Paul Triebkorn[1], Huifang Wang[1], Viktor Jirsa[1]

Institut de Neurosciences des Systèmes, Aix-Marseille Université, Marseille, France

Purpose: Current treatment options for epilepsy are medication, surgical removal of the epileptic tissue and stimulation. Success rates of surgical and stimulative interventions are in the range of 50% to 70%, leaving room for improvement. Computational modelling and dynamical systems theory can help to further our understanding about seizure dynamics and possible to provide intervention strategies.

Method: We built a high resolution personalized computational model of a patient with drug resistant focal epilepsy in the left temporal lobe. T1 weighted and diffusion MRI together with tractography were used to reconstruct the cortical surface and to estimate connections between points of the surface on the scale of $1mm^3$. A two dimensional dynamical model, called the Epileptor, was used in an excitable regime to model seizure dynamics.

Results: We first simulated reentry excitation in a toy model of two delay-coupled 2D Epileptors. Then we equipped the cortical surface with the dynamical model and explored the parameter space of local and global coupling strength. We observed self-limiting excitations, spiral waves and sustained reentry excitation. We tested two intervention strategies trying to prevent reentry. Virtual surgery was applied to the white matter by lesioning fibre tracks and removing their contribution to the connectivity of the cortex. We also demonstrated phase dependent stimulation effects through virtually implanted electrodes.

Conclusion: We demonstrated that a high resolution personalized computational model can be used to simulate epileptic dynamics and test intervention strategies on a level of resolution that is necessary for real world applications. Future studies should focus on fine tuning the parameters of the model to fit it to the individual observed empirical data and optimize the intervention.

109. Computation of Protein-Protein Interaction Kinetics using τ-RAMD

Giulia D'Arrigo[1*], Daria B. Kokh[1], Ariane Nunes-Alves[1,2], Rebecca C. Wade[1,3]

[1]Molecular and Cellular Modeling Group, Heidelberg Institute for Theoretical Studies, Schloss-Wolfsbrunnenweg 35, 69118 Heidelberg, Germany.

[2]Technical University of Berlin, Strasse des 17. Juni 135, 10623, Berlin, Germany

[3]Center for Molecular Biology (ZMBH), DKFZ-ZMBH Alliance, and Interdisciplinary Center for Scientific Computing (IWR), Heidelberg University, Im Neuenheimer Feld 282, 69120 Heidelberg, Germany.

*giulia.darrigo@h-its.org

INTRODUCTION

Neuronal signalling cascades originate, at the subcellular level, from a sequence of complex biomolecular interactions whose aberrations can cause the onset of diverse pathological conditions, including cancer. Protein- protein interactions (PPIs) are clinically relevant targets for the design of many small-molecule drugs as well as engineered proteins (e.g., antibodies or cytokines) [1]. The dissociation rate constant (k_{off}) or its reciprocal, residence time ($\tau=1/k_{off}$), is one of the key parameters that describe the duration of biomolecular interactions and its value can be optimized in the design of specific, high-affinity modulators, thus it is assuming an increasingly important role in many drug-design campaigns. However, computing kinetic rates (typically ranging from minutes to hours) is very challenging due to the limited timescale accessible with conventional molecular dynamics simulation approaches [2]. To tackle this limitation, we here report the validation and application of a computational method to estimate protein-protein dissociation rates, providing a basis for its use in kinetic modelling of neuronal signalling cascades, as well as in their modulation.

METHODS

We employed the computationally efficient τ-RAMD (τ-Random Acceleration Molecular Dynamics) method [3], which enables the observation of dissociation events in short timescale (nanosecond) molecular dynamics simulations. Following the successful application on protein-small molecule systems [4], τ-RAMD is here used to estimate the relative residence times for PPIs. Besides the computation of the dissociation rate, τ-RAMD, is here applied together with the MD-IFP (Interaction Fingerprint) post-analysis, to provide an in-depth investigation of the dissociation mechanisms (see the workflow in Figure 1). The methodology is here assessed by application to a set of well-known protein-protein complexes and a wide range of mutants [5].

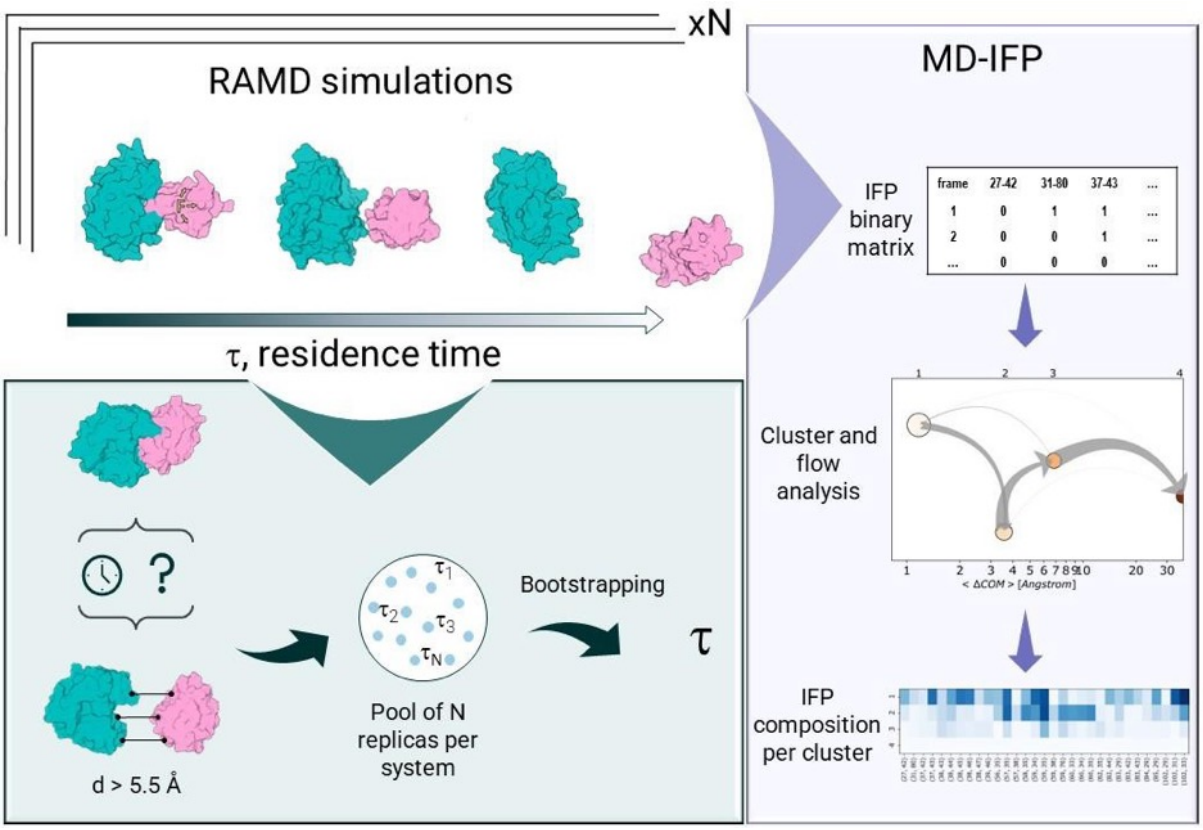

Figure 1. τ-RAMD workflow applied to protein-protein complexes. A randomly oriented force (F) is applied to one of the two proteins to facilitate the dissociation. A set of RAMD simulations are run until the dissociation of the two proteins is complete. Afterward, the RAMD trajectories are analyzed to compute the relative residence time through a bootstrapping procedure (green box) and to compute the IFPs to perform a cluster analysis for the detection of the dissociation paths and related metastable states (violet box).

RESULTS AND DISCUSSION

Our calculations show the ability of τ-RAMD to compute the relative residence time for a diverse set of protein- protein complexes in overall agreement with the experimental data (Figure 2a). The cluster analysis of the MD- IFP data provides structural insights into the unbinding mechanism and enables the detection of the metastable states along the dissociation pathway. The latter information helps to identify hot-spots to target to selectively modulate PPIs (Figure 2b). Overall, τ-RAMD is found to be a valuable approach for guiding drug and protein design and this study provides a basis for its use in the kinetic modelling of signaling cascades.

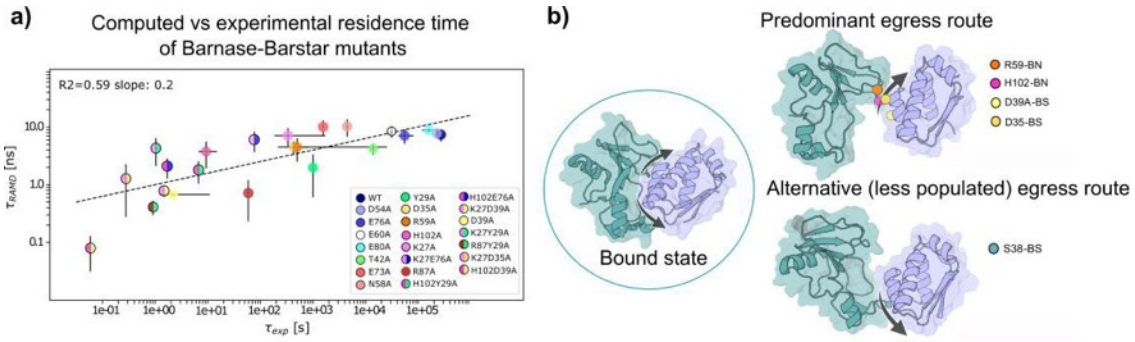

Figure 2. Results for a protein-protein complex and a set of its mutants. a) The experimental residence times computed with τ-RAMD for a set of 23 mutants of the barnase-barstar enzyme-inhibitor complex are plotted against the experimental values. b) The two main egress routes detected in the MD-IFP and cluster analyses are indicated with the key residues highlighted.

Keywords: kinetics, dissociation rate, residence time, molecular dynamics, simulation, modelling, protein-protein

ACKNOWLEDGEMENTS

We acknowledge the Human Brain Project funded by the European Union's Horizon 2020 Framework Programme for Research and Innovation under the Specific Grant Agreement No. 945539 (Human Brain Project SGA3) and the Fenix research infrastructure for providing calculation resources. We thank the Klaus Tschira Foundation for support.

REFERENCES

[1] Lu, H., Zhou, Q., He, J. et al. Recent advances in the development of protein–protein interactions modulators: mechanisms and clinical trials. Sig Transduct Target Ther. 2020; 5(1):213. doi: 10.1038/s41392-020-00315-3.

[2] Nunes-Alves A, Kokh DB, Wade RC, Recent progress in molecular simulation methods for drug binding kinetics, Curr Opin Struct Biol. 2020, 64:126-133. doi: 10.1016/j.sbi.2020.06.022

[3] Kokh DB, Amaral M, Bomke J, et al. Estimation of Drug-Target Residence Times by τ-Random Acceleration Molecular Dynamics Simulations. J Chem Theory Comput. 2018. doi: 10.1021/acs.jctc.8b00230

[4] Kokh DB, Wade RC. G Protein-Coupled Receptor-Ligand Dissociation Rates and Mechanisms from τRAMD Simulations. J Chem Theory Comput. 2021; 17(10):6610–6623. doi: 10.1021/acs.jctc.1c00641

[5] Schreiber G. Kinetic studies of protein-protein interactions. Curr Opin Struct Biol. 2002; 12(1):41-7. doi: 10.1016/s0959-440x(02)00287-7

110. Simulation of a Biophysical Morphological Realistic Model of the Inferior Olivary Nucleus in Arbor

Lennart P. L. Landmeer*^, Max C. W. Engelen*, Mario Negrello*

*Department of Neuroscience, Erasmus MC, Rotterdam, Netherlands
^Jülich Supercomputing Centre, Forschungszentrum Jülich, Jülich, Germany

Keywords: *neural simulation, network tuning, cable cell, local field potentials*

Introduction

The olivo-cerebellar loop is central in motor control and learning. Climbing fibers from the Inferior Olive (IO) neurons innervate Purkinje cell arborizations, which in turn inhibit Deep Cerebellar Nuclei (DCN), which connect back to the IO, completing the loop. Neurons from the IO show persistent subthreshold oscillations, which can synchronize via dendro-dendritic gap junctions in clusters [Loyola19]. Multiple studies exist using computational (point cell) models to characterize the IO dynamics, with a focus on the biophysics of this brain region [deGruijl12, Negrello19]. We created a novel method to generate realistic morphologies and network topologies of an *in silico* IO, allowing one to study the precise dendritic features and spatial boundary conditions that influence IO spatio-temporal pattern formation.

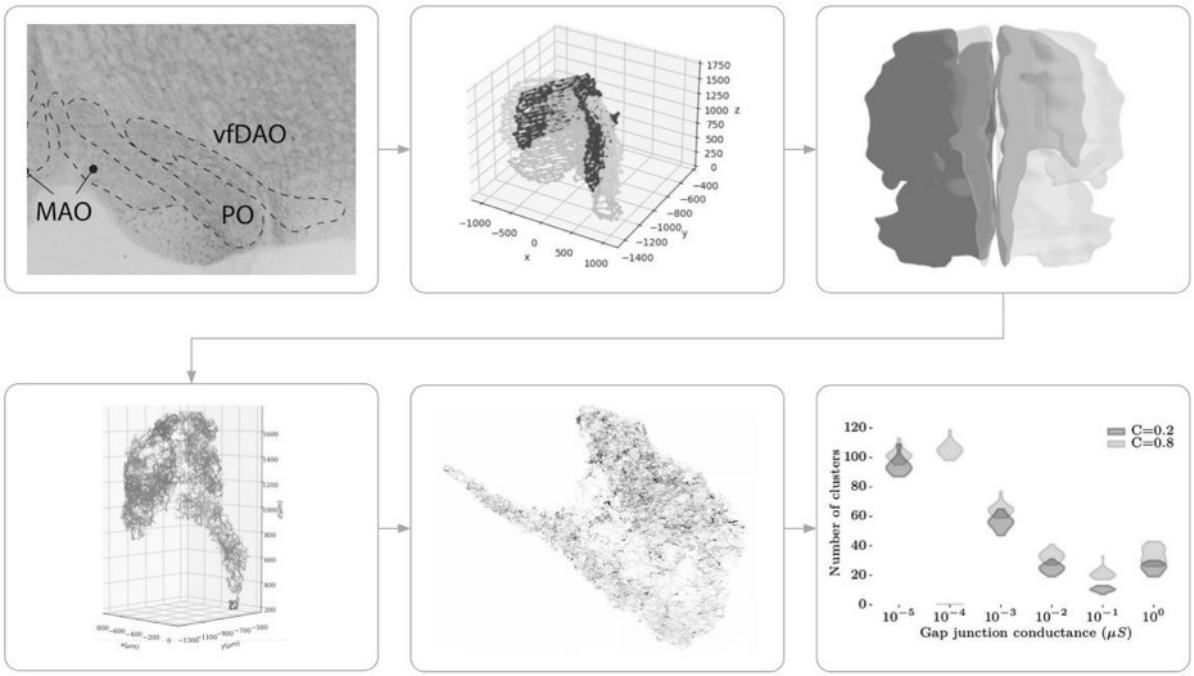

Methods

Morphological detailed digital twins of the IO were grown via a novel graph-based algorithm, mimicking experimental distributions [Leznik05, Rekling12, Vrieler19, Lefler20] and obeying spatial constraints of the IO. Spatial boundary conditions were derived from a sliced mouse IO. A

biophysical model of IO neurons was ported to the Arbor [Akar19] simulator. Evolutionary search [Hansen19] optimization of cells with similar passive impulse response was used to tune single cells subthreshold oscillations to within observed frequency, amplitude and symmetry ranges. Subsequent connection as a network led to unpredictable (but expected) loss of behavior, which was restored by a fast homeostatic control mechanism, hand tuned and developed for this purpose. Both a connected and unconnected network were simulated at the same time to allow the controller to tune both observed in-network and disconnected cellular behavior. Final networks were simulated in Arbor and local field potentials (LFP) were derived using the LFPyKit [Hagen22] library.

Results

In general, there is good agreement between *in silico* and *in vitro* dendritic statistics, even for empirical distributions that were not available to the network generation method. Sweeping over gap junction conductance, we found multiple synchronization states, suggesting that the default state of the unperturbed network is cluster synchronization. Specifically, by mapping gap junction conductance to experimentally obtained coupling coefficients, we find that the biological network is likely tuned for the critical regime between global synchrony and maximum cluster synchronization. Clustering of the network topology did not have a large effect on the amount of observed dynamically coupled clusters, but did affect the shape of these clusters considerably. LFP's obtained from a *in silico* whisker puff experiment had some similarities to experimentally obtained results, but showed that the biological network was likely more synchronized than the inferior olive network.

Discussion

Tuning of a large library of highly variable morphological cells could not be solved by tuning each cell individually. Our method, based on the grouping of similar morphologies on the basis of their passive impulse response, yielded good results but still involved manual work in tuning of hyperparameters. A more general method could be developed that also looks at channel distributions, for example, based on the workings of NEAT [Wybo18] which included linearized channels in its morphology metrics. However, the assumptions of NEAT break under subthreshold oscillations. Similarly, network tuning via individual controllers per cell leads to desired behavior, but only after considerable manual intervention. Automatic derivation of stable controller rules could use insights from machine learning and control theory for further developments. Still, our ad-hoc developed methods lead to a novel, highly detailed model of the IO that allows for insights on the effect of local topology on cluster dynamics and is the first IO model to be able to compare itself to experimental LFP data.

Acknowledgments

Tom Ruigrok for providing mouse IO contours from which the 3d model could be derived. Nora Abi Akar, Thorsten Hater and Brent Huisman for help and support with the Arbor simulator.
Gaute Einevoll and Espen Hagen for helping with LFP measurements. NVIDIA Academic Hardware Grant Program for donating an RTX6000 for CUDA development.

References

[Leznik05] Elena Leznik and Rodolfo Llinas. Role of gap junctions in synchronized neuronal oscillations in the inferior olive. Journal of neurophysiology, 94(4):2447–2456, 2005. doi: 10.1152/jn.00353.2005

[deGruijl12] De Gruijl, Jornt R., et al. "Climbing fiber burst size and olivary sub-threshold oscillations in a network setting." PLoS computational biology 8.12 (2012): e1002814. doi: 10.1371/journal.pcbi.1002814

[Rekling12] Jens C Rekling, Kristian HR Jensen, and Henrik Jahnsen. Spontaneous cluster activity in the inferior olivary nucleus in brainstem slices from postnatal mice. The Journal of Physiology, 590(7): 1547–1562, 2012. doi: 10.1113/jphysiol.2011.222570

[Wybo18] Wybo, W. A. M., Torben-nielsen, B. and Gewaltig, M. (2018) Dynamic compartmentalization in neurons enables branch-specific learning., bioRxiv, 10.1101/24. doi: 10.1101/244772.

[Aka19] Abi Akar, Nora, et al. "Arbor—a morphologically-detailed neural network simulation library for contemporary high-performance computing architectures." 2019 27th euromicro international conference on parallel, distributed and network-based processing (PDP). IEEE, 2019. doi: 10.1109/EMPDP.2019.8671560

[Loyola19] Loyola, S., et al. "Inferior olive: All ins and outs." *Handbook of the Cerebellum and Cerebellar Disorders. Cham: Springer International Publishing* (2019): 1-56. doi:10.1007/978-3- 319-97911-3_43-2

[Negrello19] Negrello, Mario, et al. "Quasiperiodic rhythms of the inferior olive." PLoS Computational Biology 15.5 (2019): e1006475. doi: 10.1371/journal.pcbi.1006475

[Vrieler19] Vrieler, Nora, et al. "Variability and directionality of inferior olive neuron dendrites revealed by detailed 3D characterization of an extensive morphological library." Brain Structure and Function 224.4 (2019): 1677-1695. doi: 10.1007/s00429-019-01859-z

[Lefler20] Yaara Lefler, Oren Amsalem, Nora Vrieler, Idan Segev, and Yosef Yarom. Using subthreshold events to characterize the functional architecture of the electrically coupled inferior olive network. elife, 9:e43560, 2020. doi: 10.7554/eLife.43560

[Hagen22] Espen Hagen and Torbjørn Vefferstad Ness. Lfpy/lfpykit: Lfpykit-0.4, February 2022. URL https://doi.org/10.5281/zenodo.6037497.

111. Hippocampal learning in Alzheimer's disease: integrating experimental data and computational modeling

Ausra Saudargiene[1*], Justinas J. Dainauskas[1,2], Hélène Marie[3], Michele Migliore[4]

[1]Neuroscience Institute, Lithuanian University of Health Sciences, Kaunas, Lithuania
[2]Department of Informatics, Vytautas Magnus University, Kaunas, Lithuania
[3]Institut de pharmacologie moléculaire et cellulaire, CNRS, Université Côte d'Azur, Valbonne, France
[4]Institute of Biophysics, National Research Council, Palermo, Italy

ausra.saudargiene@lsmuni.lt

INTRODUCTION/MOTIVATION

Alzheimer's disease (AD), a degenerative brain disorder, has a long preclinical stage and, before any clinical symptoms appear, pathological processes are observed in the hippocampus and entorhinal cortex, key brain structures responsible for memory encoding and retrieval. AD can not be prevented, halted, or cured today, and new interdisciplinary ways are urgently needed to understand and treat this devastating disease. Recent experimental evidence supports the fundamental role of AD-related peptides early in the pathology: in particular the most widely studied Amyloid beta (Aβ), and the less investigated Amyloid eta (Aη) and Amyloid precursor protein (APP) C-terminal peptide (AICD). The aim of this project is to understand the AD-related peptide-induced mechanisms of impaired learning and memory in hippocampal CA1 region in early pathology of AD by applying the integrated experimental and computational modelling approach.

METHODS

We investigated the effects of Aβ, Aη, AICD on intrinsic excitability of hippocampal CA1 pyramidal neurons and synaptic plasticity at hippocampal CA1-CA3 synapses in early pathology of AD. We developed data-driven *in silico* models of the hippocampal learning in CA1 region under AD conditions, and 1) extended the experimental evidence of Aη, Aβ, AICD-related changes in the properties of hippocampal CA1 pyramidal neuron synaptic plasticity, synaptic signal integration and neuronal excitability; 2) incorporated the effects of AD-related peptides into computational models of hippocampal synaptic plasticity to determine and explain the mechanisms of altered hippocampal function that leads to impaired learning in AD; 3) assessed the potential targets for innovative treatment of AD. We analyzed the experimental data of AD-related peptide effect on intrinsic excitability properties of CA1 pyramidal neurons using Feature Extraction Tool of the HBP Brain Simulation Platform. We built a computational model of synaptic plasticity under AD conditions and embedded it into a compartmental model of CA1 pyramidal neuron to study the development of individual synaptic strengths in clusters of

Schaffer collateral synapses and to assess the patterns of impaired learning in hippocampal pyramidal neurons.

RESULTS AND DISCUSSION

The modeling results support the experimental evidence that pathological concentrations of Aβ, Aη, and AICD cause long-term potentiation (LTP) impairment. Long-term depression (LTD) enhancement was observed in Aβ conditions. Synaptic plasticity was strongly dependent on GluN2B-NMDA receptor subunit functioning, and rescued by its partial blockade in AD. The modeling study provides insight into the complex interactions in AD pathophysiology, and suggests the conditions under which synaptic plasticity is restored. The inter-disciplinary analysis, bringing together experimentalists and modelers, helps to further unravel the neuronal mechanisms most affected by AD, build a biologically-plausible computational models of the hippocampal CA1 area under AD conditions, and suggest potential targets for pharmacological treatment of AD.

Keywords: Synaptic plasticity, Alzheimer's disease, hippocampus, CA1 pyramidal neuron, NMDA receptor, GluN2B-NMDA receptor subunit, Amyloid beta, Amyloid eta, Amyloid precursor protein C- terminal peptide.

ACKNOWLEDGEMENTS

Funding: This research is funded by the Research Council of (Lithuania), Agence Nationale de la Recherche (France) (Flagship ERA-NET Joint Transnational Call JTC 2019 in synergy with the Human Brain Project, No. S-FLAG-ERA-20-1/2020-PRO-28), the EU Horizon 2020 Framework Program for Research and Innovation (Specific Grant 945539, Human Brain Project SGA3); Fenix computing and storage resources was provided under Specific Grant Agreement No. 800858 (Human Brain Project ICEI) and a grant from the Swiss National Supercomputing Centre (CSCS) under project ID ich01.

112. Modeling and simulating spiking neurons and synaptic plasticity with NESTML

Charl Linssen[1,2*], Pooja Babu[1*], Jochen M. Eppler[1], Abigail Morrison[1-3]

[1] Simulation Lab Neuroscience, Jülich Supercomputer Centre, Institute for Advanced Simulation, Jülich-Aachen Research Alliance, Forschungszentrum Jülich GmbH

[2] Institute for Neuroscience and Medicine INM-6 / INM-10, Jülich-Aachen Research Alliance, Institute for Advanced Simulation IAS-6, Forschungszentrum Jülich GmbH

[3] Software Engineering, Department of Computer Science 3, RWTH Aachen University, Aachen, Germany

*c.linssen@fz-juelich.de, p.babu@fz-juelich.de

INTRODUCTION/MOTIVATION

NESTML is a domain-specific modeling language for neuron models and synaptic plasticity rules. It is designed to support researchers in computational neuroscience by allowing them to specify models in a precise and intuitive way. These models can subsequently be used in dynamical simulations of small or large-scale spiking neural networks, by means of high performance simulation code generated by the NESTML toolchain. NESTML features a concise yet expressive syntax, inspired by Python, making it easy to write, understand, maintain and share models. There is direct language support for (spike) events, differential equations, convolutions, stochasticity, and arbitrary algorithms using imperative programming concepts, in addition to flexible event management using handler functions and prioritization.

METHODS

Models specified in the NESTML syntax are processed by an open-source toolchain that generates fast code for a given target simulator platform. It was originally developed for NEST Simulator[1] but is being extended with support for the SpiNNaker neuromorphic hardware platform. The toolchain provides verbose model validation and transformation (optimization), fully automated ODE analysis, solver selection and solver code generation, and is extensible to new target platforms in a straightforward manner by means of templates. The toolchain is written in Python and accessible using a Python API. It can be run locally, or in a cloud environment (such as Fenix) with Jupyter Notebook as a web interface.

NESTML comes with an extensive library of neuron and synapse models. The supported neuron models include Hodgkin-Huxley and reduced variants, current and conductance-based integrate-and-fire neurons and adaptive variants. NESTML also supports synaptic plasticity rules such as spike-timing dependent plasticity (STDP) with all- to-all and nearest neighbor spike pairing, triplet STDP, and third-factor plasticity rules where STDP weight update is modulated by a postsynaptic variable such as dendritic current or dopamine concentration.

Recently added new features include support for vectors, delay-differential equations, detailed branching compartmental neurons and a Python code generation target. The software is hosted on Github[2] with continuous integration (CI) run on Github Actions. The CI runs over 100 unit and integration tests which validate the models and toolchain functionality, checking for numerical correctness of the simulation. Model documentation is automatically generated and published on ReadTheDocs in combination with other software documentation and training materials[3].

RESULTS AND DISCUSSION

NESTML makes neuron and synapse modeling accessible to neuroscience researchers without requiring a training in computer science. With increasing model complexity, models are typically re-used and evolved upon rather than starting from scratch. This means that models need to be findable, accessible, interoperable and reusable ('FAIR' principles). Findable means that in a database of potentially hundreds of model variants, the appropriate model can be easily found. Accessible models are those that do not require extensive toolchain dependencies to work with. Interoperable models are usable across different computation hardware and simulation environments. Reusability implies that the models can be easily extended and iterated upon. Furthermore, neural network models often involve a very large number of neurons and synapses, placing high demands on performance and memory consumption. Code generation allows an accessible and easy-to-use language for the user to be combined with good simulation performance; a technique that is gaining more traction within neuroscience[4].

Keywords: neural network, simulation, spiking neuron, synapse, model

ACKNOWLEDGEMENTS

This project has received funding from the Helmholtz Association through the Helmholtz Portfolio Theme "Supercomputing and Modeling for the Human Brain" and the European Union's Horizon 2020 Framework Programme for Research and Innovation under Specific Grant Agreements No. 720270, No. 785907 and No. 945539 (Human Brain Project SGA1, SGA2 and SGA3). We thank Angela Fischer for illustrations.

REFERENCES

[1] Gewaltig M-O & Diesmann M (2007) NEST (Neural Simulation Tool) Scholarpedia 2(4):1430
[2] https://github.com/nest/nestml/
[3] https://nestml.readthedocs.io/
[4] Blundell I, Brette R, Cleland TA, et al. Code Generation in Computational Neuroscience: A Review of Tools and Techniques. Frontiers in Neuroinformatics 2018; 12

113. Creating realistic networks in silico of health and disease using the Snudda softwareAbstract title

J J Johannes Hjorth[1*], Ilaria Carannante[1], Johanna Frost Nylén[2], Alexander Kozlov[1,2], Bo Bekkouche[1], Martina Scolamiero[3], Wojciech Chachólski[3], Jeanette Hellgren Kotaleski[1,2]

[1]Science for Life Laboratory, School of Electrical Engineering and Computer Science, KTH Royal Institute of Technology, SE-10044, Stockholm, Sweden [2]Department of Neuroscience, Karolinska Institute, SE-17172, Stockholm, Sweden

[3]Department of Mathematics, KTH Royal Institute of Technology, Stockholm, Sweden

* hjorth@kth.se

INTRODUCTION

Detailed computer simulations are an important tool for neuroscience. To model the connectivity of large scale networks we have developed Snudda, a software tool that based on reconstructed morphologies can place synapses between nearby neurons [1,2,3]. We have recently extended the tool with the ability to model the degeneration of neuron morphologies, seen for example in Parkinson's disease (PD) and rodent models of PD [4]. Here we present a use case of striatal network creation for healthy and diseased cases. The dendrites of D1 and D2 striatal projection neurons (dSPN, iSPN) degenerate, leading to a reduction in connectivity, while the axons of fast spiking (FS) interneurons grow as a compensatory mechanism.

METHODS

Neuron models are created based on reconstructed neuron morphologies, and electrophysiological parameters are optimised using BluePyOpt [5]. The resulting models are then placed either inside a 3D mesh representing the striatum, or in a subset of the volume. Based on the proximity of axons and dendrites, putative synapses are placed using a touch detection algorithm that voxelizes the space and looks for locations where axons and dendrites overlap. The putative synapses are then pruned based on a set of rules to match pairwise connectivity data, producing the final set of synapses. Gap junctions are also placed using a similar algorithm.

To model the neurodegenerative changes in the network each SPN had their dendrites shrunk from the dendritic tips using Treem (Hjorth et al 2021). This reduced the size and complexity of the dendritic arborisation. The original and degenerated morphologies of the neurons were then compared, and Snudda removed the synapses that were on the parts of the network that had degenerated.

The changes in the connectivity were then analysed, we investigated changes in synapse count and connection probability, but also used topological measures, such as counting the number of directed cliques.

RESULTS

We found that the decrease of the total dendritic length of dSPN and iSPN neurons, down to 70% in 6-OHDA lesioned mice and even more in human PD patients, leads to a drastic reduction in connectivity of the network. Based on the clique analysis we see that interneurons that are not degenerated become comparably more important for maintaining connectivity within the network as the dSPN and iSPN degenerate.

DISCUSSION

Here we present Snudda, a software tool for generating and simulating detailed networks of neurons, both in the healthy and in the diseased case. We demonstrate a use case of Parkinson's disease, where from morphological changes we are able to model the alterations in network connectivity. Future work will include more detailed comparisons not only of the topology, but also on the activity of the networks including models tuned both for the healthy and diseased cases.

Keywords: Parkinson's disease, striatum, detailed computer modelling

ACKNOWLEDGEMENTS

Horizon 2020 Framework Programme (945539, HBP SGA3); Vetenskapsrådet (VR-M-2020-01652); Swedish e- science Research Center (SeRC); KTH Digital Futures; EBRAINS Basal Ganglia Facility Hub. The computations were enabled by resources provided by the Swedish National Infrastructure for Computing (SNIC) at PDC KTH partially funded by the Swedish Research Council through grant agreement no. 2018-05973. We also acknowledge the use of Fenix Infrastructure resources, which are partially funded from the European Union's Horizon 2020 research and innovation programme through the ICEI project under the grant agreement No. 800858.

REFERENCES

[1] Hjorth, J. J. J., Hellgren Kotaleski, J., & Kozlov, A. (2021). Predicting synaptic connectivity for large-scale microcircuit simulations using Snudda. Neuroinformatics, 19(4), 685-701. https://doi.org/10.1007/s12021-021-09531-w

[2] Hjorth, J. J. J., Kozlov, A., Carannante, I., Frost Nylén, J., Lindroos, R., Johansson, Y., ... & Grillner, S. (2020). The microcircuits of striatum in silico. Proceedings of the National Academy of Sciences, 117(17), 9554- 9565. https://doi.org/10.1073/pnas.2000671117

[3] Frost Nylén, J., Hjorth, J. J. J., Grillner, S., & Hellgren Kotaleski, J. (2021). Dopaminergic and Cholinergic Modulation of Large Scale Networks in silico Using Snudda. Frontiers in Neural Circuits, 15, 748989. https://doi.org/10.3389/fncir.2021.748989

[4] Fieblinger, T., Graves, S., Sebel, L. et al. Cell type-specific plasticity of striatal projection neurons in parkinsonism and L-DOPA-induced dyskinesia. Nat Commun 5, 5316 (2014). https://doi.org/10.1038/ncomms6316

[5] Van Geit, W., Gevaert, M., Chindemi, G., Rössert, C., Courcol, J. D., Muller, E. B., ... & Markram, H. (2016). BluePyOpt: leveraging open source software and cloud infrastructure to optimise model parameters in neuroscience. Frontiers in neuroinformatics, 10, 17. https://doi.org/10.3389/fninf.2016.00017

114. Mean-field approximation of biophysical neuronal network to capture healthy & pathological dynamics

Abhirup Bandyopadhyay[1], Giovanni Rabuffo[1]*, Carmela Calabrese[1], Kashyap Gudibanda[1], Damien Depannemaecker[1]*, Anton I Ivanov[1], Marja-Leena Linne[2], Christophe Bernard[1], Viktor Jirsa[1], Spase Petkoski[1]

[1] Aix Marseille University, INSERM, Institute de Neuroscience des Systems, Marseille, 13005 France

[2] Faculty of Medicine and Health Technology, Tampere University, 33100 Tampere, Finland

*damien.depannemaecker@univ-amu.fr

*giovanni.rabuffo@univ-amu.fr

INTRODUCTION/MOTIVATION

Mean-field models are commonly used in network and brain modelling for their simplicity in studying dynamics. They represent a lumped description of neuronal assemblies connected by synapses, but typically do not take into account the ionic composition of the extracellular space, which can strongly affect neuronal activity[1]. In this work we included this aspect, from the single neuron level [2] to the corresponding mean-field [3] as represented in figure 1.

METHODS

This study presents a mean-field model of a population of Hodgkin-Huxley-type neurons that links the intra- and extra-cellular ion concentrations to the mean membrane potential, and the synaptic input to the population firing rate. The approach follows the method developed by *Montbrió et al [4], that is valid if the membrane potential distribution is a Lorentzian and if the equation is quadratic. With our model the the cubic shape of the reduced Hodgkin-Huxley type model is approximate with a step-wise quadratic function to match these assumptions. The derivation preserves the slow dynamics of ion concentrations. This model is compared to experimental data obtain in-vitro using low-Mg^{2+} aCSF. The eletrophysiological activities were measured using extracellular glass electrode, together with extracellular potassium concentration, using potassium-selective microelectrode.*

RESULTS AND DISCUSSION

The experimental co-recording of extracellular local field potential and extracellular [K^+] shows the correlation between pathological bursting and extra-cellular [K^+] elevation (see figure 2a). Such a dynamics is capture by the model, which can generate various brain activities by capturing the dynamics of homogeneous networks of biophysical neurons driven by an ion-exchange mechanism. It can reproduce a large repertoire of behaviors including multi-stability during simulated healthy states, pathological spiking, bursting, and depolarization block [2].

It provides a detailed biophysical level of description while describing dynamics at the neural mass scale, and thus may bridge the gap between high-level neural mass approaches and physiological parameters that drive neuronal dynamics. This approach could serve as a computational baseline to address core questions in epilepsy research. In particular, how to identify the multiscale mechanisms implicated in epileptogenicity and propagations of seizures. A first implementation connecting neural mass models into The Virtual Brain, show propagation of pathological bursts show how with a certain level of connectivity the local elevation of potassium bath concentration leads to the propagation of pathological activities (see figure 2b).

Keywords: Hodgkin–Huxley-type neurons, Mean-field model, Biophysical neural mass modeling, Multiscale neural mechanisms, Epilepsy

ACKNOWLEDGEMENTS

This research was supported by the European Union's Horizon 2020 research and innovation program under grant agreement 945539 (SGA3) Human Brain Project and by grant agreement No. 826421 Virtual Brain Cloud. CB received support from the Agence Nationale de la recherche projects ANR-17-CE37-0001-01 and ANR-20-NEUC-0005-02

REFERENCES

[1] Rasmussen R, Nicholas E, Petersen NC, Dietz AG, Xu Q, Sun Q, Nedergaard M. Cortex-wide Changes in Extracellular Potassium Ions Parallel Brain State Transitions in Awake Behaving Mice. Cell Rep. 2019 Jul 30;28(5):1182-1194.e4. doi: 10.1016/j.celrep.2019.06.082. PMID: 31365863; PMCID: PMC6790006.

[2| Damien Depannemaecker, Anton Ivanov, Davide Lillo, Len Spek, Christophe Bernard, and Viktor Jirsa. A unified physiological framework of transitions between seizures, sustained ictal activity and depolarization block at the single neuron level. Journal of Computational Neuroscience, 50(1):33–49, January 2022

[3] Abhirup Bandyopadhyay, Giovanni Rabuffo, Carmela Calabrese, Kashyap Gudibanda, Damien Depannemaecker, Anton Ivanov, Christophe Bernard, Viktor K. Jirsa, and Spase Petkoski. Mean-field approximation of network of biophysical neurons driven by conductance-based ion exchange. November 2021.

[4] *Ernest Montbrio, Diego Pazo, and Alex Roxin. Macroscopic description for networks of spiking neurons. Phys. Rev. X, 5:021028, Jun 2015*

Figure 1: Biophysically inspired neural mass model:

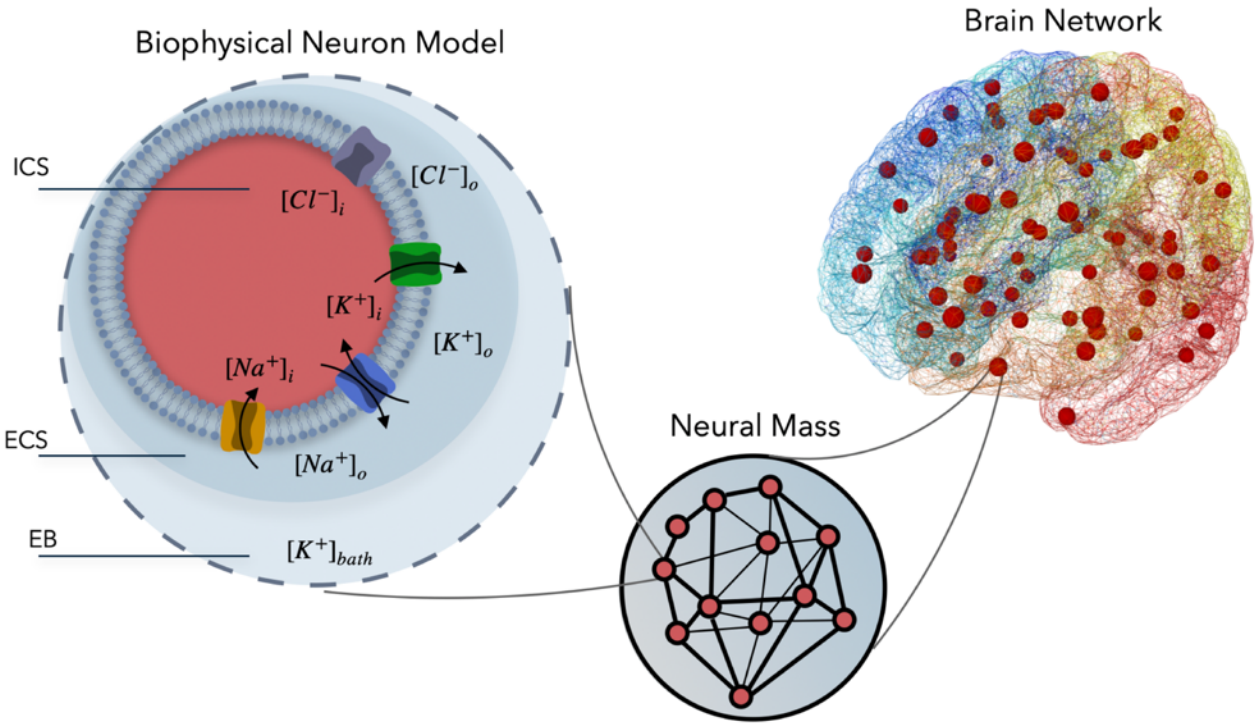

Schematic diagram of the ion channel mechanism in extracellular and intracellular space in the brain. A biophysical model of a single neuron consists of three compartments (left panel): the intracellular space (ICS; in red), the extracellular space (ECS; in dark blue), and the external bath (EB; in light blue). The ion exchange across the cellular space occurs through the ion channels: Na^+ gets inside the ICS (yellow channel), K^+ gets out (green channel), the flow of Cl^- can be bidirectional (purple channel); for the pump (blue), Na^+ gets out and K^+ gets into the ICS. A population of interacting neurons sharing the same $[K^+]_{bath}$ concentration forms a local neural mass (middle panel), for which we model the mean-field equations in this work. Brain network model (right panel) with the activity of each brain region represented by neural masses.

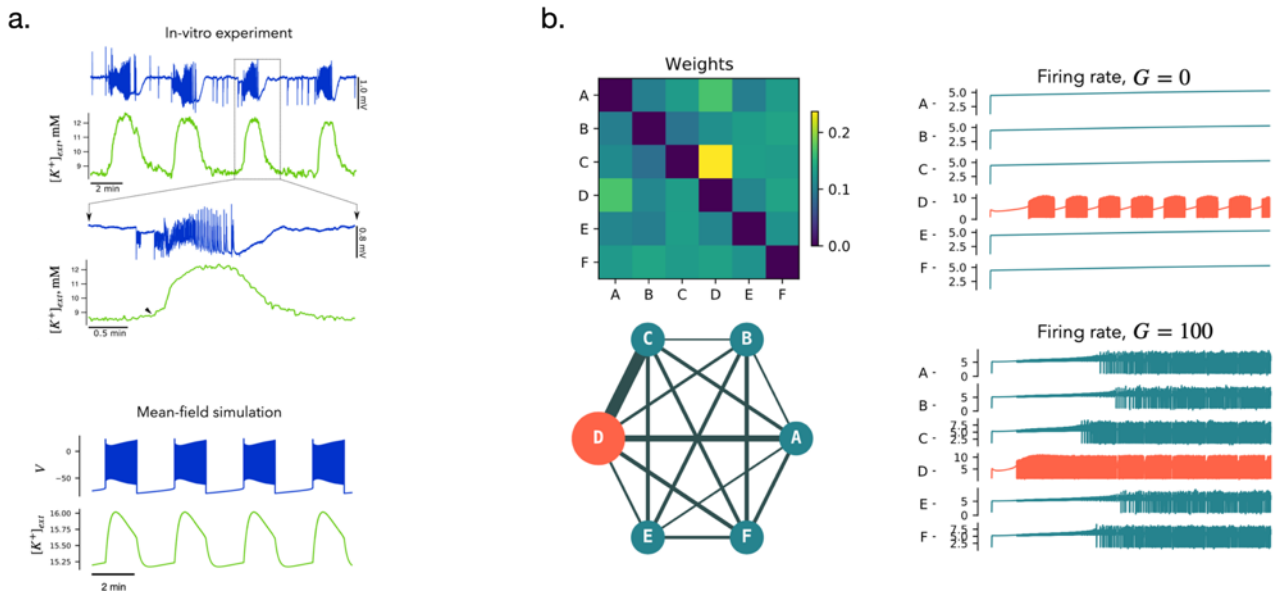

Figure 2: Comparison with experimental data and network model simulation:

(a) top: Experimental co-recording of extracellular local field potential (blue traces) and extracellular K^+ concentration (green trace). Bottom: The model qualitatively reproduces the experimentally observed oscillations showing a modulation of the amplitude of the fast oscillations during a slow oscillation cycle. (b) Network simulation of structurally connected neural mass models and propagation of pathological bursts: Structural connectivity for six all-to-all connected nodes *A, B,C, D, E, F* with random weight allocation. Each node is described by a neural mass model derived as the mean-field approximation of a

large population of HH neurons. When decoupled (Global Coupling G = 0), all the nodes operate in a 'healthy' regime with the potassium concentration in their bath set to low values $[K^+]_{bath}$ = 5.5, except for node *D* which is tuned into a pathological regime $[K^+]_{bath}$ = 15.5 characterized by the spontaneous presence of bursts. When the global coupling is sufficiently increased, the pathological value of $[K^+]_{bath}$ in node *D* generates bursts that diffuse through the connectome mimicking the spreading of a seizure.

115. Computational modeling of neuron-astrocyte interactions using the NEST simulator (AstroNeuronNets)

Jugoslava Aćimović[1*], Han-Jia Jiang[2,3*], Tiina Manninen[1], Jonas Stapmanns[2,4], Mikko Lehtimäki[1], Marja-Leena Linne[1], Markus Diesmann[2,4,5], Sacha van Albada[2,3]

[1]Faculty of Medicine and Health Technology, Tampere University, Tampere, Finland

[2]Institute of Neuroscience and Medicine (INM-6) and Institute for Advanced Simulation (IAS-6) and JARA-Institute Brain Structure-Function Relationships (INM-10), Jülich Research Centre, Jülich, Germany

[3]Institute of Zoology, Faculty of Mathematics and Natural Sciences, University of Cologne, Cologne, Germany

[4]Department of Physics, Faculty 1, RWTH Aachen University, Aachen, Germany

[5]Department of Psychiatry, Psychotherapy and Psychosomatics, School of Medicine, RWTH Aachen University, Aachen, Germany

*e-mail-address of corresponding author(s) jugoslava.acimovic@tuni.fi, h.jiang@fz-juelich.de

INTRODUCTION

Astrocytes, the most abundant glial type in the brain, have been shown to contribute to various brain functions in both developing and mature brains, and their dysfunctions are involved in a number of neurological disorders. Experimental evidence demonstrates coordinated neuronal and astrocytic activity in *in vivo* conditions [1]. Astrocytes interact with closeby synapses, neurons, other glial cells, and vasculature through complex cellular mechanisms [2]. In the cortex, astrocytes form non-overlapping domains that contain hundreds of thousands of synapses in rodents and up to million of synapses in humans [3,4]. Inside these domains, astrocytic processes are in close contact with synaptic terminals and affect synaptic transmission, plasticity, and neuronal excitability [2]. Cortical astrocytes also regulate extracellular ionic concentrations and blood flow. In order to incorporate astrocytic contributions in large-scale cortical simulations to understand different brain functions in health and disease, we need advanced computational infrastructure to model the complex astrocytic mechanisms, to integrate models with new anatomical, electrophysiological, and imaging data, and to examine how these mechanisms modulate activity in large cortical populations.

METHODS

In the past two decades, hundreds of new computational models that include neuron-astrocyte interaction mechanisms have been developed [5,6,7,8]. However, these models are rarely implemented using open-access simulation tools or shared through public platforms [8]. We developed new infrastructure for such models by

implementing an astrocyte module into NEST [9], the cellular-level simulator for large-scale brain systems included in EBRAINS. NEST, extended with our new module, allows efficient implementation and simulation of large heterogeneous populations of neurons and astrocytes [9]. The new module includes an astrocyte model with internal calcium dynamics, a synapse model for astrocyte-neuron signaling, and user-friendly and efficient high- level connectivity functions which allow probabilistic or deterministic pairing of neurons and astrocytes. This new module improves the convenience, reliability, and reproducibility of neuron-astrocyte network models and supports reuse and sharing of published models.

RESULTS AND DISCUSSION

The development of the new NEST module had three phases. In the first phase, we extended the concept of a synapse in NEST to allow interactions between the pre- and postsynaptic neurons and the neighboring astrocytic compartment. In the second phase, we developed a new method to efficiently establish interactions within large heterogeneous populations of neurons and astrocytes. In the third phase, we implemented neuron-astrocyte network models composed of several thousands of cells using the new NEST module. We first simulated these models to test and verify the correctness and efficiency of our module; next, we used these models to explore the astrocytic impact on neuronal excitability and population activity. In summary, we developed a new solution for integrating mechanisms of neuron-astrocyte interactions into large cortical circuit models. This solution is implemented as a new module in the NEST simulator and through NEST it is integrated into the EBRAINS platform. It supports development of open-access, reproducible, and efficient large-scale computational models for neuron- astrocyte networks.

Keywords: astrocyte, neuronal networks, spiking neural networks, NEST simulator, neuron-astrocyte interactions, cell population, large-scale brain systems, cellular mechanisms, simulation, neuroscience infrastructure

ACKNOWLEDGEMENTS

The study received funding as a Partnering Project (AstroNeuronNets) to the European Union's Horizon 2020 Framework Programme for Research and Innovation under the Specific Grant Agreement No. 945539 (Human Brain Project SGA3). The work is also supported by the Academy of Finland (decision Nos. 326494, 326495, and 345280).

REFERENCES

[1] Lines J, Martin ED, Kofuji P, et al. Astrocytes modulate sensory-evoked neuronal network activity. *Nat Commun* 2020;11;3689. doi:10.1038/s41467-020-17536-3

[2] Bazargani N, Attwell D. Astrocyte calcium signaling: the third wave. *Nat Neurosci* 2016;19;182-189. doi:10.1038/nn.4201

[3] Oberheim NA, Takano T, Han X, et al. Uniquely hominid features of adult human astrocytes. *J Neurosci* 2009;29;3276-3287. doi:10.1523/JNEUROSCI.4707-08.2009

[4] Zisis E, Keller D, Kanari L, et al. Digital reconstruction of the neuro-glia-vascular architecture. *Cereb Cortex* 2021;31;5686-5703. doi:10.1093/cercor/bhab254

[5] Manninen T, Aćimović J, Havela R, et al. Challenges in reproducibility, replicability, and comparability of computational models and tools for neuronal and glial networks, cells, and subcellular structur es. *Front Neuroinform* 2018;12;20. doi:10.3389/fninf.2018.00020

[6] Manninen T, Havela R, Linne ML. Computational models for calcium-mediated astrocyte functions. *Front Comput Neurosci* 2018;12;14. doi:10.3389/fncom.2018.00014
[7] Linne ML, Aćimović J, Saudargiene A, et al. Neuron–glia interactions and brain circuits. *In Computational Modelling of the Brain*. Giugliano M, Negrello M, Linaro D, eds. Cham: Springer; 2022. doi:10.1007/978-3-030- 89439-9_4
[8] Manninen T, Aćimović J, Linne ML. Analysis of network models with neuron-astrocyte interactions. *Accepted to Neuroinformatics* 2023.
[9] Spreizer S, Mitchell J, Jordan J, et al. NEST 3.3. *Zenodo* 2022. doi:10.5281/zenodo.6368024

116. Interaction schemes and spatial organization of cells in computational models of neuron-astrocyte networks

Tiina Manninen[1*], Jugoslava Aćimović[1], Marja-Leena Linne[1*]

[1]Faculty of Medicine and Health Technology, Tampere University, Tampere, Finland

*e-mail-address of corresponding author(s) tiina.manninen@tuni.fi, marja-leena.linne@tuni.fi

INTRODUCTION/MOTIVATION

Astrocytes, the largest non-neuronal cell type in the brain, have recently been shown to be involved in many brain functions, including memory and learning [1,2] and cognitive functions [3]. How astrocytes contribute to these functions is mostly not understood. We have shown with detailed mechanistic models that the cortical astrocyte can modulate synaptic long-term depression in the somatosensory cortex and thus expand the information processing capacity of the brain [4]. We have also analyzed published computational models of astrocyte-neuron interactions and the putative cellular mechanisms of these models responsible for various brain phenomena [5,6,7,8]. In this study, we focus on understanding the role of astrocytes in network functions using existing computational models.

METHODS

We study here network-level models where at least two neurons and two astrocytes interact bidirectionally. The astrocytes must include at least one intracellular calcium mechanism, and calcium dynamics must be described by a differential equation that depends on calcium itself and at least one of the other astrocytic variables. In addition, astrocytic calcium must have an impact on some signaling variable or other intracellular signal in the astrocytes. Neurons must include at least one differential equation, for example for membrane potential. In this study, we first categorize and characterize the neuron-astrocyte network models based on our detailed analysis of model components. We then show the evolution of how the models have been developed from previous models. We additionally study the models in view of the existing experimental data and present future perspectives.

RESULTS AND DISCUSSION

We analyze in total 32 models published until 2020, categorize them according to the modeled biophysical, biochemical, and cellular mechanisms, all types of functional interactions between modeled neurons and astrocytes in synaptic and non-synaptic communications, as well as inputs and outputs of the models, and develop new criteria to systematically present network-level properties in these models, such as the spatial organization of the cells and interaction schemes [8]. The largest neuron-astrocyte network models manage the computational

burden by using computationally light single cell models, whereas the smaller models utilize more detailed cell models. The interactions between neurons are represented with conventional synaptic models. In about half of the models, neurotransmitters activate astrocytes, whereas in about third of the models, gliotransmitters activate neurons. The rest of the models use more phenomenological equations in neuron-astrocyte interactions. Astrocyte-astrocyte interactions are implemented with gap junctions or extracellular diffusion. Based on our analysis, we propose how to systematically describe and categorize the properties of neuron-astrocyte interaction models and present the next steps towards understanding astrocytic contribution to different brain functions. Shortly, comprehensive data about astrocyte morphology and physiology *in vivo* is needed to be able to build biologically more detailed data-driven computational models, existing computational tools should be extended also for astrocyte research, each new model should be contrasted with other published models, and the biological choices made in the model for morphological, physiological, cell and molecular biological aspects should be clearly explained and justified.

Keywords: astrocyte, brain circuit, computational model, intracellular calcium, neuron-astrocyte interaction, neuron-astrocyte network, simulation, synapse

ACKNOWLEDGEMENTS

This study was funded by the Academy of Finland (decision Nos. 297893, 318879, 326494, 326495, and 345280) and partially by the European Union's Horizon 2020 Framework Programme for Research and Innovation under the Specific Grant Agreement Nos. 720270 (Human Brain Project SGA1), 785907 (Human Brain Project SGA2), and 945539 (Human Brain Project SGA3 and its Partnering Project AstroNeuronNets).

REFERENCES

[1] Kol A, Adamsky A, Groysman M, et al. Astrocytes contribute to remote memory formation by modulating hippocampal–cortical communication during learning. *Nat Neurosci* 2020;23;1229–1239. doi:10.1038/s41593- 020-0679-6

[2] Bohmbach K, Masala N, Schönhense EM, et al. An astrocytic signaling loop for frequency-dependent control of dendritic integration and spatial learning. *Nat Commun* 2022;13;7932. doi:10.1038/s41467-022-35620-8

[3] Santello M, Toni N, Volterra A. Astrocyte function from information processing to cognition and cognitive impairment. *Nat Neurosci* 2019;22;154–166. doi:10.1038/s41593-018-0325-8

[4] Manninen T, Saudargiene A, Linne ML. Astrocyte-mediated spike-timing-dependent long-term depression modulates synaptic properties in the developing cortex. *PLoS Comput Biol* 2020;16;e1008360. doi:10.1371/journal.pcbi.1008360

[5] Manninen T, Aćimović J, Havela R, et al. Challenges in reproducibility, replicability, and comparability of computational models and tools for neuronal and glial networks, cells, and subcellular structures. *Front Neuroinform* 2018;12;20. doi:10.3389/fninf.2018.00020

[6] Manninen T, Havela R, Linne ML. Computational models for calcium-mediated astrocyte functions. *Front Comput Neurosci* 2018;12;14. doi:10.3389/fncom.2018.00014

[7] Linne ML, Aćimović J, Saudargiene A, et al. Neuron–glia interactions and brain circuits. *In Computational Modelling of the Brain*. Giugliano M, Negrello M, Linaro D, eds. Cham: Springer; 2022. doi:10.1007/978-3-030- 89439-9_4

[8] Manninen T, Aćimović J, Linne ML. Analysis of network models with neuron-astrocyte interactions. *Accepted to Neuroinformatics* 2023.

117. A neuro-glia model to link mean-field models to the BOLD signal

Federico Tesler[1], Marja-Leena Linne[2] and Alain Destexhe[1]

[1-] Paris-Saclay University, CNRS, Paris-Saclay Institute of Neuroscience (NeuroPSI), 91400 Saclay, France
[2-] Tampere University, Faculty of Medicine and Health Technology, 33720 Tampere, Finland

INTRODUCTION/MOTIVATION

Functional magnetic resonance imaging (fMRI) relies on the coupling between neuronal and vascular activity [1], but the mechanisms behind this coupling are still under discussion. It is currently believed that glutamatergic synapses may play a central role in the coupling [2], inducing an increase of cerebral blood flow (CBF) via two main signaling pathways: a direct neuron-vascular pathway and a neuron-astrocyte-vascular pathway [3,4]. In both pathways, a glutamate induced increase in intra-cellular calcium concentrations (in neurons or astrocytes) triggers the production and release of a variety of vasomodulators which generate a dilation of nearby arterioles and an increase in CBF [3,4]. The relative relevance of these different signaling pathways is still under study. In particular, the role of astrocytes in the neurovascular coupling has it is still generating a strong debate. In addition, fMRI studies have become nowadays an essential tool to perform analyses of neuronal activity at the whole brain-level, but there is currently no biophysical detailed model designed to simulate the generation of BOLD signal at such a large scale. The goal of this work is to study the function of astrocytic calcium activity in functional hyperemia and to develop a tool to simulate the generation of BOLD signals at large scale with a biologically plausible model.

METHODS

We developed and analyzed a biologically plausible model of the neurovascular coupling based on mean-field models. Our model incorporates recent experimental findings and modelling tools at the three levels of the system: neuronal, astrocyte and vascular (see Figure 1.A for a diagram of the model). Neuronal (and synaptic) activity was modeled via a recently developed mean-field description of a network of Adaptive Exponential (AdEx) integrate-and-fire neurons [5], accessible in EBRAINS and which has been already incorporated in the TVB platform. Following experimental evidence we considered the (calcium-mediated) release of the prostaglandin PGE2 by astrocytes as the principal vasomodulator acting in the coupling [4]. The vascular system was described by a novel formulation that relates arteriole volume to cyclic-AMP concentration, together with the classical Balloon model for the BOLD signal [6] (see Figure 1.B for the dynamics of the main variables of the model).

RESULTS AND DISCUSSION

Starting from a relatively detailed description we focused on fundamental aspects of the fMRI phenomenology (such as the Hemodynamic Response Function, the linearity of the coupling and the post-stimulus undershoot) and we analyzed the role of the calcium signal in these processes. We found that a calcium-driven Hemodynamic Response Function (HRF) can be generated from our model and that it is equivalent to the one observed experimentally. We corroborated this by comparing our results with the canonical HRF (Figure 2.A). We also showed that the BOLD responds linearly with the calcium activity and we reproduced our simulations using the HRF formalism (Figure 2.B). We

found also that information transmission by the calcium signal operates mainly via frequency coding with a small contribution of amplitude modulation (Figure 2.C). Finally we found that a post-stimulus undershoot in the calcium activity can cause an undershoot in the BOLD signal (usually observed in experiments) via a decrease in CBF.

Our work opens new ways to link known alterations of astrocytic calcium signaling in neurodegenerative diseases (e.g. Alzheimer's and Parkinson's diseases) with detectable changes in the neurovascular coupling. In addition, the adoption of the mean-field description will allow to perform efficiently large-scale simulations of BOLD signals. The mean-field model used is already incorporated in the TVB platform, which makes our model easily adaptable to the existing tools in EBRAINS for whole-brain simulations.

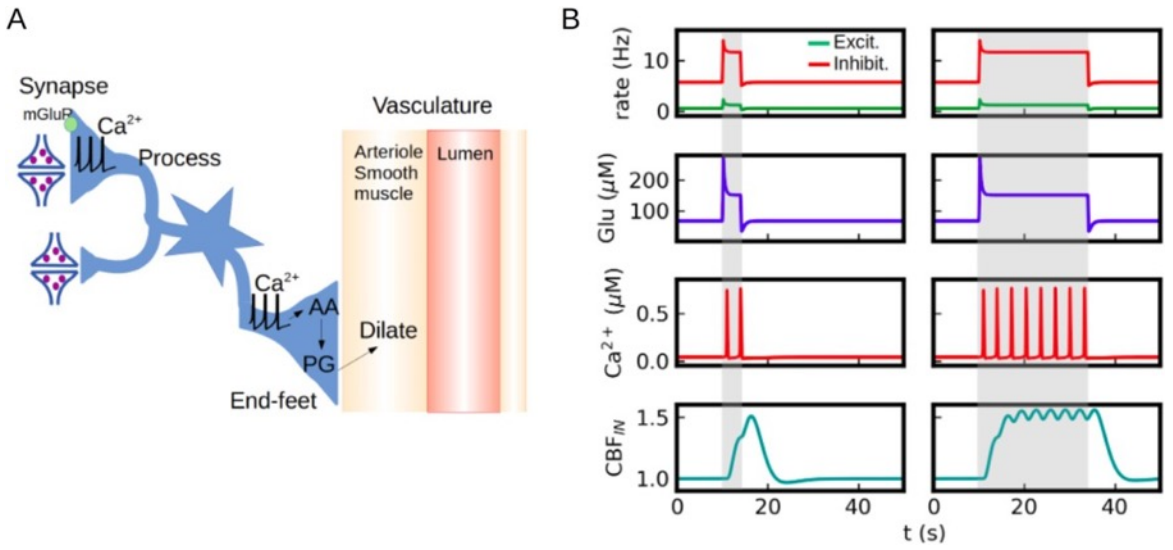

Figure 1: A) Diagram of the model describing neuronal, astrocyte and vascular dynamics. B) Time-series of the main-variables of the model (neuronal firing rates, glutamate concentration, calcium concentration and cerebral blood flow) during the application of a stimulus (indicated by the gray shaded area).

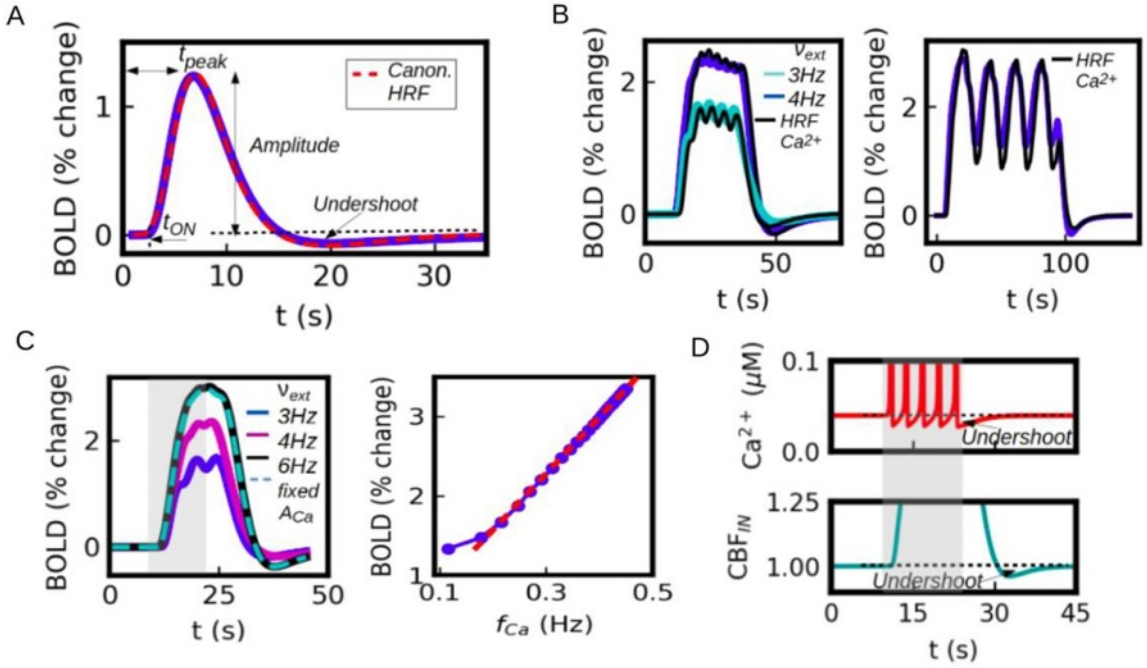

Figure 2: A) Hemodynamic response function (HRF) obtained from our model (solid blue line) and comparison with a canonical (double-gamma) HRF (dashed line). B) Results from the convolution of the HRF with the calcium activity and comparison with the simulated BOLD signal for a pulsed and oscillatory stimulus. C) Left: simulated BOLD signal for inputs of different strength. Right: amplitude of the BOLD signal as a function of astroyticic calcium oscillatory frequency. D) Post-stimulus undershoot obtained from the calcium dynamics and the corresponding undershoot observed in simulated BOLD signal.

Keywords: functional magnetic resonance, astrocytes, mean-field models, BOLD, neurovascular-coupling

ACKNOWLEDGEMENTS

Research supported by the CNRS and the European Union (Human Brain Project H2020-785907, H2020-945539).

REFERENCES

1 - S. Ogawa, T.-M. Lee, A. R. Kay, D. W. Tank, Proceedings of the National Academy of Sciences 87 (1990) 9868–9872
2 - C. Iadecola, Nature Reviews Neuroscience 5 (2004) 347–360.
3 - M. Lauritzen, Nature Reviews Neuroscience 6 (2005) 77–85
4 - D. Attwell, A. M. Buchan, S. Charpak, M. Lauritzen, B. A. MacVicar, E. A. Newman, Nature 468 (2010) 232–243.
5 - M. Di Volo, A. Romagnoni, C. Capone and A. Destexhe (2019), Neural Computation, 31, 653–680.
6 - R. B. Buxton, E. C. Wong, L. R. Frank, Magnetic Resonance in Medicine 39 (1998) 855–864

118. Converging evidence of impaired brain function in systemic lupus erythematosus: changes in perfusion dynamics and intrinsic functional connectivity

Eleftherios Kavroulakis[1*], Nicholas J. Simos[2,3], Efrosini Papadaki[1,2], George Bertsias[4,5], Despina Antypa[6], Antonis Fanouriakis[4,7], Thomas Maris [1,2], Prodromos Sidiropoulos[4], Dimitrios T Boumpas[4,7,8,9].

Affiliations: [1]Department of Radiology, School of Medicine, University of Crete, University Hospital of Heraklion, Heraklion, Crete, Greece. [2]Computational Bio-Medicine Laboratory, Institute of Computer Science, Foundation for Research and Technology - Hellas, Heraklion, Greece. [3]Computational Bio-Medicine Laboratory, Institute of Computer Science, Foundation for Research and Technology - Hellas, Heraklion, Greece. [4]Department of Rheumatology, Clinical Immunology and Allergy, School of Medicine, University of Crete, University Hospital of Heraklion, Heraklion, Crete, Greece. [5]Institute of Molecular Biology and Biotechnology, Foundation of Research and Technology-Hellas, Heraklion, Greece. [6]Department of Psychiatry, School of Medicine, University of Crete, University Hospital of Heraklion, Heraklion, Crete, Greece. [7]4th Department of Internal Medicine, Attikon University Hospital, Medical School, National and Kapodestrian University of Athens, Athens, Greece. [8]Laboratory of Autoimmunity and Inflammation, Biomedical Research Foundation of the Academy of Athens, Athens, Greece. [9]Joint Academic Rheumatology Program, and 4th Department of Medicine, Medical School, National and Kapodestrian University of Athens, Athens, Greece.

*e-mail-address of corresponding author(s): terryka21985@gmail.com

INTRODUCTION

Systemic lupus erythematosus (SLE) is a systemic autoimmune inflammatory disorder which often affects the central nervous system (CNS) [1]. Symptoms vary widely among patients with neuropsychiatric SLE (NPSLE), ranging from overt (e.g., seizures, psychosis) to subtle presentations, such as headache, depression and anxiety symptoms, and cognitive dysfunction [2]. The development of novel, advanced MRI techniques has improved sensitivity to detect hemodynamic changes, as well as functional alterations as indexed by functional brain connectivity. Resting-state functional MRI (rs-fMRI) is a non-invasive imaging technique, using blood oxygenation level– dependent (BOLD) signal, that has been widely used to investigate brain function in various CNS diseases, including NPSLE, where altered functional connectivity was shown both within and between several key brain networks [3]. Studies in patients with SLE with or without neuropsychiatric symptoms have reported altered functional connectivity both within and between several key brain networks [4 – 6]. Interestingly, rs-fMRI could provide evidence not only about neural activity, but also about regional cerebral perfusion alterations, through time-shift analysis (TSA), a promising new method that has been used to assess hemodynamics in previous studies [7-8]. According to this method, the hemodynamic transfer speed is indexed through the temporal shift of low- frequency BOLD signal fluctuations of rs-fMRI. A disturbance of local blood flow is reflected in these fluctuations as a localized delay (i.e., hemodynamic lag) or temporal gain (i.e., hemodynamic lead) in relation to the blood flow in major cerebral veins. Substantial shifts, in the order of seconds, have been shown to provide information about local brain hemodynamics similar to established MR perfusion techniques [6]. The purpose of this study was to examine changes in hemodynamics, through TSA, and functional connectivity, through intrinsic connectivity contrast (ICC), in patients with systemic lupus erythematosus (SLE) with or without neuropsychiatric manifestations.

METHODS

Participants were 44 patients with neuropsychiatric SLE (NPSLE), 20 SLE patients without such manifestations (non-NPSLE), and 35 healthy controls. Resting-state functional MRI (rs-fMRI) was used to obtain whole-brain maps of (a) perfusion dynamics derived through time shift analysis (TSA), (b) regional functional connectivity (intrinsic connectivity contrast (ICC) coefficients), and (c) hemodynamic-connectivity coupling. Group differences were assessed through independent samples t-tests, and correlations of rs-fMRI indices with clinical variables and neuropsychological test scores were, also, computed.

RESULTS AND DISCUSSION

Compared to HC, NPSLE patients demonstrated intrinsic hypoconnectivity of anterior Default Mode Network (DMN) and hyperconnectivity of posterior DMN components. These changes were paralleled by elevated hemodynamic lag. In NPSLE, cognitive performance was positively related to higher intrinsic connectivity in these regions, and to higher connectivity-hemodynamic coupling in posterior DMN components. Uncoupling between hemodynamics and connectivity in the posterior DMN was associated with worse task performance. Non-NPSLE patients displayed hyperconnectivity in posterior DMN and sensorimotor regions paralleled by relatively increased hemodynamic lag.

Adaptation of regional brain function to hemodynamic changes in NPSLE may involve locally decreased or locally increased intrinsic connectivity (which can be beneficial for cognitive function). This process may also involve elevated coupling of hemodynamics with functional connectivity (beneficial for cognitive performance) or uncoupling, which may be detrimental for the cognitive skills of NPSLE patients.

Keywords: Neuropsychiatric lupus · Resting-state fMRI · Cerebral perfusion · Time shift analysis · Intrinsic connectivity coefficient · Visuomotor capacity

ACKNOWLEDGEMENTS

Financial support for this work was provided by the Hellenic Foundation for Research and Innovation (H.F.R.I.) under the "2nd Call for H.F.R.I. Research Projects to support Post-Doctoral Researchers" (Project Number: 1220). REFERENCES

[1] Bertsias GK, Boumpas DT (2010) Pathogenesis, diagnosis and management of neuropsychiatric SLE manifestations. Nat Rev Rheumatol 6:358–367

[2] Aminiala H, Loukkola J, Peltola J, Abady M, Shoenfeld Y, Zandman-Goddard G (2001) The prevalence of neuropsychiatric syndromes in systemic lupus erythematosus. Neurology. 57:496–500

[3] Nystedt J, Mannfolk P, Jönsen A, et al. Functional connectivity changes in systemic lupus erythematosus: a resting-state study. Brain Connect 2018;8:220–34

[4] Cao ZY, Wang N, Jia JT et al (2021) Abnormal topological organization in systemic lupus erythematosus: a resting-state functional magnetic resonance imaging analysis. Brain Imag Behav 15:14– 24. https://doi.org/10.1007/s11682-019-00228-y

[5] Preziosa P, Rocca MA, Ramirez GA et al (2020) Structural and functional brain connectomes in patients with systemic lupus erythematosus. Eur J Neurol 27(1):113–1e2. https://doi.org/10.1111/ ene.14041

[6] Simos NJ, Dimitriadis SI, Kavroulakis E et al (2020) Quantitative identifcation of functional connectivity disturbances in neuropsychiatric lupus based on resting-state fMRI: a robust machine learning approach. Brain Sci 10(11):777. https://doi.org/10.3390/ brainsci10110777

[7] Amemiya S, Kunimatsu A, Saito N, Ohtomo K (2014) Cerebral hemodynamic impairment: assessment with resting-state functional MR imaging. Radiology. 270(2):548–555

[8] Khalil AA, Villringer K, Filleböck V et al (2020) Non-invasive monitoring of longitudinal changes in cerebral hemodynamics in acute ischemic stroke using BOLD signal delay. J Cereb Blood Flow Metab 40:23–34

FIGURES

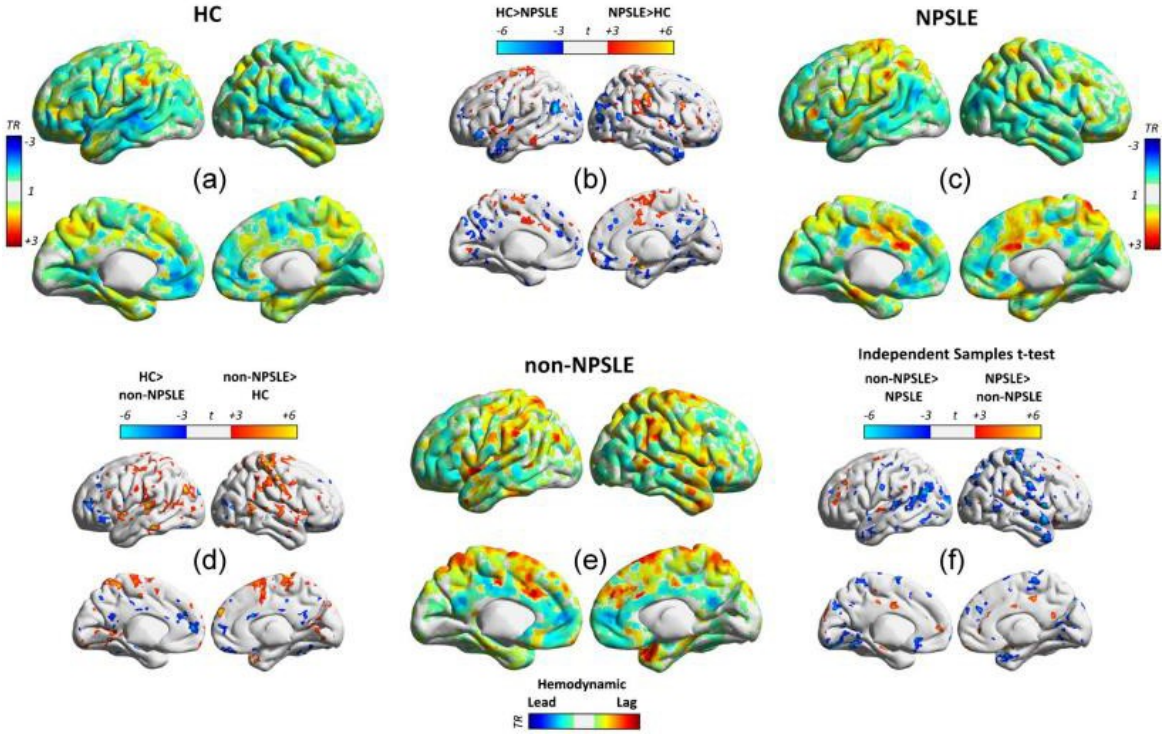

Fig. 1 Whole-brain TSA maps. a, c, e: Group TSA maps in healthy controls (HC), NPSLE and non-NPSLE patients displaying voxels that showed hemodynamic lag (positive TSA values > 1 TR) or lead (negative TSA values < − 1 TR). b, d, f: Pairwise t-contrasts on parametric TSA maps between study groups (thresholded at $p < .05$, FDR corrected with minimum cluster size of 200 voxels)

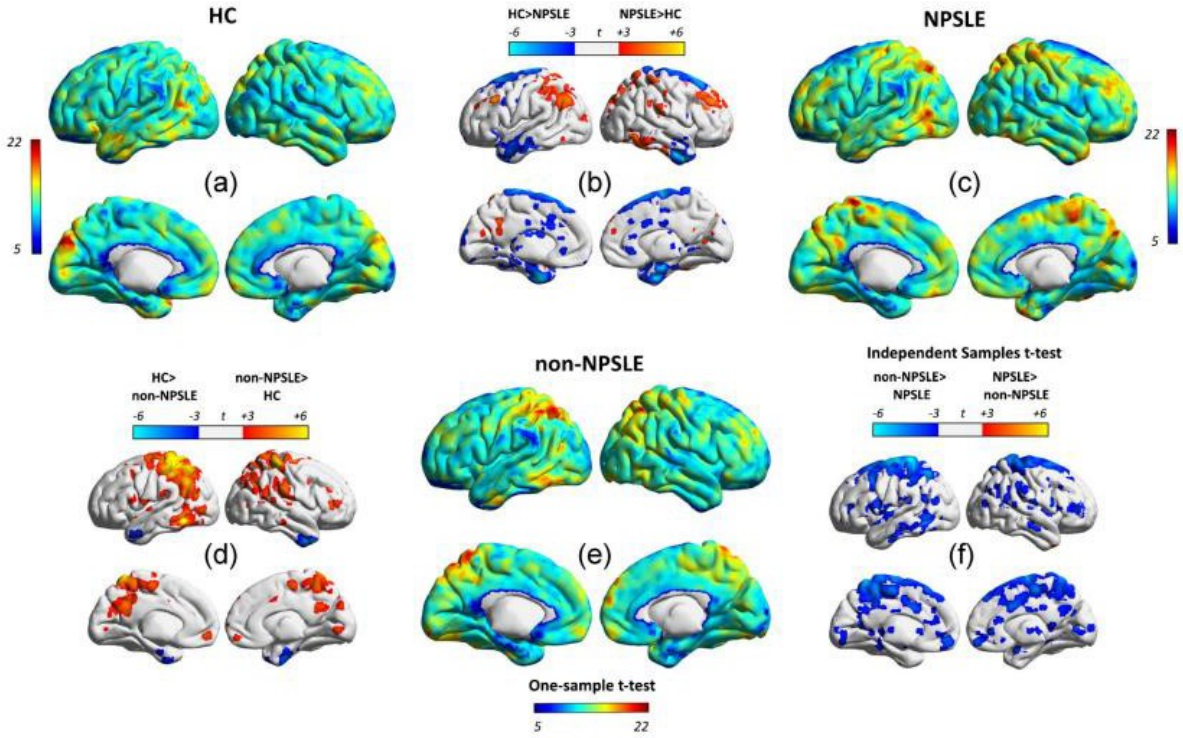

Fig. 2 Whole-brain ICC maps. a, c, e One-sample T maps in the healthy control (HC), non-NPSLE, and NPSLE groups displaying voxels with significant ICC values. b, d, f Pairwise t-contrasts on parametric ICC maps between study groups. All tests were thresholded at $p < .05$, FDR corrected, with minimum cluster size

119. Learning heterogeneous delays of spiking neurons for motion detection

Antoine Grimaldi[1*] & Laurent Perrinet[1]

[1]Institut de Neurosciences de la Timone, Aix Marseille Univ, CNRS, 27 bd Jean Moulin, Marseille, 13005, France

*antoine.grimaldi@univ-amu.fr

INTRODUCTION/MOTIVATION

The response of a biological neuron depends on the precise timing of afferent spikes. This temporal aspect of the neuronal code is essential in understanding information processing in neurobiology and applies particularly well to the output of neuromorphic hardware such as event-based cameras. However, most artificial neuronal models do not take advantage of this minute temporal dimension. Inspired by this neuroscientific observation, we develop a model for the efficient detection of temporal spiking motifs based on a layer of spiking neurons with heterogeneous synaptic delays which we apply to the computer vision task of motion detection. Indeed, the variety of synaptic delays on the dendritic tree allows to synchronize synaptic inputs as they reach the basal dendritic tree. We show this can be formalized as a time-invariant logistic regression which can be trained using labeled data. We apply this model to solve the specific computer vision problem of motion detection, and demonstrate its application to synthetic naturalistic videos transformed into event streams similar to the output of event-based cameras. In particular, we quantify how the accuracy of the model can vary with the total computational load. This end-to-end event-driven computational brick could help improve the performance of future Spiking Neural Network (SNN) algorithms and their prospective use in neuromorphic chips.

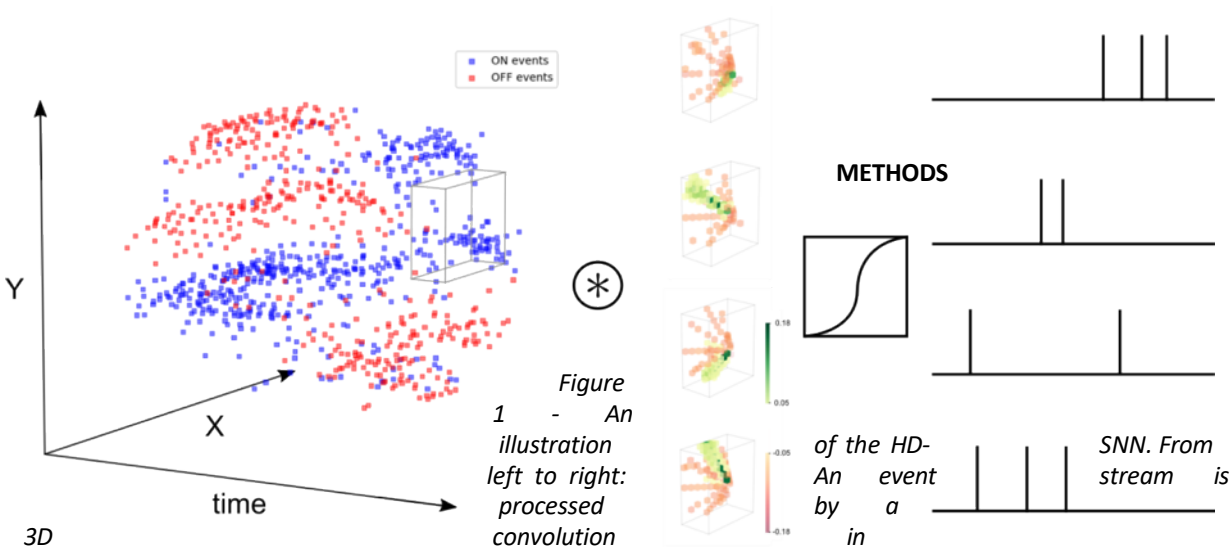

Figure 1 - An illustration of the HD-SNN. From left to right: An event stream is processed in 3D space and time by a convolution with as many kernels as the different classes of motion, here 4 kernels are represented. This convolution is followed by a MLR that gives a probability of emitting a spike for each class. A spiking mechanism like a winner-takes-all generates the output spike train.

In a previous work [1], we demonstrated that a Multinomial Logistic Regression (MLR) can be assimilated to a layer of spiking neurons with a lateral inhibition mechanism. In the present paper, we use this analogy and develop a linear-non-linear model based on a three dimensional convolution followed by a softmax function (see Figure 1). We apply this model on a motion detection task on simulated event-based recordings. To control for motion directions, we animate natural images by translating them following 8 different axes and 3 different velocities. Videos obtained with these translations are synthetically transformed to event streams according to the generative model of an event-based camera which mimics the output of retinal ganglion cells. On this dataset, we can train our model to detect motion and see if the 3D kernels make use of spiking motifs, specific for each motion direction. Once trained, we can test our model on the same type of stimuli and we also compute the accuracy of the model when pruning the weights of the kernel.

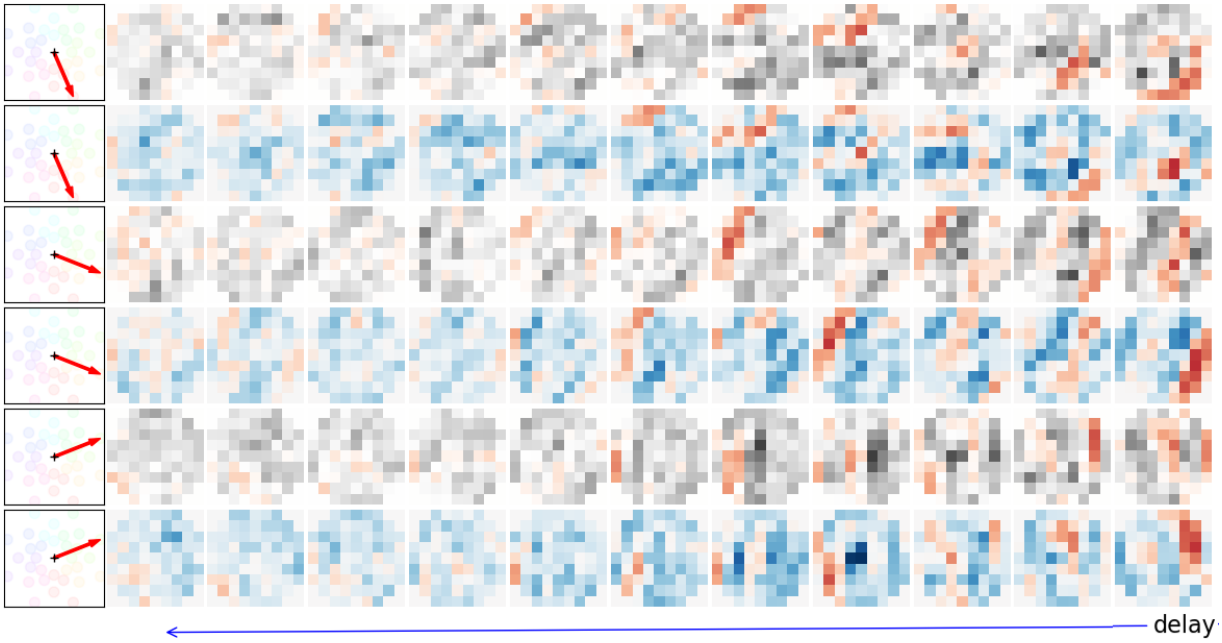

RESULTS AND DISCUSSION

Figure 2 - Representation of the weights for 3 of the 32 different learned kernels of the model as learned on natural scenes. Each pair of line correspond to the OFF and ON polarities respectively, with excitatory weights in warm colors. Delays are represented in the horizontal axis from right (zero delay) to the left (delay of 11 steps). Different kernels are selective to the different motion directions and we observe some level of orientation selectivity, where ON and OFF subfields present in a push-pull organization.

The learned model bears many similarities with neurobiological anatomical observations (see Figure 2). The event- driven computations of our method can be reduced drastically through the pruning of synapses, while maintaining top performance for classification. This shows that we may use the precise timing of spikes to enhance neural computations.

Keywords: time code, event-based computations, spiking neural networks, motion detection

REFERENCES

[1] Grimaldi, A., Boutin, V., Ieng, S. H., Benosman, R., & Perrinet, L. (2022). A robust event-driven approach to always-on object recognition.

120. Recurrent neural networks for multiscale object-based attention during contour grouping

Sami Mollard[1*], Sander M. Bothe[2,3], Pieter R. Roelfsema[1,4,5]

Affiliations:

[1]Department of Vision & Cognition, Netherlands Institute for Neuroscience, Meibergdreef 47, 1105 BA, Amsterdam, The Netherlands.

[2]Machine Learning Group, Centrum Wiskunde & Informatica, Science Park 123, 1098XG, Amsterdam, The Netherlands

[3]Swammerdam Institute for Life Sciences, University of Amsterdam, Science Park 904, 1090GE Amsterdam, Netherlands

[4]Department of Integrative Neurophysiology, Center for Neurogenomics and Cognitive Research, VU University, Amsterdam, The Netherlands.

[5]Department of Psychiatry, Academic Medical Center, Amsterdam, The Netherlands

*s.mollard@nin.knaw.nl

INTRODUCTION/MOTIVATION

Segregating objects from each other and from the background is essential for survival. At the neurophysiological level, recordings show that elements of spatially extended objects can be grouped into a coherent representation by the propagation of a tag of enhanced activity over the representation of the object [1] (Fig. 1C).

It has been shown both behaviourally and electrophysiologically that the time needed for this tag of enhanced neuronal activity to spread over the representation of the object is size invariant: it doesn't depend on the viewing distance[2,3]. This can be explained by a growth-cone model of attention where the tag can propagate at different levels of the visual hierarchy: if an object is viewed from close, its size in degrees of visual angle increases but so does the distance to distractor elements, so that the grouping can happen in neurons with bigger receptive fields (Fig 2A).

However, it remains unknown what precise neuronal circuitry are responsible for the learning and implementation of this scale-invariant tracing.

METHODS

We designed a recurrent neural network with four layers with neurons in feedforward and recurrent groups. The feedforward group represents the object at multiple scales and acts as a backbone (base-representation) on which activity spreading can take place. It also determines the scales at which grouping can happen. Units in the recurrent group spread enhanced neuronal activity over the representation of the target object, to label it as one coherent item. The activity of recurrent units is gated by units in the feedforward group with the same receptive field: if a unit in the feedforward group is inactive, the corresponding unit in the recurrent group cannot participate in the tracing process. Tracing was implemented as a disinhibitory process. Feedback and horizontal connections activate VIP interneurons that have a disinhibitory effect on their corresponding pyramidal neurons, via inhibition of SOM interneurons. Hence, tracing causes the incremental disinhibition of pyramidal units that represent the target object, which is thus serially labeled with enhanced activity.

We first pretrained two feedforward network, one for the curve-tracing task, trained to classify colinear and non-colinear elements, and one for the object-tracing task, trained to classify homogeneous image regions. Thereafter we trained the recurrent network to trace curves using reinforcement learning, analogous to the training of monkeys. Units in the recurrent groups were trained with RELEARNN, a biologically plausible learning rule local both in time and in space, inspired by the Almeida-Pineda algorithm[4–6].

RESULTS AND DISCUSSION

The network was trained to trace curves up to 7 pixels long. After training it could generalize to curves of arbitrary length, and 2D objects of arbitrary shape (Fig. 1B and 1E). As observed in the visual cortex of monkeys, the network serially labeled the target object with enhanced activity.

To probe the dynamics of attentional spreading we examined the difference in activity between the units with RFs on the target and distractor curves. We found that activity propagated slower when the target and the distractor curves were nearby, just as in the visual cortex of monkeys. Spreading made fastest progress at the higher scales, but at places where curves came in each other's vicinity, lower levels took over and spreading slowed down. For objects, as observed in human's psychophysics experiments, grouping speed depended on the size of homogeneous image regions.

Accordingly, dynamics of attentional spreading in the artificial neural network were better fit by a growth-cone-model of attention than a pixel-by-pixel model just as was measured in the visual cortex of monkeys or in human psychophysics experiments (Fig. 2B and 2C).

We show how a recurrent architecture with dedicated feedforward and recurrent pathways, in combination with disinhibitory circuits, can learn to serially propagate enhanced activity to group elements belonging to an object at different scales, with neural dynamics similar to those observed in the visual cortex of monkeys or measured in human psychophysics experiments

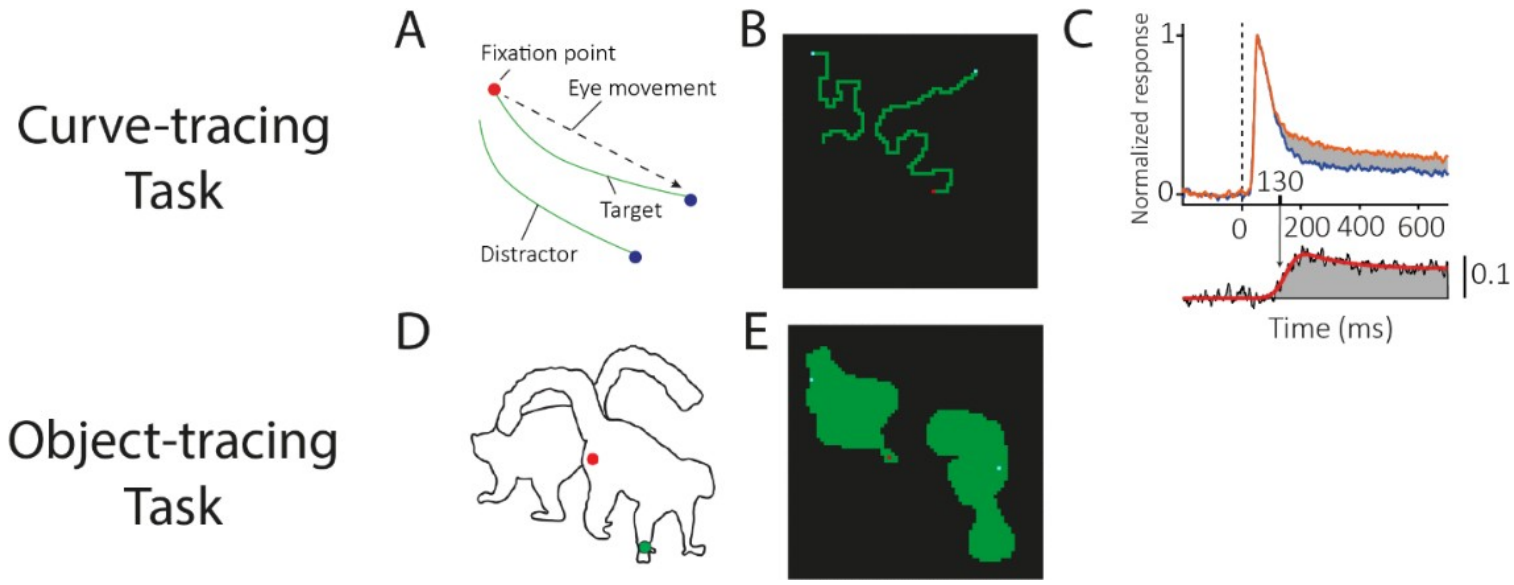

Fig 1. Example stimuli presented to the monkeys (left) and to the network (middle) and electrophysiological recordings from monkeys' visual cortex. **A,B,C** Curve-tracing task. In this task, the goal of the agent is to make an eye movement toward the blue dot connected to the red fixation point. Recordings from monkeys' visual cortex show that the target curve is identified by a tag corresponding to an enhancement of activity of neurons whose receptive field falls on the target curve (C, orange), compared to neurons whose receptive field falls on the distractor curve (C, blue). **D,E** Object-tracing task. In this task, human participants have to report whether a target (D, green dot), is on the same object as the fixation point or not while their reaction time is measured. In the version of the task adapted for the artificial network, the agent has to select the blue dot that is on the same object as the red dot.

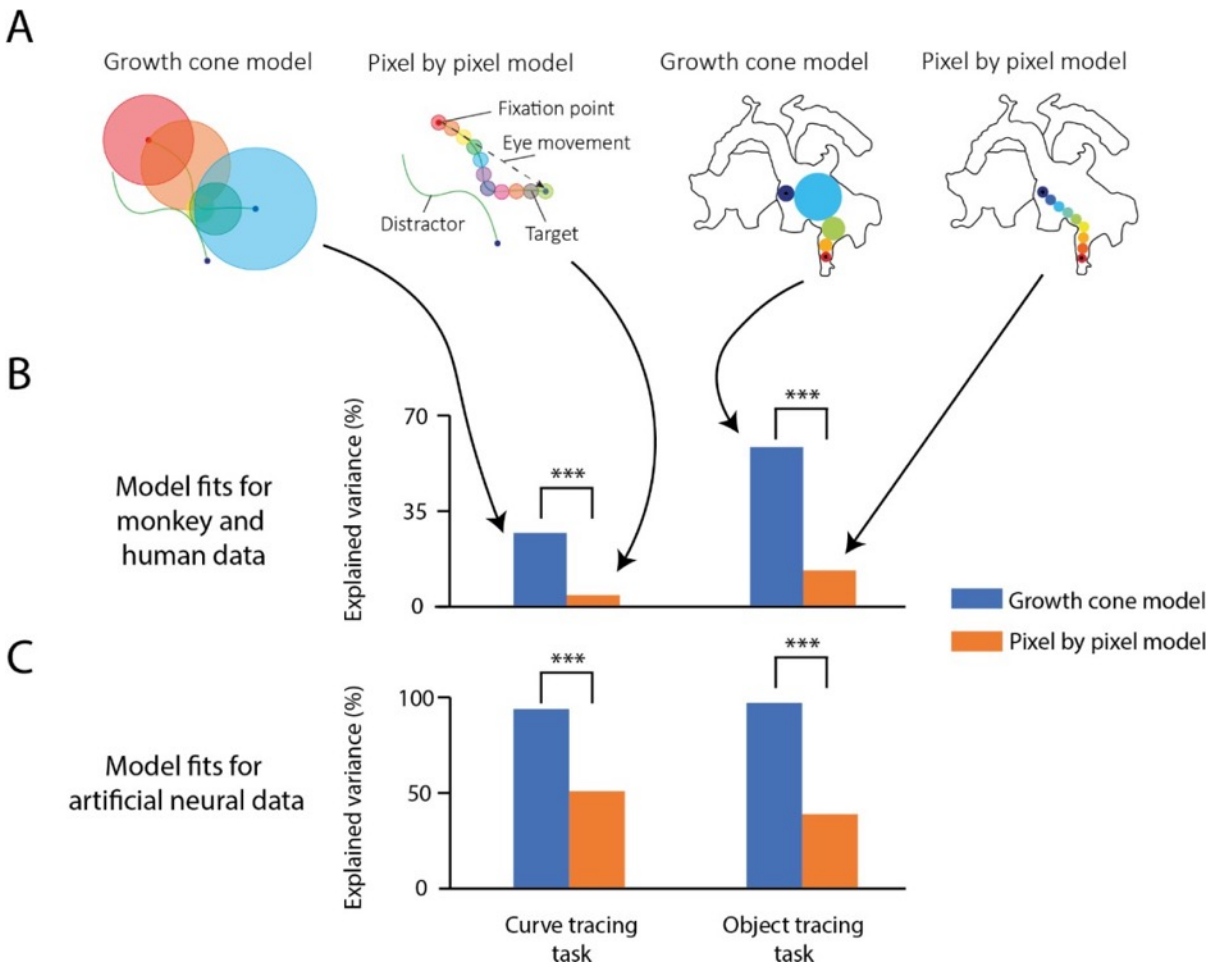

Fig 2 growth-cone model of attention explain experimental results, both in biological and artificial neural networks, better than a pixel-by-pixel model . A Model predictions. The growth cone model predicts that the speed of grouping depends on the distance between curves (curve-tracing task) or the size of homogeneous images regions (object-tracing task). The pixel by pixel model predicts that the grouping speed is constant along the shortest path between the fixation point and the target. **B** Model fits for monkey and human data. The growth-cone model better fit measured latency of response enhancement in the visual cortex of monkeys (curve-tracing task), or human reaction times (object-tracing task). **C** Model fits for artificial neural data. In both the curve-tracing task and the object-tracing task, dynamics of attentional spreading in the artificial neural network trained only on the curve-tracing task is better fit by the growth-cone model.

Keywords: Object-based attention, Recurrent neural networks, Reinforcement learning, Disinhibition ACKNOWLEDGEMENTS

This research has received funding from the European Union's Horizon 2020 Framework Programme for Research and Innovation under the Specific Grant Agreement No. 945539 (Human Brain Project SGA3). We acknowledge the use of Fenix Infrastructure resources, which are partially funded from the European Union's Horizon 2020 research and innovation programme through the ICEI project under the grant agreement No. 800858

REFERENCES

1. Roelfsema PR, Lamme VAF, Spekreijse H. Object-based attention in the primary visual cortex of the macaque monkey. *Nat 1998 3956700.* 1998;395(6700):376-381. doi:10.1038/26475
2. Pooresmaeili A, Roelfsema PR. A growth-cone model for the spread of object-based attention during contour grouping. *Curr Biol.* 2014;24(24):2869-2877. doi:10.1016/j.cub.2014.10.007
3. Jeurissen D, Self MW, Roelfsema PR. Serial grouping of 2D-image regions with object-based attention in humans. *Elife*. 2016;5(JUN2016). doi:10.7554/ELIFE.14320
4. Almeida LB. A learning rule for asynchronous perceptrons with feedback in a combinatorial environment. *Proc IEEE First Int Conf Neural Networks*. 1987;II:609-618.
5. Pineda FJ. Generalization of back-propagation to recurrent neural networks. *Phys Rev Lett*. 1987;59(19):2229-2232. doi:10.1103/PhysRevLett.59.2229
6. Brosch T, Neumann H, Roelfsema PR. Reinforcement Learning of Linking and Tracing Contours in Recurrent Neural Networks. *PLoS Comput Biol*. 2015;11(10):e1004489. doi:10.1371/journal.pcbi.1004489

121. An ANN family for systematic analysis of receptive field size and computational depth in the primate visual hierarchy

Benjamin Peters[1,2]*, Lucas Stoffl[5], Nikolaus Kriegeskorte[1,3,4]

[1]Zuckerman Mind Brain Behavior Institute, Columbia University, NY, USA, [2]Center for Cognitive Neuroimaging, Institute of Neuroscience and Psychology, University of Glasgow, UK, [3]Department of Psychology, Columbia University, NY, USA, [4]Department of Neuroscience, Columbia University, NY, USA, [5]Brain Mind Institute, Ecole polytechnique fédérale de Lausanne, Switzerland

* benjamin.peters@glasgow.ac.uk

INTRODUCTION/MOTIVATION

Deep feedforward convolutional neural network models (FCNNs) explain aspects of the representational transformations in the primate visual hierarchy. However, particular models implement idiosyncratic combinations of architectural hyperparameters, which limits theoretical progress. In particular, the size of receptive fields (RFs) and the distribution of computational path lengths (CPL; the number of nonlinearities encountered) leading up to a representational stage are confounded across layers of the same architecture (deeper layers have larger RFs) and depend on idiosyncratic choices (kernel sizes, depth, skipping connections) across architectures.

METHODS

Here we introduce HBox, a superset family of neural network architectures designed to break the confoundation of RF size and CPL. Like conventional FCNNs, an HBox model contains a feedforward hierarchy of convolutional feature maps. Unlike FCNNs, each map has a predefined RF size that can result from shorter or longer computational paths or any combination thereof (through skipping connections). We implemented a large sample of HBox models (>400) inducing representational stages with a diverse distribution of RF sizes and CPL. Using representational similarity analysis, we quantify the distribution of RF sizes and CPL in regions of interest in a large-scale human fMRI benchmark (N=8, 19-32 years, 6 females; natural scenes dataset[1]).

RESULTS AND DISCUSSION

We show that HBox representations capture an increase in receptive field size and computational path length along lower and higher-level regions in the ventral visual stream. Moreover, we find that HBox representations capture the relationship between increased receptive field size and visual eccentricity in early visual areas. The HBox architecture family illustrates how high-parametric task-performing vision models can be used systematically to gain theoretical insights into the neural mechanisms of primate vision.

KEYWORDS: convolutional neural networks, visual hierarchy, primate vision, fMRI

ACKNOWLEDGEMENTS: B.P. has received funding from the EU Horizon 2020 research and innovation programme under the Marie Skłodowska-Curie grant agreement no. 841578. This work was also supported by the National Science Foundation under Grant No. 1948004 to N.K.

REFERENCES

1. Allen EJ, St-Yves G, Wu Y, et al. A massive 7T fMRI dataset to bridge cognitive neuroscience and artificial intelligence. *Nat Neurosci.* 2022;25(1):116-126. doi:10.1038/s41593-021-00962-x

122. Object-based perception and action

Ruben van Bergen[1*] & Pablo Lanillos[1,2]

[1]Donders Institute for Brain & Cognition, Radboud University, Nijmegen, The Netherlands

[2]Cajal International Neuroscience Center, Spanish National Research Council, Madrid, Spain.

*ruben.vanbergen@donders.ru.nl

INTRODUCTION

Humans perceive and reason about the world in terms of objects[1]. Objects are the world's movable parts, as well as the natural substrate of abstract thinking and planning. In contrast, deep neural network (DNN) models of perception and action have largely ignored objects as an inductive bias, representing entire scenes in a single, unstructured representation. Recently, this has started to change with the advent of object-based DNNs for perception. However, object-based DNNs for behavior learning remain scarce (c.f. [2]) and an open challenge. Here, we present a new architecture (OBAI[3]), grounded in the principles of active inference[4,5], that extends object- based perception DNNs with action-based dynamics and goal-directed planning. Key contributions of our model over previous work[2] include the ability to plan actions efficiently in closed form, and a Bayesian filtering approach that allows the network to postdictively refine past beliefs, so that current beliefs are not irredeemably corrupted by past inference errors.

METHODS

OBAI is based on an earlier model, IODINE[6], which uses a recurrent, Siamese architecture to perform iterative variational inference on object-structured generative models. By sharing weights between subnetworks that perform inference on individual objects, the architecture capitalizes on the symmetry inherent in object-based inference. We extend this architecture with a model of action-based object dynamics, and perform temporally coupled inference simultaneously across multiple time points in a sliding window (i.e., Bayesian filtering & smoothing). Object features are represented in first- order generalized coordinates (i.e., states + derivatives). Dynamics are assumed to be approximately linear, and perturbed by actions that are operationalized as instantaneous accelerations. This formulation allows us to efficiently plan goal- directed actions within the network's latent space, by projecting the discrepancy between the current object states and their target states, onto the pseudoinverse of the action model. We trained OBAI on 50,000 4-frame videos of a simulated environment of moving, multi-colored sprite objects (Fig. 1).

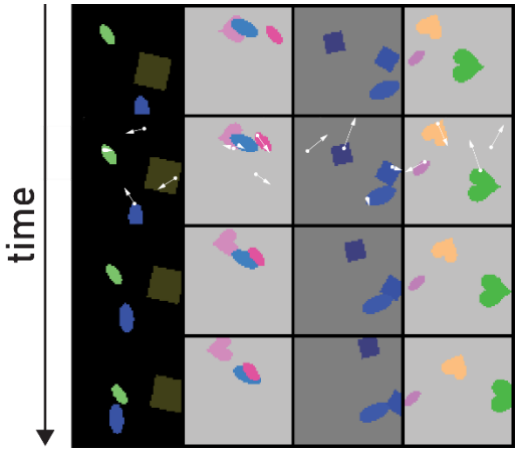

Figure 1: Example video frames (rows) from 4 instances (columns) of our simulated environment. Arrows in the second frame indicate actions (accelerations) applied at random points in the environment (actions that target the background have no effect).

Training is unsupervised, minimizing a variational ELBO loss that pushes the model to accurately reconstruct the training images, while maximizing the temporal predictability and minimizing the complexity of the object representations.

RESULTS AND DISCUSSION

We find that OBAI can accurately segment and reconstruct video frames from our synthetic environment, and performs better than an equivalent IODINE model applied to individual frames. Segmentation quality improved from 0.856 to 0.939 (Adjusted Rand Index of foreground objects; 1.0 is perfect and 0.0 is chance-level), while the mean reconstruction error decreased from 1.63×10^{-3} to 9.51×10^{-4} (mean squared error of pixel values ranging from [0, 1]). This is consistent with the idea that dynamics can provide important disambiguating cues for object perception. OBAI can also extrapolate the inferred object dynamics into the future for video frame prediction, achieving a MSE of 4.1×10^{-3} when predicting 4 frames ahead. Importantly, this predictive ability enables us to plan actions within this same abstract, compact representational space. As a first proof-of-principle for this, we show that OBAI can plan actions towards goals that are explicitly specified on a per-trial basis, by showing the model an image of a desired object configuration and letting it encode this target configuration into its latent space. (Fig. 2). With this functionality in hand, extending our method to more complex tasks (neurosymbolic planning) is only a matter of teaching a further network module to output the requisite (sequence of) target states, based on the current object representation. This will be an important breakthrough to address in future work, with the overarching goal of developing systems that reason and behave more like humans.

Keywords: Objects, Representation Learning, Active Inference, Variational Inference, Perception, Action Acknowledgments

RvB was supported by the *Spikeference* project, Human Brain Project Specific Grant Agreement 3 grant ID 643945539.

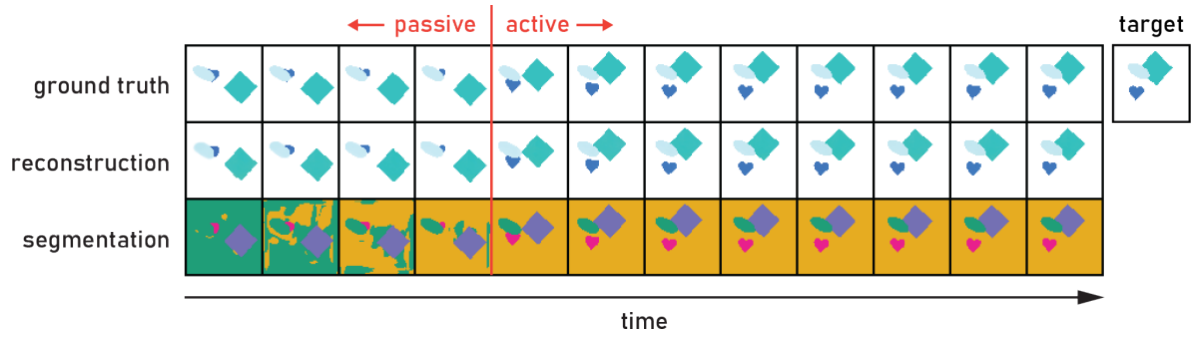

Figure 2: Results for one example trial of goal-directed action planning. Top row shows ground truth video frames rendered from the simulated environment. Middle and bottom rows show the reconstructed video frames and object segmentations produced by the model (respectively). In segmentations, colors indicate the object to which a pixel is assigned. The model spends the first four frames passively observing, before actions are permitted. The target configuration is shown to the far right.

References

1. Peters B, Kriegeskorte N. Capturing the objects of vision with neural networks. *Nat Hum Behav*. 2021;5(9):1127-1144. doi:10.1038/s41562-021-01194-6
2. Veerapaneni R, Co-Reyes JD, Chang M, et al. Entity Abstraction in Visual Model-Based Reinforcement Learning. Published online October 28, 2019. http://arxiv.org/abs/1910.12827
3. van Bergen RS, Lanillos PL. Object-based active inference. Published online September 2, 2022. http://arxiv.org/abs/2209.01258
4. Lanillos P, Meo C, Pezzato C, et al. Active Inference in Robotics and Artificial Agents: Survey and Challenges. Published online 2021:1-20. http://arxiv.org/abs/2112.01871
5. Parr T, Pezzulo G, Friston KJ. *Active Inference*. The MIT Press; 2022. doi:10.7551/mitpress/12441.001.0001
6. Greff K, Kaufman RL, Kabra R, et al. Multi-Object Representation Learning with Iterative Variational Inference. Published online 2019. http://arxiv.org/abs/1903.00450

123. Neuromorphic 3D Perception with GeNN

James P. Turner[1*], Thomas Nowotny[1]

[1]School of Engineering and Informatics, University of Sussex, Brighton, United Kingdom

*j.p.turner@sussex.ac.uk

INTRODUCTION/MOTIVATION

Neuromorphic engineering promises big improvements for power-efficiency and latency. One of the most developed neuromorphic technologies are event-based cameras. Here, we implement a GPU-accelerated version of a neuromorphic 3D perception model for visual event streams from a stereo setup of event-based cameras [1] in GeNN [2]. We demonstrate that the model correctly predicts pixelwise depth from two synthetic visual event streams that simulate the stereo setup. We use GeNN's procedural synapse creation [3] for improved runtime and memory efficiency.

METHODS

Event streams are generated from dynamic random-dot stereograms (DRDS) [1], which in turn are generated from ground-truth depth map images [4]. A single random-initialised boolean frame of size 260x346 is updated by flipping each pixel's polarity with probability 0.2. At each time step, events are generated by the modified pixels, with sign determined by the pixels' updated polarity. Left and right input event streams are then generated by shifting events respectively right (left) in the left (right) input stream by half of the corresponding depth value in a ground-truth depth map image from [4]. The resulting effect is such that neither the left nor right event streams contain any spatial scene information by themselves, however the original depth map image may be reconstructed by combining information from the two event streams.

These left and right event streams are injected into corresponding left and right retina cell populations in the neuromorphic 3D perception model [1]. The two retina populations project synapses into a leaky integrate and fire (LIF) neuron population, tuned to accumulate evidence of horizontal coincidence between spikes from each retina input. To filter out false matches, a second LIF population accumulates spike disparity evidence from coincidence detector spikes. These spikes excite disparity detector neurons representing local coordinates with matching disparity (left minus right retina coordinates), while inhibiting disparity detector neurons representing local coordinates with matching cyclopean position (left plus right retina coordinates). Mutual inhibition prevents duplicate disparity detector spikes within the same line of sight from either input retina. Event depth can then be inferred from disparity, where higher disparity indicates closer distance. See [1] for a complete description of the model.

The model is large, with two 260×346^2 coincidence populations (for each polarity), a 260×346^2

disparity population, and the aforementioned synaptic connectivity. To accelerate inference with a GPU, we used GPU-enhanced Neural Networks (GeNN) [2], which is a library for generating efficient GPU code for spiking neural network models. Due to the large number of synapses required for an input this size, we made use of GeNN's procedural connectivity mechanism [3], for generating synapses on-the-fly instead of keeping them saved to memory.

RESULTS AND DISCUSSION

Figure 1 shows the results of running the model on a synthetic office scene. The left panel is the ground truth depth map, taken from [4], which is encoded into a DRDS event-stream, as discussed above. The network output is compared to ground truth using the pixelwise sum of absolute differences (SAD) between ground truth and model prediction.

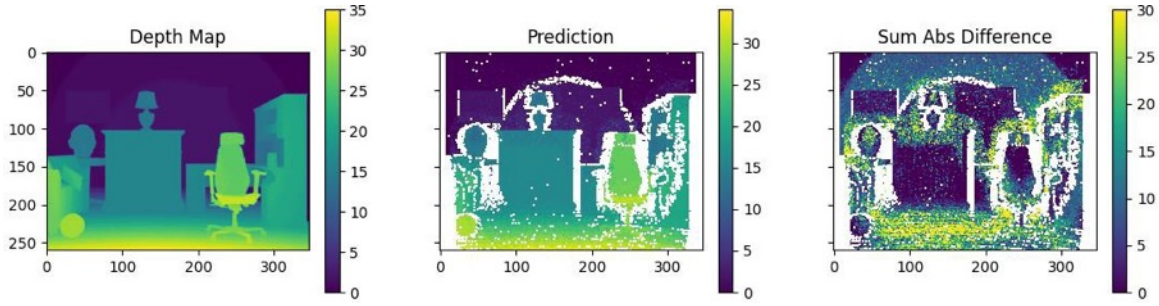

Figure 1. (left) The depth map used for evaluation and generating DRDS model inputs. Darker regions indicate lower disparity, thus more distant, regions. (middle) The depth prediction of the model. (right) SAD accuracy metric used for evaluation. Lighter indicates more error. White pixels indicate information loss in DRDS generation, where distant events are overwritten by nearby events during shifting.

Keywords: Neuromorphic, Vision, 3D, Event-Based, GeNN ACKNOWLEDGEMENTS

This work was funded by the European Union's Horizon 2020 programme under Grant Agreement 945539 (HBP SGA3).

REFERENCES

[1] Osswald M, leng SH, Benosman R, Indiveri G. A spiking neural network model of 3D perception for event-based neuromorphic stereo vision systems. Sci Rep 7, 40703 (2017). https://doi.org/10.1038/srep40703

[2] Yavuz E, Turner, J, Nowotny T. GeNN. a code generation framework for accelerated brain simulations. *Sci Rep* **6**, 18854 (2016). https://doi.org/10.1038/srep18854

[3] Knight JC, Nowotny T. Larger GPU-accelerated brain simulations with procedural connectivity. *Nat Comput Sci* **1**, 136–142 (2021). https://doi.org/10.1038/s43588-020-00022-

[4] Lee Z, Nguyen TQ. Multi-Array Camera Disparity Enhancement. *IEEE Transactions on Multimedia* **16**, 8 (2014). https://doi.org/10.1109/TMM.2014.2355131

124. DeepThickness: A Deep Learning Method for Brain MRI Cortical Thickness Estimation

Damiano Ferrari[a], Mattia Savardi[b], Alessio Fracasso[c], Lars Muckli[c], Sergio Benini[a], Alberto Signoroni[b], Michele Svanera[c,*]

[a]*Department of Information Engineering, University of Brescia, Italy*
[b]*Department of Medical and Surgical Specialties, Radiological Sciences, and Public Health – University of Brescia, Brescia, Italy*
[c]*School of Psychology & Neuroscience, University of Glasgow, UK*
[*]*Corresponding author: Michele.Svanera at glasgow.ac.uk*

1. Introduction

Studying brain anatomical deviations from normal progression along the lifespan is essential for understanding inter-individual variability and its relation to the onset and progression of several clinical conditions [1]. Among available quantitative measurements, mean *cortical thickness* across the brain has been associated with normal ageing and neurodegenerative conditions like mild cognitive impairment, Alzheimer's disease, frontotemporal dementia, Parkinson's disease, amyotrophic lateral sclerosis, and vascular cognitive impairment. Automatic techniques, such as FreeSurfer and CAT12 Toolbox, offer out-of-the-box cortical thickness estimates, but with an excessively long computational time (up to 10 hours per volume). Moreover, comparison studies have found systematic differences between these approaches [6], with discrepancies particularly pronounced in clinical data [4], questioning the reliability of these CT estimations. As more and more studies in medicine and neuroscience analyse hundreds to thousands of brain MRI scans, there is a growing need for automatic, fast, and reliable tools for cortical thickness estimation.

2. Methods

We here propose *DeepThickness*, a method for estimating cortical thickness from MRI in just a few seconds. The proposed framework, shown in Figure 1, exploits our recent achievements in deep learning segmentation methods [8, 9] for extracting grey and white matter segmentation masks and the related probability maps from an MRI T1w volume. All these volumes are given as inputs to a Convolutional Neural Network trained to compute both the external grey matter surface (or pial) level set (*LS*) and the corresponding distance set (*DS*).

In this context, the *level set* is a volumetric representation of the pial surface, in which the intensity of each voxel is the clipped signed distance (range=[−5.0, +5.0] *mm*) between the surface and the voxel itself (positive inside and negative outside the surface). Starting with a *LS*, it is possible to obtain the surface by interpolating the zero-level using the Marching Cubes algorithm [10]. Observing that in those voxels where the grey matter LS (LS_{GM}) has zero values (i.e., on the pial surface), the white matter level set (LS_{WM}) provides values of cortical thickness (since each of those LS_{WM} voxels contains the distance between the pial surface and the voxel itself), and the distance set can be computed by "intersecting" the two-level sets of grey and white matter. Therefore, we define the *DS* using the zero LS_{GM} voxels as indices for selecting the LS_{WM} interesting values, setting any other voxels to zero, and obtaining a very sparse and synthetic representation of cortical thickness.

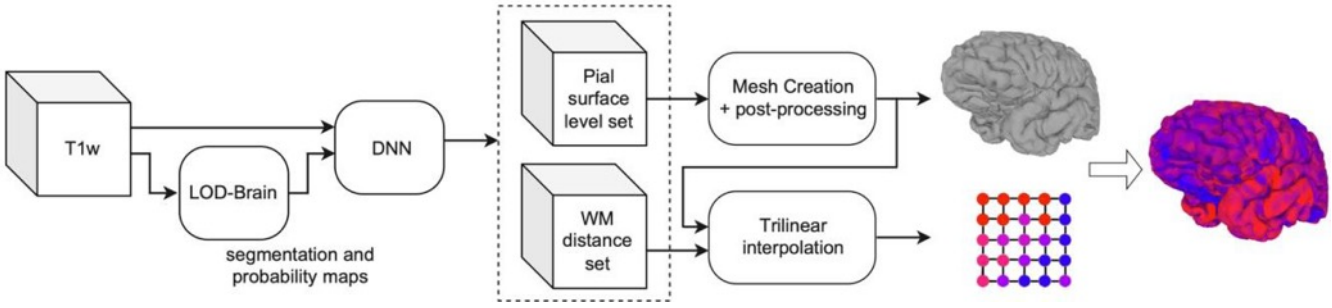

Figure 1. Framework for cortical thickness and surface estimation.

The supervised model is trained, with LS and DS volumes obtained by FreeSurfer [2] as ground truth. The network architecture resembles a 3D U-Net [5], with 4 levels of convolutional layers inspired by [3], and with two output branches predicting the pial surface and the cortical thickness. Training, validation, and testing volumes are obtained from the AOMIC dataset [7], counting 1311, 100, and 500 volumes respectively.

3. Results

In Figure 2-(a), we show qualitative results highlighting how our method performs with respect to FreeSurfer, in both the mesh generation and the cortical thickness estimation. In Figure 2-(b), we compare numerically the cortical thickness estimation distributions obtained with FreeSurfer and our method on a testing subject.

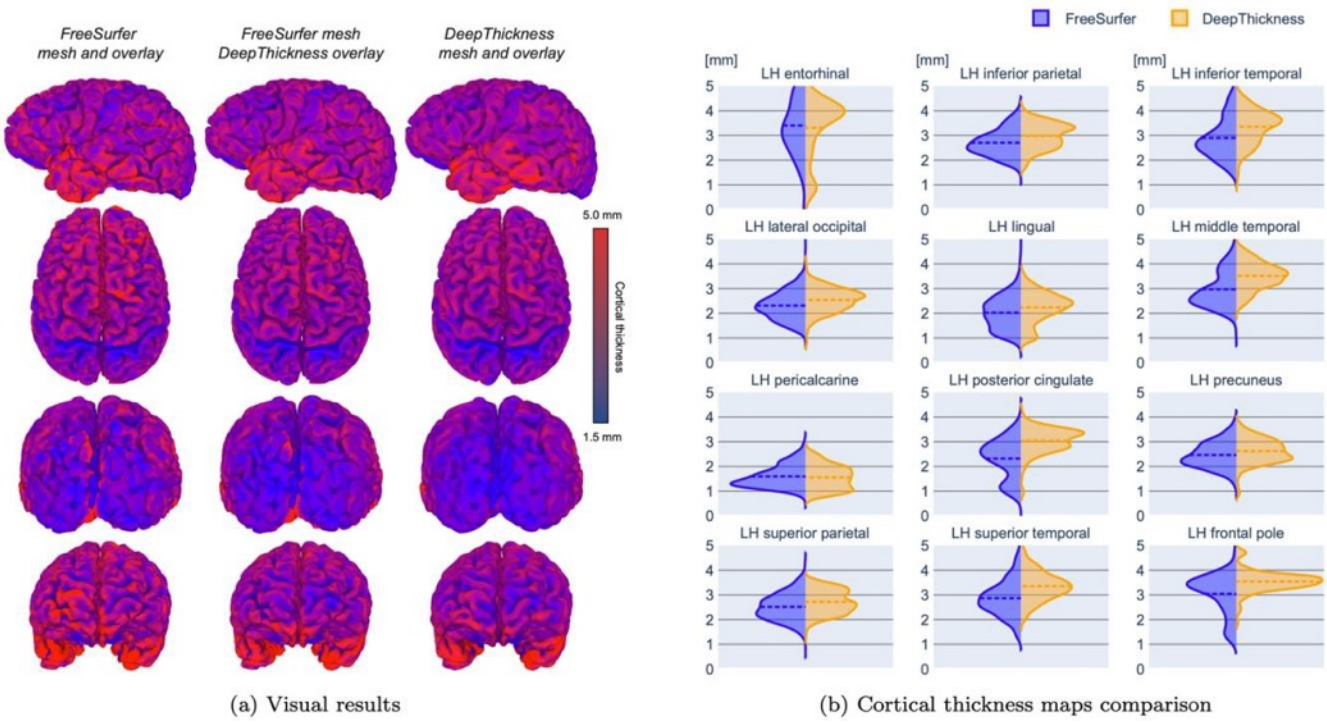

Figure 2. (a) - Visual results of FreeSurfer mesh and CT overlay, FreeSurfer mesh and DeepThickness overlay, and DeepThickness mesh and overlay. (b) - Comparison of the distributions of the cortical thickness values of 12 left hemisphere regions for FreeSurfer (blue) and DeepThickness (orange) on one testing subject in mm. Dotted lines represent average values; higher symmetry in distributions denotes higher region-wise *cortical thickness* similarity. Similar results are obtained for the right hemisphere and other subjects.

4. Conclusion

We present the first DL-based approach for cortical thickness estimation on structural MRI. The extraction of cortical thickness distributions in just a few seconds unlocks the ability to quickly draw population trajectories for thousands of healthy subjects' data, creating an atlas with different distributions for different brain areas.

Keywords: Cortical Thickness, Deep Learning, anatomical deviations, structural MRI, Alzheimer's disease, dementia.

References

[1] Richard AI Bethlehem, Jakob Seidlitz, Simon R White, Jacob W Vogel, Kevin M Anderson, Chris Adamson, Sophie Adler, George S Alexopoulos, Evdokia Anagnostou, Ariosky Areces Gonzalez, et al. Brain charts for the human lifespan. *Nature*, 604(7906):525–533, 2022. doi: 10.1038/s41586-022-04554-y.

[2] Bruce Fischl. FreeSurfer. *NeuroImage*, 62(2):774–781, 2012. ISSN 10538119. doi: 10.1016/j. neuroimage.2012.01.021.

[3] Kaiming He, Xiangyu Zhang, Shaoqing Ren, and Jian Sun. Deep Residual Learning for Image Recognition. pages 770–778, June 2016. doi: 10.1109/CVPR.2016.90.

[4] Miracle Ozzoude, Joel Ramirez, Pradeep Reddy Raamana, Melissa F Holmes, Kirstin Walker, Christopher JM Scott, Fuqiang Gao, Maged Goubran, Donna Kwan, Maria C Tartaglia, et al. Cortical thickness estimation in individuals with cerebral small vessel disease, focal atrophy, and chronic stroke lesions. *Frontiers in Neuroscience*, 14:598868, 2020. doi: 10.3389/fnins. 2020.598868.

[5] Olaf Ronneberger, Philipp Fischer, and Thomas Brox. U-Net: Convolutional Networks for Biomedical Image Segmentation. In *Medical Image Computing and Computer-Assisted Inter vention – MICCAI 2015*, Lecture Notes in Computer Science, pages 234–241, Cham, 2015. doi: 10.1007/978-3-319-24574-4 28.

[6] Rene Seiger, Sebastian Ganger, Georg S Kranz, Andreas Hahn, and Rupert Lanzenberger. Cortical thickness estimations of freesurfer and the cat12 toolbox in patients with alzheimer's disease and healthy controls. *Journal of Neuroimaging*, 28(5):515–523, 2018. doi: https: //doi.org/10.1111/jon.12521.

[7] Lukas Snoek, Maite M van der Miesen, Tinka Beemsterboer, Andries van der Leij, Annemarie Eigenhuis, and H Steven Scholte. The amsterdam open mri collection, a set of multimodal mri datasets for individual difference analyses. *Scientific Data*, 8(1):1–23, 2021.

[8] Michele Svanera, Sergio Benini, Dennis Bontempi, and Lars Muckli. CEREBRUM-7T: Fast and fully volumetric brain segmentation of 7 Tesla MR volumes. *Human brain mapping*, 42 (17):5563–5580, 2021. doi: 10.1002/hbm.25636.

[9] Michele Svanera, Mattia Savardi, Alberto Signoroni, Sergio Benini, and Lars Muckli. Fighting the scanner effect in brain mri segmentation with a progressive level-of-detail network trained on multi-site data. 2022. doi: 10.48550/ARXIV.2211.02400.

[10] Stefan van der Walt, Johannes L. Sch¨onberger, Juan Nunez-Iglesias, Fran¸cois Boulogne, Joshua D. Warner, Neil Yager, Emmanuelle Gouillart, Tony Yu, and the scikit-image con tributors. scikit-image: image processing in Python. *PeerJ*, 2:e453, 6 2014. ISSN 2167-8359. doi: 10.7717/peerj.453.

125. 7T MRI prediction from 3T MRI data: application to the IMAGEN cohort

Yuxiang Dai[1,4], Renat Jakupov[2], Frauke Nees[3], Emrah Duzel[2], He Wang[4,5], Gunter Schumann[1,6*]

[1]Centre for Population Neuroscience and Stratified Medicine (PONS), Institute of Science and Technology for Brain-Inspired Intelligence, Fudan University, Shanghai, China

[2]German Centre for Neurodegenerative Diseases (DZNE), Magdeburg site, Magdeburg, Germany

[3]Department of Medical Psychology, UKSH, University of Kiel, Germany

[4]Zhanjiang International Center for Neuroimaging (ZIC), Institute of Science and Technology for Brain- Inspired Intelligence, Fudan University, Shanghai, China

[5] Phenome Institute, Fudan University, Shanghai, China

[6]PONS Centre, Department of Psychiatry and Neuroscience, Charité University Medicine, Berlin, Germany

*gunter.schumann1961@gmail.com

Keywords: Magnetic resonance imaging, 7T MRI prediction, High frequency information, GAN

INTRODUCTION

Compared with 3T MRIs, ultra-high field 7T MRIs with higher resolution and SNR can produce images with exceptional anatomical details and can provide clearer tissue boundaries. Thus, 7T MRIs can contribute to both brain research and clinical management of brain disorders[1]. However, 7T MRIs are cost prohibitive and highly inaccessible which limit the neuroscience for more accurate analysis.

To predict satisfactory 7T-like MRIs, a few models have been proposed, including sparse learning[2-4], random forest[5], and deep learning[6-8]. However, all these methods share the following limitations: (1) they require rigid registration on gray and white matters of 3T and 7T MRIs that is quite challenging for clinical data training. (2) they often fail to capture sufficient anatomical details, and the 3D predictions are often blurred. To further tackle those limitations, we proposed a high frequency-based generative adversarial network (HF-GAN) that can predict 3D 7T-like images with sharper image contrast and better SNR based on 3T MRIs.

METHODS

We utilized the GAN network to improve image contrast, in which the generator can synthesize the 7T-like MRIs and the discriminator helps approach 7T-like to 7T MRIs (Fig. 1). To embed more detailed 7T structure into predictions, a reconstruction network for learning high frequency information from 7T MRI was introduced. Specifically, in the HF extraction module of Figure 1, we transferred the 3T or 7T MRIs into Fourier domain for

k-space data and multiplied the k-space data by the designed matrix.

In order to accurately evaluate 7T-like predictions, we made Freesurfer segmentation and statistical analysis on all paired images (3T, 7T-like and 7T), which can be seen in the Statistical Analysis of Figure 1. For sub-cortical regions, we extracted the statistical intensity values related to image contrast and conducted comparison of 3T, 7T-like and 7T. Then, we implemented the same process on cortical regions via thickness values.

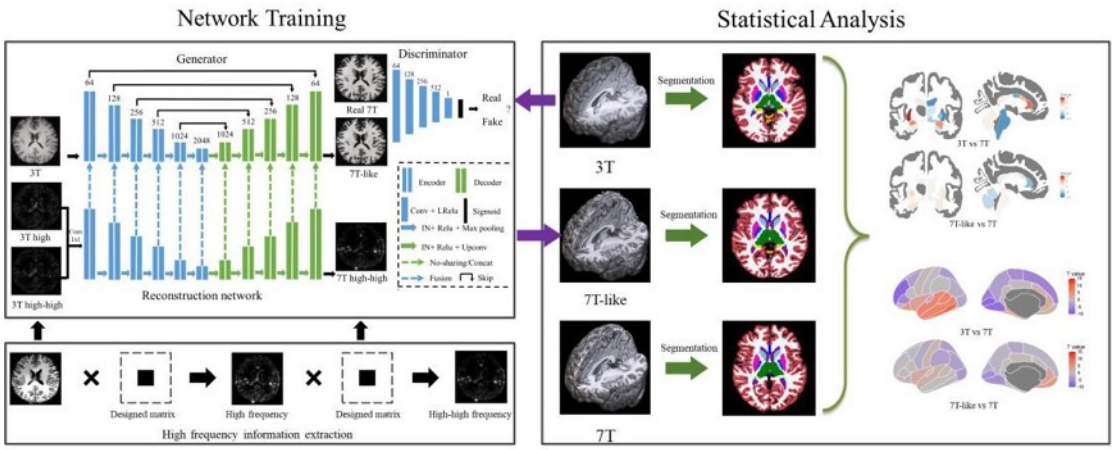

Figure 1: The framework of our proposed prediction method. The left is the network training. The right contains the testing, segmentation and statistical analysis.

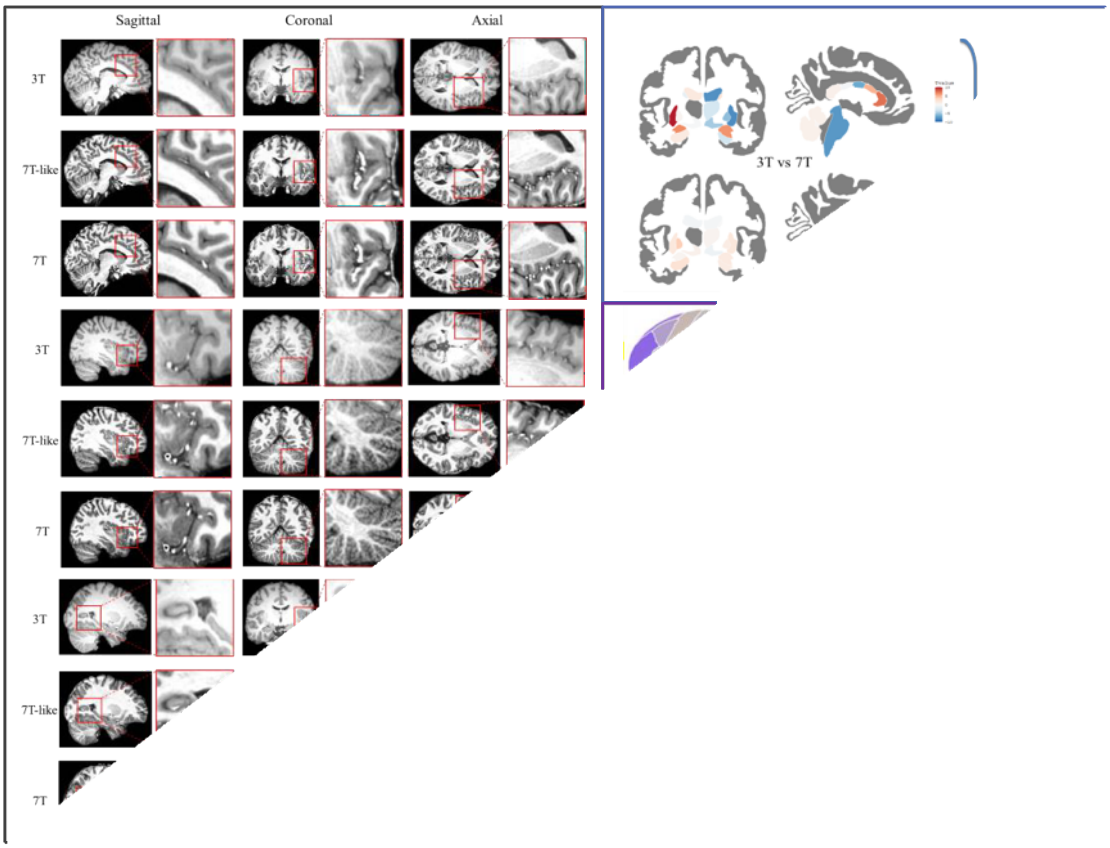

Figure 2: The visual and quantitative results of our 7T-like predictions. The left shows the visual results of three testing cases. The right demonstrates the quantitative results of

sub-cortical and cortical regions by heatmaps.

RESULTS AND DISCUSSION

Our model yields results that are very similar to those of ground truth 7T MRI thus significantly improving tissue segmentation. In the left of Figure 2, 7T-like MRIs introducing the HF information lead to better vessels representation compared with 3T MRIs. Specially, some subtle regions like cerebellum and hippocampus have significantly higher SNR than 3T MRIs. This can be attributed to the high frequency learning capability of HF-GAN. Intensity values extracted from sub-cortical regions were calculated for all 30 pairs of MRIs. In Figure 2, 7T-like predictions share much less difference with 7T compared with 3T vs 7T for most sub-cortical regions. Meanwhile, our HF-GAN performs quite well on cortical regions. For instance, according to cortical heatmaps of thickness difference in Figure 2, 7T-like temporal lobes always demonstrate much less difference with 7T.

We found out which brain regions have been significantly enhanced by our method. Based on these findings, we are applying the model to the genetics IMAGEN cohort of 2000 adolescent participants assessed with 3T (www.imagen-project.org) who have been followed up with two neuroimaging assessments. As IMAGEN has extensive behavioural and neuropsychological assessments, we expect that a more refined neuroimaging characterisation might yield new insights in the relation of brain structure, development and behaviour.

ACKNOWLEDGEMENTS

This work received support from tthe European Union-funded Horizon Europe project 'environMENTAL' (grant number: 101057429), the Horizon 2020 funded ERC Advanced Grant 'STRATIFY' (Brain network based stratification of reinforcement-related disorders) (695313) and the Human Brain Project (HBP SGA3, 945539).

REFERENCES

1. Isaacs R, Mulder J, Groot M, et al. 3 versus 7 Tesla magnetic resonance imaging for parcellations of subcortical brain structures in clinical settings. PLoS ONE, 2020, 15(11): e0236208. https://doi.org/10.1371/journal.pone.0236208

2. Bahrami K, Shi F, Zong X, et al. Hierarchical reconstruction of 7T-like images from 3T MRI using multi- level CCA and group sparsity. International Conference on Medical Image Computing and Computer- Assisted Intervention. Springer, Cham, 2015: 659-666. https://doi.org/10.1007/978-3-319-24571-3_79

3. Bahrami K, Shi F, Zong X, et al. Reconstruction of 7T-like images from 3T MRI. IEEE transactions on medical imaging, 2016, 35(9): 2085-2097. https://doi.org/10.1109/TMI.2016.2549918

4. Zhang Y, Cheng J Z, Xiang L, et al. Dual-domain cascaded regression for synthesizing 7T from 3T MRI, International Conference on Medical Image Computing and Computer-Assisted Intervention. Springer, Cham, 2018: 410-417. https://doi.org/10.1007/978-3-030-00928-1_100

5. Bahrami K, Rekik I, Shi F, et al. 7T-guided learning framework for improving the segmentation of 3T MR images, International Conference on Medical Image Computing and Computer-Assisted Intervention. Springer, Cham, 2016: 572-580. https://doi.org/10.1007/978-3-319-46723-8_66

6. Bahrami K, Shi F, Rekik I, et al. Convolutional neural network for reconstruction of 7T-like images from 3T MRI using appearance and anatomical features. Deep Learning and Data Labeling for Medical

Applications. Springer, Cham, 2016: 39-47. https://doi.org/10.1007/978-3-319-46976-8_5

7. Qu L, Zhang Y, Wang S, et al. Synthesized 7T MRI from 3T MRI via deep learning in spatial and wavelet domains. Medical image analysis, 2020, 62: 101663. https://doi.org/10.1016/j.media.2020.101663

8. Qu L, Wang S, Yap P T, et al. Wavelet-based semi-supervised adversarial learning for synthesizing realistic 7T from 3T MRI. International Conference on Medical Image Computing and Computer- Assisted Intervention. Springer, Cham, 2019: 786-794. https://doi.org/10.1007/978-3-030-32251-9_86

126. A simulating and assimilating platform for the whole human brain with applications

Wenlian Lu[1], Qibao Zheng[1], Ningsheng Xu[1], Jianfeng Feng[1,2,3,4,5*], DTB Consortium

[1] Institute of Science and Technology for Brain-Inspired Intelligence, Fudan University, Shanghai, China

[2] Key Laboratory of Computational Neuroscience and Brain-Inspired Intelligence (Fudan University), Ministry of Education, China

[3] Shanghai Center for Mathematical Sciences, Fudan University, Shanghai, China

[4] Department of Computer Science, University of Warwick, Coventry, United Kingdom

[5] Zhangjiang Fudan International Innovation Center, Shanghai, China

*Corresponding author. Email: jianfeng64@gmail.com

INTRODUCTION/MOTIVATION

We have not been able to come up a simulated whole human brain model which has roughly 100 billion neurons and these neurons are intensively interconnected via chemical junctions. The difficulty has a few facets. In neuroscience, we cannot directly measure the activities of multi-neurons in a healthy human brain. Even if we have the data of each neuronal activity available, we do not have a mathematical tool to reverse engineering to reconstruct the complex neuronal networks, which basically requires to fit/found at least multi-trillion parameters. European brain project produced two digital brains: one is the SpinNakker [1] and the other is the virtual brain [2]. The data which we can directly measure for a whole human brain is the BOLD signals for each voxel (a human brain typically has around 100,000 voxels) and the fibre connection between each measured voxel (DTI). With these available data, we intend to construct a digital twin brain (DTB) as close as possible to its biological counterpart [3].

METHODS, RESULTS AND DISCUSSION

The DTB (Fig. 1A) gives methods and platform of neuromorphic computing and statistic inference and comprises of two components. One is to construct and simulate neuronal network of human brain scale and intensively biological data driven structure on general GPU-based HPC with appreciable performance [4]. The other is to fit the brain resting-state experiment data and mimic 3 real-world functional experiment tasks by a proposed hierarchical mesoscale data assimilation method [5]. Firstly, the simulated number of neurons in a neuronal population is proportional to the grey matter volume obtained from the T1-weighted MRI image (Fig. 1B). Excitatory neurons and inhibitory neurons are included here and the ratio of the number of excitatory neurons to that of inhibitory neurons in each neuronal population is set as 4:1. Each neuron is described by the Leaky integrate and fire model with four synaptic currents (AMAP, NMDA, $GABA_A$, $GABA_B$). Second, the structural connection

probability between a pair of neuronal populations is estimated by the row-normalized fibre counts obtained from the DTI (Fig. 1B). Thirdly, the connection within each neuronal population inside a micro-column is based on neuroanatomy data [6] (Fig. 1B). Finally, with the predefined network size (86B) and in-degree scale (100). [3] provides us with details. To meet the requirement of low-latency communication between GPUs for the DTB simulation, we first propose a partitioning algorithm and a two-level routing method to balance the data traffic and reduce the degree of GPU connections (Fig. 1C). The time series of the BOLD signal for each ROI/voxel are formulated by the Balloon-Windkessel model [7], and generate the simulated BOLD signals (Fig. 1D). We proposed a framework of hierarchal mesoscale data assimilation to estimate the model parameters [5]. However, due to the huge amount of parameters (more than 10 trillion parameters for 86B neurons in total), we take each region of interest(ROI), for instance, the brain region, voxel or each layer of the micro column structure according to the resolution of the network model, and assume that the conductance parameters of the same type of the neurons in the same ROI follow the same distribution, or, equivalently, share the same hyper-parameters. The hyper- parameters are estimated and each conductance value is sampled according to the distribution with the hyperparameters. The DTB and its biological counterpart has a correlation coefficient above 0.9 in the resting state [3]. Therefore, the DTB, equipped with the hierarchal mesoscale data assimilation, can be used to conduct digital experiments to explore the phenomena at neuronal and synaptic level (dry experiment). The assimilated model can be validated by mimicking the cognitive action task by simulating the brain by the assimilated model, compared with the results of the real-world experiments (in-action experiment) (see Fig. 2).

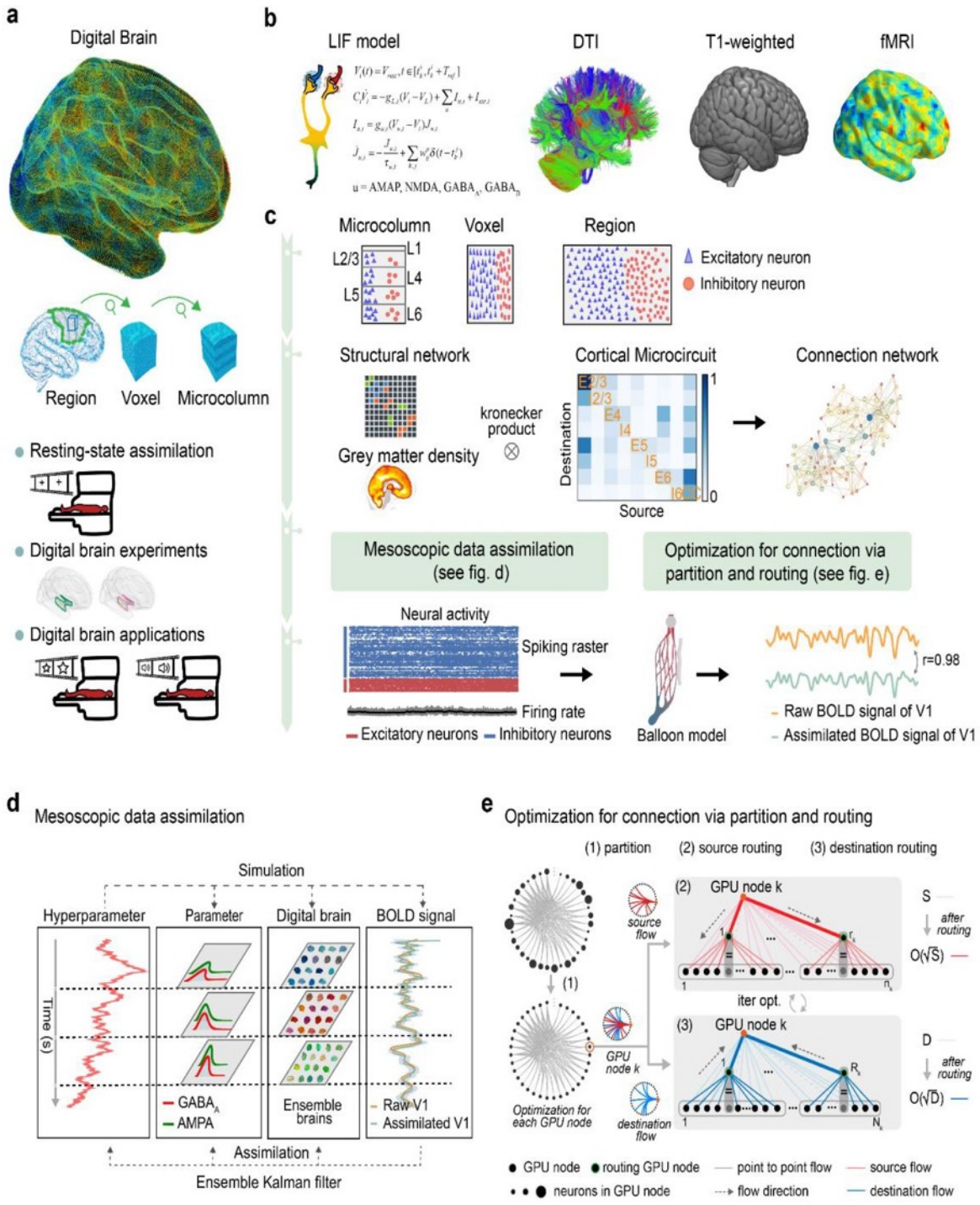

Fig. 1. Work flow of the digital twin brain (DTB). (A) The DTB is constructed with different numbers of spiking neurons to mimic the brain activity at three resolutions: regional, voxel and micro-column. The DTB containing 86 billion neurons and 10 trillion synapses is simulated on 10,000 GPU cards and achieved a time-to-solution of 560. Resting-state and task-based digital experiments were performed with the DTB (see Fig. 2 and 5). Besides, information flow and deep brain stimulation were also explored with the DTB (see Fig. 3 and 4). (B) Multi-modality MRI data (i.e., diffusion tensor imaging (DTI) and T1-weighted imaging) and a micro-column connection map were used to construct a probabilistic connection network. The micro-column is an elaborate network composed of six layers (L1, L2/3, L4, L5 and L6) and two types of neurons (excitatory and inhibitory neurons), whose inner

connections are defined based on the neuroanatomy of the primary visual cortex of the cat. (C) An illustration for our two-level routing system, with which we could balance the data traffic and reduce the degree of graphics processing 15 units (GPUs) connection. (D) The parameter and model setting for the DTB. The Leaky Integrate- and-Fire neuron model was used to model spike activity. Then the firing rate, obtained by counting the number of spikes of neural activity over a sliding window, is fed into the Ballon Windkessel model to form the time series of the simulated blood oxygenation level-dependent signal. The synaptic conductance of AMPA and GABAA are tuned to fit the empirical BOLD signal from functional MRI. (E) An illustration for our hierarchical mesoscale data assimilation method. The hierarchical brain assimilation estimated the hyperparameters by iterating two processes: simulation and filtering the hidden states by diffusion ensemble Kalman filter (EnKF). Also see Supplementary Materials for more details.

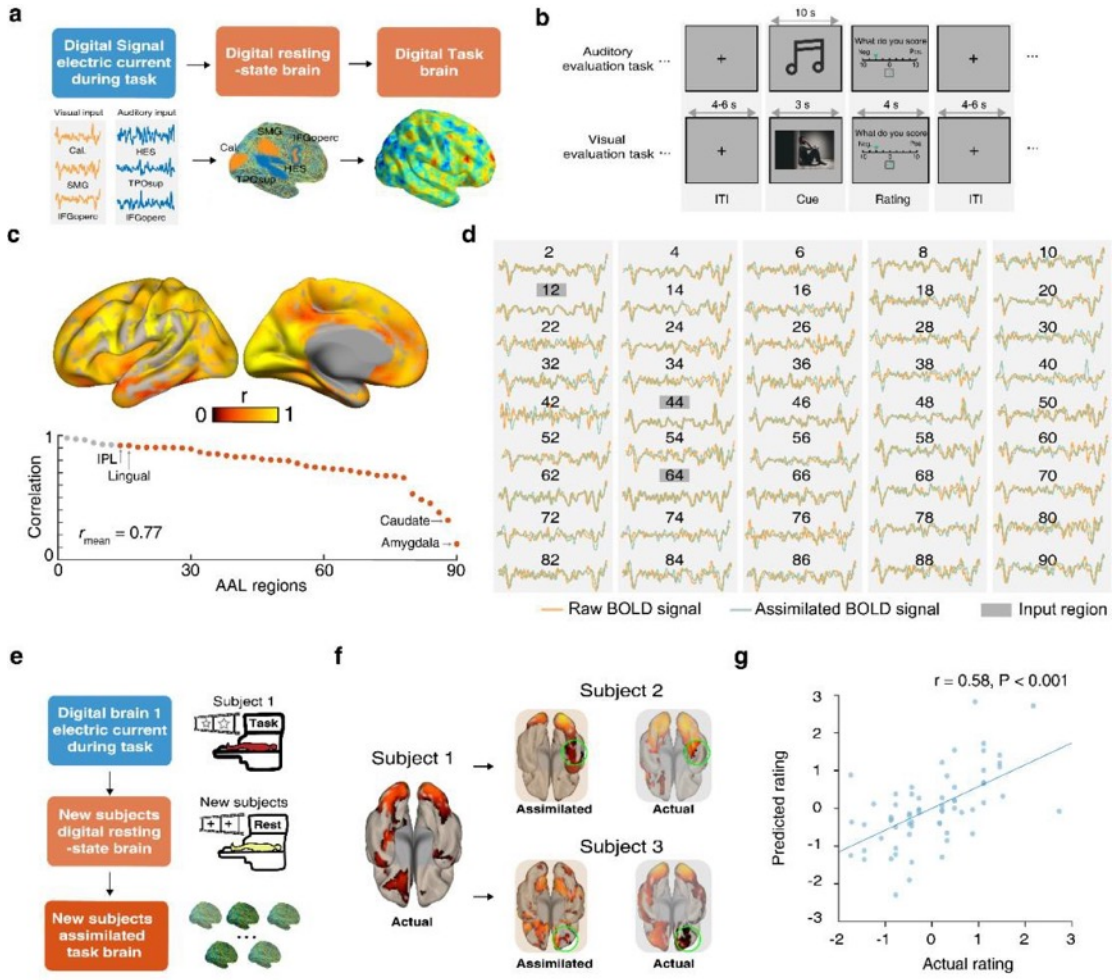

Fig. 2. DTB in action (100 M neurons, voxel version). (A) Workflow for the DTB in action. We firstly simulate the BOLD signals of the reference brain regions to obtain electric input currents. Then we injected the above currents into the DTB to yield the digital task brain. (B) A schematic illustration of the auditory and visual evaluation task.

(C) Pearson correlations between the empirical and assimilated BOLD signals at both voxel- and region-level. (D)

The illustrations of the empirical and the assimilated BOLD signals with a time lag of 4 for each region in right hemisphere during the visual evaluation task. (E) A schematic illustration of the digital brain virtual experiment, in which we injected current during the task from subject 1 into the digital resting state brain of other subjects, to yield a digital task brain of other subjects. (F) The activation patterns of the assimilated digital task brain and its corresponding biological brain. (G) The predicted performance based on the assimilated DTB of the visual evaluation task. Also see fig. S8 for the auditory evaluation task and Supplementary Materials for more details

Keywords: digital twin brain, meso-scale data assimilation, resting state, spiking neuronal networks, two-level routing method

ACKNOWLEDGEMENTS

We are working on the second version DTB: DTB2.

REFERENCES

[1]S. B. Furber, et al., The SpiNNaker Project. Proceedings of the IEEE 102, 652-665 (2014).
[2] P. Sanz Leon et al., The Virtual Brain: a simulator of primate brain network dynamics. Front Neuroinform 7, 10 (2013).
[3] W.L. Lu et al. The human digital twin brain in the resting state and in action https://arxiv.org/ftp/arxiv/papers/2211/2211.15963.pdf, (2022).
[4] X. Du et al., A Low-Latency Communication Design for Brain Simulations. IEEE Network 36, 8-15 (2022).
[5] W. Zhang, B. Chen, J. Feng, W. Lu, On a framework of data assimilation for neuronal networks. arXiv preprint arXiv:2206.02986, (2022).
[6] T. Binzegger, R. J. Douglas, K. A. Martin, A quantitative map of the circuit of cat primary visual cortex. J Neurosci 24, 8441-8453 (2004).
[7] K. J. Friston, A. Mechelli, R. Turner, C. J. Price, Nonlinear responses in fMRI: the Balloon model, Volterra kernels, and other hemodynamics. Neuroimage 12, 466-477 (2000).

127. A nonparametric tool to quantify the content of information transmitted between neural populations

Marco Celotto[1,2,3*], Jan Bím[2,4], Alejandro Tlaie[2], Vito De Feo[2,5], Stefan Lemke[2,6], Daniel Chicharro[2,7], Hamed Nili[1], Malte Bieler[8,9], Ileana L. Hanganu-Opatz[8], Tobias Donner[10], Andrea Brovelli[11], Stefano Panzeri[1,2 *]

[1] Department of Neural Information Processing, Center For Molecular Neurobiology (ZMNH), University Medical Center, Hamburg-Eppendorf, Falkenried 94, D-20251 Hamburg, Germany

[2] Neural Computation Laboratory, Istituto Italiano di Tecnologia, Rovereto (TN) 38068, Italy

[3] Department of Pharmacy and Biotechnology, University of Bologna, 40126 Bologna, Italy

[4] Datamole, s. r. o, Vítězné náměstí 577/2 Dejvice, 160 00 Praha 6, The Czech Republic.

[5] Artificial Intelligence Group, Future Health Technology Lab, School of Computer Science and Electronic Engineering, University of Essex, Colchester, UK

[6] Department of Cell Biology and Physiology, University of North Carolina, Chapel Hill, United States

[7] Department of Computer Science, City, University of London, London, UK

[8] Institute of Developmental Neurophysiology, Center for Molecular Neurobiology, University Medical Center, Hamburg-Eppendorf, 20251 Hamburg, Germany

[9] Mobile Technology Lab, School of Economics, Innovation and Technology, University College Kristiania, 0152 Oslo, Norway

[10] Section Computational Cognitive Neuroscience, Department of Neurophysiology and Pathophysiology, University Medical Center, Hamburg-Eppendorf, Martinistrasse 52, 20251 Hamburg, Germany

[11] Institut de Neurosciences de la Timone, UMR 7289, Aix Marseille Université, CNRS, 13385 Marseille, France

* marco.celotto@iit.it, s.panzeri@uke.de

INTRODUCTION

A key step for understanding how the brain processes sensory information is the ability to quantify how much of the information that a neural population X encodes about a specific feature of a sensory stimulus S is transmitted to a downstream population Y [1]. Traditional methods rely on the Wiener-Granger causality principle to quantify how much overall information is transmitted between simultaneously recorded neuronal signals. These methods include both parametric measures, such as Granger Causality, and nonparametric ones, such as information-theoretic Directed Information (DI) [2,3]. However, while these established measures allow quantifying the magnitude and directionality of information transfer, they provide no insight into the content of the information being communicated.

METHODS

In this work, we defined a new measure, which we called Feature-specific Information Transfer (FIT). FIT is a measure of information transfer that quantifies how much of the directed information transmitted between neural signals is about specific external target variables, such as a feature of a sensory stimulus S (Fig.1A,B). To define FIT, we leveraged on the mathematical framework of Partial Information Decomposition (PID) [4]. PID extends classical Shannon's information theory and allows breaking down the joint mutual information that several source variables carry about a target variable into pieces of redundant, unique and synergistic information. Within this framework, we defined FIT(S:X→Y) as the amount of information that is redundant between the past of a sender neural signal X and the present of a receiver signal Y about a specific stimulus feature S, which is also unique with respect to the past of the receiver signal Y (Fig.1C). Such definition uses PID to combine the Wiener-Granger causality principle of information transfer with the content specificity about a target variable of interest into a single measure. Since it does not make assumptions on the data distributions, FIT can be applied to any type of simultaneously recorded neural signals. We provided a permutation-based null hypothesis for FIT that can be used to identify scenarios where S induces temporally-lagged covariations in X and Y and there is no actual interaction between the two neural signals. Additionally, we defined a conditioned version of FIT, that we named cFIT. cFIT(S:X→Y | Z) quantifies the amount of FIT about S transmitted from X to Y that, at the same time, is not present in the past of a potentially confounding neural signal Z.

RESULTS AND DISCUSSION

We validated FIT on simulated data showing that it only captures information transfer that is about specific stimulus features, correctly discarding the transfer of noise between neural signals, while traditional measures of directed communication such as DI are sensitive to the transfer of both stimulus and noise. We tested the permutation based null hypothesis and the cFIT measure on simulated signals to prove how to deal with variables that could potentially act as confounder of FIT. Then, we tested FIT and cFIT on several previously published real datasets. Analyzing electroencephalographic (EEG) recordings [5,6], we could establish inter-hemispheric directed information transfer about visual features relevant for the perception of faces. Using magnetoencephalographic (MEG) recordings [7,8] we could establish sensory-specific communication (including gamma-band feedforward communication of visual information relevant for behavior). Importantly, such effects could not be revealed by traditional measures such as DI.

In summary, FIT extends previous methodologies that quantify the overall transfer of information between neural populations, providing insight on the content of communication. Our results indicate that FIT can be an important tool to unveil novel properties of sensory information processing in the brain that cannot be detected using standard measures of information transfer.

Keywords: Information transfer, sensory processing, Wiener-Granger causality, partial information decomposition, systems neuroscience

ACKNOWLEDGEMENTS

This research was supported by the European Union's Horizon 2020 Framework Programme for Research and Innovation under the Specific Grant Agreement No. 945539 (Human Brain Project SGA3). Further support was received by the NIH Brain Initiative (grants U19NS107464 and NS108410 to SP), by the European Research Council (ERC-2015-CoG 681577 to I.L.H.-O.), the German Research Foundation (Ha 4466/10-1, SPP 1665, SFB 936 B5 to I.L.H.-O), the French National Agency (ANR-18-CE28-0016-01 to AB), and the FLAG-ERA (ANR-17-HBPR-0001-02 to AB).

REFERENCES

[1] Panzeri S, Moroni M, Safaai H, Harvey C. The structures and functions of correlations in neural population codes. Nat Rev Neurosci 2022; 23(9) 551–567. doi:10.1038/s41583-022-00606-4

[2] Granger CWJ. Investigating Causal Relations by Econometric Models and Cross-spectral Methods. *Econometrica* 1969; 37(3) 424-438. doi:10.2307/1912791

[3] Massey JL. Causality, feedback and directed information. *Proc 1990 Intl Symp on Info Th and its Applications, Waikiki, Hawaii* 1990.

[4] Williams PL, Beer RD. Nonnegative Decomposition of Multivariate Information. 2010 arXiv. doi: 10.48550/arXiv.1004.2515

[5] Rousselet GA, Ince RAA, van Rijsbergen NJ, Schyns PG. Eye coding mechanisms in early human face event-specific potentials. *J Vis* 2014; 14(13) 7. doi:10.1167/14.13.7

[6] Ince RAA, Jaworska K, Gross J, et al. The Deceptively Simple N170 Reflects Network Information Processing Mechanisms Involving Visual Feature Coding and Transfer Across Hemispheres. *Cereb Cortex* 2016; 26(11), 4123–4135, doi:10.1093/cercor/bhw196

[7] Brovelli A, Badier JM, Bonini F, Bartolomei F, Coulon O, Auzias G. 2017. Dynamic reconfiguration of visuomotor- specific functional connectivity networks. *J Neurosci* 2017; 37(4), 839–853. doi:10.1523/JNEUROSCI.1672- 16.2016

[8] Wilming N, Murphy PR, Meyniel F, Donner TH. Large-scale dynamics of perceptual decision information across human cortex. *Nat Commun* 2020; 11(1) 5109. doi:10.1038/s41467-020-18826-6

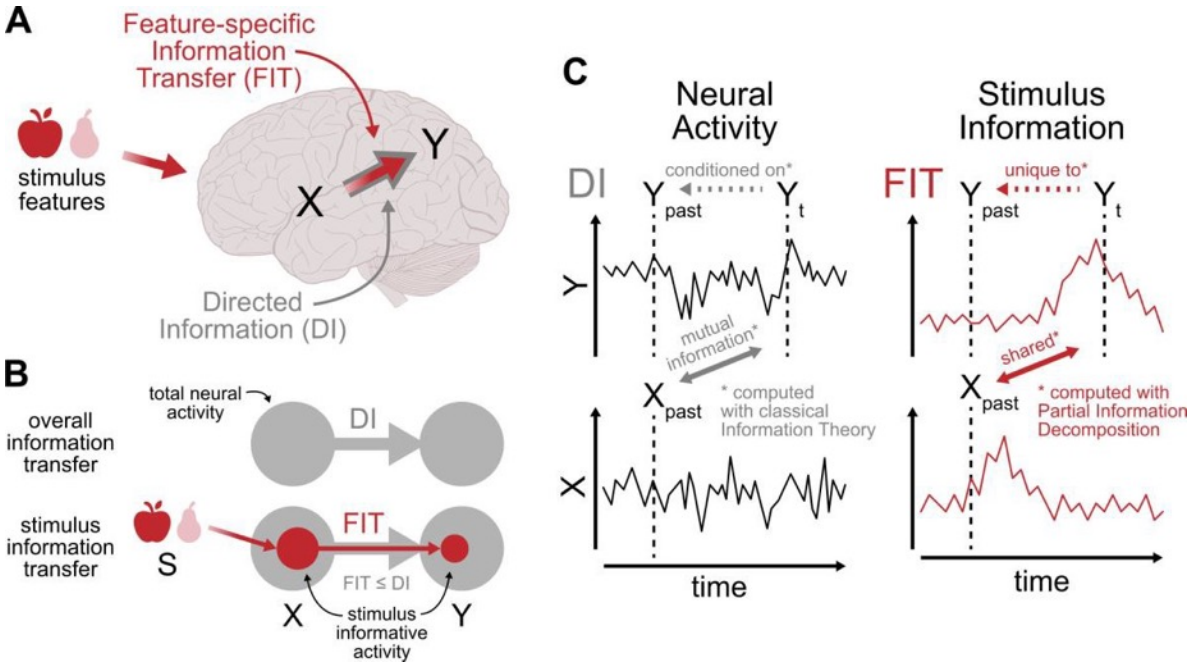

A) DI a traditional information-theoretic measure to quantify the directional information transmission between two simultaneously recorded brain areas X (sender) and Y (receiver). FIT measures the information that is transferred from

X to Y about a specific target variable, such as a feature of a sensory stimulus S. B) DI is sensitive to the total neural activity, while FIT looks specifically to the stimulus-informative neural activity. Stimulus-informative activity is a subpart of the total activity, therefore FIT is upper bounded by DI. C) Both DI and FIT satisfy the Weiner-Granger causality principle. DI is defined as the conditional mutual information between the past of X and the present of Y given the past of Y. FIT is defined within the PID framework as the stimulus-information shared by the past of X and the present of Y which, at the same time, is unique with respect to the past of Y.

128. Multidisciplinary and multiscale perspective on cortical feedback mechanisms

Lucy S. Petro[1], Michele Svanera[1], A. Tyler Morgan[2], Koen Seignette[3], Christiaan N. Levelt[3], Paolo Papale[4], Feng Wang[4], Xing Chen[5], Amparo Gilhuis[4], Pieter R. Roelfsema[4], Matthew W. Self[4], Lars Muckli[1]*

1. Centre for Cognitive NeuroImaging, School of Psychology and Neuroscience, College of Medical, Veterinary and Life Sciences, University of Glasgow, 62 Hillhead Street, Glasgow, G12 8QB, UK.
2. Section on Functional Imaging Methods, Laboratory of Brain and Cognition, National Institute of Mental Health, Bethesda, Maryland, USA.
3. Netherlands Institute for Neuroscience, Molecular Visual Plasticity Group, Royal Netherlands Academy of Arts and Sciences, Meibergdreef 47, 1105 BA Amsterdam, the Netherlands.
4. Department of Vision & Cognition, Netherlands Institute for Neuroscience (KNAW), 1105 BA Amsterdam, Netherlands.
5. Department of Ophthalmology, University of Pittsburgh School of Medicine, 203 Lothrop St, PA 15213, Pittsburgh, US
**Corresponding author: Lars.Muckli at glasgow*.ac.uk

1. Introduction

What makes a system intelligent, and what level of abstraction best captures its functional principles? We propose that the human brain must integrate internal models with external evidence, since the unique human sensorimotor skills and cognitive abilities depend on extracting information from sensory input, contextualised by our intentions and prior knowledge, and brain states. The connectomic foundations of the human cerebral cortex reveal large-scale cortical circuits organised into highly interconnected processing streams flowing backwards to and forward from sensory areas, and intra-areally between specialised functional association regions (e.g. [1]). In the awake state, the top-down negotiation of world knowledge and the bottom-up evidence of sensory information allow for the disambiguation of sensory data, optimising goal-directed behaviour, guiding flexible decision-making [2], and the simulation of imaginary content based on perceptual memory. Investigating how the integration of sensory signals with internal models maps onto cortical neuroanatomy requires a paradigm that allows us to disentangle these signals, including but not limited to top-down modulation.

2. Methods

We chose visual occlusion as a paradigmatic example where top-down knowledge provides input layers with additional contextual information beyond what is available from bottom-up thalamic input [3]. To investigate how contextual feedback processing influences neuronal activity in the primary visual cortex, we presented identical stimuli from 24 partially occluded natural scene images to mice, monkeys, humans, and a deep convolutional neural network model. This approach isolates cortical retinotopic regions that do not receive informative, direct thalamic bottom-up input, but lateral and cortical top-down input. We recorded mice activity with two-photon calcium imaging of V1 L2/3 and L5 neurons in the primary visual cortex of awake, head-fixed mice [4]. The monkey experiment is based on V1 spiking activity data recorded at comparable retinotopic locations in deep layer 5 cells [5]. In a 3T human fMRI experiment, we measured top-down activity in non-stimulated areas of V1 and V2 and compared it to visual processing models [6]. Finally, we trained an artificial model to predict the top-down projected information of occluded regions of an image in a self-supervised way [7].

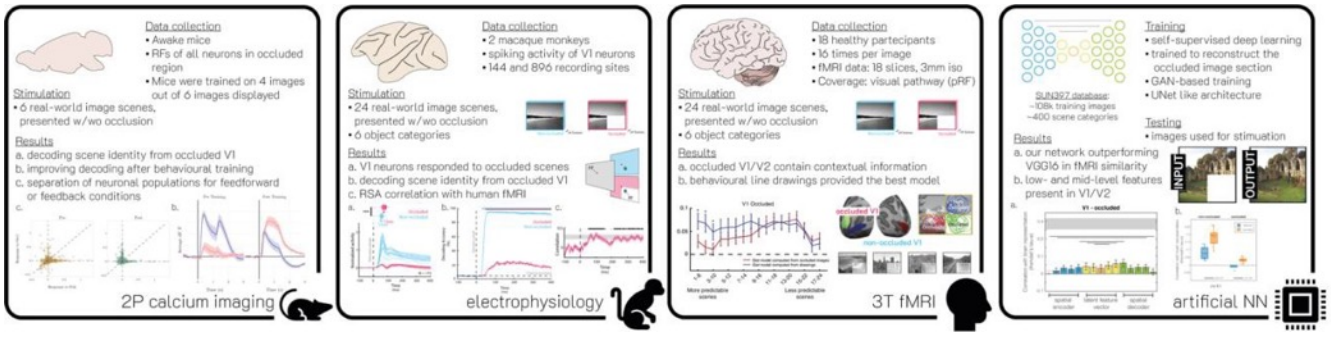

Figure 1. The same occluded images were presented to mice (6), monkeys (24), and humans (24) and while testing a self-supervised deep neural network.

3. Results

Mice: We could decode the stimulus identity from non-stimulated regions of mouse V1, with slightly improved decoding accuracy after behavioural training [4]. We also see a separation of neuronal populations responding to either feedforward or feedback conditions. Our results are consistent with a predictive processing model of visual perception.

Monkeys: We found that V1 neurons responded rapidly and selectively to occluded scenes, and contain information to decode scene identity, indicating an overlap between visually-driven and contextual responses. Using RSA [8], we showed how the structure of V1 representations of occluded scenes correlates strongly with the representations of the same scenes in humans measured with fMRI.

Humans: Consistent with our previous findings [9], we found that non-stimulated regions of human V1 and V2 contain contextual information fed back from higher visual areas. Furthermore, behavioural line drawings of subjects asked to sketch the missing information provided the best model to explain V1/V2 activities of non-stimulated occluded regions [6].

Artificial neural network: We compared the layer activations in our network to human brain activity fMRI data from V1 while viewing the same images. We found that the self-supervised network completed the task in a more brain-like manner, outperforming a classical object-recognition supervised network (VGG16) in terms of similarity to fMRI data [7].

4. Conclusion

We combined multi-species evidence from experimental and theoretical perspectives describing the information content, microcircuitry, temporal dynamics, and cognitive functions of top-down cortical streams encoding contextual information and perceptual internal models. Such multiscale empirical frameworks, validated by computational models, will be necessary if we are to confront the neuronal explanandum of cognitive functions and infer behaviour from microscale anatomy and function.

References

[1] Claus C. Hilgetag, Alexandros Goulas, and Jean-Pierre Changeux. A natural cortical axis connecting the outside and inside of the human brain. Network Neuroscience, 6(4):950–959, 10 2022. ISSN 2472-1751. doi: 10.1162/netn a 00256. URL https://doi.org/10.1162/netn_a_ 00256.

[2] Ivo Vlaev. Local choices: Rationality and the contextuality of decision-making. Brain Sciences, 8(1), 2018. ISSN 2076-3425. doi: 10.3390/brainsci8010008. URL https://www.mdpi.com/ 2076-3425/8/1/8.

[3] Fraser W Smith and Lars Muckli. Nonstimulated early visual areas carry information about surrounding

context. Proceedings of the National Academy of Sciences, 107(46):20099–20103, 2010. doi: https://doi.org/10.1073/pnas.1000233107.

[4] Koen Seignette, Christiaan N. Levelt, and Pieter Roelfsema. Paper in preparation.

[5] Paolo Papale, Feng Wang, A. Tyler Morgan, Xing Chen, Amparo Gilhuis, Lucy S. Petro, Lars Muckli, Pieter R. Roelfsema, and Matthew W. Self. Feedback brings scene information to the representation of occluded image regions in area v1 of monkeys and humans. bioRxiv, 2022. doi: 10.1101/2022.11.21.517305. URL https://www.biorxiv.org/content/early/2022/11/22/2022.11.21.517305.

[6] Andrew T. Morgan, Lucy S. Petro, and Lars Muckli. Scene representations conveyed by cortical feedback to early visual cortex can be described by line drawings. Journal of Neuroscience, 39(47):9410–9423, 2019. ISSN 0270-6474. doi: 10.1523/JNEUROSCI.0852-19.2019. URL https://www.jneurosci.org/content/39/47/9410.

[7] Michele Svanera, Andrew T. Morgan, Lucy S. Petro, and Lars Muckli. A self-supervised deep neural network for image completion resembles early visual cortex fMRI activity patterns for occluded scenes. Journal of Vision, 21(7):5–5, 07 2021. ISSN 1534-7362. doi: 10.1167/jov.21. 7.5. URL https://doi.org/10.1167/jov.21.7.5.

[8] Nikolaus Kriegeskorte, Marieke Mur, and Peter Bandettini. Representational similarity analysis - connecting the branches of systems neuroscience. Frontiers in Systems Neuroscience, 2, 2008. ISSN 1662-5137. doi: 10.3389/neuro.06.004.2008. URL https://www.frontiersin. org/articles/10.3389/neuro.06.004.2008.

[9] Lars Muckli, Federico DeA Martino, Luca Vizioli, Lucy S. Petro, Fraser W. Smith, Kamil Ugurbil, Rainer Goebel, and Essa Yacoub. Contextual feedback to superficial lay ers of v1. Current Biology, 25(20):2690–2695, 2015. ISSN 0960-9822. doi: https://doi.org/ 10.1016/j.cub.2015.08.057. URL https://www.sciencedirect.com/science/article/pii/ S0960982215010738.

129. Loss shaping enhances learning with EventProp in spiking neural networks

Thomas Nowotny[1*], James P Turner[1], James C Knight[1]

[1]School of Engineering and Informatics, University of Sussex, Brighton, UK

*t.nowotny@sussex.ac.uk

INTRODUCTION

In a recent paper [1], Wunderlich and Pehle introduced the EventProp algorithm that allows learning by gradient descent on exact gradients in spiking neural networks. Moreover, the backward pass of the EventProp algorithm is event-based so that it is a natural fit for our GPU enhanced neuronal networks (GeNN) framework [2,3]. We have, therefore, implemented EventProp in GeNN and investigated its learning performance on increasingly challenging benchmarks, including the Spiking Heidelberg Digits (SHD) classification task [4]. Using a typical loss function we observed a failure to learn the SHD task. Here we present work that analyses this failure and solves it through "loss shaping", the definition of a loss function that is specifically tuned to enable rapid and successful learning of the task.

METHODS

EventProp was implemented in the GeNN framework using the PyGeNN interface [5]. Besides user-side definitions of custom neuron and synapse models, only one minor change in GeNN was required: We introduced the new construct of a pre-synaptic action at spikes or spike-like events in order to efficiently implement the event-based backpropagation of errors in EventProp. The code is available at https://github.com/tnowotny/genn_eventprop. We also slightly extended the EventProp formalism to make explicit how to handle a larger family of loss functions of the form $L' = F\left(\int_0^T l_V(V(t), t)\, dt\right)$, where F is an at least once differentiable function, instead of the originally described $L = \int_0^T l_V(V(t), t)\, dt$.

RESULTS AND DISCUSSION

The GPU acceleration of GeNN has allowed us to test EventProp extensively on increasingly challenging learning benchmarks. We find that EventProp performs well on some tasks, such as the YinYang benchmark [6] and latency encoded MNIST [7] but for others, such as the SHD task [4] learning initially failed.

We have analysed the underlying issues in detail and discovered that they relate to the nature of the exact gradient of the employed loss functions. In particular, the exact gradient does not contain information about loss changes due to the emergence of additional spikes or the removal of spikes. It only carries information related to changes in spike times. Depending on the details of the task and the loss function, descending the exact gradient with

EventProp can, therefore, lead to the "accidental" deletion of important spikes and so to an inadvertent increase of the loss and decrease of classification accuracy.

Problems of a similar flavour are well-known and are usually solved by regularisation. However, regularisation encourages appropriate activity across all neurons whereas we found that for the SHD data specifically the most useful hidden spikes were deleted due to the employed loss function. Regularisation was hence too unspecific to recover learning.

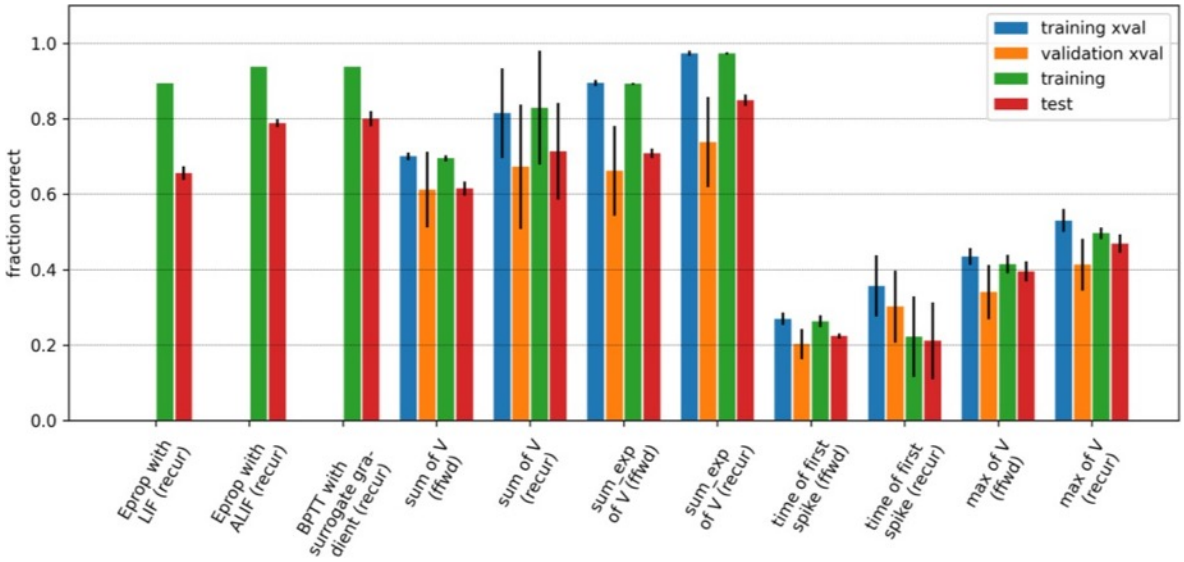

Figure 1: Summary of SHD classification results. The result for back-propagation through time with surrogate gradient is from [5] and the e-prop results from [6]. "ffwd" are feed-forward networks, "recur" recurrent networks. "xval" refers to "leave one speaker out" cross-validation. The bars are the average fraction of correctly predicted digits after 300 training epochs, for the cross-validation averaged over the 10 folds of left out speakers, for the full training and testing averaged over 10 runs with different random seeds. The error bars are standard deviations for the same repeats. In the cross-validation, mean and standard deviation are additionally averaged across two
runs with different seeds.

We have augmented the EventProp algorithm to support a wider class of loss functions and with a loss function that considers the cross-entropy of average output voltages instead of the average of the cross-entropy of output voltages, learning can be restored.

The last twist in the tale is that this new loss function results in very small gradients for hidden layer neurons because the timing of hidden spikes is now almost irrelevant when calculating the average voltage of output neurons. This in turn leads to extremely slow learning. To achieve faster learning, we therefore introduced a weighting term in the loss function that favours early useful hidden spikes and so introduces a beneficial additional gradient for input-to-hidden synapse weights. The headline classification results for SHD are shown in Figure 1. The weighted loss of averaged voltages (“sum_exp”) allows us to achieve state of the art classification accuracy.

Keywords: Spiking Neural Network, EventProp, Spiking Heidelberg Digits, Gradient Descent, Regularisation

ACKNOWLEDGEMENTS

This work was funded by the EPSRC, grants EP/P006094/1, EP/S030964/1, EP/V052241/1, and the EU, under Grant Agreement 945539 (HBP SGA3). Additionally, we gratefully acknowledge the Gauss Centre for Supercomputing e.V. (www.gauss-centre.eu) for funding this project by providing computing time through the John von Neumann Institute for Computing (NIC) on the GCS Supercomputer JUWELS at Jülich Supercomputing Centre (JSC); and the JADE2 consortium funded by the EPSRC (EP/T022205/1) for compute time on their systems.

REFERENCES

[1] Wunderlich T, Pehle C (2021) Event-based backpropagation can compute exact gradients for spiking neural networks. Scientific Reports, 11(1):12829. doi: 10.1038/s41598-021-91786-z

[2] GeNN developers, https://github.com/genn-team/genn

[3| Yavuz E, Turner J, Nowotny T (2016) GeNN: a code generation framework for accelerated brain simulations. Scientific Reports 6:18854. doi: 10.1038/srep18854

[4] Cramer B, Stradmann Y, Schemmel J, Zenke F (2022) The Heidelberg Spiking Data Sets for the Systematic Evaluation of Spiking Neural Networks. IEEE Transactions on Neural Networks and Learning Systems, 33(7):2744– 2757. doi: 10.1109/TNNLS.2020.3044364

[5] Knight JC, Komissarov A, Nowotny T (2021) PyGeNN: A Python Library for GPU-Enhanced Neural Networks. Frontiers in Neuroinformatics 15: 10. doi: 10.3389/fninf.2021.659005

[6] Kriener L, Göltz J, Petrovici MA (2022) The Yin-Yang dataset. Neuro-Inspired Computational Elements Conference, ACM, pp107–111. doi: 10.1145/3517343.3517380

[7] Y. LeCun and C. Cortes (1998) MNIST database. http://yann.lecun.com/exdb/mnist/

130. Control of slow oscillations and epileptiform discharges by photoswitchable M1 muscarinic ligands

José M. Sanchez-Sanchez[1], Fabio Riefolo[2], Almudena Barbero-Castillo[1], Rosalba Sortino[2], Luca Agnetta[3], Arnau Manasanch[1], Michael Decker[3], Pau Gorostiza[2,4,5], Maria V. Sanchez-Vives[1,5,*]

[1] Institute of Biomedical Research August Pi i Sunyer (IDIBAPS), Barcelona, Spain

[2] Institute for Bioengineering of Catalonia (IBEC), Barcelona Institute of Science and Technology. Barcelona, Spain

[3] Institute of Pharmacy and Food Chemistry. University of Würzburg, Germany

[4] CIBER-BBN, Madrid, Spain

[5] ICREA, Barcelona, Spain

* Corresponding author: jmsanchez@recerca.clinic.cat

INTRODUCTION

The transition between brain states is physiologically induced by a combination of neurotransmitters where acetylcholine (ACh) has a prominent and relevant role[1]. Cholinergic action in the cerebral cortex takes place largely through muscarinic receptors which are involved in a range of critical functions related to cognition, behavior and motor processing[2]. Specific spatiotemporal control of the ACh-receptor activation can contribute to the understanding of the role of ACh in the different cortical brain states and in its transitions[3] and to the exploration of a potential therapeutical tool. In this study, we explored the use of photopharmacology, a new approach that allows the light activation of photoswitchable drugs in the brain. Specifically, we studied the role of M_1 mAChRs on the modulation of cortical spontaneous slow oscillations (SO)(Fig. 1a) and of epileptogenic activity using a novel photoswitchable M_1 mAChR agonist, benzylquinolone-carboxylic acid–azo-iperoxo (BAI), and a M_1 mAChR antagonist, cryptozepine, respectively.

METHODS

To study the effect of BAI on cortical dynamics *in vitro*, first we obtained BAI cis-isomer, which has a lower affinity for M_1 mAChRs (inactive molecule). We applied UV light (365 nm) for 5 min to the stock dilution (100 µM BAI), then it was diluted to 1 µM

BAI and added the interphase chamber bath in the dark. Finally, white light was applied to the slice to obtain the *trans*- isomer (active molecule). In the *in vivo* experiments, BAI was delivered inside a well made over the craniotomy, following the same experimental sequence as *in vitro*[4]. In the case of cryptozepine, we performed *trans*- (less active isomer) isoform bath application in the presence of muscarinic agonist iperoxo and then slices were exposed to 365 nm light to obtain *cis*-cryptozepine (more active isoform).

RESULTS

We first characterized the *cis*- and *trans*- BAI effects on SO to identify a concentration that effectively modulated the oscillation. Once we identified this concentration (1 µM) we performed photoswitching experiments to modulate SO with light. We departed from SO as control condition and then applied 1 µM of *cis*-BAI, and, as expected, no significant changes were observed. Conversely, illumination of the slices with white light (*cis*- to *trans*- photoconversion) produced a significant increment in the oscillatory frequency (Fig. 1b). *In vivo* experiments using BAI were consistent with these results as illumination of brain containing *cis*-BAI produced a significant increase of the oscillatory frequency.

Next, we tested the effect of *trans*- and *cis*- cryptozepine in the presence of muscarinic agonist iperoxo. *In vitro* bath application of the muscarinic agonist iperoxo evoked seizure-like activity, characterized by recurrent high amplitude activity. Seizure-like activity was not affected by the application of *trans*-cryptozepine while photoconversion (*trans*- to *cis*-) led to a total blockage of epileptiform discharges.

Our results demonstrate that the light-mediated activation of the photoswitchable M_1 mAChR agonist BAI modulates the cerebral cortex network activity, inducing a significant increase in the SO frequency, *in vitro* and *in vivo*. Epileptiform seizures evoked by muscarinic agonist iperoxo were supressed by light-activation of photoswitchable M_1 mAChR antagonist cryptozepine. In conclusion, we have demonstrated a new method for modulating cortical activity of the brain. This method is based on the control of endogenous M_1 mAChR activation by means of light, but without the need of gene manipulation, as is the case in optogenetics. This opens the door to the use of photoswitchable M_1 muscarinic ligands for spatiotemporal modulation of human brain networks as a therapeutical tool.

Figures

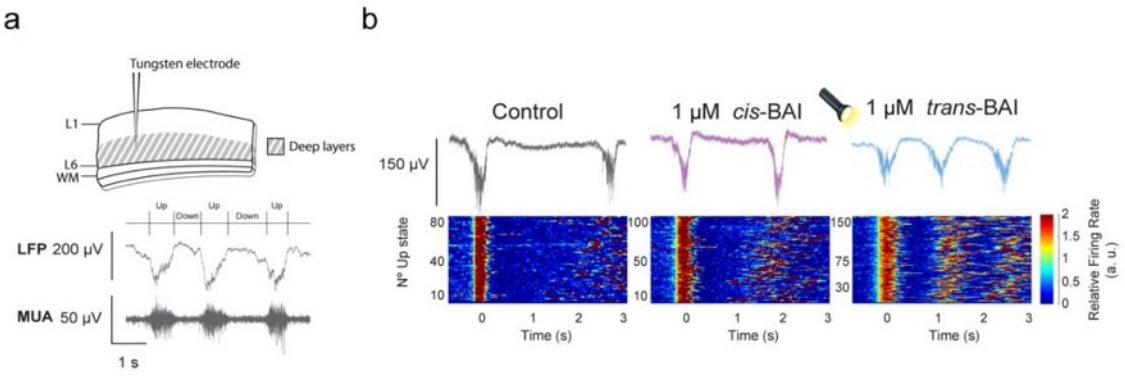

Figure 1. Effect of BAI isomers and photocontrol of slow oscillations using BAI direct illumination. (a) Cortical slice scheme and description of slow oscillations in the form of Up and Down states. (b) LFP traces (µV) and raster plot of relative firing rate (normalized MUA) during control condition, application of 1µM *cis*-BAI and photoconversion to 1µM BAI *trans*-BAI with white light.

References

1. Lee SH, Dan Y. Neuromodulation of Brain States. *Neuron*. 2012;76(1):209-222. doi:10.1016/j.neuron.2012.09.012

2. Eglen RM. Muscarinic Receptor Subtype Pharmacology and Physiology. In: *Progress in Medicinal Chemistry*. Vol 43. Elsevier; 2005:105-136. doi:10.1016/S0079-6468(05)43004-0

3. Kruse AC, Kobilka BK, Gautam D, Sexton PM, Christopoulos A, Wess J. Muscarinic acetylcholine receptors: novel opportunities for drug development. *Nat Rev Drug Discov*. 2014;13(7):549-560. doi:10.1038/nrd4295

4. Barbero-Castillo A, Riefolo F, Matera C, et al. Control of Brain State Transitions with a Photoswitchable Muscarinic Agonist. *Adv Sci*. 2021;8(14):2005027. doi:10.1002/advs.202005027

ACKNOWLEDGEMENTS

This research has received funding from the European Union's Horizon 2020 Framework Programme for Research and Innovation under the Specific Grant Agreement no. 945539 (Human Brain Project SGA3) and from the Ministerio de Economía y Competitividad/ PID2020-112947RB-I00.

131. Dynamics of ictogenic and irritative zones using machine learning of interictal epileptiform discharges

Stuart Smith[1,2,*], Jamie Norris[4,8], Gerald Cooray[2,4,5,6], Martin Tisdall[3,5], Richard Rosch[4,7], Karl Friston[4]

[1] University College London, Institute of Neurology, London, United Kingdom, [2] Great Ormond Street Hospital, Department of Clinical Neurophysiology, London, United Kingdom, [3] Great Ormond Street, Department of Neurosurgery, [4] University College London, Wellcome Centre for Human Neuroimaging, London, United Kingdom, [5] University College London, Institute of Child Health, London, United Kingdom, [6] Karolinska Institute, Department of Clinical Neurophysiology, Stockholm, Sweden, [7] Kings College London, MRC Centre for Neurodevelopmental Disorders, London, United Kingdom, [8] University College London, Institute of Health Informatics, London, United Kingdom.

*e-mail-address of corresponding author: stuart.d.w.smith@ucl.ac.uk

INTRODUCTION/MOTIVATION

Interictal epileptiform discharges (IEDs) are theorised to be transient electrographic features of excessive inhibition within the hyperexcitable cortex [1]. IEDs are seen within parts of the cortex which generate seizures (ictogenic cortex) and those which do not (irritative zone). The current literature states that a lack of IED variance indicates an ictogenic zone [2]. In contrast, patients with excess spike variance have a worse post-surgical outcome [3]. Furthermore, studies suggest that resectioning a larger proportion of the irritative zone can improve post-surgical outcomes. Still, in some patients, this needs to balance with safety and risk of cognitive deficit [4]. We wanted to answer the questions, one, can we define different groups of IEDs by their dynamics and two, do IED group dynamics differ between interictal and preictal states?

METHODS

In five patients with refractory epilepsy who underwent SEEG implantation, we clustered IEDs using a machine learning (ML) algorithm. For each cluster, we calculated inter-ictal and pre-ictal spike rates. Interictal data was collected 24 hours before the seizure and pre-ictal data one hour before the neurophysiological onset of the seizure. In addition, we calculated a z-scored spike rate. Pre-ictal spike rates were corrected using interictal Z-scores.

RESULTS AND DISCUSSION

We were able to cluster IEDs by spatial, temporal and morphological variance. The clustering of IEDs reveals significant dynamics. Cluster pre-ictal dynamics deviate from the interictal baseline and are heterogenous within the irritative cortex. In clusters within or near the ictogenic onset, the majority of clusters demonstrated a significantly increased IED rate in the hour preceding the seizure. We conclude that ML can be used to differentiate spikes and has the potential to delineate between irritable and ictogenic cortex. This information could be used to support surgical planning.

Keywords: Stereo-electroencephalography, ictogenic zone, irritable cortex, interictal epileptiform discharges, machine learning, pre-ictal states.

REFERENCES

1. Michelson HB, Wong RK. Synchronization of inhibitory neurones in the guinea-pig hippocampus in vitro. *J Physiol*. 1994;477(Pt 1):35-45.

2. Conrad EC, Tomlinson SB, Wong JN, et al. Spatial distribution of interictal spikes fluctuates over time and localizes seizure onset. *Brain*. 2020;143(2):554-569. doi:10.1093/brain/awz386

3. Klimes P, Peter-Derex L, Hall J, Dubeau F, Frauscher B. Spatio-temporal spike dynamics predict surgical outcome in adult focal epilepsy. *Clinical Neurophysiology*. 2022;134:88-99. doi:10.1016/j.clinph.2021.10.023

4. Bautista RED, Cobbs MA, Spencer DD, Spencer SS. Prediction of Surgical Outcome by Interictal Epileptiform Abnormalities During Intracranial EEG Monitoring in Patients with Extrahippocampal Seizures. *Epilepsia*. 1999;40(7):880-890. doi:10.1111/j.1528-1157.1999.tb00794.x

132. Selectively branched higher-order thalamocortical axons underlie functional forebrain subnetworks

Diana Casas-Torremocha[1+*], César Porrero[2+], Mario Rubio-Teves[2], Arnau Manasanch[1], Javier Rodríguez-Moreno[2], María García-Amado[2], Carmen Alonso[2], Lucia Prensa[2], María C. Ballesteros-Briones[3], Cristian Smerdou[3], Takahiro Furuta[4], María V. Sanchez-Vives[1,5], Francisco Clascá[2]

1. Institut d'Investigacions Biomèdiques August Pi i Sunyer (IDIBAPS), Barcelona, Spain
2. Anatomy and Neuroscience Departmet, Autonoma de Madrid University, Madrid, Spain
3. Division of Gene Therapy and Regulation of Gene Expression, CIMA, Navarra University and Idisna, Pamplona, Spain
4. Department of Oral Anatomy and Neurobiology, Osaka University, Osaka, Japan
5. Institució Catalana de Recerca i Estudis Avançats (ICREA), Barcelona, Spain

+ both authors share first authorship

*email: dicasas@recerca.clinic.cat

INTRODUCTION

The thalamus is a central hub of the forebrain networks. Thalamic axons in different nuclei target the cerebral cortex and other forebrain structures in overlapping and divergent/convergent patterns.

The best characterized thalamic projection axons are those of the "First-Order" (FO) nuclei, which orderly relay to a single area of the cortex signals from subcortical sensory or motor pathways. Thalamocortical axons from sensory relay nuclei neurons strongly innervate the middle layers of their target cortical area in a spatially focused manner. Thalamic axons arising from neurons in different domains of these nuclei are overall organized in a point-to-point fashion and thus create an isomorphic representation of the corresponding sensory receptor sheets in a primary area of the cerebral cortex [1]. On the other hand, "Higher-Order" (HO) thalamic nuclei axons mainly send back to the cortex the signals received from the cortex itself, and usually branch and innervate several separate cortical areas and often the striatum as well [2]. However, the functional logic behind the divergent and widely diverse axon arborization patterns of HO axons remains poorly understood (review in [3]).

To address this issue, we systematically compared axonal morphology and cortical targets of axons originated in different domains of the mouse posterior thalamic nucleus (Po), a HO nucleus, at the population and single-cell resolution levels. In addition, we applied electrical stimulation *in vivo* in different Po regions and recorded Local Field Potential (LFP) changes in the cortical areas that their axons target.

METHODS

Experiments were performed on adult male C57BL/6 mice. All procedures were conducted under protocols approved by Ethics Committee at Autónoma de Madrid University and Hospital Clinic of Barcelona and the competent Spanish Government agency (BOE 34/11370-421, 2013), in accordance with the European Community Council Directive 2010/63/UE.

Stereotaxic surgical procedures for anatomical experiments were conducted under deep anaesthesia. For single cell experiments, mice were electroporated with Sindbis Pal-eGFP RNA to individually label thalamic neurons and reveal the full extent of their cell axons as described by [4]. To anterogradely label axons from small populations of neurons located in restricted domains of Po, we made BDA deposits trough iontophoretic injections. For electrophysiological experiments, mice were deeply anesthetized and the extracellular LFP activity was recorded by means of 32-channel multielectrode arrays (MEA) covering the motor and somatosensory cortical areas. A stainless-steel bipolar electrode was placed in the Po nucleus and single pulses, with intensities ranging from 20 to 160 µA, were delivered to evoke responses in the cortex. Brain histological processing was performed in order to precisely identify the site of stimulation and location of the MEA contact electrodes.

RESULTS AND DISCUSSION

We demonstrated that the axons from the Po systematically branch to target several cortical (and often also striatal) domains that process sensory/motor information about the same body part. Single-cell and micropopulation tracing data reveal that Po neurons innervating domains related to the same body part are clustered together; as a result, a continuous "connectivity map" links each point of Po with multiple cortical areas, in a somatotopic fashion.

Micro-electrocorticogram recordings reveal that Po activation elicits simultaneous LFP responses in separate cortical foci, at locations that match the observed axon branching motifs. Selectively branched thalamocortical axons may thus favor activity coupling across specific subnetworks of cortical and subcortical cell populations, contributing to the creation of functional networks.

These observations reveal that HO neuronal axons may modulate functional connectivity among cortical and striatal neuronal populations involved in movement/sensation of specific body regions, revealing a new mode of interaction between the thalamus and the cortex.

Keywords: Thalamus; Cortex; Somatosensory system; Posterior nucleus; Networks

REFERENCES

[1] O'Reilly C, Iavarone E, Yi J, Hill SL. Rodent somatosensory thalamocortical circuitry: Neurons, synapses, and connectivity. Neurosci Biobehav Rev. Jul 2021;126:213-235. doi:10.1016/j.neubiorev.2021.03.015

[2] Clascá F, Porrero C, Galazo M, Rubio-Garrido P, Evangelio M. Anatomy and development of multi-specific thalamocortical axons: implications for cortical dynamics and evolution. In: Axons and brain architecture (Rockland KS, ed), pp 69–92. Amsterdam: Elsevier (2016). doi:10.1016/B978-0-12-801393-9.00004-9

[3] Clasca F. Thalamic output pathways. In: The Thalamus. Cambridge University Press, Cambridge, UK (2022). doi:10.1017/9781108674287

[4] Porrero C, Rodriguez-Moreno J, Quetglas JI, Smerdou C, Furuta T, Clasca F. A Simple and Efficient In Vivo Non-viral RNA Transfection Method for Labeling the Whole Axonal Tree of Individual Adult Long-Range Projection Neurons. Front Neuroanat. 2016;10:27. doi:10.3389/fnana.2016.00027

ACKNOWLEDGEMENTS

This research has received funding from the European Union's Horizon 2020 Framework Programme for Research and Innovation under the Specific Grant Agreement No. 785907 (Human Brain Project SGA2) and no. 945539 (Human Brain Project SGA3) and from the Ministerio de Economía y Competitividad/Fondo Europeo para el Desarrollo Regional (MINECO/FEDER) Grant BFU2017-88549 and PID2020-112947RB-I00.

133. Multimodal Brain-Phenotype Relations of the Angular Gyrus: Group Trends versus Individual Profiles

Christiane Jockwitz[1,2*], Camilla Krämer[1,2], Johanna Stumme[1,2], Paulo Dellani[1], Susanne Moebus[3], Nora Bittner[1,2], Svenja Caspers[1,2]

[1]Institute of Neuroscience and Medicine (INM-1), Research Centre Jülich, Jülich, Germany

[2]Institute for Anatomy I, Medical Faculty & University Hospital Düsseldorf, Heinrich Heine University, Düsseldorf, Germany

[3] Institute of Urban Public Health, University of Duisburg-Essen, Essen, Germany

*c.jockwitz@fz-juelich.de

INTRODUCTION

We are currently in the UN Decade of Healthy Aging, whose main goal is to understand the interindividual variability in brain aging and associated cognitive decline to enable independent living into old age. This involves using empirical data to characterize the aging brain and to develop key aging theories, which then form the basis for brain models and simulations to eventually predict individual brain changes. In this line of research, however, the question arises to what extend general principles of brain-phenotype relationships reflect individual particularities. To examine this question, we selected one region of interest, the angular gyrus (AG), which has been implied to play a key role in age-related cognitive decline [1]. We first calculated multimodal brain- phenotype relationships for the AG in a large population-based cohort of older adults, 1000BRAINS [2], after which we switched the perspective to the individual, and compared these general trends to exemplary extreme individual profiles in the same cohort.

METHODS

For the cytoarchitectonically defined AG areas PGa and PGp (part of the the JulichBrain [3]), we extracted (1) GMV (T1-weighted 3D anatomical image); (2) resting state functional connectivity (RSFC; 300 functional EPI images) and (3) structural connectivity (SC, multi-shell diffusion-weighted data) in 499 subjects (mean age = 68 ± 7 years; 1000BRAINS). We calculated multiple regressions (forward-selection) between the GMV of left and

right (l/r) PGa/PGp and a) age, b) cognitive performance, c) lifestyle and d) either GMV, SC or RSFC of all regions belonging to the JulichBrain (implemented in the EBRAINS multilevel atlas (https://ebrains.eu)). EBRAINS was consulted for characterizing the AG on the genetic and molecular level. Finally, we selected ten subjects, who fell within the highest (High#6-10) and lowest (Low#1-5) 25% of the AG GMV, derived their individual profiles and compared them to the obtained group trends.

RESULTS

Group analyses revealed heterogeneous patterns of whole-brain associations between the AG and regional GMV, RSFC and SC (Fig. 1A). EBRAINS-derived information revealed distinct genetic and molecular organization of the AG parts (Fig. 1B,C). Significant ($p < .05$) age-related decreases in GMV were evident for all AG parts, with the strongest decrease for rPGa. In addition, there was a heterogeneous relationship between AG GMV, cognition and lifestyle. For example, we found positive relations between GMV of lPGa and figural fluency and rPGa and semantic word fluency. Moreover, rPGa correlated positively with sports, while rPGp was negatively related to BMI and alcohol consumption. Focusing on the extreme individual profiles (Fig. 2B), the following can be deduced: All ten subjects deviated significantly from the regression line. For example, subject Low#3 performed below average in AG-related cognitive functions, such as semantic verbal fluency, but above average in reasoning and visual working memory. In contrast, subject High#10 shows low performance in most of the cognitive tasks assessed.

DISCUSSION

Based on the multimodal group results, the AG can be considered as a heterogeneous structure of the aged brain: First, we found the greatest decrease in GMV in rPGa, consistent with the theory that the right hemisphere has a greater age-related decrease compared with the left hemisphere [4]. Second, AG parts were associated with different cognitive abilities or lifestyles, which was complemented by both different covariance patterns of GMV, RSFC, and SC as well as genetic and molecular organization. However, especially important with respect to emerging brain modelling approaches [5] that build upon group-derived theories, individual profiles deviated considerably from the global conclusion drawn from the group study. Our findings in older adults underscore the need to carefully acknowledge generalized findings when dealing with individual conditions in clinical practice.

Keywords: Angular gyrus, Aging, Group Trends, Individual Profiles, Multimodal Imaging

ACKNOWLEDGEMENTS

This project was partially funded by the German National Cohort and the 1000BRAINS-Study of the Institute of Neuroscience and Medicine, Research Centre Jülich, Germany. We thank the Heinz Nixdorf Foundation (Germany) for the generous support of the Heinz Nixdorf Study. We thank the investigative group and the study staff of the Heinz Nixdorf Recall Study and 1000BRAINS. This project has received funding from the European Union's Horizon 2020 Research and Innovation Programme under Grant Agreement No. 945539 (HBP SGA3; SC).

The authors gratefully acknowledge the computing time granted through JARA on the supercomputer JURECA (2021) at Forschungszentrum Jülich.

REFERENCES

[1] Hirst, R.J., et al., *Gray matter volume in the right angular gyrus is associated with differential patterns of multisensory integration with aging.* Neurobiol Aging, 2021. **100**: p. 83-90.

[2] Caspers, S., et al., *Studying variability in human brain aging in a population-based German cohort- rationale and design of 1000BRAINS.* Front Aging Neurosci, 2014. **6**: p. 149.

[3] Amunts, K., et al., *Julich-Brain: A 3D probabilistic atlas of the human brain's cytoarchitecture.* Science, 2020. **369**(6506): p. 988-992.

[4] Dolcos, F., H.J. Rice, and R. Cabeza, *Hemispheric asymmetry and aging: right hemisphere decline or asymmetry reduction.* Neurosci Biobehav Rev, 2002. **26**(7): p. 819-25.

[5] Lavanga, M., et al., *The virtual aging brain: a model-driven explanation for cognitive decline in older subjects.* bioRxiv, 2022.

[6] Jockwitz, C., et al., *Characterization of the angular gyrus in an older adult population: a multimodal multilevel approach.* Brain Struct Funct, 2022.

Figure 1: **A** Brain regions being associated with GMV (Gray Matter Volume) of the AG (Angular Gyrus) subdivisions; **B** Normalized Receptor Density Fingerprints of the AG subdivisions; **C** Gene expressions of the AG subdivisions. Figure adapted from [6].

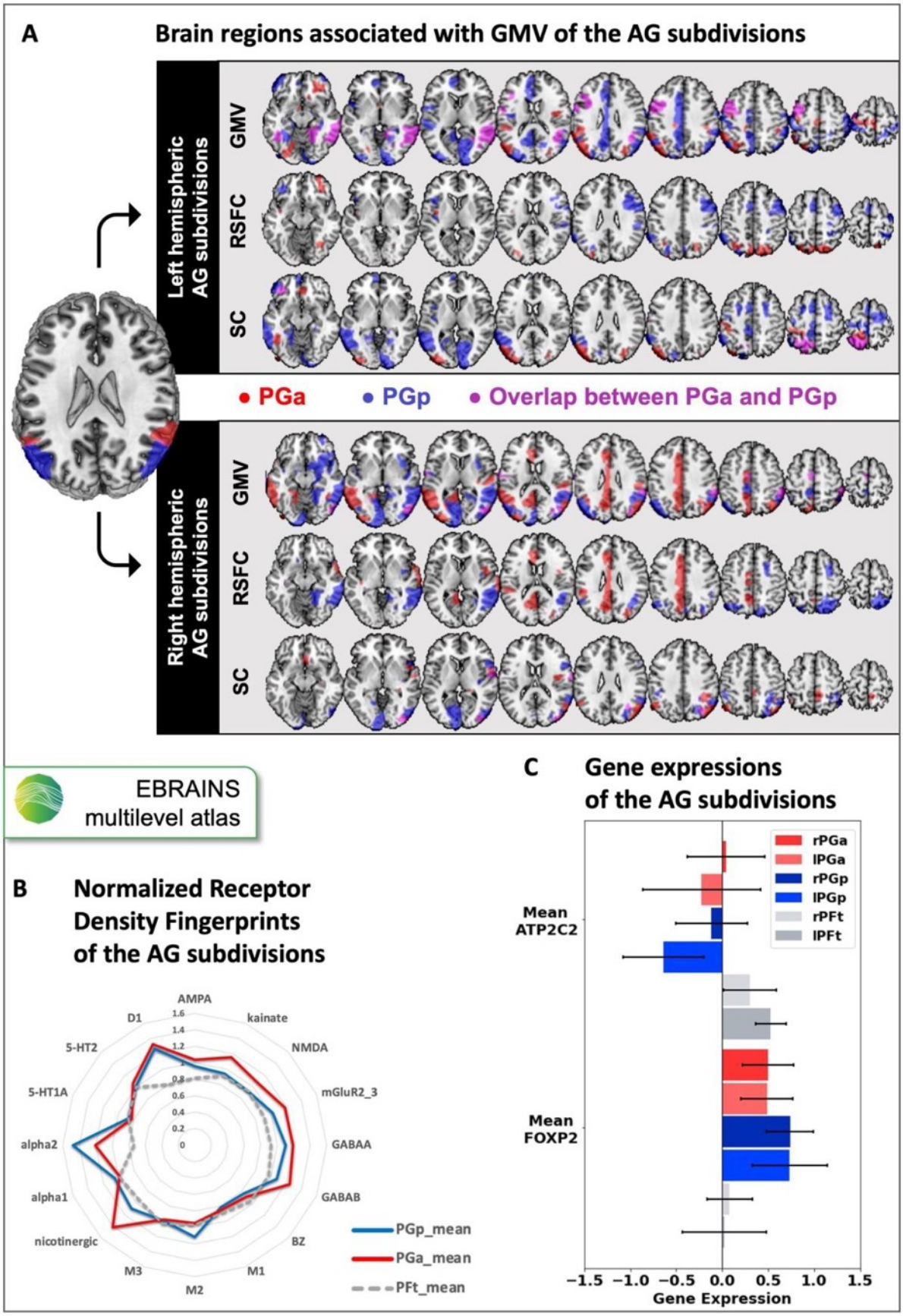

Figure 2: **A** Relation between GMV (Gray Matter Volume) of the AG (angular gyrus) subdivisions and i) Age, ii) Cognition, and iii) Lifestyle; **B** Individual profiles for Low #1-5 /High #1-5 in i) Lifestyle and ii) Cognition. Figure adapted from [6].

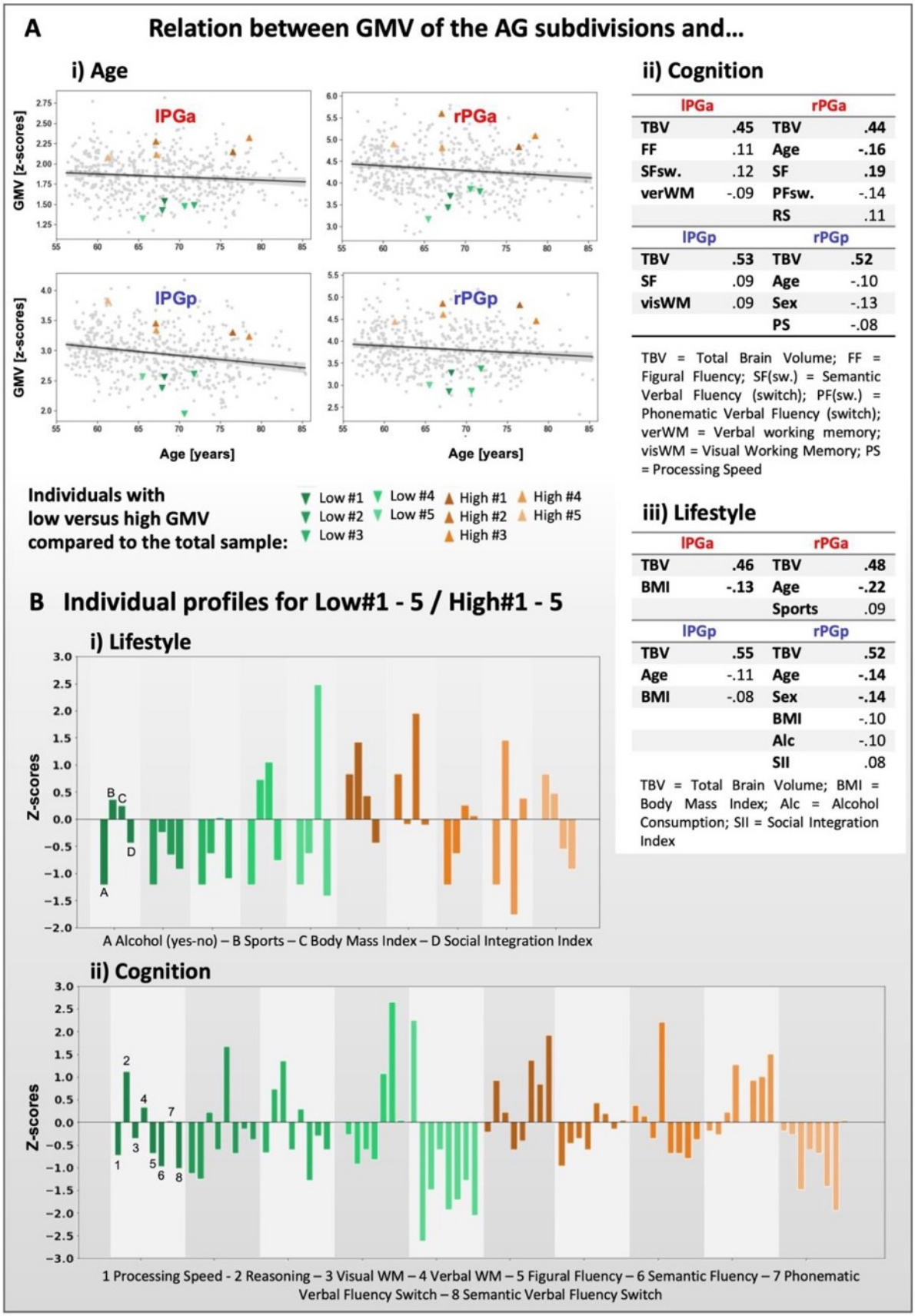

134. Mediation Analysis of neural Response's Shape

Jules Brochard[1], Etienne Combrisson[2], Jean-Philippe Lachaux[3], Andrea Brovelli[2], Jean Daunizeau[1]

1. *Paris Brain Institute, Hôpital Pitié, 47 Bd de l'Hôpital, 75013 Paris, France*
2. *Institut de Neurosciences de la Timone, Aix Marseille Université, UMR 7289 CNRS, 13005, Marseille, France*
3. *Centre de Recherche en Neurosciences de Lyon (CRNL), Institut National de la Santé et de la Recherche Médicale (INSERM), Lyon, France*

Introduction.

The two basic processes underlying perceptual decisions—how neural responses encode stimuli, and how they inform behavioural choices—have mainly been studied separately (Panzeri et al., 2017). Mediation analyses, however, can tackle these questions together by analysing neural activity as an intermediate step of behaviour production (Brochard et al., 2020). However, it remains unclear which component of a neural response supports such processing. We propose here a data-driven mediation analysis applied on the parameters of a descriptive model of neural response. This approach allowed us to identify which parameter in the neural activity (e.g. its amplitude, peak time, build-up speed) mediates the transformation of perceptual entries into behavioural production.

Methods.

We analysed intracranial EEG (IEEG) recordings of 62 pharmacoresistant epileptic patients performing a visual search task. Patients had to identify a T letter in a group of distractor letters, with varying contrast for the distractors. We compared two forms of mediation analysis (i) using information- theoretical measures applied at each time point (Combrisson et al., 2022; Cover and Thomas, 1991) and (ii) applied on the parameters of a neural-response model (Figure 1A). The model consisted of 8 free parameters identified at the single-trial level using gradient descent. Each parameter captured different components of the signal's shape: its peak time, its amplitude, its initial and finishing baselines and the concavity and window of activity of the signal before and after the peak.

Results.

We identified a network of regions mediating the effect of the task difficulty on the participant's response time. The instantaneous approach of mediation analysis revealed multiples areas in the prefrontal, visual and sensorimotor regions. The shape mediation analysis then, not only supported these results, but also revealed a mediation through the concavity of the signal in three additional areas of the temporal and motor regions (Figure 1B).

Discussion.

This work demonstrates the potential of a mediation analysis at the crossroad of data-driven and model-driven approaches. Not only did it separate behavioural effects from perceptual effects, but our work now characterises more precisely which component of a neural response support such transformative processes. While it does not establish causal links, nor does it yet use a bio-realistic

response model, our work empowers iEEG analysis in two interesting ways: 1) going beyond instantaneous activity analysis, it increases statistical efficiency by decreasing the number of statistical tests and enables scanning entire brains in search of regions of interest, 2) it decomposes the signal in interpretable features allowing for a characterisation of the region's hidden dynamics.

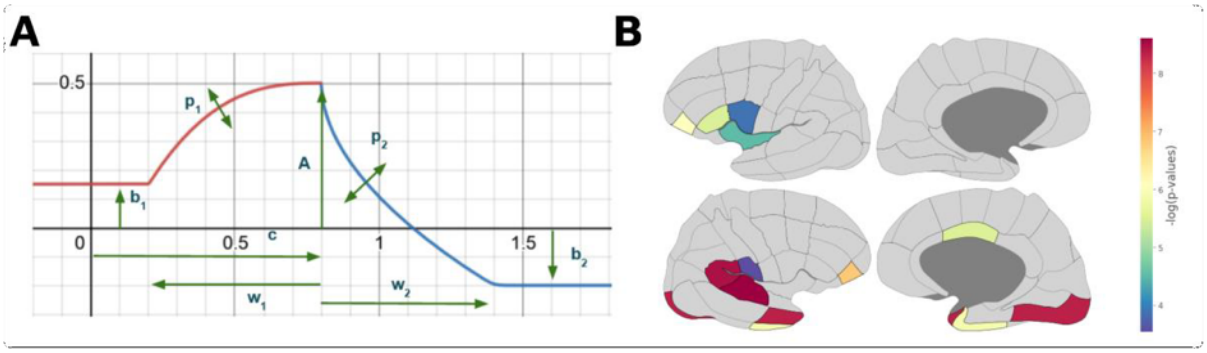

Figure 1. Neural parameters mediating task difficulty and response time **(*A*)** Model of neural response across time captured by 8 parameters fitted at the single-trial level. Namely the initial (*b1*) and finishing baseline (b2), time window of integration (*w1*) and depletion (*w2*), concavity of integration (*p1*) and depletion (*p2*), peak (*c*) and amplitude (*A*), **(B)** Network of regions for which the concavity (i.e. *p1* and *p2*) mediated the effect of task difficulty on response time (p<0.05, FDR corrected)

References

1. Brochard et al. 2020. Meet me in the middle: brain-behavior mediation analysis for fMRI experiments. preprint.
2. Combrisson, E., Allegra, M., Basanisi, R., Ince, R.A.A., Giordano, B.L., Bastin, J., Brovelli, A., 2022. Group-level inference of information-based measures for the analyses of cognitive brain networks from neurophysiological data. NeuroImage 258, 119347. https://doi.org/10.1016/j.neuroimage.2022.119347
3. Cover, T.M., Thomas, J.A., 1991. Elements of information theory. New York: Wiley.
4. Panzeri, S., Harvey, C.D., Piasini, E., Latham, P.E., Fellin, T., 2017. Cracking the Neural Code for Sensory Perception by Combining Statistics, Intervention, and Behavior. Neuron 93, 491–507. https://doi.org/10.1016/j.neuron.2016.12.036

Keywords

Mediation, perception, behaviour, intracranial EEG

Acknowledgments

This project/research has received funding from the European Union's Horizon 2020 Framework Programme for Research and Innovation under the Specific Grant Agreement No. 945539 (Human Brain Project SGA3). EC and AB were also supported by the PRC project "CausaL" (ANR-18-CE28-0016).

135. Lifestyle- & body-related differences in neurite morphology of white matter tracts in older adults

Nora Bittner[1,2*], Till Frentzel[1,2], Johanna Stumme[1,2], Maria Agan[1,2], Christiane Jockwitz[1,2], Susanne Moebus[3], Svenja Caspers[1,2]

[1]Institute for Anatomy I, Medical Faculty & University Hospital Düsseldorf, Heinrich-Heine-University, Düsseldorf, Germany; [2]Institute of Neuroscience and Medicine (INM-1), Research Centre Juelich, Juelich, Germany; [3]Institute of Urban Public Health, University of Duisburg-Essen, 45122 Essen, Germany

*e-mail-address of corresponding author: n.bittner@fz-juelich.de

INTRODUCTION/MOTIVATION

First attempts to virtually age the brain using modelling approaches have revealed promising results, but still face difficulties in reflecting the large inter-individual variability in aging and its origins, e.g. lifestyle and body-related factors. To inform more theoretical frameworks, we, here, focused on exploring the contribution of specific lifestyle habits and obesity, to the variability in connectivity of major white matter tracts [1, 2] in two studies including older adults from the population-based 1000BRAINS cohort [3]. To obtain meaningful biological insights we employed an advanced diffusion model, Neurite Orientation Dispersion and Density Imaging (NODDI; [4]), allowing the detailed analysis of white matter with specific parameters, e.g. the density and angular variation of neurites.

METHODS

The first study assessed lifestyle factors in 591 (273 females, mean age 67 □ 6.5 years) participants including smoking (pack-years), social integration, alcohol consumption (grams per week) and physical activity [5], as well as a risk score of these variables, reflecting an accumulated unfavorable lifestyle at higher values [6].

In a second study, we focused on body-related aspects, including BMI, waist-to-hip ratio (WHR) and A Body Shape Index (ABSI) in 558 participants (251 females, mean age 67 7.3 years). □

For both studies, fractional anisotropy (FA) and mean diffusivity (MD) were estimated from the diffusion tensor, neurite density from intra-cellular volume fraction (ICVF) and angular variation of neurites from orientation dispersion index (ODI). After registration of individual parameter maps onto a template (DTI-TK) and skeletonization (TBSS, [7]), associations between white matter parameters and lifestyle factors (covariates: age, sex, education and BMI) and obesity (covariates: age, education, hypertension, daily physical activity) were tested (Threshold-Free Cluster Enhancement, $p < 0.05$).

RESULTS AND DISCUSSION

In general, a more unfavourable lifestyles risk score and obesity were related to unfavourable white matter characteristics, e.g. lower FA (fig.1). Healthier lifestyle habits, e.g. higher social integration and physical activity, were related to better preserved white matter tracts, e.g. lower MD (fig.1).

Higher physical activity was associated to higher ICVF and lower ODI in almost all included major fibre tracts (fig. 1). In males but not in females, more visceral fat (WHR) correlated with lower ODI, specifically in projection fibres,

e.g. the corona radiata as well as with lower ICVF again in almost all white matter tracts included in the skeleton with greatest effects in the corticospinal tract and cerebellar peduncle.

The present results suggest that lifestyle and body-related factors may explain variability in older adults' brains,

i.e. white matter microstructure. Physical activity is generally thought of as a promising factor for healthy brain aging [8]. Here, the usage of NODDI parameters enabled a deeper mechanistical insight: The microstructural differences associated to physical activity hint at concurrent higher neurite density (ICVF) and more coherently organized axons (ODI, [9]) in many large-scale fibre tracts, which may be favourable for transmission capacities [10]. Interestingly, a link between higher WHR, as one parameter for obesity, and poorer white matter fibre tract integrity was only observed in men, but not in women. Interestingly, both lower physical activity and higher WHR showed global associations across all deep white matter tracts, thus affecting its structural integrity per se.

The current results show that age itself might be an important, but not the only factor, affecting the brain. To increase the accuracy of current model-based approaches, the need arises to include other factors, such as for instance, lifestyle, genetics and diet.

Keywords: lifestyle, body-related factors, aging, white matter fibre tracts, neurite morphology

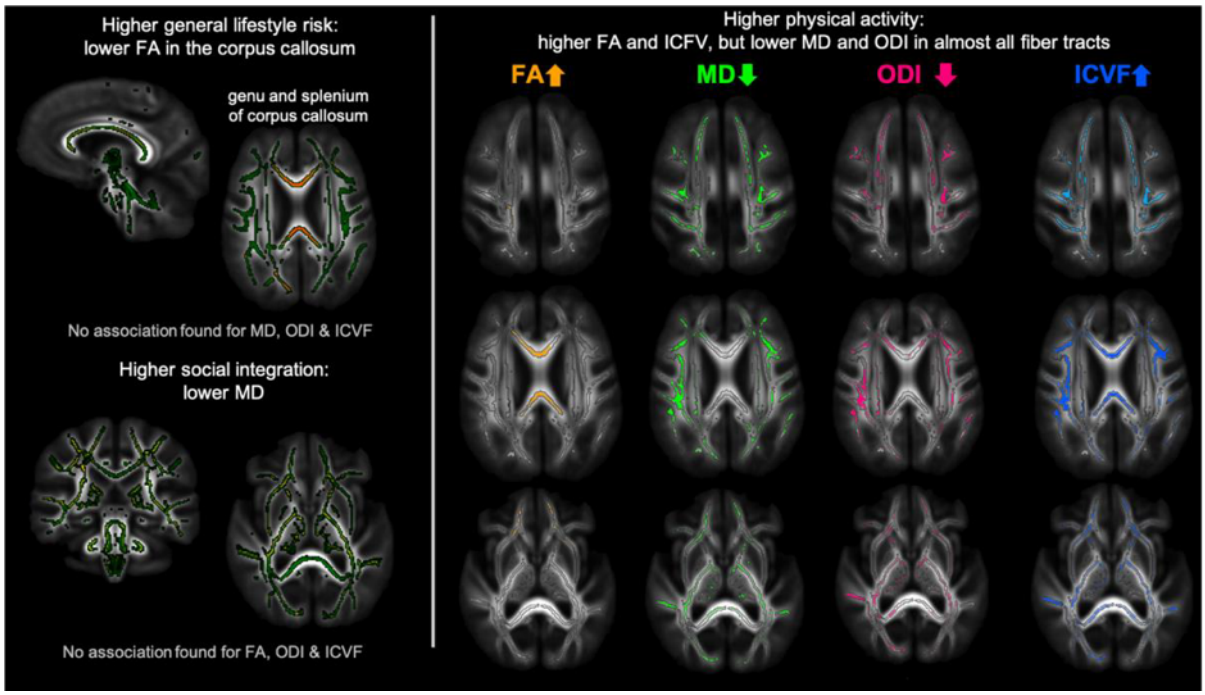

Figure 1. Selection of slices (from superior to inferior) showing the associations between lifestyle factors and voxels of the skeleton overlaid onto the mean FA image of the study sample. Convention is radiological (left is right).

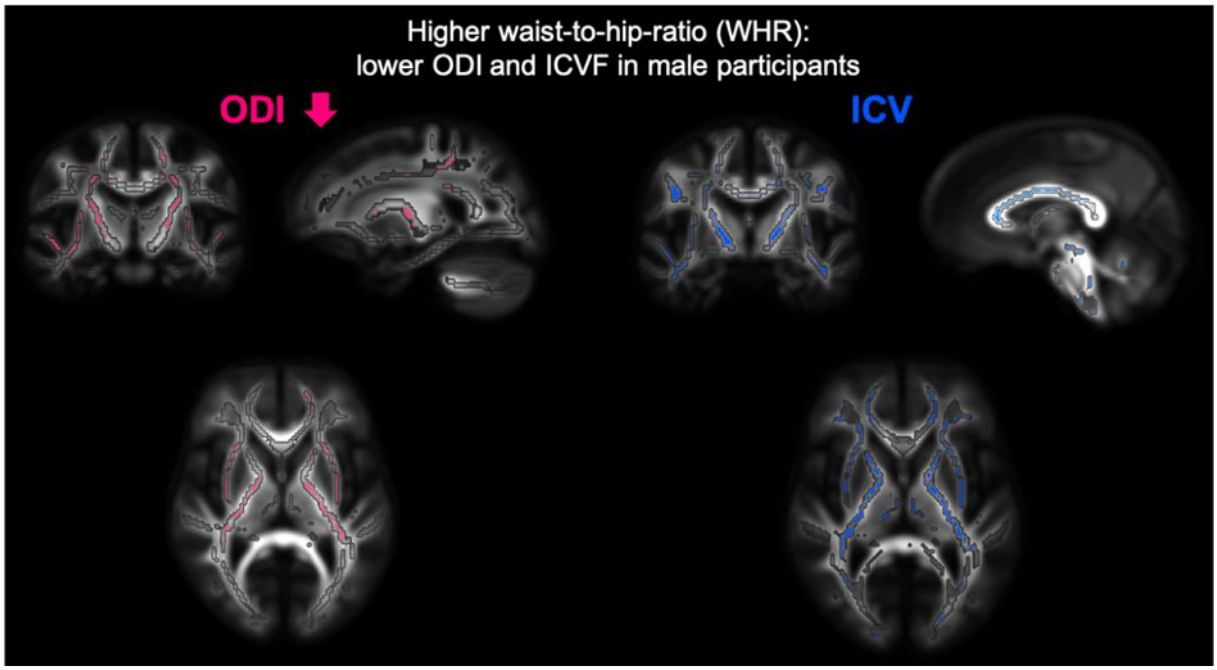

Figure 2. Selection of slices showing the associations between waist-to-hip-ratio (WHR) and voxels of the skeleton overlaid onto the mean FA image of the male participants. Convention is radiological (left is right). Results are shown of n = 302 male participants.

ACKNOWLEDGEMENTS

This project was partially funded by the German National Cohort and the 1000BRAINS-Study of the Institute of Neuroscience and Medicine, Research Centre Jülich, Germany. We thank the Heinz Nixdorf Foundation (Germany) for the generous support of the Heinz Nixdorf Study. We thank the investigative group and the study staff of the Heinz Nixdorf Recall Study and 1000BRAINS. This project has received funding from the European Union's Horizon 2020 Research and Innovation Programme under Grant Agreement No. 945539 (HBP SGA3; SC). The authors gratefully acknowledge the computing time granted through JARA on the supercomputer JURECA (2021) at Forschungszentrum Jülich.

REFERENCES

[1] Cox, S. R., Ritchie, S. J., Tucker-Drob, E. M., Liewald, D. C., Hagenaars, S. P., Davies, G., ... & Deary, I. J. (2016). Ageing and brain white matter structure in 3,513 UK Biobank participants. Nature communications, 7(1), 1-13. https://doi.org/10.1038/ncomms13629

[2] Wassenaar, T. M., Yaffe, K., van der Werf, Y. D., & Sexton, C. E. (2019). Associations between modifiable risk factors and white matter of the aging brain: insights from diffusion tensor imaging studies. Neurobiology of aging, 80, 56-70. https://doi.org/10.1016/j.neurobiolaging.2019.04.006

[3] Caspers, S., Moebus, S., Lux, S., Pundt, N., Schütz, H., Mühleisen, T. W., Gras, V., Eickhoff, S. B., Romanzetti, S., Stöcker, T., Stirnberg, R., Kirlangic, M. E., Minnerop, M., Pieperhoff, P., Mödder, U., Das, S., Evans, A. C., Jöckel, K. H., Erbel, R., ... Amunts, K. (2014). Studying variability in human brain aging in a population-based German cohort- rationale and design of 1000BRAINS. Frontiers in Aging Neuroscience, 6(JUL). https://doi.org/10.3389/fnagi.2014.00149

[4] Zhang, H., Schneider, T., Wheeler-Kingshott, C. A., & Alexander, D. C. (2012). NODDI: practical in vivo neurite orientation dispersion and density imaging of the human brain. Neuroimage, 61(4), 1000-1016. https://doi.org/10.1016/j.neuroimage.2012.03.072

[5] Ainsworth, B. E., Haskell, W. L., Herrmann, S. D., Meckes, N., Bassett, D. R., Tudor-Locke, C., ... & Leon, A. S. (2011). 2011 Compendium of Physical Activities: a second update of codes and MET values. Med Sci Sports Exerc, 43(8), 1575-1581. https://doi.org/10.1249/MSS.0b013e31821ece12

[6] Bittner, N., Jockwitz, C., Mühleisen, T. W., Hoffstaedter, F., Eickhoff, S. B., Moebus, S., ... & Caspers, S. (2019). Combining lifestyle risks to disentangle brain structure and functional connectivity differences in older adults. Nature communications, 10(1), 1-13. https://doi.org/10.1038/s41467-019-08500-x

[7] Smith, S. M., Jenkinson, M., Johansen-Berg, H., Rueckert, D., Nichols, T. E., Mackay, C. E., ... & Behrens, T. E. (2006). Tract-based spatial statistics: voxelwise analysis of multi-subject diffusion data. Neuroimage, 31(4), 1487- 1505. https://doi.org/10.1016/j.neuroimage.2006.02.024

[8] Kramer, A. F., & Colcombe, S. (2018). Fitness effects on the cognitive function of older adults: a meta-analytic study—revisited. Perspectives on Psychological Science, 13(2), 213-217. https://doi.org/10.1177/1745691617707316

[9] Timmers, I., Roebroeck, A., Bastiani, M., Jansma, B., Rubio-Gozalbo, E., & Zhang, H. (2016). Assessing microstructural substrates of white matter abnormalities: a comparative study using DTI and NODDI. PloS one, 11(12), e0167884. https://doi.org/10.1371/journal.pone.0167884

[10] Timmers, I., Zhang, H., Bastiani, M., Jansma, B. M., Roebroeck, A., & Rubio-Gozalbo, M. E. (2015). White matter microstructure pathology in classic galactosemia revealed by neurite orientation dispersion and density imaging. Journal of inherited metabolic disease, 38(2), 295-304. https://doi.org/10.1007/s10545-014-9780-x

136. Cortico-subcortical interaction and dynamical state switching in the resting brain

Michele Allegra[1,2,*], Chiara Favaretto[1,3], Alessandro Nazzi[1], Lorenzo Pini[1,3], Gustavo Deco[6,7], Andrea Brovelli[5] and Maurizio Corbetta[1,3,4]

[1] Padova Neuroscience Center (PNC), University of Padova, via Orus 2/B, 35129, Padova, Italy

[2] Department of Physics and Astronomy "Galileo Galilei", University of Padova, via Marzolo 8, 35131, Padova, Italy

[3] Department of Neuroscience (DNS), University of Padova, via Giustiniani 2, 35128, Padova, Italy

[4] Venetian Institute of Molecular Medicine (VIMM), 35128 Padova, Italy

[5] Institut de Neurosciences de la Timone UMR 7289, Aix Marseille Université, CNRS, 13005, Marseille, France

[6] Center for Brain and Cognition (CBC), Department of Information Technologies and Communications (DTIC), Pompeu Fabra University, Edifici Mercè Rodoreda, Carrer Trias i Fargas 25−27, 08005, Barcelona, Catalonia, Spain

[7] Institució Catalana de Recerca I Estudis Avançats (ICREA), Passeig Lluis Companys 23, 08010, Barcelona, Catalonia, Spain

*michele.allegra@unipd.it

INTRODUCTION/MOTIVATION

In the last decade, functional resonance imaging at rest (rs-fMRI) has revealed that functional connectivity is dynamic, as the brain continuously alternates between alternative connectivity patterns, or 'dynamical states'. However, mechanisms controlling dynamical patterns in spontaneous brain activity are poorly understood: whether specific regions play a leading role in orchestrating global changes in connectivity patterns is unclear. Most studies of dynamic connectivity have focused on cortical regions, following an underlying hypothesis is that shifts in brain states depend on highly interconnected cortical regions (hubs). Within the HBP Flag-Era 'Brainsynch- Hit' project, we leveraged a large neuroimaging database including healthy subjects and stroke patients (Washington stroke database) and focused our dynamic connectivity analysis on cortico-subcortical interactions [1]. To ensure the generality of our findings, we are currently replicating our dynamical state analysis using a large public rs-fMRI database from the Human Brain Project HBP() [4].

METHODS

Details about the Washington stroke database can be found in the original publications [2,3]. After standard preprocessing, the cortical, surface-projected time series were projected on the Gordon-Laumann atlas. As for subcortical regions, we compared a traditional parcellation (Harvard-Oxford atlas) with a recent multi-scale parcellation provided by [5]. Briefly, in our analysis we computed sliding-window functional connectivity matrices, approximated the matrices with their leading vector, and performed K-means clustering, identifying K=5 clusters

or ‘dynamical states’ common to both patients and healthy controls. We replicated the same analysis using the HCP database (the HCP website provides full details on the data).

RESULTS AND DISCUSSION

In the Washington data set, we observed that state switches are accompanied by sudden changes in cortico- subcortical coupling, We identified a set of dynamical connectivity states differing both in terms of segregation/integration between cortical networks, and icortico-subcortical connectivity patterns. Cortical regions flexibly synchronized with either limbic regions (hippocampus/amygdala), or subcortical nuclei (thalamus/basal ganglia). Focal lesions induced by stroke, especially those damaging white matter connections between basal ganglia/thalamus and cortex, provoked anomalies in the fraction times, dwell times, and transitions between states. Preliminary results on the HCP data set qualitatively reproduce the cortico-subcortical patterns identified in the previous study. Overall, our results show that brain activity at rest involves a dynamic relation between cortical regions and two main groups of subcortical regions. Overall, our findings hint at a key role of subcortical regions in global brain dynamics, and call for further investigation of cortico-subcortical interaction using data from different modalities as well as computational modelling.

Keywords: fMRI, Dynamic Functional Connectivity, Subcortical Regions, Stroke

ACKNOWLEDGEMENTS

C.F., M.A., A.B., and M.C. were supported by FLAG-ERA JTC 2017 (grant ANR-17-HBPR-0001). C.F. and M.C. were supported by Fondazione Cassa di Risparmio di Padova e Rovigo (CARIPARO) - Ricerca Scientifica di Eccellenza 2018 – (Grant Agreement number 55403). A.B. has received funding from the European Union’s Horizon 2020 Framework Programme for Research and Innovation under the Specific Grant Agreement No. 945539 (Human Brain Project SGA3). M.C. was also supported by MIUR - Departments of Excellence Italian Ministry of Research (MART_ECCELLENZA18_01); Ministry of Health Italy Brain connectivity measured with high-density electroencephalography: a novel neurodiagnostic tool for stroke - NEUROCONN (RF-2008 −12366899); H2020 European School of Network Neuroscience - euSNN, H2020-SC5-2019-2 (Grant Agreement number 869505).

REFERENCES

[1] Favaretto C, Allegra M, Deco G, Metcalf NV, Griffis JC, Shulman GL, Brovelli A, Corbetta M. Subcortical-cortical dynamical states of the human brain and their breakdown in stroke. *Nat. Comm. (2022)*, *13*(1), 5069. https://doi.org/10.1038/s41467-022-32304-1

[2] Corbetta M, Ramsey L, Callejas A, Baldassarre A, Hacker CD, Siegel JS., … , Shulman, GL. Common behavioral clusters and subcortical anatomy in stroke. *Neuron (2015)*, *85*(5), 927-941. https://doi.org/10.1016/j.neuron.2015.02.027

[3] Siegel JS, Ramsey LE, Snyder AZ, Metcalf NV, Chacko RV, Weinberger K, … , Corbetta M, Disruptions of network connectivity predict impairment in multiple behavioral domains after stroke. *PNAS (2016)*, *113*(30), E4367-E4376.https://doi.org/10.1073/pnas.1521083113

[4] Van Essen DC, Smith SM, Barch DM, Behrens TE, Yacoub E, Ugurbil K, Wu-Minn HCP Consortium. The WU-Minn human connectome project: an overview. *Neuroimage (2013)*, *80*, 62-79. https://doi.org/10.1016/j.neuroimage.2013.05.041

[5] Tian Y, Margulies DS, Breakspear M, Zalesky A. Topographic organization of the human subcortex unveiled with functional connectivity gradients. *Nat. neuroscience (2020)*, *23*(11), 1421-1432. https://doi.org/10.1038/s41593-020-00711-6

137. Linking hubs, embryonic neurogenesis, transcriptomics and diseases in human brain networks

Ibai Diez[1], Fernando Garcia-Moreno[2,3], Nayara Carral-Sainz[4], Sebastiano Stramaglia[5], Alicia Nieto-Reyes[4], Mauro D'Amato[3,6], Jesus Maria Cortes[3,7], Paolo Bonifazi[3,7,*]

[1]Gordon Center for Medical Imaging, Department of Radiology, Massachusetts General Hospital, Harvard Medical School, Boston, MA, USA.
[2]Achucarro Basque Center for Neuroscience, Scientific Park of the University of the Basque Country (UPV/EHU), Leioa, Spain.
[3]IKERBASQUE: The Basque Foundation for Science, Bilbao, Spain.
[4]Departamento de Matemáticas, Estadística y Computación, Facultad de Ciencias, Universidad de Cantabria, Santander, Spain.
[5]Dipartimento Interateneo di Fisica, Università degli Studi di Bari Aldo Moro, and INFN, Sezione di Bari, Italy.
[6]Department of Medicine and Surgery, LUM University, Casamassima, Italy,
[7]Computational Neuroimaging Lab, Biocruces-Bizkaia Health Research Institute, Barakaldo, Spain.

*e-mail-address of corresponding author Paol.bonifazi@gmail.com

INTRODUCTION/MOTIVATION

The most characteristic anatomical property of brain networks is their organization across multiple spatial scales. A key challenge is to decipher the rules of connectivity that shape brain networks in order to understand how the brain works and how traumatic or neurological damage may affect brain functionality[1]. The general structure and function of the human brain, and its internal connectivity are all the result of its developmental history, which is at the same time the product of evolution[2].

Small-world, scale-free or heavy-tailed distribution network organizations have been identified at the structural- functional level in microcircuits, and in meso- and macro-scale networks[3].

Inspired by the Barabasi-Albert model [4] which showed that the principle "the rich gets richer" (a.k.a. "preferential attachment") led to scale-free networks and hubs in real-world networks, in this work we test the hypothesis that the topology of brain networks could be shaped according to the rule that "the older gets richer", i.e. the evolutionary older circuits or those generated earlier in embryogenesis are most central in the organization of the adult brain network[5].

METHODS

Methods are fully detailed in [6]. Briefly, we segmented human brain circuits according to their first (i.e. earliest) neurogenic Time (FirsT), i.e. the post-conception day on which the first neurons of the circuit are generated (Fig. 1A). We identified 18 MACs for which a timing sequence based on their FirsT could be defined. Since MACs'

volumes span across multiple scales, we studied the brain networks on two different spatial resolutions: a low- resolution network with the 18 MACs (nodes), and a high-resolution network where MACs were decomposed in a total of 2566 regions of interest (ROIs) of similar volumes which kept the same FirsT of the corresponding MAC. We used dMRI and resting-state fMRI images acquired at 7T from N=184 healthy subjects taken from the Human Connectome project [7] to reconstruct structural-functional brain networks (see Fig. 1B). Eigenvector centrality was calculated as hubness metric for each node (ROI or MAC; Fig. 1B) and correlated to nodes' FirsT.

Brain maps of transcriptomics of 20787 genes in the adult healthy brain were reconstructed from the Allen Human Brain Atlas (AHBA) data [8] with a maximal possible resolution of 90 macro-regions each belonging to distinct MACs.

Brain maps of nodes' centrality and FirsT were correlated to transcriptomics maps. Finally, enrichment analysis was performed both on physiological biological processes and cell component annotations, and in relation to the genes causally associated to epilepsy, Alzheimer's Disease (AD), Parkinson's disease (PD) and autism spectrum disorder (ASD) based on the Genome-Wide-Association-Study (GWAS Catalogue; https://www.ebi.ac.uk/gwas/). RESULTS AND DISCUSSION

At high resolution level, we observed that FirsT reversely shaped the nodes' centrality in the structural and functional networks, where highly central nodes displayed respectively early and late FirsT (fig. 2 A1). Distinctly, the structural and functional nodes' centrality of the low-resolution MACs similarly correlated with FirsT, with higher centrality displayed in the early born MACs (fig. 2 A1). In addition, we observed that FirsT-lags reversely correlated with wiring probability and connection weight, so ROIs and MACs connected more and stronger with those at similar age (fig. 2 A2). Finally, brain transcriptomic analysis revealed also high association between genes' expression, FirsT and nodes' centrality, in respect to physiological nervous system development and synapse regulation, and to neuropathological conditions. Notably, a significant rate of genes involved in major neurological diseases such as epilepsy, Parkinson's, Alzheimers' and autism spectrum disorder displays extreme correlation values (fig. 2 B) with nodes' centrality (we especially mention high correlation for highly studied genes such as SCN1A, SNCA and APOE). The results provide a new multi-scale evidence on how neurogenesis time shapes structural and functional networks, brain nodes' centrality and their transcriptomics in patho-physiological conditions and underlie two main neurogenesis preferential wiring principles: "the older gets richer" and "preferential age attachment".

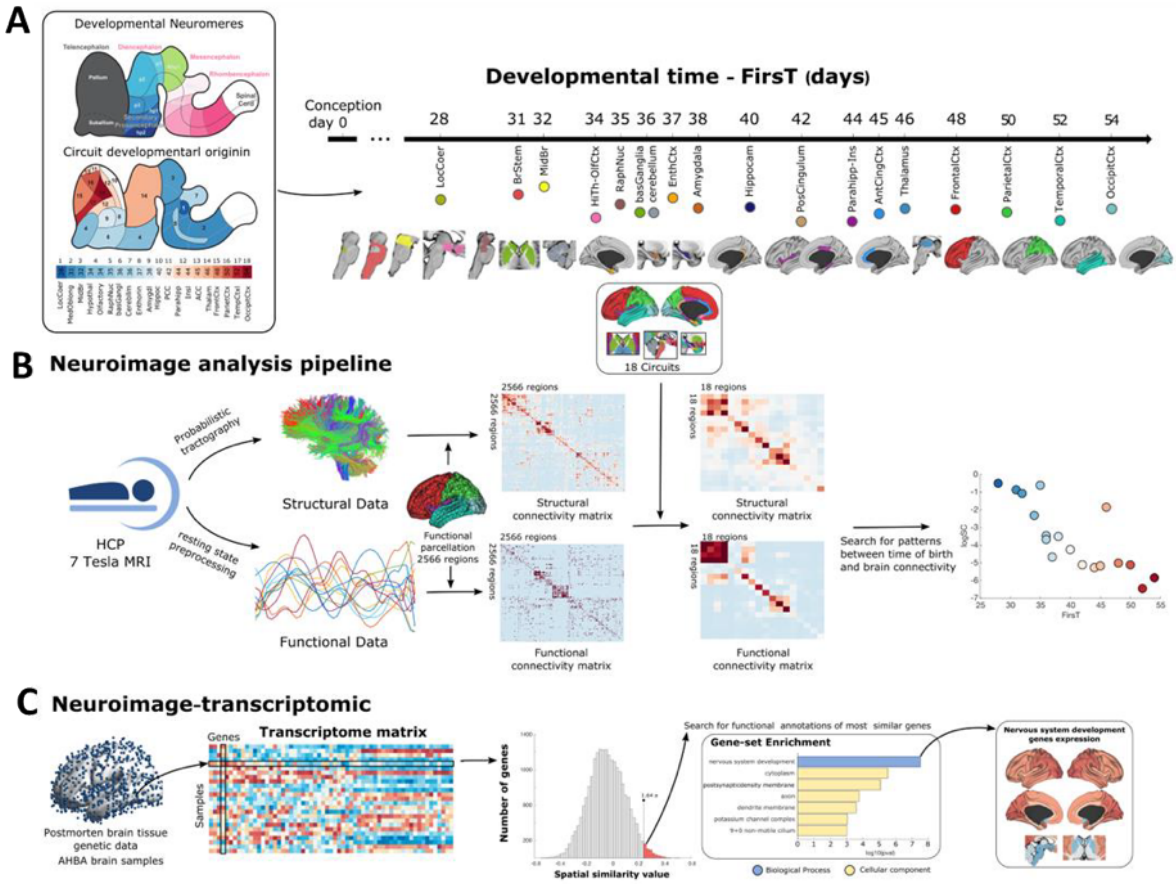

Figure 1. From the circuits' embryogenic age to brain networks and transcriptomics. (A) Sagittal schemes of the early embryonic human brain with fundamental neuromeres (top) and location of the 18 MACs (bottom). (B) Neuroimage analysis pipeline. For each subject, high- and low-resolution structural and functional networks were reconstructed respectively using probabilistic tractography and correlation on resting-state activity. The correlation between the nodes' metrics (eigenvector centrality) and embryonic age (FirsT expressed in post- conception days) was calculated. (C) Brain transcriptome data from AHBA dataset was used to search for genes with a high similarity between its spatial brain expression and brain maps of embryonic age and nodes centrality. Functional annotations of the obtained genes were further computed using overrepresentation analysis to find significantly associated biological processes and cellular components associated with maps of embryonic age and nodes' centrality.

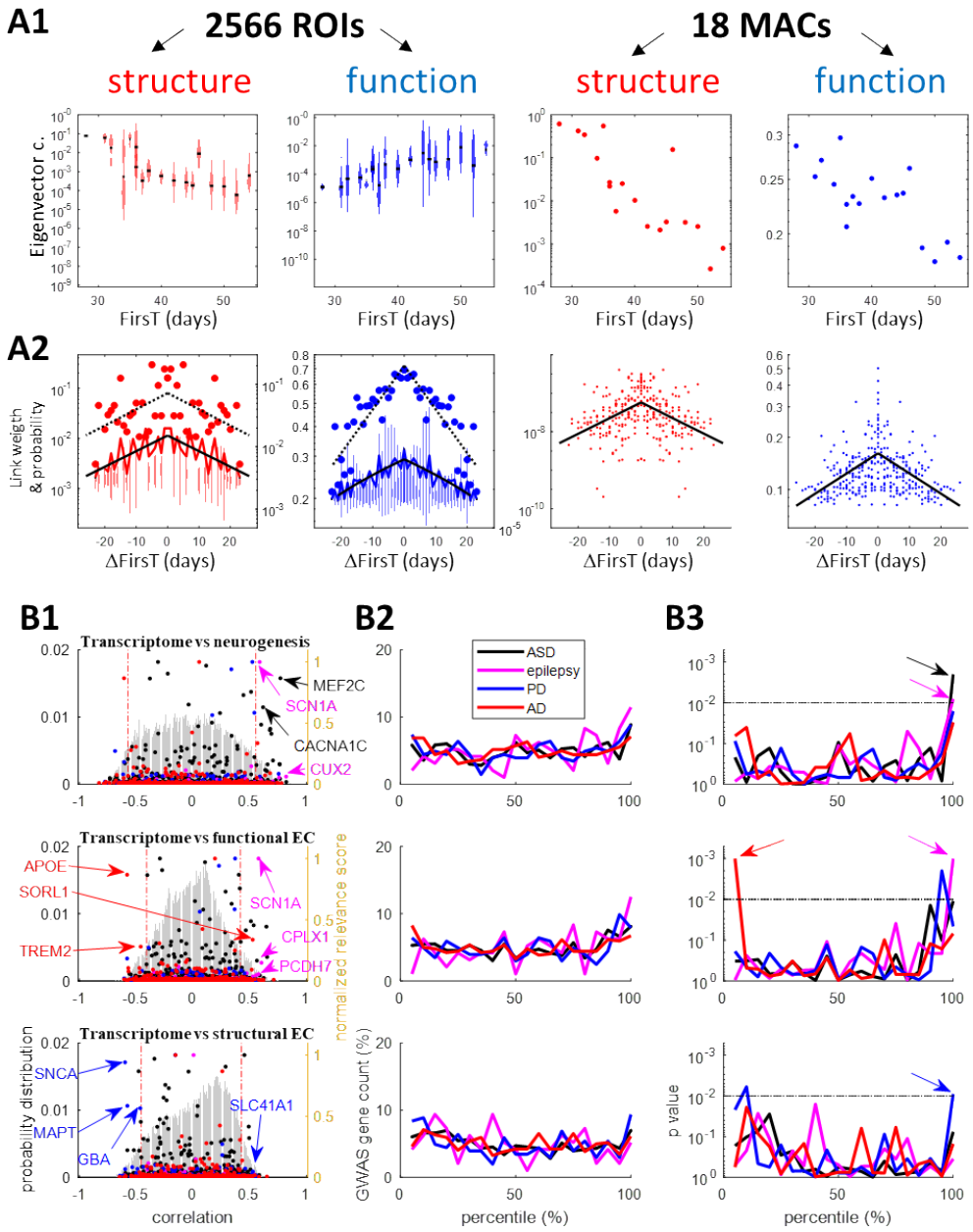

Figure 2. “older gets richer”, “age preferential attachment” and genetic causal link to major neuro-pathologies (Autism Spectrum Disorder, epilepsy, Parkinson’s and Alzheimer’s disease). A. Scatter plots of the nodes’ centrality (A1) and the links’ probability/weight (A2) relative to the FirsT, in the high (2566 ROIs) and low (18 MACs) resolution structural (red) and functional (blue) networks. The first and second columns from left represent the results for the 2,566 ROIs as violin plots, where the mean of each group (i.e. ROIs within a MAC) is plotted in black. All plots have a logarithmic scale in the y-axis. In (A2) the link weights (left y-axis) are plotted as a function of the differences of FirsT. Violin plots for the 2,566 ROIs show the link weight distributions while the solid lines plot the average values. Black solid lines show the exponential fit on the average values. The link probability is represented by the right y-axes and displayed as dots, and the broken black line showing the exponential fit. In (B) the same colour code is used for the four different diseases as shown in the inset legend of the top plot of panel (B2). For each gene the spatial expression in the brain was correlated to the spatial maps of eigenvector centrality and neurogenesis. In (B1) the probability distribution of the correlations (light gray histogram, left axis) between transcriptomics (20,787 genes) and neurogenesis (top plot), functional centrality (middle plot) and structural

centrality (bottom plot) is shown. The normalized relevance score of the GWAS genes listed for each disease (obtained from the GeneCards databases) has been plotted with dots (right axis). Vertical broken lines highlight the lowest and top five percentile interval. In (B2) the normalized count (percentage of gene per interval) of GWAS genes in five percentile intervals of the correlation distribution is plotted. IN panel (B3) the P-values of the normalized gene count in each percentile are shown. The threshold for $p<0.01$ calculated from the null model (based on a thousand reshuffled replications) which keeps into account spatial dependencies of both centrality maps and gene-expression is plotted as a broken horizontal black line. The arrows mark the extremities of the correlation distributions with a significantly higher number of GWAS-genes than what expected by chance.

Keywords: brain networks, hubness, neurogenesis, transcriptomics, older-gets-richer, age-preferential attachment, resting-state activity, tractography

KNOWLEDGEMENTS

We acknowledge the Human Brian Connectome project, Genome-wide association study and Allen Human Brain Atlas for the database of the study. PB acknowledge financial support from Ikerbasque (The Basque Foundation for Science) and from the Ministerio Economia, Industria y Competitividad (Spain) and FEDER (grant SAF2015- 69484-R, PID2021-127163NB-I00, and AI-2021-039).

REFERENCES

[1]. Fox, M. D. Mapping Symptoms to Brain Networks with the Human Connectome. *N Engl J Med* 379, 2237– 2245 (2018). doi: 10.1056/NEJMra1706158.

[2]. Cisek, P. & Hayden, B. Y. Neuroscience needs evolution. *Phil. Trans. R. Soc. B* 377, 20200518 (2022). doi: 10.1098/rstb.2020.0518.

[3]. Bassett, D. S., Khambhati, A. N. & Grafton, S. T. Emerging Frontiers of Neuroengineering: A Network Science of Brain Connectivity. *Annu. Rev. Biomed. Eng.* 19, 327–352 (2017). doi: 10.1146/annurev-bioeng-071516- 044511

[4]. Barabási, A.-L. & Albert, R. Emergence of Scaling in Random Networks. *Science* 286, 509–512 (1999). doi: 10.1126/science.286.5439.509.

[5]. van den Heuvel, M. P. & Sporns, O. Network hubs in the human brain. *Trends in Cognitive Sciences* 17, 683–696 (2013). doi: 10.1016/j.tics.2013.09.012.

[6]. Diez, I. *et al.* "Older circuits get richer": neurogenesis timeline shapes hubness and neurogenetic profiles of the adult human brain. *BioRxiv*, doi: https://doi.org/10.1101/2022.04.01.486541

[7]. Elam, J. S. *et al.* The Human Connectome Project: A retrospective. *NeuroImage* 244, 118543 (2021). doi: 10.1016/j.neuroimage.2021.118543.

[8]. Shen, E. H., Overly, C. C. & Jones, A. R. The Allen Human Brain Atlas : comprehensive gene expression mapping of the human brain. Trends in Neurosciences 35, 711–714 (2012). doi: 10.1016/j.tins.2012.09.005. Epub 2012 Oct 5.

138. Fiber enhancement and 3D orientation analysis in volume fluorescence microscopy

Michele Sorelli [1,2], Irene Costantini [2,3,4,*], Leonardo Bocchi [5], Markus Axer [6], Francesco Saverio Pavone [1,2,4], and Giacomo Mazzamuto [1,2,4]

[1] Department of Physics and Astronomy, University of Florence, Sesto Fiorentino, Italy
[2] European Laboratory for Non-Linear Spectroscopy (LENS), Sesto Fiorentino, Italy
[3] Department of Biology, University of Florence, Sesto Fiorentino, Italy
[4] National Research Council, National Institute of Optics (CNR-INO), Sesto Fiorentino, Italy
[5] Department of Information Engineering, University of Florence, Florence, Italy
[6] Institute of Neuroscience and Medicine, Research Centre Jülich, Jülich, Germany
[*] costantini@lens.unifi.it

INTRODUCTION

The combination of imaging modalities able to explore the connectivity of the human brain at micro-, meso- and macroscopic spatial scales is an established requirement for advancing our comprehension of its structural organization [1]. Increased magnetic field strengths and improved contrast models in diffusion-weighted magnetic resonance imaging (dMRI) have recently enabled the quantitative mapping of the human brain connectional anatomy with sub-millimetric resolution and refined angular accuracy [2]. However, state-of-the-art dMRI may not accurately reproduce the brain tissue microstructure within voxels which encompass challenging fiber branchings or interdigitated architectures and, thus, still requires proper validation. The development of a gold standard for investigating the brain myeloarchitectonics with single fiber resolution over extended tissue volumes is of paramount importance with respect to the generation of reliable ground truth datasets of fiber tract orientations. Two-photon confocal scanning fluorescence microscopy (TPFM) and light-sheet fluorescence microscopy (LSFM) can be used to achieve superior spatial resolutions compared to state-of-the-art polarimetry-based modalities such as 3D polarized light imaging [3]. Nevertheless, unlike the latter, volume fluorescence microscopy requires fiber orientations to be estimated via image processing methods, such as Fourier or structure tensor analysis [4]. These, however, may lead to inaccurate orientation maps as they cannot isolate myelinated fibers from the surrounding tissue. Here we introduce a novel analysis pipeline built around a 3D Frangi filter [5] which enables a multiscale enhancement and segmentation of tubular structures of varying diameters in tiled brain volume images of arbitrary size, and the generation of accurate 3D fiber orientation maps from both grey and white matter regions. The developed software tool also features the estimation of orientation distribution functions (ODFs) which may support the histological validation of modern dMRI-based tractography.

METHODS

The image processing pipeline for the 3D analysis of myelinated fiber orientations was developed in Python and is available at https://github.com/lens-biophotonics/Foa3D. Its main stages are schematized in Fig. 1. In the present work, the pipeline was tested on a mesoscale TPFM reconstruction of a human brain region in between the primary and secondary visual cortex, treated for fluorescence microscopy according to the label-free MAGIC preparation technique [6], which enhances the autofluorescence and, thus, the signal-to-background ratio of myelinated nerve fibers. 3D image stacks were acquired at a resolution of 0.88 µm x 0.88 µm x 1 µm by means of a custom-made TPFM system. The separate TPFM stacks composing the tiled reconstruction were aligned using ZetaStitcher, a software tool for large volumetric stitching [7], preliminarily compensating for their uneven spatial illumination via the retrospective CIDRE shading correction method [8], in order to suppress the grid-like stitching artifacts which would otherwise arise. Based on the available system resources, the fused image is then sliced into a batch of basic sub-volumes of adjusted size that are

processed in parallel over different CPU cores.

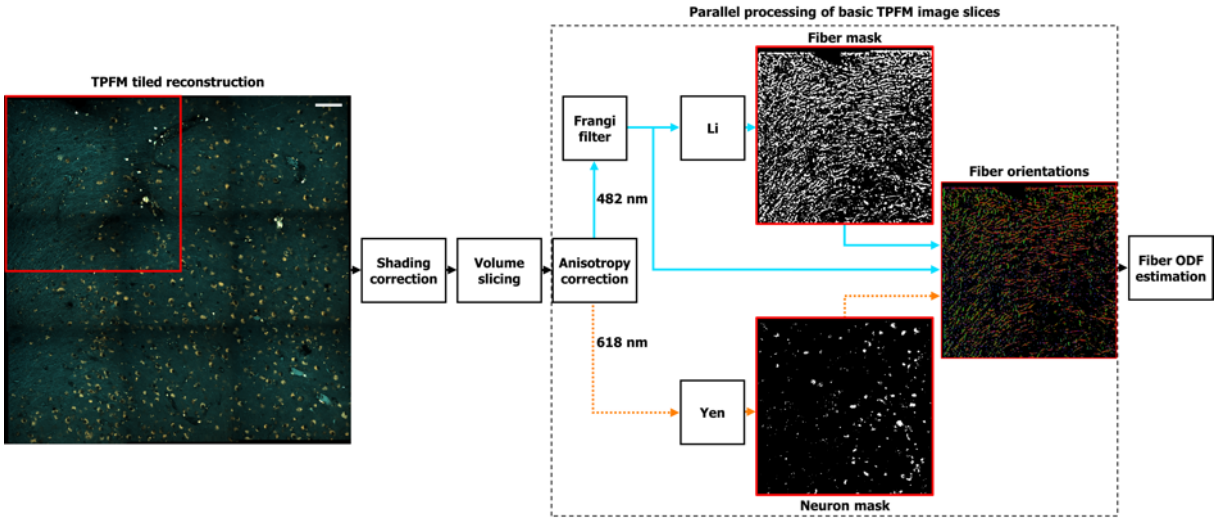

Figure 1 Block diagram schematizing the Foa3D image processing pipeline for the 3D analysis of myelinated fiber orientations in volume fluorescence microscopy; the pipeline is parallelized over basic sub-volumes of the reconstructed brain tissue sample; scale bar: 100 µm (adapted from [9]).

RESULTS AND DISCUSSION

Fig. 2 shows the typical segmentation of myelinated fibers produced by the Frangi filter with the resulting 3D fiber orientation field, and the corresponding ODF map which is finally generated using the fast analytical approach recently proposed in [10], so as to provide a comprehensive statistical characterization of the fiber tissue microstructure within larger spatial compartments of adaptable size. Despite being tested on brain samples treated with MAGIC and imaged with TPFM, the developed pipeline can be generically applied to volume images acquired using LSFM or obtained by means of specific fluorescent myelin stains such as DiD (data not shown).

Keywords: human connectome, myeloarchitectonics, fluorescence microscopy, Frangi filter, orientation distribution functions

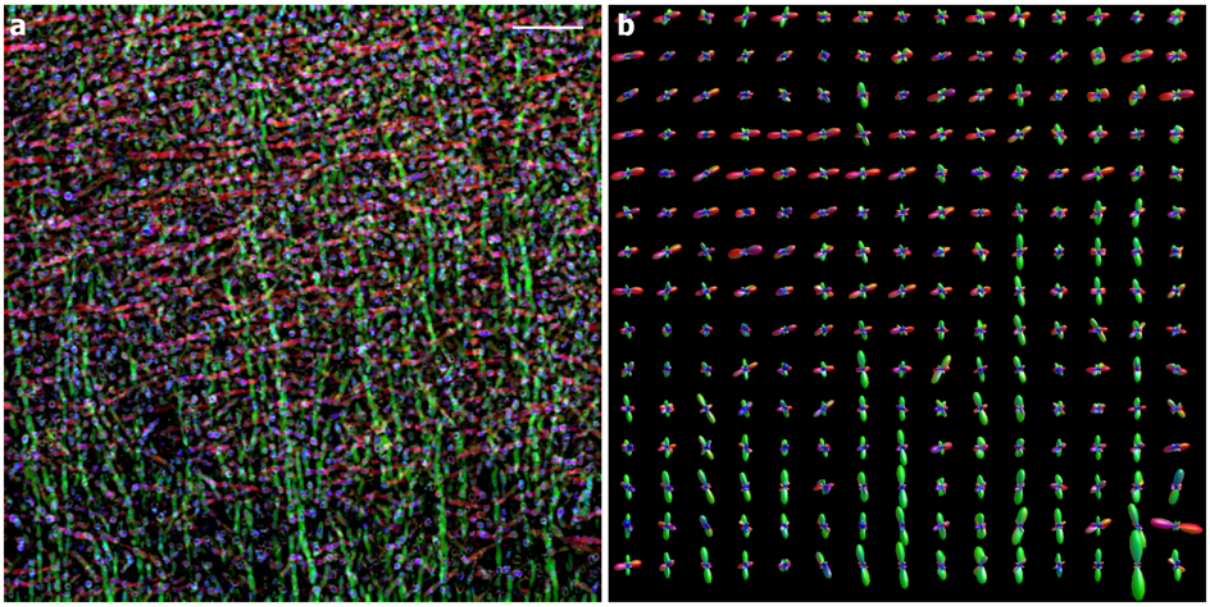

Figure 2 Frangi-based analysis of myelinated fiber orientations in a representative TPFM image stack (depth: 30 µm): a) average intensity projection of 3D fiber orientations (enhanced fiber diameters: 4 µm, 5 µm, 6 µm; resolution: 1 µm x 1 µm x 1 µm); b) fiber ODFs (resolution: 30 µm x 30 µm x 30 µm); scale bar: 50 µm.

ACKNOWLEDGEMENTS
The research leading to these results received funding from the European Union's Horizon 2020 Framework Programme for Research and Innovation under the Specific Grant Agreement No. 785907 (Human Brain Project SGA2), No. 871124 (Laserlab-Europe), and No. 945539 (Human Brain Project SGA3); the General Hospital Corporation Center of the National Institutes of Health under the award number U01 MH117023; the Italian Ministry for Education in the framework of the Euro-Bioimaging Italian Node (ESFRI research infrastructure); Fondazione CR Firenze (private foundation, project title: Human Brain Optical Mapping). The content of this work is solely the responsibility of the authors and does not necessarily represent the official views of the National Institutes of Health.

REFERENCES
[1] Yendiki, A. et al. Post mortem mapping of connectional anatomy for the validation of diffusion MRI. NeuroImage 256, 119146, DOI: 10.1016/j.neuroimage.2022.119146 (2022).

[2] Setsompop, K. et al. Pushing the limits of in vivo diffusion MRI for the Human Connectome Project. NeuroImage 80, 220-233, DOI: 10.1016/j.neuroimage.2013.05.078 (2013).

[3] Axer, M. et al. Estimating Fiber Orientation Distribution Functions in 3D-Polarized Light Imaging. Front. Neuroanat. 10, DOI: 10.3389/fnana.2016.00040 (2016).

[4] Khan, A. R. et al. 3D structure tensor analysis of light microscopy data for validating diffusion MRI. NeuroImage 111, 192–203, DOI: 10.1016/j.neuroimage.2015.01.061 (2015)

[5] Frangi, A. F., Niessen, W. J., Vincken, K. L. & Viergever, M. A. Multiscale vessel enhancement filtering. In Wells, W. M., Colchester, A. & Delp, S. (eds.) Medical Image Computing and Computer-Assisted Intervention - MICCAI'98, vol. 1496, 130–137, DOI: 10.1007/BFb0056195 (1998).

[6] Costantini, I. et al. Autofluorescence enhancement for label-free imaging of myelinated fibers in mammalian brains. Sci. Reports 11, 8038, DOI: 10.1038/s41598-021-86092-7 (2021).

[7] Mazzamuto, G. ZetaStitcher: a Software Tool for High-Resolution Volumetric Stitching (2021).

[8] Smith, K. et al. CIDRE: an illumination-correction method for optical microscopy. Nat. Methods 12, 404–406, DOI: 10.1038/nmeth.3323 (2015).

[9] Sorelli, M. et al. Fiber enhancement and 3D orientation analysis in label-free two-photon fluorescence microscopy. bioRxiv, DOI: 10.1101/2022.10.19.512531 (2022).

[10] Alimi, A. et al. Analytical and fast Fiber Orientation Distribution reconstruction in 3D-Polarized Light Imaging. Med. Image Analysis 65, 101760, DOI: 10.1016/j.media.2020.101760 (2020).

139. Closed-loop brain-inspired meta-reinforcement learning rules during cognitive inhibition control

Federica Robertazzi[1,2*], Matteo Vissani[3,4], Egidio Falotico[1,2]

[1] The BioRobotics Institute, Sant'Anna School of Advanced Studies, Pisa, 56127, Italy

[2] Department of Excellence in Robotics & AI, Sant'Anna School of Advanced Studies, Pisa, 56127, Italy

[3] Harvard Medical School, Boston, Massachusetts

[4] Department of Neurosurgery, Massachusetts General Hospital, Boston, Massachusetts

*federica.robertazzi@santannapisa.it

INTRODUCTION/MOTIVATION

Inhibition is one of the domains of the more general property of cognitive control that is the ability to adapt behavior to current demands by promoting relevant information regardless of interference with the internal urge [1]. Action inhibition is the disengagement from a motor command, and it is a necessary component in the transition between different cognitive demands.

Modern artificial agents exhibit long-standing performance in terms of accuracy and reliability when learning a single task after exposure to stationary learning trials. However, in human-real case circumstances characterized by sources of uncertainty and variability such as unpredictable cues and unexpected constraints, they are not usually able to show reactive behavior to adapt to the environment [2].

Meta-learning (ML) systems can be used to integrate flexible and efficient learning in artificial agents. In ML the inner learning loop is continuously adjusted by an outer learning system made up of meta-parameters which reveal computational changes in the artificial agent-environment interaction [3].

METHODS

Our work 4 inherits the meta-learning principles in the neuromodulation theory proposed by Doya 5 and the neural architecture developed by Khamassi and colleagues 6 for agent-environment interaction. The neuromodulation theory propounds a direct equivalence between the dynamics of the four major neurotransmitters (e.g., acetylcholine, serotonin, dopamine, and noradrenaline) and the computational role of the hyperparameters which shape the meta-learning processes (Fig.1).

In this brain-inspired meta-learning framework for inhibition cognitive control we included meta-learner representations of the distributed learning systems in the human brain, e.g., cortical areas such as prefrontal cortex and subcortical regions such as basal ganglia. We formalized brain-inspired meta-learning hyperparameters optimization rules, mimicking explicitly the dynamics and mutual interaction of the major neurotransmitters in the brain: (i) dopamine receptors D1 modulate the noradrenergic system (i.e. exploration/exploitation rate) with an inverse linear function that relates dopamine to the entropy of the probability distribution of the actions 7, (ii) dopamine receptors D2 tune the striatum neuron's excitability 8, and (iii) serotonin regulates the overall dopamine release and

the reward temporal scale 9,10.

The artificial agent was tested in two different conflictual tasks that involve different types of action inhibition 11,12: action restrain in NoGo Paradigm and action cancellation in Stop-Signal Paradigm. In the former, we evaluated the ability to withdraw a not-yet-initiated action from responding by the appearance of a hold signal before the movement execution. In the latter, we investigated the ability to cancel an initiated response triggering an unpredictable hold signal after a range of delays from the action onset.

In a subsequential work, we evaluated the role of the ratio between D1-mesocorticolimbical and D2- nigrostriatal pathways in inhibition cognitive control investigating the computational role of the dopamine meta-parameter, both in terms of concentration and efficacy.

We used the Wilson-Cowan formalism to implement the closed-loop serotonin-dopamine mutual interaction and the effect of an external background activity on the serotonin-dopamine system.

We included monotonic logarithmic coupling functions that mediate the concentration of the two neurotransmitters according to the ongoing demand of the learning in the artificial agent.

RESULTS AND DISCUSSION

The artificial agent, after the training session, learned how to adjust successfully its hyperparameters (e.g., driving the system towards exploitation regimes) in response to the appearance of the hold signal in both paradigms, and hence, showing a proper encoding of the action inhibition command (Fig.2). In particular, both right inhibition and global accuracy increased significantly during the test phase in NoGo Paradigm (Mean ± SD; training: 53.32 ± 15.51% 88 vs test: 85.22 ± 4.42%; dc = 2.060 ; Mean ± SD; training: 0% vs test: 70.67 ± 9.20%; dc = 7.675) and in Stop-Signal Paradigm (accuracy, Mean ± SD; training: 45.53 ± 15.54% vs test: 73.29 ± 4.76; dc = 1.952 ; right inhibition, Mean ± SD; training: 0% vs test: 47.83 ± 10.46%; dc = 4.555).

By considering the Stop-Signal Paradigm, high serotonin concentration acting on the dopamine release led to behavioral effects as such it shifted of the agent's behavior towards non-impulsive regimes, e.g., shorter reaction time and higher right inhibition as well as a reduction in the Stop Signal Reaction Time (SSRT), i.e., the latency of the inhibition process.

Finally, we found that changes in D1-mesocorticolimbical and D2-nigrostriatal concentration as well as efficacy (η) produced differential and asymmetrical effects in the network's activity as well as in the behavioral performance.

In the closed loop scenario, we obtained an increase of Inhibition performances in terms of right inhibition (Mean ± SD; test open-loop: 47.59 ±10.31 % vs test closed-loop: 78.96% ±8.95 %; dc = 2.442) and accuracy (Mean ± SD; test open-loop: 73.23 ±4.65 % vs test closed-loop: 89.46 ±4.42 ; dc =2.781) compared to the previous open-loop implementation, there is no difference in the stop-signal reaction time (Mean ± SD; test open-loop: 12.16 ± 1.10 % vs test closed-loop: 12.07 ± 1.04 % ; dc =0.065).

We demonstrated that brain-inspired meta-learning rules may pave the way of the design of cognitive control architectures for artificial agents that achieve more flexible and accurate behavior when conflictual inhibitory signals

are present in the non-deterministic environment.

Keywords: Meta-learning, Brain-inspired Modeling, Inhibition Cognitive Control, Basal Ganglia, Prefrontal Cortex

ACKNOWLEDGEMENTS

F.R. & E.F. have received funding from the European Union's Horizon 2020 Framework Programme for Research and Innovation under the Specific Grant Agreement No. 945539 (Human Brain Project SGA3). M.V. has received internal funding from Sant'Anna School of Advanced Studies.

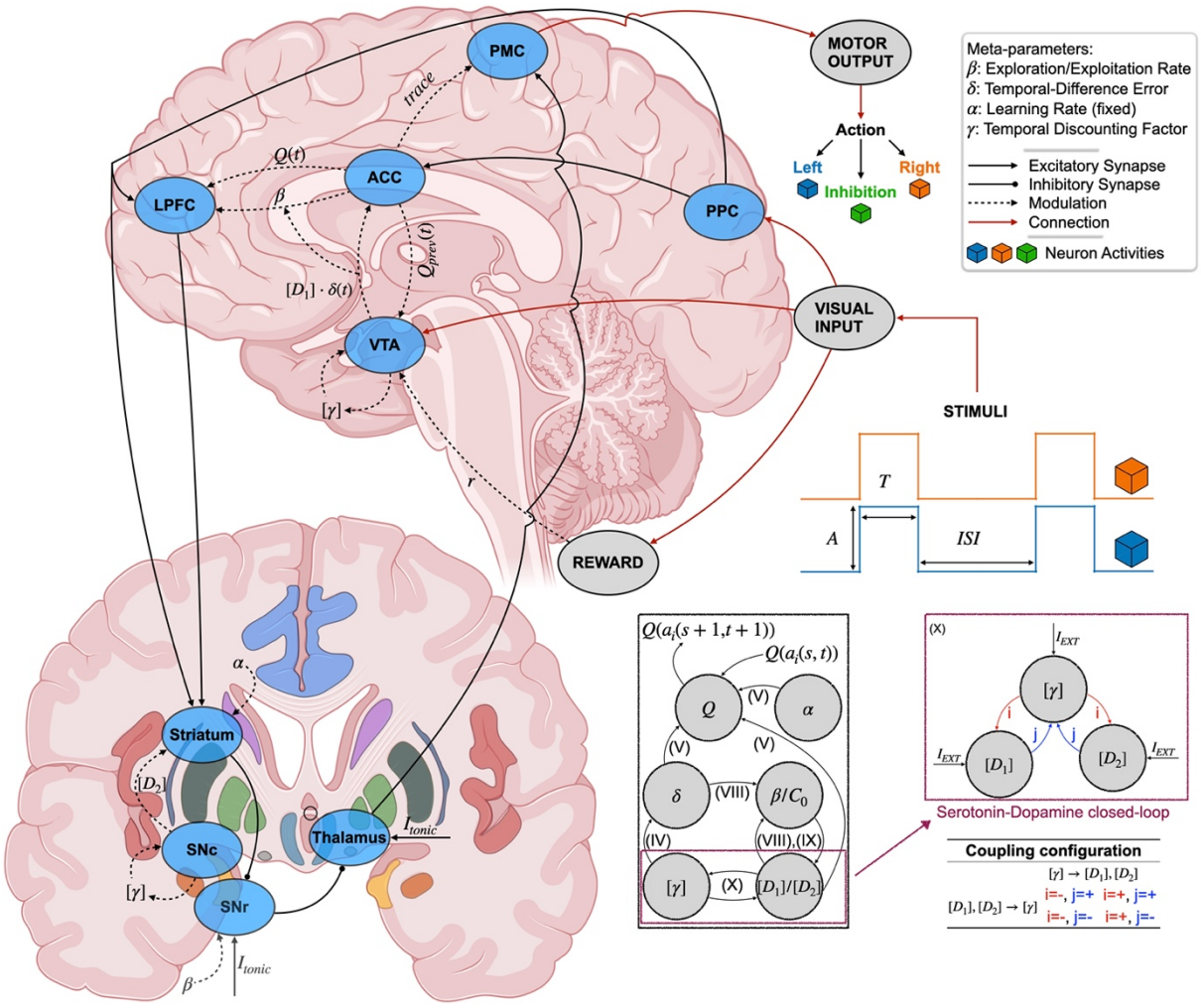

Figure 1. The model architecture inspired by 6,13 and the meta-learning mechanism based on principles of Doya's neuromodulation theory 5,14,15 are illustrated. The cubes represent the neuron's activity topographically associated with the two directions (Left (blue), Right (orange)) and action inhibition (Inhibition (Green)). Excitatory (black arrow) and inhibitory (black circle arrow) neural synapses, reinforcement learning, meta-learning mechanisms (e.g., action values $Q(t)$, dopamine $[\mathrm{D}_1]$, $[\mathrm{D}_2]$, serotonin $[\gamma]$, noradrenaline β, etc.) (black dashed arrows), and input/output connections (red line) are displayed. Stimuli are fed in the model by simulating a square wave (A (amplitude) = 1 [a.u.], T (duration) = 100 [samples], ISI (inter-stimuli interval) = 200 [samples]) for neurons codifying Left or Right movement.

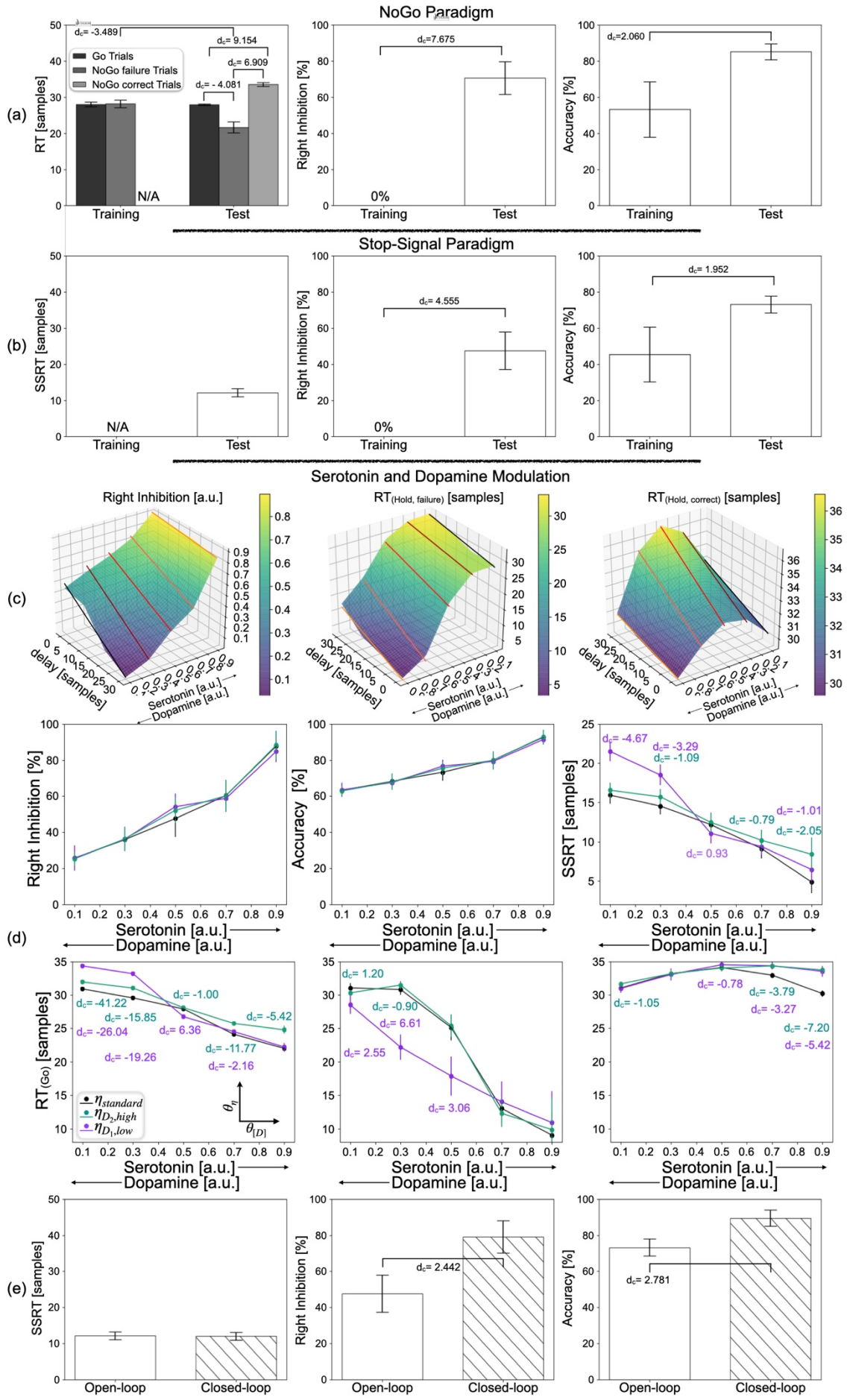

Figure 2. Performance of the simulated agent in NoGo and Stop-Signal Paradigms. Results are averaged across 40 simulations of 1000 stimuli during the training and test phases in NoGo Paradigm and Stop-Signal Paradigm. Results are expressed as Mean ± SD. Cohen's effect sizes are reported for large effects d_c. (a) Reaction time (RT), Right Inhibition and Accuracy are displayed for both training and test phases in NoGo Paradigm. (b) Stop Signal Reaction time

(SSRT), Right Inhibition and Accuracy are displayed for both training and test phases in Stop-Signal Paradigm. SSRT is not defined during the training phase as the right inhibition is 0%. The color of the bar indicates the type of trials used to compute the metrics: Go trials (black), Hold failure trials (dark gray), Hold correct trials (light gray) and all trials (white). d_c is positive/negative if the right/left group mean is higher. (c) 3D representation of the relationship among task parameters (Right Inhibition, RT(Hold,failure) and RT(Hold,correct)), delay of the hold signal $d \in \{10,20,30\}$), and serotonin concentration [γ] ∈ {0.1, 0.3, 0.5, 0.7, 0.9}.(d) Network parameters and inhibition performance metrics (RTs (Go and Hold failure and Hold correct Trials), Right Inhibition, Accuracy, SSRT) are plotted against the serotonin concentration $[\gamma] \in \{0.1, 0.3, 0.5, 0.7, 0.9\}$ averaging across all the stimuli presentation during the Hold Trials during Stop-Signal Paradigm in the test phases at low $\eta_{D_1,\,low}$(violet), $\eta_{standard}$ (black) and high $\eta_{D_2,\,high}$ (sea green) efficacy of the ratio between $[D_1]$- D1-mesocorticolimbical and D2-nigrostriata pathways in favor of D2 pathways. d_c is positive if the $\eta_{D_1,\,low}/\eta_{D_2,\,high}$ efficacy group mean is lower respect to the standard condition.(e) Comparison between open-loop condition (white) at fixed serotonin level of $[\gamma] = 0.5$ and closed-loop (hitch pattern filled) condition in the Stop-Signal Paradigm ($d \in \{10,20,30\}$).

REFERENCES

1. Dreher JC, Berman KF. Fractionating the neural substrate of cognitive control processes. *Proc Natl Acad Sci USA*. 2002;99(22):14595-14600. doi:10.1073/pnas.222193299

2. Pfeifer R, Lungarella M, Iida F. Self-Organization, Embodiment, and Biologically Inspired Robotics. *Science*. 2007;318(5853):1088-1093. doi:10.1126/science.1145803

3. Thrun S, Pratt L. Learning to Learn: Introduction and Overview. In: Thrun S, Pratt L, eds. *Learning to Learn*. Springer US; 1998:3-17. doi:10.1007/978-1-4615-5529-2_1

4. Robertazzi F, Vissani M, Schillaci G, Falotico E. Brain-inspired meta-reinforcement learning cognitive control in conflictual inhibition decision-making task for artificial agents. *Neural Networks*. 2022;154:283-302. doi:10.1016/j.neunet.2022.06.020

5. Doya K. Metalearning and neuromodulation. *Neural Netw*. 2002;15(4-6):495-506. doi:10.1016/s0893-6080(02)00044-8

6. Khamassi M, Lallée S, Enel P, Procyk E, Dominey PF. Robot Cognitive Control with a Neurophysiologically Inspired Reinforcement Learning Model. *Front Neurorobot*. 2011;5. doi:10.3389/fnbot.2011.00001

7. Humphries M. Dopaminergic control of the exploration-exploitation trade-off via the basal ganglia. *Front Neurosci*. 2012;6. doi:10.3389/fnins.2012.00009

8. Tanaka SC, Doya K, Okada G, Ueda K, Okamoto Y, Yamawaki S. Prediction of immediate and future rewards differentially recruits cortico-basal ganglia loops. *Nat Neurosci*. 2004;7(8):887-893. doi:10.1038/nn1279

9. Tanaka SC, Schweighofer N, Asahi S, et al. Serotonin Differentially Regulates Short- and Long-Term Prediction of Rewards in the Ventral and Dorsal Striatum. Lu B, ed. *PLoS ONE*. 2007;2(12):e1333. doi:10.1371/journal.pone.0001333

10. Schweighofer N, Tanaka SC, Doya K. Serotonin and the Evaluation of Future Rewards: Theory, Experiments, and Possible Neural Mechanisms. *Annals of the New York Academy of Sciences*. 2007;1104(1):289-300. doi:10.1196/annals.1390.011

11. Eagle DM, Baunez C, Hutcheson DM, Lehmann O, Shah AP, Robbins TW. Stop-Signal Reaction-Time Task Performance: Role of Prefrontal Cortex and Subthalamic Nucleus. *Cerebral Cortex*. 2008;18(1):178-188. doi:10.1093/cercor/bhm044

12. Schall JD, Palmeri TJ, Logan GD. Models of inhibitory control. *Phil Trans R Soc B*. 2017;372(1718):20160193. doi:10.1098/rstb.2016.0193

140. On-chip spike coding control: Linear-quadratic-Gaussian filtering through sparse and irregular spiking

André Rodrigues Urbano[1], Filip S. Slijkhuis[1], Mahyar Shahsavari[1], Sander Kemmink[1+], Pablo Lanillos[1,2+*]

[1] Donders Institute, Radboud University, Nijmegen, The Netherlands

[2] Cajal International Neuroscience Center, Spanish National Research Council, Madrid, Spain.

*p.lanillos@donders.ru.nl

+ Researchers contributed equally

INTRODUCTION/MOTIVATION

Understanding and artificially synthesising how animals control their bodies and adapt to the environment is one of the most important scientific and technological challenges in both neuroscience and robotics. We know that behaviour is produced through sparse and irregular spiking patterns, which provide both robust and efficient control that requires little energy. Current neural network control approaches, however, are far from energy and data efficiency and even the ones that use spikes for computations have ineficient, dense and regular spike trains. Moreover, these approaches still need complex training and optimization procedures, complicating their implementation in on-chip low-power solutions.

Here, we describe, supported by the theory of Spike Coding Networks (SCNs) [1] a novel solution for optimal estimation and control, a spike control approach that behaves as a linear-quadratic-Gaussian controller [2], which

i) can be practically deployed on neuromorphic hardware and *ii)* has the advantage of having irregular, sparse, and robust spiking activity and does not need training.

We evaluated our robust estimation and control algorithm on two classical systems—the spring-mass-damper system and the cartpole (Fig. 1), in the face of several perturbations, including input- and system-noise, system disturbances, and neural silencing.

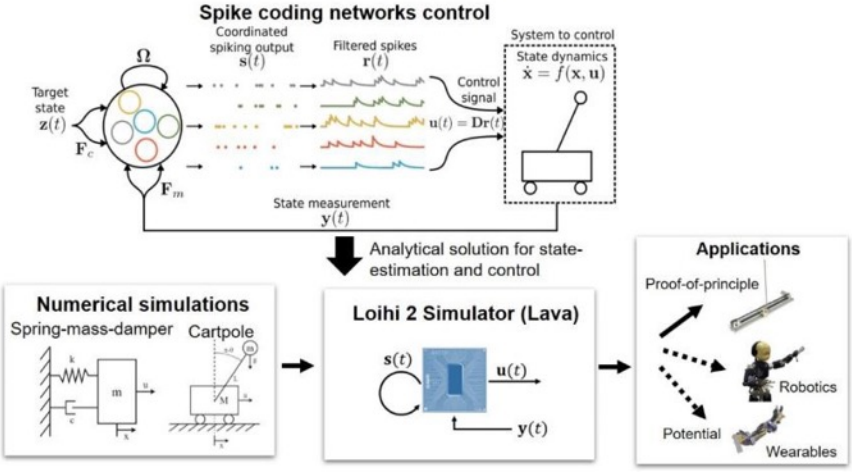

Figure 1. Spike coding control. Under the neuroscience theory of Spike Coding Networks (SCNs) we propose an estimation and control approach that can be easily deployed in neuromorphic hardware without the need for training when the

dynamical system is known. We evaluated the proposed approach in simulation using numerical simulations and Intel's Lava simulator.

METHODS

Spike Coding Network control (SCN control)

We hypothesise that these spiking patterns encode a meaningful signature related to prediction error minimization [1,2] that can be analytically computed. Given a system with state x(t) with a spiking signal s(t) emitted from a recurrent SNN, where the SNN has access to a measurement of the input y(t), a desired state z(t) and is to generate a control signal u(t), we provide a closed-form solution for estimating and controlling any (linearized) dynamical system using SNNs with recurrent connections while maintaining sparse, irregular and robust spiking activity — We refer to [3] for a detailed explanation of the method.

Neuromorphic deployment

We implement our SNN in the Lava framework and simulator which allows the use of the Loihi 2 chip as a hardware backend. This involves optimizing the algorithm so that message passing between neurons occurs only upon spiking and creating standardized functions that build a network for control of any given linear system.

We simulate it as a Process and implement a Python Process Model to simulate the Loihi behaviour on CPU.

RESULTS AND DISCUSSION

We tested the model on numerical simulations and using the Intel's Lava neuromorphic framework (Fig. 2C). The comparison of our controller against the well-known idealized LQR controller shows equivalent performance with the advantage of using spikes instead of traditional Von-Neumann architecture. As our approach does not need learning or optimization, it may provide fast and efficient task-specific on-chip spiking controllers with biologically realistic activity. Our next step is to connect the Loihi 2 to a mechanical cartpole system (Fig. 2A) to evaluate the system in a non-simulated environment.

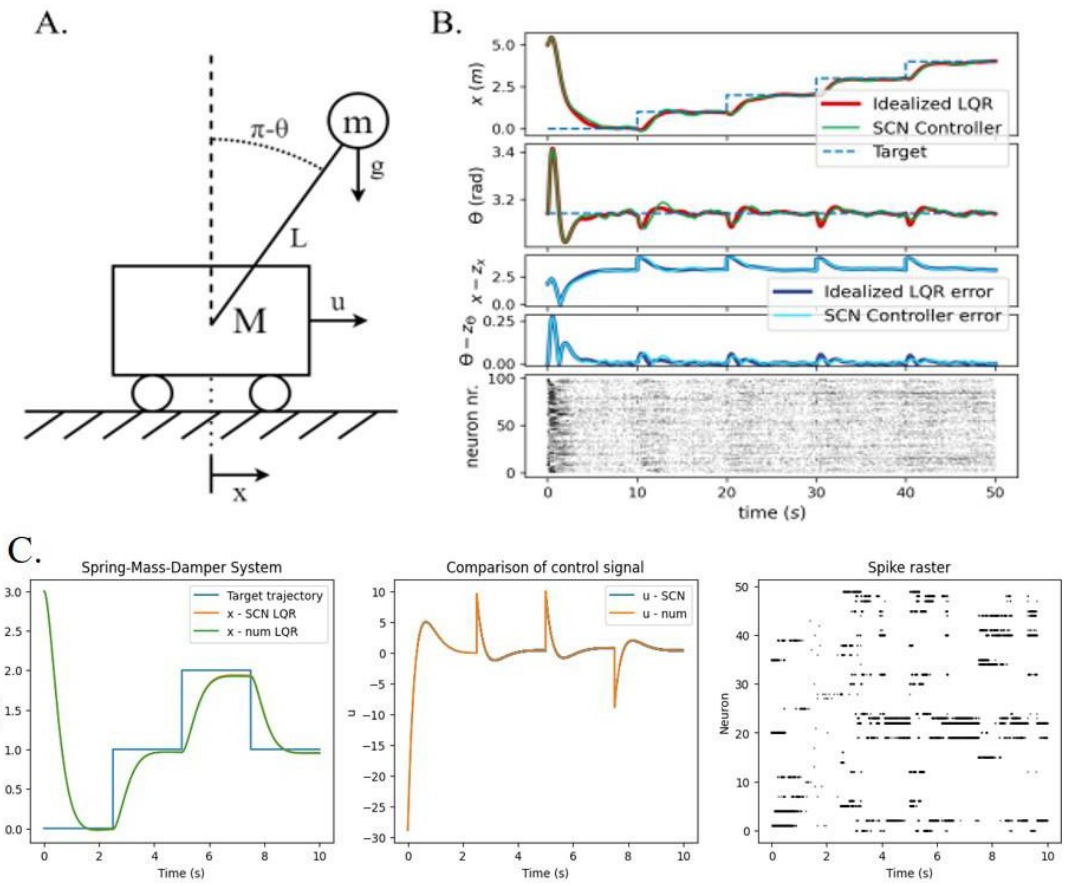

Figure 2. SCN control evaluation. (A) Cartpole definition for the numerical simulations. (B) Estimation and control of the cartpole compared to the LQR baseline (Reproduced from [3]). (C) Spring-Mass-Damper control following a reference trajectory using SCN control on the Intel's Lava simulator.

Keywords: Spiking Neural Networks, Estimation and Control, Neuromorphic hardware

ACKNOWLEDGEMENTS
This work has been partially supported by the Spikeference project, Human Brain Project Specific Grant Agreement 3 (ID: 945539).

REFERENCES

[1] Boerlin, M., Machens, C. K., & Denève, S. (2013). Predictive coding of dynamical variables in balanced spiking networks. PLoS computational biology, 9(11), e1003258.

[2] Lanillos, P., Meo, C., Pezzato, C., Meera, A. A., Baioumy, M., Ohata, W., ... & Tani, J. (2021). Active inference in robotics and artificial agents: Survey and challenges. arXiv preprint arXiv:2112.01871.

[3] Slijkhuis, F. S., Keemink, S. W., & Lanillos, P. (2022). Closed-form control with spike coding networks. arXiv preprint arXiv:2212.12887.

[4] Mancoo, A., Keemink, S., & Machens, C. K. (2020). Understanding spiking networks through convex optimization. Advances in Neural Information Processing Systems, 33, 8824-8835.

141. Neurophysiology of gaze visual orientation: a synthesis of the contribution of animal studies

Laurent Goffart[1,2*]

[1] INT, UMR 7289 CNRS AMU, Marseille, France

[2] Centre Gilles Gaston Granger, UMR 7304 CNRS AMU, Aix-en-Provence, France

*e-mail-address of corresponding author: laurent.goffart@cnrs.fr

INTRODUCTION/MOTIVATION

The appearance of an object in the visual field triggers a rapid gaze shift toward its location. This orienting response consists of a rapid rotation of the eyes, the saccade, which can be accompanied by a rotation of the head. If the target moves, the saccade is followed by a slow movement of the eyes and a catch-up saccade.

METHODS

Instead of describing the path leading from the target-evoked retinal activity to the changes in muscle tension, we shall take the reverse path. Starting from the muscle contractions, we proceeded upstream and described the tremendous organization that, in the brainstem and cerebellum, enables us to rapidly and accurately orient the foveae towards visual targets located at different eccentricities and depths. Thus, we discovered the considerable knowledge that neurophysiologists and neuroanatomists gathered during the last six decades with non-human species (mostly monkey and cat). Technical developments indeed offered the possibility to measure precisely the time course of eye and head movements and to study correlations between the firing rate of neurons and kinematic parameters (amplitude, velocity, acceleration and various differences called errors).

RESULTS AND DISCUSSION

These statistical correlation studies should not lead us to believe that a one-to-one correspondence exists between on the one hand, the multiple neuronal networks within which activities propagate, and on the other hand, the homogeneous mathematical medium with which we quantify the movements. Such a mapping is questionable insofar as contrary to the physical space, the medium of neuronal activity is neither homogeneous nor passive. Unlike most objects that we visually fixate and manipulate, the corresponding brain activity is not rigid. Even the mere spot of activity evoked by a small static object on the retina yields multiple parallel flows of activity that make its correspondence in the brain spatially distributed, temporally extended and context- dependent. Moreover, reducing the neurons or neuronal chains to units encoding geometric or kinematic relations between gaze target directions conceals not only the muscle forces and the antagonisms between muscles but also the antagonisms between the multiple channels that drive each movement.

In the majority of models proposed during the last decades, the movements were considered as driven by error signals encoding displacement vectors in physical space. These models were definitely useful to communicate

concepts and to bring a comprehensive picture of the complexity underlying the generation of movements. However, embedding geometric and kinematic notions within the inner functioning of the brain (i.e., mapping intrinsic neuronal signals with extrinsic behavioral measurements) may be neurophysiologically misleading because different constraints characterize the neurophysiological and kinematic descriptions. Rather than outcomes of processes reducing geometric or kinematic errors, the eye movements merely consist of transitions between equilibria opposing populations of neurons whose activity leads to mutually antagonist movement tendencies.

Further empirical investigation is still required to determine and explain several other issues: i.e., whether and how the networks underlying orienting movements of the eyes and head interact with those generating other types of goal-directed action such as reaching movements of the hand or locomotion; whether and how they interact with the networks involved in the navigation and the memory of locations; and whether and how they support the learning of new skills and possibly the acquisition of more abstract knowledge such as geometry or counting. With the recent multiplication of cognitive studies that use eye-tracking techniques to explore the so- called "inner space" with quantitative methods, more effort is required to characterize what exactly are those covert processes that eye movements would express.

Keywords: Neurophysiology, Neuroanatomy, Non-human primate, Brain stem, Cerebellum, Superior Colliculus, Reticular Formation, Visual orienting

ACKNOWLEDGEMENTS

This work was possible thanks to support from Centre National de la Recherche Scientifique and from the Fondation pour la Recherche Médicale.

REFERENCES

[1] Goffart L, Bourrelly C, Quinet J. Synchronizing the tracking eye movements with the motion of a visual target: Basic neural processes. Prog Brain Res 236: 243–268, 2017

[2] Goffart L, Bourrelly C, Quinton JC. Neurophysiology of visually-guided eye movements: critical review and alternative viewpoint. J Neurophysiol 120: 3234–3245, 2018.

[3| Goffart L. Kinematics and the neurophysiological study of visually-guided eye movements. Prog Brain Res 249: 375–384, 2019.

[4] Goffart L., Quinet J. & Bourrelly C. Neurophysiology of gaze orientation: Core neuronal networks. In : J. Grafman (Ed) Encyclopedia of the Human Brain, submitted

142. All-optical method to study cortical information integration in awake and anesthetized mice

Francesco Resta[*,1,2], Alessandro Scaglione[1,2], Emilia Conti[1,2,3], Giacomo Mazzamuto[2,4], Anna Letizia Allegra Mascaro[1,3], Francesco Saverio Pavone[1,2,4]

1. European Laboratory for Non-Linear Spectroscopy, University of Florence, Sesto Fiorentino 50019, Italy
2. Department of Physics and Astronomy, University of Florence, Sesto Fiorentino 50019, Italy
3. Neuroscience Institute, National Research Council, Pisa 56124, Italy
4. National Institute of Optics, National Research Council, Sesto Fiorentino 50019, Italy

*e-mail-address of corresponding author: resta@lens.unifi.it.

INTRODUCTION/MOTIVATION

Brain responsiveness and complexity are linked to the level of consciousness (Tononi et al., 2004). The combination of Transcranial Magnetic Stimulation (TMS) and hd-EEG recordings represents the gold standard method to study how the brain states affect response complexity in humans. In this framework, a preclinical analogous using lab animals would provide novel mechanistic insights into the state-dependent responsiveness of the brain.

The use of light to monitor and control neuronal activity presents numerous advantages. Compared to standard electrophysiological techniques, imaging and optogenetics are less invasive, offer higher spatial resolution and allow to target genetically selected neuronal populations. A promising approach to record and simultaneously stimulate neuronal activity in mice is using all-optical neurophysiological methods. These methods allow causal investigation of neuronal connectivity with milliseconds temporal resolution across multiple spatial scales. A powerful technique to study mesoscale connectivity in mice exploits wide-field microscopy coupled with functional fluorescence indicators (Montagni et al., 2018). This approach provides simultaneous information of neuronal ensemble activity from distributed cortical areas. At the same time, transcranial optogenetic stimulation has been demonstrated to be a powerful tool to activate neuronal clusters in the cortex (Hira et al., 2009).

However, all-optical systems that combine these techniques critically suffer for crosstalk between imaging and photostimulation, limiting the possibility to develop wide-field all-optical systems (Lim et al. 2012; Akerboom et al. 2013; Emiliani et al. 2015).

METHODS

All experiments were performed in accordance with the guidelines of the Italian Minister of Health (aut. n. 857/2021). 5 C57BL/6J adult mice (3-6 months) of both sexes were used.

Wide-field microscopy setup. Wide-field imaging and optogenetic stimulation were performed using a custom- made microscope with two excitation sources. The excitation source for jRCaMP1b was a red-light beam of emitting diodes (595 nm LED) selected by a bandpass filter (578/21 nm). The light beam was deflected by a dichroic mirror (606nm) to the 2X objective towards the skull. The excitation source for single-photon stimulation of ChR2 was a continuous wavelength (CW) laser (λ = 473 nm). The excitation beam was overlaid on the imaging pathway using a second dichroic beam splitter (FF484-Fdi01-25) before the objective. The system has a random-access scanning head with two orthogonally-mounted acousto-optical deflectors (DTSXY400). The jRCaMP1b fluorescence signal emitted was collected through a band-pass filter (630/69) and focused on a high speed complementary metal-oxide semiconductor (CMOS) camera.

RESULTS AND DISCUSSION

Here we established a crosstalk-free large-scale all-optical method combining wide-field fluorescence imaging of the red-shifted calcium indicator jRCaMP1b and transcranial optogenetic stimulation of Channelrhodopsin-2 (ChR2)(Resta et al., 2022) (fig. 1).

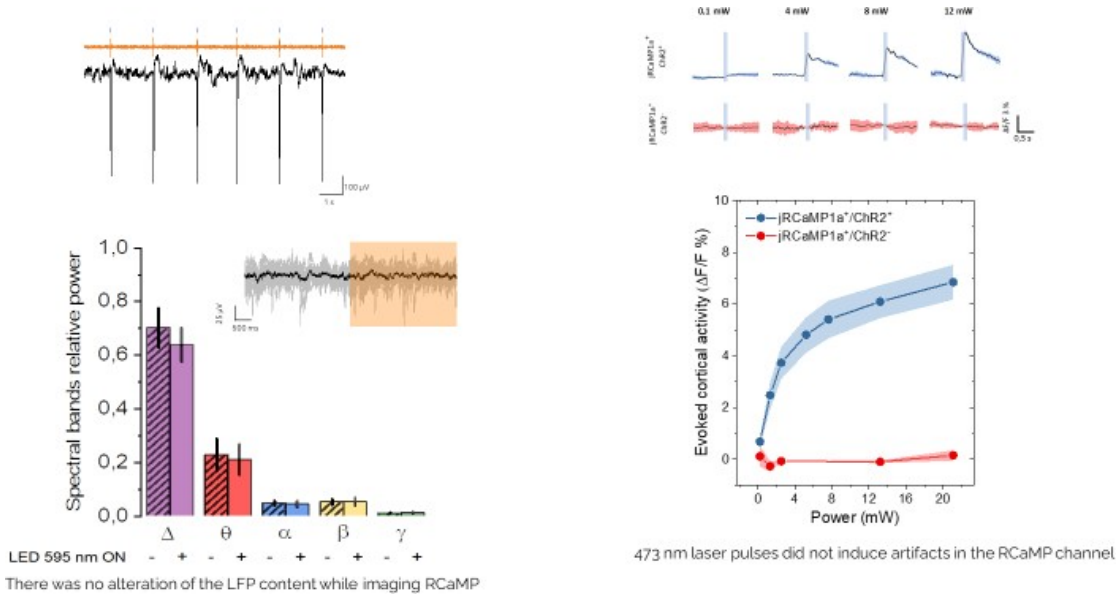

Fig.1 electrophysiological experiment showing that Wide-field imaging of RCaMP did not induce ChR2 cross-activation

To achieve a cortex-wide expression of the calcium indicator and the optogenetic actuator, we took advantage of adeno-associated virus (AAV.PHP.eb) carrying jRCaMP1b under the control of the neuronal promoter synapsin and ChR2 under the CamKIIa promoter, thus targeting only excitatory neurons. This approach gives us the possibility to visualize the stimulated neuronal activity propagation in all the dorsal cortical areas.

Results show that in awake mice, optogenetic stimulations evoke a distributed cortical response in several areas in the two hemispheres (fig. 2), whereas, during anesthesia, stimulation led to a localized response limited in space and time.

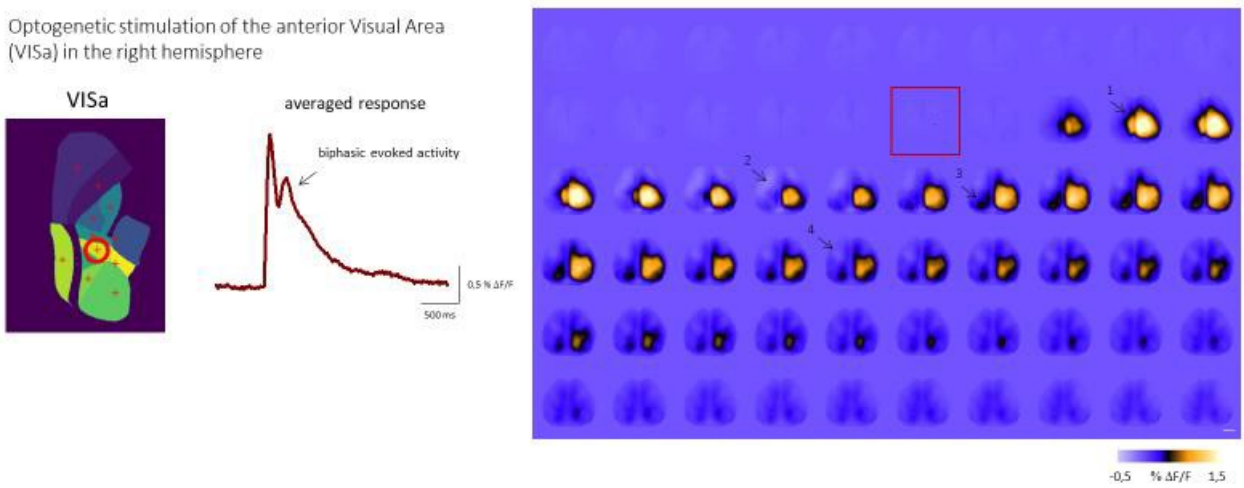

Fig. 2 All-optical causal interrogation of the dorsal cortical mantle in awake mice. Image sequence representing the cortical activation following a single pulse stimulation fo the associative area, Posterio Parietal Cortex (PPC).

These results confirm that the spatiotemporal complexity of the evoked response decreases with the levels of consciousness, as observed in pathological patients affected by disorders of consciousness (Massimini et al., 2009).

Keywords: large-scale, imaging, optogenetics, brain states, brain responsiveness

ACKNOWLEDGEMENTS

This research was supported by the European Union's Horizon 2020 Research and Innovation Framework Program under grant agreements 945539 (HBP-SGA3) and 785907 (HBP-SGA2), by the EU program H2020 EXCELLENT SCIENCE – European Research Council (ERC) under grant agreement 692943 (BrainBIT)

REFERENCES

1. Akerboom, J., Carreras Calderón, N., Tian, L., Wabnig, S., Prigge, M., Tolö, J., ... & Looger, L. L. (2013). Genetically encoded calcium indicators for multi-color neural activity imaging and combination with optogenetics. Frontiers in molecular neuroscience, 6, 2.
2. Emiliani, V., Cohen, A. E., Deisseroth, K., & Häusser, M. (2015). All-optical interrogation of neural circuits. Journal of Neuroscience, 35(41), 13917-13926.
3. Hira, R., Honkura, N., Noguchi, J., Maruyama, Y., Augustine, G. J., Kasai, H., & Matsuzaki, M. (2009). Transcranial optogenetic stimulation for functional mapping of the motor cortex. Journal of neuroscience methods, 179(2), 258-263.

4. Lim, D. H., Mohajerani, M. H., LeDue, J., Boyd, J., Chen, S., & Murphy, T. H. (2012). In vivo Large-Scale Cortical Mapping Using Channelrhodopsin-2 Stimulation in Transgenic Mice Reveals Asymmetric and Reciprocal Relationships between Cortical Areas. Frontiers in Neural Circuits, 6. https://doi.org/10.3389/fncir.2012.00011
5. Massimini, M., Boly, M., Casali, A., Rosanova, M., & Tononi, G. (2009). A perturbational approach for evaluating the brain's capacity for consciousness. Progress in brain research, 177, 201-214.
6. Montagni, E., Resta, F., Conti, E., Scaglione, A., Pasquini, M., Micera, S., ... & Pavone, F. S. (2018). Wide- field imaging of cortical neuronal activity with red-shifted functional indicators during motor task execution. Journal of Physics D: Applied Physics, 52(7), 074001.
7. Resta, F., Montagni, E., de Vito, G., Scaglione, A., Mascaro, A. L. A., & Pavone, F. S. (2022). Large-scale all- optical dissection of motor cortex connectivity shows a segregated organization of mouse forelimb representations. Cell Reports, 41(6), 111627.
8. Tononi, G. (2004). An information integration theory of consciousness. BMC neuroscience, 5, 1-22.

143. Biologically plausible gated recurrent neural networks for working memory and learning-to- learn

Alexandra R. van den Berg[1,2*], Pieter R. Roelfsema[2,3], Sander M. Bohté[1,4,5]

[1]Machine Learning Group, Centrum Wiskunde & Informatica, Amsterdam, the Netherlands

[2]Department of Vision and Cognition, Netherlands Institute for Neuroscience, Amsterdam, the Netherlands

[3]Department of Integrative Neurophysiology, Center for Neurogenomics and Cognitive Research, Vrije Universiteit, Amsterdam, the Netherlands

[4]Cognitive and Systems Neuroscience, Swammerdam Institute of Life Sciences, University of Amsterdam, Amsterdam, the Netherlands

[5]Computer Science, Rijksuniversiteit Groningen, Groningen, the Netherlands

*arvdb@cwi.nl

INTRODUCTION/MOTIVATION

Learning-to-learn is a process by which individuals accelerate their learning of novel tasks as a result of prior experience with similar tasks[1,2]. Within reinforcement learning, this ability is known as meta-reinforcement learning[3]. However, most models that carry out memory-based meta-reinforcement learning, including variants of long-short term memory, are unlikely to be implemented by the brain since they rely on training procedures that require non-local information, i.e. not available at synapses undergoing plasticity[4]. Moreover, these architectures can be unnecessarily complex[5,6] and therefore not easily interpretable[5] or mappable to the brain. AuGMEnT[7] is a biologically plausible model of working memory that only performs local computations but lacks gating mechanisms required for integration and selective forgetting of information over longer timescales, which hinders learning-to-learn. In this work we develop a biologically plausible gated recurrent architecture called RECOLLECT, which learns to memorize and forget based on locally available information and can learn-to-learn.

METHODS

RECOLLECT stands for "REinforCement learning of wOrking memory with bioLogically pLausible recurrent uniTs". It is based on a simplified version of the gated-recurrent unit (GRU) called Light-GRU[5] and the biologically plausible learning rule AuGMEnT[7]. The architecture consists of three layers: an input layer, a memory layer with candidate input, gating and memory units, and an output layer that maps memories onto Q-values. Memory units in RECOLLECT learn to represent task-relevant information as persistent activity. These memories are altered or erased at the appropriate time points, for example when a new trial has started. As in Light-GRU[5], memory units have one gate, which both manages the degree to which previous memory is retained and how much new information from candidate input units enter the memory. Once the memory has been updated, memory units

project towards output units that compute the Q-values of actions. Finally, actions are determined by a mechanism biased towards the action with the highest Q-value.

While recurrent neural networks tend to be trained with backpropagation-through-time, which utilises non-local gradients, RECOLLECT employs the AuGMEnT learning rule[7]. Synapses that contributed to the winning action of the network are tagged by means of an attentional feedback signal. Only tagged synapses are plastic and sensitive to a reward prediction error (difference between successive Q-values), delivered in the form of a global neuromodulatory signal. The gradients that are required to update the synapses are stored in synaptic traces. Therefore, each unit has access to all gradient information that is required to update its weights locally, enabling
the network to learn in a biologically plausible manner.

RESULTS AND DISCUSSION

RECOLLECT was able to successfully store task-relevant input into its memory and to sustain these memory representations over increasingly long delays on the saccade/anti-saccade task[8]. Moreover, it learned to flush its memory upon the end of trials to prevent interference with subsequent trials. Aside from its working memory capacity, RECOLLECT also acquired high performance on a two-armed reversal bandit task: a probabilistic choice task where reward probabilities associated with actions were periodically reversed[9]. It learned to initially perform explorative actions to assess which choices yielded the highest rewards, then to consistently choose the most promising action until the next reversal, and to forget previous reward mappings upon reversals. Since it could even perform this task without updating its weights, this demonstrates meta-learning. In conclusion, RECOLLECT is a biologically plausible gated recurrent network model that despite reduced computational complexity is capable of selectively retaining information, as well as learning-to-learn.

ACKNOWLEDGEMENTS

This research has received funding from the European Union's Horizon 2020 Framework Programme for Research and Innovation under the Specific Grant Agreement No. 945539 (Human Brain Project SGA3, Task 3.7).

We acknowledge the use of Fenix Infrastructure resources, which are partially funded from the European Union's Horizon 2020 research and innovation programme through the ICEI project under the grant agreement No. 800858.

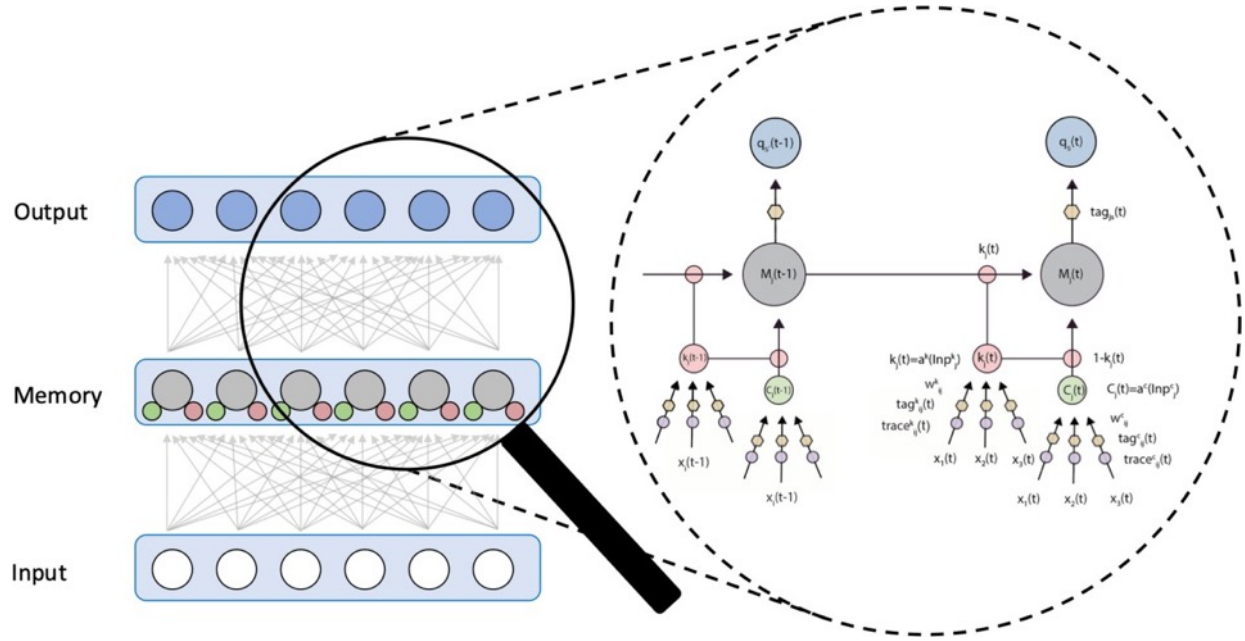

Figure 1. RECOLLECT architecture. Candidate cell units (C_j) and gates (k_j) integrate input and synapse onto memory cells (M_j). Memory cells in turn project to output units (q_k), after which a winner-takes-all mechanism determines the winning unit (q_s). Connections contributing to the winning action are made plastic by means of synaptic tags. Synaptic traces store the gradients for candidate cell states and gates, thereby making local updates feasible.

Keywords: Recurrent neural network, learning-to-learn, meta-reinforcement learning, gating, working memory, neuroscience, reinforcement learning, computational modelling

REFERENCES

[1] Harlow HF. The formation of learning sets. *Psychological Review*. 1949;56(1):51-65. doi:10.1037/h0062474
[2] Thrun S, Pratt L. Learning to Learn: Introduction and Overview. In: Thrun S, Pratt L, eds. *Learning to Learn*. Springer US; 1998:3-17. doi:10.1007/978-1-4615-5529-2_1
[3] Wang JX, Kurth-Nelson Z, Kumaran D, et al. Prefrontal cortex as a meta-reinforcement learning system. *Nature Neuroscience*. 2018;21(6):860-868. doi:10.1038/s41593-018-0147-8
[4] Lillicrap TP, Santoro A. Backpropagation through time and the brain. *Current Opinion in Neurobiology*. 2019;55:82-89. doi:10.1016/j.conb.2019.01.011
[5] Ravanelli M, Brakel P, Omologo M, Bengio Y. Light Gated Recurrent Units for Speech Recognition. *IEEE Trans Emerg Top Comput Intell*. 2018;2(2):92-102. doi:10.1109/TETCI.2017.2762739
[6] Dey R, Salem FM. Gate-variants of Gated Recurrent Unit (GRU) Neural Networks. *IEEE 60th International Midwest Symposium on Circuits and Systems (MWSCAS)*. 2017:1597-1600. doi: 10.1109/MWSCAS.2017.8053243.
[7] Rombouts JO, Bohte SM, Roelfsema PR. How Attention Can Create Synaptic Tags for the Learning of Working Memories in Sequential Tasks. *PLOS Computational Biology*. 2015;11(3):e1004060. doi:10.1371/journal.pcbi.1004060
[8] Gottlieb J, Goldberg ME. Activity of neurons in the lateral intraparietal area of the monkey during an antisaccade task. *Nat Neurosci*. 1999;2(10):906-912. doi:10.1038/13209
[9] Wang JX, Kurth-Nelson Z, Tirumala D, et al. Learning to reinforcement learn. *arXiv:161105763 [cs, stat]*. Published online January 23, 2017. Accessed August 12, 2020. http://arxiv.org/abs/1611.05763

144. Functional network complexity reflects diverse reward contexts in macaque premotor cortex

Valentina Giuffrida [1], Giampiero Bardella [1], Surabhi Ramawat [1], Isabel Beatrice Marc[1], Roberto Fontana [1], Emiliano Brunamonti [1], Pierpaolo Pani [1], **Stefano Ferraina** [1]*
[1] Department of Physiology and Pharmacology, Sapienza University, Rome, Italy;

Corresponding Author:
Stefano Ferraina* stefano.ferraina@uniroma1.it

Introduction

Motor inhibitory control is one of the executive functions controlled by areas of the frontal lobe in primates. Being able to cancel a movement when required is essential for any action in a dynamic environment. This and other forms of contextual decision-making are dependent on the information provided by the contexts. One experimental task designed to investigate these functions is the stop signal task (SST) [1]. In this standardised paradigm the subjects are required to respond to a Go signal as fast as possible, and to inhibit if an unexpected presentation of a Stop signal during the reaction time (RT) occurs. However, how context dependent information influences the neural dynamics underlying the level motor preparation is still unknown.

Methods

We recorded neuronal activity from the dorsal premotor cortex (PMd) of monkeys while they performed a modified version of the SST, as detailed in [2]. The task consisted of two trial types namely Go and Stop trials, and three different conditions depending on the reward values associated with the correct response to each trial: Go+, Stop+ and Neutral. While the Neutral condition offered an equal amount of reward for correct Go and Stop trials, the Go+ and Stop+ conditions offered an uneven reward. Compared to the Neutral condition, the reward in the Go+ was higher on successful Go trials and lower on successful Stop trials; in the Stop+, reward was the reversed, higher on successful Stop trials and lower on successful Go trials. We characterised the fractal topology of the PMd functional network built from the linear synchronization (Pearson's correlation, C) between well isolated single unit activity (SUA) in two specific task epochs (before and after the Go signal) and two specific task conditions. This approach provided an NxN (N = number of neurons) correlation matrix, the generic entry of which is the Cij between the i-th and j-th SUA time series in the chosen time window. We then interpreted the correlation matrix as the adjacency matrix of an undirected weighted graph, in which the nodes are the neurons and the weighted edges are the pairwise Cij. To quantify the topology of the network and to characterize its fractal properties across the different reward contexts of the task we employed the node-based multifractal analysis framework (NMFA) on the thresholded matrices according to percolation analysis [3;4]. NMFA, recently proposed by Xiao and colleagues [5], is a robust mathematical framework that provides a formal way to quantify the fractal properties of a network, thereby capturing the multi-scale details of its topology. It discloses the high-order connectivity patterns encrypted in the network structure and links them with its underlying intrinsic functionalities across task conditions. The main output of the NMFA is a curve, called the multifractal spectrum, f(α). The parameter α accounts for the level of complexity intrinsic to the network and therefore, f(α) describes how such complexity is distributed within the network. The degree of intrinsic complexity can be then easily expressed by a single number, α0, that is defined as the abscissa corresponding to the maximum of f(α) [6].

Results and Discussion

Figure 1 shows the normalised population SUA of correct Go trials across task conditions and epochs obtained from 68 neurons of one example recording sessions.The mean SUA is influenced by the reward context as signified by the different RTs of Go+ and Stop+ conditions. Figure 2A and 2B show f(α) and the degree of complexity α0 compared across task conditions between epochs. Results show that the neuronal dynamics in the PMd network exhibits a more

complex fractal structure during Stop+ compared to Go+ condition (One-way Anova: p<.04). We attribute the increased complexity of the Stop+ condition to the different reward contexts provided by the Cue.

Keywords: decision-making, reward, single neurons, functional connectivity, graph theory, network analysis

REFERENCES

[1] Logan, G. D., and Cowan, W. B. (1984). On the ability to inhibit thought and action: A theory of an act of control. Psychol Rev 91. doi: 10.1037/0033-295X.91.3.295

[2] Giamundo M, et al. "Neuronal activity in the premotor cortex of monkeys reflects both cue salience and motivation for action generation and inhibition." *Journal of Neuroscience* 41.36 (2021): 7591-7606.

[3] Bardella, G., Bifone, A., Gabrielli, A., Gozzi, A. & Squartini, T. Hierarchical organization of functional connectivity in the mouse brain: A complex network approach. Sci. Reports 6, 1–11,949 10.1038/srep32060 (2016).

[4] Bardella, G., Pani, P., Brunamonti, E., Giarrocco, F. & Ferraina, S. The small scale functional topology of movement control: Hierarchical organization of local activity anticipates movement generation in the premotor cortex of primates. NeuroImage 207, 10.1016/j.neuroimage.2019.116354909 (2020).

[5] Xiao, X., Chen, H. & Bogdan, P. Deciphering the generating rules and functionalities of complex networks. Sci. Reports 2021 11:1 11, 1–15, 10.1038/s41598-021-02203-4 (2021).

[6] Response inhibition in Premotor cortex corresponds to a complex reshuffle of the mesoscopic information network Bardella G., Giarrocco G, Giuffrida V., Brunamonti E., Pan P.i, Ferraina S. bioRxiv 2021.03.15.435381; doi: https://doi.org/10.1101/2021.03.15.435381 (2023).

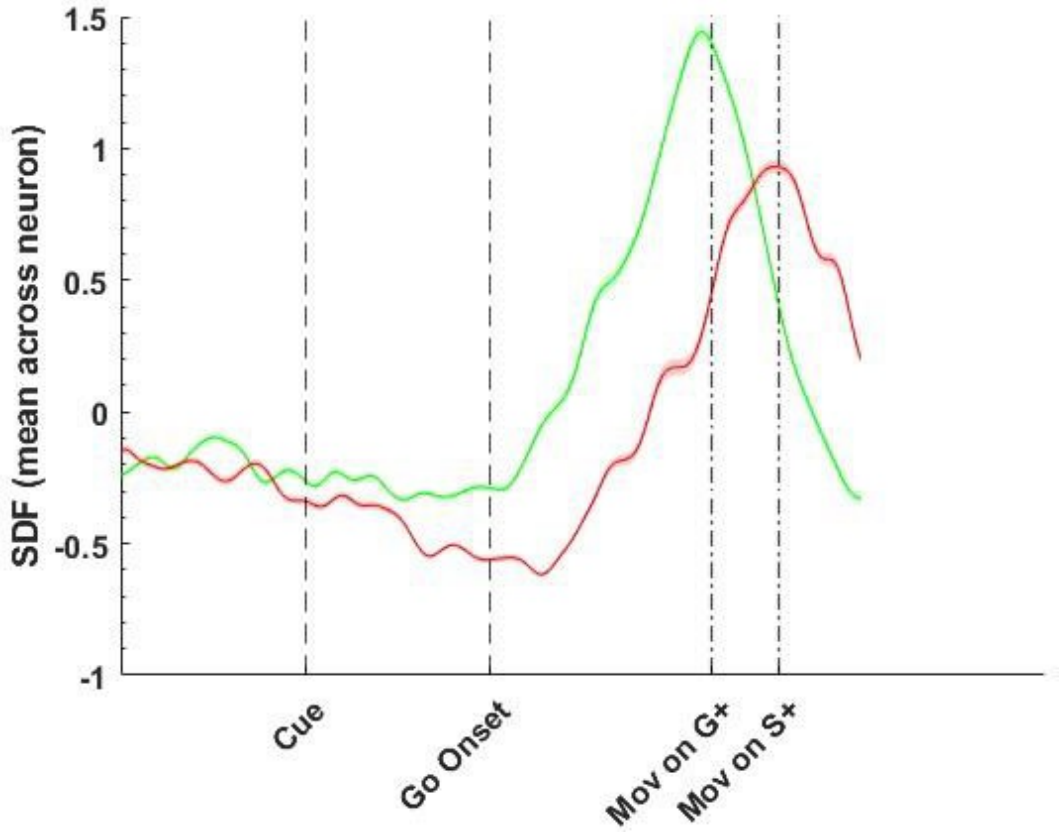

Figure 1: Normalised SUA (mean ± SEM) in the epochs [-500, -100] and [+100, +500] aligned to the Go signal for Go+ (green) and Stop+ (red) conditions. The Y-axis are z-scored units of SUA while the X-axis marks the time in ms. The vertical line labeled *Cue* shows the Cue onset and the line labeled *Go Onset* represents the Go Signal onset. The vertical lines marked *Mov on G+* and *Mov on S+* represent the average Movement onset in Go+ and Stop+ conditions respectively (Mean RT Go+
= 658 ms; Mean RT Stop+ = 785 ms).

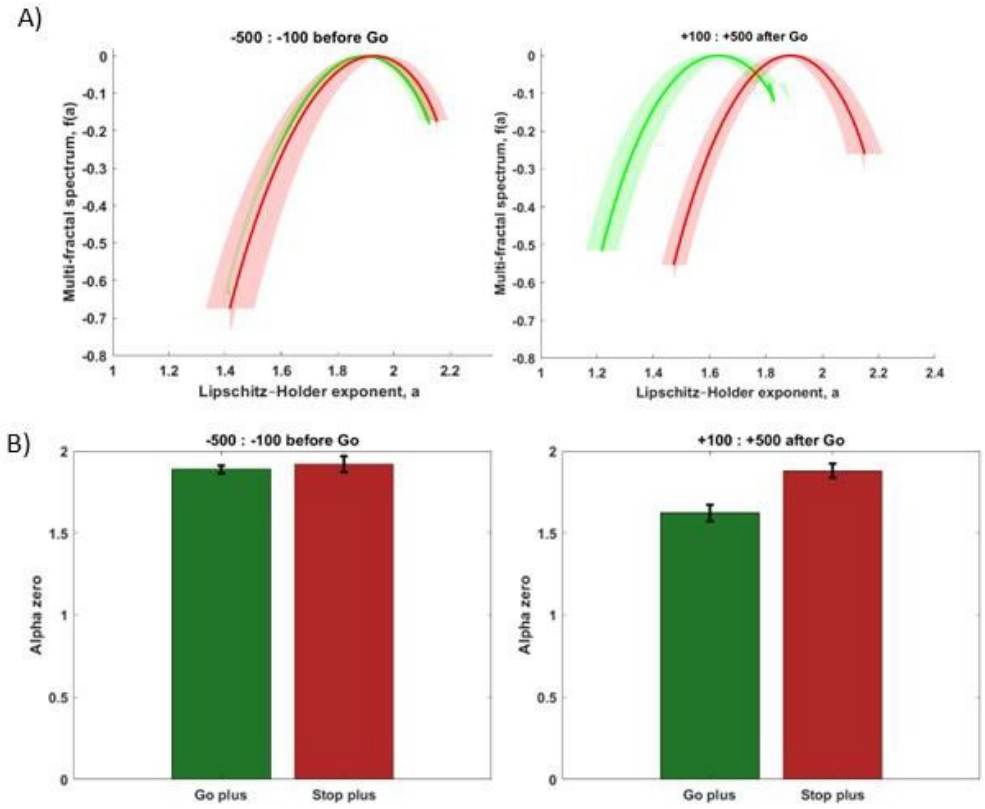

Figure 2: NMFA results: Metrics obtained from the NMFA framework compared across behavioural conditions for the epochs marked in Figure 1. **A)** the multifractal spectrum f(α) compared over epochs for Go+ (green traces) and Stop+ (red traces). **B)** the degree of structural complexity α0 averaged over trials for Go+ and Stop+ conditions.

145. Moth trajectories recorded with a lab-on-cables exhibit a Lévy flight pattern

Dominique Martinez[1,2,*]

[1]Université de Lorraine, CNRS, LORIA, 54000 Nancy, France

[2]ISM, CNRS, 13288 Marseille, France.

[*] Dominique.Martinez@loria.fr

INTRODUCTION/MOTIVATION

Despite their tiny brain, insects exhibit a rich behavioural repertoire in their daily life when foraging for food or searching for mates. Models of search processes are important not only to biology but also to applications in robotics. As an example, the characteristic "cast and surge" path of male moths tracking a pheromone source [1] led to an efficient search algorithm, named Infotaxis [2], which was successfully implemented in olfactory robots [3-4]. When external cues are available, Infotaxis exploits the scarcity of odour encounters to maximize information gain and thereby limit the search time. Yet, when no cue is present or before finding the first cue, random searches might be favoured for their lower computational cost. A special class of random walks, so-called Lévy flight, seems to be optimal for searching under restrictive conditions [5,6]. Lévy flights have been observed in many animals including humans but whether the trajectories of flying moths follow a Lévy distribution is largely unknown. This lack of knowledge is due in part to experimental difficulties in tracking moths of small size and high speed of motion. Here, we take advantage of a new technology, named lab-on-cables [7], to track free-flying moths and analyse their trajectories for correspondence with Lévy flights.

METHODS

To record free-flight trajectories we used a cable-driven robot, a.k.a. lab-on-cables [7]. Reminiscent of the SkyCam or SpiderCam [8] used to cover sports events, the lab rig supporting two cameras is mounted on cables and moves automatically with the insect (Fig. 1). The cables are actuated by motorized winches so as to keep the insect within the moving lab by minimizing the tracking error. The position of the moving lab is computed from the cable lengths. The position of the insect is computed by the embedded stereo-vision system and transmitted wireless to the control computer. To start an experiment, the insect is placed on a takeoff platform at the center of the moving lab. After takeoff, the robot tracks the insect within a workspace of 6 m long by 4 m wide and 3 m high and the insect trajectory is recorded. For analysis, the trajectories are described as a sequence of flight segments of relatively straight motion interspersed by abrupt turns. The turns are identified as changes in flight direction higher

than a given threshold Δθ. The empirical distribution $P(l)$ of the lengths l of the flight segments is plotted in logarithmic scale for correspondence with the theoretical Lévy flight distribution $P(l) \propto l^{-\mu}$. The power-law exponent μ is estimated with a linear fit in logarithmic scale and mean±SD is obtained by averaging the results over different segmentation thresholds Δθ.

RESULTS AND DISCUSSION

We recorded the trajectories of n=32 *Agrotis ipsilon* moths of ~2cm long (Fig. 1 left). Moths flew at a relatively high speed (1-3 m/sec). Moth trajectories are well described by segments of straight flight punctuated by rapid reorientations (Fig. 2 left). The length of flight segments l in logarithmic scale spans over a limited range, i.e. 1-2 decades (Fig. 2 right). The distribution has a power law scaling $P(l) \propto l^{-\mu}$ reminiscent of Lévy flight with $1 < \mu \leq$

3. By varying the segmentation threshold $\Delta\theta$, from 10° to 50°, we estimate the scaling exponent $\mu \approx 2$ (1.94 ± 0.2, mean±SD). The correspondence with Lévy strategies is striking given that a Lévy flight with $\mu = 2$ is optimal in the case of nondestructive targets [5] and performs better than Brownian strategies in the case of destructive moving targets [6]. When comparing our results with theoretical Lévy distribution however, we need to bear in mind that similarity in trajectories does not imply necessarily that the insect brain produces a Lévy search process.

Yet, it is worth noting that $\mu \approx 2$ Lévy walks can emerge from autonomous patterns of neural activity in brain-blocked Drosophila larvae [9].

REFERENCES

[1] Kennedy J.S., Marsh D. (1974) Pheromone-regulated anemotaxis in flying moths. *Science*, 184(4140):999- 1001. doi: 10.1126/science.184.4140.999

[2] Vergassola, M., Villermaux, E., and Shraiman, B. I. (2007) Infotaxis as a strategy for searching without gradients. *Nature* 445, 406–409. doi: https://doi.org/10.1038/nature05464

[3] Martinez D. (2007). On the right scent. *Nature* 445, 371–372. doi: https://doi.org/10.1038/445371a

[4] Moraud E.M and Martinez D. (2010). Effectiveness and robustness of robot infotaxis for searching in dilute conditions. *Front. Neurorobot.* 4:1. doi: 10.3389/fnbot.2010.00001

[5| Viswanathan G.M., Buldyrev S.V., Havlin S., Da Luz M.G.E., Raposo E.P., and Stanley H.E. (1999) Optimizing the success of random searches. *Nature* 401(6756):911–914, 1999. doi: https://doi.org/10.1038/44831

[6] Bartumeus F., Catalan J., Fulco U.L., Lyra M.L., Viswanathan G.M. (2002) Optimizing the encounter rate in biological interactions: Lévy versus Brownian strategies. Phys Rev Lett. 88(9):097901. doi: 10.1103/PhysRevLett.88.097901

[7| Pannequin R., Jouaiti M., Boutayeb M., Lucas P. and Martinez D. (2020) Automatic tracking of free-flying insects using a cable-driven robot. *Science Robotics* 5, eabb2890. DOI: 10.1126/scirobotics.abb2890

[8| Cone L.L., Skycam, an aerial robotic camera system. Byte magazine 10, 122–132, 1985

[9] Sims D.W., Humphries N.E., Violeta N.H., Berni M.J. (2019) Optimal searching behaviour generated intrinsically by the central pattern generator for locomotion. *eLife* 8:e50316. doi: https://doi.org/10.7554/eLife.50316

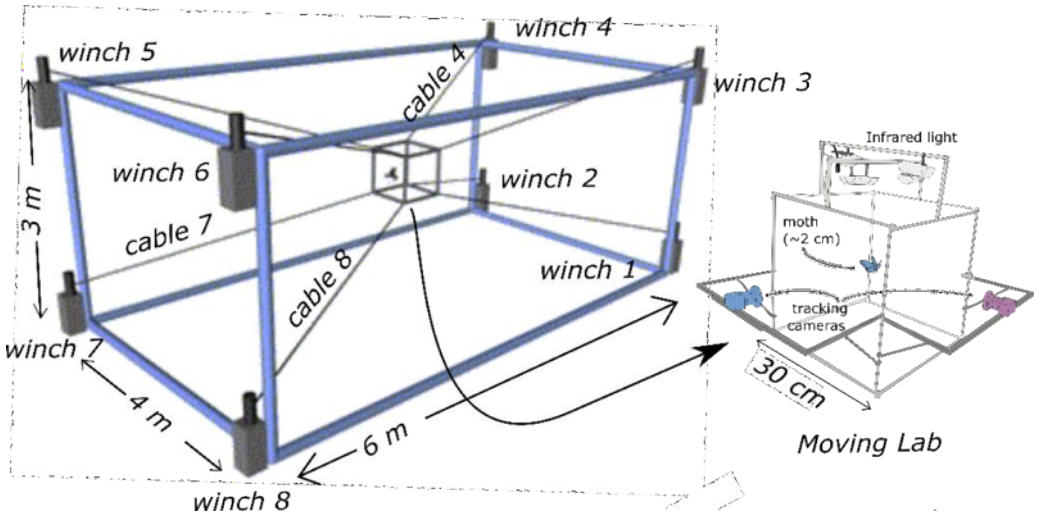

Figure 1. Collecting free-flight trajectories with a lab-on-cables. (Left) cable-driven robot for tracking free-flying insects in a workspace of 6m x 4m x 3m. (Right) Moving lab (30cm x 30cm x 30cm): Effector of the robot supporting the cameras and moving with the insect.

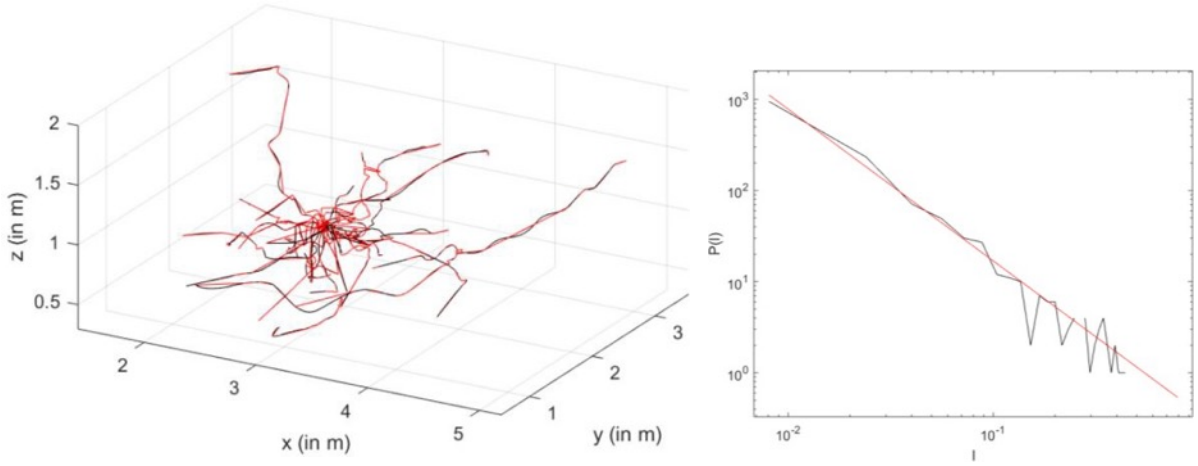

Figure 2. Correspondence with $\mu \approx \mathbf{2}$ Lévy Flights. (Left) Trajectories recorded with the lab-on-cables for n=32 moths. Raw trajectories are in black. Segmented trajectories are in red ($\Delta\theta$ = 10°). (Right) The empirical distribution $P(l)$ of the lengths l of the flight segments is in black. The linear fit with logarithmic scale is in red. The estimate of the exponent in $P(l) \propto l^{-\mu}$ is μ = 1.94 ± 0.2 (mean±SD).

Keywords: insect trajectory, Lab-on-cables, Lévy flight, search process, animal behaviour

ACKNOWLEDGEMENTS

The author thanks R. Pannequin for help with the lab-on-cables and P. Lucas for providing the insects.

146. Digital twin for upper limb closed-loop brain computer interface and exoskeleton neurorehabilitation

Alex Escalera Balcells[1], Hector Lozano[2], Nerea Irastorza[2], Andrea Sarasola[2], Carlos Escolano[1], Ander Ramos[2], Luis Montesano[1]

[1] BitBrain, Zaragoza, Spain

[2] TECNALIA, Basque Research and Technology Association BRTA, Health Unit

alex.escalera@bitbrain.com, hector.lozano@tecnalia.com, nerea.irastorza@tecnalia.com, andrea.sarasola@tecnalia.com, carlos.escolano@bitbrain.com, ander.ramos@tecnalia.com, luis.montesano@bitbrain.com

INTRODUCTION AND MOTIVATION

Near 13 million people all over the world suffer a stroke every year, around 8 million of them survive[1]. Around 85%[2] of them suffer some deficit in motor control due to the lesion. Neurorehabilitation aims to improve the recovery of severe paralysed patients using, for instance, Brain Machine Interfaces (BMI) controlling a neurprosthesis[3] to associate volition and action and promote neuroplasticity[4]. ISMORE is an exoskeleton[5] which implements a closed-loop process where the EEG-based BMI predicts movement intention and the exoskeleton mobilizes the paretic upper limb. Despite promising results, this type of rehabilitation still faces some challenges that include the variability in the brain activity of stroke survivors and the need to better study neuroplasticity mechanisms during the therapy. Indeed, therapy is pre-programed (not personalized) and sometimes slightly adapted iteratively depending on the evolution and response to treatment. The research question is whether the therapy can be fully personalized and optimized to each patient, with the available clinical history and before therapy starts.

This poster reports the progress in implementing a digital twin to personalize and optimize rehabilitation protocols and treatment prognosis. Figure 1 describes the architecture of the twin implementing a closed-loop rehabilitation system in which the biomechanical model and exoskeleton are linked to *The Virtual Brain (TVB)*[6] in a bidirectional way within the *Neuro-Robotics Platform (NRP)*[7]. The TVB supplies efferent information and provides movement directives to the biomechanical system, while the sensory information of the biomechanical system provides feedback to the brain.

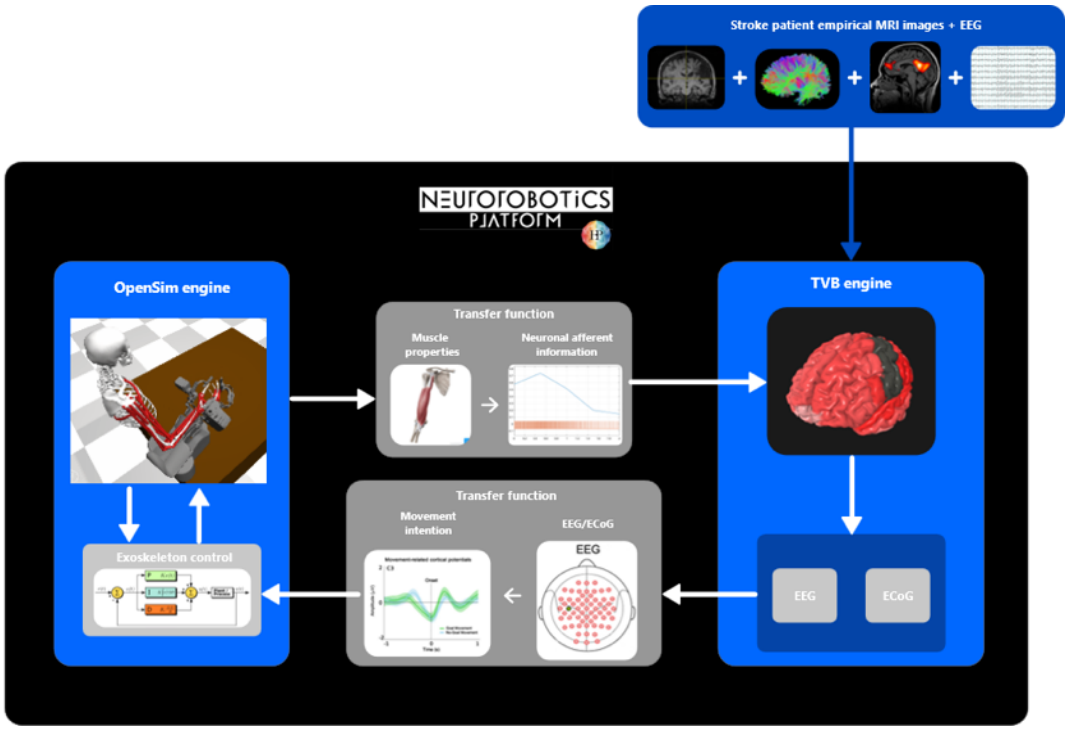

Figure 1: Overall scheme of the digital twin.

METHODS

The virtual twin uses patient neuroimage recordings: 1) MRI and DWI scans performed before the therapy starts to get information of the structural anatomy of the brain; and 2) fMRI, EEG and EMG data collected to get physiological information during motor tasks. Based on this patient anatomic and neurophysiological data, we used OpenSim to build an upper limb biomechanical model (affected by the spasticity of a stroke) coupled with a model of the ISMORE exoskeleton that mobilizes the affected arm.

In addition to this, the TVB was adapted to the patient stroke anatomy by using automated pre-processing tools[8]. We extracted a structural connectome out of the structural and diffusion images and the brain activity out of the fMRI images. The connection between the two HBP engines is done within the NRP. The afferent block models the sensory organs of the muscles and tendons. The efferent system detects movement intention out of the EEG to trigger pre-stablished motor commands executed by the exoskeleton.

RESULTS AND DISCUSSION

The current state of the digital twin development is the following. We have implemented a closed-loop simulator within the NRP that integrates in a coordinated way the TVB, the biomechanical model, and the afferent and efferent module. The TVB simulates BOLD and EEG activity taking in consideration the anatomical structure of the patient brain based on parameters optimized using Bayesian optimization[9] to maximize the correlation with the empirical functional connectivity matrix[10]. Two motor primitives simulate rehabilitation exercises (open-close hand and coordinated reaching), while afferent information in the form of neural action potentials derived from the mechanical properties of muscle length and velocity and tendon tension.

This first digital twin of a neuro-rehabilitation therapy provides opportunities for further research. It highlights the need for a full integrated model that includes volition and interaction with the peripheral nervous as well as as mechanisms to understand, modulate and cope with neural plasticity. Also, it provides simulation tools that can be directly transferred to a real physical system for validation with stroke patients.

Keywords: Neurorehabilitation, closed-loop, exoskeleton, upper limb, stroke, brain simulation, motor tasks.

ACKNOWLEDGEMENTS

This work has been supported by the HBP SGA3. REFERENCES

1. World Stroke Organization (WSO): Global Stroke Fact Sheet 2022. Accessed February 1, 2023. http://ghdx.healthdata.org/gbd-results-tool
2. López-Larraz E, Sarasola-Sanz A, Irastorza-Landa N, Birbaumer N, Ramos-Murguialday A. Brain-machine interfaces for rehabilitation in stroke: A review. *NeuroRehabilitation*. 2018;43(1):77-97. doi:10.3233/NRE- 172394
3. Lo HS, Xie SQ. Exoskeleton robots for upper-limb rehabilitation: State of the art and future prospects. *Med Eng Phys*. 2012;34(3):261-268. doi:10.1016/J.MEDENGPHY.2011.10.004
4. Warraich Z, Kleim JA. Neural Plasticity: The Biological Substrate For Neurorehabilitation. *PM&R*. 2010;2(12):S208-S219. doi:10.1016/J.PMRJ.2010.10.016
5. Sarasola-Sanz A, Irastorza-Landa N, López-Larraz E, et al. A hybrid brain-machine interface based on EEG and EMG activity for the motor rehabilitation of stroke patients. *IEEE International Conference on Rehabilitation Robotics*. Published online August 11, 2017:895-900. doi:10.1109/ICORR.2017.8009362
6. Sanz-Leon P, Knock SA, Spiegler A, Jirsa VK. Mathematical framework for large-scale brain network modeling in The Virtual Brain. *Neuroimage*. 2015;111:385-430. doi:10.1016/J.NEUROIMAGE.2015.01.002
7. Falotico E, Vannucci L, Ambrosano A, et al. Connecting artificial brains to robots in a comprehensive simulation framework: The neurorobotics platform. *Front Neurorobot*. 2017;11(JAN):2. doi:10.3389/FNBOT.2017.00002/BIBTEX
8. Schirner M, Rothmeier S, Jirsa VK, McIntosh AR, Ritter P. An automated pipeline for constructing personalized virtual brains from multimodal neuroimaging data. *Neuroimage*. 2015;117:343-357. doi:10.1016/J.NEUROIMAGE.2015.03.055
9. Martinez-Cantin R. BayesOpt: A Bayesian Optimization Library for Nonlinear Optimization, Experimental Design and Bandits. *Journal of Machine Learning Research*. 2014;15:3915-3919. Accessed February 1, 2023. https://bitbucket.org/rmcantin/bayesopt/
10. Falcon MI, Riley JD, Jirsa V, et al. The virtual brain: Modeling biological correlates of recovery after chronic stroke. *Front Neurol*. 2015;6(NOV):228. doi:10.3389/FNEUR.2015.00228/BIBTEX

147. Enhancing Neuroscience Research with Intuitive GUI Widgets in EBRAINS lab

Lia Domide[1]*, Sandra Diaz-Pier[2], Jan Fousek[3], Paula Prodan[1], Romina-Ioana Băilă[1], David Bacter[1], Rareş-Liviu Horge[1], Maria-Teodora Mişan[1], Jochen Mersmann[1]

[1] CODEMART, Cluj-Napoca, Romania

[2] Simulation and Data Lab Neuroscience - Jülich Supercomputing Centre, Jülich, Germany

[3] Institut de Neurosciences des Systèmes (INS), Inserm, Aix-Marseille University, Marseille, France

* lia.domide@codemart.ro

INTRODUCTION/MOTIVATION

The showcases developed in the last phase of the HBP are meant to illustrate the full potential of technical and scientific features offered by EBRAINS. In order to support the usability of the showcases, as well as future EBRAINS workflows, we have developed a set of modular graphic components and software solutions [1] which can be easily deployed or replicated in the EBRAINS Collaboratory within the JupyterLab.

These graphical user interfaces (GUI) components are all based on and under open source licences, supporting open neuroscience and they enable features like:

- Easy setup of models and region specific or cohort simulations
- Selection of Data sources and their links to models.
- Querying data from Siibra and the Knowledge Graph.
- Deployment and monitoring jobs on HPC resources.
- Integration of a subset of the virtual brain [2] analysis and visualisation tools [3].

METHODS

The graphical components developed, called tvb-widgets, are designed to be integrated into cells of notebooks or are part of JupyterLab extensions for direct usage in the EBRAINS Collaboratory as independent panels (Fig 2) with an appealing look and feel (3D display and interaction: Fig 1, reactive UI, drag&drop events).

The solution is modular, easy to extend and applicable to multiple showcases within EBRAINS.

For the development of these modules, we choose a Data Centred Architecture, where data is annotated, and accessed independently by the satellite components which can read or modify it. We introduce a hierarchical representation with flexible types for data and its metadata [2]; the components access shared data structures and are relatively independent —they interact only through data exchange; we get automatic orchestration as a possibility.

RESULTS AND DISCUSSION

The storyline of a showcase would start from the structural data of a patient (or cohort). HeadWidget, from the tvb-widgets module, allows the user to scroll through a Drive or Bucket, load compatible DataTypes in a 3D display, overlap multiple such structures, show them with an opacity slider, and slightly manipulate them.

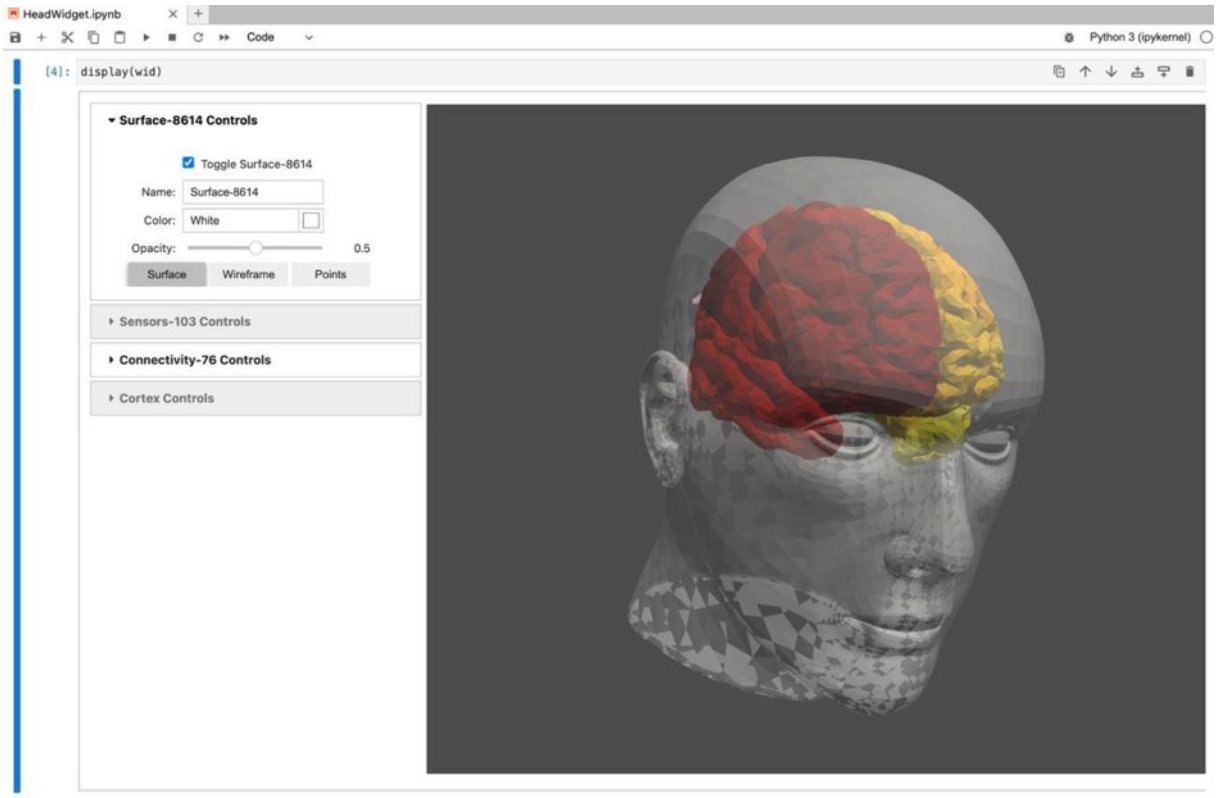

Fig.1: HeadWidget allows displaying overlapped multiple structural elements from a case, and to interact in 3D space.

tvb-ext-xircuits module would follow logically, and allow the user to build a showcase. Technically it is a JupyterLab extension[4] offering a graphical interface for creating, analysing and executing workflows inside the EBRAINS Lab. It allows users to utilise EBRAINS capabilities through a graphical programming paradigm.

The main feature of the module is the creation of workflows, by dragging components onto a canvas area and linking them together. Each component can be configured through direct input values or graphical widgets, and the users choose between executing the workflow locally or remotely on an HPC node. For each HPC execution, a job is created and submitted and it can be monitored using tvb-ext-unicore.

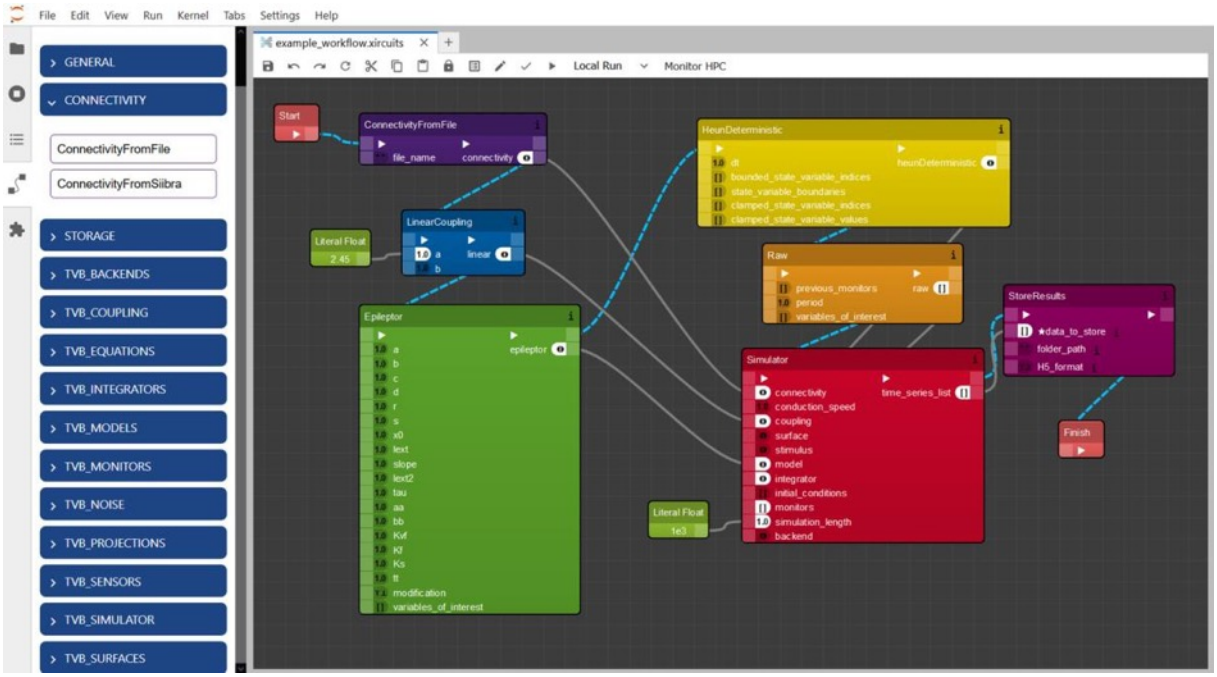

Fig.2: tvb-ext-xircuits offers an easy graphical interaction with operations and data flows directly in EBRAINS lab

tvb-ext-unicore is an EBRAINS lab extension developed to add a GUI to the py-unicore API. This extension uses reactive graphical elements for auto-refreshing status of tasks, granting the user possibility to cancel a running job and most importantly downloading results fast from the HPC to EBRAINS lab or a local user environment.

tvb-ext-bucket is another novel EBRAINS lab extension providing a file browser for the Data-Proxy straight into jupyter lab while bringing the power of drag & drop to manage files from and into local storage, EBRAINS Drive or Data-Proxy. This software completes the flow cycle, by allowing users to easily push or pull results into and from archiving for other operations.

With the development of these tools we provide users with new means to approach the EBRAINS infrastructure, make better and easier use of HPC and the showcases. We address some critical interfaces in EBRAINS such as integration of data into simulations, deployment of computing tasks to HPC, as well as visualisation and analysis of input/output data.

Keywords: widgets, showcases, JupyterLab, GUI, Datatype, virtual brain, HPC, open source

ACKNOWLEDGEMENTS

- H2020 Research and Innovation Action Grant Human Brain Project SGA3 945539
- Aix University, Marseille, Prof Dr Viktor Jirsa, Director, Institut de Neurosciences des Systèmes (INS)
- HBP Technical team for their support in deploying on EBRAINS and for other linked software modules
- We acknowledge the use of Fenix Infrastructure resources, which are partially funded from the European Union's Horizon 2020 research and innovation programme through the ICEI project under the grant agreement No. 800858.

REFERENCES

[1] TVB-WIDGETS. Dedicated EBRAINS Collaboratory page with many relevant resources (Github links, demo movies, demo notebook urls). https://wiki.ebrains.eu/bin/view/Collabs/tvb-widgets

[2] P. Sanz Leon, S. A. Knock, M. Woodman, L. Domide, J. Mersmann, A. R. McIntosh, V. Jirsa: *The Virtual Brain: a simulator of primate brain network dynamics, Frontiers in Neuroinformatics* 7:10. doi: 10.3389/fninf.2013.00010.

[3] M. Schirner, L. Domide, D. Perdikis, P. Triebkorn, L. Stefanovski, R. Pai, P. Popa, B. Valean, J. Palmer, C. Langford, A. Blickensdörfer, M. van der Vlag, S. Diaz-Pier, A. Peyser, W. Klijn, D. Pleiter, A. Nahm, O. Schmid, M. Woodman, L. Zehl, J. Fousek, S. Petkoski, L. Kusch, M. Hashemi, D. Marinazzo, J.-F. Mangin, A. Flöel, S. Akintoye, B. C. Stahl, M. Cepic, E. Johnson, G. Deco, A. R. McIntosh, C. C. Hilgetag, M. Morgan, B. Schuller, A. Upton, C. McMurtrie, T. Dickscheid, J. G. Bjaalie, K. Amunts, J. Mersmann, V. Jirsa, P. Ritter - *Brain simulation as a cloud service: The Virtual Brain on EBRAINS* - NeuroImage 2022, doi.org/10.1016/j.neuroimage.2022.118973.

[4] XIRCUITS. An open source Jupyter lab extension with generic workflows. Original code is here: https://github.com/XpressAI/xircuits and our customised fork for EBRAINS lab usage is here: https://github.com/the-virtual-brain/tvb-ext-xircuits

148. Bringing the Analysis Workflow for 3D-PLI Data with Oblique Measurements to HPC

Benning, Kai[1,2*]; Matuschke, Felix[1]; Müller, Andreas[3]; Schober, Martin[1]; Kooijmans, Roxana[1,4]; Amunts, Katrin[1,5]; Axer, Markus[1,2]

[1]Institute of Neuroscience and Medicine-1 (INM-1), Forschungszentrum Jülich, Jülich, Germany [2]Department of Physics, School of Mathematics and Natural Sciences, Bergische Universität Wuppertal, Wuppertal, Germany

[3] Simulation and Data Lab Neuroscience, Jülich Supercomputing Centre, Institute for Advanced Simulation, Forschungszentrum Jülich, Jülich, Germany

[4]Vision and Cognition, Netherlands Institute for Neuroscience, The Dutch Academy for Arts and Science, Amsterdam, The Netherlands

[5]C. and O. Vogt Institute for Brain Research, Medical Faculty, Heinrich-Heine University Düsseldorf, Düsseldorf, Germany

*k.benning@fz-juelich.de

INTRODUCTION

3D Polarized Light Imaging (3D-PLI) enables the reconstruction of the brain's fiber architecture at micrometer resolution[1–4]. By measuring the transmitted light intensity of polarized light through unstained histological sections, the in-plane orientation (Direction) of both myelinated and unmyelinated fibers and their respective birefringent strength (Retardation) can be obtained. Recently, we have built 3D-PLI microscopes that provide additional measurements from oblique views. This makes the determination of the fibers' out-of-plane orientation (Inclination) possible due to the varying Direction and Retardation because of the change in perspective. Therefore, every scanned voxel can be attributed to a 3D fiber orientation vector.

In recent years, the analysis of 3D-PLI data obtained under oblique views has been enabled by applying Least- Squares Analysis[5] and refined by the introduction of a Bayesian approach with prior Markov-Chain Monte-Carlo (MCMC) Sampling[6,7] to obtain point estimates of orientation as well as credible intervals of 3D fiber orientation angles. While these algorithms were validated on a limited number of brain sections, their application to a series of 3,000 sections (covering an entire human brain) needs a well-defined automated high-performance computing (HPC)-based workflow. Here, we present a working implementation of such a workflow.

METHODS

A deep-frozen brain is cut into 50 µm thin sections using a cryostat-microtome. During sectioning, Blockface images are acquired and serve as a volume reconstruction target. The unstained brain sections undergo 3D-PLI scanning[1,2] (Figure 1, Step 1) under one flat and four oblique views. The resulting five image stacks are calibrated to address inhomogeneities in the illumination of the sample (Figure 1, Steps 2 and 3).

Next, Fourier analysis is applied to obtain the sample's Transmittance, Direction, and Retardation maps[1,2]. The resulting Transmittance of the flat measurement can be used as the moving image in the registration process to the undistorted space of the Blockface images (Figure 1, Step 4). In a pre-masking step, laboratory labels and sealing marks are eliminated (Figure 1, Step 5). This is a prerequisite for the Gray Matter-White Matter (GM- WM) segmentation[8] (Figure 1, Step 6) and the denoising step (Figure 1, Step 8) because both algorithms are based on the statistics of the image pixels[7,9]. Furthermore, the different perspectives of the oblique views must be accounted for to allow voxel-wise analysis (Figure 1, Step 7).

The directional analysis consists of a point estimate of each orientation for each measurement voxel, following the estimation of Credible Intervals (Figure 1, Step 9). While the Least Square Fitting can be performed on unmasked measurement stacks, the Bayesian approach is only performed on a representative subset of the image[7]. In the final step, the point estimates of the 3D fiber orientations are combined and visualized in the fiber orientation map (Figure 1, Step 10).

The automatic registration of the histological measurement to the Blockface image and the WM-GM segmentation enables easy reconstruction of the 3D volume inside the undistorted laboratory space (Figure 2, upper row) and enables the reconstruction of the obtained voxel-wise fiber orientations (Figure 2, lower row) with respect to this reference. It creates an interface for further integration and comparison of microscopical and MR data.

RESULTS AND DISCUSSION

The presented workflow enables efficient usage of Jülich's JURECA supercomputer and storage facilities as provided by FENIX[10]. In its current state, it utilizes CPU and GPU resources. Consequently, the automated processing of 3D-PLI images without manual intervention has been achieved and is now applicable to large-scale datasets.

FIGURE 1

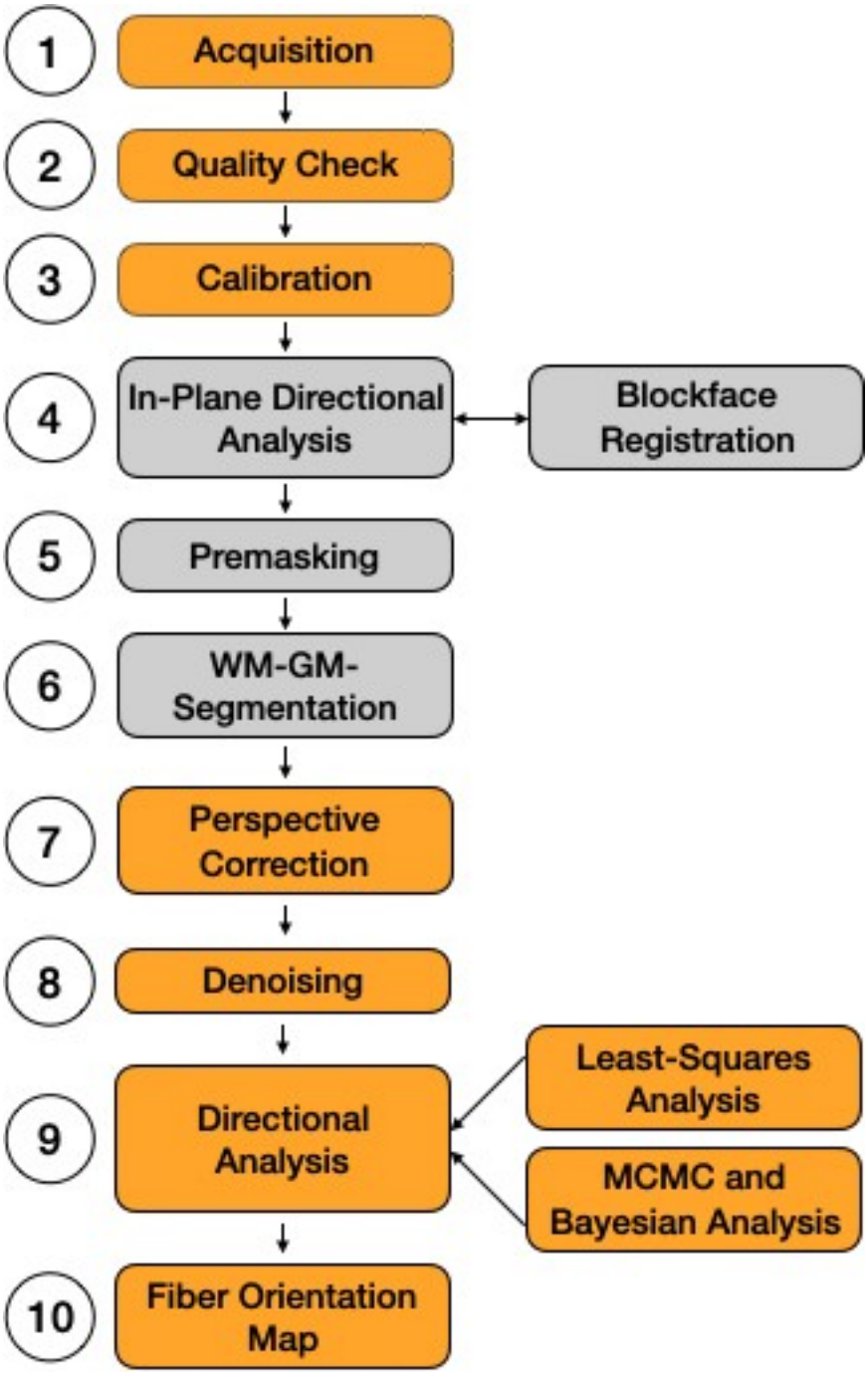

Figure 1: Workflow diagram of the Analysis Workflow of 3D-PLI Data with oblique views: The yellow steps require both the flat views and the oblique views, while the grey ones utilize the flat views only.

FIGURE 2

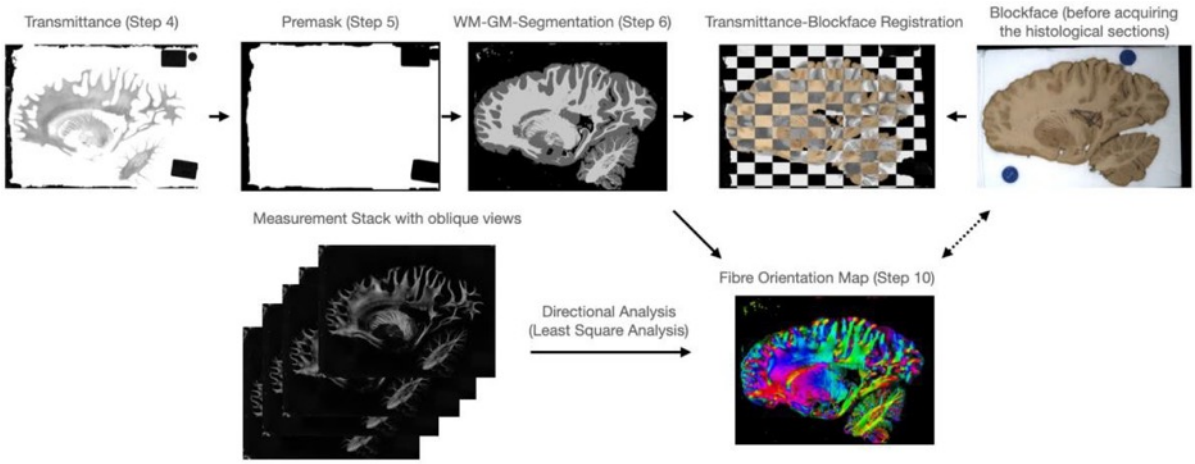

Figure 2: Segmentation and Alignment of 3D-PLI Data: The Transmittance image is registered to the Blockface image for spatial reference. Additionally, Premasking and WM-GM-Segmentation allow further anatomical comparisons. The Directional Analysis resulting in the Fiber Orientation Map (FOM) can be warped to the Blockface space by applying the transformation yielding from the first row.

Keywords: Polarized Light Imaging, Workflow, Histological Sections, HPC, Directional Analysis

FUNDING

This project has received funding from the European Union's Horizon 2020 Framework Program for Research and Innovation under the Specific Grant Agreement No. 945539 (Human Brain Project SGA3).

ACKNOWLEDGEMENTS

The authors gratefully acknowledge the computing time granted through JARA on the supercomputer JURECA at Forschungszentrum Jülich.

REFERENCES

1. Axer M, Amunts K, Grässel D, et al. A novel approach to the human connectome: Ultra-high resolution mapping of fiber tracts in the brain. *NeuroImage*. 2011;54(2):1091-1101. doi:10.1016/j.neuroimage.2010.08.075

2. Axer M, Grässel D, Kleiner M, et al. High-Resolution Fiber Tract Reconstruction in the Human Brain by Means of Three-Dimensional Polarized Light Imaging. *Front Neuroinform*. 2011;5. doi:10.3389/fninf.2011.00034

3. Axer M, Amunts K. Scale matters: The nested human connectome. *Science*. 2022;378(6619):500-504. doi:10.1126/science.abq2599

4. Stacho M, Herold C, Rook N, et al. A cortex-like canonical circuit in the avian forebrain. *Science*. 2020;369(6511):eabc5534. doi:10.1126/science.abc5534

5. Schmitz D, Muenzing SEA, Schober M, et al. Derivation of Fiber Orientations From Oblique Views Through Human Brain Sections in 3D-Polarized Light Imaging. *Front Neuroanat*. 2018;12:75. doi:10.3389/fnana.2018.00075

6. Schmitz D, Lippert T, Amunts K, Axer M. Quantification of fiber orientation uncertainty in polarized light imaging of the human brain. 2020;11312:1131239. doi:10.1117/12.2548935

7. Schmitz D, Benning K, Schubert N, Minnerop M, Amunts K, Axer M. Fast data-driven computation and intuitive visualization of fiber orientation uncertainty in 3D-polarized light imaging. *Front Phys*. 2022;10:958364. doi:10.3389/fphy.2022.958364

8. Reuter JA, Menzel M. PLImig (PLI Mask and Inclination Generation). https://github.com/3d-pli/PLImig

9. Benning K, Menzel M, Reuter JA, Axer M. Independent Component Analysis for Noise and Artifact Removal in Three-Dimensional Polarized Light Imaging. In: Amunts K, Grandinetti L, Lippert T, Petkov N, eds. *Brain- Inspired Computing*. Lecture Notes in Computer Science. Springer International Publishing; 2021:90-102. doi:10.1007/978-3-030-82427-3_7

10. Alam SR, Bartolome J, Carpene M, Happonen K, Lafoucriere JC, Pleiter D. Fenix: a Pan-European federation of supercomputing and cloud e-infrastructure services. *Commun ACM*. 2022;65(4):46-47. doi:10.1145/3511802

149. Synaptic proteome database and Bioconductor tools Synaptome.db and BioNAR to facilitate building and analysis of customised synaptic PPI networks

Oksana Sorokina[1*], Colin McLean[4], Anatoly Sorokin[2], T. Ian Simpson[1], J Douglas Armstrong[1,3]

[1] School of informatics, University of Edinburgh, UK., [2] Biological Systems Unit, Okinawa Institute of Science and Technology, Okinawa, Japan, [3]Computational Biomedicine Institute (IAS-5 / INM-9), Forschungszentrum Jülich, Jülich, Germany. [4]Health Economics and Data Science at the Institute for Genetics and Cancer, University of Edinburgh, UK

*To whom correspondence should be addressed.

Introduction

The proteomes of the presynaptic and postsynaptic compartments mediate information processing in the brain via complex and highly dynamic molecular networks. We curated 58 proteomic studies from 2000 to 2021, to produce a comprehensive dataset describing >8000 proteins expressed at the mammalian synapse[1].

Each synaptic component was annotated with relevant metadata based on the respective study (author, year, method, subcellular compartment and brain region) and associated with function and disease information according to Gene Ontology and Human Disease Ontology. Furthermore, the protein–protein interactions (PPI) were obtained based on combined human, mouse and rat data from publicly available databases. The resulting database/network model is available in a SQLite implementation (SynaptomeDB) from Edinburgh
DataShare https://doi.org/10.7488/ds/3771 and EBRAINS.

To make the database widely accessible we developed synaptome.db package, which allows building customised synaptic PPI networks based on metadata [2]. To support and facilitate further analysis of obtained PPI networks with respect to disease-related molecular complexes we developed the package BioNAR. Both packages are available from Bioconductor release 3.16:
https://bioconductor.org/packages/release/bioc/html/BioNAR.html and
https://bioconductor.org/packages/release/data/annotation/html/synaptome.db.html.

Results

Synaptome db. enables direct access to the data from within the R environment, providing a simple API for extracting the data from the database. Main functionalities include:

- Information about specific genes, including the most frequent user queries: When? and by whom? was my favourite gene (or list of genes) identified? Was my gene/list found pre- or post-synaptically? and how often? Was it found in a specific brain region? and which diseases it is associated with?
- Prioritisation. Synaptome.db allows extracting the "most likely synaptic" subset of proteins in each dataset, enabling custom filters for the proteins that have been identified more frequently than others, thus, may correspond to higher confidence synaptic networks.
- Building customised PPIs. The package supports the extraction of PPIs for the gene list (list of EntrezIDs or gene names) or entire compartment/brain region and their export in a form of a network graph or a table.

To enable rapid and systematic analysis of biologic networks we designed **BioNAR.** The package integrates and complements existing R packages and fills the methodological gaps necessary to interrogate biomedical networks with respect to functional and disease domains. As a result, we provide a detailed topologically based network analysis pipeline, enabling the researcher to load networks generated and/or annotated using their lab's own meta-data, thus making the tool as widely applicable and flexible as possible. Package allows to predict a protein's impact within multiple complexes, and enables the co-occurrence of meta-data, i.e., diseases and functions, to be estimated across the network and which can identify clusters whose components are likely to share common function and mechanisms.

Figure 1 illustrates the main functionalities of BioNAR.

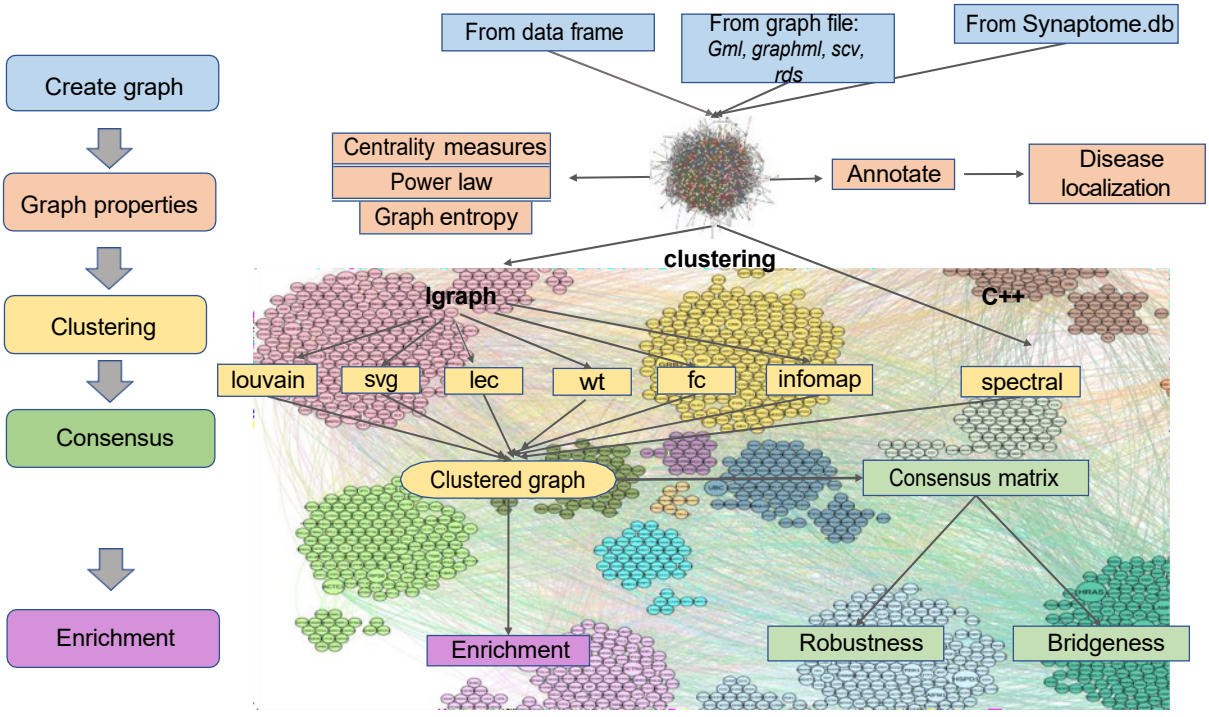

Discussion

We developed synaptome.db package to provide a simple and intuitive access to the SynaptomeDB and allow quick and convenient retrieval of information for specific gene(s) and building the PPIs for synaptic subset on fly. We developed BioNAR package to get useful insight from the PPI network based on topology and metadata, providing new insights into the molecular basis of synaptic transmission and the molecular basis of neurological diseases.

Anowledgement

This research has received funding from the European Union's Horizon 2020 Framework Programme for Research and Innovation [No 945539 (Human Brain Project SGA3)], and Cancer Research UK [No CTRQQR-2021\100006 (Cancer Research UK Scotland Centre)].

1. Sorokina, O., et al., *A unified resource and configurable model of the synapse proteome and its role in disease.* Scientific Reports, 2021. **11**(1): p. 9967.
2. Sorokina, O., A. Sorokin, and J.D. Armstrong, *Synaptome.db: A Bioconductor package for synaptic proteomics data.* Bioinformatics Advances, 2022.

150. Estimating brain connectome for modeling deep brain stimulation effect in Parkinson's disease

Gustavas Davidavicius[1], Paul Jan Triebkorn[2], Andrius Radziunas[3], Jan Fousek[2], Justinas J. Dainauskas[4], Vytautas Kucinskas[4], Daniel K. Wójcik[5], Viktor Jirsa[2], Ausra Saudargiene[4*]

[1]Department of Informatics, Vytautas Magnus University, Kaunas, Lithuania

[2]Institut de neurosciences des systemes, University Aix Marseille Université, Marseille, France

[3]Department of Neurosurgery, Hospital of Lithuanian University of Health Sciences Kauno klinikos, Kaunas, Lithuania

[4]Neuroscience Institute, Lithuanian University of Health Sciences, Kaunas, Lithuania

[5]Nencki Institute of Experimental Biology PAS, Warsaw, Poland

*ausra.saudargiene@lsmuni.lt

INTRODUCTION/MOTIVATION

Parkinson's disease (PD) is a degenerative brain condition in which the patient develops uncontrollable, involuntary movements. The best available treatment to date is deep brain stimulation (DBS) of subcortical nuclei. DBS, if successful can have life-changing improvements in PD symptoms, however, the postsurgical results can vary by a large margin. The main goal of this study is to build personalized PD patient connectomes to be used for simulating brain activity in The Virtual Brain (TVB) platform. The long-term aim is to build a model to predict the outcomes of DBS treatment in PD patients.

METHODS

Ten patients with PD were operated on with subthalamic nucleus (STN) DBS implantation. T1 and diffusion-weighted magnetic resonance images (MRI) were collected before the surgery and a postoperative computerized tomography (CT) scan was performed. Tissue segmentation and reconstruction of cortical surfaces were performed using Freesurfer's recon-all pipeline for processing the structural T1 MRI scan. Diffusion-weighted images were artifact-corrected, constrained spherical deconvolution and tractography was performed using the MRtrix3 toolbox. The structural parcellation of the T1 MRI scan was projected onto the diffusion-weighted images. The Desikan and DISTAL atlases were used to obtain a structural connectome. The precise location of the DBS electrode was identified from the postsurgical CT and projected onto the T1 image.

RESULTS AND DISCUSSION

The PD patient T1 MRI neuroimaging data was used to build an individualized virtual brain model. The brain connectome including subcortical areas of interest for PD – STN, globus pallidus internal, and globus pallidus external, was computed. The resulting virtual brain model was enhanced with the

projection of the DBS electrode, to determine the location and volume of tissue affected by electric stimulation.

The resulting model will be used to model PD patient brain under DBS in the TVB platform. The simulation of the neuronal activity will be achieved by equipping a dynamic neural mass model to every node of the connectome. The virtualized DBS electrodes will be used to model the dynamics of perturbations resulting from the stimulation. Individualized patient virtual brain modelling will improve our understanding of the varying results in the DBS treatment of PD.

Keywords: Parkinson's disease, connectome, deep brain stimulation, The Virtual Brain

ACKNOWLEDGEMENTS

Funded by the EU Horizon 2020 Framework Program Human Brain Project (EBRAINS Voucher Call 2020 project Prediction of neurosurgical treatment outcomes in Parkinson's disease).

151. Normalizing the brain connectome for communication through synchronization

Spase Petkoski*, and Viktor Jirsa

Affiliations: [1]Aix Marseille Univ, INSERM, INS, Inst Neurosci Syst, UMR 1006, Marseille, France

*e-mail-address of corresponding author(s) spase.petkoski@univ-amu.fr

INTRODUCTION/MOTIVATION

Networks in neuroscience determine how brain function unfolds, and their perturbations lead to psychiatric disorders and brain disease. Brain networks are characterized by the connectomes, which comprise the totality of all connections, and are commonly described by graph theory. This approach is deeply rooted in a particle view of information processing, based on the quantification of informational bits such as firing rates. Oscillations and brain rhythms demand, however, a wave perspective of information processing based on synchronization.

METHODS

Networks of oscillators, are often used to study dynamical systems for which the local activity is multidimensional and nonlinear [1]. They have been conceptualized to be responsible for the communication in the brain through coherence [2] and synchronization [3], Fig. 1 (A), but this aspect is still unlinked on the network level to the features of the structural links, i.e. weights and time delays, that shape the synchronization of the brain network [4].

When the time delays are comparable to the timescale of the intrinsic oscillations, they need to be included in the analysis of network dynamics. To go beyond the static representation of networks, we use the insight that the impact of the direct link in the phase difference between oscillators can be separated from the rest of the network. We extend traditional graph theory to a dual, particle-wave, perspective, integrate time delays due to finite transmission speeds, and derive a normalization of the connectome, Fig. 1.

RESULTS AND DISCUSSION

Normalized wave coupling $w^{(f)}_{ij} = w_{ij} \cos \Omega \tau_{ij}$ scales the static weight w_{ij} between the regions i and j at frequency Ω, by including the impact of the time delay τ_{ij}. When applied to the data base of the Human Connectome project, we explain the emergence of frequency-specific network cores including the visual and default mode networks [5], Fig. 2. These findings are robust across human subjects (N=100) [6] and are a fundamental network property within the wave picture.

The normalized connectome comprises the particle view in the limit of infinite transmission speeds and opens the applicability of graph theory to a wide range of novel network phenomena, including physiological and pathological brain rhythms. These two perspectives are orthogonal, but not incommensurable, when understood within the novel here proposed generalized framework of structural connectivity.

Keywords: Synchronization, Time delays, Spectral activation patterns, Resting state networks, Oscillations

ACKNOWLEDGEMENTS

This research was supported by the European Union's Horizon 2020 research and innovation program under grant agreement No. 945539 (SGA3) Human Brain Project, and by grant agreement No. 826421 Virtual Brain Cloud.

REFERENCES

[1] Pikovsky, A., Rosenblum, M., & Kurths, J. (2001). Synchronization : a universal concept in nonlinear sciences. Cambridge University Press.

[2] Fries, P. (2015). Rhythms for Cognition: Communication through Coherence. Neuron, 88(1), 220–235. https://doi.org/10.1016/j.neuron.2015.09.034

[3| Palva, S., & Palva, J. M. (2012). Discovering oscillatory interaction networks with M/EEG: Challenges and breakthroughs. Trends in Cognitive Sciences, 16(4), 219–229. https://doi.org/10.1016/j.tics.2012.02.004

[4] Petkoski, S., & Jirsa, V. K. (2019). Transmission time delays organize the brain network synchronization. Philosophical Transactions of the Royal Society A: Mathematical, Physical and Engineering Sciences, 377(2153), 20180132.

[5] Petkoski, S., & Jirsa, V. K. (2022). Normalizing the brain connectome for communication through synchronization. *Network Neuroscience*, *6*(3), 722-744.

[6] Van Essen, D. C., Smith, S. M., Barch, D. M., Behrens, T. E. J., Yacoub, E., & Ugurbil, K. (2013). The WU-Minn Human Connectome Project: An overview. *NeuroImage*, *80*, 62–79.

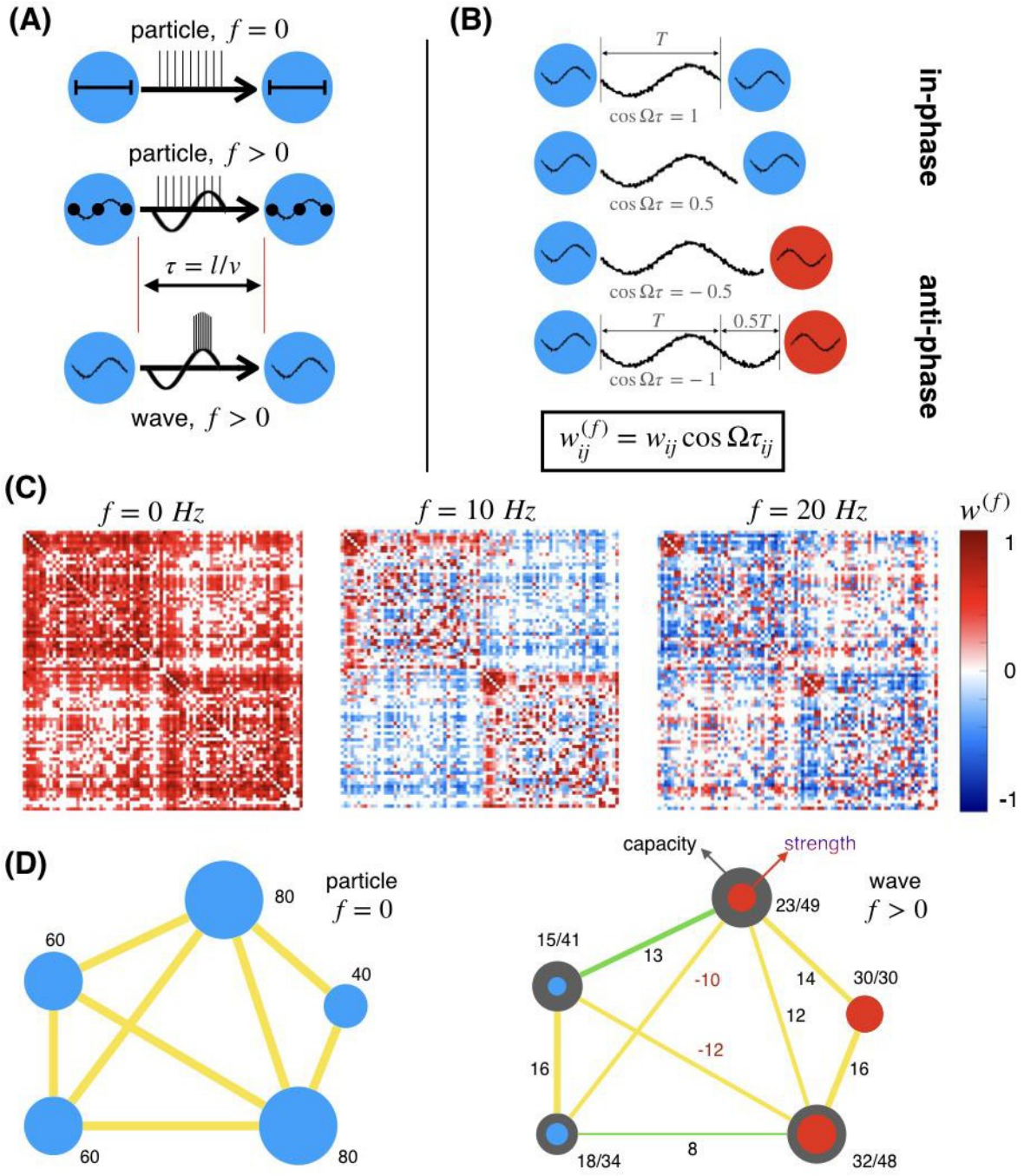

Figure 1. Spatio-temporal network organization and wave coupling weights for synchronized networks. (A) Particle (static or frequency-independent) and wave (synchronization-dependent) interactions with delay τ, due to distance *l*, and propagation velocity *v*. (top) Transmission of packets over non-oscillatory local dynamics; (middle) a particle type of transmission that does not depend on the coherence (e.g. during strong perturbation) and is thus independent of the underlying oscillatory dynamics; (bottom) the communication is dependent on the synchronization. (B) In-and anti-phase synchronization for fixed frequency and different time-delays for 2 oscillators and the wave coupling weight. (C) Wave couplings for a human and connectome at different frequencies. (D) Wave couplings and spectral strength and capacity for a particle and for wave communication. Links contributing positively (negatively) to the synchronization are yellow (green). Lines have width proportional to the absolute wave coupling strength (shown next to the links) and the size of the circles corresponds to the nodes spectral capacity (dark) and strength (colored), both shown for each node.

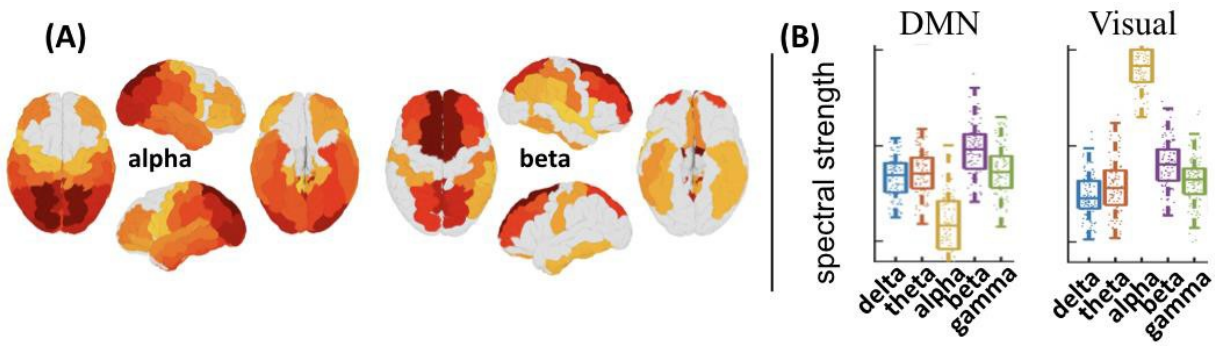

Figure 2. Mean spectral cortical activity of 100 healthy subjects. Mean spectral strength is shown across regions and frequencies, and the proportion of the activation (power) of Visual and Default Mode Networks (DMN) is projected in each of the bands.

152. Frites: a Python package for functional connectivity analysis and group-level statistics of neurophysiological data

Etienne Combrisson[1], Ruggero Basanisi[1], Vinicius Lima Cordeiro[1, 2], Michele Allegra[1, 3, 4], Bruno L. Giordano[1], Andrea Brovelli[1]

1. *Institut de Neurosciences de la Timone, Aix Marseille Université, UMR 7289 CNRS, 13005, Marseille, France*
2. *Institut de Neurosciences des Systèmes, Aix-Marseille Université, UMR 1106 Inserm, 13005, Marseille, France*
3. *Dipartimento di Fisica e Astronomia "Galileo Galilei", Università di Padova, via Marzolo 8, Padova 35131, Italy*
4. *Padua Neuroscience Center, Università di Padova, via Orus 2, Padova 35131, Italy*

Introduction. A standard approach in brain networks analysis involves the characterisation of brain regions and inter-areal interactions that participate in cognitive processes [1]. Here, we present a novel statistical framework and Python toolbox for both the analysis of local task-related activations and functional connectivity (FC) in task-related conditions [2, 3].

Methods and Results. The Python toolbox called *Frites* (Framework for Information Theoretical analysis of Electrophysiological data and Statistics) allows the inference of task-related inter-areal interactions from multi-channel and multimodal neurophysiological signals (M/EEG, intracranial EEG) using information theoretical methods and group-level statistical approaches. Frites is equipped with a set of information theoretic tools for the analysis of interactions between brain signals and their relation with experimental task-related variables. By default, Frites is using the Gaussian Copula Mutual-Information [4] to study the relation between either local brain activity and inter-areal FC with experimental variables (i.e., cognitive tasks). For what concerns FC measures, the toolbox allows the estimate of dynamic (i.e., time-resolve), undirected (e.g., mutual information) and directed (e.g., Granger causality) FC on a single-trial basis [5, 6]. For statistical inferences, the package integrates a non-parametric permutation-based statistical framework to perform group-level inferences on non-negative measures of information. The toolbox includes different methods that cope with multiple-comparison correction problems, such as test- and cluster-wise p-value corrections. The implemented framework also supports both fixed- and random-effect models to adapt to inter-individuals and inter-sessions variability. Frites provides a set of workflows that integrate several analysis steps. Those workflows take as inputs the neural data coming from single or multi-participants (or single / multi sessions), estimate the amount of information shared between the brain data and the external variable, at each brain region and time bins, and finally perform network-level statistical inference, corrected for multiple comparisons. Frites is currently present in the EBRAINS Knowledge Graph and installed in the EBRAINS cloud environment.

Discussion. Frites is a Python software combining information-theoretical approaches with flexible group-level analyses for the investigation of cognitive brain networks. It is now accessible from EBRAINS services and it will be further integrated with future EBRAINS modelling and data analysis

services.

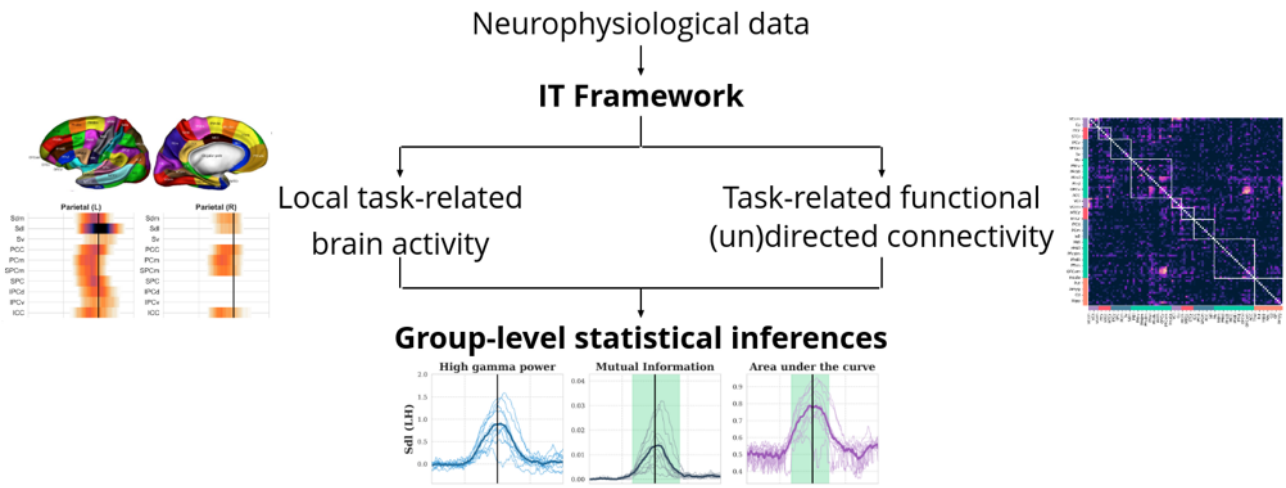

Figure 1. Overall structure of Frites. Frites proposes a single group-level statistical inference and neuroinformatics framework for the analysis of local task-related activations and functional connectivity (FC) measures starting from neurophysiological data (LFP, iEEG, MEG, EEG).

Keywords. Functional connectivity, MEG, EEG, iEEG, LFP, cognition, brain networks, group-level statistics.

References

1. Battaglia D, Brovelli A (2020). Functional connectivity and neuronal dynamics: insights from computational methods. In The Cognitive Neurosciences, Sixth Edition (The MIT Press) by David Poeppel (Editor), George R. Mangun (Editor), Michael S. Gazzaniga (Editor)
2. Combrisson E, Allegra M, Basanisi R, Ince RAA, Giordano BL, Bastin J, Brovelli A (2022). Group-level inference of information-based measures for the analyses of cognitive brain networks from neurophysiological data. Neuroimage, 258:119347. doi: 10.1016/j.neuroimage.2022.119347
3. Combrisson E, Basanisi R, Cordeiro VL, Ince RAA, Brovelli A (2022). Frites: A Python package for functional connectivity analysis and group-level statistics of neurophysiological data. Journal of Open Source Software 7 (79), 3842. doi: 10.21105/joss.03842
4. Ince RAA et al (2016) A statistical framework for neuroimaging data analysis based on mutual information estimated via a Gaussian copula. Human Brain Mapping 38(3):1541-1573. doi: 10.1002/hbm.23471
5. Brovelli A, Badier JM, Bonini F, Bartolomei F, Coulon O, Auzias G (2017). Dynamic reconfiguration of visuomotor-related functional connectivity networks. Journal of Neuroscience, 37(4):839-853. doi: 10.1523/JNEUROSCI.1672-16.2016
6. Brovelli A, Chicharro D, Badier J-M, Wang H, Jirsa V (2015). Characterization of cortical networks and corticocortical functional connectivity mediating arbitrary visuomotor mapping. Journal of Neuroscience, 35(37):12643–12658. doi: 10.1523/JNEUROSCI.4892-14.2015

Keywords

Brain networks, Functional Connectivity, intracranial EEG, MEG,

Acknowledgments

This project/research has received funding from the European Union's Horizon 2020 Framework Programme for Research and Innovation under the Specific Grant Agreement No. 945539 (Human Brain Project SGA3). EC and AB were also supported by the PRC project "CausaL" (ANR-18-CE28-0016).

153. Task T1.12 (WP1): Data-driven and model-based workflows for inference and validation of task-related brain network models

Andrea Brovelli[1], Jules Brochard[2], Marco Celotto[3], Etienne Combrisson[1], Jean Daunizeau[2], Olivier David[4], Gustavo Deco[5,6], Anira Escrichs[5, 6], Matthieu Gilson[1], Jean-Philippe Lachaux[7], Stefano Panzeri[4, 8], Petra Ritter[9]

1. Institut de Neurosciences de la Timone, Aix Marseille Université, UMR 7289 CNRS, 13005, Marseille, France
2. Paris Brain Institute (ICM), Paris, France
3. Neural Computation Laboratory, Istituto Italiano di Tecnologia, Rovereto (TN) 38068, Italy
4. Institut de Neuroscience des Systèmes, Aix Marseille Université, UMR 1106 Inserm, 13005, Marseille, France
5. Computational Neuroscience Group, Center for Brain and Cognition, Department of Information and Communication Technologies, Universitat Pompeu Fabra, Barcelona, Catalonia, Spain.
6. Institució Catalana de la Recerca i Estudis Avancats (ICREA), Barcelona, Catalonia, Spain.
7. Lyon Neuroscience Research Center, EDUWELL Team, INSERM UMRS 1028, CNRS UMR 5292, Université Claude Bernard Lyon 1, Université de Lyon, Lyon F-69000, France
8. Department of Neural Information Processing, Center For Molecular Neurobiology (ZMNH), University Medical Center, Hamburg-Eppendorf, Falkenried 94, D-20251 Hamburg, Germany
9. Berlin Institute of Health at Charité—Universitätsmedizin Berlin, Charitéplatz, Berlin, Germany

Introduction. Our vision is that whole-brain models will lead to ground-breaking applications when they will be able to formalise how perception and action emerge from dynamic interactions between specialised brain regions and circuits. Within WP1 of HBP (SGA3), Task T1.12 aims at providing the theoretical foundations and neuroinformatics tools to: i) infer behaviorally-relevant brain responses, inter-areal interactions and information routing patterns and ii) validate brain models of task-related local activations and network interactions that account for such empirical evidence.

Methods and Results. Here we present an overview of most recent achievements of Task T1.12 linking model-free and model-based approaches for the analysis and modelling of brain network dynamics and interactions. Our approach was tested on data from the Human Intracranial Database (HID), a collection of stereotactic electroencephalography (sEEG) data in epileptic patients, performing eight behavioural tasks [1]. The first study proposes a combined brain-behaviour mediation analysis with statistical models of evoked brain responses to identify which features of brain activity mediate the processing of sensory information and behavioural responses. The shade mediation analysis pipeline was tested on intracranial EEG high-gamma activity (HGA) recorded from epileptic patients, while performing a visual search task and preliminary results are shown at a HBP poster [2]. The second study [3, 4] presents a novel statistical framework and Python toolbox for the analysis of functional connectivity (FC) in task-related conditions. The Python toolbox called *Frites* (Framework for Information Theoretical analysis of Electrophysiological data and Statistics) allows the inference of task-related inter-areal interactions from multi-channel and multimodal neurophysiological signals (M/EEG, intracranial EEG) using information theoretical methods and group-level statistical approaches. Using these tools, we computed group-level FC from iEEG during a visual search task and performed statistical analyses to infer which interareal interactions differentiate between two task conditions that differ in difficulty. The third study introduces a new FC measure, called Feature-specific Information Transfer (FIT), which quantifies how much of the directed information transmitted between neural signals is about specific external target variables, such as a feature of a sensory stimulus S. The FIT measure can be combined with network-level statistical analyses to infer task-related information routing patterns. Results are presented at the poster session of the HBP Summit [5]. The fourth study presents whole-brain model inversion based on FC matrices computed from iEEG data during task-related

conditions [6]. Notably, a whole-brain Hopf model was built using empirical anatomical DTI and iEEG data parcellated according to the MarsAtlas parcellation scheme. The simulated data was calculated using Gaussian-Copula mutual information between each pair of brain areas, and fitting was improved by optimising the effective connectivity (EC). We successfully simulated the empirical sEEG data for different reaction times (fast, middle, and slow) and two difficulty levels of the visual task (easy and hard). We found differences underlying EC, that is, different mechanisms underlying task difficulty levels. The last study was interested in inferring interareal axonal propagation delays and excitatory and inhibitory synaptic time constants at the whole cortical level using neural mass models whose parameters were inverted from iEEG responses to direct cortical stimulations (F-TRACT database) [7]. These new neurophysiological brain maps have been added to the knowledge graph of EBRAINS for re-use in whole brain models, e.g. for informational graph theory analyses [8].

Discussion. Overall, we presented an integrated set of workflows for the analysis and modelling of task-related brain networks. The workflows include both data-driven and model-based methods for inference and validation of task-related brain network models. Several components are already present into EBRAINS and future work will focus on the correct integration within the EBRAINS infrastructures. In particular, future integration initiatives will aim at bridging the gap between additional modelling and validation initiatives within EBRAINS, and potentially integration with the cloud and HPC services of EBRAINS thanks to the collaboration with the team of Petra Ritter.

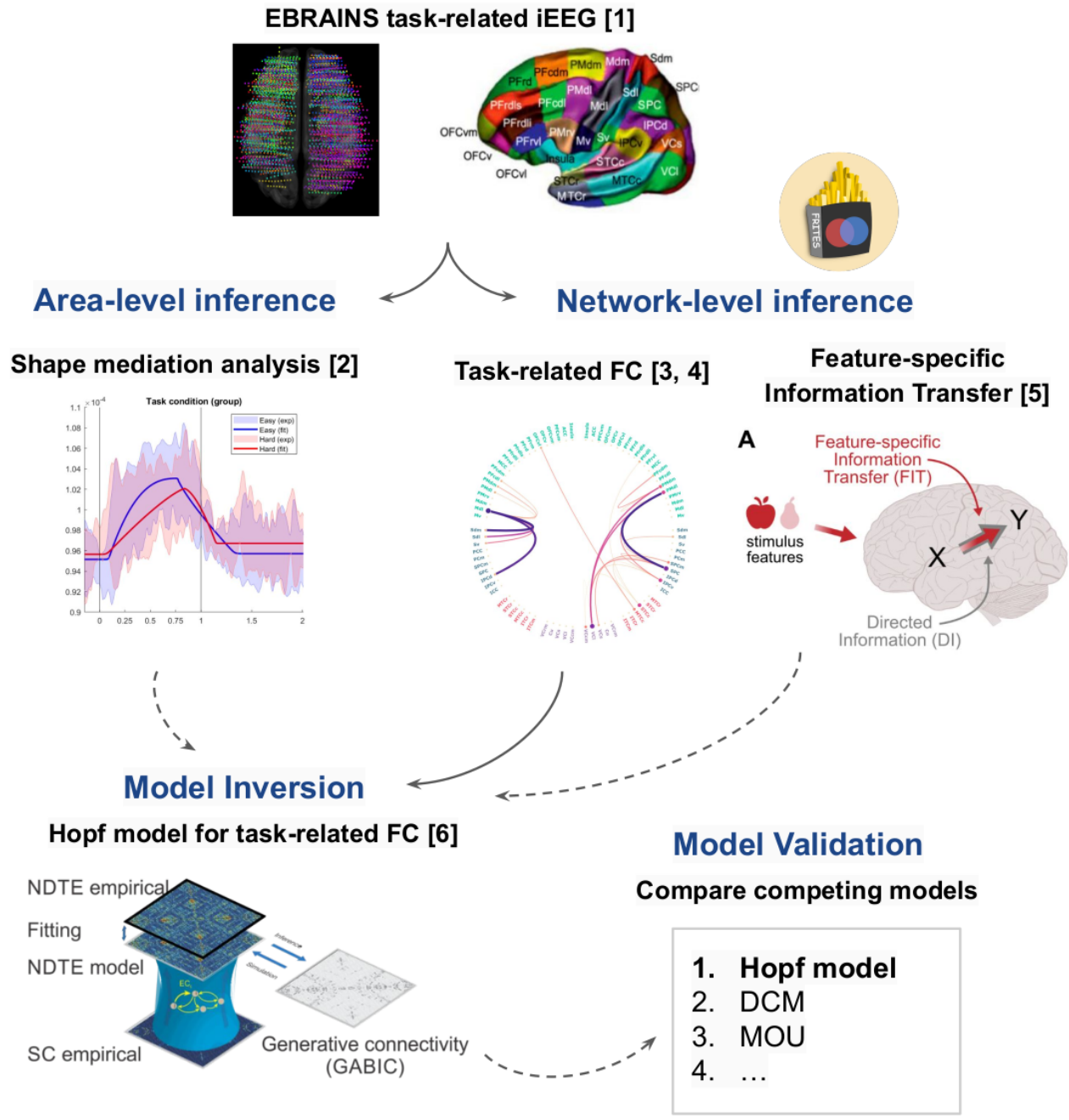

Figure 1. Workflows for inference of network-level properties and validation of whole-brain models.

References

1. Lachaux, J.-P., Rheims, S., Chatard, B., & Bertrand, O. (2022). Human Intracranial Database (release-4) [Data set]. EBRAINS. https://doi.org/10.25493/WNHQ-TM0
2. Brocard J, Combrisson E, Lachaux JP, Brovelli A, Daunizeau J (HBP poster). Mediation analysis of neural response's shape.
3. Combrisson E, Allegra M, Basanisi R, Ince RAA, Giordano BL, Bastin J, Brovelli A (2022). Group-level inference of information-based measures for the analyses of cognitive brain networks from neurophysiological data. Neuroimage, 258:119347. doi: 10.1016/j.neuroimage.2022.119347
4. Combrisson E, Basanisi R, Cordeiro VL, Ince RAA, Brovelli A (2022). Frites: A Python package for functional connectivity analysis and group-level statistics of neurophysiological data. Journal of Open Source Software 7 (79), 3842. doi: 10.21105/joss.03842

5. Celotto M, Bím J, Tlaie A, De Feo V, Lemke S, Chicharro D, Nili H, Bieler M, Hanganu-Opatz IL, Donner T, Brovelli A, Panzeri (HBP poster). A nonparametric tool to quantify the content of information transmitted between neural populations.
6. Escrichs A, Combrisson E, Brovelli A, Deco G (in preparation). Generative whole-brain models for intracortical iEEG during visual tasks in epileptic patients.
7. Lemaréchal JD, Jedynak M, Trebaul L, Boyer A, Tadel F, Bhattacharjee M, Deman P, Tuyisenge V, Ayoubian L, Hugues E, Chanteloup-Forêt B, Saubat C, Zouglech R, Reyes Mejia GC, Tourbier S, Hagmann P, Adam C, Barba C, Bartolomei F, Blauwblomme T, Curot J, Dubeau F, Francione S, Garcés M, Hirsch E, Landré E, Liu S, Maillard L, Metsähonkala EL, Mindruta I, Nica A, Pail M, Petrescu AM, Rheims S, Rocamora R, Schulze-Bonhage A, Szurhaj W, Taussig D, Valentin A, Wang H, Kahane P, George N, David O; F-TRACT consortium. A brain atlas of axonal and synaptic delays based on modelling of cortico-cortical evoked potentials. Brain. 2022 Jun 3;145(5):1653-1667. doi: 10.1093/brain/awab362.
8. Seguin C, Jedynak M, David O, Mansour L S, Sporns O, Zalesky A (in press) Communication dynamics in the human connectome shape the cortex-wide propagation of direct electrical stimulation. Neuron.

Keywords

Brain networks, functional connectivity, intracranial EEG, MEG, causal whole-brain modelling, effective connectivity

Acknowledgments

This project/research has received funding from the European Union's Horizon 2020 Framework Programme for Research and Innovation under the Specific Grant Agreement No. 945539 (Human Brain Project SGA3).

154. SpecSeg: cross-spectral power based segmentation of neurons in chronic calcium imaging datasets

Leander de Kraker[1], Koen Seignette[1#], Premnath Thamizharasu[1#], Bastijn J. G. van den Boom[2,4], Ildefonso Ferreira Pica[1], Ingo Willuhn[2,4], Christiaan N. Levelt[1,2]*, & Chris van der Togt[1]

[1] *Dept. Of Molecular Visual Plasticity,*

[2] *Dept. Of Neuromodulation and Behavior, Meibergdreef 47, 1105 BA Amsterdam, the Netherlands,*

[3] *Department of Molecular and Cellular Neurobiology, Center for Neurogenomics and Cognitive Research, VU University Amsterdam, de Boelelaan 1085, 1081 HV*

[4] *Department of Psychiatry, Amsterdam UMC, Meibergdreef 5, 1105 AZ, University of Amsterdam*

* Corresponding author: c.levelt@nin.knaw.nl

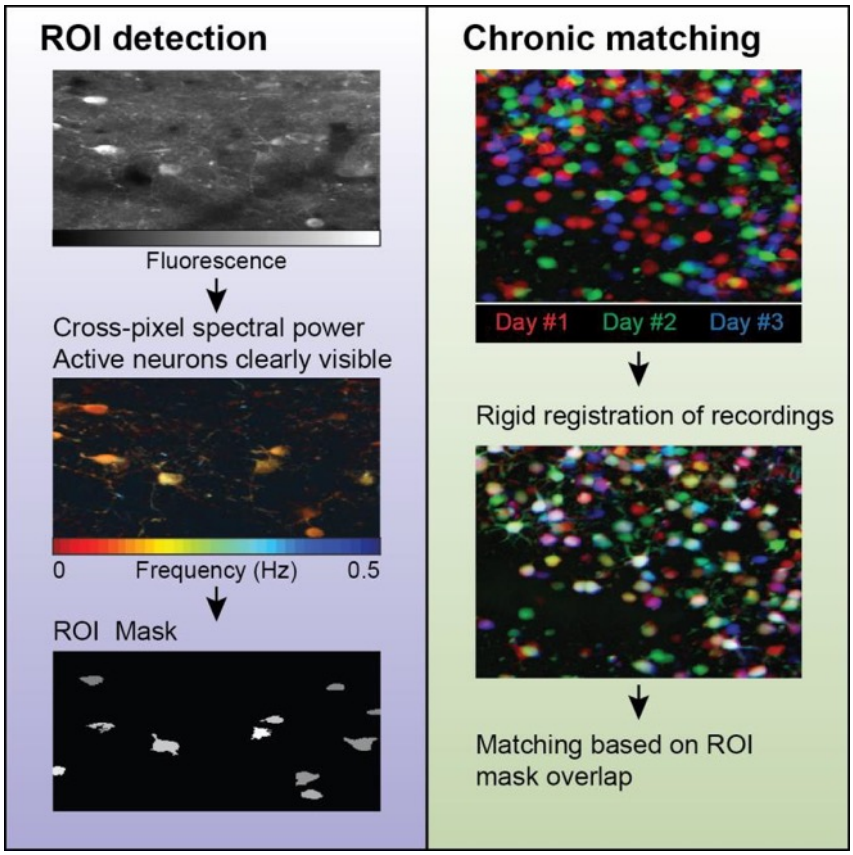

INTRODUCTION

2-photon calcium recordings are becoming massive and powerful methods are needed to extract the neurons and their responses from the data. We created the Spectral Segmentation toolbox, to:

1) segment regions of interest (ROIs) representing neuronal structures,

2) inspect data and edit ROIs,

3) extract data with neuropil subtraction, and

4) match ROIs in sequential recordings.

Figure 1. summary of the analysis pipeline.

METHODS

The ROI identification is based on two steps. First, cross-spectral power between each pixel and its eight neighbors is calculated to create images in which active neurons are clearly visible. The ROIs are then automatically created with constraints set by the user, like size and signal strength. After the automatic process ROIs can be edited or added with a user interface. This user interface also enables inspection of the raw data in many ways. The calcium signal traces from ROIs can be extracted and neuropil corrected. ROIs from different recordings can be matched together by registering the spectral images and calculating the ROI overlaps.

RESULTS & DISCUSSION

The software can reliably detect active neurons and dendrites and gives insight into the data. It enables chronic tracking of individual neurons in calcium imaging experiments over periods from days to multiple months. The software pipeline is available on GitHub at github.com/Leveltlab/SpectralSegmentation.

Key words: Calcium imaging, ROI segmentation, pre-processing

References

[1] Leander de Kraker, Koen Seignette, Premnath Thamizharasu, Bastijn J.G. van den Boom, Ildefonso Ferreira Pica, Ingo Willuhn, Christiaan N. Levelt, Chris van der Togt, (2022) SpecSeg is a versatile toolbox that segments neurons and neurites in chronic calcium imaging datasets based on low-frequency cross-spectral power, Cell Reports Methods, 2022, 100299, ISSN 2667-2375, https://doi.org/10.1016/j.crmeth.2022.100299.

155. Layer-specific plasticity of feedforward and contextual neuronal populations in mouse visual cortex

Koen Seignette[1], Paolo Papale[2], Leander de Kraker[1], Maaike van der Aa[1], Paul Neering[1,2], Chris van der Togt[1,2], Matt Self[2], Christiaan N. Levelt[1,3,*]

1. Department of Molecular Visual Plasticity, Netherlands Institute for Neuroscience (KNAW), 1105 BA Amsterdam, Netherlands.
2. Department of Vision & Cognition, Netherlands Institute for Neuroscience (KNAW), 1105 BA Amsterdam, Netherlands.
3. Department of Molecular and Cellular Neurobiology, Center for Neurogenomics and Cognitive Research, VU University, Amsterdam, the Netherlands.

* Corresponding author: c.levelt@nin.knaw.nl

INTRODUCTION

Our brains are extremely efficient in interpreting and responding to constant streams of highly complex sensory information. One increasingly influential concept of how the brain achieves this is predictive coding. It views the brain as a hypothesis-testing machine that compares an internal model of the environment with sensory inputs it receives. It tries to minimize the difference between the two by calculating errors in the prediction and using these to update the internal model. This requires neurons that encode the internal representation, and those that encode prediction errors. Identifying the cell types that encode prediction errors or internal representations has been extremely challenging, mainly because responses to visual inputs and predictions are strongly intertwined. Here, we used occlusion of natural visual scenes to separate visual and predictive responses across layer 2/3 (L23) and layer 5 (L5) in mouse primary visual cortex (V1) and study the effect of visual training on these responses.

METHODS

We recorded activity from L23 or L5 neurons in mouse V1 using chronic two-photon and widefield calcium imaging in awake mice (Fig 1A). We mapped population- and single cell receptive fields (RFs)

and then presented six (partially) occluded and full natural scenes (Fig 1B). In order to study the effects of learning, we then trained mice to detect a subset of these natural scenes in full condition while leaving the others out. This resulted in familiarity with some, but not other images. We then again recorded single-cell responses to full and occluded scenes after training. Finally, we used a convolutional neural network (CNN) to model visual responses and maximally excited inputs (MEIs) to compare visual properties between populations of neurons. For all analyses we only included neurons that had their RFs in the occluded region of the images (Fig 1B).

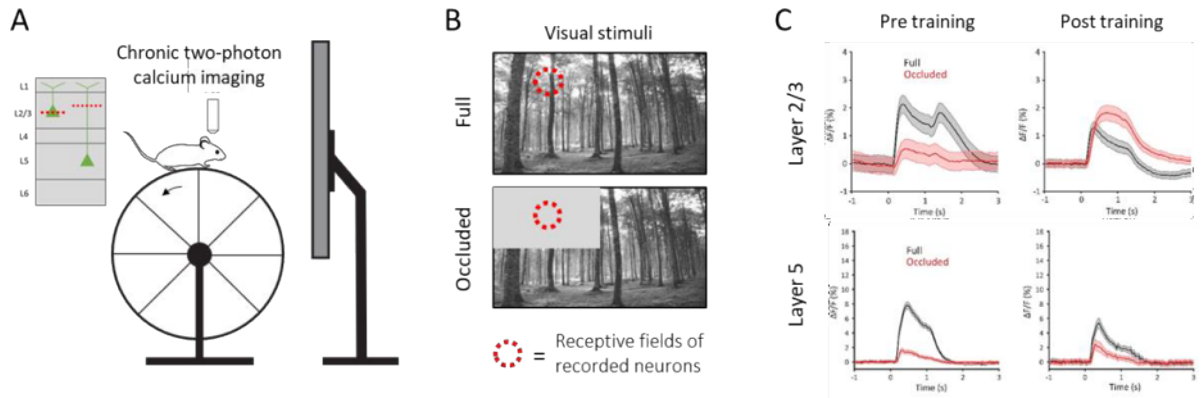

Figure 1. Experimental setup (A-B) and summary of main results (C).

RESULTS

In L23 we found neurons that either responded to the full images or to the occluded images, in line with the presence of positive and negative prediction neurons. Perceptual training induced strong plasticity of these responses, decreasing responses to full images but increasing those to familiar images. Responses to novel images (full or occluded) were strongly enhanced. In L5, neurons responding to the full images dominated and showed similar, but stronger plasticity than layer 23 neurons. Responses to occluded stimuli were weaker and did not change with experience. Finally, decoding image identity from occluded responses was possible both in L23 and L5, and slightly increased after training in L23.

CONCLUSION

Our results suggest that like human and monkey visual cortex (see poster 96), mouse V1 neurons can encode visual contextual information in the absence of FF input. These responses are experience- dependent and are in line with the presence of positive and negative prediction error neurons in L23 and possibly internal representation neurons in layer 5.

156. Data-driven analysis of brain's resting-state manifold

Anastasios-Polykarpos Athanasiadis[1*], Jan Fousek[1], Marmaduke Woodman[1], Spase Petkoski[1], Viktor Jirsa[1]

Affiliations: [1]Theoretical Neuroscience Group, Institut de Neurosciences des Systèmes, Marseille, France.
*e-mail-address: anastasios-polykarpos.ATHANASIADIS@univ-amu.fr

INTRODUCTION/MOTIVATION

The brain activity measured by fMRI is linked to the output of the cognitive activity performed by the subjects under study. This type of activity is considered to be the top layer of processing and subsequently it is considered to make up the `brain states' which are thought to emerge from the interactions among brain areas[1]. Here, we spatiotemporally decompose synthetic and empirical fMRI BOLD recordings during rest into substates that are characterized in their own activity space and are further exposed on the manifold of the whole-brain activity.

METHODS

The temporal decomposition of the data is done with the aim of getting the dynamic functional connectivity (dFC) states[2], which come with the use of sliding temporal windows. We identify co-fluctuation (CF) events which happen as traces of highly-correlated activity across the brain[3] and we apply PCA, PHATE and T-PHATE to reconstruct the manifolds. The analysis goes from the "top" layer (`brain state' output) to the "networks" level, where more details of the dynamics are expected to be apparent. The spatial decomposition is done following a novel method which combines PHATE and Spectral Clustering to split the brain into networks of most synergetic regions that exhibit homogeneous profiles of activity (Figure 1). The first principal component (PC1) of each profile explains the vast variance of each profile and its scores reflect the essence of the activity. Combining these PC1s the manifolds of the dFC states are extracted.

In parallel, the phase portrait of each network can be viewed based on each PC1. Following the framework of Structured Flows on Manifolds (SFM)[4] we are attempting to find the flow on the manifolds. Clearer manifestation of the flow should happen around the areas where the deterministic component of the underlying slow-timescale dynamics is stronger. These areas were considered to be around the CF events which take place away from the core of the manifold. There, the lines of the flow are expected to be less dense and the fast-time scale dynamics weaker.

RESULTS & DISCUSSION

Resting-state from the synthetic and empirical data show similar topological organization with the CF events at the boundaries of the manifolds. Splitting the regions into non-overlapping sub-networks of similar activation profiles gives access to more localized dynamics and the manifolds of the separate dFC states. Phase portraits reveal the mechanisms of the flow, which can be characterized by single or multiple attractors. This is first demonstrated with the synthetic data, where the exploration of the manifold is driven by local bistabillity. In the second part, the same procedure for the areas around CF events leads to phase portraits that expose the structured flow that governs the slow-time scale dynamics of the resting state (Figure 2). Signatures of bistability can be explained by the activity of sensory areas which transitions from high (sensitivity to external stimuli) to low (mind-wandering). The characterization of the flow on the manifold of the resting state allows better understanding of different metrics that describe the brain at rest. Comparison with the synthetic data from the brain network model, offers better understanding of the generative mechanisms of macroscopic brain dynamics. Keywords: resting-state, manifolds, flow, dFC, co-fluctuation events

REFERENCES

[1] McIntosh AR. Towards a network theory of cognition. *Neural Networks*. 2000;13(8-9):861-870. doi:10.1016/s0893-6080(00)00059-9 [Accessed February 2, 2023].

[2] Hansen ECA, Battaglia D, Spiegler A, Deco G, Jirsa VK. Functional connectivity dynamics: Modeling the switching behavior of the resting state. *NeuroImage*. 2015;105:525-535. doi:10.1016/j.neuroimage.2014.11.001 [Accessed February 2, 2023].

[3| Esfahlani FZ, Jo Y, Faskowitz J, et al. High-amplitude cofluctuations in cortical activity drive functional connectivity. *Proceedings of the National Academy of Sciences*. 2020;117(45):28393-28401. doi:10.1073/pnas.2005531117 [Accessed February 2, 2023].

[4] Jirsa V. Structured Flows on Manifolds as guiding concepts in brain science. *Selbstorganisation – ein Paradigma für die Humanwissenschaften*. Published online 2020:89-102. doi:10.1007/978-3-658-29906-4_6 [Accessed February 2, 2023].

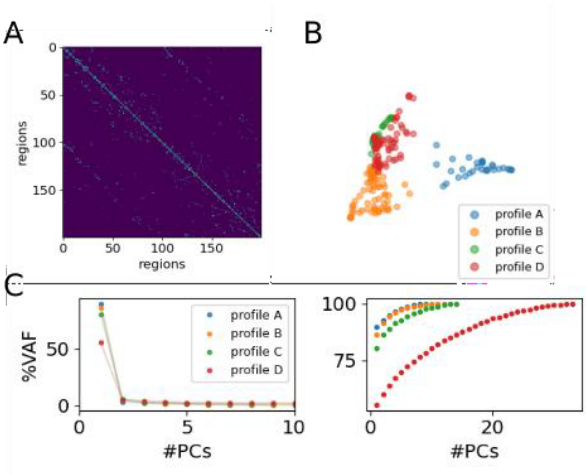

Figure 1. A: Affinity matrix of regions calculated by PHATE when applied to cluster the regions based on the similarity of their dynamics. B: Spectral clustering of the affinity matrix splits the regions into networks which make up profiles of homogeneous and distinctive activity. C: The first principal components dominate the activity's variance for obtained subnetworks, thus validating the clustering procedure.

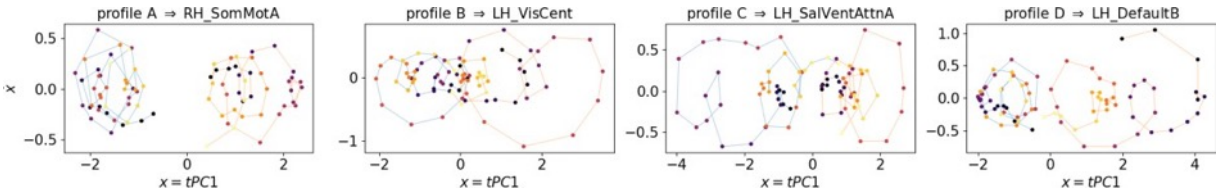

Figure 2. Phase portraits reveal the flow of the slow-time scale dynamics of each profile, which is dominated by the mentioned networks. Color-coded is the time-evolution before and after the CF (purple to yellow).

157. Characterizing thalamic sodium accumulation in focal epilepsy to better inform patients' modelling

Roy A.M. Haast[1,2,*], Mohamed Mounir El Mendili[1,2], Julia Makhalova[1,2,3], Lucas Gauer[1,2], Benoit Testud[1,2], Alexandre Cabane[1,2], Arnaud Le Troter[1,2], Jean-Philippe Ranjeva[1,2], Wafaa Zaraoui[1,2], Fabrice Bartolomei[3,4] & Maxime Guye[1,2]

[1]Aix Marseille University, CNRS, CRMBM, Marseille, France; [2]APHM, Hôpital Universitaire Timone, CEMEREM, Marseille, France; [3]Department of Epileptology and Clinical Neurophysiology, APHM La Timone Hospital, Marseille, France; [4]INS, INSERM UMR 1106, Aix-Marseille University, Marseille, France
*roy.haast@univ-amu.fr

INTRODUCTION/MOTIVATION

Sodium (^{23}Na) MRI provides relevant functional information on neuronal energetic status and cell viability[1]. In the context of focal epilepsy, sodium accumulation has been observed in cortical regions characterized by high epileptogenicity[2], and inclusion of ^{23}Na information appeared promising to improve Virtual Epileptic Patient (VEP) performance[3]. The involvement of the thalamus and its structural abnormalities in patients[4–6], motivated us to investigate thalamic sodium accumulation and assess its specificity based on epilepsy type and/or thalamic segment. The perspective is to include this information the VEP framework.

METHODS

A total of 21 temporal lobe epilepsy (TLE, mean age ± SD: 33±11 yrs, 8 males), 16 non-TLE (NTLE, 34±13 yrs, 9 males) and 22 healthy controls (H, 37±15 yrs, 10 males) were recruited. All patients underwent a comprehensive pre-surgical work-up including a SEEG recording for grouping in TLE and NTLE (prefrontal, insular-opercular, central-premotor or posterior) based on epileptogenic zone network topography[7].

For each subject, ^{1}H-MRI B_1^+, T_1 (0.6 mm^3) and multi-echo ^{23}Na (3 mm^3) data were acquired using a whole-body 7T scanner (Siemens Healthineers, Erlangen, Germany) and ^{1}H 1Tx/32Rx (Nova Medical, Wilmington, USA) and dual-tuned ^{23}Na/^{1}H QED birdcage coils, respectively[2]. The multi-echo ^{23}Na images were fitted using a bi- exponential model and normalized relative to signals from reference tubes to compute whole-brain total sodium concentration (TSC) maps[8]. In parallel, post-hoc B_1^+ corrected T_1 data were skull-stripped for automatic segmentation of the thalamus and its nuclei using the 7TAMIBrain atlas[6,9]. Gray matter density-weighted TSC averages were calculated in ^{23}Na image space for left and right thalami separately, and their posterior, lateral and medial segments (Fig. 1A). Average T_1 and total volume were extracted in T_1 space[6].

While TSC averages were only significantly modulated by estimated total intracranial volume (eTIV, calculated by FreeSurfer, Fig. 1B), estimates were corrected for age, sex, hemisphere and eTIV effects (to match T_1 and volume correction) based on the controls data using the confounds Python package[10]. After z-scoring with respect to controls, group-wise, ipsi- vs.contralateral differences in thalamic (segments) and associations with clinical parameters were explored using ANOVA, (Bonferroni-corrected) pairwise comparisons and correlation analyses as implemented in the *pingouin* Python package.

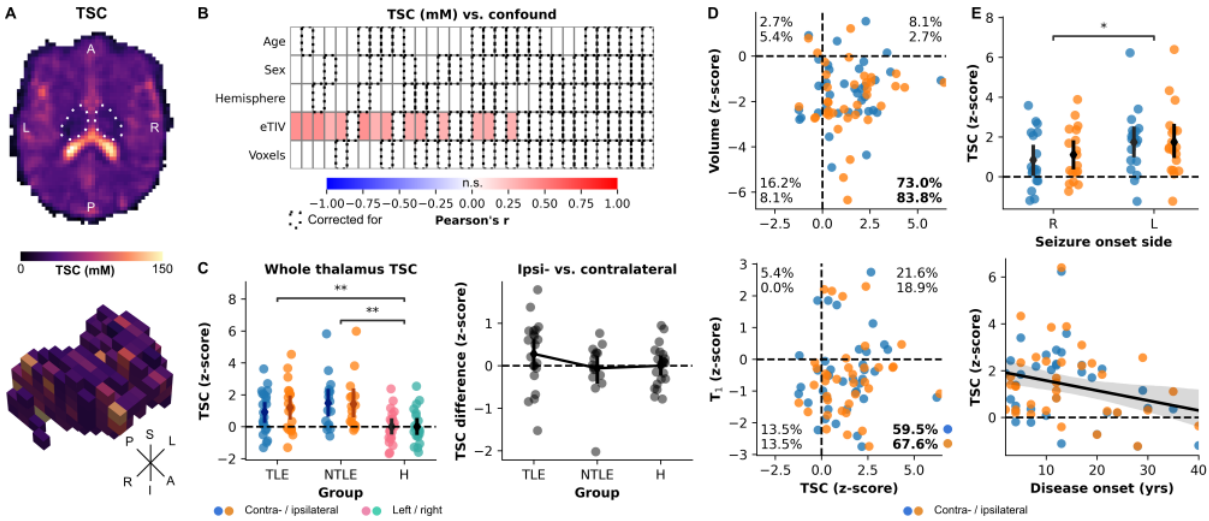

Fig. 1 - Whole thalamus total sodium concentration. (A) Example total sodium concentration (TSC) maps for an axial slice (top) and thalamus in 3D (bottom). (B) Impact of confounding factors on TSC estimates. Here, columns represent all possible combinations of confounding factors (delineated using dashed outlines) during correction with cell color indicating the correlation strength between thalamic TSC and each confounding factor (rows). (C) Thalamic TSC (left, color-coded for side) and ipsilateral-contralateral differences (right) per group (x-axis). (D) Overlap with volume (top) and T1 (bottom) changes. (E) Impact of seizure onset side (top) and disease onset (bottom) on thalamic TSC, color-coded for ipsi- and contralateral side.

RESULTS AND DISCUSSION

Thalamic TSC differed significantly between groups (p<.001) with increased TSC in both TLE (p<.01) and NTLE patients (p<.01), while unilateral increases appeared more pronounced in TLE patients (Fig. 1C). Increased TSC overlaps with decreased T_1 and volume (Fig. 1D) in these patients both ipsi- and contralaterally. With respect to clinical characteristics (Fig.1E), TSC was higher in patients with a left seizure onset zone especially (p<.05), and earlier disease onset (r=-.26, p<.05).

Analyses per thalamic segment (Fig. 2A, based on >29 voxels/subject) did not reveal clear spatial differences across the thalamus with similar group patterns as at the whole thalamus scale. Nonetheless, the medial segment appeared uniquely impacted in the NTLE patients while in TLE the strongest TSC increase was observed in the lateral segment (Fig. 2B).

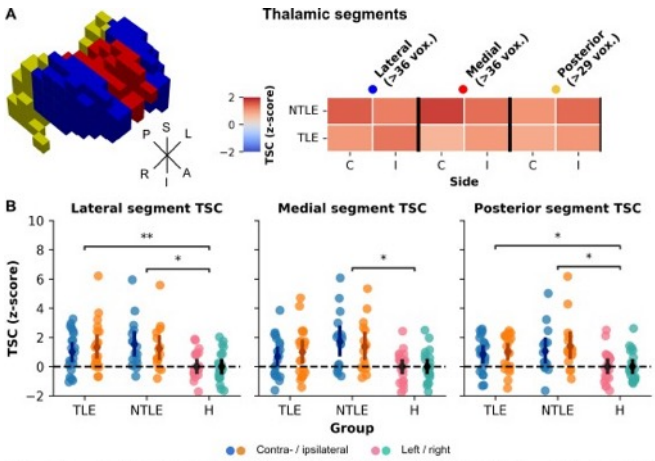

Fig. 2 - Thalamic segments' total sodium concentrations. (A) Example segmentation of the thalamus into lateral, medial and posterior segments and corresponding total sodium concentration (TSC) estimates per group and side (ipsi- vs. contralateral; i.e., I vs. C). (B) Statistical evaluation of group-wise (x-axes) differences per segment (left to right), color-coded for side.

The observed increase in thalamic TSC follows previously observed tissue degeneration (e.g.,

volume decrease)[5] and microstructural changes (i.e., shortened T_1)[6] and indicate changes in neuronal integrity. This effect seems strongest in patients with left hemisphere seizure and earlier disease onset. Finally, our analyses provide first estimates of differential TSC increase across posterior, lateral and medial segments between patient groups. Together, these findings suggest that the extent of thalamic sodium accumulation might depend on clinical and/or SEEG characteristics and potentially provide additional priors to enhance VEP performance.

Keywords: Focal epilepsy, thalamus, sodium, ultra-high field MRI, Virtual Epileptic Patient

ACKNOWLEDGEMENTS

We would like to thank the patients and control participants who agreed to take part in this study. The study was financially supported by the French government under the "Programme Investissements d'Avenir", Excellence Initiative of Aix-Marseille University -A*MIDEX (AMX-19IET-004), 7TEAMS Chair, EPINOV (ANR-17-RHUS-0004) and the European Union's Horizon 2020 Framework Program HBP (SGA3-945539). Author RAMH is supported by a Marie-Curie Postdoctoral Fellowship (101061988) for this work.

REFERENCES

1. Thulborn, K. R. Quantitative sodium MR imaging: A review of its evolving role in medicine. *NeuroImage* 168, 250–268. doi: 10.1016/j.neuroimage.2016.11.056 (2018).
2. Azilinon, M. *et al.* Combining sodium MRI, proton MR spectroscopic imaging, and intracerebral EEG in epilepsy. *Human Brain Mapping.* doi: 10.1002/hbm.26102 (2022).
3. Azilinon, M. *et al.* Brain sodium MRI-derived priors support the estimation of epileptogenic zones using personalized model-based methods in Epilepsy. 2022.12.14.22283389 Preprint at https://doi.org/10.1101/2022.12.14.22283389 (2022).
4. Pizzo, F. *et al.* The Ictal Signature of Thalamus and Basal Ganglia in Focal Epilepsy: A SEEG Study. *Neurology* 96, e280–e293. doi: 10.1212/WNL.0000000000011003 (2021).
5. Keller, S. S. *et al.* Thalamotemporal impairment in temporal lobe epilepsy: a combined MRI analysis of structure, integrity, and connectivity. *Epilepsia* 55, 306–315. doi: 10.1111/epi.12520 (2014).
6. Haast, R. A. *et al.* Multi-scale structural alterations of basal ganglia in focal epilepsy as demonstrated by 7T MRI. 2022.11.01.514655 Preprint at https://doi.org/10.1101/2022.11.01.514655 (2022).
7. Bartolomei, F. *et al.* Defining epileptogenic networks: Contribution of SEEG and signal analysis. *Epilepsia* 58, 1131–1147. doi: 10.1111/epi.13791 (2017).
8. Grimaldi, S. *et al.* Increased Sodium Concentration in Substantia Nigra in Early Parkinson's Disease: A Preliminary Study With Ultra-High Field (7T) MRI. *Frontiers in Neurology* 12, 715618. doi: 10.3389/fneur.2021.715618 (2021).
9. Brun, G. *et al.* Automatic segmentation of deep grey nuclei using a high-resolution 7T magnetic resonance imaging atlas-Quantification of T1 values in healthy volunteers. *Eur J Neurosci* 55, 438–460. doi: 10.1111/ejn.15575 (2022).
10. Raamana, P. R. Conquering confounds and covariates in machine learning with the python library confounds. (2020) doi:10.5281/zenodo.3701528.

158. Multiscale responsiveness following microstimulation of the prefrontal and parietal cortices in wakefulness and anaesthesia

Abhilash Dwarakanath[1], Majid Khalili-Ardali[1], Rodrigo Cofre[5], Chloe Duprat[5], Marion Gay[1], Maxime Roustan[1], Stanislas Dehaene[1,4], Bechir Jarraya[1,2,3], Alain Destexhe[7], Theofanis I Panagiotaropoulos[1]

[1] Cognitive Neuroimaging Unit, INSERM, CEA, Université Paris-Saclay, NeuroSpin center, Gif/Yvette, France

[2] University of Versailles Saint-Quentin-en-Yvelines, Université Paris-Saclay, Versailles, France

[3] Neuromodulation Unit, Foch Hospital, Suresnes, France

[4] Collège de France, Université Paris-Sciences-Lettres (PSL), Paris, France

[5] CNRS, Paris-Saclay University, Institute of Neuroscience (NeuroPSI), Saclay, France

Introduction

Understanding the effects of anaesthesia on cortical signal propagation could lead to a better understanding of different states and mechanisms of (un)consciousness. Previous studies using whole-brain imaging techniques such as BOLD-fMRI, and EEG have demonstrated that the repertoire of cortical states drastically diminishes under anaesthesia[1,2]. Moreover, anaesthesia results in reduced large-scale complexity of cortical activity elicited by trans-cranial magnetic stimulation (tCMS) and deep brain stimulation (DBS), *vis a vis* wakefulness, using methods such as the Perturbation Complexity Index (PCI)[3,4]. However, studies that specifically target the fronto-parietal loop[5,6], which is thought to be central to conscious access [7–9] and crucial for awareness, are rare.

Results and Discussion

Here we recorded from Utah arrays chronically implanted in the ventrolateral prefrontal (vlPFC) and posterior parietal (PPC) cortices, in three male macaque monkeys, respectively. Scalp potentials were also recorded simultaneously from eleven EEG channels. Furthermore, intracortical microstimulation was delivered to the centre of the 10x10 Utah Array at different amplitudes (ranging between 1µA to 100µA), during wakefulness, light and deep anaesthesia. At the mesoscale, we found that the microstimulation-

induced evoked response (broadband local field potentials - 0.1-250Hz) during wakefulness was significantly stronger in amplitude, and lasted longer in time (following the end of the pulse-train), than during light anaesthesia. However, the evoked response during deep anaesthesia was stronger than during light anaesthesia, but weaker than during wakefulness. Coupled with the observation of burst suppression periods during deep anaesthesia, we attribute this paradoxical finding to increased cortical sensitivity during periods of cortical silence[10]. Next, we found that the amplitude of the evoked response was distance- dependent for different levels of consciousness. We quantified this modulation of signal propagation as the pre/post modulation of signal energy (l2 norm). We found that it was similar in proximal and distal populations under quiet wakefulness, while under anaesthesia, it dropped off sharply across distance, showing that anaesthesia restricts the mesoscale spread of the elicited cortical activity[11].

At the macro-scale, the EEG-evoked response pattern was similar to intracranial recordings on electrodes closer to the stimulation site. However, these evoked responses displayed the opposite polarity on the contralateral electrodes, but only above a certain amplitude threshold. Furthermore, these responses were positively correlated with the stimulation intensity (non-linearly), while the depth of anaesthesia negatively impacted the amplitude of the evoked response.

Finally, to model the mesoscale results, we used a 2D array of mean-field models (of AdEx type) which can display asynchronous (awake-like) or synchronous slow-wave (anaesthesia-like) dynamics, and can reproduce the above-observed enhanced response to stimuli in the asynchronous state, compared to slow-wave states. This model was also tested on different types of slow-waves, to simulate the "depth" of anaesthesia. The model is compatible with TVB and runs on EBRAINS.

Taken together, our results suggest that signal propagation during anaesthesia is disrupted at multiple scales (meso and large-scale) following microstimulation of the prefrontal and parietal cortices. This effect may underlie a similar disruption in multiscale integrative processes that are potentially crucial for the mechanisms of sensory (un)awareness.

Keywords

Consciousness, anaesthesia, signal propagation, simultaneous recordings, intracortical microstimulation, Utah arrays, mesoscale, TVB, cortical states, mean-field models.

Acknowledgements

We would like to thank Mr Raghuram HV for his assistance during the experiments. This work received funding by INSERM, CEA, the European Union's Horizon 2020 Framework Programme for Research and Innovation under the Specific Grant Agreement No. 945539 (Human Brain Project SGA3), a grant from Templeton World Charity Foundation, Inc (TWCF0562) to Theofanis Panagiotaropoulos and the Bettencourt-Schueller Foundation.

References

1. Uhrig L, Dehaene S, Jarraya B. Cerebral mechanisms of general anesthesia. *Ann Fr Anesth Reanim*. 2014;33(2):72-82. doi:10.1016/j.annfar.2013.11.005

2. Barttfeld P, Uhrig L, Sitt JD, Sigman M, Jarraya B, Dehaene S. Signature of consciousness in the dynamics of resting-state brain activity. *Proc Natl Acad Sci USA*. 2015;112(3):887-892. doi:10.1073/pnas.1418031112

3. Sarasso S, Rosanova M, Casali AG, et al. Quantifying cortical EEG responses to TMS in (un)consciousness. *Clin EEG Neurosci*. 2014;45(1):40-49. doi:10.1177/1550059413513723

4. Casali AG, Gosseries O, Rosanova M, et al. A theoretically based index of consciousness independent of sensory processing and behavior. *Sci Transl Med*. 2013;5(198):198ra105. doi:10.1126/scitranslmed.3006294

5. Lee U, Ku S, Noh G, Baek S, Choi B, Mashour GA. Disruption of frontal-parietal communication by ketamine, propofol, and sevoflurane. *Anesthesiology*. 2013;118(6):1264-1275. doi:10.1097/ALN.0b013e31829103f5

6. Pal D, Dean JG, Liu T, et al. Differential role of prefrontal and parietal cortices in controlling level of consciousness. *Curr Biol*. 2018;28(13):2145-2152.e5. doi:10.1016/j.cub.2018.05.025

7. Del Cul A, Dehaene S, Reyes P, Bravo E, Slachevsky A. Causal role of prefrontal cortex in the threshold for access to consciousness. *Brain*. 2009;132(Pt 9):2531-2540. doi:10.1093/brain/awp111

8. Bor D, Seth AK. Consciousness and the prefrontal parietal network: insights from attention, working memory, and chunking. *Front Psychol*. 2012;3:63. doi:10.3389/fpsyg.2012.00063

9. Odegaard B, Knight RT, Lau H. Should a few null findings falsify prefrontal theories of conscious perception? *J Neurosci*. 2017;37(40):9593-9602. doi:10.1523/JNEUROSCI.3217-16.2017

10. Kroeger D, Amzica F. Hypersensitivity of the anesthesia-induced comatose brain. *J Neurosci* 27

(39) 10597-10607; DOI: https://doi.org/10.1523/JNEUROSCI.3440-07.2007

11. Lee U, Mashour GA, Kim S, Noh G-J, Choi B-M. Propofol induction reduces the capacity for neural information integration: implications for the mechanism of consciousness and general anesthesia. *Conscious Cogn*. 2009;18(1):56-64. doi:10.1016/j.concog.2008.10.005

159. Identification and neuromodulation of consciousness states: experimental and clinical considerations

Glenn J.M. van der Lande[1,2*], Diana Casas-Torremocha[3], Francisco Clasca[4], Gustavo Deco[5,6], Pau Gorostiza[6,7,8], Olivia Gosseries[1,2], Steven Laureys[1,2,9,10], Arnau Manasanch[3], Jorge F. Mejías[11], Rajanikant Panda[1,2], Fabio Riefolo[8], Maria V. Sanchez-Vives[3,6], Bertrand Thirion[12], Gorka Zamora-López[5], Jitka Annen[1,2]

[1]GIGA-Consciousness, Coma Science Group, University of Liège, Liège, Belgium
[2]Centre du Cerveau[2], University Hospital of Liège, Liège, Belgium
[3]Institut d'Investigacions Biomèdiques August Pi i Sunyer (IDIBAPS), Barcelona 08036, Spain
[4]Department of Anatomy and Neuroscience, School of Medicine, Universidad Autónoma de Madrid, Madrid 28029, Spain
[5]Computational Neuroscience Group, Center for Brain and Cognition, Universitat Pompeu Fabra, Barcelona, Spain [6]Institució Catalana de la Recerca i Estudis Avançats (ICREA), Barcelona, Spain
[7]Biomedical Research Networking Center in Bioengineering, Biomaterials, and Nanomedicine (CIBER-BBN), Madrid 28029, Spain
[8]Institute for Bioengineering of Catalonia (IBEC), Barcelona Institute of Science and Technology, Barcelona 08028, Spain
[9]Joint International Research Unit on Consciousness, CERVO Brain Research Centre, U Laval CANADA
[10]International Consciousness Science Institute, Hangzhou Normal University, Hangzhou, CHINA
[11]Swammerdam Institute for Life Sciences, University of Amsterdam, Science Park 904, 1098XH Amsterdam, Netherlands
[12]Inria, CEA, Université Paris-Saclay, Paris, France

*Corresponding author (Glenn J.M. van der Lande) email: glenn.vanderlande@uliege.be

Introduction

Experimental and clinical studies of consciousness identify brain states (i.e., transient, relevant features of the brain associated with the state of consciousness) in a non-systematic manner. Moreover, the identification of brain states is not consistently coupled to research into the induction of state changes, even though this coupling may provide outstanding opportunities for targeted induction of changes in the state of consciousness. This review aims to outline important and consistent findings related to identification and modulation of transitions across brain states in consciousness research. In turn, this is crucial for the diagnosis and treatment of patients with a disorder of consciousness (DoC).

Methods

We have coordinated our efforts towards a multiscale and multi-methodology in both the human and animal domain approach in order to systematically explore how to induce brain state transitions. The resulting outlook could eventually be used in the clinic with DoC patients. We first scrutinize the identification of brain states associated with consciousness and unconsciousness (e.g., DoC and anesthesia). Next, we show the effects of neuromodulation (i.e., pharmacology, photopharmacology, non-invasive brain stimulation like transcranial direct current stimulation (tDCS), and invasive brain stimulation like deep brain stimulation (DBS)) in relation to alterations of brain states and the potential induction of state changes in the spectrum of consciousness. Furthermore, this narrative review is supported by data by being part of the Live Paper innovation initiative within the Human Brain Project, meaning that it is possible to follow a link tointeract, through EBRAINS, with data and figures illustrating the concepts.

Results

We show that in DoC the frequencies in which the brain operates are slowed down and that the pattern of functional communication in the brain is sparser, less efficient and less complex[1]. The results also highlight

damaged resting state networks, in particular the default mode network, or decreased connectivity in long-range connections or in the thalamocortical loop. These findings are similar to those found under anesthesia or in animal models, highlighting their importance to clinical advancement.
Moreover, we show that anesthesia and animal models offer excellent experimental control.

Therapeutic approaches to DoC, through pharmacology (e.g., amantadine, zolpidem[2]), non-invasive brain stimulation (e.g., tDCS[3]) or invasive brain stimulation (e.g., DBS[4]) have shown some effectiveness. It seems that the deteriorated features of the brain found in the first part may improve in response to these neuromodulatory approaches yet targeting often remains non-specific. On the other hand, neuromodulatory techniques like DBS and photopharmacology[5] that allow for excellent spatial and temporal control, offer outstanding opportunities for the further investigation of neuromodulation and induction of brain states. Given the similarities of affected brain states across DoC, anesthesia and animal models the latter play a major role in the development of targeted treatments.

Discussion

The fields of brain state identification and neuromodulation of brain states with relation to consciousness are showing fascinating developments. This paves the way for increased coupling of both fields, where brain states could be identified in a more predictive setting, and this could be followed by theory and empirical testing of neuromodulatory techniques inducing changes. Moreover, there is compelling evidence for the benefits of the integration of computational modelling in such studies. This review further helps to identify where challenges and opportunities lay for the clinical translation of our findings. All in all, this review shows that the field of brain state research of states of consciousness, as well as its manipulation through neuromodulation, is maturing with clear opportunities for future research.

Keywords: Consciousness, brain states, neuromodulation, disorders of consciousness, anesthesia, animal models, humans, live paper

Acknowledgements

This project/research has received funding from the European Union's Horizon 2020 Framework Programme for Research and Innovation under the Specific Grant Agreement No. 945539 (Human Brain Project SGA3).

References

1. Demertzi A, Tagliazucchi E, Dehaene S, et al. Human consciousness is supported by dynamic complex patterns of brain signal coordination. *Sci Adv*. 2019;5:1-12. doi:10.1126/sciadv.aat7603
2. Edlow BL, Sanz LRD, Polizzotto L, et al. Therapies to Restore Consciousness in Patients with Severe Brain Injuries: A Gap Analysis and Future Directions. *Neurocrit Care*. 2021;35:68-85. doi:10.1007/s12028-021-01227-y
3. Mensen A, Bodart O, Thibaut A, et al. Decreased Evoked Slow-Activity After tDCS in Disorders of Consciousness. *Front Syst Neurosci*. 2020;14(September). doi:10.3389/fnsys.2020.00062
4. Redinbaugh MJ, Phillips JM, Kambi NA, et al. Thalamus modulates consciousness via layer-specific control of cortex. *Neuron*. 2020;106(1):66-75. doi:10.1016/j.neuron.2020.01.005.Thalamus
5. Barbero-Castillo A, Riefolo F, Matera C, et al. Control of Brain State Transitions with a Photoswitchable Muscarinic Agonist. *Adv Sci*. 2021;8(14):1-11. doi:10.1002/advs.202005027

160. Circuit and network dynamics of the human cerebral cortex in vitro

Joana Covelo[1*], Alessandra Camassa[1], Jose Manuel Sanchez-Sanchez[1], Arnau Manasanch[1], Leonardo Dalla Porta[1], Rita M. Robles[1], Nathalia Cancino-Fuentes[1], Almudena Barbero-Castillo[1], Silvia Tapia-Gonzalez[2,3], Mar Carreño[4], Estefania Conde[4], Pedro Roldán[4], Jordi Rumià Arboix[4], Javier DeFelipe[2,3], Maria V. Sanchez- Vives[1,5]

Affiliations: [1]Institut d'Investigacions Biomèdiques August Pi i Sunyer (IDIBAPS), Barcelona, Spain
[2]Centro De Tecnología Biomédica, Universidad Politécnica de Madrid, Madrid, Spain
[3]Instituto Cajal (CSIC), Consejo Superior De Investigaciones Científicas, Madrid, Spain
[4]Unidad de Epilepsia, Hospital Clinic, Barcelona, Spain
[5]Institució Catalana de Recerca i Estudis Avançats (ICREA), Barcelona, Spain
*e-mail-address of corresponding author(s): joana.covelo@gmail.com

INTRODUCTION/MOTIVATION

The complexity of the cellular makeup and function of the human brain is remarkable and distinct from non- human species[1]. As such, studies adopting human models are of great importance to move forward in the understanding of human cortical dynamics. So far, electrophysiology and histochemical experiments in human cortical slices have revealed important principles of network and cellular physiology of human cells (for a review regarding epileptic tissue, see [2]). However, previous studies often focused on the microscopic level, offering a scarce view of population and local network activity. To research on circuit dynamics, it is essential to resort to larger scale recordings, such as multielectrode array (MEA) recordings[3]. Here, our goal was to provide a two- dimensional characterization of human cortical dynamics in cortical slices during spontaneous cortical activity and following pharmacological and electrical modulation.

METHODS

Samples of human cortical tissue were obtained during surgery of epileptic (EP) or brain tumour patients (TP) and cut into 400µm-thick coronal slices. We simultaneously recorded the extracellular local field potentials of multiple cortical columns and layers using MEA (40 slices from 12 samples) during spontaneous and evoked activity. Excitability levels were modulated using 0.5–8µM bicuculline methiodide (BMI), a $GABA_A$ receptor antagonist which blocks fast inhibition. We also applied exogenous Electric Fields (EFs,+/-1-5V/m), which shift the resting membrane potential (ca.0.5mV per 2V/m[4]). Following electrophysiological recording, cortical layers were histologically reconstructed. The alignment of recording sites with cytoarchitectonic areas allowed the

spatiotemporal profiling of cortical spiking events, including the directionality of influence (Granger causality) between sites.

RESULTS AND DISCUSSION

Human slices expressed spontaneous slow oscillations (SO), which are characterized by periods of activity (Up- states) interspersed by periods of silence (Down-states), at a frequency <1Hz[5] (Fig 1). Activity from slices obtained from EP displayed shorter Up-states (<0.2s) with higher firing rates and longer Down-states, when compared to activity from the TP tissue. Histological investigation revealed that the cortical structure of our samples was preserved, not corresponding to dysplasia or tumoral tissue. As such, the differences observed between the cortex of EP and TP may reflect intrinsic functional changes and/or the impact of seizures.

Additionally, we found layer-specific dynamics consistent with findings from other mammals [6], with Up-states initiating preferentially in deep cortical layers. Measuring the Granger causal influence between layers, we also found a greater causality from deep (d) to superficial (s) layers (d to s=$2.2x10^{-3}$, s to d=$0.6x10^{-3}$), indicating the same preferred direction of the flow of information.

BMI application resulted in shorter Up-states, higher firing rates and more synchronized discharges. In fact, neurons in the peritumoral tissue following BMI application had similar firing rates to those in the epileptic one. Hence, GABAergic blockade increased network excitability and induced strong network synchronization. Network excitability was also modulated using EFs. Positive EFs resulted in an increase in SO frequency, while negative EFs led to decreased SO frequency, illustrating how human emergent cortical activity can be finely tuned exogenously (e.g., tDCS). A similar network response to the different levels of excitability has also been described in animal models[7]–[9], taking their translation to medical applications one step further.

The characterization of cortical dynamics at different levels of excitability broadens our understanding of human cortex network mechanisms and mesoscale organization. Comprehending the basic properties of the human cortex is a crucial first step towards the development of effective treatment strategies.

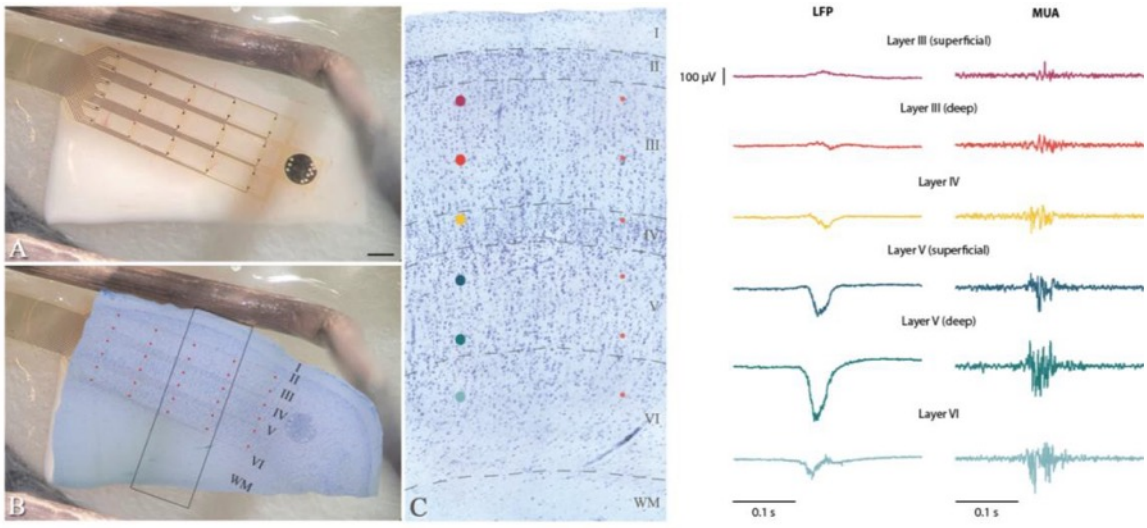

Fig 1. Human cerebral cortex in vitro Human slices recorded with a multielectrode array (A) covering multiple cortical layers and columns. (B) Histological reconstruction allowed the alignment of recording sites with cytoarchitectonic areas. (C) Local field potential (LFP) and multiunit activity (MUA) of one cortical column expressing spontaneous slow wave activity.

Keywords: Human, Cortical Dynamics, Brain Slices, in vitro, Slow Oscillations, Up States

ACKNOWLEDGEMENTS

Funded by euSNN MSCA-ITN-ETN H2020-860563, HBP-SGA3 No.945539, CORTICOMOD PID2020-112947RB-I00 and PRE2018-086203.

REFERENCES

[1] K. Lee *et al.*, «Human in vitro systems for examining synaptic function and plasticity in the brain», *J. Neurophysiol.*, vol. 123, n.º 3, pp. 945-965, mar. 2020, doi: 10.1152/jn.00411.2019.

[2] M. Avoli, J. Louvel, R. Pumain, y R. Köhling, «Cellular and molecular mechanisms of epilepsy in the human brain», *Prog. Neurobiol.*, vol. 77, n.º 3, pp. 166-200, oct. 2005, doi: 10.1016/j.pneurobio.2005.09.006.

[3] R. S. G. Jones, A. B. da Silva, R. G. Whittaker, G. L. Woodhall, y M. O. Cunningham, «Human brain slices for epilepsy research: Pitfalls, solutions and future challenges», *J. Neurosci. Methods*, vol. 260, pp. 221-232, feb. 2016, doi: 10.1016/j.jneumeth.2015.09.021.

[4] F. Fröhlich y D. A. McCormick, «Endogenous Electric Fields May Guide Neocortical Network Activity», *Neuron*, vol. 67, n.º 1, pp. 129-143, jul. 2010, doi: 10.1016/j.neuron.2010.06.005.

[5] M. Steriade, A. Nunez, y F. Amzica, «A novel slow (< 1 Hz) oscillation of neocortical neurons in vivo: depolarizing and hyperpolarizing components», *J. Neurosci.*, vol. 13, n.º 8, pp. 3252-3265, ago. 1993, doi: 10.1523/JNEUROSCI.13-08-03252.1993.

[6] C. Capone *et al.*, «Slow Waves in Cortical Slices: How Spontaneous Activity is Shaped by Laminar Structure», *Cereb. Cortex*, vol. 29, n.º 1, pp. 319-335, ene. 2019, doi: 10.1093/cercor/bhx326.

[7] M. V. Sanchez-Vives *et al.*, «Inhibitory modulation of cortical up states», *J. Neurophysiol.*, vol. 104, n.º 3, pp. 1314-1324, sep. 2010, doi: 10.1152/jn.00178.2010.

[8] A. Barbero-Castillo *et al.*, «Proceedings #31: Cortical Network Complexity under Different Levels of Excitability Controlled by Electric Fields», *Brain Stimul. Basic Transl. Clin. Res. Neuromodulation*, vol. 12, n.º 2, pp. e97-e99, mar. 2019, doi: 10.1016/j.brs.2018.12.200.

[9] M. D'Andola, M. Giulioni, V. Dante, P. Del Giudice, y M. V. Sanchez-Vives, «Control of cortical oscillatory frequency by a closed-loop system», *J. NeuroEngineering Rehabil.*, vol. 16, p. 7, ene. 2019, doi: 10.1186/s12984-018-0470-z.

161. The Virtual Basal Ganglia

Carola Sales-Carbonell[1], Damien Depannemaecker[1], Kashyap Gudibanda[1], Jan Fousek[1], Hiba Sheheitli[1] and Viktor K. Jirsa[1*]

[1]Institut de Neurosciences des Systèmes (INS), Inserm, Aix-Marseille University, Marseille 13005, France
[*]Corresponding author e-mail-address: viktor.jirsa@univ-amu.fr

INTRODUCTION

Dopamine is a powerful neuromodulator that regulates a plethora of higher brain functions, including motor control, cognition and emotions, by modulating neuronal excitability and synaptic inputs of a wide range of neurons across the brain [1]. Specifically, dopamine exerts different effects via D1- and D2-type dopamine receptors, with distinct spatial distributions, and with different affinities which endow sensitivity to different timescales and input characteristics [2]. The basal ganglia is a network of subcortical nuclei that has a central role on dopamine synthesis and function and its emergent activity is integrated in the whole-brain dynamics through the basal ganglia-thalamo-cortical circuit [3]. Particular dopamine signaling dysfunctions within this circuit are selectively implicated in several neuropsychiatric disorders such as Parkinson's disease [4]. The relationship between large-scale brain activity and behavior (or clinical symptoms) can inform on how distinct behaviors arises from the coordinated activity between neural populations. How dopaminergic neuromodulation regulates brain-wide activity remains largely unknown [5]. In the last recent years much effort has been put into developing data-driven, large-scale brain activity theoretical models such as The Virtual Brain (TVB) [6]. TVB allows for personalized patient's brain modeling and has been proven to be a valuable tool for translational brain research. However, until now, few have been the attempts to implement neuromodulation in TVB. Here we aim to provide TVB with dopaminergic modulation with a bottom-up strategy using knowledge on how dopamine receptors function at the microscale, single-cell level, to investigate the role of dopamine receptors activity in regulating large-scale neural dynamics and behavior in health and Parkinson's disease.

METHODS

Precisely, we developed a new module in TVB, which includes a basal ganglia-thalamo-cortical circuit. Each node in the virtual basal ganglia-thalamo-cortical network represents a distinct cell population described by a local neural activity obtained with a mean-field model derived for an all-to-all coupled neural network of adaptive quadratic integrate-and-fire (aQIF) neurons [7]. Each neuron is modelled by a four-dimensional system consisting of one equation for membrane excitability, one equation for spike frequency adaptation plus two equations accounting for inhibitory and excitatory conductance-based synaptic inputs. To model D1- and D2-type dopamine receptors specific modulation of neural excitatory and inhibitory synaptic inputs we used a published, data-informed aQIF spiking neuron model, extended to account for dopaminergic modulation [8]. The corresponding mean-field model is based on the Lorentzian ansatz approach [9] recently adapted for the aQIF model [10].

RESULTS AND DISCUSSION

We showed that, for a single population node, the resulting mean-field description is capable of qualitatively and quantitatively describing the collective dynamics of the neural network, including transition between tonic firing and bursting. We are currently tuning the model parameters to assess how the emergent network dynamics of each of the coupled nodes in the virtual basal ganglia-thalamo-cortical circuit succeeds to recover the expected physiological dynamics in healthy and pathological dopamine signaling conditions. Altogether, we are presenting a new multiscale TVB approach that will allow for modeling: 1. Specific D1- and D2-type dopamine receptors modulation at a cellular microscale level and; 2. The corresponding derived macroscale realistic brain activity readouts. This new tool will help elucidate the mechanisms by which dopamine modulates large-scale brain activity in health and Parkinson's disease and will set the path to provide with a suitable in silico model for pharmacological development and discovery for dopamine-related neurological and psychiatric diseases.

Keywords: Neuromodulation, dopamine, basal ganglia, Parkinson's disease, The Virtual Brain, adaptive quadratic integrate-and-fire neuron, mean-field model

REFERENCES

[1] Peters, KZ, Cheer, JF, Tonini, R (2021). Modulating the Neuromodulators: Dopamine, Serotonin, and the Endocannabinoid System. Trends in Neurosciences, 44(6): 464-477, DOI: 10.1016/j.tins.2021.02.001.

[2] Dayan, P (2012). Twenty-Five Lessons from Computational Neuromodulation. Neuron, 76(1): 240-256, DOI: 10.1016/j.neuron.2012.09.027.

[3] Alexander, GE, Crutcher, MD, DeLong, MR (1991). Chapter 6 Basal ganglia-thalamocortical circuits: Parallel substrates for motor, oculomotor, "prefrontal" and "limbic" functions. In: H.B.M. Uylings ed., Progress in Brain Research, Elsevier: CG Van Eden, De Bruin, JPC, Corner, MA, Feenstra, MGP, 85: 119-146, DOI: 10.1016/S0079-6123(08)62678-3.

[4] Bernheimer, H, Birkmayer, W, Hornykiewicz, O, Jellinger, K, Seitelberger, F (1973). Brain dopamine and the syndromes of Parkinson and Huntington Clinical, morphological and neurochemical correlations. Journal of the Neurological Sciences, 20(4): 415-455, DOI: 10.1016/0022-510X(73)90175-5.

[5] Grillner S, Robertson B, Kotaleski JH. Basal Ganglia-A Motion Perspective. Compr Physiol. 2020 Sep 24;10(4):1241-1275, DOI: 10.1002/cphy.c190045. PMID: 32969510.

[6] Sanz-Leon, P, Knock, SA, Spiegler, A, Jirsa, VK (2015). Mathematical framework for large-scale brain network modeling in The Virtual Brain. *NeuroImage, 111:* 385–430, DOI: 10.1016/j.neuroimage.2015.01.002**.**

[7] Izhikevich, EM (2003). Simple model of spiking neurons. IEEE Transactions on Neural Networks, 14(6): 1569–1572, DOI: 10.1109/TNN.2003.820440.

[8] Humphries MD, Lepora N, Wood R, Gurney K (2009). Capturing dopaminergic modulation and bimodal membrane behaviour of striatal medium spiny neurons in accurate, reduced models. Frontiers in Computational Neuroscience, 3:26, DOI: 10.3389/neuro.10.026.2009.

[9] Montbrió, E, Pazó, D, Roxin, A (2015). Macroscopic description for networks of spiking neurons. Physical Review X, 5(2), DOI: 10.1103/Phys-RevX.5.021028.

[10] Chen L, Campbell SA (2022). Exact mean-field models for spiking neural networks with adaptation. Journal of Computational Neuroscience 50: 445-469, DOI: 10.1007/s10827-022-00825-9.

162. The “motor-way” to decision-making: the role of premotor oscillatory activity in cue-guided choice

- Department of Psychology, University of Bologna, Cesena, Italy
  Sara Garofalo sara.garofalo@unibo.it
  Gianluca Finotti g.finotti@unibo.it
  Luigi A.E. Degni luigialbertdegni2@unibo.it
  Daniela Dalbagno daniela.dalbagno2@unibo.it
  Marco Badioli marco.badioli2@studio.unibo.it
  Francesca Starita francesca.starita2@unibo.it
  Giuseppe di Pellegrino g.dipellegrino@unibo.it

- Institut des Sciences Cognitives Marc Jeannerod, Neuropsychology of Action Lab
  Lara Bardi lara.bardi@isc.cnrs.fr
  Yulong Huang yulong.huang@isc.cnrs.fr Angela
  Sirigu sirigu@isc.cnrs.fr

- Netherlands Institute for Neuroscience, Social Brain Lab
  Valeria Gazzola v.gazzola@nin.knaw.nl

Introduction

Environmental cues (like the logo of a diner) exert a powerful influence on our daily choices. Although intrinsically neutral, such cues acquire predictive and motivational value through their pairing with a rewarding outcome (e.g., food) and, thus, bias future choices by triggering reward-seeking behavior [1–3] However, the mechanism through which such reward-associated cues exert their influence on human choice is yet to be clarified.

We propose that intimate and bidirectional links between decision, behavior and the cortical motor system may be at the core of this phenomenon. More precisely, we hypothesize that the extent to which a reward-associated cue bias choice is associated with motor-related changes in brain rhythms in response to the presentation of such cues.

Methods

42 participants completed a Pavlovian-to-Instrumental Transfer (PIT) task [4–6] while the electroencephalographic (EEG) signal was acquired.

The PIT task was structured in three phases: (1) Instrumental conditioning phase, in which the participant learned two response-outcome associations (R1O1 and R2O2); (2) Pavlovian Conditioning phase, in which the participant learned the association between four reward-associated conditioned stimuli (CS) and their

respective outcome (CS1→O1, CS2→O2, CS3→O3, CS-→no outcome); (3) Transfer phase, in which the influence of the conditioned stimulus (CS) on the instrumental response was tested (e.g. CS1: R1 or R2?) under extinction (i.e., no reward is delivered). Crucially, while CS1 and CS2 predicted an outcome previously earned by a specific instrumental action (CS+ action), CS+3 predicted rewarding an outcome that was never associated with an instrumental action (CS+ no-action). The CS- served as an unrewarded control condition.

Changes in premotor activity were measured by means of oscillatory activity recorded from electrodes over the premotor cortex, contralateral to the hand used to perform the action (i.e., FC3 electrode for right hand and FC4 electrode for left hand).

Results

Behavioral results confirmed a robust PIT effect across subjects. Analysis of the oscillatory activity revealed decreased beta power and increased theta power in the premotor areas contralateral (but not ipsilateral) to the hand performing the action, selectively associated with the CS+ action condition, as compared to the CS+ no-action and CS- conditions. This activation was observed during the deliberation period, before action execution.

Discussion

These results show the early involvement of premotor activity in cue-guided decision-making, thus supporting the idea - in line with the work on motor cognition and embodied decision-making [7,8] - that the motor system is not downstream to the decision process, but actively contributes to the influence that reward-associated cues can exert on choice processes.

Keywords

reinforcement learning, motor system, cue-guided choice, decision-making, reward

References

1. Dolan RJ, Dayan P. Goals and Habits in the Brain. Neuron. 2013;80: 312–325. doi:10.1016/j.neuron.2013.09.007
2. Doya K. Modulators of decision making. Nat Neurosci. 2008;11: 410–6. doi:10.1038/nn2077
3. Dalley JW, Everitt BJ, Robbins TW. Impulsivity, Compulsivity, and Top-Down Cognitive Control. Neuron. 2011;69: 680–694. doi:10.1016/j.neuron.2011.01.020
4. Garofalo S, Battaglia S, Starita F, di Pellegrino G. Modulation of cue-guided choices by transcranial direct current stimulation. Cortex. 2021;137: 124–137. doi:10.1016/j.cortex.2021.01.004
5. Degni LA, Dalbagno D, Starita F, Benassi M, di Pellegrino G, Garofalo S. General Pavlovian-to-Instrumental Transfer in humans: evidence from Bayesian inference. Front Behav Neurosci. 2022.
6. Cartoni E, Balleine B, Baldassarre G. Appetitive Pavlovian-instrumental Transfer: A review.

Neurosci Biobehav Rev. 2016;71: 829–848. doi:10.1016/j.neubiorev.2016.09.020

7. Casartelli L, Chiamulera C. The motor way: Clinical implications of understanding and shaping actions with the motor system in autism and drug addiction. Cogn Affect Behav Neurosci. 2016;16: 191–206. doi:10.3758/s13415-015-0399-7

8. Lepora NF, Pezzulo G. Embodied Choice: How Action Influences Perceptual Decision Making. Daunizeau J, editor. PLOS Comput Biol. 2015;11: e1004110. doi:10.1371/journal.pcbi.1004110

Acknowledgments

This research is part of the Human Brain Project (FLAG-ERA JTC 2019) titled “The "Motor-way" to Decision-Making: how the motor system drives cue-triggered decisions” (MoDeM)

163. Neural Mechanism of Cue-triggered Decision-making: the Role of the Motor System

Yulong Huang[a,b], Lara Bardi[a], Chen Qu[b], Michel Desmurget[a], Giuseppe di Pellegrino[c], Sara Garofalo[c], Francesca Starita[c], Valeria Gazzola[cd], and Angela Sirigu[a,f†]

[a]Institute of Cognitive Sciences Marc Jeannerod CNRS, UMR 5229, & University of Lyon 1, France

[b]South China Normal University, Department of Psychology, China

[c]Department of Psychology, University of Bologna, Italy

[d]Social Brain Lab, Netherlands Institute of Neuroscience, Netherlands

[e]Department of Psychology, University of Amsterdam, Netherlands

[f] iMind Center of Excellence for Autism, Le Vinatier Hospital, France

Introduction

Environmental stimuli influence our daily decisions, even when they are irrelevant to our current goals. This influence can be adaptive when such cues facilitate the rapid detection of environmental opportunities[1]. However, it can sometimes be maladaptive when the elicited course of action is either no longer appropriate, or difficult to control. This can be observed in compulsive behaviors [2,3]. Crucially, the neural mechanisms through which some cues bias the decision process remain debated [4,5]. In the current functional magnetic resonance imaging (fMRI) study, we hypothesize that the motor system plays a key role in cue-triggered decision-making.

Methods

Thirty-eight right-handed participants (after preprocessing N=31, age=20.36±2.36SD, female=15) performed a variant of the Pavlovian-to-Instrumental Transfer task (PIT) in the MRI scanner. The day before the experimental session, rewards were individually tailored for each participant so that the selected rewards had equal liking and wanting scoring (scale 1-9). A functional localization task in which subjects saw either a circle, square, or cross on the screen asking them to prepare a right-hand, left-hand, or no response, was performed to locate the motor preparation network. During two Pavlovian learning phases, occurring before and after an Instrumental learning phase, participants were asked to passively observe some color cues (CS1, CS2, CS3, CS-) coupled with food rewards (O1, O2, O3, O-). During instrumental learning, some of the rewards (O1 and O2) also became associated with a manual response (R1, R2): Participants press the left or right key on each trial to obtain a reward (R1->O1, R2->O2). In the transfer phase, the slot machine will light up a color cue and participants could freely produce as many responses as they wanted (both left- and right-hand) (see **Fig. 1**)

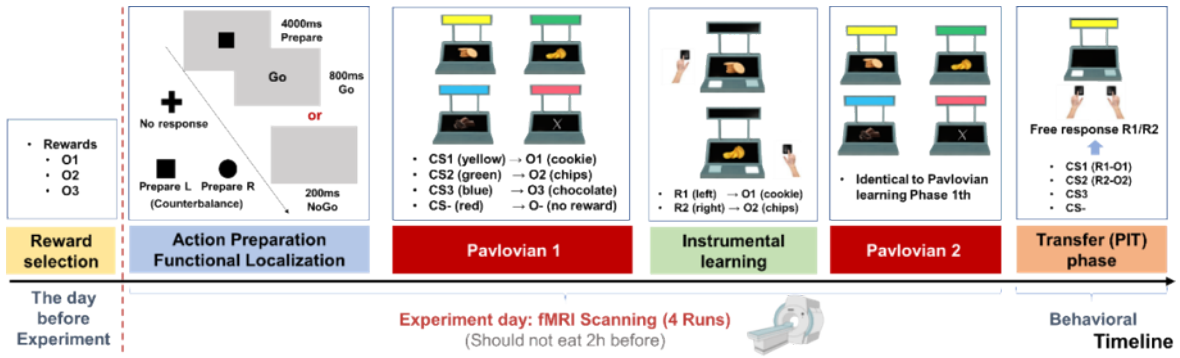

Figure. 1. Experimental timeline and task illustration.

Results

At the behavior level, CS1 and CS2, which were coupled with a reward that was previously associated with a manual response elicited the production of more corresponding actions during the transfer phase (i.e., CS1->R1, CS2->R2), indicating an action-specific PIT effect (**Fig.2A**, $t_{(30)}$=4.563, Cohen's d=0.820, p<0.001). Moreover, we found a higher number of responses when CS3 was presented, relative to CS− (Fig.2B, $t_{(30)}$=2.266, Cohen's d=0.407, p=0.031), indicating a reward-related general PIT effect. At the neural level (**Fig.2C**), during the second Pavlovian phase, we found that color cues that were indirectly associated with a response (CS1 and CS2) led to the significant activation of the Superior parietal and Postcentral cortex, a key region for motor intention and action control [6,7], as compared to CS3. This effect was absent in the first Pavlovian phase. Further functional localization-based ROIs analysis (**Fig.2D**) showed the action-related CS+ activate the Left pre-supplementary motor area (preSMA) only in the second Pavlovian phase (CS1>CS3: $t_{(30)}$=1.964, Cohen's d=0.353, p=0.021).

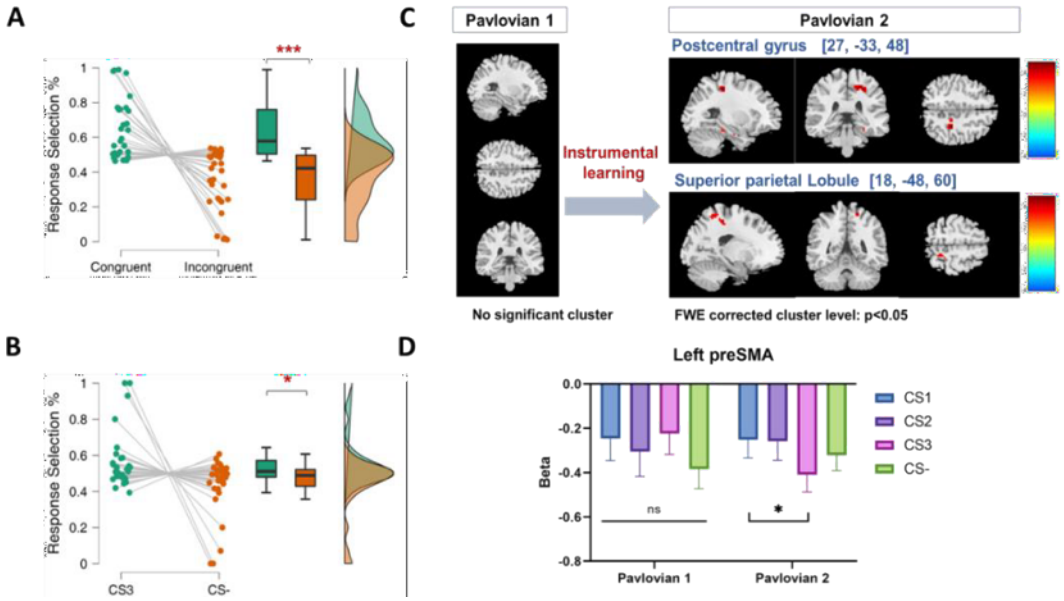

Figure. 2. Behavioral results of transfer phase A) Specific PIT effect and B) General PIT effect; C) Whole brain analysis results of the first and second Pavlovian phases (voxel-wise threshold of p<0.001, family-

wise error corrected at the cluster level. D) Functional localization-based region of interest analysis results. *<0.05, ***<0.001

Discussion

Our current results suggest that the underlying neural substrates of motor processes might be pivotal in cue-triggered decision-making, enriching the understanding of the neural processes that could mediate the transition from adaptive to maladaptive cue-triggered decisions.

Keywords ： Pavlovian-to-Instrumental Transfer (PIT) task; Cue-trigger decision making; Functional magnetic resonance imaging (fMRI); Motor system

Acknowledgment: This research is part of the Human Brain Project (FLAG-ERA JTC 2019) titled “The "Motor-way" to Decision-Making: how the motor system drives cue-triggered decisions” (MoDeM)

Reference:

1. Cartoni, E., Balleine, B., & Baldassarre, G. (2016). Appetitive Pavlovian-instrumental transfer: a review. Neuroscience & Biobehavioral Reviews, 71, 829-848. DOI: https://doi.org/10.1016/j.neubiorev.2016.09.020
2. Holmes, N. M., Marchand, A. R., & Coutureau, E. (2010). Pavlovian to instrumental transfer: a neurobehavioural perspective. Neuroscience & Biobehavioral Reviews, 34(8), 1277-1295. DOI: https://doi.org/10.1016/j.neubiorev.2010.03.007
3. Casartelli, L., & Chiamulera, C. (2016). The motor way: clinical implications of understanding and shaping actions with the motor system in autism and drug addiction. Cognitive, Affective, & Behavioral Neuroscience, 16(2), 191-206. DOI: https://doi.org/10.3758/s13415-015-0399-7
4. Seabrooke, T., Hogarth, L. & Mitchell, C. J. The propositional basis of cue-controlled reward seeking. Q. J. Exp. Psychol. 69, 2452–2470 (2016). DOI: https://doi.org/10.1080/17470218.2015.1115885
5. Prevost, C., Liljeholm, M., Tyszka, J. M. & O’Doherty, J. P. Neural Correlates of Specific and General Pavlovian-to-Instrumental Transfer within Human Amygdalar Subregions: A High-Resolution fMRI Study. J. Neurosci. 32, 8383–8390 (2012). DOI: https://doi.org/10.1523/JNEUROSCI.6237-11.2012
6. Desmurget, M., Reilly, K. T., Richard, N., Szathmari, A., Mottolese, C., & Sirigu, A. (2009). Movement intention after parietal cortex stimulation in humans. science, 324(5928), 811-813. DOI: 10.1126/science.1169896
7. Mendelsohn, A., Pine, A., & Schiller, D. (2014). Between thoughts and actions: motivationally salient cues invigorate mental action in the human brain. Neuron, 81(1), 207-217. DOI: https://doi.org/10.1016/j.neuron.2013.10.019

164. Looking at previous cue sites reactivates value coding for serial evaluation in orbitofrontal cortex

Demetrio Ferro[1,2,*], Anna Rifé Mata[1,2], Tyler Cash-Padgett[3], Maya Zhe Wang[3], Benjamin Hayden[3], Rubén Moreno Bote[1,2]

[1] Center for Brain and Cognition, Universitat Pompeu Fabra, 08002, Barcelona, ES;

[2] Department of Information and Communication Technologies, Universitat Pompeu Fabra, 08002, Barcelona, ES;

[3] Department of Neuroscience, Center for Magnetic Resonance Research, University of Minnesota, Minneapolis, MN55455, USA

*corresponding author, e-mail: demetrio.ferro@upf.edu

INTRODUCTION/MOTIVATION

Whenever facing dislocated options to choose, we tend to sequentially direct our gaze to each of them, until we commit to a decision[1,2]. Studies about the behavioral role of gaze allocation suggest longer inspections for the most valuable options[3-6], but the effects of allocating gaze on neural activity during decision-making is unknown. We aimed at detecting value encoding in orbito-frontal (OFC) cells, combined with task-relevant gaze patterns, to investigate the modulatory effects of gaze position on neural activity at multiple task conditions. We assessed that value encoding for sequentially presented offers mainly occurs during offer presentation and choice deliberation, for ipsi-lateral gaze allocation. By analyzing delay times following each offer presentation, we found that subjects preferentially looked at screen locations where best offer previously occurred, and exclusively re-activated the encoding of the best offer value for ipsi-lateral visual inspection.

METHODS

We simultaneously recorded eye and neural data during a risky reward gambling task (Fig.1A). The task is performed by two macaque monkeys and consists in the sequential presentation of two alternative offers on either screen side (*offer1*/*offer2*, 400ms), interleaved with blank screen delay times (*delay1*/*delay2*, 600ms). Choice is performed by holding fixation on the chosen offer for at least 200ms. The monkeys correctly performed the task by accurately detecting best offer (Fig.1B) and gazing to meaningful locations throughout task execution (Fig. 1C). We fit a logistic model of choice (Fig.1D) with regressors: expected value (*EV*) of left/right offers (EV_L/EV_R), their variance σ_L^2 or σ_R^2, and order of presentation (s_{LR}=1 if trial starts with left offer, 0 otherwise). *EV* is the product of reward magnitude *m* and probability *p*; σ^2 is computed as $mp\ (1-p)$. We included the fraction of time spent looking at the right screen side $f_R=t_R/(t_R+t_L)$, with t_R (t_L) being the time on right (left) side. For the encoding of the *EV*s in OFC, we regressed the spike count η of each of $n=248$ cells in 10 ms bins with a linear rate model to EV_L or EV_R (Fig.2A,B). The empirical fraction of significant cells is compared to the distribution of $n=1000$ trial order shuffles and deemed significant if >95th percentile threshold. The analysis is repeated by combination with eye data, for which trials are classified as looking left (or right) based on average horizontal eye position being negative (or positive) (Fig.2C,D).

RESULTS AND DISCUSSION

Subjects directed their gaze to offers during their presentation, and shifted if most recent offer was less valuable, so that more time was spent on most valuable offer. By factoring out value-related variables, we found that more time was devoted to the chosen offer, suggesting that gaze allocation plays a causal role in decision making, beyond value-based contingencies. Surprisingly, the same pattern occurs during delay times. Despite the screen was blank, subjects directed gaze where valuable offers were previously shown. We find that EV encoding mainly occurred during presentation, or at later times, before and during choice deliberation (Fig.2A,B). Investigating EV encoding in opposite inspection sides (look left, look right), we find that the respective offer is significantly encoded in OFC if and only if the subject directs gaze to ipsilateral screen side (Fig2.C,D), in line with overt visual search for sensory input integration[1-3]. Strikingly, we find that if subjects looked back at first offer location during the second delay, the encoding of the first offer EV significantly increased, possibly implying the reactivation of offer re-evaluation for that offer (Fig.2C,D). Combining our results, we provide evidence that eye position reflects and internal deliberation process possibly modulating the encoding of currently (re-)evaluated content, providing a new window to study the hidden dynamics of decision making.

Keywords: decision making, reward gambling, value encoding, orbitofrontal cortex, re-evaluation, visual inspection

REFERENCES

[1] Thomas, A.W., Molter, F. and Krajbich, I., 2021. *Elife*, *10*, pp. e57012. doi: 10.7554/eLife.57012

[2] Krajbich, I., Armel, C. and Rangel, A., 2010. *Nat. Neuroscience*, *13*(10), pp.1292-1298, doi: 10.1038/nn.2635;

[3] McGinty, V.B., Rangel, A. and Newsome, W.T., 2016. *Neuron*, *90*(6), pp.1299-1311, doi: 10.1016/j.neuron.2016.04.045;

[4] Padoa-Schioppa, C. and Assad, J.A., 2006. *Nature*, *441*(7090), pp.223-226; doi: 10.1038/nature04676;

[5] Strait, C.E., Blanchard, T.C. and Hayden, B.Y., 2014. *Neuron*, *82*(6), pp.1357-1366; doi: 10.1152/jn.00325.2015;

[6] Rich, E.L. and Wallis, J.D., 2016. *Nat. Neuroscience*, *19*(7), pp.973-980. doi: 10.1038/nn.4320;

Figures

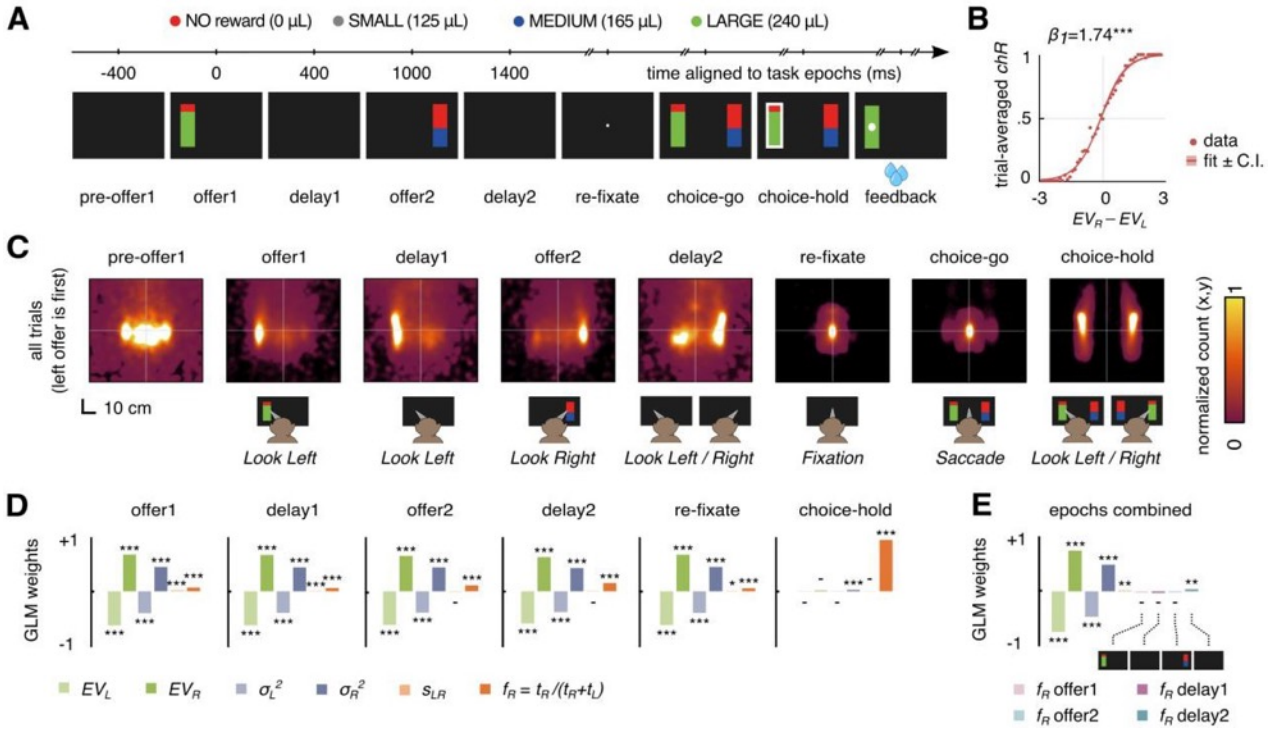

Figure 1. Task, choice, and gaze position during execution. A. Timeline of the gambling task for a sample trial. Reward offers are sequentially presented at opposite screen sides for 400 ms (*offer1/offer2*), each followed by 600 ms delay time (*delay1/delay2*). Visual stimuli consist of vertical bars whose height cues to reward probability *p*, and color cues to reward size *m* = medium (blue), large (green) or small (safe, always had *p*=1, gray). Choice is performed after *choice- go* cue by gazing to either side for at least 200 ms (*choice-hold*). Reward size, probability and order of presentation are randomized across trials. Data are anchored to first offer on left side, so all data are horizontally mirrored in trials that started with right offer. B. Fraction of choices for right offer (ch_R), higher when right offer had higher EV compared to left offer. Solid line shows logistic fit (logit(ch_R) = $\beta_0 + \beta_1 (EV_R - EV_L)$), shaded areas show ±95% Confidence Interval (C.I.).

C. Heatmap of eye position during the task execution. The main gaze pattern follows the sequential presentation of offers. At delay times, subjects either looked to most recent presented location (*delay1*) or at best offer side (*delay2*).

D. Logistic model of choice (logit(ch_R)= $\beta_0+\beta_1 EV_L+\beta_2 EV_R+\beta_3 \sigma_L^2+\beta_4 \sigma_R^2+\beta_5 s_{LR}+\beta_6 f_R$). The fraction of time spent inspecting right screen side f_R has impact on choosing right offer in all epochs, even including value related (EV_L, EV_R, σ_L^2, σ_R^2) and presentation order (s_{LR}) regressors. E. Same as D, but pooling f_R regressors in all *offer/delay* epochs to assess their weight on the choice. B-E. Trials n=5971 (Subject 1: n=2463; Subject 2 n=3328). Significance: *p<0.05, **p<0.01, ***p<0.001.

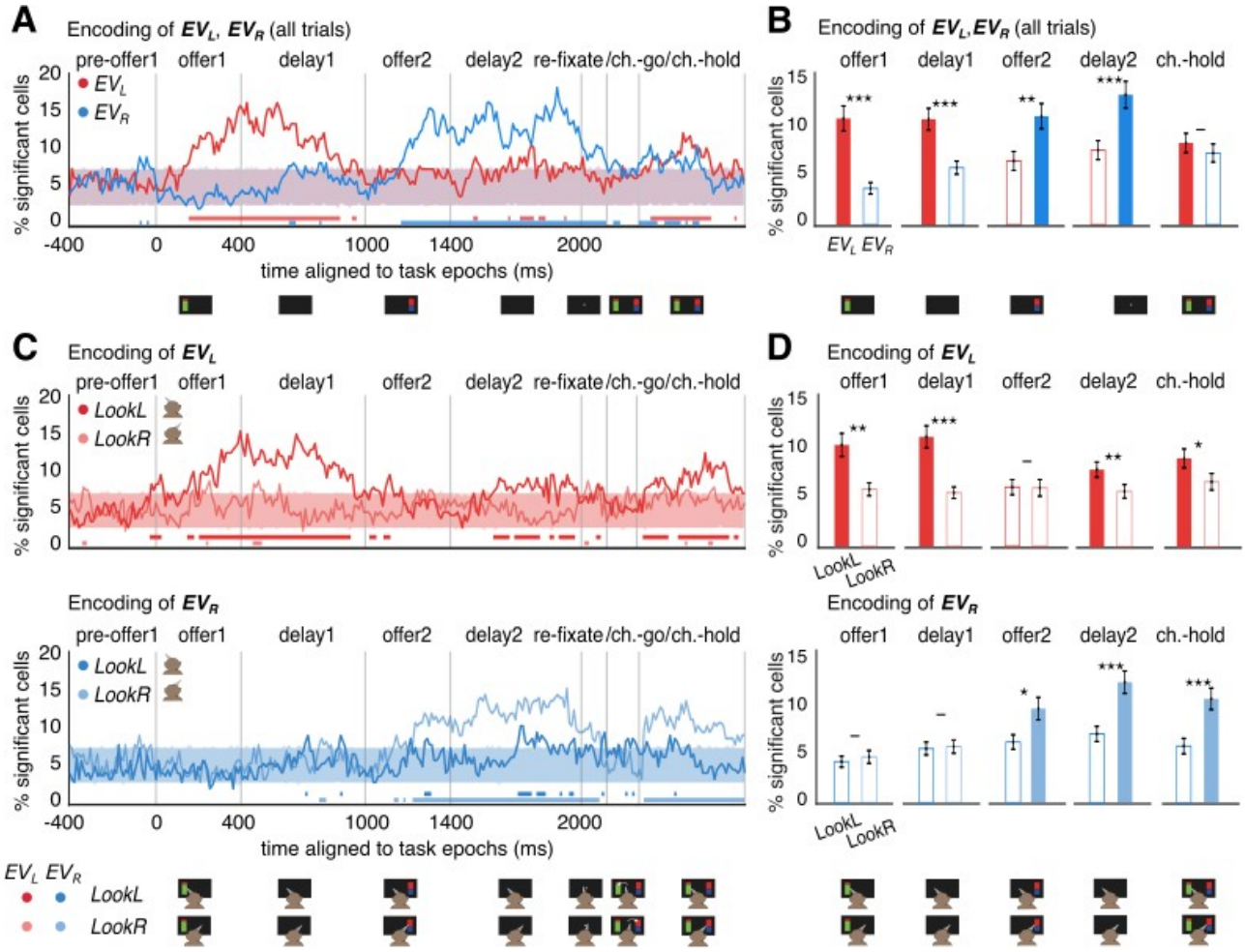

Figure 2. Analyses of neural spike count coding of reward offer EV and the effects of visual inspection on either screen side. A. Fraction of cells showing significant encoding of offer expected value (EV_L, EV_R), independently fit to linear models for the spike count η as $\eta=\beta_0+\beta_1 EV_L$ (red), or $\eta=\beta_0+\beta_1 EV_R$ (blue). The regression is applied independently for each cell (*n=31±5.85* mean ± s.e.m. cells per session, *n=248* in total), including all trials (*n=746.38±87.29* mean ± s.e.m trials per session, *n=5971* in total); Solid lines show the empirical results in each time bin; shaded areas (overlaid, in opacity) cover the 5th to 95th percentile of significant fraction of cells encoding the respective *EV* obtained via *n=1000* trial order permutations; bottom lines report consecutive runs of time bins with significant encoding of EV_L or EV_R (assessed as fraction of cells above the 95th percentile of trial-order shuffles). B. Time-averaged fraction of cells showing significant encoding of offer *EV*s, matching results in B. The significance of empirical values is assessed as exceeding of the 95th percentile of the same values run over *n=1000* trial-order shuffles of the data (non-significant bars are in white). Results for the fraction of cells for EV_L and EV_R are compared via non-parametric tests (Wilcoxon signed-rank test), significance:

- n.s., *p<0.01, **p<0.01, ***p<0.001. C. Top: same as A but focusing on EV_L and comparing trial subsets where subjects mostly *LookL* (negative average eye position for current bin, in red) with trials where subjects mostly *LookR* (positive average eye position, in light red). Bottom: same as B but focusing on EV_R and comparing *LookL* trials (blue) with *LookR* trials (light blue). D. Top: same as B but focusing on EV_L and comparing *LookL* with *LookR* trials. Bottom: same as C but focusing on EV_R and comparing *LookL* with *LookR* trials.

165. A multisensory profile protocol: spatial and postural virtual reality subsets applied to vestibular disorders

Angela Julienne[1,3*], Stéphane Besnard[1,2] (MD, PhD)

[1] Unité de Recherche VERTEX 7480, Université de Caen, Caen, France
[2] Service ORL, Centre Hospitalier Universitaire de Caen, Caen, France
[3] Virtualis VR, Montpellier, France

*Corresponding author e-mail address: angelajulienne@hotmail.fr

INTRODUCTION

Vertigo is one of the most common causes of consultation in the adult population and particularly in the geriatric community [1]. Vestibular patients, manifesting vertigo, constitute a rather heterogeneous group because of the diversity of symptoms, the intensity of these symptoms and the existence or not of comorbidities (psychological, somatic, cognitive, etc.)[2–4]. Numerous studies have shown cognitive and postural deficits in vestibular disorders[5–7].In fact, these disorders can be considered as a multisensory syndrome; which has a significant impact on psychological, cognitive and social aspects leading to varied and sometimes lasting disabling states. However, patients' management is punctuated by uncertainties and misdiagnosis; moreover, cognitive and postural consequences remain unexplored in clinical practice. Other aspects of vestibular dysfunction need to be considered. Therefore, a multisensory profile protocol, associated with virtual reality (VR), was developed using a new software in order to explore higher cognitive functions. In fact, this immersive tool offers user- friendly test programming as well as automated tracking and analysis compared to current tools used to investigate human cognition. The feasibility was studied as well to investigate patients understanding of the paradigms and their relevance.

METHODS

Based on a literature review, we selected tests and programmed a multisensory computerized assessment protocol evaluating different aspects of vestibular dysfunction which are not considered in classic clinical evaluation. In this paper, the spatial and cognitive components will be presented. The patients were tested using spatial and postural paradigms associated with VR. The spatial cognitive component consists of a simple and complex virtual reality maze task. The postural component consists of a static and dynamic task associated with virtual reality. The protocol is currently still being implemented in persons with chronic vestibular disorders. Following assessment, the patients had to respond to a questionnaire in order to measure the study feasibility. The next phase will consist of implementing the protocol in healthy individuals. The spatial and postural subsets will be thus validated in healthy individuals and vestibular patients.

RESULTS AND DISCUSSION

We recruited 16 patients (12 F, 51 ± 13 years old) suffering from chronic vestibular disorders. Following assessment, the patients had to respond to a questionnaire in order to measure the study feasibility. There were 12 respondents of which 67 percent said that they would be willing to participate in another similar study using VR. These results provide a preliminary overview of a multisensory assessment as well as its acceptance by patients and relevance. In fact, user-friendly, automated tests and real-life constraining environments are components integrated using the software and thus facilitating human

cognition assessment. The spatial and postural subsets are associated with virtual reality paradigms to represent ecological situations and reflect difficulties encountered by patients. This protocol will continue being tested on vestibular patients and healthy individuals to create a database and guide health policymakers by providing information on specific sensory profiles and cognitive impairments for optimizing diagnostic and therapeutic purposes.

Keywords: Multisensory profile, Vestibular disorders, Virtual reality, Computer-based Software, Human cognition.

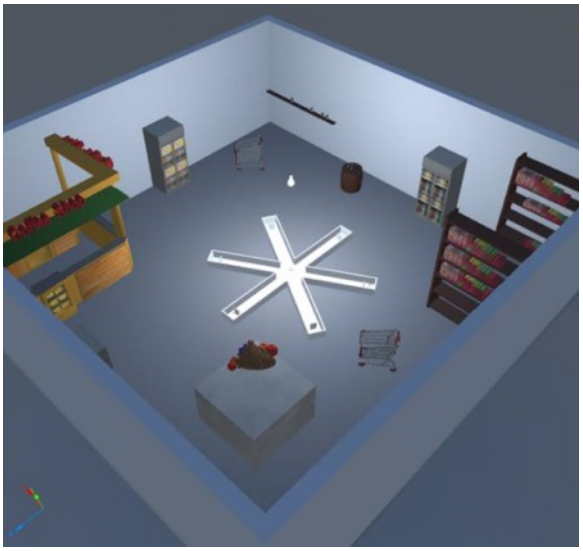

Figure 1. Radial Arm Maze (Complex Spatial task) configured in supermarket environment. The subject was placed at the centre of the six armed maze and had to learn to find two rewards located in different arms. The distance travelled and latency were recorded. This task allowed the evaluation of reference memory and working memory.

REFERENCES

1. Bisdorff A, Bosser G, Gueguen R, Perrin P. The epidemiology of vertigo, dizziness, and unsteadiness and its links to co-morbidities. *Front Neurol*. 2013;4 MAR(March):1-7. doi:10.3389/fneur.2013.00029

2. Lahmann C, Henningsen P, Brandt T, et al. Psychiatric comorbidity and psychosocial impairment among patients with vertigo and dizziness. *J Neurol Neurosurg Psychiatry*. 2014;86(3):302-308. doi:10.1136/jnnp-2014-307601

3. Jacob RG, Furman JM. Psychiatric consequences of vestibular dysfunction. *Curr Opin Neurol*. 2001;14(1):41-46. doi:10.1097/00019052-200102000-00007

4. Limburg K, Sattel H, Radziej K, Lahmann C. DSM-5 somatic symptom disorder in patients with vertigo and dizziness symptoms. *J Psychosom Res*. 2016;91:26-32. doi:10.1016/j.jpsychores.2016.10.005

5. Popp P, Wulff M, Finke K, Rühl M, Brandt T, Dieterich M. Cognitive deficits in patients with a chronic vestibular failure. *J Neurol*. 2017;264(3). doi:10.1007/s00415-016-8386-7

6. Whitney SL, Marchetti GF, Schade AI. The relationship between falls history and computerized dynamic posturography in persons with balance and vestibular disorders. *Arch Phys Med Rehabil*. 2006;87(3):402-407. doi:10.1016/j.apmr.2005.11.002

7. Bisdorff A, von Brevern M, Lempert T, Newman-Toker DE. Classification of vestibular symptoms: Towards an international classification of vestibular disorders. *J Vestib Res*. 2009;19(1-2):1-13. doi:10.3233/VES-2009-0343

166. Role of the Motor Cortex and Social Environment in Cue-Triggered Decision-Making: Insights from Single-Pulse TMS and Action Observation

Junjie Wei[1], Cas Teurlings[1], Sara Garofalo[2], Francesca Starita[2], Lara Bardi[3], Yulong Huang[3], Angela Sirigu[3], Giuseppe Di Pellegrino[2] and Valeria Gazzola[1]

[1] Netherlands Institute for Neuroscience, Amsterdam, Netherlands
[2] Department of Psychology, University of Bologna, Bologna, Italy
[3] Institut des Sciences Cognitives Marc Jeannerod, Neuropsychology of Action Lab, Paris, France

Introduction

Environmental cues play an important role in our daily life by influencing decision-making and guiding behaviors (Bray et al., 2008). The most common paradigm to investigate the influence of environmental cues on decision-making is the Pavlovian Instrumental Transfer (PIT) task, which could test the transfer effects between Pavlovian cues (e.g., colors) and instrumental actions (e.g., pressing left or right buttons) via the same reward (specific transfer) or similar rewards associated with the Pavlovian cue (general transfer). In this process, Lepora et al (2015) stressed the motor system is not just responsible for physically executing actions, but is also involved in making decisions. It plays a causal role in decision-making based on cues. While there is a close relationship between decision-making, behavior and motor system, the current research on this topic is still sparse, and to what extent a conclusion could be generalized to the role of the premotor cortex is unclear in this process. Therefore, we set two Pavlovian phases before (Pav1) and after (Pav2) instrumental learning in the current experiment, aiming to investigate whether the premotor cortex is deeply involved in building associations between behavioral and environmental cues. By measuring the motor evoked potentials (MEP) induced by single-pulse transcranial magnetic stimulation (TMS) during the PIT task, we aim to explore the role of the premotor cortex in the decision-making of the PIT task. We hypothesize that there will be an increase in cortical excitability, measured from the premotor cortex, in the second Pavlovian phase (Pav2) compared to the first (Pav1). Because we expect that the instrumental phase affects the motor representation of the cue related to that specific action (specific PIT).

Methods

40 healthy adults (M = 24.63, SD = 4.60) were recruited. 38 of these completed the whole task and MEP data collection. Each participant was asked to fill out an online questionnaire first to assess their liking of the food stimuli from a preselected list of 40 snack foods. The resting motor threshold (RMT) and the intensity of single-pulse TMS were estimated for each subject to set the individualized stimulation strength before the experiment. Then they were asked to play a tailored PIT paradigm based on their three favorite snacks to ensure that the food reward in the paradigm was highly attractive to the participant. Individual MEP data was recorded in two Pavlovian phases before and

after the instrumental phase, including behavioral data from the transfer PIT phase.

Results

Behavioral results revealed, tested with a paired samples t-test, a specific transfer effect ($t(75) = 8.61$, $p<0.0001$), both in CS1 ($t(37) = 4.95$, $p<0.0001$) and CS2 conditions ($t(37) = 7.51$, $p<0.0001$). There was a marginally significant difference between the number of responses in the CS3 condition (M±SD=151.7±65.82) and in the CS- condition (M±SD=135.4±70.94) in the general PIT effect ($t(37) = 2.019$, $p=0.0507$). For the MEP data, a repeated ANOVA analysis was conducted, but no significant differences were found between conditions (conditioned stimulus, left and right hemisphere for the first Pavlovian phase and the second Pavlovian phase).

Discussion

The behavioral results of our PIT task provide evidence to illustrate that environmental cues could influence our decision-making (PIT effect). However, the investigated role of the motor cortex before and after building the association between action and food rewards (difference in MEP amplitudes) did not lead to any significant results. In the current experiment, we did not use neural navigation, and participants' inattentive head movement during the experiment may have affected the MEP results. In the future, different observational techniques that could compare between brain regions or size of activity within the motor cortex (e.g., BOLD fMRI) could help us better understand the changes during the PIT task.

Acknowledgement:

This research is part of the Human Brain Project (FLAG-ERA JTC 2019) titled “The "Motor- way" to Decision-Making: how the motor system drives cue-triggered decisions” (MoDeM).

Keywords

< motor cortex> < PIT> < MEP>

Reference

[1]. Bray, S., Rangel, A., Shimojo, S., Balleine, B., & O'Doherty, J. P. (2008). The neural mechanisms underlying the influence of pavlovian cues on human decision making. J Neurosci, 28(22), 5861-5866. https://doi.org/10.1523/JNEUROSCI.0897-08.2008

[2]. Lepora, Nathan F.; Pezzulo, Giovanni; Daunizeau, Jean (2015). Embodied Choice: How Action Influences Perceptual Decision Making. PLOS Computational Biology, 11(4), e1004110–. doi:10.1371/journal.pcbi.1004110

167. Laminar feedback signals in visual cortex related to an anticipated future during navigation

Yulia Lazarova*[1,2*], Angus Paton*[1,2], Lucy S. Petro[1,2], Lars Muckli[1,2]

[1]Centre for Cognitive Neuroimaging, School of Psychology and Neuroscience, College of Medical, Veterinary and Life Sciences, University of Glasgow, Glasgow, United Kingdom, G12 8QB.

[2] Imaging Centre for Excellence, Queen Elizabeth University Hospital, University of Glasgow, G51 4LB.

y.lazarova.1@research.gla.ac.uk

INTRODUCTION/MOTIVATION

We rely on pre-existing models of the world accumulated through past experiences to form internal representations of our present environment. In addition to facilitating perception in the present, these models enable us to engage in prospective thoughts and mental simulations unrelated to the immediate environment. Traces of both streams of thought have been found to coexist and share some neuronal mechanisms at the earliest level of cortical processing [1][2]. It is still a challenge to understand the mechanisms that allow the parallel existence of these two streams of thought while at the same time keeping the perception of reality and imagination segregated. We used 7T fMRI and a navigation task to investigate on a laminar level the two codes of information – related to the present and to the anticipated future.

METHODS

We used a VR headset to familiarise participants with a virtual environment prior to scanning. The environment consisted of four contextually different rooms (a kitchen, an office, a bedroom, and a game room) arranged in a plus shape configuration (Fig .1A). We recorded BOLD responses in a series of experiments using 3T and 7T fMRI while participants were presented with videos simulating navigation through the environment. Directional cues elicited expectations for an upcoming room that the participant was not presently viewing but could generate prospective thoughts about (Fig. 1B). The lower right quadrant of the video was hidden behind an occluder, blocking feedforward input to the corresponding patch of the visual cortex. We applied MVPA analysis to probe the contents of the activation in the non-stimulated areas of the visual cortex. We were interested whether the classifier could successfully decode the anticipated future room even before it was presented. In a subsequent control study, we removed the direction cue to prevent the anticipation of the upcoming room.

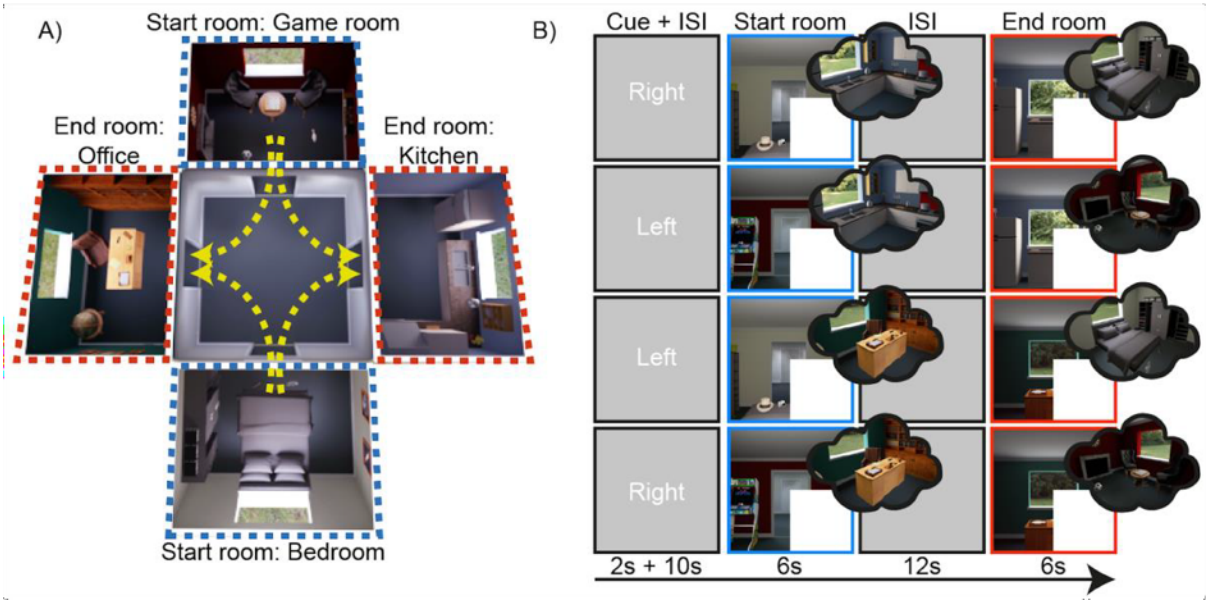

Figure 1. (A) An aerial perspective of the virtual environment. The yellow arrows denote the trajectories of navigation videos. **(B) Experimental design.** A direction cue is shown to the subject for 2s followed by a 10s inter-stimulus interval. The start room video is then shown for 6s, depicting a first- person perspective moving out of the start room (Game room/Bedroom) into the centre room. A 12s inter-stimulus interval precedes the end room video moving into the end room (Kitchen/Office). The bottom right quadrant of the video stimuli is occluded.

RESULTS AND DISCUSSION

The classifier could successfully decode the anticipated future room based on activity from non-stimulated patches of area V2 and V3 (Fig.2 A). Upon removing the direction cue at the start of navigation, the classifier performance dropped to chance level. This suggests that information about the future is driven by predictions formed in higher order areas and is conveyed to the visual cortex via feedback cortical pathways. Our 7T study reviled traces of information about the future room specifically in the deep and superficial cortical layers of V2 and deep layers of V3 (Fig. 2 B, C). This finding is in line with previous studies identifying deep and superficial layers to be the main target of feedback connections [3]. Our results further add to findings from animal model studies which point to the importance of layer-spanning pyramidal neurons for the integration of feedforward and feedback processing [4]. Information about the present room in non-stimulated patches of the visual cortex was decodable only at the end of the navigation path but not at the start. This finding raises the question of potential competition between the two codes of information which is yet to be answered in future studies.

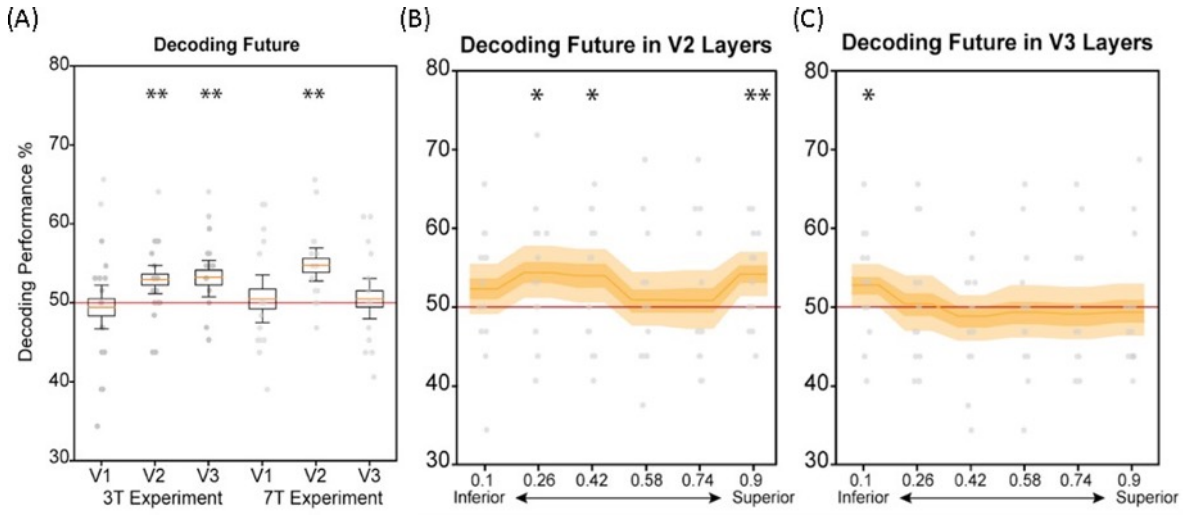

Figure 2. Classification results for decoding the identity of the future room from occluded voxels.

(A) Results from the 3T (N=20) and the 7T (N=15) study for all ROIs. (B) Decoding accuracy of the future room across cortical depths of area V2. (C) Decoding accuracy of the future room across cortical depths of area V3.

Keywords: fMRI, cortical layers, cortical feedback processing, navigation, visual cortex, VR

ACKNOWLEDGEMENTS

This project has received funding from the European Union's Horizon 2020 Framework Programme for Research and Innovation under the Specific Grant Agreement No. 720270, 785907 and 945539 (Human Brain Project SGA1, SGA2 and SGA3), and the Biotechnology and Biological Sciences Research Council (BBSRC) 'Layer-specific cortical feedback'.

REFERENCES

[1| Monaco, S., Malfatti, G., Culham, J. C., Cattaneo, L., & Turella, L. (2020). Decoding motor imagery and action planning in the early visual cortex: Overlapping but distinct neural mechanisms. *NeuroImage*. https://doi.org/10.1016/j.neuroimage.2020.116981

[2] Huang, Y., Jiao, B., Wang, Y., Li, J., Liu, M., & Zhang, D. (2021). Parallel neural representation shared by visual perception and mental imagery. *Journal of Vision*. https://doi.org/10.1167/jov.21.9.2443

[3] Self, M. W., van Kerkoerle, T., Goebel, R., & Roelfsema, P. R. (2019). Benchmarking laminar fMRI: Neuronal spiking and synaptic activity during top-down and bottom-up processing in the different layers of cortex. In *NeuroImage*. https://doi.org/10.1016/j.neuroimage.2017.06.045

[4] Larkum, M. E., Petro, L. S., Sachdev, R. N. S., & Muckli, L. (2018). A Perspective on Cortical Layering and Layer-Spanning Neuronal Elements. In *Frontiers in Neuroanatomy*. https://doi.org/10.3389/fnana.2018.00056

…

168. Laminar dynamics in the awakening sensory cortex

Antonio Pazienti[1*], Mariel Müller[2], Umberto Olcese[2], Maurizio Mattia[1]

Affiliations: [1]Istituto superiore di sanità, viale Regina Elena 299, 00161 Rome, Italy

[2] Cognitive and Systems Neuroscience Group, Swammerdam Institute for Life Sciences, University of Amsterdam, Science Park 904, 1098XH Amsterdam, The Netherlands

*e-mail-address of corresponding author: antonio.pazienti@iss.it

INTRODUCTION

Neuronal activity in brain networks unfolds across a multitude of spatiotemporal scales, due to the brain's hierarchical organization and to the constraints given by the need to bidirectionally interact with the environment. The bottom-up flow of information from sensory to associative areas and the top-down feedback in the opposite direction follow specific and almost complementary laminar and inter-areal trajectories [1]. The effectiveness in the percolation and transformation of information across these pathways is known to underlay our capability of conscious processing [2].

However, the mechanistic underpinnings of the sleep/wake cycle, in which consciousness is lost and recovered and the working regime of our brain changes dramatically, are still widely unknown. Long-range functional connectivity, for instance, is widely modulated across these global transitions in brain state [3,4], while local connectivity appears to be preserved [5]. Yet, spiking activity in the thalamus and deep cortical layers correlates with consciousness level [6]. A state-dependent modulation of cross-laminar temporal dynamics has been also found at the macroscale, on top of infra-slow rhythms [7]. Thus, changes in the activity occur both at the macro- and microscopic level as a function of the brain state, yet it remains poorly understood how global state transitions such as between wakefulness and anaesthesia unfold.

Here, we focused on the laminar spatiotemporal unfolding of isoflurane-induced slow-wave activity (SWA) and on its modifications during the awakening process. To this purpose, we simultaneously recorded the activity of several neuronal assemblies probed across all cortical layers, and in both a primary and a higher sensory area during the transitions from awake to isoflurane-induced SWA and vice versa.

METHODS

Experiments were performed in head-fixed mice (N=12). Following habituation to head-fixation, two dual-shank laminar probe recordings (Neuronexus A2x16-10mm-100-500-177CM32) were performed in primary visual cortex V1 and posterior parietal cortex PPC, identified via intrinsic signal imaging. Probe location was verified post- mortem via histological reconstruction. Recordings were done across behavioural states, using the following sequence: wakefulness (30 min), anaesthesia induction, progressive decrease of isoflurane concentration: 0.5%, 0.3% and 0% (awakening); for each level there was 15 min of induction and 30 min of stable recording. From the

raw recordings, LFP and MUA signals were extracted. Ad-hoc Matlab (The Mathworks) scripts were used for further analyses.

RESULTS AND DISCUSSION

We characterized the activity propagation both across cortical layers and between the two cortical areas we recorded. Fading of anaesthesia wass accompanied by increasingly complex and rapid patterns, whose main modes of propagation travelled from posterior to medial-lateral areas and vice versa. At the same time, the wakening process showed emerging instances of asynchronous, generalized spiking activity. Spectral analysis showed that the neuronal activity shifted from infra-slow (around 0.1 Hz) to slow (1 Hz), to the theta range (6-8 Hz) while going from high isoflurane levels to wakefulness.

Importantly, when characterizing the simultaneous propagation of the activity across the layers and across the cortical surface, we found that the timing with which layer 5, 6 and 2/3 are entrained changes depending on the global state, with the involvement of layer 2/3 (L2/3) showing the biggest changes when recovering from anaesthesia. Critically, this occursed specifically for feedback propagation (PPC to V1). Specifically, the delay with which the spiking activity coming from layer 5 propagated to L2/3 got smaller when the global state approached awakening.

Our results shed new light on the interplay between local (at the level of single neurons) and global dynamics involved in the feedforward and feedback signalling in the transition to and from consciousness.

Keywords: Sensory processing, laminar computation, isoflurane, sleep, slow-wave activity, consciousness, anaesthesia.

REFERENCES

[1] Markov NT, Ercsey-Ravasz M, Van Essen DC, Knoblauch K, Toroczkai Z, Kennedy H. 2013. Cortical high-density counterstream architectures. Science (80-) 342:1238406. doi:10.1126/science.1238406

[2] Mashour GA, Roelfsema P, Changeux J, Dehaene S. 2020. Conscious processing and the global neuronal workspace hypothesis. Neuron 105:776–798. doi:10.1016/j.neuron.2020.01.026

[3] Barttfeld P, Uhrig L, Sitt JD, Sigman M, Jarraya B, Dehaene S. 2015. Signature of consciousness in the dynamics of resting- state brain activity. Proc Natl Acad Sci USA 112:887–92. doi:10.1073/pnas.1418031112

[4] Demertzi A, Tagliazucchi E, Dehaene S, Deco G, Barttfeld P, Raimondo F, Martial C, Fernández-Espejo D, Rohaut B, Voss HU, Schiff ND, Owen AM, Laureys S, Naccache L, Sitt JD. 2019. Human consciousness is supported by dynamic complex patterns of brain signal coordination. Sci Adv 5:eaat7603. doi:10.1126/sciadv.aat7603

[5] Olcese U, Bos JJ, Vinck M, Lankelma J V, van Mourik-Donga LB, Schlumm F, Pennartz CM. 2016. Spike-based functional connectivity in cerebral cortex and hippocampus: loss of global connectivity is coupled to preservation of local connectivity during Non-REM Sleep. J Neurosci 36:7676–92. doi:10.1523/JNEUROSCI.4201-15.2016

[6] Redinbaugh MJ, Phillips JM, Kambi NA, Afrasiabi M, Raz A, Saalmann YB. 2020. Thalamus modulates consciousness via layer- specific control of cortex. Neuron 0:1–10. doi:10.1016/j.neuron.2020.01.005

[7] Mitra A, Kraft A, Wright P, Acland B, Snyder AZ, Rosenthal Z, Czerniewski L, Bauer A, Snyder L, Culver J, Lee J-M, Raichle ME. 2018. Spontaneous infra-slow brain activity has unique spatiotemporal dynamics and laminar structure. Neuron 1–9. doi:10.1016/j.neuron.2018.03.015

169. Simulating the emergence of conscious and unconscious states at the whole-brain level (Showcase 3)

Maria Sacha[1], Jennifer Goldman[1], Nuria Tort-Colet[1], Federico Tesler[1], Rodrigo Cofre[1], Letizia Allegra Mascaro[2], Francesco Resta[2], Elena Montagni[2], Mavi Sánchez-Vives[3], Marcello Massimini[4,5], Alain Destexhe[1]*

Affiliations:
[1]Paris-Saclay University, CNRS, Paris-Saclay Institute of Neuroscience (NeuroPSI), 91400 Saclay, France
[2]European Laboratory for Non-Linear Spectroscopy (LENS), 50019 Sesto Fiorentino FI, Italy
[3]Institut d'Investigacions Biomèdiques August Pi i Sunyer (IDIBAPS), 08036 Barcelona, Spain
[4]Department of Biomedical and Clinical Sciences "L. Sacco", Università degli Studi di Milano, Italy
[5]IRCCS, Fondazione Don Carlo Gnocchi, 20148 Milan, Italy

*e-mail-address of corresponding author: alain.destexhe@cnrs.fr

INTRODUCTION

Conscious and unconscious states are characterized by differences in whole brain dynamics as well as differences in the microscale of single neurons. The awake brain generates high frequency, asynchronous neuronal activity, corresponding to sustained but irregular firing patterns of single neurons, defined as Asynchronous Irregular (AI). On the contrary, during unconscious states like non- rapid eye movement (NREM) sleep or anesthesia, the dynamics switch to synchronous slow-wave activity, as a result of neurons oscillating between hyperpolarized (Down) and depolarized (Up) states [1,2]. In addition to these discernable spontaneous dynamics, a state-dependent response of the brain to external stimuli is observed, with complex patterns of stimulus propagation evoked during wakefulness as opposed to diminished responsiveness during slow-wave activity [3–5]. In Showcase 3 of the Human Brain Project, whole-brain models of this paradigm were implemented in three different species, the human, mouse and macaque.

METHODS

The paradigms are demonstrated by simulations constructed in EBRAINS, consisting of the implementation of AdEx mean-field models into The Virtual Brain (TVB) [6,7]. This model could reproduce two activity states, asynchronous and synchronized slow-waves, as well as their responsiveness.

In the case of human, experiments using transcranial magnetic stimulation (TMS) were replicated, in order to show this differential brain responsiveness between wakefulness and slow-wave sleep or anesthesia, quantified by the Perturbational Complexity Index (PCI) [4]. This paradigm could be equally simulated in the cases of monkey and mouse brain. In the latter case, the mice model could be further compared to calcium imaging experiments, displaying a decrease of PCI with the depth of the anesthesia and the emergence of slow waves[8].

RESULTS AND DISCUSSION

The TVB - AdEx mean-field model was able to reproduce the occurrence of empirically observed patterns of spontaneous and evoked macroscopic brain dynamics between conscious and unconscious states,

across three different species. The advantage of the AdEx mean-field model is two-fold. Firstly, this model has been conceived to capture the asynchronous and slow-wave states, which are central in the studying of different level of consciousness. Secondly, a great feature of the mean-field model is that it enables the assessment of the impact of altering microscopic parameters on a whole-brain level. We show here the example of simulating whole brain slow-wave activity, following changes in synaptic receptor parameters, either by enhancing GABA-A receptors (propofol, barbiturates, isoflurane), or by reducing glutamate (NMDA) receptors (ketamine, xenon)[9]. In both cases, these actions can lead to the emergence of slow-wave dynamics, mimicking the action of these anesthetics.

In conclusion, we demonstrate that the EBRAINS-based TVB-Adex model is a powerful tool to investigate the effect of drugs (anesthetics) on the emergence of activity at the whole brain level, as well as capturing its responsiveness to external inputs and the way information about these inputs is propagated across the brain, which appears to be an important correlate of the level of consciousness. Future work will address the signs of consciousness based on monkey fMRI experiments, as well as in human patients in coma or minimal states of consciousness.

Keywords: whole-brain simulation, mean-field model, spontaneous activity, evoked responses, wakefulness, slow-wave sleep, anaesthesia, unconscious states

ACKNOWLEDGEMENTS

Research supported by the CNRS and the European Union (Human Brain Project H2020-785907, H2020-945539)

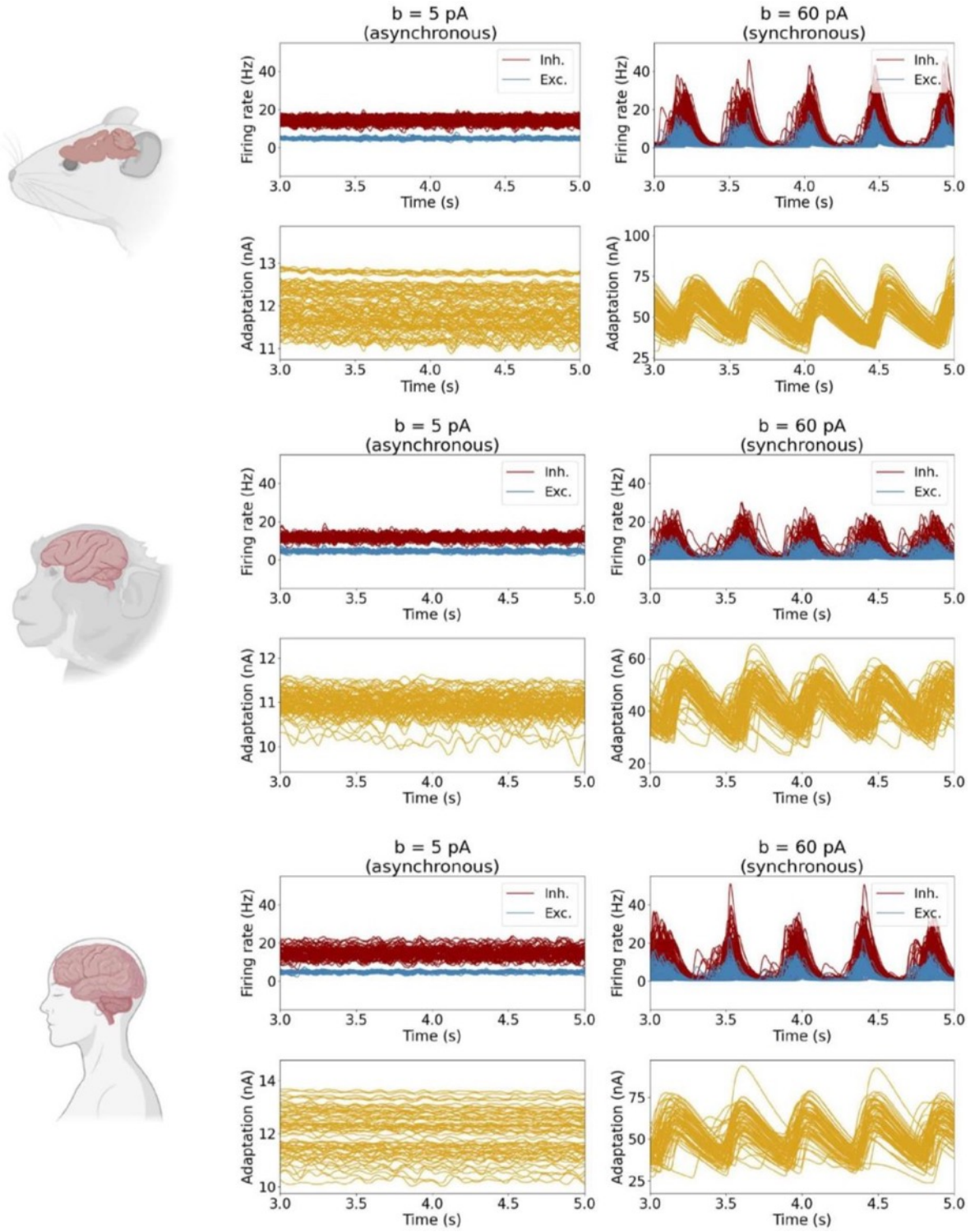

Figure 1: Simulations of spontaneous whole-brain dynamics using of the TVB-AdEx mean-field model reproducing awake (left column) and deep sleep (right column) states in the mouse, macaque and human. The time traces of the firing rates of inhibitory and excitatory populations (red and blue) and adaptation current (gold) of each of the nodes are plotted, representing 98 brain regions for the mouse, 84 for the macaque and 76 for the human. For low spike frequency adaptation (be = 5 pA) asynchronous brain activity emerges, while by increasing the adaptation (be = 60pA) the dynamics switch to synchronous, slow-wave activity.

REFERENCES

1. Niedermeyer E, da Silva FHL. *Electroencephalography: Basic Principles, Clinical Applications, and Related Fields*. Lippincott Williams & Wilkins; 2005.

2. Goldman JS, Tort-Colet N, di Volo M, et al. Bridging Single Neuron Dynamics to Global Brain States. *Front Syst Neurosci*. 2019;13:75. doi:10.3389/FNSYS.2019.00075/BIBTEX

3. Casali AG, Gosseries O, Rosanova M, et al. A theoretically based index of consciousness independent of sensory processing and behavior. *Sci Transl Med*. 2013;5(198). doi:10.1126/SCITRANSLMED.3006294

4. Massimini M, Ferrarelli F, Huber R, Esser SK, Singh H, Tononi G. Breakdown of cortical effective connectivity during sleep. *Science*. 2005;309(5744):2228-2232. doi:10.1126/SCIENCE.1117256

5. Dasilva M, Camassa A, Navarro-Guzman A, et al. Modulation of cortical slow oscillations and complexity across anesthesia levels. *Neuroimage*. 2021;224. doi:10.1016/J.NEUROIMAGE.2020.117415

6. Volo M di, Romagnoni A, Capone C, Destexhe A. Biologically Realistic Mean-Field Models of Conductance-Based Networks of Spiking Neurons with Adaptation. *Neural Comput*. 2019;31(4):653-680. doi:10.1162/neco_a_01173

7. Goldman JS, Kusch L, Aquilue D, et al. A comprehensive neural simulation of slow-wave sleep and highly responsive wakefulness dynamics. *Front Comput Neurosci*. 2023;16:190. doi:10.3389/FNCOM.2022.1058957/BIBTEX

8. Brockmeyer T, Friederich HC, Schmidt U. Advances in the treatment of anorexia nervosa: a review of established and emerging interventions. *Psychol Med*. 2018;48(8):1228-1256. doi:10.1017/S0033291717002604

9. Hemmings HC, Akabas MH, Goldstein PA, Trudell JR, Orser BA, Harrison NL. Emerging molecular mechanisms of general anesthetic action. *Trends Pharmacol Sci*. 2005;26(10):503-510. doi:10.1016/j.tips.2005.08.006

170. Apparent divergence of EEG signal diversity and information integration in rats during anaesthesia

A.S. Nilsen*[1], A. Arena[1], J.F. Storm[1]

Affiliations: [1] Physiology section, Department of Molecular Medicine, Institute of Basic Medical Sciences, University of Oslo.

*andresni@medisin.uio.no

INTRODUCTION

To investigate proposed mechanisms underlying loss of consciousness, it is important to extend approaches used in humans to rodents. Perturbational complexity index (PCI) has been promoted as a metric of "capacity for consciousness" in humans[1], but PCI is technically demanding and impractical for some clinical purposes. Therefore, a measure based on spontaneous EEG recordings is desired. We aimed to compare PCI directly with spontaneous EEG-based measures of signal diversity and integrated information in rats during wakefulness and while undergoing different forms of general anesthesia. Such a direct comparison seems to be lacking so far.

METHODS

Adult male Sprague-Dawley rats (*n* = 12) were chronically implanted with 16 epidural electrodes placed in a symmetric grid covering most of the dorsal neocortical surface (Figure 1A), for EEG recording during normal rest and general anaesthesia with either (1) ketamine, (2) propofol, or, (3) sevoflurane. See [2] for more details. Spontaneous EEG data was analysed in terms of signal diversity (Lempel-Ziv complexity; LZc, Amplitude Coalition Entropy; ACE, Synchrony Coalition Entropy: SCE - see e.g. [3]), power spectrum slope in the 20-40 Hz range (SE_{20-40} - see e.g. [4]), and measures of information integration (decoder based integrated information; $\mathbf{\Phi}^*$, geometric integrated information; $\mathbf{\Phi}^G$, stochastic interaction; SI, multi mutual information given covariance; MI, mutual integrated information; MII - see e.g. [5]).

The measures were compared to each other and to the state transition-based perturbational complexity index (PCI^{ST} - see [6]).

RESULTS

All measure of signal diversity (except SCE), $SE_{20\text{-}40}$, and measures of information integration were significantly rank-order correlated with PCI^{ST} ($|\rho| > .318$, $p < .05$) across rats and conditions (Figure 1E). The measures LZc, ACE, $SE_{20\text{-}40}$, and $\mathbf{\Phi}^{G}$, were all able to differentiate wakefulness from propofol and sevoflurane anaesthesia (Wilcoxon S-R. test; $Z = 0$, $p < 0.005$), but only PCI^{ST}, SCE, and $\mathbf{\Phi}^{G}$ were able to differentiate wakefulness from ketamine anaesthesia ($Z < 2$, $p < 0.05$). All measures besides SCE showed the same relative absolute difference between wakefulness and anaesthesia (% diff. wake vs. propofol > sevoflurane > ketamine - see Figure 1D). However, while measures of signal diversity and PCI^{ST} decreased in anaesthesia as expected, measures of information integration increased, contrary to expectations. Post-hoc analysis showed that an increase in network integration during anaesthesia, and a decrease in segregation (Figure 1F) predicted the level of change in the measures used. Applying the same analysis on a range of auto-regressive models (Figure 2A) made to investigate the relationship between structural properties of a network and measures of information integration [7] further supported these results (Figure 2B).

DISCUSSION

We observed that signal diversity measures based on spontaneous EEG can accurately distinguish between wakefulness and different anesthetics in a similar way as the perturbational index, PCI^{ST}. However, contrary to expectations, we found that measures of information integration increased during anesthesia. While estimates of structural integration (increase in anesthesia) and segregation (decrease in anesthesia) predicted the observed changes in measures based on spontaneous EEG, the connectivity changed in the opposite direction compared to connectivity measures based on evoked responses[2]. This is surprising given the contemporary understanding of the effect of anesthesia on corticocortical connectivity (e.g. [8]). We speculate that our results may be explained by either a decrease in specificity in information processing (i.e. reduced differentiation) during propofol and sevoflurane anesthesia, but not in ketamine anesthesia, or that thalamocortical projections are preserved during propofol and sevoflurane anesthesia while long-range corticocortical connectivity is disrupted as is argued in previous studies.

Keywords: EEG, consciousness, anaesthesia, rat, PCI, integrated information, signal diversity, connectivity, neuroscience

ACKNOWLEDGEMENTS

We thank Bjørn Erik Juel, PhD, for valuable comments and assistance during analysis. This research was funded by the ConsciousBrainConcepts project under the Life Science Convergence Projects initiative of University of Oslo, and the European Union's Horizon 2020 Framework Programme for Research and Innovation under the Specific Grant Agreements No. 945539 (Human Brain Project SGA3), No. 785907 (Human Brain Project SGA2; JFS, ASN, BEJ), and the Norwegian Research Council (NRC grant 262950/F20). ASN performed the analysis and wrote the manuscript. AA gathered the data and helped design the analytical pipeline. JFS lead the project. All authors contributed to the manuscript.

REFERENCES

[1] Casali AG, Gosseries O, Rosanova M, Boly M, Sarasso S, Casali KR, et al. A theoretically based index of consciousness independent of sensory processing and behavior. *Sci Transl Med*. 2013;5(198):198ra105. doi:10.1126/scitranslmed.3006294

[2] Arena A, Comolatti R, Thon S, Casali AG, Storm JF. General anesthesia disrupts complex cortical dynamics in response to intracranial electrical stimulation in rats. *eneuro*. Published online 2021:ENEURO.0343-20.2021. doi:10.1523/eneuro.0343-20.2021

[3] Schartner M, Seth A, Noirhomme Q, Boly M, Bruno MA, Laureys S, et al. Complexity of multi-dimensional spontaneous EEG decreases during propofol induced general anaesthesia. *PLoS One*. 2015;10(8). doi:10.1371/journal.pone.0133532

[4] Colombo MA, Napolitani M, Boly M, Gosseries O, Casarotto S, Rosanova M, et al. The spectral exponent of the resting EEG indexes the presence of consciousness during unresponsiveness induced by propofol, xenon, and ketamine. *Neuroimage*. 2019;189:631-644. doi:10.1016/j.neuroimage.2019.01.024

[5] Kitazono J, Oizumi M. Practical PHI Toolbox for Integrated Information Analysis.; 2018. doi:10.6084/m9.figshare.3203326

[6] Comolatti R, Pigorini A, Casarotto S, Fecchio M, Faria G, Sarasso S, et al. A fast and general method to empirically estimate the complexity of brain responses to transcranial and intracranial stimulations.
Brain Stimul. 2019;12(5):1280-1289. doi:10.1016/j.brs.2019.05.013

[7] Mediano PAM, Seth AK, Barrett AB. Measuring Integrated Information: Comparison of Candidate Measures in Theory and Simulation. *Entropy*. 2018 Dec 25;21(1):17. doi: 10.3390/e21010017

[8] Hudetz AG. General anesthesia and human brain connectivity. *Brain Connect*. 2012;2(6):291-302. doi:10.1089/brain.2012.0107

FIGURES

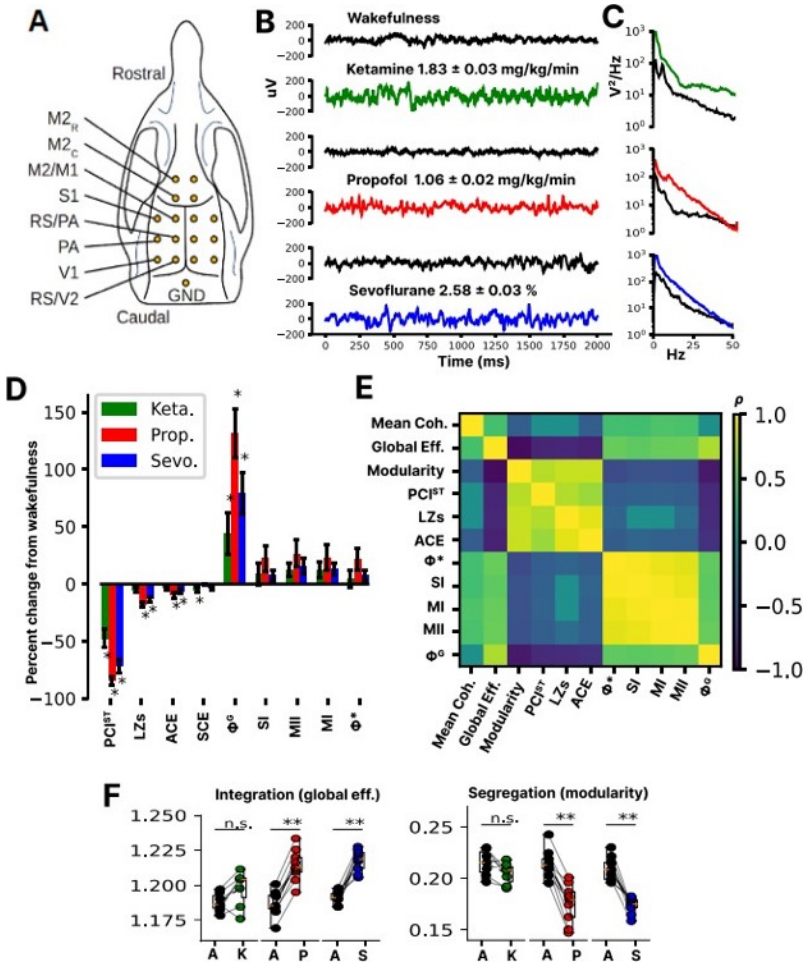

Figure 1. A) Overview of electrode placement. **B)** Example of raw traces from a single rat and single channel ($M2_R$). **C)** Power spectral density over channels for a single rat. **D)** Percentwise change from wakefulness for measures of signal diversity, PCI, and integrated information. **E)** Spearman's rank-order correlation matrix between measures, across all rats and conditions. **F)** Estimate of structural integration (global efficiency) and structural segregation (modularity) of the directed connectivity (as estimated by the directed transfer function) during wakefulness and anesthesia. Abbreviations: ρ; Spearman's correlation, **LZs**; Lempel-Ziv single channel complexity, **PCIST**; perturbational complexity index on state transitions, **Φ^G**; geometric integrated information, **SE_{20-40}**; spectral exponent (calculated in the 20-40 Hz range), **ACE**; amplitude coalition entropy, **SCE**; synchrony coalition entropy, **Φ^***; mismatched decoding based integrated information, **SI**; stochastic interaction, **MI**; multi mutual information given covariance, **MII**; mutual integrated information, **Mean Coh**; mean absolute coherence across channels.

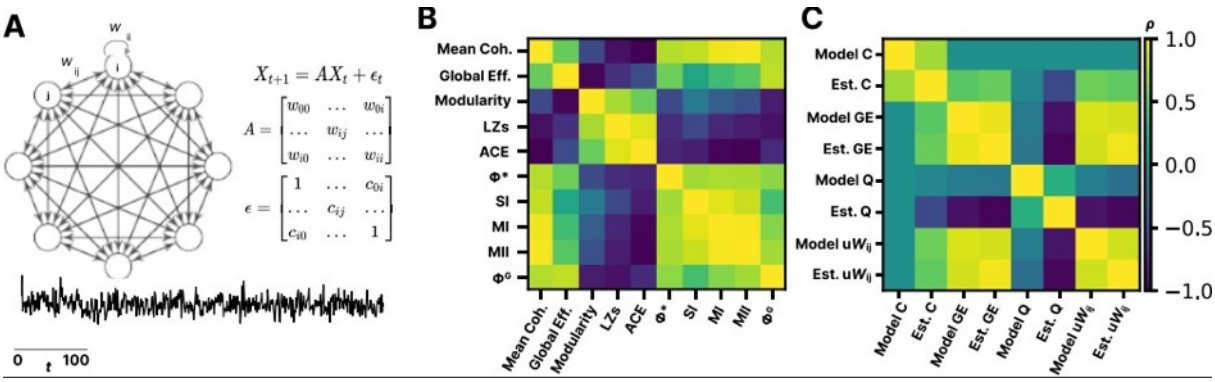

Figure 2. A) Overview of the auto-regressive model inspired by [7], **B)** Spearman's rank-order correlation matrix between measures and estimated network properties based on the directed transfer function (DTF), across all generated models, **C)** and over estimated (est.) network properties based on DTF and on the networks' underlying (model) connectivity (matrix A in panel A). Abbreviations: ρ; Spearman's correlation, **LZs**; Lempel-Ziv single channel complexity, **Φ^G**; geometric integrated information, **SE_{20-40}**; spectral exponent (calculated in the 20-40 Hz range), **ACE**; amplitude coalition entropy, **SCE**; synchrony coalition entropy, **Φ^***;

mismatched decoding based integrated information, **SI**; stochastic interaction, **MI**; multi mutual information given covariance, **MII**; mutual integrated information, **Mean Coh**; mean absolute coherence across channels, **C**; correlated noise factor, $\boldsymbol{W}_{ij}$; connection weight, **Q**; modularity estimated with the Louvain method, **GE**; global efficiency (i.e. mean inverse shortest path length).

171. Experimentation, Learning and Dialogue: a novel approach to dual use of concern in brain research

Inga Ulnicane

Centre for Computing and Social Responsibility, De Montfort University, Leicester, UK inga.ulnicane@dmu.ac.uk

INTRODUCTION/MOTIVATION

New technologies usually are developed with the best intentions in mind. However, history of technology shows that afterwards they occasionally are put to harmful or malicious uses. This is typically known as a dual use problem, namely, that all technologies – including brain research – can be put to socially beneficial as well as harmful uses (Ulnicane 2020). More narrowly, dual use is understood as civil-military dichotomy, where technologies can have applications both in civil and military domains. The EU Framework Programme for research and innovation, which also funds the Human Brain Project (HBP), stipulates that all research it funds should have an exclusive focus on civil applications. In addition to complying with the contractual obligations about exclusive focus on civil applications, the HBP Ethics and Society team in collaboration with scientists and stakeholders within and beyond the project has developed a novel approach to dual use of concern issues (Ulnicane et al 2022). This approach considers a broader range of potential concerns that brain research might raise in political, security, intelligence and military domains (Aicardi et al 2018).

METHODS

To identify and address dual use of concern in brain research, the HBP Ethics and Society team uses Responsible Research and Innovation (RRI) approach, which aims to align research and innovation with societal needs (Stahl et al 2021). To identify and address potential concerns, RRI approach focuses on anticipation, reflection, engagement and action. These activities require interdisciplinary collaborations bringing together expertise, insights and perspectives from various disciplines including neuroscience, computing, social sciences and humanities (Aicardi et al 2020). The HBP has established a number of forums for such interdisciplinary collaborations including a project-wide Dual Use Working Group that collaborates closely with the Ethics Rapporteur Programme, HBP Education programme and the Ethics and Society team (Ulnicane et al 2022). These forums provide safe spaces and networks of support that allow to raise and discuss any potential concerns in a safe and supportive environment that encourages mutual learning and experimentation. Identifying any potential concerns is a part of an ongoing and open-ended dialogue rather than a checklist or a box-ticking exercise (Stahl 2019).

RESULTS AND DISCUSSION

Our experience from these interdisciplinary collaborations suggests that in order to identify and address a broader range of potential concerns, it is important 1) to productively combine research and practice, where research on

governance of emerging technologies provides background and ideas for novel methods, while practice raises questions for future research; 2) to closely integrate activities of anticipation, reflection, engagement and action; and 3) to undertake an experimental approach which allows to flexibly engage with emerging and uncertain issues (Ulnicane et al 2022). This approach to dual use of concern developed by the HBP Ethics and Society team has been well received (Ienca et al 2018), including invitations to present it at the Horizon Europe Foresight Network of the European Commission and to provide training on dual use issues for another FET project.

Keywords: dual use of concern, misuse, brain research, Responsible Research and Innovation, ethics, governance, emerging technology, interdisciplinary collaboration

ACKNOWLEDGEMENTS

This research has received funding from the EU's Horizon 2020 Research Programme under Grant Agreements No.720270 (HBP SGA1), No.785907 (HBP SGA2), No. 945539 (HBP SGA3).

REFERENCES

[1] Aicardi, Christine, Simisola Akintoye, B. Tyr Fothergill, Manuel Guerrero, Gudrun Klinker, William Knight, Lars Klüver, et al. 2020. "Ethical and Social Aspects of Neurorobotics." *Science and Engineering Ethics* 26 (5): 2533–2546. doi:10.1007/s11948-020-00248-8

[2] Aicardi, Christine, Lise Bitsch, Nicklas Bang Bådum, Saheli Datta, Kathinka Evers, Michele Farisco, Tyr Fothergill, et al. 2018. "Opinion on 'Responsible Dual Use' Political, Security, Intelligence and Military Research of Concern in Neuroscience and Neurotechnology." Zenodo. doi:10.5281/zenodo.4588601

[3| Ienca, Marcello, Fabrice Jotterand, and Bernice S. Elger. 2018. "From Healthcare to Warfare and Reverse: How Should We Regulate Dual-Use Neurotechnology?" *Neuron* 97 (2): 269–274. doi:10.1016/j.neuron.2017.12.017

[4] Stahl, Bernd Carsten, Simisola Akintoye, B. Tyr Fothergill, Manuel Guerrero, Will Knight, and Inga Ulnicane. 2019. "Beyond Research Ethics: Dialogues in Neuro-ICT Research." *Frontiers in Human Neuroscience* 13. doi:10.3389/fnhum.2019.00105

[5] Stahl, Bernd Carsten, Simisola Akintoye, Lise Bitsch, Damian Eke, Michele Farisco, Karin Grasenick, Manuel Guerrero, William Knight, Tonii Leach, Sven Nyholm, George Ogoh, Achim Rosemann, Arleen Salles, Julia Trattnig and Inga Ulnicane. 2021. "From Responsible Research and Innovation to Responsibility by Design." *Journal of Responsible Innovation* 8(2): 175-198 https://doi.org/10.1080/23299460.2021.1955613

[6] Ulnicane, Inga. 2020. "Governance of Dual Use Research in the EU: The Case of Neuroscience." In *Emerging Security Technologies and EU Governance: Actors, Practices and Processes*, edited by Antonio Calcara, Raluca Csernatoni, and Chantal Lavallée, 1 edition, 177–191. London; New York, NY: Routledge. https://doi.org/10.4324/9780429351846-12

[7] Ulnicane, Inga, Tara Mahfoud and Arleen Salles. 2022. "Experimentation, learning, and dialogue: an RRI- inspired approach to dual-use of concern." *Journal of Responsible Innovation*. https://doi.org/10.1080/23299460.2022.2094071

172. The EBRAINS Italian national node: multiscale, multimodal and multimodel approach for integrated services

Francesco S. Pavone[1,*], Giulia Adembri[2]

[1] European Laboratory for Non-Linear Spectroscopy. LENS - University of Florence, Italy
[2] INO-CNR, Firenze, Italy

*pavone@lens.unifi.it

INTRODUCTION/MOTIVATION

The analysis of the relationship between neural anatomical structures and the emerging functional properties is a crucial step for the advancement of modern Neuroscience. The integration through multimodal approaches of advanced electrophysiological recordings, imaging and modelling techniques to address the structure -function conundrum is now opening promising perspectives in health and neurotechnology. This long-term vision is the backbone of the EBRAINS Italian national node, which offers an integrated approach encompassing Multiscale, Multimodal and Multimodel analyses (3M) to provide Health, Neuroscientific and Industrial communities access to services in the EBRAINS framework.

The understanding of brain structures and functions has been significantly improved owing to modern imaging techniques such as magnetic resonance imaging (MRI) at the macroscale and optical imaging at the micro and mesoscale. At the same level, novel signal recordings methods such as high-density integrated silicon-technologies and genetically encoded activity probes have shed light on molecular, cellular and biophysical building blocks at multiple temporal resolution. The data generated with these techniques can be integrated with multiscale modelling workflows that can go either from micro to macro and vice-versa to simulate brain functions with an unprecedented range of spatio-temporal scales. Data-driven models of brain activity allow conceptual integration, provide the basis for prediction and validation and can be potentially brought up to the generation of effective

brain digital twins. The integration of data and models is the basis for the Italian node toward the effective implementation of the EBRAINS targets.

METHODS

The EBRAINS Italian National Node (EINN) will move along a multiscale spatiotemporal concept offering a 3M approach in which the structure-function dichotomy can be explored using advanced methods implemented and accessed through various facilities distributed within the national EBRAINS ecosystem. The EINN is led by the Consiglio Nazionale delle Ricerche (CNR) and interacts with many national bodies. The "EBRAINS Italian Community (EIC)" consortium is one of them. It embraces 15 research institutions, working on the involvement of stakeholders and communities in order to support the national node. Together with that, EINN interacts with the consortium of institutes, most of them also included in EIC, involved in the EBRAINS-Italy Infrastructure (a National Project connected to the "European Recovery Funds Action"), in which 23 operative units are creating services for data production, storage and curation, analysis and modelling tools including neuromorphic and neurorobotics, and innovative genetically-encoded molecular tools for translational applications, as well as a training and innovation facility, all of which propaedeutic to the creation of the Italian National Node services.

On top of that, EINN also interacts with the neuroscience National Communities, Hospital Networks, industries and governmental bodies.

The Italian National Node will be keen in securing adequate and sustainable funding to provide tools and services to the EBRAINS RI by continuous interaction with national and regional governing bodies as well as biotech and pharma companies to set up tailored services.

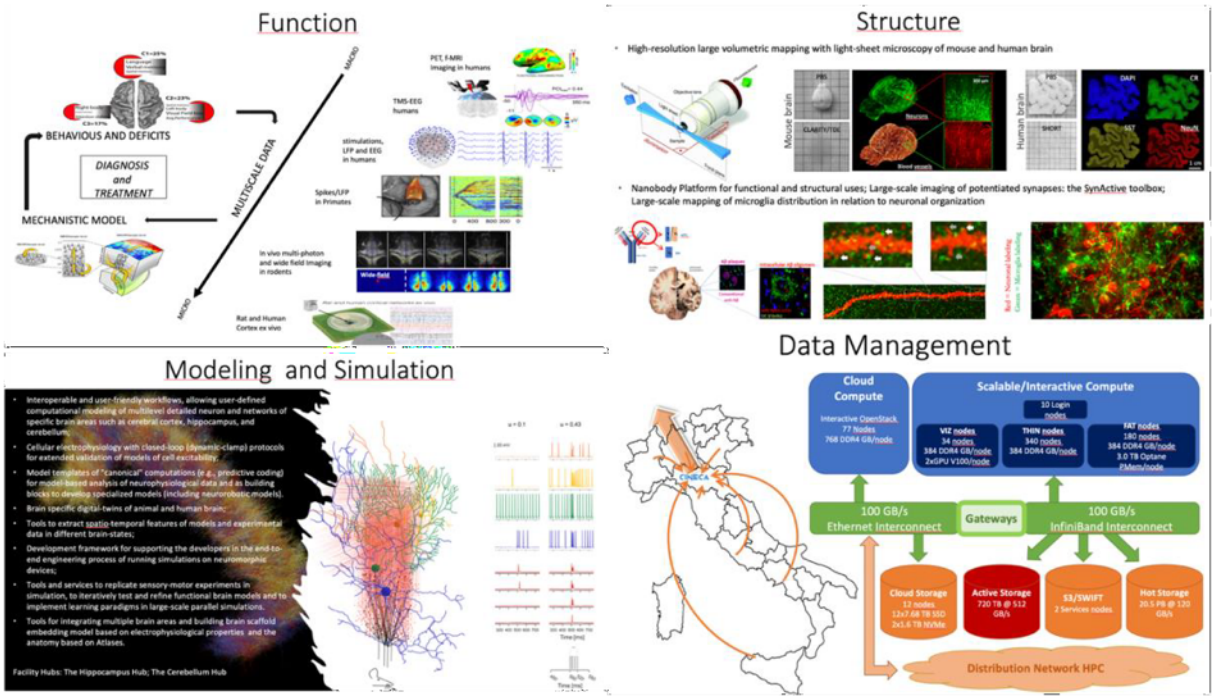

Fig.1

RESULTS AND DISCUSSION

The EBRAINS Italian National Node has moved along this 3M vision and the partners are implementing service pipelines integrating customized 3M data production, data analysis, data curation and data management, together with modelling, simulation and neurorobotic platforms. Furthermore, a service for training and innovation center will be made available for the development and use of *ad hoc* training instruments, both on-site and in remote (e.g., e-learning) and to promote dissemination and interactions with academic, institutional and industrial partners. The EINN proposes integrated data services that feed modelling and simulation in line with the original EBRAINS proposition of connecting distributed research infrastructures for neuroscience toward a new era of neuroscience research.

Keywords:

EBRAINS

Italian national node

multiscale multimodal

multimodel

ACKNOWLEDGEMENTS

This project was supported by the European Union's Horizon 2020 Framework Programme for Research and Innovation under the Specific Grant Agreement No. 945539 (Human Brain Project SGA3), the European Union's Research and Innovation Program Horizon Europe under grant agreement No 101079717 (EBRAINS-PREP), and the Project IR11– EBRAINS-Italy - M4C2 Line 3.1 of the PNRR, Action 3.1.1 – Funded by European Commission – NextGenerationEU (CUP B51E22000150006)

REFERENCES

The full list of institution involved in the EBRAINS ecosystem

- Consiglio Nazionale delle Ricerche (CNR)
- Cineca Interuniversity Consortium (CINECA)
- European Brain Research Institute Rita Levi-Montalcini Foundation (EBRI)
- Istituto Nazionale di Fisica Nucleare (INFN)
- European Laboratory for Non Linear Spectroscopies (LENS)
- Polytechnic University of Turin (POLITO)
- Scuola Normale Superiore of Pisa (SNS)
- Sant'Anna School of Advanced Studies and Specialization (SSSA)
- University of Milan (UMIL)
- University of Pavia (UNIPV)
- Istituto Italiano di Tecnologia (IIT)
- Istituto Superiore di Sanità (ISS)
- Polytechnic University of Milan (POLIMI)
- Sapienza University of Rome (UNIROMA1)
- University of Naples Federico II (UNINA)
- International School for Advanced Studies (SISSA)
- University of Padua (UNIPD)
- University of Modena and Reggio Emilia (UNIMORE)
- University of Turin (UNITO)

- University of Naples Parthenope (UNINAP)
- IRCSS San Camillo Hospital
- University of Sassari (UNISS)
- University of Florence

173. EBRAINS Spanish Node

Guillermo Velasco[1*]

[1] Centro de Apoyo a la Innovación Tecnológica, UPM, Madrid, Spain

*guillermo.velasco@upm.es

One major objective of the EBRAINS SPAIN is to increase the interaction and links between its members and other neuroscientific actors worldwide to generate opportunities for joint research and optimize the agenda of services to be integrated and offered through EBRAINS.

The activities of the EBRAINS Spanish Node are designed to generate a much more profound understanding of the EBRAINS´ mission by other national players, including patients and the public, thus contributing to a broader perception of the social, economic, and medical benefits of human brain research.

The EBRAINS Spanish Node is presently formed by different universities, research centers, hospitals, and industrial companies operating in neuroscience and neuro-technology. The members are immersed in diverse research initiatives, including, among many others, the combination of functional brain imaging techniques with patient injury data, pharmacology, genetics and intracranial registries to analyse human brain functions; the study of new non-pharmacological treatments for movement disorders, in particular for Parkinson's disease; the development of diagnostic tools to evaluate non-invasive and translational image-based biomarkers in neurodegenerative diseases; the elaboration of prognostic tools based on artificial intelligence; the three-dimensional reconstruction of the structure of brain tissue to provide data on brain 3D synaptic organization; or the use of multiphotonic stimulation, with non-invasive infrared light, to target pharmacological actions. The Node may also provide access to various and comprehensive computational imaging biobanks for brain research.

The synergies associated to these research initiatives will contribute to position the Node as a strategic pillar of the Spanish Neuroscience system and facilitate a progressive alignment of its work to the European Commission policies and programs in Neuroscience, particularly in relation to the fight against brain diseases.

Keywords: EBRAINS, Research infrastructure, Neuroscience, Neurotechnology